

Reactivity and Structural Characterization of Alkylolithium
and Amidolithium Reagents

By Chi-Cheung Su

B.S., Tsinghua University, 2008

A Dissertation Submitted in Partial Fulfillment of the
Requirements for the Degree of Doctor of Philosophy in
the Department of Chemistry at Brown University

Providence, Rhode Island

May 2014

© Copyright 2014 by Chi-Cheung Su

This dissertation by Chi-Cheung Su is accepted in its present form by the Department of Chemistry as satisfying the dissertation requirement for the degree of Doctor of Philosophy.

Date _____
Paul G. Williard, Advisor

Recommended to the Graduate Council

Date _____
David E. Cane, Reader

Date _____
Christopher T. Seto, Reader

Approved by the Graduate Council

Date _____
Peter M. Weber, Dean of the Graduate School

Curriculum Vitae

Chi-Cheung Su was born in Hong Kong on March 29th, 1986. In August 2004, he entered Tsinghua University with a full tuition scholarship for four years. He graduated in July 2008 with a Bachelor of Science degree in Chemistry. In the fall of 2008, he enrolled at Brown University pursuing the degree of Doctor of Philosophy in the Department of Chemistry. He was awarded a fellowship from the department in 2009. He was accepted into Professor Williard's research group and started his research on organolithium compounds in January 2009.

Publications

1. Su, C.; Williard, P. G. "Isomerization of Allyl Ethers Initiated by Lithium Diisopropylamide", *Org. Lett.* **2010**, *12*, 5378-5381.
2. Beng, T. K.; Tyree, W. S.; Parker, T.; Su, C.; Williard, P. G.; Gawley, R. E. "Dynamics of Catalytic Resolution of 2-Lithio-N-Boc-piperidine by Ligand Exchange", *J. Am. Chem. Soc.* **2012**, *134*, 16845-16855.
3. Su, C.; Hopson, R.; Williard, P. G. "Crystal Structure and Solution State Characterization of Lithium (*S*)-(1-(bis(2-methoxyethyl)amino)-3-methylbutan-2-yl)(methyl)amide", *J. Org. Chem.* **2013**, *78*, 7288-7292.
4. Su, C.; Hopson, R.; Williard, P. G. "Characterization of Hexameric and Octameric *sec*-Butyllithium/*sec*-Butoxide Mixed Aggregates", *Eur. J. Inorg. Chem.* **2013**, *24*, 4136-4141.

5. Su, C.; Hopson, R.; Williard, P. G. “Characterization of Cyclopentyllithium and Cyclopentyllithium Tetrahydrofuran Complex”, *J. Am. Chem. Soc.* **2013**, *135*, 12400-12406.
6. Su, C.; Li, W.; Hopson, R.; Williard, P. G. “Mixed Aggregates of an Alkyl Lithium Reagent and a Chiral Lithium Amide Derived from *N*-Ethyl-*O*-Triisopropylsilyl Valinol”, *J. Am. Chem. Soc.* **2013**, *135*, 14367-14379.
7. Su, C.; Hopson, R.; Williard, P. G. “Isotopically Enriched ^{13}C Diffusion-Ordered NMR Spectroscopy – Analysis of Methyl lithium”, *J. Org. Chem.* **2013**, *78*, 11733-11746.
8. Su, C.; Guang, J.; Williard, P. G. “Crystal Structures of Lithiated *N*-Alkylanilides: From Tetra-solvated Dimer to Tri-solvated Monomer”, *J. Org. Chem.* Revision pending for final acceptance.
9. Su, C.; Williard, P. G. “Facile Preparation of Carbamoyl Chlorides from Tertiary *N*-allyl Amines with Triphosgene”, submitted.
10. Su, C.; Guang, J.; Li, W.; Wu, K.; Liu, C.; Hopson, R.; Williard, P. G. “Chiral Lithium Diamides Derived from Linked *N*-isopropyl Valinol or Alaninol”, submitted.
11. Su, C.; Liu, C.; Hopson, R.; Williard, P. G. “Chiral Lithium Amide Aggregates”, submitted.
12. Su, C.; Liu, Q.; Williard, P. G. “Characterization of hexameric lithium diethylamino propenolate and its mixed aggregates with lithium *n*-butoxide”, manuscript in preparation.

To My Family

Acknowledgments

First of all, I would like to express my sincere gratitude to my advisor Professor Paul G. Williard for always guiding, supporting and encouraging me into the field of chemical research. He has offered me invaluable opportunities to pursue my research interest and conduct intriguing projects. His unlimited knowledge and sharp insight in chemistry was a constant inspiration and motivating factor in my research. Nothing could be accomplished without his guidance in these five years.

I also want to thank Professor David E. Cane, Professor Christopher T. Seto and Professor J. William Suggs for not only being my committee members, but also providing excellent suggestions and teaching me valuable knowledge of chemistry. I also thank Professor Matthew B. Zimmt for instructing me with the knowledge of physical organic chemistry.

I would like to acknowledge Professor Robert E. Gawley for his sharing of in-depth knowledge about lithiated piperidine and Professor Renzo Luisi for his teaching on the chemistry of aziridines and *sec*-butyllithium.

I am very grateful to Dr. Russell Hopson for his intensive support with the NMR experiments and paper correction. I also thank Dr. Tun-li Shen for his help with the mass spectroscopy.

It is so fortunate for me to work in Williard's group. I thank Dr. Indrek Reile for educating me with the practical skills of organic synthesis. I also thank Dr. Weibin Li and Dr. Gerald Kagan for sharing me with their ample knowledge of diffusion-ordered spectroscopy. I also need to thank Ms. Jie Guang for her help and discussion about NMR

experiments. I thank Mr. Satoshi Umezu for teaching me the chemistry of ynolates and Japanese language. I also appreciate the help from Mr. Chang Liu for the synthesis of Diamino diethers.

Finally, I am very indebted to all of my family members for their understanding, support, and encouragement all these years.

Table of Contents

Chapter 1. General Introduction	1
1.1 Brief introduction of organolithium compounds	2
1.2 Methods for the determination of aggregation and solvation states	4
1.2.1 X-Ray crystallography for the determination of solid state structures	4
1.2.2 Multinuclear one- and two-dimensional NMR spectroscopy	5
1.2.3 Diffusion-ordered NMR spectroscopy for the formula weight determination	6
1.3 The scope and overview of this thesis	10
1.4 References	12
Chapter 2. Isomerization of allyl ethers initiated by lithium diisopropylamide	15
2.1 Abstract.....	16
2.2 Introduction	16
2.3 Results and Discussion	17
2.3.1 Isomerization of allyl ethers by lithium diisopropylamide	17
2.3.2 Isomerization of allyl ethers by different lithium amides	20
2.3.3 Comparison of <i>t</i> -BuOK and LDA initiated isomerization.....	21
2.4 Conclusion	23
2.5 Experimental Section.....	23
2.6 References	37
Chapter 3. Isotopically enriched ¹³C diffusion-ordered NMR spectroscopy – analysis of methyllithium	38

3.1 Abstract.....	39
3.2 Introduction	39
3.3 Results and Discussion	42
3.3.1 Design, synthesis and <i>D-FW</i> analysis protocol of the ¹³ C labeled internal reference system for DOSY NMR.....	42
3.3.2 Analysis of methyllithium and methyllithium-tertiary diamine complexes in diethyl ether	49
3.4 Conclusion	67
3.5 Experimental Section.....	68
3.6 Acknowledgement	77
3.7 References	78

Chapter 4. Characterization of cyclopentyllithium and cyclopentyllithium

tetrahydrofuran complex.....	81
4.1 Abstract.....	82
4.2 Introduction	82
4.3 Results and Discussion	84
4.3.1 Characterization of cyclopentyllithium in solid- and solution-states	84
4.3.2 Characterization of cyclopentyllithium/THF complex in solid- and solution- states	91
4.4 Conclusion	95
4.5 Experimental Section.....	96
4.6 Acknowledgement	99

4.7 References	100
----------------------	-----

Chapter 5. Characterization of hexameric and octameric <i>sec</i>-butyllithium/<i>sec</i>-butoxide mixed aggregates.....	102
5.1 Abstract.....	103
5.2 Introduction	103
5.3 Results and Discussion	104
5.3.1 Characterization of hexameric <i>s</i> -BuLi/ <i>s</i> -BuOLi mixed aggregate	104
5.3.2 Characterization of octameric <i>s</i> -BuLi/ <i>s</i> -BuOLi mixed aggregate	110
5.4 Conclusion	113
5.5 Experimental Section.....	114
5.6 Acknowledgement	117
5.7 References	118

Chapter 6. Crystal structure and solution state characterization of lithium (S)-(1-(Bis(2-methoxyethyl)amino)-3-methylbutan-2-yl)(methyl)amide	120
6.1 Abstract.....	121
6.2 Introduction	121
6.3 Results and Discussion	122
6.4 Conclusion	128
6.5 Experimental Section.....	128
6.6 Acknowledgement	131
6.7 References	132

Chapter 7. Mixed aggregates of an alkyllithium reagent and a chiral lithium amide derived from <i>N</i>-ethyl-<i>O</i>-triisopropylsilyl valinol	134
7.1 Abstract.....	135
7.2 Introduction	135
7.3 Results and Discussion	137
7.3.1 Solid state structure of 2:2 mixed aggregate of lithiated (<i>S</i>)- <i>N</i> -ethyl-3-methyl-1-(triisopropylsilyloxy)butan-2-amine and cyclopentyllithium.....	137
7.3.2 Solution state characterization of a 2:2 mixed aggregate of cyclopentyllithium and the chiral lithium amide derived from <i>N</i> -ethyl- <i>O</i> -triisopropylsilyl valinol	139
7.3.3 Solution state characterization of a 2:2 mixed aggregate of <i>n</i> -butyllithium and the chiral lithium amide derived from <i>N</i> -ethyl- <i>O</i> -triisopropylsilyl valinol.....	145
7.3.4 Solution state characterization of a 2:2 mixed aggregate of isopropyllithium and the chiral lithium amide derived from <i>N</i> -ethyl- <i>O</i> -triisopropylsilyl valinol	150
7.3.5 Solution state characterization of a 2:2 mixed aggregate of <i>s</i> -butyllithium and the chiral lithium amide derived from <i>N</i> -ethyl- <i>O</i> -triisopropylsilyl valinol.....	155
7.4 Conclusion	160
7.5 Experimental Section.....	161
7.6 Acknowledgement	166
7.7 References	166
Chapter 8. Chiral lithium diamides derived from linked <i>N</i>-isopropyl valinol or alaninol	169
8.1 Abstract.....	170

8.2 Introduction	170
8.3 Results and Discussion	172
8.3.1 Crystal structure of dilithiated (2 <i>S</i> ,2' <i>S</i>)-1,1'-(butane-1,4-diylbis(oxy))bis(<i>N</i> -isopropylpropan-2-amine)	173
8.3.2 Crystal structure of dilithiated (2 <i>S</i> ,2' <i>S</i>)-1,1'-(pentane-1,5-diylbis(oxy))bis(<i>N</i> -isopropylpropan-2-amine)	175
8.3.3 Crystal structure of dilithiated (2 <i>S</i> ,2' <i>S</i>)-1,1'-(heptane-1,7-diylbis(oxy))bis(<i>N</i> -isopropyl-3-methylbutan-2-amine).....	177
8.3.4 Crystal structure of dilithiated (2 <i>S</i> ,2' <i>S</i>)-1,1'-(pentane-1,5-diylbis(oxy))bis(<i>N</i> -isopropyl-3-methylbutan-2-amine).....	179
8.4 Conclusion	180
8.5 Experimental Section.....	181
8.6 Acknowledgement	185
8.7 References	186
Chapter 9. Crystal structures of lithium <i>N</i>-alkylanilides: from tetra-solvated dimer to tri-solvated monomer	188
9.1 Abstract.....	189
9.2 Introduction	189
9.3 Results and Discussion	191
9.3.1 Tetrahydrofuran tetra-solvated dimers of various lithium anilides.....	191
9.3.2 Tetrahydropyran, methyltetrahydrofuran and <i>N,N</i> -diethylpropionamide tetra-solvated dimers of lithium <i>N</i> -methylanilide	194

9.3.3 Dimethoxymethane tetra-solvated dimers of two lithium <i>N</i> -alkylanilides	197
9.3.4 Dimethyltetrahydrofuran di-solvated dimer of lithium <i>N</i> -methylanilide.....	198
9.3.5 Tetrahydrofuran tri-solvated monomers of lithium <i>N</i> -isopropylanilide and <i>N</i> - diphenylamide	199
9.3.6 Tetrahydrofuran tri-solvated dimer of lithium <i>N</i> -isobutylanilide and tetrahydro- furan di-solvated dimer of lithium <i>N</i> -neopentylanilide	201
9.4 Conclusion	203
9.5 Experimental Section.....	204
9.6 Acknowledgement	206
9.7 References	207
Chapter 10. The Mixed Aggregates of Chiral Lithium Amides	209
10.1 Abstract.....	210
10.2 Introduction	210
10.3 Results and Discussion	213
10.3.1 Solution State Characterization of the 2:2 Mixed Aggregate of Lithiated Chiral Amine 7 and <i>n</i> -BuLi (10)	213
10.3.2 Solution State Characterization of the Mixed Aggregates of Lithiated Chiral Amine 8 and <i>n</i> -BuLi (11 and 12).....	220
10.3.3 Solution State Characterization of the Mixed Aggregate of Lithiated Chiral Amine 9 and <i>n</i> -BuLi 13 and Homodimer 14	226
10.4 Conclusion	231
10.5 Experimental Section.....	232

10.6 Acknowledgement	235
10.7 References	236
Appendix A. CCDC numbers for all crystal structures.....	239
Appendix B. Supporting information for Chapter 2.....	241
Appendix C. Supporting information for Chapter 3.....	275
Appendix D. Supporting information for Chapter 4.....	307
Appendix E. Supporting information for Chapter 5.....	326
Appendix F. Supporting information for Chapter 6.....	359
Appendix G. Supporting information for Chapter 7	372
Appendix H. Supporting information for Chapter 8	403
Appendix I. Supporting information for Chapter 10.....	407

List of Figures

Figure 1.1. The PGSE pulse sequence.....	7
Figure 2.1. (1a) Definition of α and β positions and R' group of the allyl ethers. (1b) An example of allyl ether without β branched chain. (1c) An example of allyl ether with only one β branched chain. (1d) An example of allyl ether with two β branched chains	18
Figure 3.1. ^{13}C DOSY of BEN , IR1 , IR2 , IR3 and 1 at 20 °C.....	45
Figure 3.2. <i>D-FW</i> analysis of ^{13}C DOSY data. Internal references are shown as solid squares and <i>N</i> -Boc-piperidine 1 is shown as open square.....	46
Figure 3.3. ^{13}C DOSY of BEN , IR1 , IR2 , IR4 and 1 at 20 °C.....	48
Figure 3.4. <i>D-FW</i> analysis of ^{13}C DOSY data. Internal references are shown as solid squares and <i>N</i> -Boc-piperidine 1 is shown as open square.....	48
Figure 3.5. NMR spectra of 0.06 M $^{13}\text{CH}_3^6\text{Li}$ DEE solution at -40 °C. ^6Li spectrum are depicted in (a) and ^{13}C spectrum is depicted in (b).....	51
Figure 3.6. ^{13}C DOSY of $^{13}\text{CH}_3^6\text{Li}$ DEE solution at -40 °C.....	52
Figure 3.7. <i>D-FW</i> analysis of ^{13}C DOSY data. Internal references are shown as black squares and the tetra-solvated tetramer 3 is shown as the white square.....	53
Figure 3.8. ^{13}C spectra of $^{13}\text{CH}_3^6\text{Li}$. (a) represents the ^{13}C spectrum of 0.12 M $^{13}\text{CH}_3^6\text{Li}$ in DEE at -70°C. (b) represents the ^{13}C spectrum of 0.12 M $^{13}\text{CH}_3^6\text{Li}$ in DEE with 3 equiv TMEDA at -40°C. (c) represents the ^{13}C spectrum of 0.12 M $^{13}\text{CH}_3^6\text{Li}$ in DEE with 3 equiv TMEDA at -70°C	55
Figure 3.9. ^6Li NMR spectrum of 0.12 M $^{13}\text{CH}_3^6\text{Li}$ DEE solution with 3 equiv TMEDA at -70 °C.	55
Figure 3.10. ^{13}C DOSY of $^{13}\text{CH}_3^6\text{Li}$ DEE solution with 3 equiv TMEDA at -50 °C.....	56
Figure 3.11. <i>D-FW</i> analysis of ^{13}C DOSY data. Internal references are shown as black squares	

and the MeLi-TMEDA dimer 7 is shown as the white square.....	56
Figure 3.12. ^{13}C NMR spectra of TMCDA titration of 0.15 M $^{13}\text{CH}_3^6\text{Li}$ DEE solution at $-40\text{ }^\circ\text{C}$. 3 represents the resonance of tetramer 3 ; 4 represents the resonance tetramer 4 ; 10 represents the resonance of dimer 10 and 11 represents the resonance of mixed dimer 11	58
Figure 3.13. NMR spectra of 0.15 M $^{13}\text{CH}_3^6\text{Li}$ DEE solution with 2 equiv TMCDA at $-40\text{ }^\circ\text{C}$. ^{13}C spectrum is depicted in (a) and ^6Li spectrum is depicted in (b).....	59
Figure 3.14. ^{13}C DOSY of $^{13}\text{CH}_3^6\text{Li}$ DEE solution with 2 equiv TMCDA at $-40\text{ }^\circ\text{C}$	60
Figure 3.15. <i>D-FW</i> analysis of ^{13}C DOSY data. Internal references are shown as black squares and the MeLi-TMCDA dimer 10 is shown as the white square.	60
Figure 3.16. NMR spectra of 0.09 M $^{13}\text{CH}_3^6\text{Li}$ DEE solution with 2 equiv DMB at $-40\text{ }^\circ\text{C}$. ^{13}C spectrum is depicted in (a) and ^6Li spectrum is depicted in (b).....	62
Figure 3.17. <i>D-FW</i> analysis of ^{13}C DOSY data. Internal references are shown as black squares and the MeLi-DMB dimer 12 is shown as the white square	63
Figure 3.18. NMR spectra of 0.21 M $^{13}\text{CH}_3^6\text{Li}$ DEE solution with 2 equiv PMDTA at $-70\text{ }^\circ\text{C}$. ^{13}C spectrum is depicted in (a) and ^6Li spectrum is depicted in (b).....	64
Figure 3.19. <i>D-FW</i> analysis of ^{13}C DOSY data. Internal references are shown as black squares and the MeLi-PMDTA dimer 14 is shown as the white square.	65
Figure 3.20. NMR spectra of 0.08 M $^{13}\text{CH}_3^6\text{Li}$ DEE solution with 3 equiv (-)-sparteine at $-40\text{ }^\circ\text{C}$. ^{13}C spectrum is depicted in (a) and ^6Li spectrum is depicted in (b).....	66
Figure 3.21. <i>D-FW</i> analysis of ^{13}C DOSY data. Internal references are shown as black squares and the MeLi-SP dimer 15 is shown as the white square	67
Figure 4.1. Crystal structure of hexameric cyclopentyllithium. Thermal ellipsoid plots are at the 50% probability level. Hydrogen atoms have been omitted for clarity. Crystallographic	

asymmetric unit atoms labeled and C(1) – Li interatomic distances displayed.....	84
Figure 4.2. Variable temperature ^1H NMR (400 MHz) spectra of 1.07 M c-PenLi in toluene- d_8 . H represents the methine signal of c-PenLi in hexamer, T represents the signal in tetramer. .	86
Figure 4.3. ^1H NMR (400 MHz) spectra of 1.07 M, 0.73 M and 0.54 M c-PenLi in toluene- d_8 at 15 °C. H represents the methine signal of c-PenLi hexamer, T represents the signal of tetramer.....	86
Figure 4.4. The van 't Hoff plot of reaction (1).....	89
Figure 4.5. ^1H DOSY of c-PenLi toluene- d_8 solution at -25 °C.....	89
Figure 4.6. D-FW analysis of ^1H DOSY data. Internal references are shown as black squares, the tetrameric c-PenLi is shown as the green square and the hexameric c-PenLi is shown as the white square.....	90
Figure 4.7. Crystal structure of tetrameric cyclopentyllithium/THF complex. Thermal ellipsoid plot shown at the 50% probability level. Hydrogen atoms have been omitted for clarity. Crystallographic asymmetric unit atoms labeled and C(1) – Li interatomic distances displayed.....	92
Figure 4.8. Variable temperature ^6Li NMR spectra of natural abundant c-PenLi/THF complex in toluene- d_8	93
Figure 4.9. ^1H DOSY of c-PenLi/THF complex in toluene- d_8 solution at -35 °C.	94
Figure 4.10. D-FW analysis of ^1H DOSY data of c-PenLi/THF complex in toluene- d_8 solution at -35 °C. Internal references are shown as solid squares and the c-PenLi/THF complex is shown as open square.	94
Figure 5.1. Variable temperature ^1H NMR (400 MHz) spectra of 0.49 M <i>s</i> -BuLi in toluene- d_8 . H represents the methine signal of <i>s</i> BuLi in hexamer, T represents the signal in tetramer and M ₁ represents the signal in <i>s</i> -BuLi/ <i>s</i> -BuOLi mixed hexamer.....	105

Figure 5.2. The van 't Hoff plot of reaction (1).....	106
Figure 5.3. The ^1H NMR (400 MHz) spectra of the methine of 0.49 M <i>s</i> -BuLi in toluene- d_8 , showing the initial <i>s</i> -BuLi solution (c, d), solution after 2 μL <i>s</i> -BuOH was added (a) and solution after exposing in dioxygen atmosphere for 10 minutes (b)	108
Figure 5.4. ^1H DOSY of <i>s</i> -BuLi toluene- d_8 solution at $-20\text{ }^\circ\text{C}$	108
Figure 5.5. <i>D</i> -FW analysis of ^1H DOSY data. Internal references are shown as solid squares and the complexes are shown as open squares.	110
Figure 5.6. ^1H NMR spectra of sec-butanol titration of 0.49 M <i>s</i> -BuLi toluene- d_8 solution at $-20\text{ }^\circ\text{C}$. H represents the resonance of <i>s</i> -BuLi in hexamer; T represents the resonance <i>s</i> -BuLi in tetramer; M_1 represents the resonances of <i>s</i> -BuLi and <i>s</i> -BuOLi in mixed hexamer; M_2 represents the resonances of <i>s</i> -BuLi and <i>s</i> -BuOLi in mixed octamer; S represents the resonances of <i>s</i> -BuOLi in pure <i>s</i> -BuOLi aggregates.....	111
Figure 5.7. Variable temperature ^1H NMR (400 MHz) spectra of 2:7 <i>s</i> -BuOLi to <i>s</i> -BuLi toluene- d_8 solution. M_1 represents the resonances of <i>s</i> -BuLi and <i>s</i> -BuOLi in mixed hexamer; M_2 represents the resonances of <i>s</i> -BuLi and <i>s</i> -BuOLi in mixed octamer.....	112
Figure 5.8. ^1H DOSY of <i>s</i> -BuLi/ <i>s</i> -BuOLi toluene- d_8 solution at $-20\text{ }^\circ\text{C}$. The ratio of <i>s</i> -BuOLi to <i>s</i> -BuLi is 2:7 in (a) and 5:3 in (b).	113
Figure 6.1. Crystal structure of lithiated (<i>S</i>)- N^1,N^1 -bis(2-methoxyethyl)- $N^2,3$ -dimethylbutane-1,2-diamine 4 . Thermal ellipsoid plots are at the 50% probability level. Hydrogen atoms have been omitted for clarity.	123
Figure 6.2. ^6Li NMR of [^6Li] Amide 1	125
Figure 6.3. ^1H DOSY of lithiated amine 1	126
Figure 6.4. <i>D</i> -FW analysis of ^1H DOSY data. Internal references are shown as solid squares and	

lithiated amine 1 is shown as open square.....	127
Figure 7.1. Crystal structure of the mixed aggregate of lithiated (<i>S</i>)- <i>N</i> -ethyl-3-methyl-1-(triisopropylsilyloxy)butan-2-amine and <i>c</i> -PenLi 6a	138
Figure 7.2. ¹ H NMR spectra of chiral amine 5 titration of 0.47 M <i>c</i> -Pen ⁶ Li toluene- <i>d</i> ₈ solution at -50 °C. H represents the resonance of <i>c</i> -Pen ⁶ Li in hexamer; T represents the resonance <i>c</i> -Pen ⁶ Li in tetramer; 6a represents the resonance of the 2:2 mixed aggregate 6a	139
Figure 7.3. ⁶ Li NMR spectra of chiral amine 5 titration of 0.47 M <i>c</i> -Pen ⁶ Li toluene- <i>d</i> ₈ solution at -50 °C. H represents the resonance of <i>c</i> -Pen ⁶ Li in hexamer; T represents the resonance <i>c</i> -Pen ⁶ Li in tetramer; 6a represents the resonances of the 2:2 mixed aggregate 6a . Smaller peaks are unknown species.....	140
Figure 7.4. ¹ H { ⁶ Li} HMBC of 6a in toluene- <i>d</i> ₈ at -50 °C.	141
Figure 7.5. ¹³ C NMR of carbon atom 1 of mixed aggregate 6a in toluene- <i>d</i> ₈ at -50 °C.	142
Figure 7.6. ¹ H DOSY of mixed aggregate 6a in toluene- <i>d</i> ₈ at -50 °C.....	143
Figure 7.7. <i>D</i> -FW analysis of ¹ H DOSY data. Internal references are shown as solid squares and mixed aggregate 6a is shown as open square.....	144
Figure 7.8. ¹ H NMR spectra of chiral amine 5 titration of 0.45 M <i>n</i> -Bu ⁶ Li toluene- <i>d</i> ₈ solution at -50 °C. 6b represents the resonance of the 2:2 mixed aggregate 6b	146
Figure 7.9. ⁶ Li NMR spectra of chiral amine 5 titration of 0.45 M <i>n</i> -Bu ⁶ Li toluene- <i>d</i> ₈ solution at -50 °C. 6b represents the resonance of the 2:2 mixed aggregate 6b	146
Figure 7.10. ¹ H{ ⁶ Li} HMBC of 6b in toluene- <i>d</i> ₈ at -50 °C....	147
Figure 7.11. ¹³ C NMR of carbon atom 1 of mixed aggregate 6b in toluene- <i>d</i> ₈ at -50 °C.....	147
Figure 7.12. ¹ H DOSY of mixed aggregate 6b in toluene- <i>d</i> ₈ at -50 °C.	149
Figure 7.13. <i>D</i> -FW analysis of ¹ H DOSY data. Internal references are shown as solid squares and	

mixed aggregate 6b is shown as open square.....	149
Figure 7.14. ^1H NMR spectra of chiral amine 5 titration of 0.35 M <i>i</i> -Pr ^6Li toluene- d_8 solution at -50 °C. 6c represents the resonance of the 2:2 mixed aggregate 6c	151
Figure 7.15. ^6Li NMR spectra of chiral amine 5 titration of 0.35 M <i>i</i> -Pr ^6Li toluene- d_8 solution at -50 °C. 6c represents the resonance of the 2:2 mixed aggregate 6c	151
Figure 7.16. $^1\text{H}\{^6\text{Li}\}$ HMBC of 6c in toluene- d_8 at -50 °C.....	152
Figure 7.17. ^{13}C NMR of carbon atom 2 of mixed aggregate 6c in toluene- d_8 at -50 °C	153
Figure 7.18. ^1H DOSY of mixed aggregate 6c in toluene- d_8 at -50 °C.....	154
Figure 7.19. <i>D</i> -FW analysis of ^1H DOSY data. Internal references are shown as solid squares and mixed aggregate 6c is shown as open square.	155
Figure 7.20. ^1H NMR spectra of chiral amine 5 titration of 0.38 M <i>s</i> -Bu ^6Li toluene- d_8 solution at -50 °C. H represents the resonance of <i>s</i> -Bu ^6Li in hexamer; T represents the resonance <i>s</i> -Bu ^6Li in tetramer; M represents mixed aggregate of <i>s</i> -Bu ^6Li / <i>s</i> -BuO ^6Li and 6d represents the resonance of the 2:2 mixed aggregate 6d	156
Figure 7.21. ^6Li NMR spectra of chiral amine 5 titration of 0.38 M <i>s</i> -Bu ^6Li toluene- d_8 solution at -50 °C. H represents the resonance of <i>s</i> -Bu ^6Li in hexamer; T represents the resonance <i>s</i> -Bu ^6Li in tetramer; M represents mixed aggregate of <i>s</i> -Bu ^6Li / <i>s</i> -BuO ^6Li and 6d represents the resonance of the 2:2 mixed aggregate 6d	157
Figure 7.22. $^1\text{H}\{^6\text{Li}\}$ HMBC of 6d in toluene- d_8 at -50 °C.	157
Figure 7.23. ^1H DOSY of mixed aggregate 6d in toluene- d_8 at -50 °C	159
Figure 7.24. <i>D</i> -FW analysis of ^1H DOSY data. Internal references are shown as solid squares and mixed aggregate 6d is shown as open square.....	159
Figure 8.1. Crystal structure of DEE coordinated dilithiated chiral diamino diethers 11a .	

Thermal ellipsoid plots are at the 50% probability level. Hydrogen atoms have been omitted for clarity.....	175
Figure 8.2. Crystal structure of DEE coordinated dilithiated chiral diamino diethers 11b . Thermal ellipsoid plots are at the 50% probability level. Hydrogen atoms have been omitted for clarity.....	175
Figure 8.3. Crystal structure of DEE coordinated dilithiated chiral diamino diethers 12a . Thermal ellipsoid plots are at the 50% probability level. Hydrogen atoms have been omitted for clarity.....	176
Figure 8.4. Crystal structure of THF coordinated dilithiated chiral diamino diethers 12b . Thermal ellipsoid plots are at the 50% probability level. Hydrogen atoms have been omitted for clarity.....	176
Figure 8.5. (a) Distances between alkyl chains of 11a . (b) Distances between alkyl chains of 12a	177
Figure 8.6. Crystal structure of DEE coordinated dilithiated chiral diamino diether 13a . Thermal ellipsoid plots are at the 50% probability level. Hydrogen atoms have been omitted for clarity.....	178
Figure 8.7. Crystal structure of THF coordinated dilithiated chiral diamino diether 13b . Thermal ellipsoid plots are at the 50% probability level. Hydrogen atoms have been omitted for clarity.....	179
Figure 8.8. Distances between alkyl chains of 13a	179
Figure 8.9. Crystal structure of DEE coordinated dilithiated chiral diamino ethers 14 . Thermal ellipsoid plots are at the 50% probability level. Hydrogen atoms have been omitted for clarity.	180
Figure 9.1. Crystal structure of THF solvated lithium <i>N</i> -methylanilide 10 . Thermal ellipsoid plots	

are at the 50% probability level. Hydrogen atoms have been omitted for clarity	193
Figure 9.2. Crystal structure of THF solvated lithium <i>N</i> -ethylanilide 11 . Thermal ellipsoid plots are at the 50% probability level. Hydrogen atoms have been omitted for clarity.....	193
Figure 9.3. Crystal structure of THF solvated lithium indolide 12 . Thermal ellipsoid plots are at the 50% probability level. Hydrogen atoms have been omitted for clarity	194
Figure 9.4. Crystal structure of THF solvated lithium tetrahydroquinolide 13 . Thermal ellipsoid plots are at the 50% probability level. Hydrogen atoms have been omitted for clarity.....	194
Figure 9.5. Crystal structure of THP solvated lithium <i>N</i> -methylanilide 14 . Thermal ellipsoid plots are at the 50% probability level. Hydrogen atoms have been omitted for clarity.....	195
Figure 9.6. Crystal structure of MeTHF solvated lithium <i>N</i> -methylanilide 15 . Thermal ellipsoid plots are at the 50% probability level. Hydrogen atoms have been omitted for clarity.....	196
Figure 9.7. Crystal structure of DEPA solvated lithium <i>N</i> -methylanilide 16 . Thermal ellipsoid plots are at the 50% probability level. Hydrogen atoms have been omitted for clarity.....	196
Figure 9.8. Crystal structure of DME solvated lithium <i>N</i> -methylanilide 17 . Thermal ellipsoid plots are at the 50% probability level. Hydrogen atoms have been omitted for clarity.....	198
Figure 9.9. Crystal structure of DME solvated lithium <i>N</i> -ethylanilide 18 . Thermal ellipsoid plots are at the 50% probability level. Hydrogen atoms have been omitted for clarity	198
Figure 9.10. Crystal structure of DMTHF solvated lithium <i>N</i> -methylanilide 19 . Thermal ellipsoid plots are at the 50% probability level. Hydrogen atoms have been omitted for clarity	199
Figure 9.11. Crystal structure of THF solvated lithium <i>N</i> -diphenylamide 20 . Thermal ellipsoid plots are at the 50% probability level. Hydrogen atoms have been omitted for clarity.....	200
Figure 9.12. Crystal structure of THF solvated lithium <i>N</i> -isopropylanilide 21 . Thermal ellipsoid plots are at the 50% probability level. Hydrogen atoms have been omitted for clarity	200

Figure 9.13. Crystal structure of THF solvated lithium <i>N</i> -isobutylanilide 22 . Thermal ellipsoid plots are at the 50% probability level. Hydrogen atoms have been omitted for clarity.....	202
Figure 9.14. Crystal structure of THF solvated lithium <i>N</i> -neopentylanilide 23 . Thermal ellipsoid plots are at the 50% probability level. Hydrogen atoms have been omitted for clarity.....	202
Figure 10.1. ¹ H NMR spectra of chiral amine 7 titration of 0.2 M <i>n</i> -Bu ⁶ Li toluene- <i>d</i> ₈ solution at -40 °C. H represents the resonance of <i>n</i> -Bu ⁶ Li hexamer; I represents the resonances of impurities and mixed aggregates of <i>n</i> -Bu ⁶ Li and <i>n</i> -BuO ⁶ Li; 10 represents the resonances of the 2:2 mixed aggregate 10	214
Figure 10.2. ⁶ Li NMR spectra of chiral amine 7 titration of 0.2 M <i>n</i> -Bu ⁶ Li toluene- <i>d</i> ₈ solution at -40 °C. H represents the resonance of <i>n</i> -Bu ⁶ Li hexamer; I represents the resonances of impurities and mixed aggregates of <i>n</i> -Bu ⁶ Li and <i>n</i> -BuO ⁶ Li; 10 represents the resonances of the 2:2 mixed aggregate 10	214
Figure 10.3. ¹ H DOSY of mixed aggregate 10 in toluene- <i>d</i> ₈ at -40 °C.....	216
Figure 10.4. D-FW analysis of ¹ H DOSY data. Internal references are shown as solid squares and mixed aggregate 10 is shown as open square.	217
Figure 10.5. Crystal structures of the mixed aggregates 2a and 6a	218
Figure 10.6. ¹ H NMR spectra of chiral amine 8 titration of 0.2 M <i>n</i> -Bu ⁶ Li toluene- <i>d</i> ₈ solution at -40 °C. H represents the resonance of <i>n</i> -Bu ⁶ Li in hexamer; I represents the resonances of impurities and mixed aggregates of <i>n</i> -Bu ⁶ Li and <i>n</i> -BuO ⁶ Li; 11 represents the resonances of the 2:2 mixed aggregate 11 ; 12 represents the resonances of the 2:1 mixed trimer 12	221
Figure 10.7. ⁶ Li NMR spectra of chiral amine 8 titration of 0.2 M <i>n</i> -Bu ⁶ Li toluene- <i>d</i> ₈ solution at -40 °C. H represents the resonance of <i>n</i> -Bu ⁶ Li in hexamer; I represents the resonances of impurities and mixed aggregates of <i>n</i> -Bu ⁶ Li and <i>n</i> -BuO ⁶ Li; 11 represents the resonances of the	

2:2 mixed aggregate 11 ; 12 represents the resonances of the 2:1 mixed trimer 12	222
Figure 10.8. $^1\text{H} \{^6\text{Li}\}$ HMBC of 11 and 12 in toluene- d_8 at -40°C	222
Figure 10.9. ^{13}C NMR of carbon atoms 1 and 7 of mixed aggregates 11 and 12 in toluene- d_8 at -40°C	223
Figure 10.10. ^1H DOSY of mixed aggregates 11 and 12 in toluene- d_8 at -40°C	224
Figure 10.11. D-FW analysis of ^1H DOSY data. Internal references are shown as solid squares and mixed aggregate 11 is shown as green square and mixed trimer 12 is shown as the white square.....	225
Figure 10.12. ^1H NMR spectra of chiral amine 9 titration of 0.2 M $n\text{-Bu}^6\text{Li}$ toluene- d_8 solution at -40°C . H represents the resonance of $n\text{-Bu}^6\text{Li}$ in hexamer; I represents the resonances of impurities and mixed aggregates of $n\text{-Bu}^6\text{Li}$ and $n\text{-BuO}^6\text{Li}$; 13 represents the resonances of the 2:1 mixed trimer 13 ; 14 represents the resonances of homodimer 14	227
Figure 10.13. ^6Li NMR spectra of chiral amine 9 titration of 0.2 M $n\text{-Bu}^6\text{Li}$ toluene- d_8 solution at -40°C . H represents the resonance of $n\text{-Bu}^6\text{Li}$ in hexamer; I represents the resonances of impurities and mixed aggregates of $n\text{-Bu}^6\text{Li}$ and $n\text{-BuO}^6\text{Li}$; 13 represents the resonances of the 2:1 mixed trimer 13 ; 14 represents the resonances of homodimer 14	227
Figure 10.14. $^1\text{H} \{^6\text{Li}\}$ HMBC of 13 and 14 in toluene- d_8 at -40°C	228
Figure 10.15. ^{13}C NMR of carbon atoms 1 of mixed trimer 13 in toluene- d_8 at -40°C	228
Figure 10.16. ^1H DOSY of mixed trimer 13 and homodimer 14 in toluene- d_8 at -40°C	230
Figure 10.17. D-FW analysis of ^1H DOSY data. Internal references are shown as black squares, mixed trimer 13 is shown as white square and homodimer 14 is shown as the green square.	230

List of Tables

Table 2.1. LDA catalyzed isomerization of various allyl ether.	19
Table 2.2. Isomerization of (allyloxy)cycloheptane by different amides	20
Table 2.3. Comparison of <i>t</i> -BuOK and LDA initiated isomerization	21
Table 3.1. <i>D</i> -FW Analysis of ¹³ C DOSY of BEN, IR1, IR2, IR3 and 1 at 20 °C.	46
Table 3.2. <i>D</i> -FW Analysis of ¹³ C DOSY of BEN, IR1, IR2, IR4 and 1 at 20 °C	48
Table 3.3. <i>D</i> -FW Analysis of ¹³ C DOSY of BEN, IR1, IR2, IR4, 3 and 4 at -40 °C.....	53
Table 3.4. <i>D</i> -FW Analysis of ¹³ C DOSY of BEN, IR1, IR2, IR4 and 7 at -50 °C.....	55
Table 3.5. <i>D</i> -FW Analysis of ¹³ C DOSY of BEN, IR1, IR2, IR4 and 10 at -40 °C.....	61
Table 3.6. <i>D</i> -FW Analysis of ¹³ C DOSY of BEN, IR1, IR2, IR4, 12 and 13 at -40 °C.....	63
Table 3.7. <i>D</i> -FW Analysis of ¹³ C DOSY of BEN, IR1, IR2, IR4, 14 at -40 °C	65
Table 3.8. <i>D</i> -FW Analysis of ¹³ C DOSY of BEN, IR1, IR2, IR4, 15 at -40 °C	67
Table 4.1. Concentrations of cyclopentyllithium (c-PenLi) complexes and the equilibrium constant (K) at 15 °C in toluene- <i>d</i> ₈	87
Table 4.2. Concentrations of different cyclopentyllithium complexes as a function of temperature in toluene- <i>d</i> ₈	88
Table 4.3. ¹ H and ¹³ C signal assignments of hexameric and tetrameric c-PenLi in toluene- <i>d</i> ₈	89
Table 4.4. <i>D</i> -FW analysis of ¹ H DOSY data.....	90
Table 4.5. ¹ H and ¹³ C signal assignments of c-PenLi solvated by THF in toluene- <i>d</i> ₈	93
Table 4.6. <i>D</i> -FW analysis of ¹ H DOSY data.....	95
Table 5.1. Concentrations of <i>s</i> -BuLi complexes and the equilibrium constant (K) at -30 °C in toluene- <i>d</i> ₈	106
Table 6.1. ¹ H and ¹³ C signal assignments of lithiated amine 1	124

Table 6.2. <i>D-FW</i> analysis of ^1H DOSY data.....	127
Table 7.1. ^1H and ^{13}C signal assignments of mixed aggregate 6a	142
Table 7.2. <i>D-FW</i> analysis of ^1H DOSY data of 6a	144
Table 7.3. ^1H and ^{13}C signal assignments of mixed aggregate 6b	148
Table 7.4. <i>D-FW</i> analysis of ^1H DOSY data of 6b	150
Table 7.5. ^1H and ^{13}C signal assignments of mixed aggregate 6c	153
Table 7.6. <i>D-FW</i> analysis of ^1H DOSY data of 6c	154
Table 7.7. ^1H and ^{13}C signal assignments of mixed aggregate 6d	158
Table 7.8. <i>D-FW</i> analysis of ^1H DOSY data of 6d	160
Table 10.1. ^1H and ^{13}C signal Assignments of Mixed Aggregate 10	216
Table 10.2. <i>D-FW</i> Analysis of ^1H DOSY Data of 10	217
Table 10.3. ^1H and ^{13}C signal Assignments of Mixed Aggregates 11 and 12	223
Table 10.4. <i>D-FW</i> Analysis of ^1H DOSY Data of 11 and 12	225
Table 10.5. ^1H and ^{13}C signal Assignments of Mixed Aggregate 13 and Homodimer 14	229
Table 10.6. <i>D-FW</i> Analysis of ^1H DOSY Data of 13 and 14	230
Table 10.7. Aggregation states of different lithium chiral amide/ <i>n</i> -BuLi complexes	231

List of Schemes

Scheme 2.1. The PGSE pulse sequence.	17
Scheme 2.2. (1a) Definition of α and β positions and R' group of the allyl ethers. (1b) An example of allyl ether without β branched chain. (1c) An example of allyl ether with only one β branched chain. (1d) An example of allyl ether with two β branched chains.....	20
Scheme 2.3. Allyl ethers isomerization catalyzed by <i>t</i> -BuOK.....	21
Scheme 2.4. Isomerization of 2a catalyzed by LDA and <i>t</i> -BuOK.....	23
Scheme 3.1. Synthesis of ^{13}C labeled internal references	44
Scheme 3.2. Synthesis of ^{13}C labeled <i>N</i> -Boc-piperidine 1	45
Scheme 3.3. Synthesis of internal reference derived from squalene.....	47
Scheme 3.4. MeLi tetramer 3 and MeLi-LiI mixed tetramer 4	50
Scheme 3.5. MeLi-TMEDA dimer 7 , cyclic trimer 8 and cyclic oligomer 9	56
Scheme 3.6. MeLi-TMCDA homodimer 10 and MeLi-LiI-TMCDA heterodimer 11	58
Scheme 3.7. MeLi-LiI cyclic trimers and oligomers	58
Scheme 3.8. MeLi-DMB homodimer 12 and MeLi-LiI-DMB heterodimer 13	62
Scheme 3.9. MeLi-PMDTA homodimers 14a and 14b	64
Scheme 3.10. Synthesis of internal reference derived from squalene.....	66
Scheme 4.1. The equilibrium reaction of the hexameric and tetrameric complexes of <i>c</i> -PenLi...	86
Scheme 5.1. The equilibrium reaction of the hexameric and tetrameric complexes of <i>s</i> -BuLi ..	106
Scheme 6.1. Synthesis and Crystallization of lithium amide 1	123
Scheme 7.1. The trimeric 2:1 complexes 2 , 3 and the homodimer 4	136
Scheme 7.2. The 2:2 Ladder Structure Mixed Aggregates 6	137
Scheme 8.1. The trimeric complexes 2 and the homodimer 3	171

Scheme 8.2. The equivalently solvated dimer 5 and non-equivalently solvated dimer 6	172
Scheme 8.3. Synthesis of chiral diamino ethers 7, 8, 9 and 10	173
Scheme 8.4. Crystallization of dilithiated chiral diamino ethers 7, 8, 9 and 10 in ethereal solvents.....	173
Scheme 9.1. Equilibrium of lithium anilide aggregates (1-5).....	190
Scheme 9.2. Crystallization of THF tetra-solvated lithium anilides 10, 11, 12 and 13	192
Scheme 9.3. The <i>trans</i> structure of lithium anilides 10, 11, 12 and 13	193
Scheme 9.4. Branched chains of <i>N</i> -alkylanilines.....	201
Scheme 10.1. The Trimeric 2:1 Complexes 2,3 and the Homodimer 4	211
Scheme 10.2. The 2:2 Ladder Structure Mixed Aggregates 6	212
Scheme 10.3. Chiral amines 7, 8 and 9	213
Scheme 10.4. Numbering and labeling scheme of chiral amines.....	219

Chapter 1

General Introduction

1.1 Brief introduction of organolithium compounds

It is undisputable that organolithium reagents are among the most widely used reagents in organic synthesis. The reagents are employed in many reaction methodologies, such as deprotonation of weakly acidic protons, alkylation, nucleophilic addition, rearrangement, epoxide opening, lithium halogen exchanges and transmetalation.¹ Moreover, the development of asymmetric addition and deprotonation furthered the versatility of organolithium compounds.² More recently, organolithium reagents are extensively used not only in academic laboratories, but also in pharmaceutical and chemical industries.³

Organolithium compounds are well known to form aggregates in solid, solution and gaseous state.^{1e,2n,4} The strongly polarized Li-X (X = C, N, O) bond is generally believed to be the origin for aggregate formation.^{1c,e,5} Organolithium compounds tend to maximize the number of Li-X interactions for the sake of minimizing the electrostatic energy. Many studies revealed that the reactivity and stereoselectivity of organolithium compounds are highly dependent on their aggregation and solvation state.⁶ Thus, any such information regarding these intermediate states can enhance our understanding and ability to tailor these reactions to the desired products. Alkylolithiums and lithium amides, being the source of most organolithium compounds, are the major foci of this thesis.

Alkylolithium reagents are obtained mainly by the reaction of lithium metal with alkyl halides. Alternatively, reagents such as methylolithium and phenylolithium can be synthesized by the reaction of the corresponding alkyl halide with a more reactive alkylolithium such as *n*-butylolithium and *tert*-butylolithium at -78° C.¹ Alkylolithium reagents are the major source of most organolithium reagents because they can efficiently

generate a wide variety of carbanions such as lithium amide, acetylide and alkoxide. Moreover, the low boiling point alkane by-product is a saturated hydrocarbon that is inert to most of the reactions.

Owing to their strong nucleophilicity, alkyllithium reagents are not normally used in the deprotonation of compounds such as ketones and esters, which are prone to nucleophilic attack. Thus, non-nucleophilic organolithium amide bases such as lithium diisopropylamide and lithium hexamethyldisilazide have long been widely employed in the deprotonation of those compounds.⁷ Chiral lithium amide bases, which are usually derived from enantiopure amino acids and tartaric acids, were later developed for asymmetric addition and deprotonation.² Recently, chiral lithium amide bases have also gained significant application in the catalytic dynamic resolution for enantioselective synthesis.^{2n,8}

1.2 Methods for the determination of aggregation and solvation states

The aggregation state of organolithium reagents is diverse, ranging from monomer, dimer to hexamer, octamer or even polymer. The solvation state of organolithium compounds can also be varied. The lithium atom in an organolithium complex can be solvated by one, two, or even three solvent molecules.^{1e,9} Besides the inherent structure of the organolithium reagents, several parameters including temperature, concentration, solvent and additional salts are found to control the aggregation and solvation states of the reagents.¹⁰

X-ray crystallography and NMR spectroscopy are two major means for establishing the aggregation and solvation states of organolithium reagents.

1.2.1 X-Ray crystallography for the determination of solid-state structures

The ability to obtain a definitive solid-state structure renders x-ray crystallography the most important and widely used technique in determining the solid-state structure of organolithium compounds.¹ Moreover, the crystal structure determined by x-ray diffraction (XRD) often serves as a guide for the solution structure determination.

Although x-ray crystallography is very useful in structural analysis of organolithium, the technique also suffers from certain limitations. First of all, obtaining suitable single crystals is not guaranteed. Many organolithium complexes are not able to form crystals, whereas some of the complexes can only form powder-like precipitates. Besides, crystallization is a delicate process that requires precise control of various factors

including temperature, concentration, solvent, time and even glassware. A slight difference in the condition of crystallization may make the process futile. Secondly, most of the reactions involving organolithium reagents are performed in solution.¹ It is not guaranteed that the crystal structure determined represents the only or the major species in solution. It is possible that the crystal structure represents only one among several species or even insignificant in solution. Thirdly, x-ray crystallography cannot provide any information for the dynamic process of the organolithium reagents in solution.

Despite the fact that x-ray crystallography has certain limitations, it is still one of the most prominent techniques in revealing the aggregation and solvation states of organolithium compounds. Crystal structures are especially valuable in elucidating the structure of complicated aggregates.

1.2.2 Multinuclear one and two dimensional NMR spectroscopy

Nuclear magnetic resonance (NMR) spectroscopy is of utmost importance in revealing the solution structures of organolithium complexes. This powerful instrument not only allows us to detect a variety of nuclei (^1H , ^{13}C , ^{15}N , ^{31}P , ^{19}F , ^6Li , ^7Li) in solution, but also provides us with the information of interaction between different nuclei.

The one dimensional NMR experiments for the detection of the chemical environment of different nuclei allows us to have a general idea of number of species present. Sometimes, isotopically labeled compounds are synthesized to obtain a clear picture of the chemical environment of the atom concerned. For example, lithium-6 labeled complexes were used extensively instead of natural abundance lithium which

contains 93% ^7Li and 7% ^6Li in the NMR spectroscopy because the quadrupole moment of ^6Li is much smaller than ^7Li resulting in significantly narrower linewidths.¹¹ Moreover, the coupling between ^6Li and ^{13}C provides important clues for the structural elucidation of alkyllithiums in solution.

The two dimensional NMR techniques offer details about the interaction between different nuclei. Such details are critical in determining the solution structure of organolithium complexes. Heteronuclear multiple bond correlation (HMBC) is used to map the long range scalar interaction between ^6Li and ^1H , a technique that is critical in mixed aggregate characterization and solvation state studies.¹² Heteronuclear Overhauser effect spectroscopy (HOESY) is used to detect the dipolar, or “through space” coupling between protons and lithium atoms.¹³ Exchange spectroscopy (EXSY) is used to detect the interchange of lithium atoms and is useful in revealing the dynamic processes.¹⁴

1.2.3 Diffusion-ordered NMR spectroscopy for the formula weight determination

The conventional NMR techniques discussed above provide us valuable information about the structures of organolithium complexes; however, the conventional NMR experimental results are usually not enough to establish solution structures of the complexes unambiguously because several possible structures are consistent with the results. To tackle the problem, a pseudo two dimensional NMR technique called diffusion-ordered spectroscopy (DOSY), often referred to as “chromatography by NMR”, was introduced to the organometallic field.¹⁵ It is found to be highly useful in revealing the formula weight, aggregation and solvation states of organolithium complexes.

In 1964, Stejskal and Tanner reported the first use of a pulsed gradient spin-echo (PGSE) sequence to measure the diffusion coefficients of molecules in solution.¹⁶ The application of the PGSE sequence was limited until thirty years later, when Johnson and Morris incorporated the PGSE sequence in a pseudo two dimensional NMR experiment in which chemical shift is displayed horizontally, while the vertical axis represents diffusion coefficient.¹⁷ The pseudo 2D NMR experiment is called diffusion-ordered spectroscopy (DOSY). As depicted in Figure 1, the PGSE sequence consists of a standard spin-echo pulse sequence with the insertion of two identical gradient pulses.¹⁸ The signal attenuation (I/I_0) of the PGSE experiment and the self-diffusion coefficient have an exponential relationship as the following theoretical equation (1) in which I and I_0 represent the signal intensity at the echo with and without the gradient pulses respectively, γ is the gyromagnetic ratio of the nucleus, g represents the gradient strength, δ is the duration of gradient pulse, Δ represents the diffusion time and D is the self-diffusion coefficient. In practice, by adjusting the gradient strength, a series of signal attenuation data will be observed. Self-diffusion coefficient is deduced from the exponential decay curve by fitting the signal attenuation data into equation (1) with g as the variable factor.¹⁹

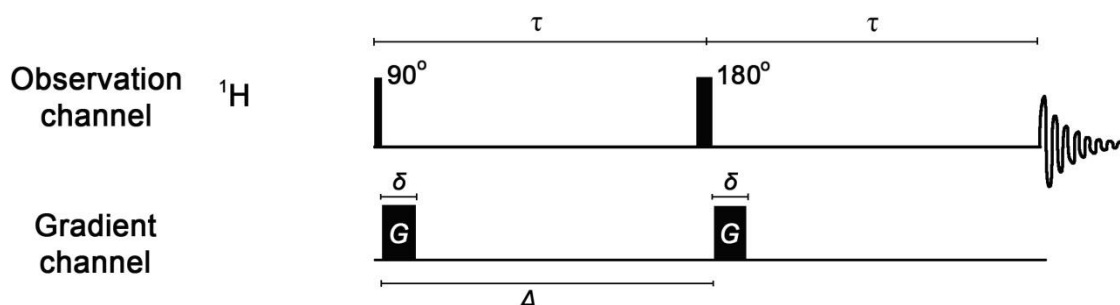


Figure 1.1. The PGSE pulse sequence.

$$\frac{I}{I_0} = \exp[-D(\gamma\delta g)^2(\Delta - \frac{\delta}{3})] \quad \text{Equation (1)}$$

To evaluate the formula weight of an unknown complex in solution by its diffusion coefficient, diffusion coefficient-formula weight (*D-FW*) analysis is implemented. The idea of *D-FW* analysis was proposed by Dr. Keresztes in his thesis and was achieved by Dr. Li through the introduction of internal reference system.²⁰ The theory of *D-FW* analysis is based on the Stokes-Einstein equation ($D = kT/6\pi\eta r$) where k is the Boltzmann constant, T represents the temperature, η is the viscosity of the solution and r is the hydrodynamic radius. After making two important assumptions, equation (2) is deduced from the Stokes-Einstein equation. One of the assumptions is that the molecules concerned are spherical, and so the hydrodynamic radius is proportional to the molecular volume. Another assumption is very similar density between the molecules concerned, so that the molecular volume is proportional to formula weight. In equation (2), ρ is the density and FW is the formula weight. After taking the logarithm on both sides of equation (2), empirical equation ($\log D = A \log FW + C$) is deduced. Since A and C are constants for a single experiment, their values can be calculated by measuring the diffusion coefficients of a series of internal references with known formula weights. Thus, the formula weight of an unknown complex can be obtained by substituting its diffusion coefficient into the empirical equation.

$$D = \frac{kT}{6\pi\eta} \left(\frac{4\pi\rho}{3FW} \right)^{\frac{1}{3}} \quad \text{Equation (2)}$$

For a successful DOSY experiment with *D-FW* analysis, a suitable internal reference system must be employed. The criteria for internal references include: (a) lack of

reactivity and coordinating ability towards the analyte; (b) easily recognizable resonances that are not overlapping with resonances of the molecules concerned; (c) solubility in the NMR solvents; (d) desirable formula weight range for correlation; (e) suitable spin-lattice relaxation time (T_1 time constant).²¹

1.3 The scope and overview of this thesis

This thesis focuses on the reactivity and structure determination of various organolithium reagents. The development of ^{13}C labeled internal reference system for DOSY *D-FW* analysis and its use in elucidating the solution structures of organolithium complexes have also been addressed.

We started to investigate the Wittig rearrangement²² of allyl ethers with alkyllithium reagents and discovered the isomerization reaction of allyl ethers initiated by lithium diisopropylamide (LDA). Allylic ethers can be isomerized efficiently with very high stereoselectivity to (*Z*)-propenyl ethers by LDA or other lithium secondary amide. It was discovered that the conversion rate decreases significantly with more sterically hindered allylic ethers. Therefore, the isomerization methodology also provides an efficient means to regioselectively isomerize the less steric hindered allyl ether group to (*Z*)-propenyl ether.

The discussion of structural analysis of organolithium complexes begins in chapter 3. We successfully developed a ^{13}C labeled internal reference system for ^{13}C DOSY. The technique was applied in establishing the aggregation and solvation states of methyllithium with several widely used tertiary diamines.

Chapter 4 discusses the characterization of unsolvated cyclopentyllithium and its tetrahydrofuran complex through X-ray crystallography and various NMR techniques. Cyclopentyllithium exists as hexamer and tetramer equilibrating with each other in hydrocarbon solvents, whereas a tetrahydrofuran tetrasolvated tetramer is the dominant species in tetrahydrofuran solution.

The investigation of another secondary alkyllithium, *sec*-butyllithium is presented in chapter 5. It is revealed that both commercially available and laboratory prepared *sec*-butyllithium contains a small amount of *sec*-butoxide. A mixed hexamer of *sec*-butyllithium and *sec*-butoxide is present when the percentage of *sec*-butoxide is low. Upon addition of *sec*-butoxide, a mixed octamer of *sec*-butyllithium and *sec*-butoxide appears.

The discussion of chiral lithium amides begins at chapter 6. The solid and solution structures of lithiated (*S*)- N^1, N^1 -bis(2-methoxyethyl)- $N^2, 3$ -dimethylbutane-1,2-diamine were characterized. This chiral lithium amide forms a dimer in both solid and solution state.

In chapter 7, the characterization of mixed aggregates of an alkyllithium reagent and a chiral lithium amide derived from *N*-ethyl-*O*-triisopropylsilyl valinol is presented. The results of x-ray crystallography and a variety of NMR experiments reveal that identical dimeric, ladder-type, mixed aggregates are the major species at a stoichiometric ratio of 1:1 lithium chiral amide to alkyllithium in toluene- d_8 solution.

Chapter 8 discusses the solid-state structures of four different chiral diamino diethers synthesized from *N*-isopropyl valinol or alaninol. The crystal structures of the lithium chiral diamido diethers reveal one monomer and six dimeric structures that are solvated by ethereal solvents.

In chapter 9, the solid-state characterization of a series of lithium *N*-alkylanilines solvated by different ethereal solvents is presented. The crystal structures include tetra-solvated, tri-solvated and di-solvated dimers and tri-solvated monomers.

Chapter 10 discusses the effect of the steric hindrance of different chiral lithium amides on the aggregation state of the mixed complexes between lithiated chiral amines and *n*-BuLi.

1.4 References

(1) (a) Stowell, J. C., *Carbanions In Organic Synthesis*; Wiley: New York, **1979**. (b) Trost, B. M., Fleming, I., Eds. *Comprehensive Organic Synthesis*; Pergamon: Oxford, **1991**. (c) Clayden, J. *Organolithiums: Selectivity for Synthesis*; Pergamon: Oxford, **2002**. (d) Hodgson, D. *Organolithiums in Enantioselective Synthesis*; Springer: New York, **2003**. (e) Rappoport, Z., Marek, I., Eds. *The Chemistry of Organolithium Compounds*; John Wiley & Sons, Ltd.: West Sussex, **2004**. (f) Mahrwald, R., *Modern Aldol Reactions*; Wiley-VCH: Weinheim, **2004**.

(2) (a) Whitesell, J. K.; Felman, S. W. *J. Org. Chem.* **1980**, *45*, 755-756. (b) Eleveld, M. B.; Hogeveen, H. *Tetrahedron Lett.* **1984**, *45*, 5187-5190. (c) Shirai, R.; Tanaka, M.; Koga, K. *J. Am. Chem. Soc.* **1986**, *108*, 543-545. (d) Cain, C. M.; Cousins, R. P. C.; Coumbarides, G.; Simpkins, N. S. *Tetrahedron* **1990**, *46*, 523-544. (e) Bhuniya, D.; DattaGupta, A.; Singh, V. K. *J. Org. Chem.* **1996**, *61*, 6108-6113. (f) Corruble, A.; Valnot, J.-Y.; Maddaluno, J.; Duhamel, P. *Tetrahedron: Asymmetry* **1997**, *8*, 1519-1523. (g) Simpkins, N. S.; Hume, S. C. *J. Org. Chem.* **1998**, *63*, 912-913. (h) Corruble, A.; Valnot, J.-Y.; Maddaluno, J.; Duhamel, P. *J. Org. Chem.* **1998**, *63*, 8266-8275. (i) Matsuo, J.; Odashima, K.; Kobayashi, S. *Org. Lett.* **1999**, *1*, 345-348. (j) Arvidsson, P. I.; Davidsson, O.; Hilmersson, G. *Tetrahedron: Asymmetry* **1999**, *10*, 527-534. (k) De Sousa, S. E.; O'Brien, P.; Pilgram, C. D. *Tetrahedron* **2002**, *58*, 4643-4654. (l) Flinois, K.; Yuan, Y.; Bastide, C.; Harrison-Marchand, A.; Maddaluno, J. *Tetrahedron* **2002**, *58*, 4707-4716. (m) Rodeschini, V.; Simpkins, N. S.; Wilson, C. *J. Org. Chem.* **2007**, *72*, 4265-4267. (n) Gawley, R. E., Siegel, J., *Stereochemical Aspects of Organolithium Compounds: Topics in Stereochemistry, Volume 26*; John Wiley & Sons: New York, **2009**. (o) Stivala, C. E.; Zakarian A. *J. Am. Chem. Soc.* **2011**, *133*, 11936-11939.

(3) Wu, G.; Huang, M. *Chem. Rev.* **2006**, *106*, 2596-2616.

(4) (a) Setzer, W. N.; Schleyer, P. von R. *Adv. Organomet. Chem.* **1985**, *24*, 353-451. (b) Plavsic, D.; Srzic, D.; Klasinc, L. *J. Phys. Chem.* **1986**, *90*, 2075-2080. (c) Seebach, D. *Angew. Chem. Int.*

Ed. **1988**, 27, 1624-1654. (d) Kahn, J. D.; Haag, A.; Schleyer, P. vonR. *J. Phys. Chem.* **1986**, 92, 212-220. (e) Boche, G. *Angew. Chem. Int. Ed.* **1989**, 28, 277-297. (f) Abdul-Sada, A. K.; Greenway, A. M.; Seddon, K. R. *J. Orgmet. Chem.* **1989**, 375, C17-C19. (g) Weiss, E. *Angew. Chem. Int. Ed.* **1993**, 31, 1501-1523.

(5) (a) Streitwieser, A., Jr. *J. Orgmet. Chem.* **1978**, 156, 1-3. (b) Schlosser, M., *Organometallics in Synthesis Third Manual*; John Wiley & Sons, Ltd.: Hoboken, **2013**.

(6) (a) West, P.; Waack, R.; Purmort, J. I. *J. Am. Chem. Soc.* **1970**, 92, 840-845. (b) McGarrity, J. F.; Ogle, C. A.; Brich, Z.; Loosli, H. *J. Am. Chem. Soc.* **1985**, 107, 1810-1815. (c) Bates, T. F.; Clarke, M. T.; Thomas, R. D. *J. Am. Chem. Soc.* **1988**, 110, 5109-5112. (d) Sato, D.; Kawasaki, H.; Shimada, I.; Arata, Y.; Okamura, K.; Date, T.; Koga, K. *J. Am. Chem. Soc.* **1992**, 114, 761-763. (e) Ogle, C. A.; Johnson IV, H. C.; Wang, X. L.; Strickler, F. H.; Bucca, D.; Gordon III, B. *Macromolecules* **1995**, 28, 5184-5191. (f) Lucht, B. L.; Bernstein, M. P.; Remenar, J. F.; Collum, D. B. *J. Am. Chem. Soc.* **1996**, 118, 10707-10718. (g) Reich, H. J.; Green, D. P.; Medina, M. A.; Goldenberg, W. S.; Gudmundsson, B. O.; Dykstra, R. R.; Phillips, N. H. *J. Am. Chem. Soc.* **1998**, 120, 7201-7210. (h) Arvidsson, P. I.; Hilmersson, G.; Ahlberg, P. *J. Am. Chem. Soc.* **1999**, 121, 1883-1887. (i) Arvidsson, P. I.; Hilmersson, G.; Davidsson, O. *Chem.—Eur. J.* **1999**, 5, 2348-2355. (j) Rutherford, J. L.; Hoffmann, D.; Collum, D. B. *J. Am. Chem. Soc.* **2002**, 124, 264-271. (k) Sott, R.; Granander, J.; Hilmersson, G. *Chem.—Eur. J.* **2002**, 8, 2081-2087. (l) Jones, A. C.; Sanders, A. W.; Bevan, M. J.; Reich, H. J. *J. Am. Chem. Soc.* **2007**, 129, 3492-3493. (m) Pate, F.; Duguet, N.; Oulyadi, H.; Harrison-Marchand, A.; Fressigne, C.; Valnot, J.; Lasne, M.; Maddaluno, J. *J. Org. Chem.* **2007**, 72, 6982-6991. (n) Liu, J.; Li, D.; Sun, C.; Williard, P. G.; *J. Org. Chem.* **2008**, 73, 4045-4052. (o) Lecachey, B.; Duguet, N.; Oulyadi, H.; Fressigne, C.; Harrison-Marchand, A.; Yamamoto, Y.; Tomioka, K.; Maddaluno, J. *Org. Lett.* **2009**, 11, 1907-1910. (p) Kolonko, K. J.; Wheritt, D. J.; Reich, H. J. *J. Am. Chem. Soc.* **2011**, 133, 16774-16777.

(7) (a) Collum, D.; McNeil, A. J.; Ramirez, A. *Angew. Chem. Int. Ed.* **2007**, 46, 3002-3017. (b) Lucht, B.; Collum, D. *Acc. Chem. Res.* **1999**, 32, 1035-1042. (c) Snieckus, V. *Chem. Rev.* **1990**, 90, 879-933.

(8) (a) Beng, T. K.; Gawley, R. E. *J. Am. Chem. Soc.* **2010**, 132, 12216-12217. (b) Beng, T. K.; Tyree, W. S.; Parker, T.; Su, C.; Williard, P. G.; Gawley, R. E. *J. Am. Chem. Soc.* **2012**, 134, 16845-16855.

(9) Elschenbroich, C., *Organometallics*; Wiley-VCH: Weinheim, **2006**.

(10) (a) Lewis, H. L.; Brown, T. L. *J. Am. Chem. Soc.* **1970**, 92, 4664-4670. (b) Kimura, B. Y.; Brown, T. L. *J. Orgmet. Chem.* **1971**, 26, 57-67. (c) Novak, D. P.; Brown, T. L. *J. Am. Chem. Soc.* **1972**, 94, 3793-3798. (d) Jackman, L. M.; DeBrosse, C. W. *J. Am. Chem. Soc.* **1983**, 105, 4177-4184. (e) Barr, D.; Clegg, W.; Mulvey, R. E.; Snaith, R. *J. Chem. Soc., Chem. Commun.* **1984**, 285-287. (f) Romesberg, F. E.; Gilchrist, J. H.; Harrison, A. T.; Fuller, D. J.; Collum, D. B. *J. Am. Chem. Soc.* **1991**, 113, 5751-5757. (g) Collum, D. B. *Acc. Chem. Res.* **1992**, 25, 448-454. (h) Corset, J.; Froment, F.; Lautie, M. F.; Ratovelomanana, N.; Seyden-Penne, J.; Strzalko, T.; Roux-Schmit, M. C. *J. Am. Chem. Soc.* **1993**, 115, 1684-1694. (i) Abbotto, A.; Streitwieser, A. *J. Am. Chem. Soc.* **1995**, 117, 6358-6359. (j) Reich, H. J.; Kulicke, K. J. *J. Am. Chem. Soc.* **1995**, 117, 6621-6622. (k) Reich, H. J.; Kulicke, K. J. *J. Am. Chem. Soc.* **1996**, 118, 273-274. (l) Remenar, J. F.; Lucht, B. L.; Collum, D. B. *J. Am. Chem. Soc.* **1997**, 119, 5567-5572. (m) Rutherford, J. L.; Collum, D. B. *J. Am. Chem. Soc.* **2001**, 123, 199-202. (n) Rutherford, J. L.; Hoffmann, D. Collum, D. B. *J. Am. Chem. Soc.* **2002**, 124, 264-271. (o) Liou, L. R.; McNeil, A. J.; Ramirez, A.; Toombes, G. E. S.; Gruver, J. M.; Collum, D. B. *J. Am. Chem. Soc.* **2008**, 130, 4859-4868. (p) De

Vries, T. S.; Goswami, A.; Liou, L. R.; Gruver, J. M.; Jayne, E.; Collum, D. B. *J. Am. Chem. Soc.* **2009**, *131*, 13142-13154. (q) Hoepker, A. C.; Gupta, L.; Ma, Y.; Fagggin, M. F.; Collum, D. B. *J. Am. Chem. Soc.* **2011**, *132*, 7135-7151. (r) Tomasevich, L. L.; Collum, D. B. *J. Org. Chem.* **2013**, *78*, 7498-7507.

(11) Jackman, L. M.; Cizmeciyan, D.; Williard, P. G.; Nichols, M. A. *J. Am. Chem. Soc.* **1993**, *115*, 6262-6267.

(12) (a) Kagan, G.; Li, W.; Sun, C.; Hopson, R.; Williard, P. G. *J. Org. Chem.* **2011**, *76*, 65-70. (b) Kagan, G.; Li, W.; Li, D.; Hopson, R.; Williard, P. G. *J. Am. Chem. Soc.* **2011**, *133*, 6596-6602.

(13) (a) Bauer, W.; Mueller, G.; Pi, R.; Schleyer, P. v. R. *Angew. Chem.* **1986**, *98*, 1130-1132. (b) Bauer, W.; Clark, T.; Schleyer, P. v. R. *J. Am. Chem. Soc.* **1987**, *109*, 970-977. (c) Hoffmann, D.; Bauer, W.; Schleyer, P. v. R. *J. Chem. Soc., Chem. Commun.* **1990**, 208-211. (d) Hilmersson, G.; Davidsson, O. *J. Orgmet. Chem.* **1995**, *489*, 175-179. (e) Schade, S.; Boche, G. *J. Orgmet. Chem.* **1998**, *550*, 359-379. (f) Gschwind, R. M.; Rajamohanam, P. R.; John, M.; Boche, G. *Organometallics*. **2000**, *19*, 2868-2873. (g) Alam, T. M.; Pedrotty, D. M.; Boyle, T. J. *Magn. Reson. Chem.* **2002**, *40*, 361-365.

(14) (a) Meier, B. H.; Ernst, R. R. *J. Am. Chem. Soc.* **1979**, *101*, 6441-6442. (b) Jeener, J.; Meier, B. H.; Bachman, P.; Ernst, R. R. *J. Chem. Phys.* **1979**, *71*, 4546-4553. (c) Riddell, F. G.; Bremner, M.; Strange, J. H. *Magn. Reson. Chem.* **1994**, *32*, 118-121. (d) Cahill, L. S.; Chapman, R. P.; Britten, J. F.; Goward, G. R. *J. Chem. Phys. B* **2006**, *110*, 7171-7177.

(15) (a) Li, D.; Hopson, R.; Li, W.; Liu, J.; Williard, P. G. *Org. Lett.* **2008**, *10*, 909-911. (b) Li, D.; Kagan, G.; Hopson, R.; Williard, P. G. *J. Am. Chem. Soc.* **2009**, *131*, 5627-5634. (c) Li, D.; Keresztes, I.; Hopson, R.; Williard, P. G. *Acc. Chem. Res.* **2009**, *42*, 270-280.

(16) Stejskal, E. O.; Tanner, J. E. *J. Chem. Phys.* **1965**, *42*, 288-292.

(17) Morris, K. F.; Johnson Jr., C. S. *J. Am. Chem. Soc.* **1992**, *114*, 3139-3141.

(18) Cohen, Y.; Avram, L.; Frish, L. *Angew. Chem. Int. Ed.* **2005**, *44*, 520-554.

(19) Carrara, C.; Viel, S.; Delaurent, C.; Ziarelli, F.; Excoffier, G.; Caldarelli, S. *J. Magn. Reson.* **2008**, *194*, 303-306.

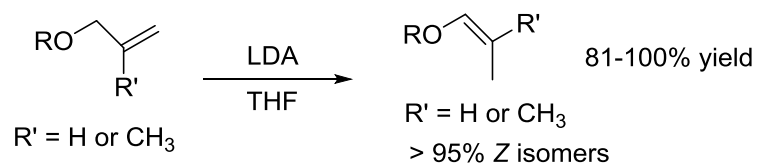
(20) (a) Kagan, G.; Li, W.; Hopson, R.; Williard, P. G. *Org. Lett.* **2009**, *11*, 4818-4821. (b) Kagan, G.; Li, W.; Hopson, R.; Williard, P. G. *Org. Lett.* **2010**, *12*, 520-523. (c) Li, W.; Kagan, G.; Yang, H.; Cai, C.; Hopson, R.; Sweigart, D. A.; Williard, P. G. *Org. Lett.* **2010**, *12*, 2698-2701. (d) Li, W.; Kagan, G.; Yang, H.; Cai, C.; Hopson, R.; Dai, W.; Sweigart, D. A.; Williard, P. G. *Organometallics*. **2010**, *29*, 1309-1311. (e) Socha, A. M.; Kagan, G.; Li, W.; Hopson, R.; Sello, J. K.; Williard, P. G. *Energy Fuels* **2010**, *24*, 4518-4521. (g) Lecachey, B.; Oulyadi, H.; Lameiras, P.; Harrison-Marchand, A.; Gerard, H.; Maddaluno, J. *J. Org. Chem.* **2010**, *75*, 5976-5983.

(21) In DOSY experiment, the duration of gradient pulse (d_{20}) must be shorter than the T_1 time of nucleus concerned. Alternatively, the relaxation delay (d_1) time is required to be at least 1.5 times of T_1 time.

(22) Schollkopf, U. *Angew. Chem. Int. Ed.* **1970**, *9*, 763-773.

Chapter 2

Isomerization of allyl ethers initiated by lithium diisopropylamide



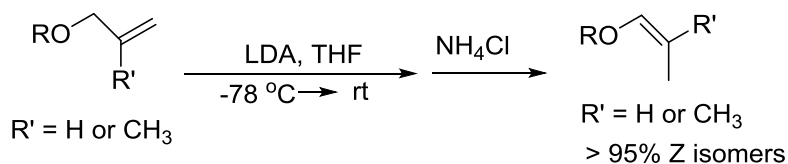
2.1 Abstract

Lithium diisopropylamide (LDA) promotes virtually quantitative conversion of allylic ethers to (*Z*)-propenyl ethers. It was discovered that allylic ethers can be isomerized efficiently with very high stereoselectivity to (*Z*)-propenyl ethers by LDA in THF at room temperature. The reaction time for the conversion increases with more sterically hindered allylic ethers. Different amides were also compared with LDA for their ability to effect this isomerization.

2.2 Introduction

Vinyl ethers are important synthetic intermediates in numerous reactions such as isoxazoline synthesis¹, cycloaddition² and cross aldol reactions³. Moreover, vinyl ethers can be easily photopolymerized to produce polymers that are used as photocurable coatings, inks, and adhesives.⁴ An efficient preparation of vinyl ethers is to prepare allyl ethers by O-alkylating an alcohol with allyl bromide followed by isomerization.⁵ Such isomerization reactions have been studied and are divided into two categories: base catalyzed⁶ and transition metal catalyzed reactions.⁷ Ruthenium and iridium complexes are reported to catalyze the conversion of allyl ethers stereoselectively to *trans* vinyl ethers.⁷⁻⁹ Although it is convenient to use transition metal complexes, the methods suffer from the fact that both ruthenium and iridium are expensive and are not suitable for large scale reactions. While iron and molybdenum complex catalyzed isomerization reactions have also been reported, both reactions produced mixtures of *cis* and *trans* isomers.^{5,10} For the base catalyzed reactions, the most widely used method is to treat the allyl ethers

with potassium tert-butoxide (*t*-BuOK) in dimethyl sulfoxide (DMSO) solution. Although the method achieved varying degrees of success,^{5,11-13} it is limited by the fact that heating is usually required for the isomerization reaction.^{6a,12-13} Moreover, since the reaction is exothermic, an increase in temperature will cause the equilibrium to shift back to the allyl ethers.¹⁴ Butyllithium has also been reported to isomerize allyl ethers,¹⁵ but the yields were relatively low due to the fact that deallylation¹⁶ or Wittig rearrangement¹⁷ may occur. An efficient method of allyl ether isomerization initiated by LDA (Scheme 2.1) and a comparison of a series of *t*-BuOK initiated isomerization reactions with the LDA initiated isomerization were illustrated in this chapter.



Scheme 2.1. Isomerization of allyl ethers initiated by LDA

2.3 Results and Discussion

2.3.1 Isomerization of allyl ethers by lithium diisopropylamide

In 1970, Dimmel and Gharpure reported the use of sodium amide in dimethoxyethane to isomerize allyl phenyl ether to (*Z*)-(prop-1-en-1-yloxy)benzene in 54% yield.¹⁸ To the best of our knowledge, this is the first allyl ether isomerization using an amide base. Lithium diisopropylamide can also effect this isomerization readily in ethereal solvents such as THF and dimethoxyethane. Other allyl ethers have also been investigated and these results are summarized in Table 2.1.

Branched chains at the β -position (Figure 2.1) of the allyl ethers reduce the rate of isomerization depending on the extent of substitution and steric bulk of the branched chain. Allyl ethers with no β branched chain (Table 2.1, entries 1-5, 7) isomerize much faster than other allyl ethers with β branched chains. Allyl ethers having only one β branched chain (Table 2.1, entries 6, 8) react faster than those with two β branched chains (Table 2.1, entry 10). When β branched chains are on both sides of the allyl ether (Table 2.1, entry 11), the isomerization rate decreases drastically. The results suggest that steric hindrance in β position plays an important role in the rate of isomerization. Moreover, the allyl ether derived from borneol (Table 2.1, entry 9) isomerizes much faster than that derived from isoborneol (Table 2.1, entry 10), presumably due to the fact that the allyl group from the former one experiences less steric hindrance than the allyl group of the latter one.

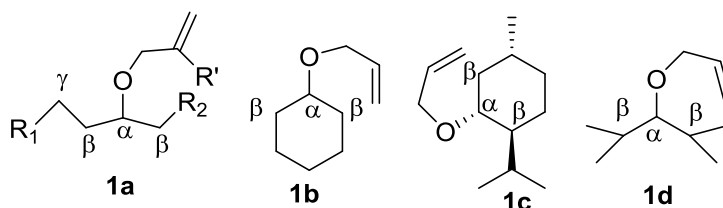
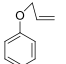
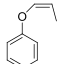
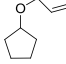
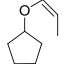
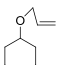
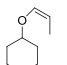
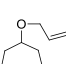
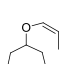
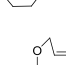
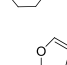
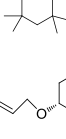
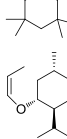
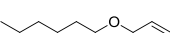
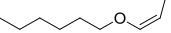
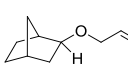
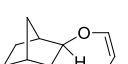
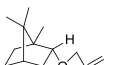
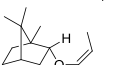
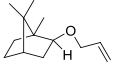
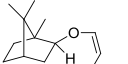
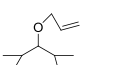
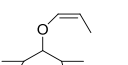
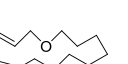
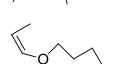
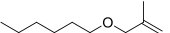
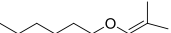


Figure 2.1. (1a) Definition of α and β positions and R' group of the allyl ethers. (1b) An example of allyl ether without β branched chain. (1c) An example of allyl ether with only one β branched chain. (1d) An example of allyl ether with two β branched chains.

The isomerization rate slows down when R' is a methyl group instead of a proton (Figure 2.1, **1a**). However, the effect of γ branched chain (Figure 2.1, **1a**) on reaction rate is small compared to the effect of β branched chain. The isomerization reaction for allyl ether derived from 3,3,5,5-tetramethylcyclohexanol (Table 2.1, entry 5) was done within 45 minutes and was much faster than that of menthol derived allyl ether (Figure 2.1, **1c**).

Table 2.1. LDA catalyzed isomerization of various allyl ether^a

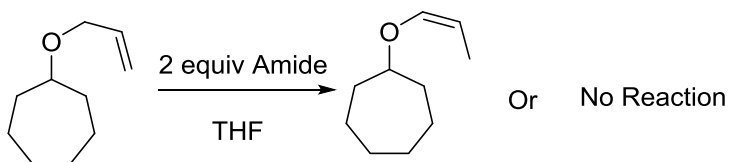
entry	allyl ether	amount of LDA	time	product	yield
1		2 equiv	0.75 h		88%
2		2 equiv	0.67 h		83%
3		2 equiv	0.75 h		88%
4		2 equiv	0.75 h		99%
5		2 equiv	0.75 h		100%
6		2 equiv	1.5 h		100%
7		2 equiv	0.67 h		92%
8		2 equiv	1.0 h		89%
9		2 equiv	1.5 h		95%
10		4 equiv	4.5 h		100%
11		6 equiv	21 h		87%
12		4 equiv	1.5 h		100%
13	TBSO-allyl	2 equiv	3.5 h	TBSO-isomerized allyl	81%
14		2 equiv	1.2 h		100%
15	TBSO-allyl	2 equiv	4 h	TBSO-isomerized allyl	85%

^a A solution of diisopropylamine in dry THF was cooled to -78 °C, 1 equiv n-BuLi in n-pentane was added dropwise, and the resulting solution was allowed to cool down in -78 °C bath for 5 min before the allyl ether was added drop by drop to the solution. The solution was allowed to warm up and stand at room temperature for the corresponding amount of time before being quenched with saturated ammonium chloride solution.

We suspect that the yields of the reactions of enol ethers with lower boiling points appear lower and are correlated with the boiling points of the enol ethers, because some loss of the lower boiling products was unavoidable upon work up.

2.3.2 Isomerization of allyl ethers by different lithium amides

Several different amide bases have also been tested for their ability to effect this isomerization reaction. The allyl ether derived from cycloheptanol (Scheme 2.2) was chosen as the model substrate for surveying the effectiveness of different amides because it has no β branched chain and its relative high boiling point. The results are summarized in Table 2.2.



Scheme 2.2. Isomerization of (allyloxy)cycloheptane initiated by different amides

Table 2.2. Isomerization of (allyloxy)cycloheptane by different amides

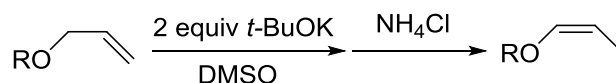
Entry	amide	time	yield
1		0.75 h	100%
2		1.75 h	93%
3 ^a		8 h	97%
4	NaNH ₂	No Reaction	
5	LiNH ₂	No Reaction	
6	LiHMDS	No Reaction	

^a 5 equiv lithium amide base was used.

Lithium bis(trimethylsilyl)amide (LiHMDS) failed to initiate the reaction. Neither lithium nor sodium amide effected this rearrangement. The reaction time for entry 3 was significantly longer than that of entries 1 and 2 probably because the lithium ion was internally solvated.¹⁹

2.3.3 Comparison of *t*-BuOK and LDA initiated isomerization

Several experiments using *tert*-butoxide/DMSO (Scheme 2.3) have been done and the results were compared to the LDA initiated isomerization (Table 2.3).



Scheme 2.3. Allyl ethers isomerization catalyzed by *t*-BuOK

Table 2.3. Comparison of *t*-BuOK and LDA initiated isomerization

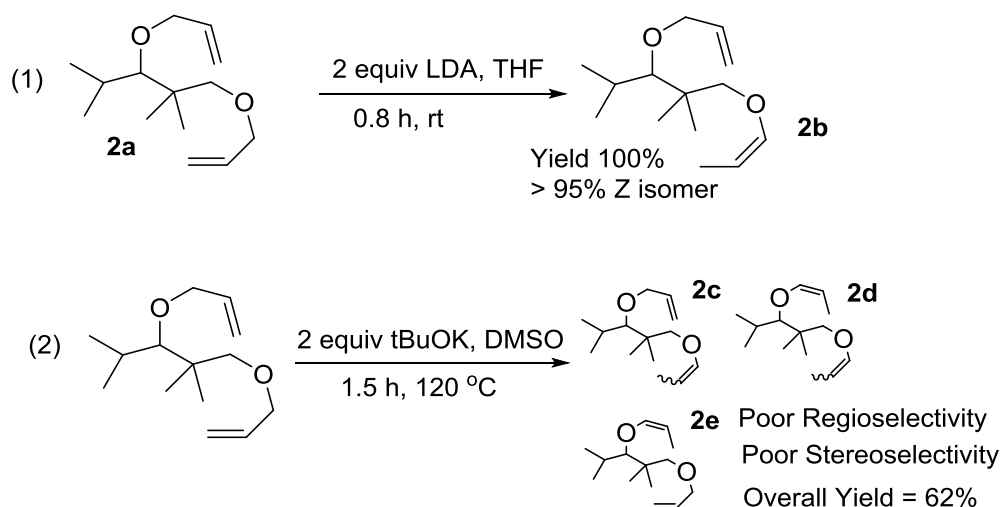
entry	allyl ether	base	time	temp.	ratio ^a
1		<i>t</i> -BuOK	1 h	60 °C	0
2		<i>t</i> -BuOK	4 h	60 °C	0
3		<i>t</i> -BuOK	2 h	120 °C	2.6 ^b
4		<i>t</i> -BuOK	4 h	120 °C	0.56 ^b
5		LDA	0.5 h	r.t.	All Enol Ether
6		LDA	4 h	r.t.	1.5

^a ratio = amount of enol ether/ amount of starting allyl ether

^b The end mixture/ starting allyl ether is less than 60%.

Entries 1-4 in Table 2.3 highlight that heating (higher than 60 °C) is required for *t*-BuOK catalyzed reactions. Although the isomerization of allyl ethers can be done at 120 °C, the rate of reaction is far slower than that of LDA catalyzed isomerization (Table 2.3, entries 5-6). Besides, for *t*-BuOK catalyzed reactions, the mass of the resulting mixtures of enol and allyl ethers recovered were less than 60% of the starting allyl ethers. We suggest that this is likely due to the high temperature of the reaction mixtures allowing the allyl ethers to volatilize or decompose. Therefore, it is clear that the LDA catalyzed isomerization is more effective than that which utilizes *t*-BuOK.

A comparison of LDA and *t*-BuOK in the isomerization of **2a** was carried out to highlight the advantage of LDA catalyzed isomerization over *t*-BuOK (Scheme 2.4). LDA regioselectively isomerizes the less steric hindered allyl ether group to *Z*-propenyl ether yield completely stereo- selectivity in quantitative yield. However, the *t*-BuOK catalyzed isomerization of **2a** was not as regio- and stereo- selective as the LDA catalyzed one as shown by the ¹³C NMR spectrum of the products (see supporting information). By comparing the spectrum of the product from the isomerization of **2a** by LDA with that of pure **2a**, we note that one of the two allyl groups has been selectively isomerized to a propenyl group. However, the spectrum of the products of *t*-BuOK catalyzed isomerization of **2a** shows that a mixture of *E* and *Z* propenyl ether isomers is formed from the less steric hindered allyl ether group. Moreover, a significant amount of the more steric hindered allyl group was isomerized to propenyl ether before the less hindered allyl group has been isomerized.



Scheme 2.4. Isomerization of **2a** catalyzed by LDA and *t*-BuOK

2.4 Conclusion

The LDA isomerization reaction outlined above provides a convenient, inexpensive and highly efficient method for the isomerization of allyl ethers to propenyl ethers. Future work will focus on studying the kinetics of the reaction with a goal of unveiling a more detailed mechanism of the complexes involved in this isomerization reaction.

2.5 Experimental Section

2.5.1 Materials and methods. THF and DME were used from a dry solvent dispensing system. DMSO was distilled from calcium hydride under a reduced pressure. Diisopropylamine was distilled from sodium hydride. Solvents for extraction and chromatography were technical grade. Unless otherwise stated, purchased chemicals (Aldrich, Acros, Alfa Aesar) were used as received. All reactions under anhydrous conditions were conducted using flame- or oven-dried glassware and standard syringe

techniques under an atmosphere of argon.

NMR spectra were recorded at either 300 MHz or 400 MHz using CDCl₃ as the solvent. Chemical shifts are reported in ppm and were referenced to residual protonated solvent for ¹H-NMR (δ 7.27 ppm for CHCl₃) and ¹³C-NMR (δ 77.00 ppm for CDCl₃). Data are represented as follows: chemical shift (multiplicity [br = broad, s = singlet, d = doublet, t = triplet, q = quartet, m = multiplet], integration, coupling constants in Hz). High-resolution mass spectra were obtained using electron impact or fast atom bombardment ionization methods.

2.5.2 General procedures for the synthesis of the allyl ethers. Allyl phenyl ether was bought from Aldrich directly. For the synthesis of other allyl ethers, it can be divided into three types.

Type I) (Table 2.1, entries 2-12 and compound **2a**) The starting alcohol (1 equiv) was dissolved in dry THF under an atmosphere of nitrogen at 0 °C. To this solution was added sodium hydride (1.3 equiv; 2.6 equiv for entry 12 and **2a**) and the mixture was allowed to stir for 10 minutes at 0 °C. After adding allyl bromide (1.3 equiv; 2.6 equiv for entry 12 and **2a**), the solution was then allowed to stir at room temperature for 30 minutes and reflux overnight. The reaction was quenched by the addition of saturated ammonium chloride solution. The mixture was then extracted with diethyl ether three times and the organic phase was washed with water, brine and dried over NaSO₄. The solvent was removed by rotary evaporation and purification was performed by vacuum distillation except entries 2, 8 and entry 11 which were purified by flash column chromatography and simple distillation respectively.

Type II) (Table 2.1, entries 13, 15) To a solution of *tert*-butyldimethylsilyl

chloride (1 equiv) in dry THF under an atmosphere of nitrogen was added imidazole (2.4 equiv). The solution was stirred for 5 minutes before allyl alcohol or 2-methylprop-2-en-1-ol (1.4 equiv) was added. The resulting mixture was allowed to stir for 2 days before being quenched by saturated ammonium chloride solution. The mixture was then extracted with diethyl ether three times and the organic phase was washed with water, brine and dried over NaSO₄. The solvent was removed by rotary evaporation and purification was performed by flash column chromatography.

Type III) (Table 2.1, entry 14) To a solution of 2-methylprop-2-en-1-ol (1 equiv) in dry THF under an atmosphere of nitrogen at 0 °C was added sodium hydride (1 equiv). The mixture was stirred at 0 °C for 10 minutes before adding 1-bromohexane (1 equiv). The reaction was stirred at room temperature for 30 minutes and was refluxed overnight. The reaction was quenched by the addition of saturated ammonium chloride solution. The mixture was then extracted with diethyl ether three times and the organic phase was washed with water, brine and dried over NaSO₄. The solvent was removed by rotary evaporation and purification was performed by flash column chromatography.

(Allyloxy)cyclopentane (Table 2.1, entry 2). (Allyloxy)cyclopentane was prepared as described above from cyclopentanol (0.50 g, 5.8 mmol). Purification (Hexanes : EtOAc = 25: 1) gave a light yellow oil (0.59 g, 4.7 mmol, 81 %). ¹H NMR (CDCl₃, 300 MHz) δ 6.02-5.80 (m, 1H), 5.26 (d, 1H, *J* = 16.6 Hz), 5.14 (d, 1H, *J* = 10.0 Hz), 4.01-3.85 (m, 3H), 1.82-1.40 (m, 8H); ¹³C NMR (CDCl₃, 75 MHz) δ 135.5, 116.3, 80.9, 69.8, 32.3, 23.6; HRMS-EI (M⁺) calcd for C₈H₁₄O 126.1045, found 126.1042.

(Allyloxy)cyclohexane (Table 2.1, entry 3). (Allyloxy)cyclohexane was prepared as described above from cyclohexanol (9.62 g, 96.0 mmol). Purification (bp = 36-37 °C, 8

mmHg) gave a colorless oil (10.8 g, 77.1 mmol, 80%). ^1H NMR (CDCl_3 , 300 MHz) δ 6.00-5.83 (m, 1H), 5.25 (d, 1H, $J = 17.2\text{Hz}$), 5.14 (d, 1H, $J = 10.2\text{Hz}$), 4.06-3.94 (m, 2H), 3.35-3.20 (m, 1H), 2.00-1.06 (m, 10H); ^{13}C NMR (CDCl_3 , 75 MHz) δ 169.3, 155.1, 144.6, 129.7, 128.1, 126.9, 80.0, 67.0, 66.8, 66.7, 49.3, 46.0, 42.6, 35.0, 28.4; MS m/z 140 (M^+), 97, 83, 67, 58, 55.

(Allyloxy)cycloheptane (Table 2.1, entry 4). (Allyloxy)cycloheptane was prepared as described above from cycloheptanol (1.92 g, 16.8 mmol). Purification (bp = 54-56 °C, 8 mmHg) gave a colorless oil (2.07 g, 13.4 mmol, 80 %). ^1H NMR (CDCl_3 , 400 MHz) δ 5.99-5.85 (m, 1H), 5.26 (dd, 1H, $J = 17.2, 1.2\text{ Hz}$), 5.21-5.10 (d, 1H, $J = 9.5\text{ Hz}$), 3.99-3.93 (m, 2H), 3.47 (quintet, 1H, $J = 4.0\text{Hz}$), 1.95-1.83 (m, 2H), 1.71-1.49 (m, 8H) , 1.44-1.31 (m, 2H); ^{13}C NMR (CDCl_3 , 100 MHz) δ 135.7, 116.2, 79.5, 69.1, 33.9, 28.4, 23.0; HRMS-EI (M^+) calcd for $\text{C}_{10}\text{H}_{18}\text{O}$ 154.1358, found 154.1355.

5-(allyloxy)-1,1,3,3-tetramethylcyclohexane (Table 2.1, entry 5). 5-(allyloxy)-1,1,3,3-tetramethylcyclohexane was prepared as described above from 3,3,5,5-tetramethyl-cyclohexanol (4.1 g, 26.3 mmol). Purification (bp = 78-80 °C, 8 mmHg) gave a colorless oil (3.6 g, 18.4 mmol, 70 %). ^1H NMR (CDCl_3 , 400 MHz) δ 6.00-5.87 (m, 1H), 5.27 (d, 1H, $J = 16.2\text{ Hz}$), 5.15 (d, 1H, $J = 9.9\text{ Hz}$), 4.02 (d, 2H, $J = 4.92\text{ Hz}$), 3.65-3.52 (m, 1H), 1.78 (d, 2H, $J = 11.6\text{Hz}$), 1.27-1.17 (m, 1H), 1.12-0.87 (m, 15H); ^{13}C NMR (CDCl_3 , 100 MHz) δ 135.6, 116.3, 77.3, 69.0, 51.8, 45.3, 35.2, 32.3, 27.9; HRMS-EI (M^+) calcd for $\text{C}_{13}\text{H}_{24}\text{O}$ 196.1827, found 196.1822.

(1*S*,2*R*,4*R*)-2-(allyloxy)-1-isopropyl-4-methylcyclohexane (Table 2.1, entry 6). (1*S*,2*R*,4*R*)-2-(allyloxy)-1-isopropyl-4-methylcyclohexane was prepared as described above from (-)-menthol (2.50 g, 16.0 mmol). Purification (bp = 78-79 °C, 8 mmHg) gave

a colorless oil (2.56 g, 13.1 mmol, 82 %). ^1H NMR (CDCl_3 , 300 MHz) δ 6.04-5.85 (m, 1H), 5.26 (d, 1H, $J = 17.2$ Hz), 5.14 (d, 1H, $J = 10.2$ Hz), 4.21-4.06 (m, 1H), 3.99-3.82 (m, 1H), 3.08 (dt, 1H, $J = 10.4, 4.1$ Hz), 2.35-2.17 (m, 1H), 2.17-2.04 (m, 1H), 1.74-1.55 (m, 2H), 1.46-1.18 (m, 2H), 1.12-0.71 (m, 14H); ^{13}C NMR (CDCl_3 , 75 MHz) δ 135.8, 116.3, 78.7, 69.5, 48.3, 40.5, 34.6, 31.5, 25.5, 23.4, 22.3, 21.0, 16.2; HRMS-EI (M^+) calcd for $\text{C}_{13}\text{H}_{24}\text{O}$ 198.1827, found 198.1821.

1-(allyloxy)hexane (Table 2.1, entry 7). 1-(allyloxy)hexane was prepared as described above from 1-hexanol (3.25 g, 31.9 mmol). Purification (bp = 36-37 °C, 8 mmHg) gave a colorless oil (3.69 g, 26.0 mmol, 82 %). ^1H NMR (CDCl_3 , 400 MHz) δ 5.99-5.85 (m, 1H), 5.27 (dd, 1H, $J = 17.2, 1.6$ Hz), 5.16 (d, 1H, $J = 10.3$ Hz), 4.00-3.93 (m, 2H), 3.96 (t, 2H, $J = 6.7$ Hz), 1.66-1.52 (m, 2H), 1.41-1.24 (m, 6H), 0.89 (t, 3H, $J = 6.64$ Hz); ^{13}C NMR (CDCl_3 , 100 MHz) δ 135.1, 116.6, 71.8, 70.5 31.7, 29.7, 25.9, 22.6, 14.0; HRMS-EI (M^+) calcd for $\text{C}_9\text{H}_{18}\text{O}$ 142.1358, found 142.1360.

(1S,2S,4R)-2-(allyloxy)bicyclo[2.2.1]heptane (Table 2.1, entry 8). (1S,2S,4R)-2-(allyloxy)bicyclo[2.2.1]heptane was prepared as described above from (1S,2S,4R)-bicyclo[2.2.1]heptan-2-ol (0.50g, 4.5mmol). Purification (Hexanes: EtOAc = 30:1) gave a light yellow oil (0.62g, 4.1mmol, 91%). ^1H NMR (CDCl_3 , 400 MHz) δ 6.02-5.35 (m, 1H), 5.26 (dd, 1H, $J = 22.9, 2.2$ Hz), 5.14 (dd, 1H, $J = 13.2, 1.1$ Hz), 4.02-3.86 (m, 2H), 3.45-3.35 (m, 1H), 2.37-2.29 (m, 1H), 2.29-2.20 (m, 1H), 1.65-1.33 (m, 5H), 1.16-0.91 (m, 2H); ^{13}C NMR (CDCl_3 , 100 MHz) δ 135.5, 116.2, 82.1, 69.3, 40.4, 39.6, 35.2, 34.8, 28.5, 24.6; HRMS-EI (M^+) calcd for $\text{C}_{10}\text{H}_{16}\text{O}$ 152.1201, found 152.1206.

(1S,2R,4S)-2-(allyloxy)-1,7,7-trimethylbicyclo[2.2.1]heptane (Table 2.1, entry 9). (1S,2R,4S)-2-(allyloxy)-1,7,7-trimethylbicyclo[2.2.1]heptane was prepared as described

above from (1*S*,2*R*,4*S*)-1,7,7-trimethylbicyclo[2.2.1]heptan-2-ol (6.5 g, 42 mmol). Purification (bp = 68-70 °C, 8 mmHg) gave a colorless oil (6.8 g, 35 mmol, 83%). ¹H NMR (CDCl₃, 300 MHz) δ 6.03-5.82 (m, 1H), 5.28 (d, 1H, *J* = 17.1 Hz), 5.15 (d, 1H, *J* = 9.1 Hz), 4.11-3.99 (m, 1H), 3.99-3.82 (m, 1H), 3.73-3.55 (m, 1H), 2.21-1.93 (m, 2H), 1.83-1.55 (m, 2H) , 1.35-1.13 (m, 2H) , 1.12-0.96 (m, 1H) , 0.96-0.75 (m, 9H); ¹³C NMR (CDCl₃, 75 MHz) δ 135.9, 115.7, 84.3, 70.8, 49.2, 47.8, 45.0, 36.3, 28.2, 26.7, 19.8, 18.8, 14.0; HRMS-EI (M⁺) calcd for C₁₃H₂₂O 194.1671, found 194.1668.

(1*S*,2*S*,4*S*)-2-(allyloxy)-1,7,7-trimethylbicyclo[2.2.1]heptane (Table 2.1, entry 10). (1*S*,2*S*,4*S*)-2-(allyloxy)-1,7,7-trimethylbicyclo[2.2.1]heptane was prepared as described above from (1*S*,2*S*,4*S*)-1,7,7-trimethylbicyclo[2.2.1]heptan-2-ol (3.0 g, 20 mmol). Purification (bp = 65-68 °C, 8 mmHg) gave a colorless oil (3.1 g, 16 mmol, 82%). ¹H NMR (CDCl₃, 400 MHz) δ 5.96-5.82 (m, 1H), 5.26 (dd, 1H, *J* = 17.2, 1.6 Hz), 5.11 (d, 1H, *J* = 10.5 Hz), 4.03-3.93 (m, 1H), 3.91-3.81 (m, 1H), 3.29-3.22 (m, 1H), 1.82-1.42 (m, 5H), 1.05-0.95 (m, 5H), 0.91 (s, 3H), 0.81 (s, 3H); ¹³C NMR (CDCl₃, 100 MHz) δ 135.9, 115.3, 107.6, 86.5, 83.8, 69.8, 49.2, 46.5, 45.1, 38.7, 34.5, 27.3, 20.24, 20.20, 11.9; HRMS-EI (M⁺) calcd for C₁₃H₂₂O 194.1671, found 194.1662.

3-(allyloxy)-2,4-dimethylpentane (Table 2.1, entry 11). 3-(allyloxy)-2,4-dimethylpentane was prepared as described above from 2,4-dimethylpentan-3-ol (2.0 g, 17 mmol). Purification (bp = 125 °C, 760 mmHg) gave a colorless oil (2.2 g, 14 mmol, 82%). ¹H NMR (CDCl₃, 300 MHz) δ 6.04-5.86 (m, 1H), 5.26 (d, 1H, *J* = 17.2 Hz), 5.12 (d, 1H, *J* = 10.3 Hz), 4.12-4.04 (m, 2H), 2.70 (t, 1H, *J* = 5.6 Hz), 1.91-1.73 (m, 2H), 0.99-0.85 (m, 12H); ¹³C NMR (CDCl₃, 75 MHz) δ 135.6, 115.9, 90.7, 74.8, 30.8, 20.3, 17.7; MS *m/z* 155 (M-H⁺), 113, 71, 57, 55.

1,6-bis(allyloxy)hexane (Table 2.1, entry 12). 1,6-bis(allyloxy)hexane was prepared as described above from hexane-1,6-diol (3.5 g, 29.7 mmol). Purification (bp = 96-98 °C, 8 mmHg) gave a colorless oil (4.6 g, 23 mmol, 78 %). ¹H NMR (CDCl₃, 400 MHz) δ 5.99-5.85 (m, 2H), 5.26 (d, 2H, *J* = 17.2 Hz), 5.16 (d, 2H, *J* = 10.0 Hz), 4.00-3.92 (m, 4H), 3.42 (t, 4H, *J* = 6.5 Hz), 1.66-1.54 (m, 4H), 1.44-1.33 (m, 4H); ¹³C NMR (CDCl₃, 100 MHz) δ 135.0, 116.7, 71.8, 70.3, 29.7, 26.0; HRMS-FAB (*M* + Na⁺) calcd for C₁₂H₂₂O₂ 221.1518, found 221.1522.

(Allyloxy)(tert-butyl)dimethylsilane (Table 2.1, entry 13). (Allyloxy)(tert-butyl)dimethylsilane was prepared as described above from tert-butylchlorodimethylsilane (1.2 g, 8.0 mmol). Purification (Hexanes : EtOAc = 30 : 1) gave a colorless oil (1.0 g, 5.8 mmol, 73 %). ¹H NMR (CDCl₃, 300 MHz) δ 6.01-5.85 (d, 1H), 5.27 (d, 1H, *J* = 17.0 Hz), 5.08 (d, 1H, *J* = 9.0 Hz), 4.26-4.16 (m, 2H), 0.93 (s, 9H), 0.08 (s, 6H); ¹³C NMR (CDCl₃, 75 MHz) δ 137.5, 113.9, 64.1, 25.9, 18.4, -5.3; MS *m/z* 172 (*M*⁺), 115, 99, 85, 75, 73, 59, 57.

1-((2-methylallyl)oxy)hexane (Table 2.1, entry 14). 1-((2-methylallyl)oxy)hexane was prepared as described above from 2-methylprop-2-en-1-ol (0.77 g, 10.7mmol). Purification (Hexanes : EtOAc = 20 : 1) gave a colorless oil (1.31 g, 8.40 mmol, 78 %). ¹H NMR (CDCl₃, 400 MHz) δ 4.95 (s, 1H), 4.88 (s, 1H), 3.87 (s, 2H), 3.38 (t, 2H, *J* = 6.6 Hz), 1.99-1.21 (m, 11H), 0.89(t, 3H, *J* = 5.9 Hz); ¹³C NMR (CDCl₃, 100 MHz) δ 142.6, 111.7, 74.7, 70.2, 31.7, 29.7, 25.9, 22.6, 19.4, 14.0; HRMS-EI (*M* +) calcd for C₁₀H₂₀O 156.1514, found 156.1502.

Tert-butyl dimethyl((2-methylallyl)oxy)silane (Table 2.1, entry 15). Tert-butyl dimethyl((2-methylallyl)oxy)silane was prepared as described above from tert-

butylchlorodimethylsilane (0.60 g, 4.0 mmol). Purification (Hexanes : EtOAc = 30 : 1) gave a colorless oil (0.50 g, 2.7 mmol, 68%). ¹H NMR (CDCl₃, 400 MHz) δ 4.99 (s, 1H), 4.81 (s, 1H), 4.05 (s, 2H), 1.71 (s, 3H), 0.94 (s, 9H), 0.09 (s, 6H); ¹³C NMR (CDCl₃, 100 MHz) δ 145.0, 109.5, 67.2, 26.3, 19.3, 18.8, -5.0; HRMS-EI (M + Na) calcd for C₁₀H₂₂O₂Si 186.1440, found 186.1431.

1,3-bis(allyloxy)-2,2,4-trimethylpentane (2a). 1,3-bis(allyloxy)-2,2,4-trimethylpentane was prepared as described above from 2,2,4-trimethylpentane-1,3-diol (4.0 g, 27 mmol). Purification (bp = 78-80 °C, 8 mmHg) gave a colorless oil (5.80 g, 25.7 mmol, 93 %). ¹H NMR (CDCl₃, 300 MHz) δ 6.02-5.84 (m, 2H), 5.27 (d, 2H, *J* = 17.2 Hz), 5.14 (m, 2H), 4.18-3.92 (m, 4H), 3.31 (d, 1H, *J* = 8.6 Hz), 3.15-3.04 (m, 2H), 2.00-1.86 (m, 1H), 1.07-0.85 (m, 12H); ¹³C NMR (CDCl₃, 75 MHz) δ 135.8, 135.3, 116.2, 115.3, 87.4, 77.9, 74.7, 72.1, 40.5, 28.9, 24.6, 22.3, 21.1, 17.9; MS *m/z* 227 (M + H⁺), 183, 127, 113, 112, 85, 71, 57, 55.

2.5.3 General procedures for the isomerization of the allyl ethers (Table 2.1 and 2a) to vinyl ethers by LDA in THF. Under an argon atmosphere, a pentane solution of *n*-butyllithium (2 equiv) was added dropwise to a solution of diisopropylamine (2 equiv) in dry THF (4 mL) at -78 °C. After stirring for 5 min, the solution was allowed to warm to 0 °C for 2 min and was then re-cooled to -78 °C. Allyl ether (1 equiv; except Table 2.1, entries 10-12) was added dropwise to the mixture at -78 °C and the mixture was allowed to stir for 5 min at -78 °C before warming up to room temperature. The reaction time of the mixture varied between different kinds of allyl ethers (Table 2.1). After being stirred for the corresponding time, the reaction mixture was quenched by saturated ammonium chloride solution. The mixture was then extracted with diethyl ether three times and the

organic phase was washed with water, brine and dried over NaSO₄. The solvent was first removed by rotary evaporation and then by oil pump yielding a yellow liquid which was then characterized by NMR spectroscopy and HRMS.

(Z)-(prop-1-en-1-yloxy)benzene (Table 2.1, entry 1). (Z)-(prop-1-en-1-yloxy)benzene (187 mg, 88 %) was obtained from (allyloxy)benzene (165 mg) as described above. ¹H NMR (CDCl₃, 400 MHz) δ 7.28-7.30 (m, 2H), 7.10-7.00 (m, 3H), 6.41 (d, 1H, *J* = 4.4 Hz), 4.91 (m, 1H), 1.75 (d, 3H, *J* = 5.9 Hz); ¹³C NMR (CDCl₃, 100 MHz) δ 157.5, 140.8, 129.5, 122.3, 116.1, 107.5, 9.4; HRMS-EI (M +) calcd for C₉H₁₀O 134.0732, found 134.0728.

(Z)-(prop-1-en-1-yloxy)cyclopentane (Table 2.1, entry 2). (Z)-(prop-1-en-1-yloxy)cyclopentane (151 mg, 83 %) was obtained from (allyloxy)cyclopentane (182 mg) as described above. ¹H NMR (CDCl₃, 400 MHz) δ 5.98-5.94 (dq, 1H, *J* = 6.2 Hz, 1.6 Hz), 4.41 (m, 1H), 4.23 (m, 1H), 1.75 (m, 6H), 1.57 (m, 5H); ¹³C NMR (CDCl₃, 100 MHz) δ 144.3, 101.5, 82.9, 32.6, 23.5, 9.2; HRMS-EI (M +) calcd for C₈H₁₄O 126.1045, found 126.1041.

(Z)-(prop-1-en-1-yloxy)cyclohexane (Table 2.1, entry 3). (Z)-(prop-1-en-1-yloxy)cyclohexane (182 mg, 88 %) was obtained from (allyloxy)cyclohexane (207 mg) as described above. ¹H NMR (CDCl₃, 300 MHz) δ 6.02-5.90 (d, 1H, *J* = 4.8 Hz), 4.45-4.30 (m, 1H), 3.64-3.45 (m, 1H), 1.90-1.10 (m, 13H), 2.49 (dd, 1H, *J* = 5.6, 12.4 Hz), 2.41 (dd, 1H, *J* = 7.5, 12.4), 1.42 (s, 9H); ¹³C NMR (CDCl₃, 75 MHz) δ 114.2, 101.0, 78.9, 32.3, 25.6, 23.6, 9.3; HRMS-EI (M +) calcd for C₉H₁₆O 140.1201, found 140.1205.

(Z)-(prop-1-en-1-yloxy)cycloheptane (Table 2.1, entry 4). (Z)-(prop-1-en-1-yloxy)cycloheptane (202 mg, 99 %) was obtained from (allyloxy)cycloheptane (205 mg) as

described above. ^1H NMR (CDCl_3 , 300 MHz) δ 6.00-5.92 (d, 1H, $J = 6.2$ Hz), 4.44-4.32 (m, 1H), 3.84-3.72 (m, 1H), 1.96-1.32 (m, 15H); ^{13}C NMR (CDCl_3 , 75 MHz) δ 144.5, 101.1, 81.8, 34.2, 28.3, 22.7, 9.3; HRMS-EI (M^+) calcd for $\text{C}_{10}\text{H}_{18}\text{O}$ 154.1358, found 154.1356.

(Z)-1,1,3,3-tetramethyl-5-(prop-1-en-1-yloxy)cyclohexane (Table 2.1, entry 5). (Z)-1,1,3,3-tetramethyl-5-(prop-1-en-1-yloxy)cyclohexane (0.19 g, 100 %) was obtained from 5-(allyloxy)-1,1,3,3-tetramethylcyclohexane (0.19 g) as described above. ^1H NMR (CDCl_3 , 400 MHz) δ 6.07-6.00 (d, 1H, $J = 6.2$ Hz), 4.44-4.34 (m, 1H), 3.90-3.78 (m, 1H), 1.83-1.73 (m, 2H), 1.62-1.54 (m, 3H), 1.31-0.89 (m, 16H); ^{13}C NMR (CDCl_3 , 100 MHz) δ 144.3, 100.9, 75.9, 51.6, 45.4, 34.9, 32.3, 28.0, 9.3; HRMS-EI (M^+) calcd for $\text{C}_{13}\text{H}_{24}\text{O}$ 196.1827, found 196.1824.

(1S,2R,4R)-1-isopropyl-4-methyl-2-((Z)-prop-1-en-1-yloxy)cyclohexane (Table 2.1, entry 6). (1S,2R,4R)-1-isopropyl-4-methyl-2-((Z)-prop-1-en-1-yloxy)cyclohexane (0.20 g, 100 %) was obtained from (1S,2R,4R)-2-(allyloxy)-1-isopropyl-4-methylcyclohexane (0.20 g) as described above. ^1H NMR (CDCl_3 , 400 MHz) δ 6.04-5.99 (dq, 1H, $J = 6.2$ Hz, 1.6 Hz), 4.38-4.30 (m, 1H), 3.35 (dt, 1H, $J = 10.7, 4.3$ Hz), 2.21-2.10 (m, 1H), 2.05-1.96 (m, 1H), 1.69-1.59 (m, 5H), 1.45-1.32 (m, 2H), 1.06-0.76 (m, 11H); ^{13}C NMR (CDCl_3 , 100 MHz) δ 114.8, 100.2, 81.3, 47.8, 41.6, 34.4, 31.6, 25.9, 23.6, 22.2, 20.8, 16.4, 9.3; HRMS-EI (M^+) calcd for $\text{C}_{13}\text{H}_{24}\text{O}$ 196.1827, found 196.1819.

(Z)-1-(prop-1-en-1-yloxy)hexane (Table 2.1, entry 7). (Z)-1-(prop-1-en-1-yloxy)hexane (180 mg, 92 %) was obtained from 1-(allyloxy)hexane (195 mg) as described above. ^1H NMR (CDCl_3 , 400 MHz) δ 5.98-5.91 (d, 1H, $J = 4.2$ Hz), 4.43-4.32 (m, 1H), 3.76-3.68 (t, 2H, $J = 6.6$ Hz), 1.67-1.54 (m, 5H), 1.42-1.24 (m, 6H), 0.94-0.85

(t, 3H, $J = 6.5$ Hz); ^{13}C NMR (CDCl_3 , 100 MHz) δ 145.6, 100.7, 72.1, 31.6, 29.7, 25.5, 22.6, 14.0, 9.2; HRMS-EI (M^+) calcd for $\text{C}_9\text{H}_{18}\text{O}$ 142.1358, found 142.1360.

(1*S*,2*S*,4*R*)-2-((*Z*)-prop-1-en-1-yloxy)bicyclo[2.2.1]heptane (Table 2.1, entry 8). (1*S*,2*S*,4*R*)-2-((*Z*)-prop-1-en-1-yloxy)bicyclo[2.2.1]heptane (125 mg, 89 %) was obtained from (1*S*,2*S*,4*R*)-2-(allyloxy)bicyclo[2.2.1]heptane (140 mg) as described above. ^1H NMR (CDCl_3 , 400 MHz) δ 5.98-5.93 (dq, 1H, $J = 6.2$ Hz, 1.6 Hz), 4.45-4.37 (m, 1H), 3.70-3.65 (m, 1H), 2.34-2.24 (m, 2H), 1.64-1.40 (m, 8H), 1.15-0.59 (m, 3H); ^{13}C NMR (CDCl_3 , 100 MHz) δ 144.1, 101.5, 83.8, 41.3, 39.3, 35.2, 34.7, 28.5, 24.2, 9.3; HRMS-EI (M^+) calcd for $\text{C}_{10}\text{H}_{16}\text{O}$ 152.1201, found 152.1206.

(1*S*,2*R*,4*S*)-1,7,7-trimethyl-2-((*Z*)-prop-1-en-1-yloxy)bicyclo[2.2.1]heptane (Table 2.1, entry 9). (1*S*,2*R*,4*S*)-1,7,7-trimethyl-2-((*Z*)-prop-1-en-1-yloxy)bicyclo[2.2.1]heptane (185 mg, 95 %) was obtained from (1*S*,2*R*,4*S*)-2-(allyloxy)-1,7,7-trimethylbicyclo[2.2.1]heptane (195 mg) as described above. ^1H NMR (CDCl_3 , 400 MHz) δ 5.99-5.94 (dq, 1H, $J = 6.1$ Hz, 1.6 Hz), 4.39-4.31 (m, 1H), 3.94-3.88 (m, 1H), 2.25-2.14 (m, 1H), 2.10-2.01 (m, 1H), 1.79-1.58 (m, 5H), 1.33-1.21 (m, 2H), 1.15-1.07 (m, 1H), 0.94-0.84 (m, 9H); ^{13}C NMR (CDCl_3 , 100 MHz) δ 145.8, 100.4, 86.6, 49.5, 48.0, 45.0, 36.4, 28.1, 26.7, 19.8, 18.8, 13.8, 9.4; HRMS-EI (M^+) calcd for $\text{C}_{13}\text{H}_{22}\text{O}$ 194.1671, found 194.1668.

(1*S*,2*S*,4*S*)-1,7,7-trimethyl-2-((*Z*)-prop-1-en-1-yloxy)bicyclo[2.2.1]heptane (Table 2.1, entry 10). (1*S*,2*S*,4*S*)-1,7,7-trimethyl-2-((*Z*)-prop-1-en-1-yloxy)bicyclo[2.2.1]heptane (0.20 g, 100 %) was obtained from (1*S*,2*S*,4*S*)-2-(allyloxy)-1,7,7-trimethylbicyclo[2.2.1]heptane (0.20g) as described above. ^1H NMR (CDCl_3 , 400 MHz) δ 5.95-5.88 (dq, 1H, $J = 6.2$ Hz, 1.6 Hz), 4.35-4.26 (m, 1H), 3.59-3.52 (m, 1H), 1.90-

1.47 (m, 8H), 1.08-0.80 (m, 11H); ^{13}C NMR (CDCl_3 , 100 MHz) δ 145.7, 99.7, 88.9, 49.5, 46.6, 45.0, 38.7, 33.9, 27.2, 20.2, 20.0, 11.8, 9.3; HRMS-EI (M^+) calcd for $\text{C}_{13}\text{H}_{22}\text{O}$ 194.1671, found 194.1665.

(Z)-2,4-dimethyl-3-(prop-1-en-1-yloxy)pentane (Table 2.1, entry 11). (Z)-2,4-dimethyl-3-(prop-1-en-1-yloxy)pentane (180 mg, 87 %) was obtained from 3-(allyloxy)-2,4-dimethylpentane (207 mg) as described above. ^1H NMR (CDCl_3 , 400 MHz) δ 6.02-5.93 (d, 1H, $J = 6.2$ Hz), 4.22-4.11 (m, 1H), 3.00-2.90 (m, 1H), 1.95-1.80 (m, 2H), 1.64-1.55 (m, 3H), 0.98-0.83 (m, 12H); ^{13}C NMR (CDCl_3 , 100 MHz) δ 149.3, 97.7, 93.5, 30.9, 20.4, 17.9, 9.6; HRMS-EI (M^+) calcd for $\text{C}_{10}\text{H}_{20}\text{O}$ 156.1514, found 156.1510.

1,6-bis((Z)-prop-1-en-1-yloxy)hexane (Table 2.1, entry 12). 1,6-bis((Z)-prop-1-en-1-yloxy)hexane (192 mg, 100 %) was obtained from 1,6-bis(allyloxy)hexane (192 mg) as described above. ^1H NMR (CDCl_3 , 400 MHz) δ 6.02-5.91 (dq, 2H, $J = 8.2$ Hz, 2.2 Hz), 4.44-4.33 (m, 2H), 3.85-3.68 (m, 4H), 1.82-1.36 (m, 14H); ^{13}C NMR (CDCl_3 , 100 MHz) δ 145.6, 100.8, 71.9, 29.7, 25.6, 9.2; HRMS-EI (M^+) calcd for $\text{C}_{12}\text{H}_{22}\text{O}_2$ 198.1620, found 198.1612.

(Z)-tert-butyldimethyl(prop-1-en-1-yloxy)silane (Table 2.1, entry 13). (Z)-tert-butyldimethyl(prop-1-en-1-yloxy)silane (160 g, 81 %) was obtained from (allyloxy)(tert-butyl)dimethylsilane (198 mg) as described above. ^1H NMR (CDCl_3 , 400 MHz) δ 6.25-6.17 (dq, 1H, $J = 4.1$ Hz, 1.6 Hz), 4.57-4.46 (m, 1H), 1.63-1.55 (dd, 3H, $J = 6.7$, 1.6 Hz), 0.94 (s, 9H), 0.14 (s, 6H); ^{13}C NMR (CDCl_3 , 100 MHz) δ 139.3, 104.8, 25.7, 18.3, 8.9, -5.4; HRMS-EI (M^+) calcd for $\text{C}_9\text{H}_{20}\text{OSi}$ 172.1283, found 172.1288.

1-((2-methylprop-1-en-1-yl)oxy)hexane (Table 2.1, entry 14). 1-((2-methylprop-1-en-1-yl)oxy)hexane (140 mg, 100 %) was obtained from 1-((2-methylallyl)oxy)hexane

(140 mg) as described above. ^1H NMR (CDCl_3 , 400 MHz) δ 5.79 (s, 1H), 3.65 (t, 2H, $J = 6.6$ Hz), 1.68-1.47 (m, 8H), 1.42-1.23 (m, 6H), 0.89 (t, 3H, $J = 6.6$ Hz); ^{13}C NMR (CDCl_3 , 100 MHz) δ 140.1, 110.1, 71.8, 31.6, 29.7, 25.56, 25.59, 19.5, 14.9, 14.0; HRMS-EI (M^+) calcd for $\text{C}_{10}\text{H}_{20}\text{O}$ 156.1514, found 156.1518.

***Tert*-butyldimethyl((2-methylprop-1-en-1-yl)oxy)silane (Table 2.1, entry 15).** *Tert*-butyldimethyl((2-methylprop-1-en-1-yl)oxy)silane (0.17 g, 85 %) was obtained from *tert*-butyldimethyl((2-methylallyl)oxy)silane (0.20 g) as described above. ^1H NMR (CDCl_3 , 400 MHz) δ 6.04 (s, 1H), 1.61 (s, 3H), 1.54 (s, 3H), 0.93 (s, 9H), 0.12 (s, 6H); ^{13}C NMR (CDCl_3 , 100 MHz) δ 133.5, 113.3, 25.7, 19.3, 18.2, 14.7, -5.3; HRMS-EI (M^+) calcd for $\text{C}_{10}\text{H}_{22}\text{OSi}$ 186.1440, found 186.1431.

(*Z*)-3-(allyloxy)-2,2,4-trimethyl-1-(prop-1-en-1-yloxy)pentane (Isomerization of 2a). (*Z*)-3-(allyloxy)-2,2,4-trimethyl-1-(prop-1-en-1-yloxy)pentane (0.194 g, 0.86 mmol, 100 %) was obtained from 1,3-bis(allyloxy)-2,2,4-trimethyl-pentane (0.194 g, 0.86 mmol) as described above. ^1H NMR (CDCl_3 , 300 MHz) δ 6.01-5.83 (m, 2H), 5.26 (d, 1H, $J = 17.1$ Hz), 5.10 (d, 1H, $J = 10.4$ Hz), 4.40-4.26 (m, 1H), 4.19-3.90 (m, 2H), 3.63 (d, 1H, $J = 9.3$ Hz), 3.36 (d, 1H, $J = 9.4$ Hz), 3.12 (s, 1H), 2.03-1.85 (m, 1H), 1.63-1.51 (m, 3H), 1.08-0.82 (m, 12H); ^{13}C NMR (CDCl_3 , 75 MHz) δ 146.4, 135.6, 115.4, 100.0, 87.3, 79.4, 74.7, 40.9, 28.8, 24.7, 22.2, 20.5, 17.9, 9.2; MS m/z 226 (M^+), 183, 157, 127, 125, 113, 111, 85, 71, 69, 57, 55.

2.5.4 General procedures for the isomerization of the allyl ethers (Table 2.3) to vinyl ethers by *t*-BuOK in DMSO. Under an argon atmosphere, potassium *t*-butoxide (2 equiv) purchased directly from Aldrich was dissolved in 3 mL dry DMSO at room temperature. To this solution was added allyl ether (1 equiv) and the reaction mixture was

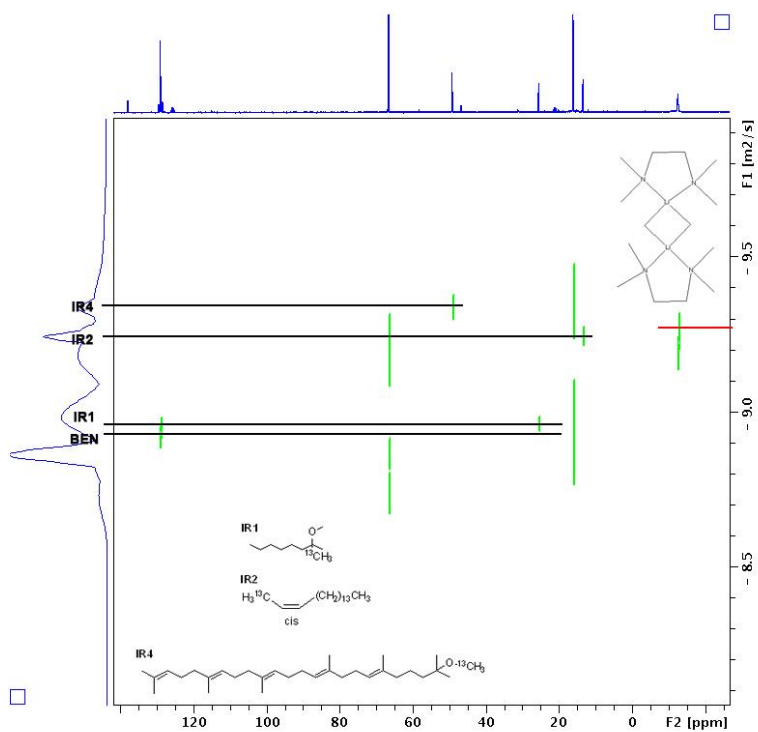
stirred at room temperature, 60 °C or 120 °C for the amount of time shown in Table 2.3. The reaction mixture was quenched by saturated ammonium chloride solution. The mixture was then extracted with diethyl ether three times and the organic phase was washed with water, brine and dried over NaSO₄. The solvent was first removed by rotary evaporation and then by oil pump yielding a light yellow liquid which was then characterized by NMR spectroscopy to determine the ratio between the starting allyl ether and vinyl ether product.

2.6 References

- (1) Krompiec, S.; Bujak, P.; Szczepankiewicz W. *Tetrahedron Lett.* **2008**, *49*, 6071-6074.
- (2) (a) Greene A.E.; Charbonnier F. *Tetrahedron Lett.* **1985**, *26*, 5525-5528; (b) Harmata M.; Lee D. R.; Barnes, C. L. *Org. Lett.* **2005**, *7*, 1881-1883.
- (3) Kawano, Y.; Fujisawa, H.; Mukaiyama, T. *Chem. Lett.* **2005**, *34*, 614-615.
- (4) (a) Sangermano, M.; Malucelli, G.; Bongiovanni R.; Pirola, A.; Annby, U.; Rehnberg, N. *Eur. Polym. J.* **2002**, *38*, 655-659; (b) Crivello, J.V.; Lohden, G. *J. Polym. Sci. Part A: Polym. Chem.* **1996**, *34*, 1015-1024; (c) Crivello, J.V.; Lohden, G. *J. Polym. Sci. Part A: Polym. Chem.* **1996**, *34*, 2051-2062. (d) Kim, W.G.; Ahn, H.K.; Lee, H.W.; Kim, S.H.; Crivello, J.V. *Opt. Mater.* **2002**, *21*, 343-347.
- (5) Crivello, J.V.; Kong, S.. *J. Org. Chem.* **1998**, *63*, 6745-6748.
- (6) (a) Mereyala, H.B.; Gurralla, S.R.; Mohan, S.K. *Tetrahedron* **1999**, *55*, 11331-11342; (b) Price, C.C.; Snyder, W. H. *J. Am. Chem. Soc.* **1961**, *83*, 1773; (c) Taskinen, E.; Laine, M.; *Structural Chem.* **1997**, *8*, 367-372.
- (7) (a) Ohmura, T.; Shirai, Y.; Yamamoto, Y. Miyaura, N. *Chem Commun.* **1998**, 1337-1338; (b) Krompiec, S.; Kuznik, N.; Urbala, M.; Rzepa, J. *J. Mol Catal. Chem.* **2006**, *248*, 198-209; (c) Carless, H.A.; Haywood, D.J. *J. Chem. Soc. Chem. Commun.* **1980**, 980-981.
- (8) Suzuki, H.; Koyama, Y.; Morooka, Y.; Ikawa, T. *Tetrahedron Lett.* **1979**, *16*, 1415-1418.
- (9) Ohmura T.; Yamamoto Y.; Miyaura, N. *Organometallics* **1999**, *18*, 413-416.
- (10) Tatsumi, T.; Hashimoto, K.; Tominaga, H. *J. Organomet. Chem.* **1983**, *252*, 105-112.
- (11) Endo, K.; Otsu, T. *Polymer* **1991**, *32*, 2856-2861.
- (12) Evans, D. A.; Kvaerno, L.; Dunn, T. B.; Beauchemin, A.; Raymer, B.; Mulder, J. A.; Olhava, E. J.; Juhl, M.; Kagechika, K.; Favor, D. A. *J. Am. Chem. Soc.* **2008**, *130*, 16295-16309.
- (13) Davis, C.E.; Duffy, B.C.; Coates, R.M. *J. Org. Chem.* **2003**, *68*, 6935-6943.
- (14) Taskinen, E. *J. Chem. S., Perkin Trans. 2.* **2001**, 1824-1834.
- (15) Harmata, M.; Lee, D.R.; Barnes, C.L. *Org. Lett.* **2005**, *7*, 1881-1883.
- (16) Bailey, W.F.; England, M.D.; Mealy, M.J.; Thongsornkleeb, C.; Teng, L. *Org. Lett.* **1999**, *2*, 489-491.
- (17) Schollkopf, U. *Angew. Chem. Int. Ed.* **1970**, *9*, 763-773.
- (18) Dimmel, D.R.; Gharpure, S.B. *J. Am. Chem. Soc.* **1971**, *93*, 3991-3996.
- (19) (a) Fraenkel, G.; Chen, X.; Chow, A.; Gallucci, J.C.; Liu, H. *J. Org. Chem.* **2005**, *70*, 9131-9138. (b) Fraenkel, G.; Gallucci, J.; Liu, H. *J. Am. Chem. Soc.* **2006**, *128*, 8211-8216.

Chapter 3

Isotopically Enriched ^{13}C Diffusion-Ordered NMR Spectroscopy – Analysis of Methylithium



3.1 Abstract

The development of isotopic labeled ^{13}C diffusion-ordered NMR spectroscopy (DOSY) NMR with diffusion coefficient-formula weight (*D-FW*) analysis and its application in characterizing the aggregation state of methyllithium aggregates and complexes with several widely used diamines are presented in this chapter. Commercially available ^{13}C labeled benzene and several easily synthesized ^{13}C labeled compounds using ^{13}C labeled iodomethane as the isotopic source are developed as internal references for diffusion – formula weight analysis (*D-FW*). The technique greatly expands the applicability of DOSY *D-FW* analysis to a much wider variety of compounds because of isotopic labeling. These results reveal that methyllithium exists as a tetrasolvated tetramer in diethyl ether and exclusively as bis-solvated dimers with chelating diamines.

3.2 Introduction

Diffusion-ordered NMR spectroscopy (DOSY) with the application of diffusion coefficient-formula weight (*D-FW*) correlation analysis is an efficient method for determination of formula weights of complexes in solution.¹ We have been developing DOSY NMR with internal references for the determination of formula weights of reactive complexes by *D-FW* correlation analysis.² A linear regression plot of the logarithms of NMR determined relative diffusion coefficients against the known formula weights of added reference compounds allows us to deduce the formula weight of unknown complexes. We have successfully utilized this technique to probe the aggregation state and the solvation state of several organometallic complexes. A major focus of our group

is to expand this *D*-FW DOSY methodology for the structural analysis of alkali metal complexes in solution. Until now, our group has successfully developed internal references for ^{13}C , ^{31}P DOSY and both hydrophilic and hydrophobic references for ^1H DOSY. Moreover, we have also developed physically separated reference systems in order to physically separate the reference and the analyte solutions.³ The internally referenced ^1H DOSY technique is used because of its simplicity and fast acquisition time. However, the technique often suffers from the drawback of overlapping resonances in the chemical shift dimension owing to the relatively narrow frequency range of ^1H NMR. Although ^{31}P DOSY has a very wide chemical shift range and fast acquisition time due to its 100% natural abundance, it is constrained to complexes containing phosphorus atoms. ^{13}C INEPT DOSY with *D*-FW analysis was developed by our group five years ago and proved to be useful in characterizing the aggregation states of an LDA-THF complex and a dimeric chiral lithium amide derived from (*S*)-*N*-isopropyl-*O*-triisopropylsilyl valinol. Although the wide range of the ^{13}C spectrum provides ample separation for the resonances with similar structures, the very low natural abundance (1.1 %) and long relaxation times of ^{13}C nuclei render ^{13}C DOSY with *D*-FW analysis a very long experiment. For example, a sample with reasonably high concentration (1 M) requires at least six hours for the signal acquisition. Such lengthy experiments preclude the analysis of short-lived intermediates. In an attempt to address this problem, the development and use of ^{13}C labeled internal references for *D*-FW analysis is described. The labeled internal references are either commercially available or can be synthesized readily using relatively inexpensive ^{13}C labeled iodomethane. The use of ^{13}C labeled DOSY greatly reduces the experiment time affording the analysis of less concentrated and short-lived

intermediates, which are easily identified in the pool of carbon resonances. Moreover, the cost and labor required to prepare isotopically labeled materials is offset because standard, protonated solvents can be used in place of expensive deuterated solvents such as diethyl ether and *n*-pentane. This is especially beneficial in experiments described herein in which the NMR solvents are also used as the solvent in the reactions to prepare the analytes.

The development and use of ^{13}C labeled DOSY NMR to establish the aggregation state of methyllithium solvated by various diamines by *D-FW* analysis are also discussed. This is significant because organolithium reagents are the most widely used reagents in organic synthesis.⁴ Alkylolithium reagents are typically utilized to generate a wide variety of carbanions such as lithium amides, acetylides and alkoxides. Moreover, the low boiling point alkane formed as a by-product is inert to most of the reactions and easily eliminable. It has become evident that the reactivity and reaction pathways of these alkylolithium reagents are related to their aggregation state⁵ and also to the formation of mixed aggregates⁶. Hence knowledge of the aggregation and solvation state helps optimize the reactivity of these reagents and provides the starting point for development of reaction mechanisms.

Methyllithium is not normally used in hydrocarbon solvents without a coordinating ligand due to its low solubility. In diethyl ether and tetrahydrofuran, it exists as a solvated tetramer in both solution and solid states.⁷ Single crystal x-ray diffraction studies revealed that methyllithium is a tetrameric polymer in the presence of *N,N,N',N'*-tetramethylethylenediamine (TMEDA)⁸ or 1,3,5-trimethyl-1,3,5-triazacyclo-hexane (TMTAC)⁹ in solid state, while it is a dimer in the presence of (-)-sparteine or *N,N,N',N'*-tetramethyl-

1,2-diaminocyclohexane (TMCDA) in solid state.¹⁰ However, there is no evidence that the solution state structure of methyllithium solvated by common diamine ligand is the same as that in solid state. Numerous calculations of possible structures and bonding in methyllithium aggregates were reported.¹¹ Previous NMR studies and spectroscopic studies of methyllithium are also reported.¹² Herein, we demonstrate that methyllithium forms dimeric complexes in diethyl ether solution in the presence of common diamine ligands including TMEDA, TMCDA, (-)-sparteine, 3,7-dimethyl-3,7-diazabicyclo-[3.3.1]nonane (*N,N'*-dimethylbispidine) and *N,N,N',N',N''*-pentamethyldiethylenetriamine (PMDTA). The formation of dimeric structures is corroborated by ¹³C-⁶Li coupling and ¹³C labeled DOSY results.

In this chapter, the design, synthesis and the *D-FW* analysis protocol of the ¹³C labeled internal reference system for DOSY NMR are first presented. Next their utility in characterizing the tetrasolvated tetramer of methyllithium in diethyl ether and in determining bis-solvated, dimeric structures of methyllithium in diethyl ether in the presence of diamines is demonstrated.

3.3 Results and Discussion

3.3.1 Design, synthesis and *D-FW* analysis protocol of the ¹³C labeled internal reference system for DOSY NMR

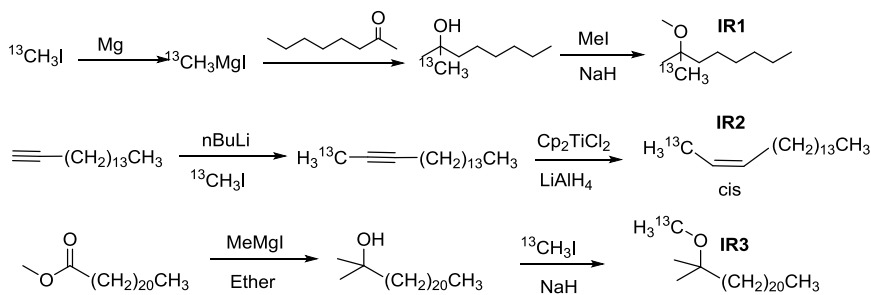
The criteria for internal molecular weight references include lack of either or both reactivity and coordinating ability toward the analyte, easily recognizable resonances, solubility in NMR solvents and desirable formula weight range.² For the isotopically

labeled compounds, internal references must also be easily obtainable from relatively inexpensive labeled sources. In ^1H and regular ^{13}C DOSY, many commercially available aromatic and alkene compounds satisfy these criteria.² However, several of the corresponding reference compounds that we have utilized previously (benzene, cyclooctene, 1-tetradecene and squalene) are not all readily available with ^{13}C isotopic enrichment with the exception of benzene. The syntheses of these ^{13}C labeled compounds require unnecessary effort and are expensive. Therefore, we sought new internal, ^{13}C labeled references that are easily prepared with isotopic enrichment.

Design and Synthesis of ^{13}C labeled Internal References. We chose benzene- $^{13}\text{C}_6$ (BEN) as our first internal reference because it is the cheapest ^{13}C labeled aromatic compound that is inert to our analyte. Additionally a very small quantity is required for each experiment since it has six labeled carbon atoms. Cyclooctene, 1-tetradecene and squalene are not useful because their ^{13}C labeled analogues are not available commercially and ^{13}C labeled, synthetic precursors are expensive. Therefore, we focused on developing three new internal references using ^{13}C labeled iodomethane as the starting material because this material represents a relatively inexpensive ^{13}C atom source. These materials are depicted as **IR1-3** in Scheme 3.1.

Although two different ethers are used in our internal reference system, *i.e.* **IR1** and **IR3**, we determined that they are not competitive in coordinating to methyl lithium aggregates since most of the experiments we performed were conducted in ethereal solvents. The concentration of these ethereal, ^{13}C labeled internal references is many orders of magnitude less than the solvent. Additionally these ethers are sterically hindered. Alternatively a significant amount of a strong chelating ligand such as TMEDA

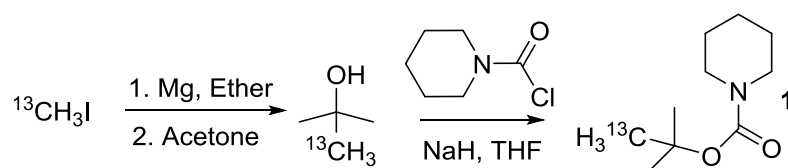
and PMDTA was also present in several experiments. Furthermore, it has been shown that the coordinating power of diethyl ether, THF or common diamine ligands to alkyl lithium reagents is much stronger than methyl *tert*-butyl ether (MTBE).^{2g,13} Since the ethers we used as internal references are even more hindered than MTBE, it is reasonable to assume that they do not coordinate with our complexes significantly in diethyl ether or THF to an observable extent.



Scheme 3.1. Synthesis of ^{13}C labeled internal references

***D-FW* Analysis of the ^{13}C Labeled Internal Reference System.** DOSY NMR separates resonances by their diffusion coefficients as is typically depicted along the vertical axis is a two dimensional plot. Chemical shifts are typically displayed along the horizontal axis. These spectra are presented as typical two-dimensional NMR plots; however, in this experiment only a single Fourier transform in the chemical shift dimension is utilized.¹⁴ We first applied DOSY NMR with internal references for the determination of formula weights of reactive complexes correlation analysis to study *n*-BuLi aggregates without the *D-FW* protocol.¹⁵ Subsequently, we have incorporated *D-FW* analysis into the experiment.^{2c} A linear regression plot of the logarithm of relative diffusion coefficients determined by DOSY NMR against known formula weights of reference standards is used to extrapolate the formula weight of observable complexes.

We use ^{13}C labeled *N*-Boc-piperidine **1** synthesized from piperidine-1-carbonyl chloride and ^{13}C labeled *tert*-butanol (Scheme 3.2) to establish the effectiveness of this ^{13}C labeled, internal reference system.¹⁶ Thus ^{13}C labeled *N*-Boc-piperidine and the ^{13}C labeled internal references depicted in Scheme 3.1 were dissolved in a mixture of diethyl ether and cyclohexane and all ^{13}C labeled atoms are easily discernible and assigned in the ^{13}C DOSY (Figure 3.1). A subsequent the *D*-FW analysis as shown in Figure 3.2 displays a high correlation ($r^2 = 0.985$) and based upon this, the predicted formula weight of labeled *N*-Boc-piperidine is 179.2 g mol^{-1} which is indeed very close to the actual formula weight of 186.3 g mol^{-1} (3.8% difference).



Scheme 3.2. Synthesis of ^{13}C labeled *N*-Boc-piperidine **1**

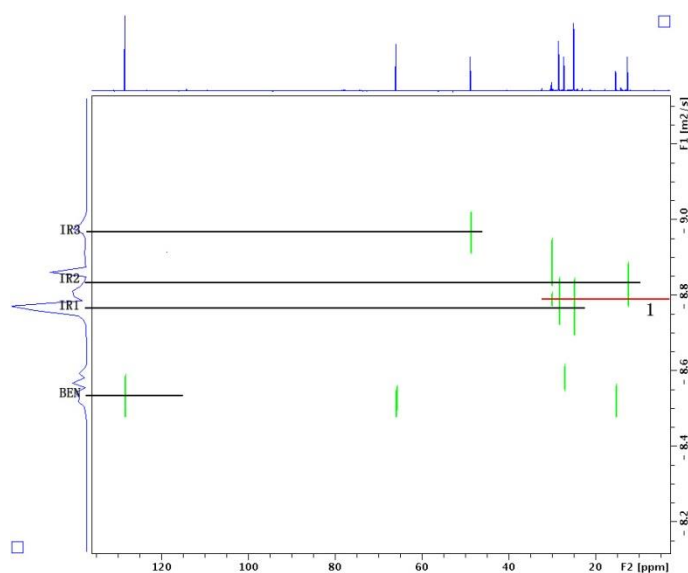


Figure 3.1. ^{13}C DOSY of **BEN**, **IR1**, **IR2**, **IR3** and **1** at $20\text{ }^\circ\text{C}$.

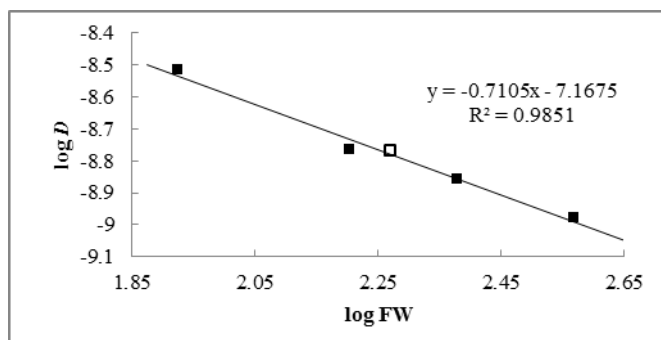


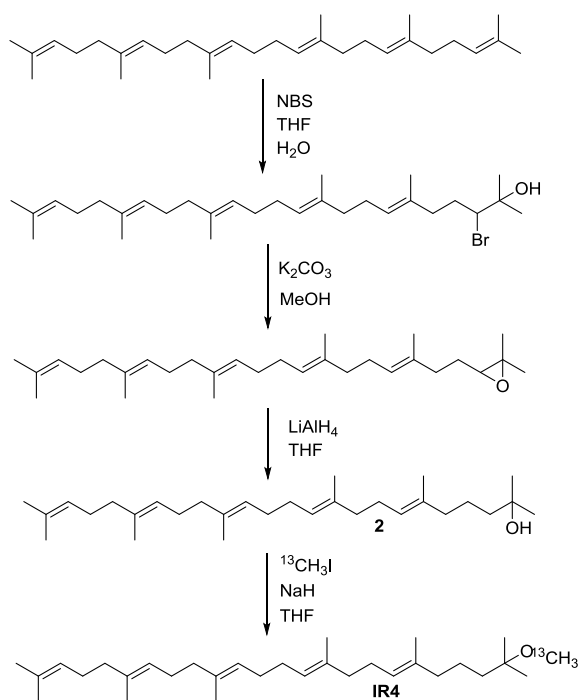
Figure 3.2. *D*-FW analysis of ^{13}C DOSY data. Internal references are shown as solid squares and *N*-Boc-piperidine **1** is shown as open square.

Table 3.1. *D*-FW Analysis of ^{13}C DOSY of **BEN**, **IR1**, **IR2**, **IR3** and **1** at 20 °C

entry	Compd	FW (gmol^{-1})	$10^{-9}D$ (m^2/s)	Predicted FW (gmol^{-1})	% error
1	BEN	84.07	3.050	78.98	6.1
2	IR1	159.3	1.716	177.4	-11.4
3	IR2	239.4	1.383	240.4	-0.4
4	IR3	369.7	1.055	351.9	4.8
5	1	186.3	1.704	179.2	3.8

Modification of the ^{13}C Labeled Internal Reference System. The high correlation ($r^2 = 0.985$) of the internal reference system given in Table 3.1 coupled with the small error in the prediction of formula weight of the ^{13}C labeled internal reference system established for us its validity to predict formula weights using ^{13}C labeled compounds. We note however that internal reference compound **IR3**, which is a solid at room temperature, precipitates easily from diethyl ether when the temperature drops below 0 °C. Since the investigation of organolithium complexes is usually performed significantly below 0 °C, **IR3** was replaced by another internal reference that remains soluble at low temperature. For simple ^1H *D*-FW analysis, we typically utilize squalene as our highest formula weight reference. Hence, in lieu of synthesizing ^{13}C labeled squalene itself, we

can readily modify squalene into the ^{13}C labeled internal reference compound **IR4** depicted in Scheme 3.3. Thus tertiary alcohol **2** is readily prepared from squalene in a few simple steps and yields **IR4** easily upon reaction with ^{13}C labeled iodomethane (Scheme 3.3). Compound **IR4** has a formula weight of 443.8 gmol^{-1} and is a liquid at room temperature. There is no precipitation observed for the diethyl ether solution of **IR4** at $-60\text{ }^{\circ}\text{C}$.



Scheme 3.3. Synthesis of internal reference derived from squalene

D-FW Analysis of the new ^{13}C labeled internal reference system. The analysis and verification experiment described above was repeated utilizing **IR4** as the highest molecular weight standard. The ^{13}C DOSY spectrum is depicted in Figure 3.3. The *D-FW* plot of the internal references also produces an excellent correlation and the *D-FW* analysis yields a predicted formula weight of ^{13}C -*N*-Boc-piperidine **1** as 198.4 gmol^{-1} (Figure 3.4, Table 3.2).

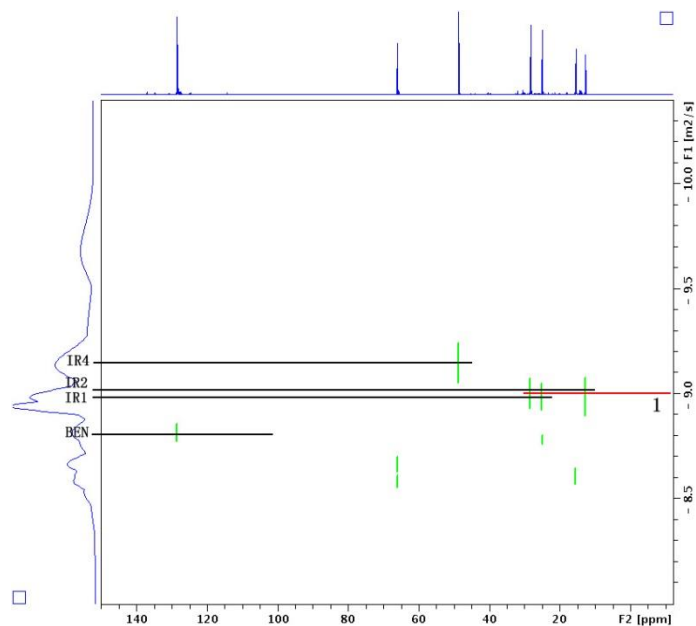


Figure 3.3. ^{13}C DOSY of **BEN**, **IR1**, **IR2**, **IR4** and **1** at 20 °C.

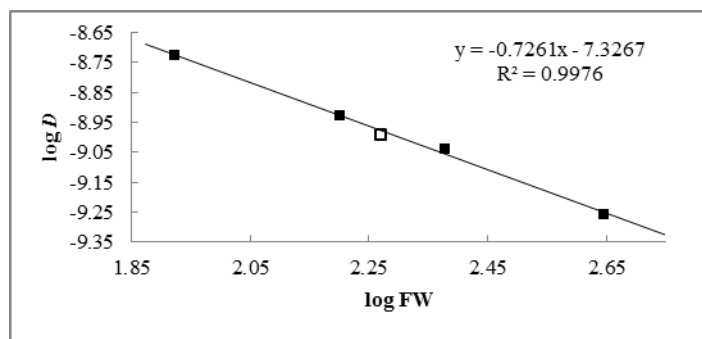


Figure 3.4. *D*-FW analysis of ^{13}C DOSY data. Internal references are shown as solid squares and *N*-Boc-piperidine **1** is shown as open square.

Table 3.2. *D*-FW Analysis of ^{13}C DOSY of **BEN**, **IR1**, **IR2**, **IR4** and **1** at 20 °C

entry	Compd	FW (gmol^{-1})	$10^{-10} D$ (m^2/s)	Predicted FW (gmol^{-1})	% error
1	BEN	84.07	18.69	85.21	-1.4
2	IR1	159.3	11.80	160.5	-0.8
3	IR2	239.4	9.150	227.9	4.8
4	IR4	443.8	5.526	456.4	-2.8
5	1	186.3	10.12	198.4	-6.5

Replacement of **IR3** by **IR4** greatly expands the temperature range for the application of this ^{13}C labeled internal reference DOSY protocol. Therefore, we turned our attention to the use of these ^{13}C labeled internal reference compounds for the DOSY analyses of the methyllithium diamine complexes at $-20\text{ }^{\circ}\text{C}$ to $-40\text{ }^{\circ}\text{C}$. As a caveat we note that since the internal references **IR1**, **IR3** and **IR4** are ethers, this fact cannot be overlooked when they are used for the study of reactive organolithium complexes in pure hydrocarbon solvents in the absence of any additional coordinating ligands or solvents. However, as noted previously, these references are indeed applicable in the investigation of many organolithium compounds and reactions since these reagents and reactions are usually performed in ethereal solvents with the addition of a stoichiometric amount of a strongly coordinating ligand such as a chelating diamine.

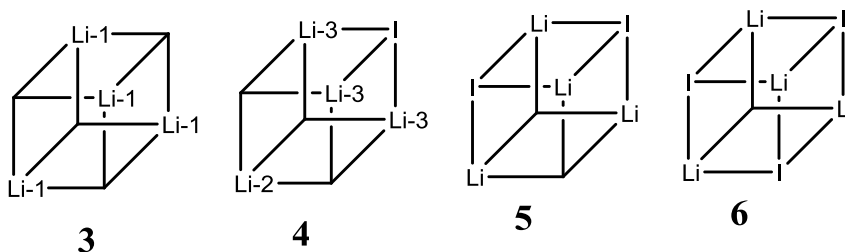
3.3.2 Analysis of methyllithium and methyllithium-tertiary diamine complexes in diethyl ether

To demonstrate the utility of these ^{13}C labeled internal reference materials, we choose to determine the aggregate state of methyllithium (MeLi) dissolved in diethyl ether (DEE) with and without the presence of several tertiary diamine ligands. Hence we describe comprehensive results of DOSY-*D*-FW analysis of the ^{13}C labeled methyllithium in diethyl ether solution.

Characterization of $^{13}\text{CH}_3^6\text{Li-DEE}$ tetramer. Double labeled (^{13}C , ^6Li) methyllithium was prepared using Maddaluno's method except that DEE was used instead of tetrahydrofuran-*d*₈.^{1a} We typically observe approximately 5–10 % lithium iodide present

in the MeLi solution utilizing this procedure.

In 1972, Brown and coworkers demonstrated that MeLi exists as a tetramer $(\text{MeLi})_4$ **3** and as a $(\text{MeLi})_3(\text{LiI})_1$ mixed tetramer **4** in diethyl ether in the presence of lithium iodide (Scheme 3.4).^{5a} Later, Gunther and coworkers reported mixed tetramers **5** and **6** when the mole ratio of LiI to MeLi approaches 1:1.^{5c} Our ^6Li NMR spectrum of the $^{13}\text{CH}_3^6\text{Li}$ -DEE solution at $-30\text{ }^\circ\text{C}$ showed two distinct peaks depicted in Figure 5. Since the mole ratio of LiI to MeLi is far less than 1:1, the presence of tetramer **5** or **6** is not significant. Therefore, we assign the large downfield peak in the ^6Li spectrum to Li-1 in the tetramer **3** and the small upfield peak to Li-3 in the $(\text{MeLi})_3(\text{LiI})_1$ mixed tetramer **4**.^{5a,b} According to Brown and Gunther, Li-2 of tetramer **3** appears as a downfield shoulder of the Li-1 peak at $-70\text{ }^\circ\text{C}$. However, we cannot resolve the shoulder peak at $-40\text{ }^\circ\text{C}$ possibly because of fast intramolecular exchange as mentioned by Brown. The ^{13}C spectrum of $^{13}\text{CH}_3^6\text{Li}$ -DEE solution displays two distinct peaks in the upfield region. The peaks at -12.9 ppm and -13.7 ppm are assigned to the resonances of the methyl group of tetramer **3** and tetramer **4** respectively.



Scheme 3.4. MeLi tetramer **3** and MeLi-LiI mixed tetramer **4**

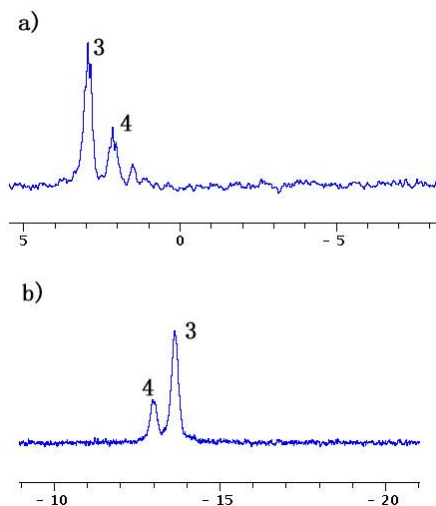


Figure 3.5. NMR spectra of 0.06 M $^{13}\text{CH}_3^6\text{Li}$ DEE solution at $-40\text{ }^\circ\text{C}$. ^6Li spectrum are depicted in (a) and ^{13}C spectrum is depicted in (b).

The ^{13}C DOSY spectrum of this $^{13}\text{CH}_3^6\text{Li}$ DEE solution with added internal references is reproduced in Figure 3.6. The correlation between $\log \text{FW}$ and $\log D$ of the linear regression is very high ($r^2 > 0.99$) and the predicted formula weight for the resonance at -13.7 ppm is 407.8 gmol^{-1} which is very close to the formula weight of the tetrameric $^{13}\text{CH}_3^6\text{Li}$ with each lithium atom coordinated to a single DEE (384.7 gmol^{-1} , -6.0% difference). However, the predicted formula weight for the resonance at -12.9 ppm is 408.8 gmol^{-1} , which represents a 17.5% difference from the calculated formula weight (495.5 gmol^{-1}) of tetra-solvated tetramer **4** (Figure 3.7, Table 3.3). We suggest that the high inaccuracy in the formula weight prediction of tetra-solvated tetramer **4** is very likely due to the presence of highly dense iodine atom in the complex.

We note that an alternative explanation for the formula weight of the tetramer **4** deduced from the D -FW analysis is consistent with a tris-solvated tetramer rather than a tetra solvated tetramer. The formula weight of an unknown complex is deduced from its experimental diffusion coefficient through the linear regression plot of the logarithms of

NMR determined diffusion coefficients against the known formula weights of known reference compounds according to the empirical equation $\log D = A \log FW + C$. The validity of the empirical equation depends on the similarity of the density of internal references and complexes.² From a comparison of the densities of many crystal structures of organolithium complexes, it is apparent that the density of tetramer **4** is very different from the density of tetramer **3** and also from the density of the internal references owing to the incorporation of the iodine atom. Therefore, the predicted formula weight that is deduced from the linear regression plot deviates significantly from the calculated formula weight of tetra-solvated tetramer **4** as we have previously observed in analyzing compounds containing heavy atoms and whose density differs significantly from the reference standards. Our results for the tetramer **3** comport with those of both Brown and Gunther as expected with the enhancement that they permit a determination of the solvation state directly. Furthermore, these results serve to demonstrate a limitation of the D -FW analysis when applied to compounds that differ significantly in density.

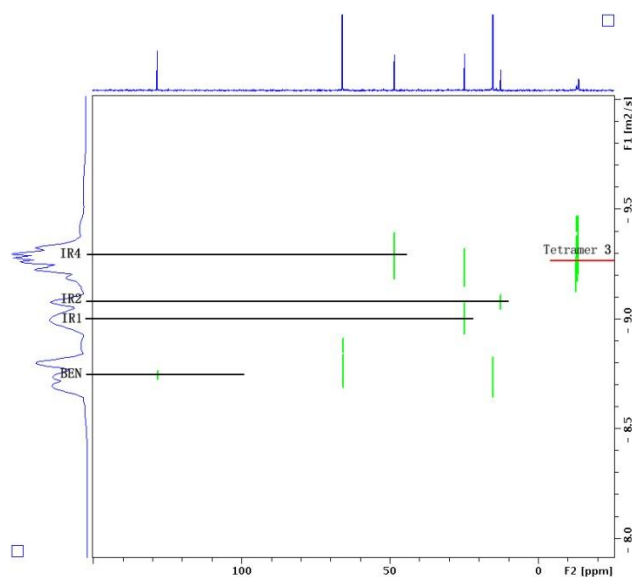


Figure 3.6. ^{13}C DOSY of $^{13}\text{CH}_3$ ^6Li DEE solution at $-40\text{ }^\circ\text{C}$.

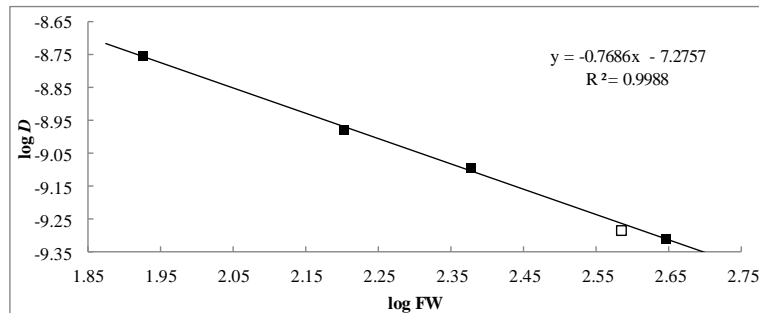


Figure 3.7. *D*-FW analysis of ^{13}C DOSY data. Internal references are shown as black squares and the tetra-solvated tetramer **3** is shown as the white square.

Table 3.3. *D*-FW Analysis of ^{13}C DOSY of **BEN**, **IR1**, **IR2**, **IR4**, **3** and **4** at $-40\text{ }^{\circ}\text{C}$

entry	Compd	FW (gmol^{-1})	$10^{-10} D$ (m^2/s)	Predicted FW (gmol^{-1})	% error
1	BEN	84.07	17.72	83.21	1.0
2	IR1	159.3	10.50	164.4	-3.2
3	IR2	239.4	8.013	233.7	2.4
4	IR4	443.8	4.882	445.2	-0.3
5	3 ^a	384.7 ^a	5.223	407.8	-6.0
6	4 ^b	495.5 ^b	5.213	408.8	17.5

^a384.7 gmol^{-1} is the formula weight of $(^{13}\text{CH}_3^6\text{Li})_4(\text{DEE})_4$ complex.

^b495.5 gmol^{-1} is the formula weight of $(^{13}\text{CH}_3^6\text{Li})_3\text{I}(\text{DEE})_4$ complex.

Characterization of $^{13}\text{CH}_3^6\text{Li}$ complexes with TMEDA, (rac)-TMCDA, *N,N'*-Dimethylbispidine, PMDTA or (-)-Sparteine. For these analyses, samples were prepared by adding the tertiary amines separately to $^{13}\text{CH}_3^6\text{Li}$ DEE solutions at $-40\text{ }^{\circ}\text{C}$ as described. Individual results and interpretation of each separate experiment are provided.

Upon addition of 3 equiv of TMEDA, the two peaks of complexes **3** and **4** disappeared and were replaced by a new peak at -12.7 ppm. The new peak resolved into a quintet with $J = 8.2$ Hz, when the temperature was lowered to $-70\text{ }^{\circ}\text{C}$ (Figure 3.8). As depicted in Figure 3.9, the ^6Li spectrum of $^{13}\text{CH}_3^6\text{Li}$ DEE solution with 3 equiv TMEDA at $-70\text{ }^{\circ}\text{C}$ is a triplet with $J = 8.0$ Hz. Clearly these results suggest the formation of an oligomeric, methyllithium-TMEDA complex. Within this complex, the single carbon of

methyl lithium interacts with two lithium atoms and each lithium atom interacts with two carbon atoms. Although the structure of dimer **7** as depicted in Scheme 3.5 is consistent with the NMR results, it is not the only possible structure because the cyclic trimer **8** and higher order cyclic oligomers are also consistent with these NMR spectra. However, it is noteworthy that these NMR results are inconsistent with the structure of the methyl lithium-TMEDA complex determined by x-ray diffraction analysis by Weiss.⁶ The tetrameric methyl lithium unit observed for the crystal structure would appear as a septet for the ¹³C and a quintet for the ⁶Li spectrum.

To establish the dimeric nature of the MeLi-TMEDA complex, we performed a ¹³C DOSY with ¹³C labeled internal references **IR1**, **IR2** and **IR4**. Isotopic labeling with ¹³C was necessary in this experiment because the natural abundance ¹³C spectrum with non-labeled internal references required a relatively high concentration (> 1.0 M and much precipitation was observed when the DEE solution of 1.0 M MeLi with 3 equiv TMEDA was kept at -40 °C for the time required to complete this experiment, approximately 6-8 hours. Moreover, ¹H DOSY and ¹³C DOSY with regular internal references required the use of expensive DEE-*d*₁₀ as solvent and this became prohibitive on a routine basis.

The ¹³C DOSY spectrum with the isotopically labeled sample is depicted in Figure 3.10. The *D*-FW plot exhibits a reliably high ($r^2 > 0.99$) correlation. The predicted formula weight for the resonance of MeLi-TMEDA complex at -12.7 ppm is 288.6 gmol⁻¹, which represents a 4.4 % difference from the calculated formula weight 276.5 gmol⁻¹ for dimer **7** (Figure 3.11, Table 3.4). However, the calculated formula weight of cyclic trimer **8** is 414.8 gmol⁻¹, a 30.4 % difference from the observed formula weight. Therefore, we

rule out the possibility that the MeLi-TMEDA complex in DEE solution as a cyclic trimer or a higher oligomer.

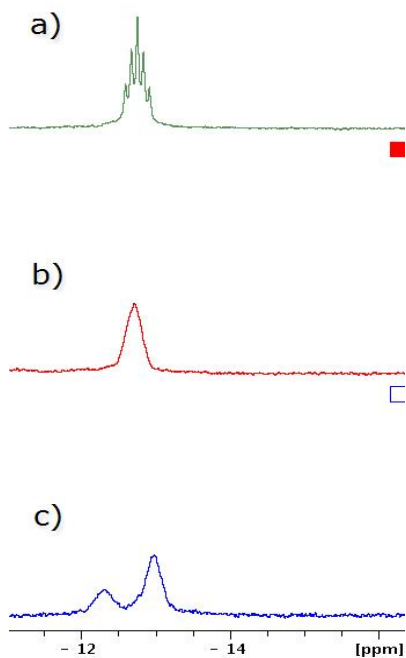


Figure 3.8. ^{13}C spectra of $^{13}\text{CH}_3^6\text{Li}$. (a) represents the ^{13}C spectrum of 0.12 M $^{13}\text{CH}_3^6\text{Li}$ in DEE at -70°C . (b) represents the ^{13}C spectrum of 0.12 M $^{13}\text{CH}_3^6\text{Li}$ in DEE with 3 equiv TMEDA at -40°C . (c) represents the ^{13}C spectrum of 0.12 M $^{13}\text{CH}_3^6\text{Li}$ in DEE with 3 equiv TMEDA at -70°C .

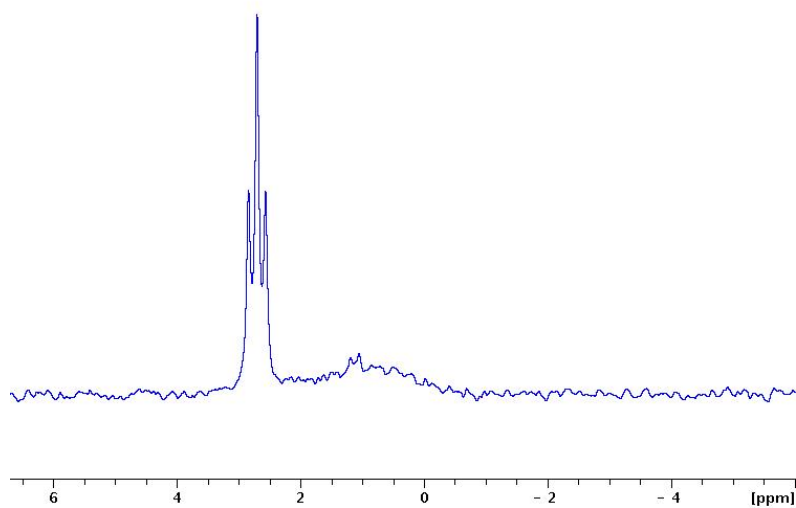
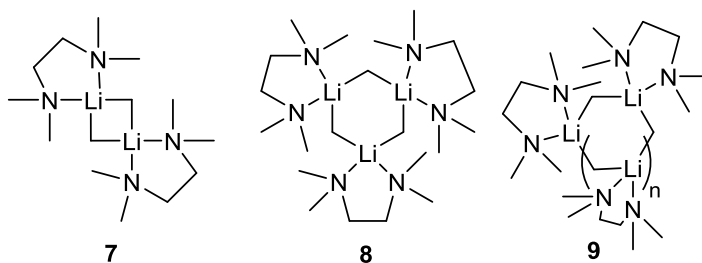


Figure 3.9. ^6Li NMR spectrum of 0.12 M $^{13}\text{CH}_3^6\text{Li}$ DEE solution with 3 equiv TMEDA at -70°C .



Scheme 3.5. MeLi-TMEDA dimer **7**, cyclic trimer **8** and cyclic oligomer **9**

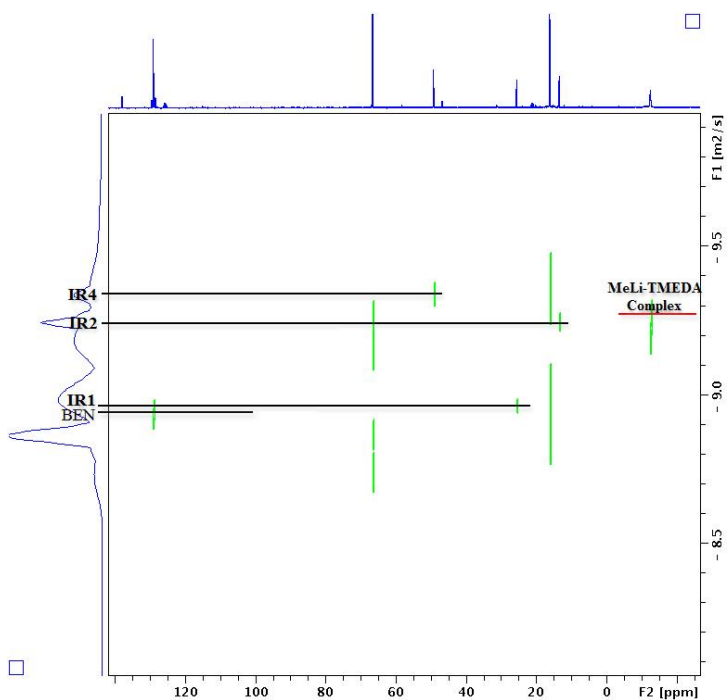


Figure 3.10. ^{13}C DOSY of $^{13}\text{CH}_3^6\text{Li}$ DEE solution with 3 equiv TMEDA at -50°C .

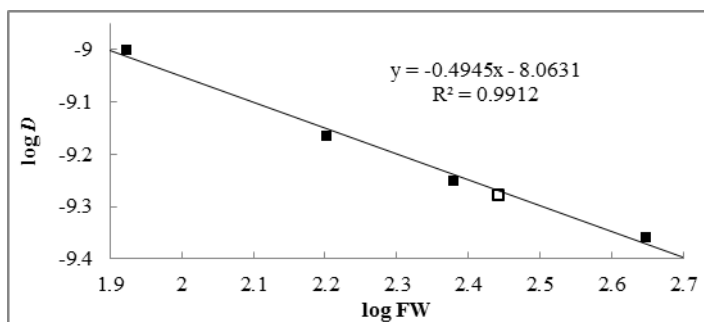


Figure 3.11. D -FW analysis of ^{13}C DOSY data. Internal references are shown as black squares and the MeLi-TMEDA dimer **7** is shown as the white square.

Table 3.4. *D*-FW Analysis of ^{13}C DOSY of **BEN**, **IR1**, **IR2**, **IR4** and **7** at $-50\text{ }^\circ\text{C}$

entry	Compd	FW (g mol^{-1})	$10^{-10} D$ (m^2/s)	Predicted FW (g mol^{-1})	% error
1	BEN	84.07	9.944	79.40	5.6
2	IR1	159.3	6.838	169.3	-6.3
3	IR2	239.4	5.613	233.7	-5.4
4	IR4	443.8	4.367	445.2	5.5
5	7 ^a	276.5 ^a	5.253	288.6	-4.4
6	8 ^b	414.8 ^b	5.253	288.6	30.4

^a276.5 g mol^{-1} is the formula weight of dimer ($^{13}\text{CH}_3^6\text{Li}$)₂(TMEDA)₂ **7**.

^b414.8 g mol^{-1} is the formula weight of trimer ($^{13}\text{CH}_3^6\text{Li}$)₃(TMEDA)₃ **8**.

Racemic TMCDA was added to the $^{13}\text{CH}_3^6\text{Li}$ DEE solution at $-40\text{ }^\circ\text{C}$ to the extent of 2 equiv of TMCDA per MeLi.¹⁷ Upon addition of 0.25 equiv TMCDA, the resonance assigned to the (MeLi)₃(Li)₁ mixed tetramer **4** disappeared and two new peaks emerge at -9.5 and -11.0 ppm. As more TMCDA was added to the sample, the peak at -11.0 ppm increased at the expense of the resonance of tetramer **3**. Meanwhile, the intensity of peak at -9.5 ppm did not change significantly. These results are consistent with the formation of a MeLi-TMCDA complex with a resonance at -11.0 ppm and a (MeLi)_m(Li)_n-TMCDA mixed complex with resonance at -9.5 ppm. The major peak at -11.0 ppm appears as a quintet with $J = 7.7$ Hz whereas we interpret the minor peak at -9.5 ppm as two quintets with $J = 9.8$ Hz overlapping with each other. The major resonance in the ^6Li spectrum of the sample is a triplet with $J = 7.7$ Hz, whereas the minor peak is a doublet with $J = 9.7$ Hz (Figure 3.13). Taken together, these one dimensional NMR results support the formation of homodimer **10** as the resonance at -11.0 ppm and heterodimer **11** as the resonance at -9.5 ppm (Scheme 3.6). Because racemic TMCDA was used in the experiment, two diastereomeric heterodimers **11** can be formed. We suggest that

formation of diastereomers of complex **11** accounts for the appearance of the resonance at -9.5 ppm as two overlapping quintets.

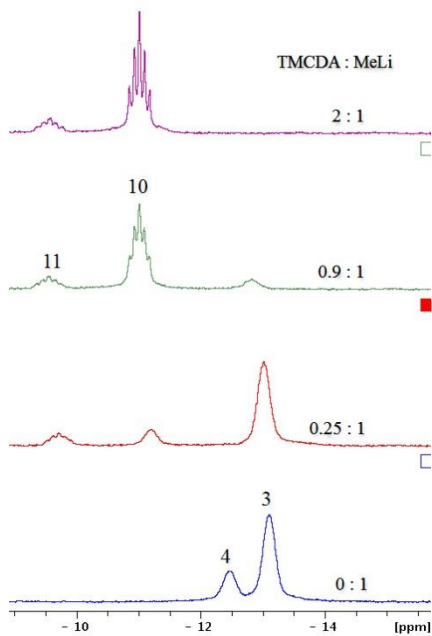
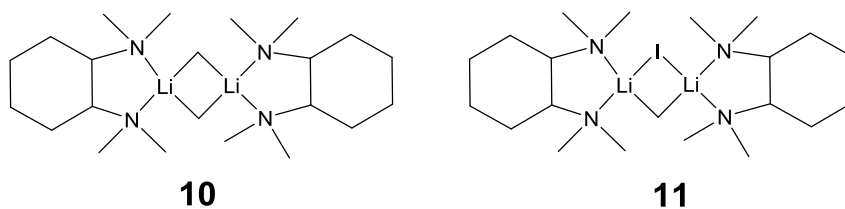
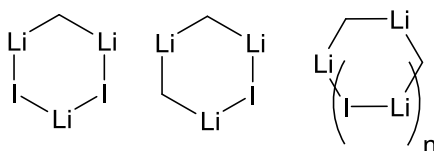


Figure 3.12. ^{13}C NMR spectra of TMCDA titration of 0.15 M $^{13}\text{CH}_3^6\text{Li}$ DEE solution at $-40\text{ }^\circ\text{C}$. 3 represents the resonance of tetramer **3**; 4 represents the resonance tetramer **4**; 10 represents the resonance of dimer **10** and 11 represents the resonance of mixed dimer **11**.



Scheme 3.6. MeLi-TMCDA homodimer **10** and MeLi-LiI-TMCDA heterodimer **11**



Scheme 3.7. MeLi-LiI cyclic trimers and oligomers

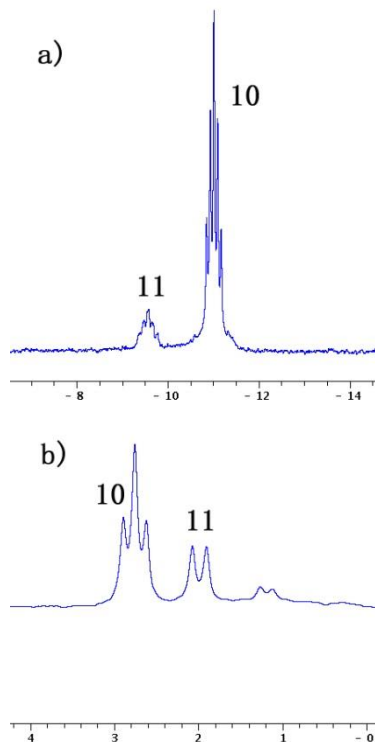


Figure 3.13. NMR spectra of 0.15 M $^{13}\text{CH}_3^6\text{Li}$ DEE solution with 2 equiv TMCDA at $-40\text{ }^\circ\text{C}$. ^{13}C spectrum is depicted in (a) and ^6Li spectrum is depicted in (b).

In analogy to the MeLi-TMEDA complex, these one dimensional NMR results for the MeLi-TMCDA complex are also consistent with a cyclic trimer or higher cyclic oligomer. However, the NMR results of MeLi-LiI-TMCDA mixed complex are not consistent with any mixed cyclic trimer or cyclic oligomer depicted in Scheme 3.7. Thus, we performed ^{13}C DOSY with ^{13}C labeled internal references to establish the dimeric structure of the MeLi-TMCDA complex in DEE. This ^{13}C DOSY spectrum is depicted in Figure 3.14. The extrapolated formula weight for the resonance at -11.0 ppm is 359.3 gmol^{-1} , a 6.6 % difference from the calculated formula weight 384.7 gmol^{-1} for the dimer **10** (Figure 3.15, Table 3.5). This experiment establishes that the major species in the sample is the MeLi-TMCDA dimer **10**, which represents the same motif as the crystal structure obtained by Strohmann.⁸ The low intensity of the minor peak prevented us from conducting a *D-FW*

analysis because we were unable to obtain a reasonable attenuation in the DOSY experiment.

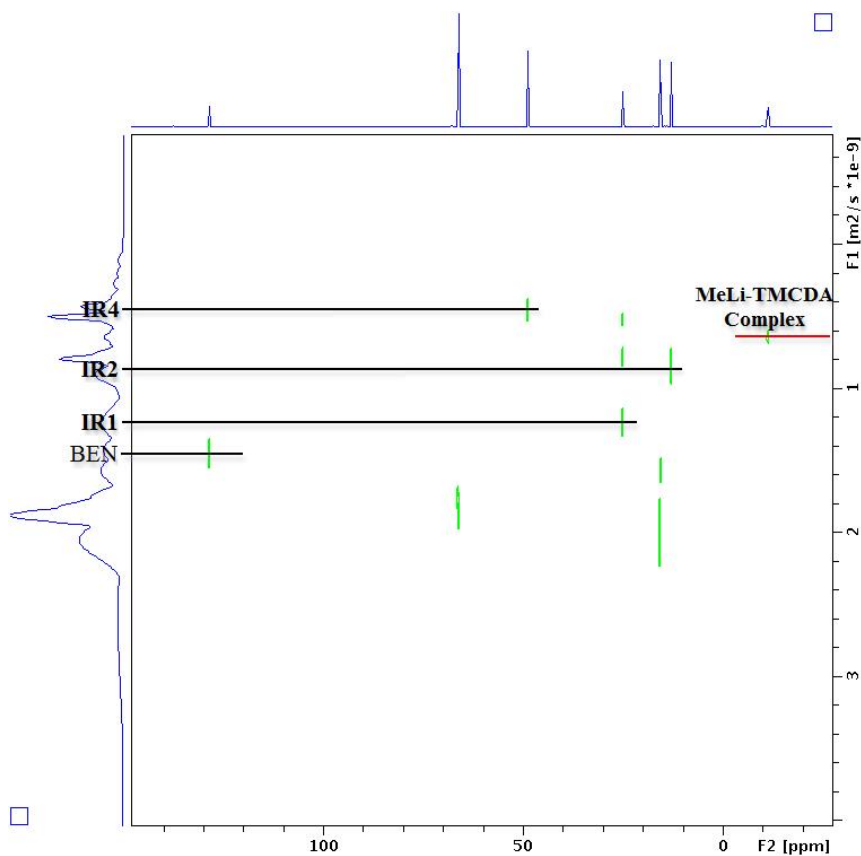


Figure 3.14. ^{13}C DOSY of $^{13}\text{CH}_3^6\text{Li}$ DEE solution with 2 equiv TMCDA at $-40\text{ }^\circ\text{C}$.

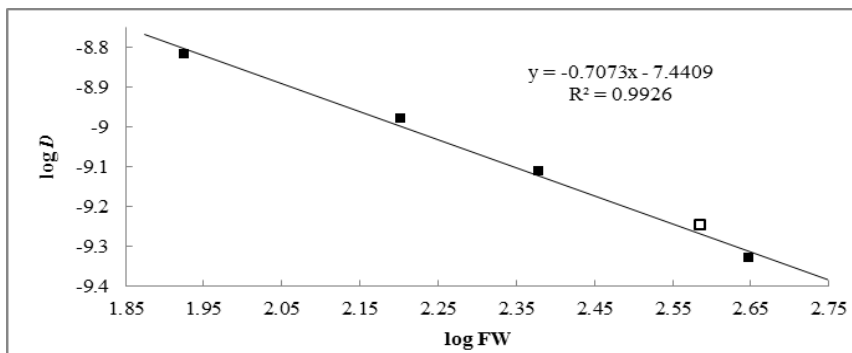


Figure 3.15. D -FW analysis of ^{13}C DOSY data. Internal references are shown as black squares and the MeLi-TMCDA dimer **10** is shown as the white square.

Table 3.5. *D-FW* Analysis of ^{13}C DOSY of **BEN**, **IR1**, **IR2**, **IR4** and **10** at $-40\text{ }^{\circ}\text{C}$

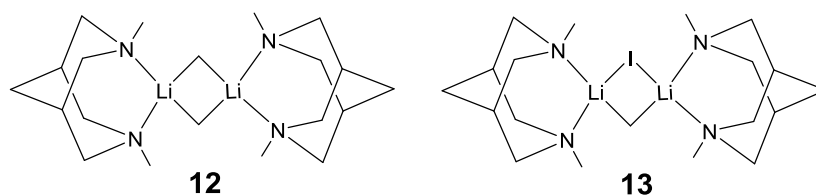
entry	Compound	FW (g mol^{-1})	$10^{-10} D$ (m^2/s)	Predicted FW (g mol^{-1})	% error
1	BEN	84.07	15.18	88.70	-5.5
2	IR1	159.3	10.48	169.3	6.0
3	IR2	239.4	7.747	233.7	4.1
4	IR4	443.8	4.691	445.2	-5.1
5	10^a	384.7 ^a	5.643	359.3	6.6

^a384.7 g mol^{-1} is the formula weight of dimer ($^{13}\text{CH}_3^6\text{Li}$)₂(TMCD A)₂ **10**.

A sample was prepared by addition of 2 equiv *N, N'*-dimethylbispidine (DMB) to a $^{13}\text{CH}_3^6\text{Li}$ DEE solution at $-40\text{ }^{\circ}\text{C}$. Two quintets appeared in the upfield region of the ^{13}C spectrum after the addition of *N, N'*-dimethylbispidine (Figure 3.16a). The major peak at -14.0 ppm with $J = 8.3\text{ Hz}$ is assigned as the methyllithium carbon of complex **12** whereas the minor peak at -12.3 ppm with $J = 10.1\text{ Hz}$ is assigned as the methyllithium carbon of complex **13** (Scheme 3.8). The assignment of the carbon signals is supported by the ^6Li NMR which consist of a major triplet ($J = 8.2\text{ Hz}$) and a minor doublet ($J = 10.1\text{ Hz}$), see Figure 3.16b. Obviously, the ^6Li doublet is coupled to the ^{13}C quintet at -12.3 ppm while the ^6Li triplet is coupled to the ^{13}C quintet at -14.0 ppm . The splitting and coupling constants support our assignment as complexes **12** and **13** respectively. It is noteworthy that a significant peak emerged at -4.1 ppm after the addition of DMB. We believe that this new peak corresponds to the ^{13}C labeled methane from the reaction between methyllithium and the water introduced with DMB. Moreover, there is also a sharp peak located downfield of the resonances of complex **12** and **13** in the ^6Li spectrum which is likely to be the corresponding resonance of lithium hydroxide.

^{13}C DOSY *D-FW* analysis with the ^{13}C labeled internal references verified the assignment as a dimer. The extrapolated formula weight for the resonance at -14.0 ppm is 361.3 g mol^{-1} differs from the calculated formula weight 352.6 g mol^{-1} of the homodimer

12 by 2.5%, see Figure 3.17 and Table 3.6. However, the extrapolated formula weight of the peak at -12.3 ppm is 309.7 g mol^{-1} , a 33.2 % difference from the calculated formula weight 463.5 g mol^{-1} of heterodimer **13**. Similar to the tetramer **4**, heterodimer **13** contains an iodine atom that makes the density of the complex differ significantly from the internal references. Therefore, the extrapolated formula weight differs significantly from the calculated one. Notwithstanding the major discrepancy in the *D-FW* analysis of **13**, it is evident that homodimer **12** is formed and is the major species upon addition of DMB into the MeLi DEE solution.



Scheme 3.8. MeLi-DMB homodimer **12** and MeLi-LiI-DMB heterodimer **13**

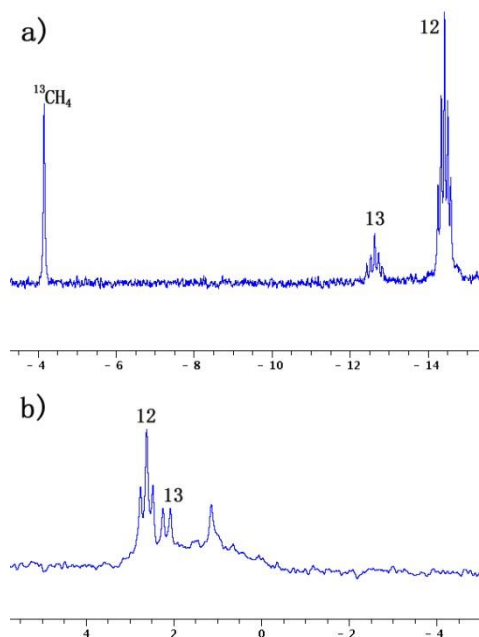


Figure 3.16. NMR spectra of 0.09 M $^{13}\text{CH}_3^6\text{Li}$ DEE solution with 2 equiv DMB at $-40\text{ }^\circ\text{C}$. ^{13}C spectrum is depicted in (a) and ^6Li spectrum is depicted in (b).

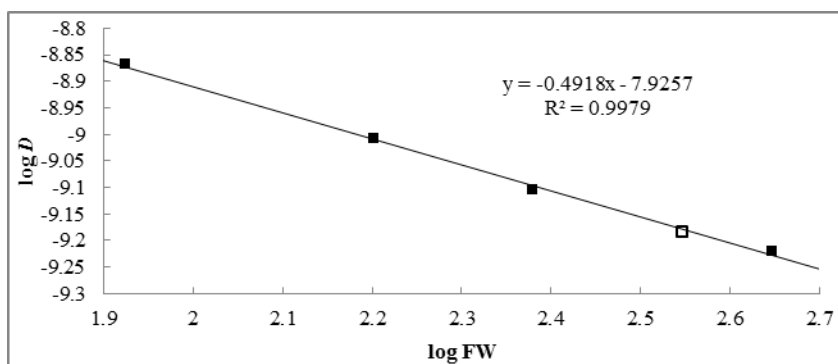


Figure 3.17. *D*-FW analysis of ^{13}C DOSY data. Internal references are shown as black squares and the MeLi-DMB dimer **12** is shown as the white square.

Table 3.6. *D*-FW Analysis of ^{13}C DOSY of **BEN**, **IR1**, **IR2**, **IR4**, **12** and **13** at $-40\text{ }^\circ\text{C}$

entry	Compd	FW (g mol^{-1})	$10^{-10} D$ (m^2/s)	Predicted FW (g mol^{-1})	% error
1	BEN	84.07	13.52	82.81	1.5
2	IR1	159.3	9.815	158.8	0.3
3	IR2	239.4	7.842	250.6	-4.7
4	IR4	443.8	6.002	431.7	2.7
5	12 ^a	352.6 ^a	6.551	361.3	-2.5
6	13 ^b	463.5 ^b	7.067	309.7	33.2

^a352.6 g mol^{-1} is the formula weight of homodimer ($^{13}\text{CH}_3^6\text{Li}$)₂(DMB)₂ **12**. ^b463.5 g mol^{-1} is the formula weight of heterodimer ($^{13}\text{CH}_3^6\text{Li}$)I(DMB)₂ **13**.

A sample was prepared by adding 2 equiv PMDTA into a $^{13}\text{CH}_3^6\text{Li}$ DEE solution at $-40\text{ }^\circ\text{C}$ followed by cooling to $-70\text{ }^\circ\text{C}$ which resolved the splitting of ^{13}C resonances coupled with ^6Li . As depicted in Figure 3.18, the carbon spectrum of this sample is a quintet at -11.6 ppm ($J = 8.1\text{ Hz}$) and a small broad peak at -8.8 ppm . The major peak in the ^6Li spectrum is a triplet ($J = 7.9\text{ Hz}$) and the minor is a small broad peak at $-70\text{ }^\circ\text{C}$. These results are consistent with the formation of homodimer **14a** or **14b** depicted in Scheme 3.9. However, we are not able to differentiate between **14a** and **14b**. In light of the results of MeLi-LiI-diamine complexes previously described, it is not unreasonable to assign the minor resonance as the MeLi-LiI-PMDTA heterodimer; however, there is no

definitive evidence to support this assignment. The ^{13}C DOSY *D*-FW formula weight derived from the resonance at -11.6 ppm is 377.5 gmol^{-1} and differs by 3.4 % from the calculated formula weight 390.7 gmol^{-1} of the homodimer **14**, see Figure 3.19 and Table 3.7.

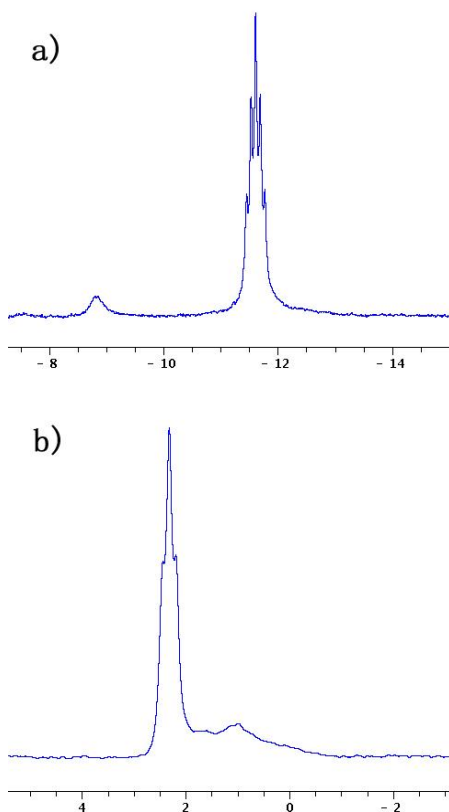
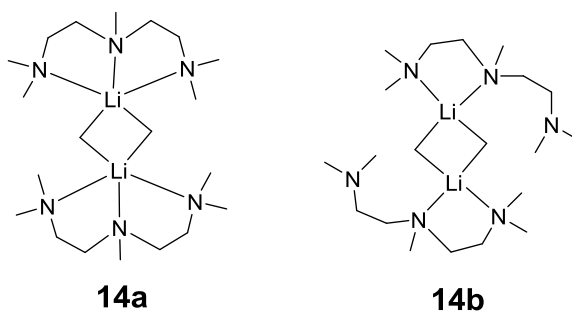


Figure 3.18. NMR spectra of 0.21 M $^{13}\text{CH}_3^6\text{Li}$ DEE solution with 2 equiv PMDTA at $-70\text{ }^\circ\text{C}$. ^{13}C spectrum is depicted in (a) and ^6Li spectrum is depicted in (b).



Scheme 3.9. MeLi-PMDTA homodimers **14a** and **14b**

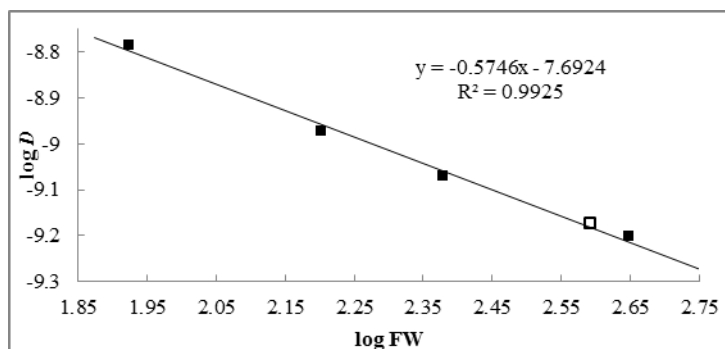


Figure 3.19. *D*-FW analysis of ^{13}C DOSY data. Internal references are shown as black squares and the MeLi-PMDTA dimer **14** is shown as the white square.

Table 3.7. *D*-FW Analysis of ^{13}C DOSY of **BEN**, **IR1**, **IR2**, **IR4**, **14** at $-40\text{ }^\circ\text{C}$

entry	Compd	FW (g mol^{-1})	$10^{-10} D$ (m^2/s)	Predicted FW (g mol^{-1})	% error
1	BEN	84.07	16.41	79.66	5.2
2	IR1	159.3	10.64	169.3	-6.3
3	IR2	239.4	8.503	250.1	-4.5
4	IR4	443.8	6.298	421.7	5.0
5	14^a	390.7 ^a	6.712	377.5	3.4

^a390.7 g mol^{-1} is the formula weight of homodimer $(^{13}\text{CH}_3^6\text{Li})_2(\text{PMDTA})_2$ **14a** or **14b**.

The (-)-sparteine complex was prepared by adding 3 equiv (-)-sparteine into a $^{13}\text{CH}_3^6\text{Li}$ DEE solution at $-40\text{ }^\circ\text{C}$. After the addition of sparteine, the resonances of tetramers **3** and **4** disappeared and a new quintet ($J = 8.1\text{ Hz}$) appeared at -8.1 ppm as depicted in Figure 3.20. A small broad peak next to the quintet is present in this ^{13}C spectrum. The ^6Li spectrum consists of a major triplet ($J = 8.4\text{ Hz}$) and some minor peaks that were not characterized. Strohmann and coworkers characterized the crystal structure of a homodimer of MeLi and (-)-sparteine.⁹ Our NMR spectra are consistent with the same homodimer **15**, see Scheme 3.10. We suggest that the small broad peak at -7.2 ppm

is the resonance of the methyl lithium in the MeLi-LiI heterodimer **16**, although we have no clear evidence for this. The formula weight for the resonance at -8.1 ppm determined by ^{13}C DOSY *D*-FW analysis is 462.9 gmol^{-1} , a 9.7 % difference from the calculated formula weight 512.9 gmol^{-1} of the homodimer **15**, see Figure 3.21 and Table 3.8. Therefore, we conclude that the structure of the MeLi-sparteine in solution is the same as the solid-state structure.

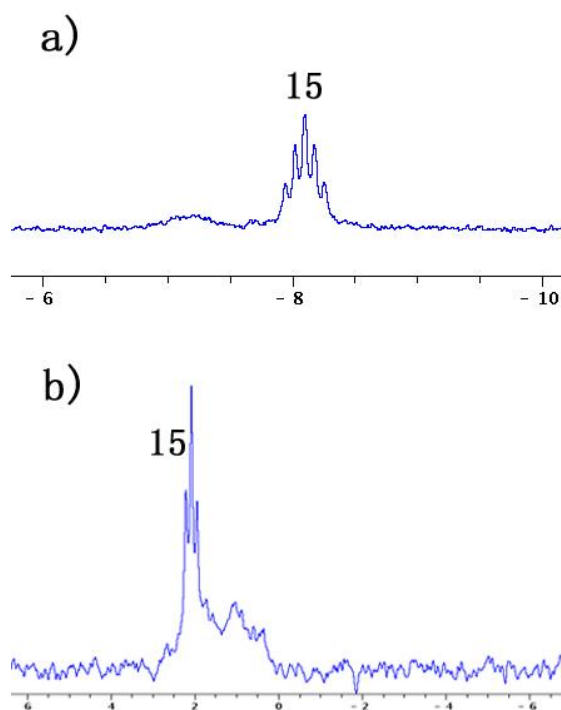
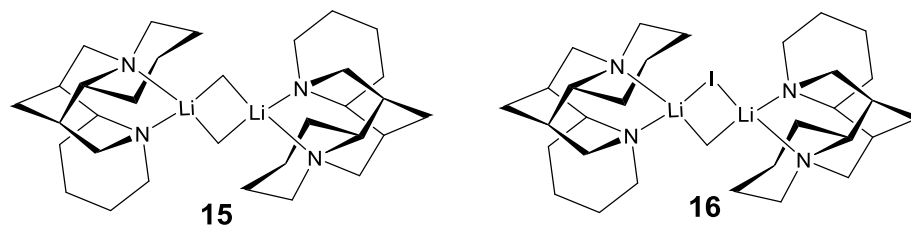


Figure 3.20. NMR spectra of 0.08 M $^{13}\text{CH}_3^6\text{Li}$ DEE solution with 3 equiv (-)-sparteine at $-40\text{ }^\circ\text{C}$. ^{13}C spectrum is depicted in (a) and ^6Li spectrum is depicted in (b).



Scheme 3.10. MeLi-SP homodimers **15** and MeLi-LiI-SP heterodimer **16**

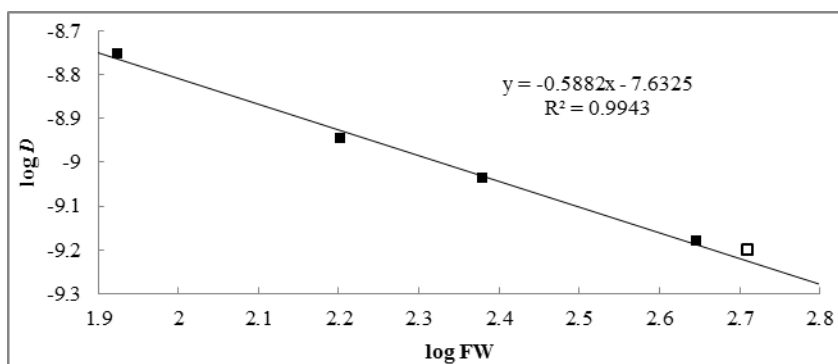


Figure 3.21. *D*-FW analysis of ^{13}C DOSY data. Internal references are shown as black squares and the MeLi-SP dimer **15** is shown as the white square.

Table 3.8. *D*-FW Analysis of ^{13}C DOSY of **BEN**, **IR1**, **IR2**, **IR4**, **15** at $-40\text{ }^\circ\text{C}$

entry	Compd	FW (g mol^{-1})	$10^{-10} D$ (m^2/s)	Predicted FW (g mol^{-1})	% error
1	BEN	84.07	17.69	80.14	4.7
2	IR1	159.3	11.35	170.4	-7.0
3	IR2	239.4	9.202	243.5	-1.7
4	IR4	443.8	6.605	427.9	3.6
5	15 ^a	512.9 ^a	6.306	462.9	9.7

^a512.9 g mol^{-1} is the formula weight of homodimer ($^{13}\text{CH}_3^6\text{Li}$)₂(SP)₂ **15**.

3.4 Conclusion

The successful development of ^{13}C labeled internal reference correlated DOSY with *D*-FW analysis is a significant step forward for the DOSY *D*-FW analysis, because it extends the applicability of the technique for the study of reactive intermediates or sensitive complexes. It is especially important when ^1H DOSY cannot be used owing to the overlap of resonances in the ^1H spectra. Isotopically enriched ^{13}C internal referenced DOSY is clearly preferable to natural abundance ^{13}C internal referenced DOSY because samples with relatively low concentration ($< 1\text{ M}$) and compounds that decompose in the

time required for natural abundance ^{13}C spectra can be analyzed. Moreover, analysis of the ^{13}C spectrum is considerably simplified because the isotopically enriched ^{13}C labeled compounds are readily identified and assigned effortlessly. Furthermore, the use of ^{13}C labeled internal reference DOSY is strongly preferable because the solvents used in the preparation of the sample are normal protonated solvents instead of expensive deuterated solvents such as diethyl ether- d_{10} and methylcyclopentane- d_{12} .

The solution structures of methyllithium complexes with various common tertiary diamines were characterized by utilizing ^{13}C - ^6Li double labeled methyllithium, as well as the ^{13}C labeled internal reference DOSY with D -FW analysis. These NMR results prove that the methyllithium - diamine complexes are homodimeric in solution. Furthermore, evidence was also obtained for the presence of minor amounts of mixed dimeric complexes consisting of one equivalent of MeLi and one equivalent of LiI with the N,N,N',N' -tetramethyl-1,2-diaminocyclohexane and N,N' -dimethylbispidine samples. These results not only demonstrate the validity of the newly formulated ^{13}C labeled internal reference DOSY, but also further our knowledge of the methyllithium - diamine complexes in solution state. These results are important to the interpretation of the mechanism and reactivity of methyllithium.

3.5 Experimental Section

3.5.1 Procedure for NMR Experiments. NMR samples of methyllithium complexes were prepared in tubes sealed with rubber septa and parafilm. NMR tubes were evacuated, flame-dried and filled with argon before use. ^1H chemical shifts were

referenced to toluene- d_8 at 7.09 ppm, and ^{13}C chemical shifts were referenced to toluene- d_8 at 137.86 ppm. For the NMR spectra of pure internal references and ^{13}C labeled *N*-Boc-piperidine, ^1H chemical shifts were referenced to the chloroform peak at 7.27 ppm in the ^1H spectrum and the peak at 77.0 ppm in the ^{13}C spectrum or alternatively to the benzene peak at 7.16 ppm, and the benzene- d_6 peak at 128.36 ppm. All NMR experiments were acquired on a 400 MHz spectrometer equipped with a z-axis gradient amplifier and an ATMA BBO probe with a z-axis gradient coil. Maximum gradient strength was 0.214 T/m. ^1H -DOSY was performed using the standard `dstebpgp3s` program, employing a double stimulated echo sequence, bipolar gradient pulses for diffusion, and 3 spoil gradients. Diffusion time was 200 ms, and the rectangular gradient pulse duration was 600-800 μs . Gradient recovery delays were 200 μs . Individual rows of the quasi-2-D diffusion databases were phased and baseline corrected. Actual diffusion coefficients used for *D*-FW analysis were obtained with commercial software using the T1/T2 analysis module.

The ^{13}C labeled internal references were first mixed in a ratio of 1:6:6:6 for BEN, **IR1**, **IR2**, and **IR4** respectively (a ratio of 1:6:6:6 for BEN, **IR1**, **IR2**, and **IR3** respectively). The mixed internal references were titrated into the NMR tube and monitored by ^{13}C NMR. The titration was stopped when the peak intensity of benzene was about a half of the major methyllithium carbon peak.

3.5.2 Preparation of *n*-Bu ^6Li solution. The *n*-Bu ^6Li solution was prepared in heptane according to the method that we've previously employed.^{2j}

3.5.3 Preparation of double labeled (^{13}C , ^6Li) methyllithium DEE solution. The double labeled (^{13}C , ^6Li) methyllithium was prepared according to Maddaluno.^{1a} A

solution of 1 equiv *n*-Bu⁶Li was added dropwise to 60 μL ¹³CH₃I dissolved in 1.5 mL pentane at -78 °C in a centrifugation tube. The solution was then stirred at -30 °C until white precipitates formed. After that, the mixture was stirred at 0 °C for 20 minutes before centrifuging for 15 minutes, followed by removal of the solvent with a syringe. The solid residue was placed under vacuum for 30 minutes, followed by the addition of 2.5 mL of diethyl ether yielding a 0.1 M – 0.2 M methyllithium solution. The mixture was transferred to an NMR tube via a syringe with the intervention of a PTFE filtration owing to the presence of a small amount of white solid precipitate in the solution. An additional 0.05 mL toluene-*d*₈ was added to the NMR samples to facilitate deuterium locking.

3.5.4 Preparation of tertiary diamines. TMEDA, PMDTA and (-)-sparteine are commercially available. Racemic TMCDA was prepared according to Collum's method.^{9b} *N,N'*-dimethylbispidine was prepared according to Zones¹⁸ by reaction of *N*-methyl-4-piperidone with a mixture of acetic acid, paraformaldehyde and methylamine hydrochloride. The resulting oil was then reduced to *N,N'*-dimethylbispidine by Wolff-Kischner reduction.

3.5.5 Synthesis of 2-methoxy-2-methyloctane-1-¹³C IR1. Step 1: To a flame-dried two-neck round bottom flask fitted with a condenser under argon atmosphere was placed 0.16 g magnesium (6.6 mmol, 1.4 equiv) and then 8 mL anhydrous diethyl ether was added with stirring. A solution of 0.836 g ¹³CH₃I (5.85 mmol, 1.25 equiv) dissolved in 5 mL diethyl ether was added dropwise to the magnesium DEE mixture using a syringe pump at room temperature. After the addition, the grey mixture was allowed to stir for 30 minutes at room temperature before transferring to a flame-dried 50 mL round bottom

flask flushed with argon and cooled to 0 °C. A solution of 0.60 g 2-octanone (4.68 mmol, 1 equiv) in 5 mL anhydrous DEE was slowly added to the grey methylmagnesium iodide solution using a syringe pump at 0 °C. After that, the reaction mixture was allowed to stir at room temperature overnight before quenching with 5 mL 0.5 M HCl. The mixture was extracted with 20 mL Et₂O three times and the combined organic phase was washed by 10 mL brine and dried over anhydrous Na₂SO₄. The solvent was then removed by rotary evaporation. The resulting 2-methyloctan-2-ol-1-¹³C was used in the next step without further purification.

Step 2: Into a flame-dried flask was placed 0.75 g 60 % sodium hydride (18.7 mmol, 4 equiv) in mineral oils under argon atmosphere. The solid was washed by 5 mL dry pentane three times before adding 12 mL anhydrous THF and 2-methyloctan-2-ol-1-¹³C obtained in the previous step. The resulting solution was then refluxed for 1 hour before adding 1.00 g iodomethane (7.05 mmol, 1.5 equiv). This reaction mixture was then refluxed overnight and quenched with 5 mL saturated ammonium chloride at 0 °C. The mixture was extracted with 20 mL pentane three times and the combined organic phase was washed by 10 mL brine and dried over anhydrous Na₂SO₄. The solvent was then removed by rotary evaporation. The residue was purified chromatographically on a flash column with 150 mL pentane. After the removal of solvent, 0.47 g **IR1** (2.95 mmol, 63 %) was obtained as colorless oil. ¹H NMR (CDCl₃, 400 MHz) δ 3.18 (s, 3H), 1.49-1.39 (m, 2H), 1.36-1.19 (m, 9.5H), 0.98 (s, 1.5H), 0.89 (t, 3H, *J* = 6.9 Hz); ¹³C NMR (CDCl₃, 100 MHz) δ 74.8, 74.4, 49.0, 39.8, 31.9, 29.9, 25.0, 23.8, 22.7, 14.1; MS *m/z* 158 [M-H]⁻, 144, 86, 74, 69, 56, 45.

3.5.6 Synthesis of (Z)-heptadec-2-ene-1-¹³C IR2. Step 1: A solution of 1.2 equiv *n*-BuLi was added slowly to a solution of 0.55 g 1-hexadecyne (2.5 mmol, 1 equiv) dissolved in 20 mL anhydrous THF in a flame-dried bottom flask under argon atmosphere and cooled to -78 °C. After 5 minutes, the reaction mixture was warmed up to room temperature and stirred for 30 minutes. The resulting solution was placed in an ice bath and 0.53 g ¹³CH₃I (3.7 mmol, 1.5 equiv) was added all at once. The resulting solution was stirred at room temperature for 2 hours before quenching with 5 mL of saturated ammonium chloride. The mixture was extracted with 20 mL hexanes three times and the combined organic phase was washed by 10 mL brine and dried over anhydrous Na₂SO₄. The solvent was then removed by rotary evaporation. The resulting heptadec-2-yne-1-¹³C was used in the next step without further purification.

Step 2: The heptadec-2-yne-1-¹³C was reduced to (Z)-heptadec-2-ene-1-¹³C by Ashby's method.¹⁹ To a solution of 0.060 g titanocene dichloride (0.24 mmol, 0.1 equiv) dissolved in 12 mL THF in a flame-dried flask under argon atmosphere was added the resulting heptadec-2-yne-1-¹³C at room temperature. The resulting solution was allowed to stir for 20 minutes before cooling down to 0 °C. After that, 0.19 g lithium aluminum hydride (5.0 mmol, 2 equiv) mixed with 2 mL anhydrous THF was added slowly to the reaction mixture. The resulting mixture was allowed to stir at room temperature overnight before cooling back to 0 °C. The reaction was then quenched by adding 1 mL water and then 4 mL 0.5 M HCl. The mixture was extracted with 20 mL hexanes three times and the combined organic phase was washed by 10 mL brine and dried over anhydrous Na₂SO₄. The solvent was then removed by rotary evaporation. The residue was purified by a flash column with 150 mL hexanes. After the removal of solvent, 0.49 g **IR2** (2.1 mmol, 83 %)

was obtained as colorless oil. ^1H NMR (CDCl_3 , 400 MHz) δ 5.50-5.32 (m, 2H), 2.09-2.00 (m, 2H), 1.63 (dd, 3H, $J = 125, 6.2$ Hz), 1.36-1.17 (m, 24H), 0.91 (t, 3H, $J = 7.0$ Hz); ^{13}C NMR (CDCl_3 , 100 MHz) δ 130.9, 123.7, 123.4, 31.9, 29.7, 29.7, 29.6, 29.4, 29.3, 22.7, 21.1, 17.9, 14.4, 14.1, 13.8, 13.6, 12.7; HRMS-EI m/z : $[\text{M}]^+$ Calcd for $\text{C}_{16}^{13}\text{CH}_{34}$: 239.2689, found: 239.2682.

3.5.7 Synthesis of 2-(methoxy- ^{13}C)-2-methyltricosane IR3. Step 1: To a flame-dried two-neck round bottom flask fitted with a condenser under argon atmosphere was placed 0.41 g magnesium (17 mmol) and then 25 mL anhydrous diethyl ether was added and stirring initiated. A solution of 2.00 g iodomethane (14 mmol) dissolving in 10 mL diethyl ether was added dropwise to the magnesium DEE mixture at room temperature using a syringe pump. After the addition, the grey mixture was allowed to stir for 30 minutes at room temperature before transferring to a flame-dried round bottom flask flushed with argon at 0 °C. A solution of 1.75 g methyl behenate (4.93 mmol) dissolved in 10 mL DEE was slowly added to the grey methylmagnesium iodide solution using a syringe pump at 0 °C. After that, the reaction mixture was allowed to stir at room temperature overnight before quenching with 15 mL 0.5 M HCl. The mixture was extracted with 40 mL Et_2O three times and the combined organic phase was washed by 30 mL brine and dried over anhydrous Na_2SO_4 . The solvent was then removed by rotary evaporation. The resulting solid was recrystallized in ethyl acetate to yield 2-methyltricosan-2-ol.

Step 2: Into a flame-dried flask was placed 0.23 g 60 % sodium hydride (5.7 mmol, 4 equiv) in mineral oils under argon atmosphere. The solid was washed by 2.5 mL dry pentane three times before adding 10 mL anhydrous THF and 0.50 g solid 2-

methyltricosan-2-ol (1.4 mmol, 1 equiv). The resulting solution was refluxed for 4 hours before adding 0.30 g $^{13}\text{CH}_3\text{I}$ (2.1 mmol, 1.5 equiv). The resulting solution was then refluxed overnight before quenching with 5 mL saturated ammonium chloride at 0 °C. The mixture was extracted with 30 mL hexanes three times and the combined organic phase was washed by 20 mL brine and dried over anhydrous Na_2SO_4 . The solvent was removed by rotary evaporation. The residue was purified chromatographically on a flash column with 150 mL hexanes. After the removal of solvent, 0.45 g **IR3** (1.2 mmol, 86 %) was obtained as white solid. ^1H NMR (Benzene- d_6 , 400 MHz) δ 3.06 (d, 3H, $J = 139$ Hz), 1.46-1.39 (m, 4H), 1.39-1.23 (m, 36H), 1.09 (s, 6H), 0.92 (t, 3H, $J = 6.5$ Hz); ^{13}C NMR (Benzene- d_6 , 100 MHz) δ 74.5, 74.5, 49.2, 40.9, 40.9, 32.7, 31.1, 30.6, 30.5, 30.2, 25.5, 25.5, 24.6, 23.5, 14.7.

3.5.8 Synthesis of (6E,10E,14E,18E)-23-(methoxy- ^{13}C)-2,6,10,15,19,23-hexamethyltetracosan-2,6,10,14,18-pentaene IR4. **IR4** was synthesized from 2,2-dimethyl-3-((3E,7E,11E,15E)-3,7,12,16,20-pentamethylhenicosa-3,7,11,15,19-pentaen-1-yl)oxirane, which was made by Tsangarakis' method from commercially available squalene.²⁰

Step 1: To a solution of 1.40 g 2,2-dimethyl-3-((3E,7E,11E,15E)-3,7,12,16,20-pentamethylhenicosa-3,7,11,15,19-pentaen-1-yl)oxirane (3.28 mmol) dissolved in 20 mL anhydrous THF in a flame-dried round bottom under argon atmosphere was added slowly 0.25 g lithium aluminum hydride (6.6 mmol) mixed with 4 mL anhydrous THF at 0 °C. The reaction mixture was allowed to stir at room temperature overnight before quenching with 5 mL 0.5 M HCl at 0 °C. The mixture was extracted with 30 mL Et_2O three times and the combined organic phase was washed by 10 mL brine and dried over anhydrous Na_2SO_4 . The solvent was then removed by rotary evaporation. Purification by flash

column chromatography (7 : 1 Hexanes to EtOAc) yielded 1.24 g (6*E*,10*E*,14*E*,18*E*)-2,6,10,15,19,23-hexamethyltetracos-6,10,14,18,22-pentaen-2-ol (2.89 mmol) as light yellow oil.

Step 2: Into a flame-dried flask was placed 0.19 g 60 % sodium hydride (4.8 mmol, 4 equiv) in mineral oil under argon atmosphere. The solid was washed by 2 mL dry pentane three times before adding 10 mL anhydrous THF and 0.50 g (6*E*,10*E*,14*E*,18*E*)-2,6,10,15,19,23-hexamethyltetracos-6,10,14,18,22-pentaen-2-ol (1.2 mmol, 1equiv). The resulting solution was refluxed for 1 hour before adding 0.25 g ¹³CH₃I (1.7 mmol, 1.5 equiv). The resulting solution was then refluxed overnight before quenching with 5 mL saturated ammonium chloride at 0 °C. The mixture was extracted with 30 mL hexanes three times and the combined organic phase was washed by 20 mL brine and dried over anhydrous Na₂SO₄. The solvent was then removed by rotary evaporation. The residue was purified chromatographically on a flash column with 250 mL hexanes. After the removal of solvent, 0.45 g **IR4** (1.0 mmol, 83 %) was obtained as light yellow oil. ¹H NMR (CDCl₃, 400 MHz) δ 5.21-5.06 (m, 5H), 3.19 (d, 3H, *J* = 140 Hz), 2.14-2.06 (m, 5H), 2.06-1.89 (m, 12H), 1.71 (s, 3H), 1.65-1.58 (m, 15H), 1.46-1.40 (m, 5H), 1.16 (s, 6H); ¹³C NMR (CDCl₃, 100 MHz) δ 135.1, 134.9, 134.9, 131.2, 124.4, 124.4, 124.3, 124.3, 74.6, 58.5, 57.6, 55.7, 49.0, 40.1, 39.8, 39.8, 39.7, 39.3, 39.3, 28.3, 26.8, 26.7, 25.7, 25.0, 22.2, 17.7, 16.0, 16.0, 15.8; MS *m/z* 443 [M]⁺, 413, 341, 273, 231, 203, 175, 143, 137, 107, 95, 81, 69, 55.

3.5.9 Synthesis of 2-methylpropan-2-yl-1-¹³C piperidine-1-carboxylate 1. The synthesis of 2-methylpropan-2-yl-1-¹³C piperidine-1-carboxylate **1** was divided into 3 steps.

Step 1: A solution of 0.250 g 1-allylpiperidine (2.00 mmol, 1 equiv) was prepared by dissolution in 5 mL dry DCM under an atmosphere of argon at 0 °C. To this solution was added dropwise 0.207 g triphosgene (0.698 mmol, 0.35 equiv) dissolved in 2 mL DCM.²¹ The solution was allowed to warm to room temperature and stirred for 4 hours. Water was then added to the reaction mixture and the resulting solution was then extracted with 20 mL DCM three times. The combined organic phase was washed with saturated sodium bicarbonate solution and brine and dried over NaSO₄. The solvent was removed by rotary evaporation and then by oil pump to yield the piperidine-1-carbonyl chloride. The resulting piperidine-1-carbonyl chloride was used in step 3 without further purification.

Step 2: To a flame-dried two-neck round bottom flask fitted with a condenser under argon atmosphere was placed 0.12 g magnesium (4.9 mmol, 2.5 equiv) and then 10 mL anhydrous diethyl ether was added and stirring initiated. A solution of 0.642 g ¹³CH₃I (4.49 mmol, 2.25 equiv) dissolving in 5 mL diethyl ether was added dropwise to the magnesium DEE mixture using a syringe pump at room temperature. After the addition, the grey mixture was allowed to stir for 30 minutes at room temperature before transferring to a flame-dried 50 mL round bottom flask flushed with argon at 0 °C. A solution of 0.170 g acetone (2.99 mmol, 1.5 equiv) in 5 mL anhydrous DEE was slowly added to the grey methylmagnesium iodide solution using a syringe pump at 0 °C. After that, the reaction mixture was allowed to stir at room temperature for 4 hours before quenching with 5 mL 0.5 M HCl. The mixture was extracted with 20 mL Et₂O three times and the combined organic phase was washed by 5 mL brine and dried over anhydrous Na₂SO₄. The solvent was then removed by simple distillation at 45 °C until no more ether

distilled out. The resulting 2-methylpropan-2-ol-1-¹³C was used in next step without further purification.

Step 3: To a flame-dried flask was placed 0.32 g 60 % sodium hydride (8.0 mmol, 4 equiv) in mineral oil under an argon atmosphere. The solid was washed by 3 mL dry pentane three times before adding 20 mL anhydrous THF and the 2-methylpropan-2-ol-1-¹³C obtained in step 2. The resulting mixture was refluxed for 1 hour before adding the piperidine-1-carbonyl chloride all at once. The mixture was then refluxed overnight before cooling down to room temperature and quenched by 1M ammonium chloride solution. The mixture was then extracted with 30 mL ethyl acetate three times and the organic phase was washed with brine and dried over NaSO₄. The solvent was removed by rotary evaporation and then by oil pump yielding a light yellow liquid of 2-methylpropan-2-yl-1-¹³C piperidine-1-carboxylate **1** (0.32 g, 1.7 mmol, 86%) which was then characterized by NMR spectroscopy and GC-MS. Further purification by flash column with 200 mL 10:1 Hexanes to EtOAc yielded 0.27 g colorless 2-methylpropan-2-yl-1-¹³C piperidine-1-carboxylate **1**. ¹H NMR (CDCl₃, 400 MHz) δ 3.35 (t, 4H, *J* = 5.4 Hz), 1.45 (d, 2H, *J* = 126 Hz), 1.62-1.40 (m, 12H; ¹³C NMR (CDCl₃, 100 MHz) δ 154.9, 79.3, 78.8, 44.6, 28.5, 25.7, 24.5; HRMS-EI *m/z*: [M]⁺ Calcd for ¹³CC₉H₁₉NO₂: 186.1444, found: 186.1442.

3.6 Acknowledgement

The author thanks Dr. Russell Hopson for his helpful suggestions.

3.7 References

(1) (a) Lecachey, B.; Oulyadi, H.; Lameiras, P.; Harrison-Marchand, A.; Gerard, H.; Maddaluno, J. *J. Org. Chem.* **2010**, *75*, 5976-5983. (b) Consiglio, G. B.; Queval, P.; Harrison-Marchand, A.; Mordini, A.; Lohier, J.; Delacroix, O.; Gaumont, A.; Gerard, H.; Maddaluno, J.; Oulyadi, H. *J. Am. Chem. Soc.* **2011**, *133*, 6472-6480. (c) Armstrong, D. R.; Garcia-Alvarez, P.; Kennedy, A. R.; Mulvey, R. E.; Robertson, S. D. *Chem. Eur. J.* **2011**, *17*, 6725-6730. (d) Li, W.; Chung, H.; Daeffler, C.; Johnson, J. A.; Grubbs, R. H. *Macromolecules*, **2012**, *45*, 9595-9603.

(2) (a) Li, D.; Hopson, R.; Li, W.; Liu, J.; Williard, P. G. *Org. Lett.* **2008**, *10*, 909-911. (b) Li, D.; Kagan, G.; Hopson, R.; Williard, P. G. *J. Am. Chem. Soc.* **2009**, *131*, 5627-5634. (c) Li, D.; Keresztes, I.; Hopson, R.; Williard, P. G. *Acc. Chem. Res.* **2009**, *42*, 270-280. (d) Kagan, G.; Li, W.; Hopson, R.; Williard, P. G. *Org. Lett.* **2009**, *11*, 4818-4821. (e) Kagan, G.; Li, W.; Hopson, R.; Williard, P. G. *Org. Lett.* **2010**, *12*, 520-523. (f) Socha, A. M.; Kagan, G.; Li, W.; Hopson, R.; Sello, J. K.; Williard, P. G. *Energy Fuels* **2010**, *24*, 4518-4521. (g) Kagan, G.; Li, W.; Sun, C.; Hopson, R.; Williard, P. G. *J. Org. Chem.* **2011**, *76*, 65-70. (h) Kagan, G.; Li, W.; Li, D.; Hopson, R.; Williard, P. G. *J. Am. Chem. Soc.* **2011**, *133*, 6596-6602. (i) Su, C.; Hopson, R.; Williard, P. G. *J. Org. Chem.* **2013**, *78*, 7288-7292. (j) Su, C.; Hopson, R.; Williard, P. G. *Eur. J. Inorg. Chem.* **2013**, ASAP. (k) Su, C.; Hopson, R.; Williard, P. G. *J. Am. Chem. Soc.* **2013**, *135*, ASAP.

(3) (a) Li, W.; Kagan, G.; Yang, H.; Cai, C.; Hopson, R.; Sweigart, D. A.; Williard, P. G. *Org. Lett.* **2010**, *12*, 2698-2701. (b) Li, W.; Kagan, G.; Yang, H.; Cai, C.; Hopson, R.; Dai, W.; Sweigart, D. A.; Williard, P. G. *Organometallics*. **2010**, *29*, 1309-1311.

(4) (a) Collum, D. B.; McNeil, A. J.; Ramirez, A. *Angew. Chem. Int. Ed.* **2007**, *46*, 3002-3017. (b) Wu, G.; Huang, M. *Chem. Rev.* **2006**, *106*, 2596-2616. (c) Rappoport, Z.; Marek, I., Eds. *The Chemistry of Organolithium Compounds*; John Wiley & Sons, Ltd.: West Sussex, **2004**. (d) Hodgson, D. *Organolithiums in Enantioselective Synthesis*; Springer: New York, **2003**. (e) Clayden, J. *Organolithiums: Selectivity for Synthesis*; Pergamon: Oxford, **2002**. (f) Lucht, B.; Collum, D. *Acc. Chem. Res.* **1999**, *32*, 1035-1042. (g) Trost, B. M., Fleming, I., Eds. *Comprehensive Organic Synthesis*; Pergamon: Oxford, **1991**. (h) Snieckus, V. *Chem. Rev.* **1990**, *90*, 879-933.

(5) (a) Ince, H. H.; Dedeoglu, B.; Gul, S.; Aviyente, V.; Coldham, I. *Mol. Phys.* **2012**, *110*, (6), 353-359. (b) Khartabil, H. K.; Gros, P. C.; Fort, Y.; Ruiz-Lopez, M. F. *J. Am. Chem. Soc.* **2010**, *132*, (7), 2410-2416. (c) Riggs, J. C.; Singh, K. J.; Yun, M.; Collum, D. B. *J. Am. Chem. Soc.* **2008**, *130*, (41), 13709-13717. (d) Jones, A. C.; Sanders, A. W.; Bevan, M. J.; Reich, H. J. *J. Am. Chem. Soc.* **2007**, *129*, 3492-3493. (e) Yakimansky, A.; Wang, G.; Janssens, K.; Van Beylen, M. *Polymer* **2003**, *44*, (21), 6457-6463. (f) Rutherford, J. L.; Hoffmann, D.; Collum, D. B. *J. Am. Chem. Soc.* **2002**, *124*, 264-271. (g) Reich, H. J.; Green, D. P.; Medina, M. A.; Goldenberg, W. S.; Gudmundsson, B. O.; Dykstra, R. R.; Phillips, N. H. *J. Am. Chem. Soc.* **1998**, *120*, 7201-7210. (h) Lucht, B. L.; Bernstein, M. P.; Remenar, J. F.; Collum, D. B. *J. Am. Chem. Soc.* **1996**, *118*, 10707-10718. (i) Ogle, C. A.; Johnson IV, H. C.; Wang, X. L.; Strickler, F. H.; Bucca, D.; Gordon III, B. *Macromolecules* **1995**, *28*, 5184-5191. (j) Bates, T. F.; Clarke, M. T.; Thomas, R. D. *J. Am. Chem. Soc.* **1988**, *110*, 5109-5112. (k) McGarrity, J. F.; Ogle, C. A.; Brich, Z.; Loosli, H. *J. Am. Chem. Soc.* **1985**, *107*, 1810-1815. (l) West, P.; Waack, R.; Purmort, J. I. *J. Am. Chem. Soc.* **1970**, *92*, 840-845.

(6) Khartabil, H. K.; Gros, P. C.; Fort, Y.; Ruiz-Lopez, M. F. *J. Am. Chem. Soc.* **2010**, *132*, (7), 2410-2416. (b) Khartabil, H. K.; Gros, P. C.; Fort, Y.; Ruiz-Lopez, M. F. *J. Org. Chem.* **2008**, *73*,

(23), 9393-9402. (c) Walfort, B.; Lameyer, L.; Weiss, W.; Herbst-Irmer, R.; Bertermann, R.; Rocha, J.; Stalke, D. *Chem. - Eur. J.* **2001**, *7*, (7), 1417-1423.

(7) (a) Fox, T.; Hausmann, H.; Gunther, H. *Magn. Reson. Chem.* **2004**, *42*, 788-794. (b) Ogle, C. A.; Huckabee, B. K.; Johnson IV, H. C.; Sims, P. F.; Winslow, S. D. *Organometallics* **1993**, *12*, 1960-1963. (c) Novak, D. P.; Brown, T. L. *J. Am. Chem. Soc.* **1972**, *94*, 3793-3798.

(8) Koster, H.; Thoennes, D.; Weiss, E. *J. Organometal. Chem.* **1978**, *160*, 1-5.

(9) Kamps, I.; Neumann, B.; Stammeler, H.-G.; Mitzel, N. W. *Organometallics* **2010**, *29*, 4746-4748.

(10) (a) Strohmam, C.; Strohfeltd, K.; Schildbach, D.; McGrath, M. J.; O'Brien, P. *Organometallics* **2004**, *23*, 5389-5391. (b) Strohmam, C.; Gessner, V. H. *J. Am. Chem. Soc.* **2007**, *129*, 8952-8953.

(11) (a) Khartabil, H. K.; Gros, P. C.; Fort, Y.; Ruiz-Lopez, M. F. *J. Org. Chem.* **2008**, *73*, (23), 9393-9402. (b) Ohta, Y.; Demura, A.; Okamoto, T.; Hitomi, H.; Nagaoka, M. *J. Phys. Chem. B* **2006**, *110*, (25), 12640-12644. (c) Gerard, H.; De la Lande, A.; Maddaluno, J.; Parisel, O.; Tuckerman, M. E. *J. Phys. Chem. A* **2006**, *110*, (14), 4787-4794. (d) Fressigne, C.; Lautrette, A.; Maddaluno, J. *J. Org. Chem.* **2005**, *70*, (20), 7816-7828. (e) Jemmis, E. D.; Gopakumar, G. *Chem. Organolithium Compd.* **2004**, *1*, 1-45. (f) Verstraete, P.; Deffieux, A.; Fritsch, A.; Rayez, J. C.; Rayez, M. T. *J. Mol. Struct. THEOCHEM* **2003**, *631*, 53-66. (g) Ponec, R.; Roithova, J.; Girones, X.; Lain, L.; Torre, A.; Bochicchio, R. *J. Phys. Chem. A* **2002**, *106*, (6), 1019-1025. (h) Kwon, O.; Sevin, F.; McKee, M. L. *J. Phys. Chem. A* **2001**, *105*, (5), 913-922. (i) Frischknecht, A. L.; Milner, S. T. *J. Chem. Phys.* **2001**, *114*, (2), 1032-1050. (j) Grotjahn, D. B.; Pesch, T. C.; Brewster, M. A.; Ziurys, L. M. *J. Am. Chem. Soc.* **2000**, *122*, (19), 4735-4741. (k) Kirschenbaum, L. J.; Howell, J. M. *Struct. Chem.* **1998**, *9*, (5), 327-337. (l) Kirschenbaum, L. J.; Howell, J. M.; Singman, E. L. *Struct. Chem.* **1996**, *7*, (1), 79-83.

(12) (a) Pate, F.; Oulyadi, H.; Harrison-Marchand, A.; Maddaluno, J. *Organometallics* **2008**, *27*, (14), 3564-3569. (b) Knorr, R.; Menke, T.; Ferchland, K.; Mehlstaebli, J.; Stephenson, D. S. *J. Am. Chem. Soc.* **2008**, *130*, (43), 14179-14188. (c) Gohaud, N.; Begue, D.; Pouchan, C. *Chem. Phys.* **2005**, *310*, (1-3), 85-96.

(13) (a) Remenar, J. F.; Lucht, B. L.; Collum, D. B. *J. Am. Chem. Soc.* **1997**, *119*, 5567-5572. (b) Lucht, B. L.; Collum, D. B. *J. Am. Chem. Soc.* **1996**, *118*, 2217-2225.

(14) (a) Morris, K. F.; Johnson, C. S., Jr., *J. Am. Chem. Soc.* **1992**, *114*, (2), 776-777. (b) Morris, K. F.; Johnson, C. S., Jr., *J. Am. Chem. Soc.* **1992**, *114*, (8), 3139-3141.

(15) Keresztes, I.; Williard, P. G. *J. Am. Chem. Soc.* **2000**, *122*, 10228-10229.

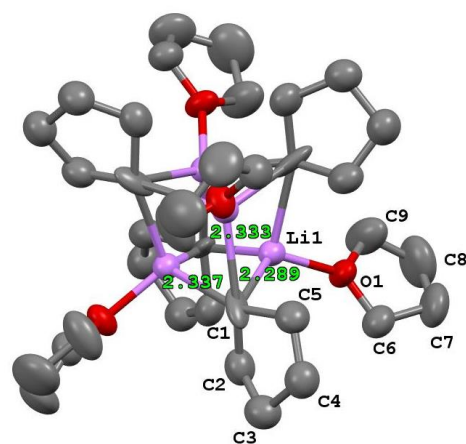
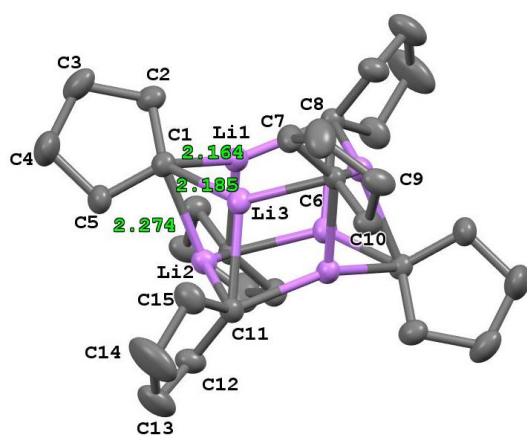
(16) This particular urethane was selected for analysis because it is a precursor and analog of synthetically useful carbanions: *c.f.* Beng, T. K.; Tyree, W. S.; Parker, T.; Su, C.; Williard, P. G.; Gawley, R. E. *J. Am. Chem. Soc.* **2012**, *134*, (40), 16845-16855.

(17) It is curious that the use of optically pure TMCDA in this experiment leads to extensive precipitation precluding the possibility of performing the NMR analyses.

- (18) Wagner, P.; Nakagawa, Y.; Lee, G. S.; Davis, M. E.; Elomari, S.; Medrud, R. C.; Zones, S. I. *J. Am. Chem. Soc.* **2000**, *122*, 263-273.
- (19) Ashby, E. C.; Noding, S. A. *J. Org. Chem.* **1980**, *45*, 1035-1041.
- (20) Tsangarakis, C.; Raptis, C.; Arkoudis, E.; Stratakis, M. *Adv. Synth. Catal.* **2008**, *350*, 1587-1600.
- (21) Su, C.; Williard, P.G. submitted for publication.

Chapter 4

Characterization of cyclopentyllithium and cyclopentyllithium tetrahydrofuran complex



4.1 Abstract

The solid-state structures of unsolvated, hexameric cyclopentylolithium and tetrameric cyclopentylolithium tetrahydrofuran solvate were determined by single-crystal X-ray diffraction. Cyclopentylolithium easily crystallized in hydrocarbon solvents. Solution-state structural analyses of cyclopentylolithium and cyclopentylolithium–tetrahydrofuran complexes in toluene- d_8 were also carried out by diffusion-ordered NMR spectroscopy with diffusion coefficient–formula weight correlation analyses and other one- and two-dimensional NMR techniques. The solution-state studies suggest that unsolvated cyclopentylolithium exists as hexamer and tetramer equilibrating with each other. Upon solvation with tetrahydrofuran, cyclopentylolithium exists mostly as a tetrahydrofuran tetrasolvated tetramer.

4.2 Introduction

Organolithium reagents are among the most widely used reagents in the synthesis of organic compounds.¹ Alkylolithium reagents are the source of most organolithium reagents because they can efficiently generate a wide variety of carbanions such as lithium amide, acetylide and alkoxide. Moreover, the low boiling point alkane by-product is a saturated hydrocarbon that is inert to most of the reactions. Secondary alkylolithium reagents are usually used for the deprotonation of very weakly acidic protons such as aryl and alkylolithium.^{1,2} Although they are not as nucleophilic as primary alkylolithium reagents, secondary alkylolithium reagents can also be used as nucleophiles and used for metal lithium exchange.^{1,3} It is evident that the reactivity and preferred

reaction pathways of these alkyllithium reagents are related to their aggregation and solvation states^{1,4} thus, any such information regarding these intermediate states can enhance our understanding and ability to tailor these reactions to the desired products. Herein we present the structural characterization in both solid and solution of cyclopentyllithium, a secondary alkyllithium reagent.

The deprotonation reactions of alkyllithium reagents are often carried out in the presence of ethereal solvents such as tetrahydrofuran (THF) and diethyl ether, to increase the reactivity of the reagents. However, it is well known that alkyllithium reagents α -deprotonate ethereal solvents.^{1,5} Therefore, it is not easy to obtain the crystal structure of alkyllithium adducts with tetrahydrofuran. The first crystal structures of *n*-butyllithium were reported twenty years ago including the THF solvated tetramer.⁶ After that, only two structures of THF-solvated alkyllithium reagents have been published.⁷ However, these two published structures are primary alkyllithium reagents possibly because secondary alkyllithium reagents react more readily with THF. Because cyclopentyllithium crystallizes readily, we were able to obtain the crystal structure of its complex with tetrahydrofuran. This is the first crystal structure of a secondary alkyllithium-THF complex although a few internally chelated and mixed aggregate secondary alkyl lithium containing structures are known.⁸ Moreover, characterization of the cyclopentyllithium/THF complex in toluene-*d*₈ solution is also described using various one- and two-dimensional NMR techniques on the dissolved crystal.

4.3 Results and Discussion

4.3.1 Characterization of cyclopentyl lithium in solid- and solution-states

Cyclopentyl lithium can be easily synthesized by reacting chlorocyclopentane with lithium in cyclohexane or heptane under argon atmosphere. Owing to the greater solubility of cyclopentyl lithium in cyclohexane, yields were always greater than obtained in heptane under otherwise analogous conditions.

Crystal structure of cyclopentyl lithium. Cyclopentyl lithium is easily crystallized in hydrocarbon solvents. When freshly made cyclopentyl lithium cyclohexane solution or heptane solution is stored at $-20\text{ }^{\circ}\text{C}$ overnight, a significant amount of colorless cyclopentyl lithium crystals are obtained and the concentration of cyclopentyl lithium cyclohexane solution decreases from 2.0 M to 0.6 M. Crystallization provides highly pure, crystalline secondary alkyl lithium in good yield. The X-ray structure determination reveals that cyclopentyl lithium is hexameric in solid state (Figure 4.1) similar to those of *n*-butyllithium,^{9a} isopropyllithium,^{9b} and cyclohexyllithium^{9c}.

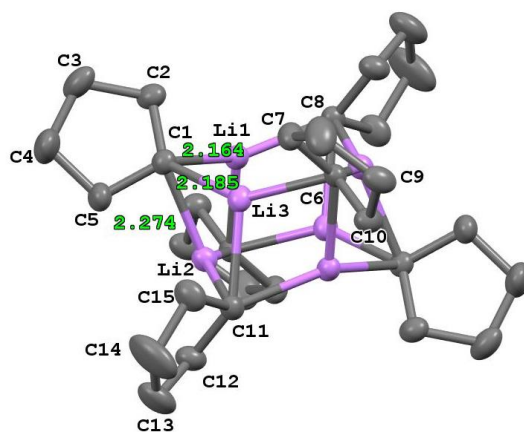
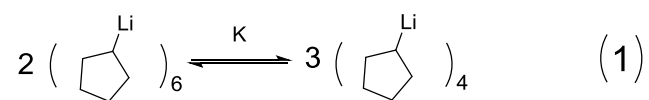


Figure 4.1. Crystal structure of hexameric cyclopentyl lithium. Thermal ellipsoid plots are at the 50% probability level. Hydrogen atoms have been omitted for clarity. Crystallographic asymmetric unit atoms labeled and C(1) – Li interatomic distances displayed.

Characterization of cyclopentyllithium in solution. After obtaining the crystal structure of cyclopentyllithium, we focused on the solution-state structure of cyclopentyllithium because most of the reactions are conducted in solution. Solution-state characterization of cyclopentyllithium was carried out by applying various one- and two-dimensional NMR techniques on a solution of the crystal dissolved in toluene- d_8 . The sample was prepared by dissolving dry crystals of cyclopentyllithium which had been washed by anhydrous pentane twice in toluene- d_8 which is unreactive to alkyllithium reagents in the absence of coordinating ligand such as THF or *N,N,N',N'*-tetramethyl ethylenediamine (TMEDA) at room temperature.¹⁰

We first examined the ^1H NMR of cyclopentyllithium in toluene- d_8 . The proton NMR shows two separate peaks in the methine region of cyclopentyllithium. It is believed that the two peaks originated from two different aggregates. To characterize the peaks, a variable-temperature NMR study with 1-dodecene (DDE) as internal reference was carried out and the result is shown in Figure 4.2. When the temperature increases from -10 °C to -25 °C, the resonance at -0.77 ppm decreases significantly in intensity as the resonance at -1.14 ppm increases. The concentration of the two aggregates can be easily determined by comparing the integrations of internal standard and the methine signals.^{10a} We assigned the resonance at -0.77 ppm as hexamer and -1.14 ppm as tetramer because the concentration of tetramer increases upon elevation of temperature in the equilibrium reaction **1** depicted in Scheme 4.1. We conducted a dilution experiment at 15 °C (Figure 4.3) to verify our assignment and this result is summarized in Table 4.1.



Scheme 4.1. The equilibrium reaction of the hexameric and tetrameric complexes of c-PenLi

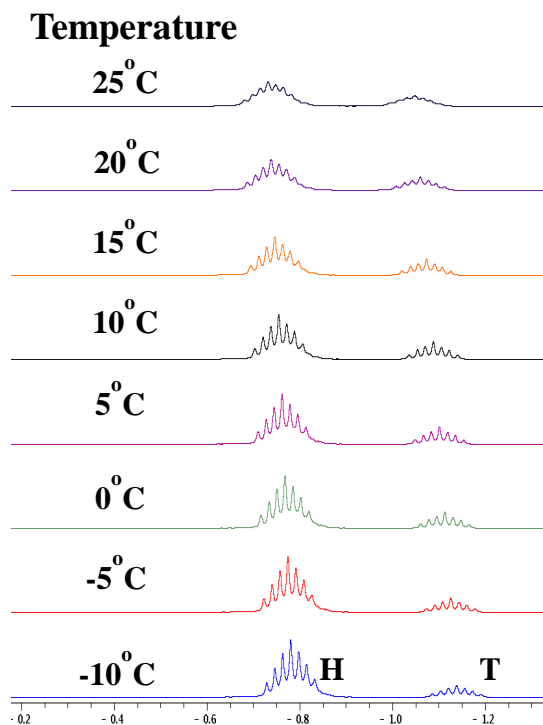


Figure 4.2. Variable temperature ^1H NMR (400 MHz) spectra of 1.07 M c-PenLi in toluene- d_8 . H represents the methine signal of c-PenLi in hexamer, T represents the signal in tetramer.

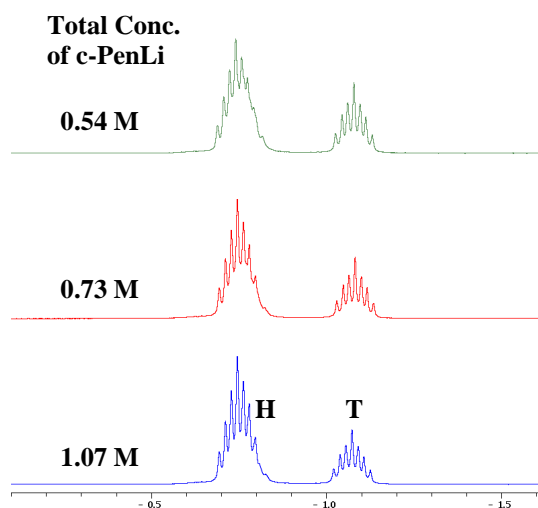


Figure 4.3. ^1H NMR (400 MHz) spectra of 1.07 M, 0.73 M and 0.54 M c-PenLi in toluene- d_8 at 15 °C. H represents the methine signal of c-PenLi hexamer, T represents the signal of tetramer.

Table 4.1. Concentrations of cyclopentyllithium (c-PenLi) complexes and the equilibrium constant (K) at 15 °C in toluene-*d*₈.

[c-PenLi] _a at -1.14 ppm, M	[c-PenLi] _b at -0.77 ppm, M	$K = \frac{([c-PenLi]_a/4)^3}{([c-PenLi]_b/6)^2}$
0.272	0.798	0.0178 M
0.203	0.529	0.0169 M
0.164	0.381	0.0170 M

These results support our assignment of the resonances because the calculated equilibrium constants are very similar according to K_{eq} given in Table 4.1. We then determined the enthalpy (ΔH) and entropy (ΔS) of the equilibrium of reaction **1** by a van't Hoff plot (Figure 4.4). The concentrations and equilibrium constants of reaction **1** at different temperatures were determined by variable-temperature ¹H NMR with 1-dodecene as internal reference, and the results are shown in Table 4.2. The van't Hoff plot has an excellent correlation ($R^2 > 0.99$). The enthalpy and entropy are calculated to be 38.2 kJmol⁻¹ and 99.7 Jmol⁻¹K⁻¹ respectively. Comparison of the thermodynamic data for cyclopentyllithium with those of *sec*-butyllithium¹¹ reveals that the ΔH of *sec*-butyllithium is 64.8 kJmol⁻¹ or 1.7 times higher than that of cyclopentyllithium whereas ΔS of *sec*-butyllithium is 262 Jmol⁻¹K⁻¹ or 2.6 times that of the ΔS of cyclopentyllithium. This is consistent with the fact that the hexamer is the major species in cyclopentyllithium toluene solution, whereas tetramer is the major species for *sec*-butyllithium at room temperature.

A series of ¹H and ¹³C NMR experiments including ¹H-NMR, ¹³C-NMR, COSY, HSQC, and HMBC were then conducted for the sake of ¹H and ¹³C signal assignment. First, we identified the resonances of methylene protons on carbon 2, 3, 4 and 5 through COSY NMR, and the carbon signals were then assigned using HSQC NMR. The results

are summarized in Table 4.3. We then carried out diffusion-ordered NMR spectroscopy (DOSY) and diffusion coefficient-formula weight (*D-FW*) correlation analyses to evaluate the formula weight of the aggregates. We applied DOSY NMR with internal references for the determination of formula weights of reactive complexes by *D-FW* correlation analysis. The formula weight of an unknown complex is deduced by its diffusion coefficient through the linear regression plot of the logarithms of NMR determined diffusion coefficients against the known formula weights of the references.¹² Benzene (BEN, 78.11 gmol⁻¹), cyclooctene (COE, 110.2 gmol⁻¹), 1-tetradecene (TDE, 196.4 gmol⁻¹) and squalene (SQU, 410.7 gmol⁻¹) were used as internal references.

The resonances of methylene protons of *c*-PenLi from 1.0 to 2.5 ppm overlapped with those from the internal references; thus, distinct peaks from the methine protons were selected for our *D-FW* analysis (Figure 4.5).

Table 4.2. Concentrations of different cyclopentyllithium complexes as a function of temperature in toluene-*d*₈.

Temp. (°C)	1/Temp. (x10 ⁻³ K ⁻¹)	Conc. of <i>c</i> -PenLi ^a at -0.77 ppm, C ₁ (M)	Conc. of <i>c</i> -PenLi ^a at -1.14 ppm, C ₂ (M)	$K = \frac{(C_2/4)^3}{(C_1/6)^2}$ (x10 ⁻³ M)	ln K
-10.0	3.80	0.870	0.179	4.24	-5.46
-5.0	3.73	0.857	0.198	5.86	-5.14
0.0	3.66	0.848	0.221	8.39	-4.78
5.0	3.60	0.826	0.235	10.6	-4.54
10.0	3.53	0.812	0.257	14.5	-4.24
15.0	3.47	0.798	0.272	17.8	-4.03
20.0	3.41	0.793	0.308	26.1	-3.64
25.0	3.35	0.763	0.328	33.9	-3.38

^aThe concentration was expressed as monomer units.

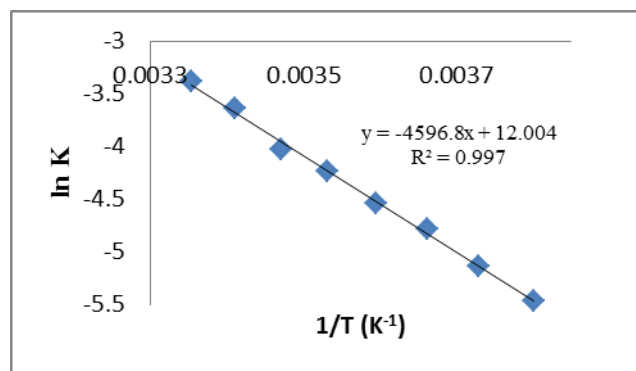
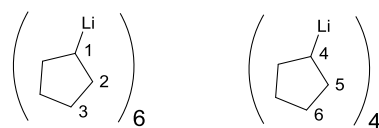


Figure 4.4. The van 't Hoff plot of reaction (1)

Table 4.3. ^1H and ^{13}C signal assignments of hexameric and tetrameric *c*-PenLi in toluene- d_8 .



Carbon atom	^{13}C (ppm)	^1H (ppm)
1	26.3	-0.78
2	34.7	1.09, 2.00
3	28.7	1.52, 1.76
4	21.8	-1.16
5	34.7	0.87, 1.93
6	28.8	1.79, 1.57

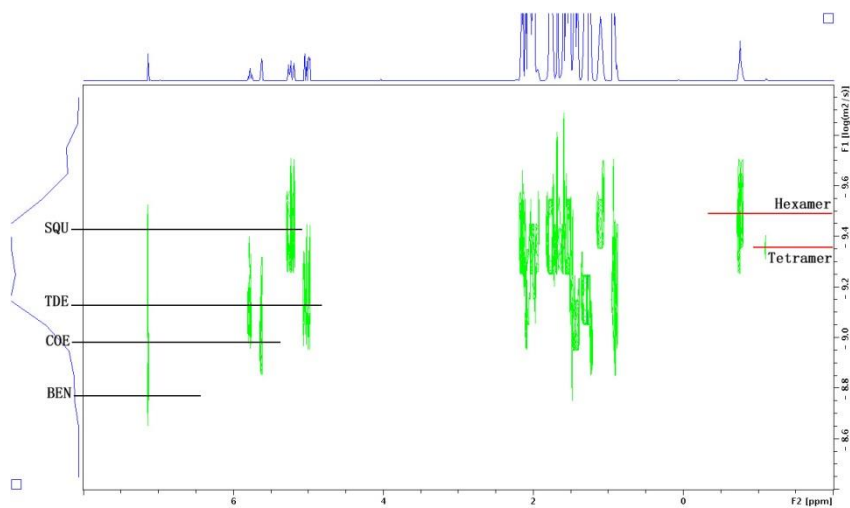


Figure 4.5. ^1H DOSY of *c*-PenLi toluene- d_8 solution at $-25\text{ }^\circ\text{C}$.

The correlation between $\log FW$ and $\log D$ of the linear regression is very high ($r^2 > 0.99$), and the predicted formula weight for the resonance at -0.77 ppm is 443.5 g mol^{-1} , which is very close to the formula weight of the hexameric *c*-PenLi (456.4 g mol^{-1} , 2.8% difference). The predicted formula weight for the resonance at -1.14 ppm is 309.1 g mol^{-1} which is only 1.6% different from the formula weight (304.3 g mol^{-1}) of the tetrameric *c*-PenLi (Figure 4.6, Table 4.4). Therefore, our DOSY result is consistent with the equilibrium reaction **1** of *c*-PenLi in toluene- d_8 and our hexamer-tetramer peak assignments.

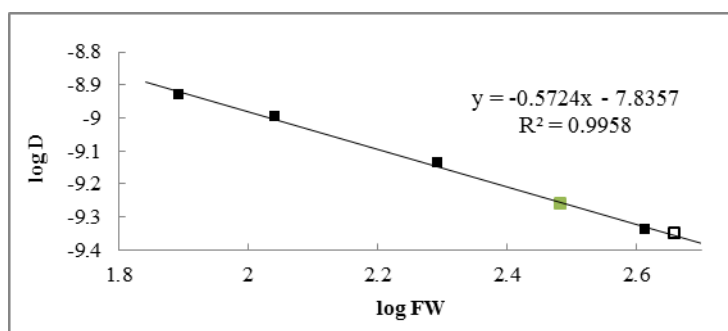


Figure 4.6. *D*-FW analysis of ^1H DOSY data. Internal references are shown as black squares, the tetrameric *c*-PenLi is shown as the green square and the hexameric *c*-PenLi is shown as the white square.

Table 4.4. *D*-FW analysis of ^1H DOSY data

entry	Compd	FW (g mol^{-1})	$10^{-10}D$ (m^2/s)	Predicted FW (g mol^{-1})	% error
1	BEN	78.11	11.73	81.84	-4.8
2	COE	110.2	10.07	106.8	3.1
3	TDE	196.4	7.311	186.9	4.8
4	SQU	410.7	4.569	424.9	-3.5
5	<i>c</i> -PenLi ^a	456.4 ^a	4.458	443.5	2.8
6	<i>c</i> -PenLi ^b	304.3 ^b	5.482	309.1	-1.6

^a456.4 g mol^{-1} is the formula weight of hexameric *c*-PenLi complex.

^b304.3 g mol^{-1} is the formula weight of tetrameric *c*-PenLi complex.

4.3.2 Characterization of cyclopentylolithium/THF complex in solid- and solution-states

Cyclopentylolithium/THF complex is easily crystallized in pentane. It exists as tetramer $(c\text{-PenLi})_4(\text{THF})_4$ in the solid state. Solution-state characterization of the complex dissolved in toluene- d_8 at low temperature reveals that tetrasolvated tetramer $(c\text{-PenLi})_4(\text{THF})_4$ is also the dominant species in solution.

Crystal structure of cyclopentylolithium/THF complex. Cyclopentylolithium/THF crystals suitable for X-ray diffraction are easily grown from pentane solution. After the addition of THF to the pentane solution of $c\text{-PenLi}$, the solution is stored at $-20\text{ }^\circ\text{C}$ for 2 hours and colorless crystals are obtained. These crystals only last for a few hours and the solution turns from colorless to yellow. We presume that this results from decomposition of THF by $c\text{-PenLi}$. X-ray diffraction analysis of the $c\text{-PenLi}/\text{THF}$ crystal indicates a tetrameric $c\text{-PenLi}$ aggregate with all lithium atoms coordinated to THF (Figure 4.7). Until now, only three crystal structures of primary alkylolithium/THF complexes have been reported, and they are also tetrasolvated tetramers with each lithium atom coordinated to THF.^{6,7} To the best of our knowledge, this is the first crystal structure of a secondary alkylolithium solvated by THF.

Characterization of cyclopentylolithium/THF complex in solution. Because it is important to understand the solution-state structure of cyclopentylolithium/THF complex, we conducted a series of NMR experiments to characterize the complex. The sample was prepared by dissolving the crystal of $c\text{-PenLi}/\text{THF}$ complex into toluene- d_8 at $-78\text{ }^\circ\text{C}$. All experiments were carried out below $-30\text{ }^\circ\text{C}$ to prevent significant reaction of $c\text{-PenLi}$ with THF or toluene.

Unlike the unsolvated *c*-PenLi toluene solution, there is only one major peak in the methine region of *c*-PenLi for the THF solvated *c*-PenLi solution. To verify that only one dominant species exists for the THF solvate, we performed a low temperature ^6Li NMR study on the *c*-PenLi/THF complex in which the lithium atoms are of natural abundance (Figure 4.8). The ^6Li spectra show one dominant peak and a small minor peak for the sample through $-30\text{ }^\circ\text{C}$ to $-90\text{ }^\circ\text{C}$.

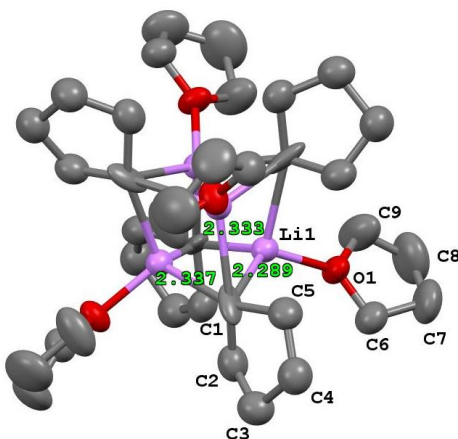


Figure 4.7. Crystal structure of tetrameric cyclopentyllithium/THF complex. Thermal ellipsoid plot shown at the 50% probability level. Hydrogen atoms have been omitted for clarity. Crystallographic asymmetric unit atoms labeled and C(1) – Li interatomic distances displayed.

We again carried out a series of ^1H - and ^{13}C -NMR experiments including ^1H -NMR, ^{13}C -NMR, COSY, HSQC, and HMBC to assign the ^1H and ^{13}C signals. The signals of methylene protons on carbon 2 and 3 were first identified by using COSY NMR, and the carbon resonances were then figured out by HSQC NMR. The result is summarized in Table 4.5. Diffusion-ordered NMR spectroscopy and *D*-FW correlation analysis were also performed to determine the formula weight of the *c*-PenLi/THF complex. Benzene, cyclooctene, 1-tetradecene, and squalene were used as internal references in this ^1H DOSY experiment, and the distinct peak from the methine proton of the *c*-PenLi/THF

complex was selected for our *D-FW* analysis because of the overlap of resonances from the internal references with the complex (Figure 4.9).

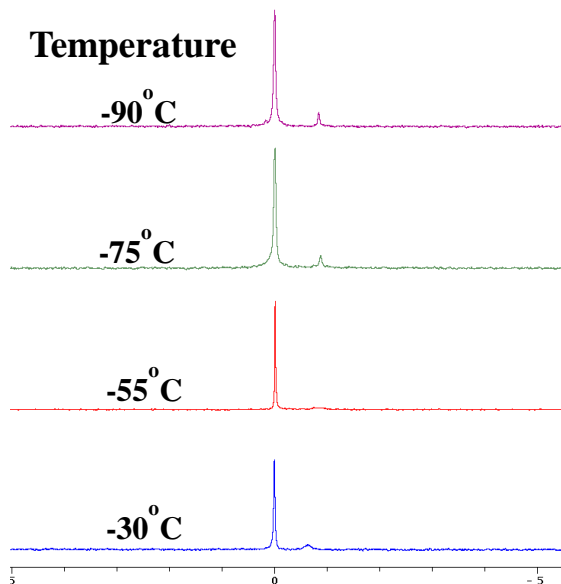
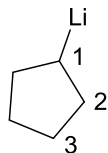


Figure 4.8. Variable temperature ${}^6\text{Li}$ NMR spectra of natural abundant *c*-PenLi/THF complex in toluene- d_8 .

Table 4.5. ${}^1\text{H}$ and ${}^{13}\text{C}$ signal assignments of *c*-PenLi solvated by THF in toluene- d_8



Carbon atom	${}^{13}\text{C}$ (ppm)	${}^1\text{H}$ (ppm)
1	23.8	-0.62
2	35.9	1.48, 2.29
3	29.4	1.66, 2.01

The correlation of the linear regression is high ($r^2 = 0.99$) and the predicted formula weight from the *c*-PenLi methine resonance is 538.4 gmol^{-1} which is 9.2% different from the formula weight 592.7 gmol^{-1} of complex $(c\text{-PenLi})_4(\text{THF})_4$ (Figure 4.10, Table 4.6). The predicted formula weight is within the typical 10% error range for the *D-FW*

analysis.¹¹ However, lowering of the predicted formula weight may also result from the influence of a small amount of dimer because we also observe a small, unassigned peak in the ⁶Li NMR. Moreover, it is known that *n*-butyllithium exists as dimer and tetramer in THF solution;¹³ therefore, it would not be surprising if a small amount of dimer is present in the *c*-PenLi/THF toluene-*d*₈ solution. Nevertheless, it is evident that the solid state structure (*c*-PenLi)₄(THF)₄ is the dominant species in solution.

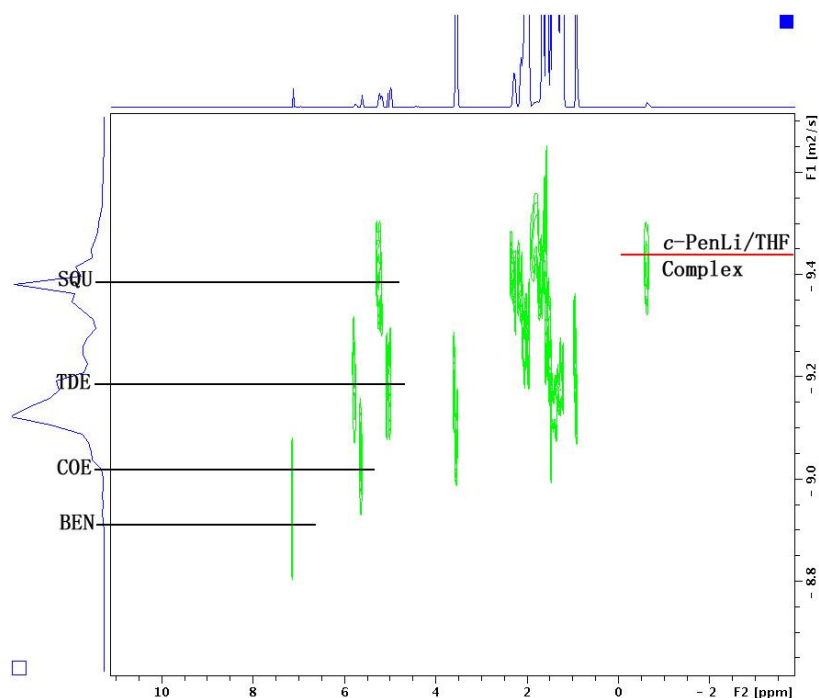


Figure 4.9. ¹H DOSY of *c*-PenLi/THF complex in toluene-*d*₈ solution at -35 °C.

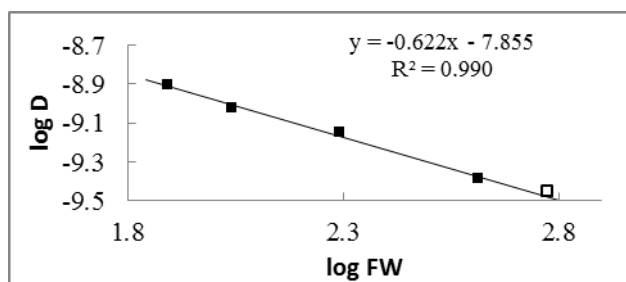


Figure 4.10. *D*-FW analysis of ¹H DOSY data of *c*-PenLi/THF complex in toluene-*d*₈ solution at -35 °C. Internal references are shown as solid squares and the *c*-PenLi/THF complex is shown as open square.

Table 4.6. *D*-FW analysis of ¹H DOSY data

entry	Compd	FW (g mol ⁻¹)	10 ⁻¹⁰ D (m ² /s)	Predicted FW (g mol ⁻¹)	% error
1	BEN	78.11	12.41	77.33	1.0
2	COE	110.2	9.54	116.1	-5.3
3	TDE	196.4	7.10	183.1	6.8
4	SQU	410.7	4.14	422.4	-2.8
5	c-PenLi ^a	592.7 ^a	3.54	539.6	9.2

^a592.7 g mol⁻¹ is the formula weight of (c-PenLi)₄(THF)₄ complex.

4.4 Conclusion

Cyclopentyllithium is easily crystallized in hydrocarbon solvent. This crystallization conveniently provides a process to obtain highly pure secondary alkyllithium reagent suitable for solution-state characterization and also for synthetic applications. X-ray diffraction reveals the hexameric nature of the cyclopentyllithium whereas it exists as both a tetramer and a hexamer in hydrocarbon solvents. Moreover, cyclopentyllithium/tetrahydrofuran complex crystallizes readily from pentane at -20 °C, and the crystal structure is a tetrameric c-PenLi aggregate with each lithium atom coordinated to THF forming the tetrasolvated, tetrameric aggregate (c-PenLi)₄(THF)₄. This same (c-PenLi)₄(THF)₄ tetramer is also the dominant species in solution.

The characterization of cyclopentyllithium in both solid and solution not only furthers our understanding of secondary alkyllithium reagents, but also provides us the mechanistic insight of the reaction of cyclopentyllithium.

4.5 Experimental Section

4.5.1 Procedures for NMR Experiments. NMR samples were prepared in tubes sealed with rubber septa and parafilm. NMR tubes were evacuated *in vacuo*, flame-dried and filled with argon before use. ^1H chemical shifts were referenced to toluene- d_8 at 7.09 ppm, and ^{13}C chemical shifts were referenced to toluene- d_8 at 137.86 ppm. All NMR experiments were acquired on a 400 MHz spectrometer equipped with a z-axis gradient amplifier and an ATMA BBO probe with a z-axis gradient coil. Maximum gradient strength was 0.214 T/m. ^1H -DOSY was performed using the standard `dstebpgp3s` program, employing a double stimulated echo sequence, bipolar gradient pulses for diffusion, and 3 spoil gradients. Diffusion time was 200 ms, and the rectangular gradient pulse duration was 1200 μs . Gradient recovery delays were 200 μs . Individual rows of the quasi-2-D diffusion databases were phased and baseline corrected. Actual diffusion coefficients used for D-FW analysis were obtained with commercial software using the T1/T2 analysis module.

The cyclopentyllithium (c-PenLi) sample was prepared by dissolving dry crystals in toluene- d_8 . The crystals were kept at $-78\text{ }^\circ\text{C}$ in a cold bath immediately after removing from a $-20\text{ }^\circ\text{C}$ freezer, the solvent was removed by syringe and the crystals were washed twice with anhydrous pentane. After the removal of solution by syringe, the crystals were kept in a dry ice-acetonitrile bath and evacuated for 1 hour. Toluene- d_8 was then added to the crystals under an argon atmosphere. The solution was allowed to stir at $-42\text{ }^\circ\text{C}$ for 20 min before transferring into a sealed NMR tube via syringe.

The cyclopentyllithium/THF sample can be prepared by dissolving dry crystals in toluene- d_8 or by adding anhydrous tetrahydrofuran into a toluene- d_8 solution of

cyclopentyllithium. The crystals were kept at $-78\text{ }^{\circ}\text{C}$ in a cold bath immediately after removing from a $-20\text{ }^{\circ}\text{C}$ freezer, the solvent was removed by syringe and the crystals were washed with anhydrous pentane. After the removal of solution by syringe, the crystals were then kept at $-78\text{ }^{\circ}\text{C}$ and evacuated for 20 min. Toluene- d_8 (0.6 mL) was then added to the crystals under argon atmosphere. The resulting solution was transferred into a sealed NMR tube via syringe at $-78\text{ }^{\circ}\text{C}$. Alternatively, tetrahydrofuran was added via syringe into a sealed NMR tube of cyclopentyllithium toluene- d_8 at $-78\text{ }^{\circ}\text{C}$. After the addition, the NMR tube was shaken vigorously at $-78\text{ }^{\circ}\text{C}$ before the signal acquisition.

For the variable temperature experiments in determining equilibrium constant and thermodynamic data, 51.1 mg of 1-dodecene was added via syringe to 0.650 mL of cyclopentyllithium toluene- d_8 solution to accurately measure the concentration of the cyclopentyllithium toluene- d_8 solution.

The internal references (in a ratio of 1:3:3:1 for BEN, COE, TDE, and SQU, respectively) were titrated into the NMR tube and monitored by $^1\text{H-NMR}$. The titration was stopped when the peak intensity of benzene was similar to the methine peak of c-PenLi.

4.5.2 Synthesis of cyclopentyllithium.¹⁴ About 1.00 g (144 mmol) of finely cut Li metal was placed into a flame-dried flask with a condenser attached and flushed with argon. The condenser was fitted with a serum septum and sealed with parafilm. The metal was washed by adding 10 mL of dry pentane to the flask via syringe. The flask was placed in an ultrasound bath for 15 minutes. Pentane was then removed via syringe. This was repeated until the washings were clear, with no white solid suspended in the wash (3

times). Dry cyclohexane or heptane (10 mL) was added to the flask, and the flask was placed in an oil bath at 50 °C with stirring. A drop of methyl *tert*-butyl ether was added to 6.33 g (60.5 mmol) of chlorocyclopentane, and the resulting solution was added via syringe to the hot lithium metal cyclohexane or heptane mixture over a period of 2.5 hours using a syringe pump. After the addition of chlorocyclopentane, the mixture was stirred overnight at room temperature, after which a purple slurry was obtained. The suspension was transferred via syringe to a clean, flame-dried vial flushed with argon and fitted with a serum septum. The vial was centrifuged until the solid was separated. The supernatant was transferred to a second identical vial and centrifuged again. The supernatant was transferred to a third identical vial. This cyclopentyllithium solution in cyclohexane or heptane was titrated using 2,2-diphenylacetic acid in tetrahydrofuran and found to be 2.0 M and 1.4 M for the cyclohexane solution and heptane solution respectively.

4.5.3 Crystallization of cyclopentyllithium. Cyclopentyllithium can be easily crystallized from hydrocarbons by storing freshly made cyclopentyllithium cyclohexane solution or heptane solution at -20 °C overnight. A significant amount of colorless cyclopentyllithium crystals are obtained. XRD quality crystals are obtained directly from the heptane solution of cyclopentyllithium. Alternatively, the crystals were re-dissolved in toluene and the solution was stored at -20 °C for a few days before the appearance of colorless cyclopentyllithium crystals.

4.5.4 Crystallization of cyclopentyllithium tetrahydrofuran adduct. To a 0.2 mL cyclopentyllithium heptane solution in a flame-dried vial under argon atmosphere at -20 °C was added 2 mL anhydrous pentane. After 5 min, 0.1 mL of THF was added to the

solution. The solution was shaken vigorously at -20 °C and stored at -20 °C. Colorless XRD quality crystals appeared after 2 hours.

4.6 Acknowledgement

The author thanks Dr. Russell Hopson.

4.7 References

- (1) (a) Rappoport, Z., Marek, I., Eds. *The Chemistry of Organolithium Compounds*; John Wiley & Sons, Ltd.: West Sussex, 2004. (b) Clayden, J. *Organolithiums: Selectivity for Synthesis*; Pergamon: Oxford, 2002. (c) Hodgson, D. *Organolithiums in Enantioselective Synthesis*; Springer: New York, 2003. (d) Trost, B. M., Fleming, I., Eds. *Comprehensive Organic Synthesis*; Pergamon: Oxford, 1991. (e) Wu, G.; Huang, M. *Chem. Rev.* **2006**, *106*, 2596–2616. (f) Collum, D. B.; McNeil, A. J.; Ramirez, A. *Angew. Chem. Int. Ed.* **2007**, *46*, 3002-3017. (g) Lucht, B.; Collum, D. *Acc. Chem. Res.* **1999**, *32*, 1035-1042. (h) Snieckus, V. *Chem. Rev.* **1990**, *90*, 879-933.
- (2) (a) Evans, D. A.; Andrews, G. C. *Acc. Chem. Res.* **1974**, *7*, 147-155. (b) Still, W. C.; Macdonald, T. L. *J. Am. Chem. Soc.* **1974**, *96*, 5561-5563. (c) Carbone, G.; O'Brien, P.; Hilmersson, G. *J. Am. Chem. Soc.* **2010**, *132*, 15445-15450. (d) Coldham, I.; Leonori, D. *Org. Lett.* **2008**, *10*, 3923-3925. (e) Wu, S.; Lee, S.; Beak, P. *J. Am. Chem. Soc.* **1996**, *118*, 715-721. (f) Lutz, G. P.; Du, H.; Gallagher, D. J.; Beak, P. *J. Org. Chem.* **1996**, *61*, 4542-4554. (g) Herbert, S. A.; Arnott, G. E. *Org. Lett.* **2009**, *11*, 4986-4989.
- (3) (a) Crandall, J. K.; Clark, A. C. *J. Org. Chem.* **1972**, *37*, 4236-4242. (b) Al-Aseer, M. A.; Allison, B. D.; Smith, S. G. *J. Org. Chem.* **1985**, *50*, 2715-2719. (c) Schrock, R. R.; Shih, K.; Dobbs, D. A.; Davis, W. M. *J. Am. Chem. Soc.* **1995**, *117*, 6609-6610. (d) Schrock, R. R.; Seidel, S. W.; Mosch-Zanetti, N. C.; Dobbs, D. A.; Shih, K.; Davis, W. M. *Organometallics* **1997**, *16*, 5195-5200. (e) Weber, L.; Meyer, M.; Stammer, H.; Neumann, B. *Organometallics* **2003**, *22*, 5063-5068. (f) Toba, T.; Murata, K.; Futamura, J.; Nakanishi, K.; Takahashi, B.; Takemoto, N.; Tomino, M.; Nakatsuka, T.; Imajo, S.; Goto, M.; Yamamura, T.; Miyake, S.; Annoura, H. *Bioorg. Med. Chem.* **2012**, *20*, 2850-2859. (g) Chai, G.; Fu, C.; Ma, S. *Org. Lett.* **2012**, *14*, 4058-4061. (h) Green, J. C.; Brown, E. R.; Pettus, T. R. R. *Org. Lett.* **2012**, *14*, 2929-2931. (i) Narayan, R.; Frohlich, R.; Wurthwein, E. *J. Org. Chem.* **2012**, *77*, 1868-1897. (j) Fournier, A. M.; Clayden, J. *Org. Lett.* **2012**, *14*, 142-145. (k) Tait, M.; Donnard, M.; Minassi, A.; Lefranc, J.; Bechi, B.; Carbone, G.; O'Brien, P.; Clayden, J. *Org. Lett.* **2013**, *15*, 34-37.
- (4) (a) West, P.; Waack, R.; Purmort, J. I. *J. Am. Chem. Soc.* **1970**, *92*, 840-845. (b) McGarrity, J. F.; Ogle, C. A.; Brich, Z.; Loosli, H. *J. Am. Chem. Soc.* **1985**, *107*, 1810-1815. (c) Bates, T. F.; Clarke, M. T.; Thomas, R. D. *J. Am. Chem. Soc.* **1988**, *110*, 5109-5112. (d) Ogle, C. A.; Johnson IV, H. C.; Wang, X. L.; Strickler, F. H.; Bucca, D.; Gordon III, B. *Macromolecules* **1995**, *28*, 5184-5191. (e) Lucht, B. L.; Bernstein, M. P.; Remenar, J. F.; Collum, D. B. *J. Am. Chem. Soc.* **1996**, *118*, 10707-10718. (f) Reich, H. J.; Green, D. P.; Medina, M. A.; Goldenberg, W. S.; Gudmundsson, B. O.; Dykstra, R. R.; Phillips, N. H. *J. Am. Chem. Soc.* **1998**, *120*, 7201-7210. (g) Rutherford, J. L.; Hoffmann, D.; Collum, D. B. *J. Am. Chem. Soc.* **2002**, *124*, 264-271. (h) Jones, A. C.; Sanders, A. W.; Bevan, M. J.; Reich, H. J. *J. Am. Chem. Soc.* **2007**, *129*, 3492-3493.
- (5) Stanetty, P.; Mihovilovic, M. D. *J. Org. Chem.* **1997**, *62*, 1514-1515.
- (6) (a) Nichols, M. A.; Williard, P. G. *J. Am. Chem. Soc.* **1993**, *115*, 1568-1572. (b) Barnett, N. D. R.; Mulvey, R. E.; Clegg, W.; O'Neil, P. A. *J. Am. Chem. Soc.* **1993**, *115*, 1573-1574.
- (7) (a) Ogle, C. A.; Huckabee, B. K.; Johnson, H. C. I. V.; Sims, P. F.; Winslow, S. D.; Pinkerton, A. A. *Organometallics* **1993**, *12*, 1960-1963. (b) Kottke, T.; Lagow, R. J.; Hoffmann, D.; Thomas, R. D. *Organometallics* **1997**, *16*, 789-792.
- (8) (a) Klumpp, G. W.; Geurink, P. J. A.; Spek, A. L.; Duisenberg, A. J. M. *J. Chem. Soc., Chem.*

Commun., **1983**, 814-816. (b) Spek, A. L.; Duisenberg, A. J. M.; Klumpp, G. W.; Geurink, P. J. A. *Acta Crystallographica, Section C: Cryst. Struct. Commun.*, **1984**, C40, 372-374. (c) Moene, W.; Vos, M.; De Kanter, F. J. J.; Klumpp, G. W.; Spek, A. L. *J. Am. Chem. Soc.* **1989**, *111*, 3463-3465. (d) Ahlbrecht, H.; Boche, G.; Harms, K.; Marsch, M.; Sommer, H. *Chem. Ber.* **1990**, *123*, 1853-1858. (e) Williard, P. G.; Sun, C. *J. Am. Chem. Soc.* **1997**, *119*, 11693-11694. (f) Strohmman, C.; Strohfeltdt, K.; Schildbach, D. *J. Am. Chem. Soc.* **2003**, *125*, 13672-13673. (g) Strohmman, C.; Gessner, V. H. *J. Am. Chem. Soc.* **2007**, *129*, 8952-8953. (h) Strohmman, C.; Gessner, V. H.; Damme, A. *J. Chem. Soc., Chem. Commun.*, **2008**, 3381-3383.

(9) (a) Kottke, T.; Stalke, D. *Angew. Chem., Int. Ed.* **1993**, *32*, 580-582. (b) Siemeling, U.; Redecker, T.; Neumann, B.; Stammeler, H. *J. Am. Chem. Soc.* **1994**, *116*, 5507-5508. (c) Zenger, R.; Rhine, W.; Stucky, G. *J. Am. Chem. Soc.* **1974**, *116*, 6048-6055.

(10) (a) Hoye, T. R.; Eklov, B. M.; Voloshin, M. *Org. Lett.* **2004**, *6*, 2567-2570. (b) Wetzel, T. G.; Dehnen, S.; Roesky, P. W. *Organometallics* **1999**, *18*, 3835-3842. (c) Gausing, W.; Wilke, G. *Angew. Chem., Int. Ed.* **1978**, *17*, 371-372.

(11) (a) Fraenkel, G.; Henrichs, M.; Hewitt, M.; Su, B. M. *J. Am. Chem. Soc.* **1984**, *106*, 255-256. (b) Su, C.; Hopson, R.; Williard, P. G. *Eur. J. Inorg. Chem.* **2013**, *24*, 4136-4141.

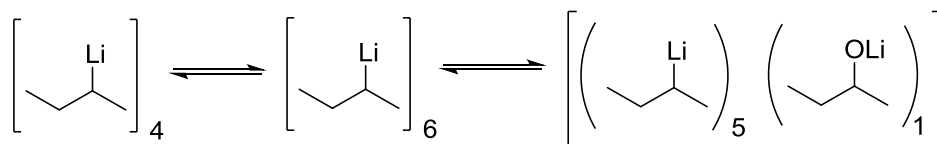
(12) (a) Li, D.; Hopson, R.; Li, W.; Liu, J.; Williard, P. G. *Org. Lett.* **2008**, *10*, 909-911. (b) Li, D.; Sun, C.; Williard, P. G. *J. Am. Chem. Soc.* **2008**, *130*, 11726-11736. (c) Li, D.; Sun, C.; Liu, J.; Hopson, R.; Williard, P. G. *J. Org. Chem.* **2008**, *73*, 2373-2381. (d) Liu, J.; Li, D.; Sun, C.; Williard, P. G. *J. Org. Chem.* **2008**, *73*, 4045-4052. (e) Li, D.; Kagan, G.; Hopson, R.; Williard, P. G. *J. Am. Chem. Soc.* **2009**, *131*, 5627-5634. (f) Li, D.; Keresztes, I.; Hopson, R.; Williard, P. G. *Acc. Chem. Res.* **2009**, *42*, 270-280. (g) Kagan, G.; Li, W.; Hopson, R.; Williard, P. G. *Org. Lett.* **2009**, *11*, 4818-4821. (h) Kagan, G.; Li, W.; Hopson, R.; Williard, P. G. *Org. Lett.* **2010**, *12*, 520-523. (i) Li, W.; Kagan, G.; Yang, H.; Cai, C.; Hopson, R.; Sweigart, D. A.; Williard, P. G. *Org. Lett.* **2010**, *12*, 2698-2701. (j) Li, W.; Kagan, G.; Yang, H.; Cai, C.; Hopson, R.; Dai, W.; Sweigart, D. A.; Williard, P. G. *Organometallics*. **2010**, *29*, 1309-1311. (k) Socha, A. M.; Kagan, G.; Li, W.; Hopson, R.; Sello, J. K.; Williard, P. G. *Energy Fuels* **2010**, *24*, 4518-4521. (l) Kagan, G.; Li, W.; Sun, C.; Hopson, R.; Williard, P. G. *J. Org. Chem.* **2011**, *76*, 65-70. (m) Kagan, G.; Li, W.; Li, D.; Hopson, R.; Williard, P. G. *J. Am. Chem. Soc.* **2011**, *133*, 6596-6602. (n) Lecachey, B.; Oulyadi, H.; Lameiras, P.; Harrison-Marchand, A.; Gerard, H.; Maddaluno, J. *J. Org. Chem.* **2010**, *75*, 5976-5983. (o) Consiglio, G. B.; Queval, P.; Harrison-Marchand, A.; Mordini, A.; Lohier, J.; Delacroix, O.; Gaumont, A.; Gerard, H.; Maddaluno, J.; Oulyadi, H. *J. Am. Chem. Soc.* **2011**, *133*, 6472-6480.

(13) (a) Li, W.; Kagan, G.; Hopson, R.; Williard, P. G. *ARKIVOC* **2011**, 180-187. (b) Keresztes, I.; Williard, P. G. *J. Am. Chem. Soc.* **2000**, *122*, 10228-10229. (c) McGarrity, J. F.; Ogle, C. A. *J. Am. Chem. Soc.* **1985**, *107*, 1805-1810.

(14) Smith, W. N.; (Metallgesellschaft A.-G.). Application: DE, 1969, 8 pp (German patent).

Chapter 5

Characterization of hexameric and octameric *sec*-butyllithium/*sec*-butoxide mixed aggregates



5.1 Abstract

Solution state characterization of *sec*-butyllithium in toluene-*d*₈ was conducted by utilizing a variety of NMR experiments including diffusion-ordered NMR spectroscopy (DOSY) with diffusion coefficient-formula weight correlation analyses and other one- and two-dimensional NMR techniques. Those results suggest that *sec*-butyllithium exists primarily as a mixture of tetramer and hexamer in hydrocarbon solvents. However, the presence of roughly 2-5 % by mole ratio in all samples of lithium *sec*-butoxide in both commercially available and laboratory synthesized *sec*-butyllithium solution due to the reaction with adventitious dioxygen will lead to the formation of a 1:5 *sec*-butoxide/*sec*-butyllithium mixed hexamer. A *sec*-butoxide/*sec*-butyllithium mixed octamer will emerge when the proportion of butoxide to butyllithium increases.

5.2 Introduction

Organolithium reagents are among the most widely used reagents in organic synthesis.¹ Alkyl-lithium reagents, especially butyllithiums, are the source of most organolithium reagents since they can efficiently generate a wide variety of carbanions such as lithium amide, acetylide and alkoxide.¹ Moreover, the gaseous by-product butane is a saturated hydrocarbon which can be easily eliminated. As a result, butyllithium reagents have been a focus of research of several groups for more than 40 years.^{1,2} Unlike *n*-butyllithium (*n*-BuLi) and *tert*-butyllithium (*t*-BuLi), the racemic nature of *sec*-butyllithium (*s*-BuLi) makes it hard to form single crystal. Until now, only two crystal structures containing *s*-BuLi were reported³ and thus, solution state studies play a critical

role in revealing the aggregation state of *s*-BuLi.^{2f,1,4} By using ⁶Li and ¹³C NMR, Fraenkel and his coworkers proposed that *s*BuLi in hydrocarbon media exists as a mixture of hexamer and tetramer with a tiny amount of dimer at very high concentration.⁵ However, the assignment cannot be established unambiguously because the experimental results are also consistent with other possible complexes. Moreover, McGarrity and his coworkers showed that *n*-BuLi commonly contains *n*-butoxide because of its reaction with dioxygen⁶ and the *n*-butoxide can readily form mixed tetramers with *n*-BuLi in tetrahydrofuran (THF). They also showed that there are rate differences between *n*-BuLi aggregates and *n*BuLi/Lithium butoxide mixed aggregates toward the reaction of *n*-BuLi with benzaldehyde.⁷ Being a similar species, it will not be surprising if a substoichiometric amount of lithium *sec*-butoxide (*s*-BuOLi) is present in a *s*-BuLi solution. We find that a small amount of *s*-BuOLi is present in both brand new commercial and laboratory synthesized *s*-BuLi solutions. The preparation of butoxide free *s*-BuLi solution appears to be very difficult since there is no known method to crystallize *s*-BuLi. The mixed aggregate formation of *s*BuLi/*s*BuOLi and the characterization of hexameric and octameric *s*BuLi/*s*BuOLi mixed aggregates are presented. A variety of mixed aggregates are reported although the influence of these species remains uncertain.⁸

5.3 Results and Discussion

5.3.1 Characterization of hexameric *s*-BuLi/*s*-BuOLi mixed aggregate

We first examined the ¹H NMR of *s*-BuLi in toluene-*d*₈ which is unreactive to alkyl lithium reagents in the absence of coordinating ligand such as THF or *N,N,N',N'*-

tetramethylethylenediamine (TMEDA) at room temperature.⁹ The proton NMR shows 3 peaks in the methine region of *s*-BuLi. In an attempt to reveal the nature of the peaks, variable-temperature NMR study with 1-dodecene (DDE) as internal reference was carried out and the result was shown in Figure 5.1. Upon decrease in temperature, the resonance at -1.16 ppm decreases significantly in intensity and the resonance at -0.88 ppm increases clearly while the middle resonance at -0.97 ppm has no significant change. The total concentration of *s*-BuLi is determined by comparing the integrations of internal standard and the methine signals,^{9a} while the ratios between the three peaks were obtained by Lorentzian deconvolution,¹⁰ and thus, the concentration of each species could be determined. According to Fraenkel's report, *s*-BuLi exists mainly as a hexamer and a tetramer in hydrocarbon solvents,⁵ accordingly we assigned the peak at -0.88 ppm as a hexamer and at -1.16 ppm as tetramer. In order to verify our assignment, a dilution experiment at -30 °C was performed and the result is summarized in Table 5.1.

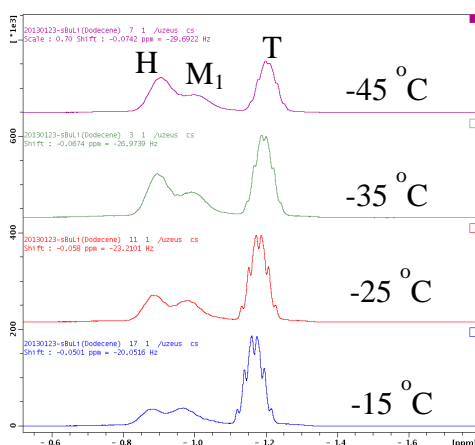
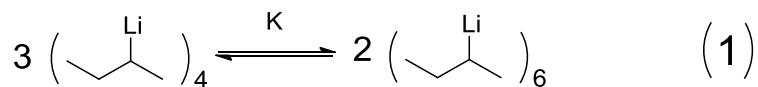


Figure 5.1. Variable temperature ¹H NMR (400 MHz) spectra of 0.49 M *s*-BuLi in toluene-*d*₈. H represents the methine signal of *s*BuLi in hexamer, T represents the signal in tetramer and M₁ represents the signal in *s*-BuLi/*s*-BuOLi mixed hexamer.



Scheme 5.1. The equilibrium reaction of the hexameric and tetrameric complexes of *s*-BuLi

Table 5.1. Concentrations of *s*-BuLi complexes and the equilibrium constant (K) at -30 °C in toluene-*d*₈

[<i>s</i> BuLi] _{total} , M	[<i>s</i> BuLi] _a at -0.88 ppm, M	[<i>s</i> BuLi] _b at -1.16 ppm, M	$K = \frac{([s-BuLi]_a/6)^2}{([s-BuLi]_b/4)^3}$
0.487	0.113	0.246	1.54 M ⁻¹
0.332	0.068	0.176	1.47 M ⁻¹
0.248	0.048	0.135	1.71 M ⁻¹

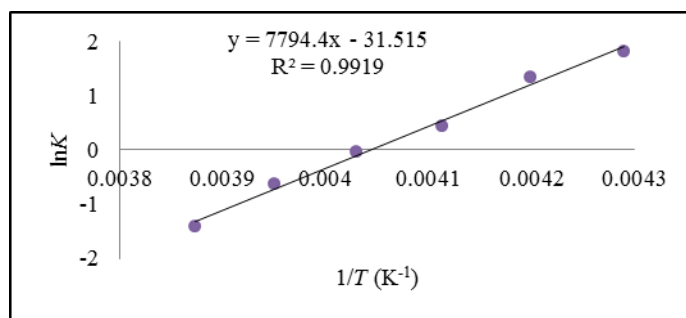


Figure 5.2. The van 't Hoff plot of reaction (1).

The result supports our peak assignment because the calculated equilibrium constants are very similar. The enthalpy (ΔH) and entropy (ΔS) of the equilibrium reaction 1 (Scheme 5.1) were then determined by linear regression (Figure 5.2). The enthalpy and entropy were calculated to be -64.8 kJmol⁻¹ and -262 Jmol⁻¹K⁻¹ respectively. Compared with the cyclopentane solution of *s*-BuLi in which the ΔH and ΔS are -29 kJmol⁻¹ and -117 Jmol⁻¹K⁻¹ respectively,⁵ the toluene solution of *s*BuLi favors the formation of

hexamer when the temperature is below $-27\text{ }^{\circ}\text{C}$ and favors the formation of tetramer when the temperature is above $-27\text{ }^{\circ}\text{C}$.

There is evidence that butyllithium can react with adventitious dioxygen to form butoxide which is known to form mixed aggregates with butyllithium⁶ and thus, it is very probable that the unknown peak at -0.97 ppm may belong to a mixed aggregate. To substantiate this prediction, we deliberately added pure dioxygen gas or *sec*-butanol into *s*-BuLi samples. Upon the addition of dioxygen or *sec*-butanol, the intensity of the unknown peak increases simultaneously with a peak at 3.44 ppm which is the methine proton of *s*-BuOLi (Figure 5.3).

This observation confirms that the unknown peak at -0.97 ppm belongs to the methine proton of *s*-BuLi in a *s*-BuLi/*s*-BuOLi mixed aggregate. The fact that the ratio of the integration of the methine peak of *s*BuOLi to *s*BuLi is about 1 to 5 leads to the conclusion that it is a 5:1 mixed hexamer. Thomas and her coworkers reported that *t*-BuLi can form 1:5 and 2:4 *t*-BuLi/*t*-BuOLi mixed hexamers;¹¹ however, their interpretation was based on the hexameric nature of *t*-BuOLi can exist as hexamer or octamer in hydrocarbon solvents as reported by Henderson.¹²

In order to unambiguously establish the hexameric structure of the mixed aggregate, diffusion-ordered NMR spectroscopy (DOSY) and diffusion coefficient-formula weight (*D*-FW) correlation analyses were conducted to evaluate the formula weight of the mixed aggregate. Our group previously applied DOSY NMR with internal references for the determination of formula weights of reactive complexes by *D*-FW correlation analysis. The linear regression plot of the logarithms of NMR determined diffusion coefficients

against the known formula weights of the references is used to deduce the formula weight of unknown complex from its diffusion characteristics.¹³ In this proton DOSY experiment, benzene (BEN, 78.11 g/mol), cyclooctene (COE, 110.2 g/mol), 1-tetradecene (TDE, 196.4 g/mol) and squalene (SQU, 410.7 g/mol) were added to the sample solution as our internal references.

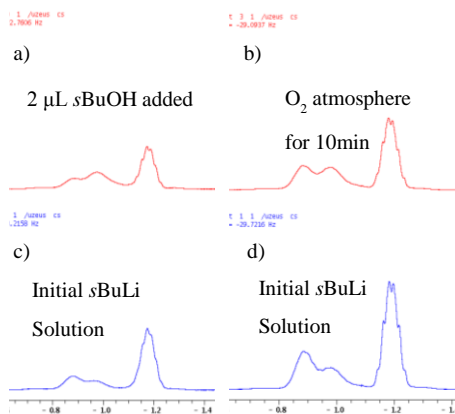


Figure 5.3. The ^1H NMR (400 MHz) spectra of the methine of 0.49 M *s*-BuLi in toluene- d_8 , showing the initial *s*-BuLi solution (c, d), solution after 2 μL *s*-BuOH was added (a) and solution after exposing in dioxygen atmosphere for 10 minutes (b).

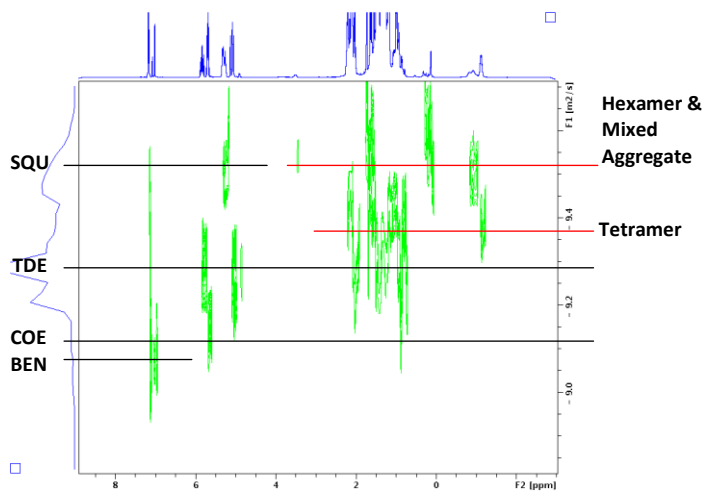


Figure 5.4. ^1H DOSY of *s*-BuLi toluene- d_8 solution at $-20\text{ }^\circ\text{C}$

After the addition of internal references into the toluene- d_8 solution of *s*-BuLi, the signals of methyl and methylene protons of *s*-BuLi and *s*-BuOLi from 1.0 to 2.5 ppm were overlapped with the signals from the internal references; thus, distinct peaks from the methine protons were picked for our *D*-FW analysis. As seen in the DOSY spectrum (Figure 5.4), the methine peaks of *s*-BuOLi and *s*-BuLi have very similar diffusion coefficients.

The correlation between \log FW and $\log D$ of the linear regression is very high ($r^2 > 0.99$) and the predicted formula weight for the resonance of tetrameric *s*-BuLi (-1.16 ppm) is 255.7 gmol^{-1} which is very close to actual value 256.2 gmol^{-1} (0.2 % error) (Figure 5.5). The predicted formula weight for the resonance of hexameric *s*-BuLi (-0.88 ppm) is 401.2 gmol^{-1} (4.4 % error) and the predicted formula weight for the resonance of the mixed aggregate at -0.97 ppm is 401.9 gmol^{-1} which is very close to the formula weight of the 1:5 *s*-BuOLi /*s*-BuLi (400.3 gmol^{-1} , 1.0 % error). The predicted formula weight for the resonances of the mixed aggregate at 3.6 ppm is found to be 426.0 gmol^{-1} (6.4 % error). Given the intrinsic 10 % error in the formula weight prediction of the DOSY technique,¹³ we were unable to distinguish the 1:5 mixed hexamer (ROLi)(RLi)₅ from the 2:4 mixed hexamer (ROLi)₂(RLi)₄ by the predicted molecular weight solely. However, the integral ratio of the methine peak of *s*-BuOLi to *s*-BuLi is approximately 1 to 5 when there is less than 0.08 equivalent *s*-BuOLi. This indicates that 1:5 mixed hexamer should be the major species. The integral ratio cannot be determined when there is more than 0.08 equivalent *s*-BuOLi in the solution because a new mixed aggregate peak overlaps seriously with the *s*-BuLi methine peaks of other aggregates. We also note that the butoxide proportion in *s*-BuOLi/*s*-BuLi mixed hexamer (1:5) is significantly lower than

the *t*-BuOLi/*t*-BuLi mixed hexamer (5:1 or 4:2) reported by Thomas¹¹ because the decrease in steric hindrance of the butyl group allows a higher ratio of butyllithium in the complex.

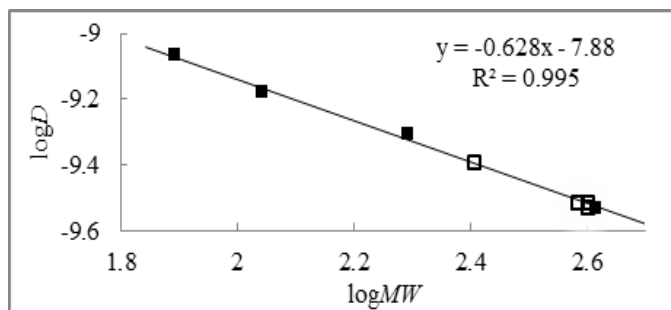


Figure 5.5. *D*-FW analysis of ¹H DOSY data. Internal references are shown as solid squares and the complexes are shown as open squares.

5.3.2 Characterization of octameric *s*-BuLi/*s*-BuOLi mixed aggregate

When more than 0.1 equivalent of *s*-BuOH was added to the *s*-BuLi solution, a small peak emerged at 3.63 ppm and its intensity continued to increase when more *s*-BuOH was added (Figure 5.6). Moreover, a methine peak of *s*-BuLi at -1.06 ppm was observed to increase with the ascending *s*-BuOLi peak. The result indicated another type of *s*-BuOLi/*s*-BuLi mixed aggregate was formed. The fact that the new peak at 3.63 ppm which can only belong to the methine proton of *s*-BuOLi increases at the expense of the methine peak of *s*-BuOLi of the mixed hexamer when the temperature decreases from -20 °C to -40 °C indicates that the new mixed aggregate should be larger than a hexamer (Figure 5.7).

To establish the aggregation state of the new mixed aggregate in solution, we applied the same ¹H DOSY and *D*-FW analysis to the *s*-BuOLi/*s*-BuLi toluene-*d*₈ solution. Two

weight of 464.3 gmol^{-1} which is significantly smaller than the experimental results. Consequently, an octameric structure is proposed for the structure of the new mixed aggregate. However, it is not obvious whether the mixed aggregate is a 2:6 *s*-BuOLi/*s*-BuLi mixed octamer which has a formula weight of 544.5 gmol^{-1} or a 4:4 mixed octamer (576.4 gmol^{-1}) because our *D*-FW DOSY technique has an intrinsic 10 % error. The integrations of the methine peaks in the ^1H NMR spectrum cannot be compared quantitatively as noted above. We believe that this new aggregate is more likely to be a 4:4 mixed complex because a 2:6 mixed aggregate should have a higher intensity methine peak of *s*-BuLi and the mixed octamer may possibly adopt the same pattern as the crystal structure of $(n\text{-BuLi})_4(t\text{-BuOLi})_4$ octamer obtained by Boche;^{8b} however, no definitive evidence is present. Nevertheless, it is evident that a *s*-BuOLi/*s*-BuLi mixed octamer is present when there is between 0.08 to 2 equivalent of *s*-BuOLi in the toluene solution of *s*-BuLi. The characterization of an octamer in solution state by conventional ^6Li - ^{13}C coupling is exceptionally difficult because the outermost peaks of the multiplets can hardly be distinguished¹¹ and the racemic nature of *s*-BuLi further complicates the spectra.

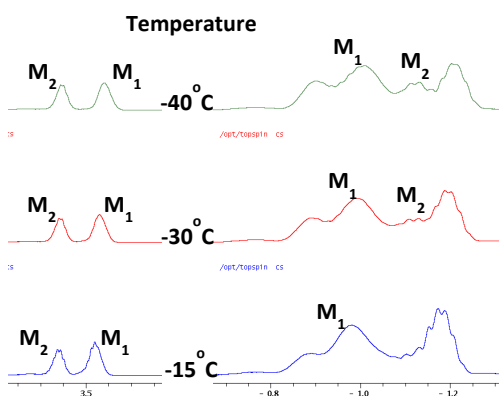


Figure 5.7. Variable temperature ^1H NMR (400 MHz) spectra of 2:7 *s*-BuOLi to *s*-BuLi toluene- d_8 solution. M_1 represents the resonances of *s*-BuLi and *s*-BuOLi in mixed hexamer; M_2 represents the resonances of *s*-BuLi and *s*-BuOLi in mixed octamer.

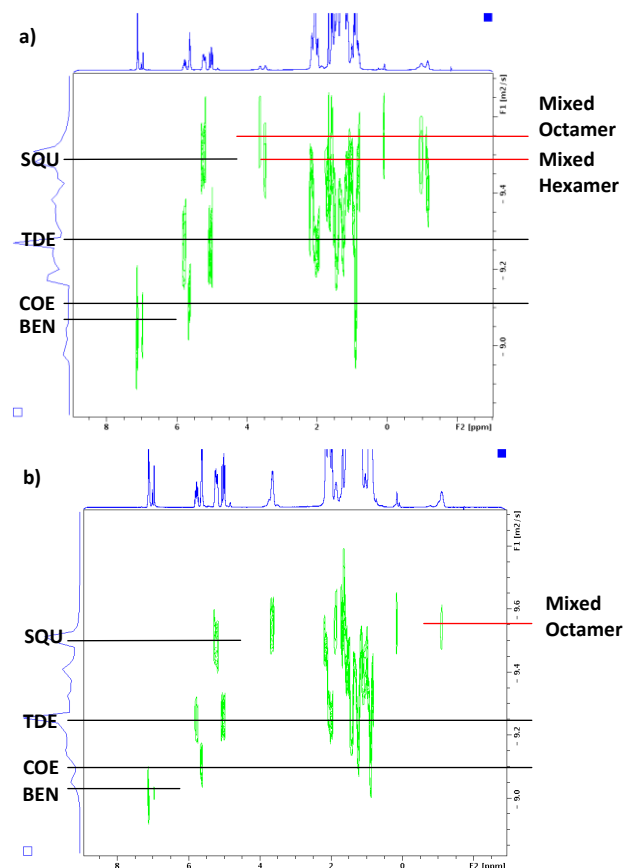


Figure 5.8. ^1H DOSY of *s*-BuLi/*s*-BuOLi toluene- d_8 solution at $-20\text{ }^\circ\text{C}$. The ratio of *s*-BuOLi to *s*-BuLi is 2:7 in (a) and 5:3 in (b).

5.4 Conclusion

In summary, *s*-BuLi exists mainly as a mixture of tetramer and hexamer in hydrocarbon solvents. However, the presence of a small amount of *s*-BuOLi in both commercially available and laboratory synthesized *s*BuLi solution due to the reaction of *s*-BuLi with adventitious dioxygen definitely leads to the formation of a 1:5 *s*-BuOLi/*s*-BuLi mixed hexamer that is difficult to avoid. A mixed *s*-BuOLi/*s*-BuLi mixed octamer will emerge when the proportion of *s*-BuOLi to *s*-BuLi increases. The effectiveness of DOSY NMR with *D*-FW correlation analyses over the conventional ^6Li - ^{13}C coupling

experiments in revealing the aggregation states of the *s*-BuOLi/*s*-BuLi complexes is clearly useful in this analysis.

5.5 Experimental Section

The values of concentration were expressed as monomer units unless otherwise specified.

The *sec*-butanol used in the NMR experiments was distilled over calcium hydride under nitrogen gas and stored over 4 Å molecular sieves prior to usage.

The 2-chlorobutane used in the synthesis of *sec*-butyllithium was dried over anhydrous calcium chloride under nitrogen gas and stored over 4 Å molecular sieves prior to usage.

5.5.1 Procedures for NMR Experiments. NMR samples were prepared in tubes sealed with rubber septa cap purchased from Aldrich and parafilm. NMR tubes were evacuated *in vacuo*, flame-dried and filled with argon before use. ¹H chemical shifts were referenced to toluene-*d*₈ at 7.09 ppm and ¹³C chemical shifts were referenced to toluene-*d*₈ at 137.86 ppm. All NMR experiments were acquired on a Bruker DRX400 spectrometer equipped with an Accustar z-axis gradient amplifier and an ATMA BBO probe with a z-axis gradient coil. Maximum gradient strength was 0.214 T/m. ¹H DOSY was performed using the standard Bruker dstebppg3s program, employing a double stimulated echo sequence, bipolar gradient pulses for diffusion, and 3 spoil gradients. Diffusion time was 200 ms, and the rectangular gradient pulse duration was 800 μs. Gradient recovery delays were 200 μs. Individual rows of the quasi-2-D diffusion

databases were phased and baseline corrected. Actual diffusion coefficients used for *D*-FW analysis were obtained in the Bruker Topspin software using the T1/T2 analysis module. Lorentzian deconvolution was performed on the overlapping methine protons using t Bruker's Topspin 3.2 software.

The *sec*-butyllithium (*s*-BuLi) toluene-*d*₈ solution was prepared by either commercially available *sec*-butyllithium cyclohexane solution (Aldrich, 1.4 M) or laboratory synthesized *sec*-butyllithium cyclohexane solution (1.06 M). The samples were prepared in two methods:

Method 1: About 200 μ L of the *s*-BuLi cyclohexane solution was added via syringe to a NMR tube (A PTFE filter purchased from VWR International was required for preparing the sample from commercial *s*-BuLi solution because the solution was milky with some solid materials even though it was brand new). Toluene-*d*₈ was added via syringe to bring the total volume up to 600 μ L.

Method 2: After the addition of 200 μ L *s*-BuLi cyclohexane solution to a NMR tube, the NMR tube was evacuated in vacuo for 30 minutes at 0 °C in order to remove the cyclohexane. After filling with argon, toluene-*d*₈ was added via syringe to bring the total volume up to 600 μ L or 650 μ L.

Method 2 was implemented for most of the time because the spectrum obtained was cleaner due to the elimination of cyclohexane.

For the variable temperature experiments in determining equilibrium constant and thermodynamic data, about 20 mg of 1-dodecene was added via syringe to the solution in

order to accurately measure the concentration of the *s*-BuLi toluene-*d*₈ solution. The exact mass of 1-dodecene added was accurately measured.

The concentration of *s*-BuLi was about 0.4 M. The internal references (in a ratio of 1:3:3:1 for BEN, COE, TDE, and SQU, respectively) were titrated into the NMR tube and monitored by ¹H NMR. The titration was stopped when the peak intensity of benzene was about half that of *s*-BuLi.

5.5.2 Synthesis of *s*-BuLi. About 1.00 g (144 mmol) of finely cut Li metal was placed into a flame-dried flask with a condenser attached that was flushed with argon. The condenser was fitted with a serum septum and sealed with parafilm. The metal was washed with dry pentane by adding 10 mL of pentane to the flask via syringe. The flask was then placed in an ultrasound bath for 15 minutes. Pentane was then removed via syringe. This was repeated until the washings were clear, with no white solid suspended in the wash (3 times). Dry cyclohexane (10 mL) was added to the flask and the flask was placed in an oil bath at 50 °C with stirring. A drop of methyl *tert*-butyl ether was added to 5.60 g (60.5 mmol) of 2-chlorobutane and the resulting solution was added via syringe to the hot lithium metal cyclohexane mixture in 2.5 hours using a syringe pump. After the addition of 2-chlorobutane, the mixture was stirred overnight at room temperature, after which a purple slurry was obtained. The suspension was transferred via syringe to a clean, flame-dried vial flushed with argon and fitted with a serum septum. The vial was centrifuged until the solid was separated. The supernatant was transferred to a second identical vial and centrifuged again. The supernatant was transferred to a third identical vial. This *s*-BuLi solution in cyclohexane was titrated using 2,2-diphenylacetic acid in tetrahydrofuran and found to be 1.06 M. Note worthily, the light yellow transparent

*s*BuLi solution turned milky after sitting in a -20 °C freezer for about 7 to 14 days. NMR samples were prepared from the transparent *s*-BuLi solution.

5.6 Acknowledgement

The author wishes to thank Dr. Russell Hopson for his advice.

5.7 References

- (1) a) Z. Rappoport, I. Marek, (Eds.) *The Chemistry of Organolithium Compounds*; John Wiley & Sons, Ltd.: West Sussex, 2004; b) J. Clayden, *Organolithiums: Selectivity for Synthesis*; Pergamon: Oxford, 2002; c) D. Hodgson, *Organo-lithiums in Enantioselective Synthesis*; Springer: New York, 2003; d) B. M. Trost, I. Fleming, (Eds.) *Comprehensive Organic Synthesis*; Pergamon: Oxford, 1991; e) G. Wu, M. Huang, *Chem. Rev.* **2006**, *106*, 2596–2616.
- (2) a) Z. K. Cheema, G. W. Gibson, J. F. Eastham, *J. Am. Chem. Soc.* **1963**, *85*, 3517-3518; b) T. L. Brown, *Acc. Chem. Res.* **1968**, *1*, 23–31; c) L. D. McKeever, R. Waack, *J. Chem. Soc. D* **1969**, 750-751; d) M. Y. Darensbourg, B. Y. Kimura, G. E. Hartwell, T. L. Brown, *J. Am. Chem. Soc.* **1970**, *92*, 1236-1242; e) T. L. Brown, *Pure Appl. Chem.* **1970**, *23*, 447-462; f) J. M. Catala, G. Clouet, J. Brossas, *J. Organomet. Chem.* **1981**, *219*, 139-143; g) R. D. Thomas, M. T. Clarke, R. M. Jensen, T. C. Young, *Organometallics*, **1986**, *5*, 1851-1857; h) R. D. Thomas, R. M. Jensen, T. C. Young, *Organometallics* **1987**, *6*, 565-571; i) W. Bauer, W. R. Winchester, P. von Rague Schleyer, *Organometallics* **1987**, *6*, 2371-2379; j) O. Eppers, H. Gunther, *Tetrahedron Lett.* **1989**, *30*, 6155-6158. k) K. Bergander, R. He, N. Chandrakumar, O. Eppers, H. Gunther, *Tetrahedron* **1994**, *50*, 5861-5868; l) J. M. Saa, G. Martorell, A. Frontera, *J. Org. Chem.* **1996**, *61*, 5194-5195; m) P. Stanetty, M. D. Mihovilovic, *J. Org. Chem.* **1997**, *62*, 1514-1515; n) G. T. DeLong, D. Hoffmann, H. D. Nguyen, R. D. Thomas, *J. Am. Chem. Soc.* **1997**, *119*, 11998-11999; o) D. Hoffmann, D. B. Collum, *J. Am. Chem. Soc.* **1998**, *120*, 5810-5811; p) J. L. Rutherford, D. Hoffmann, D. B. Collum, *J. Am. Chem. Soc.* **2002**, *124*, 264-271; q) G. Hilmersson, B. Malmros, *Chem. Eur. J.* **2001**, *7*, 337-341; r) B. Qu, D. B. Collum, *J. Am. Chem. Soc.* **2006**, *128*, 9355-9360; s) A. C. Jones, A. W. Sanders, M. J. Bevan, H. J. Reich, *J. Am. Chem. Soc.* **2007**, *129*, 3492-3493; t) C. Strohmam, V. H. Gessner, *Angew. Chem. Int. Ed.* **2007**, *46*, 8281-8283.
- (3) a) P. Williard, C. Sun, *J. Am. Chem. Soc.* **1997**, *119*, 11693-11694; b) C. Strohmam, V. H. Gessner, *J. Am. Chem. Soc.* **2007**, *129*, 8952-8953.
- (4) a) J. B. Smart, R. Hogan, P. A. Scherr, Linda Ferrier, J. P. Oliver; *J. Am. Chem. Soc.*, **1972**, *94*, 8371–8375; b) S. Bywater, P. Lachance, D. J. Worsfold, *J. Phys. Chem.* **1975**, *79*, 2148-2153.
- (5) G. Fraenkel, M. Henrichs, M. Hewitt, B. M. Su, *J. Am. Chem. Soc.*, **1984**, *106*, 255-256.
- (6) J. F. McGarrity, C. A. Ogle, *J. Am. Chem. Soc.*, **1985**, *107*, 1805-1810.
- (7) J. F. McGarrity, C. A. Ogle, Z. Brich, H. R. Loosli, *J. Am. Chem. Soc.*, **1985**, *107*, 1810-1815.
- (8) a) Seebach, D. *Angewandte Chemie* **1988**, *100*, 1685-1715; b) M. Marsch, K. Harms, L. Lochmann, G. Boche, *Angew. Chem. Int. Ed.* **1990**, *29*, 308-309; c) Hoffman, D.; Kottke, T.; Lagow, R. J.; Thomas, R. D. *Angew. Chem., Int. Ed.* **1998**, *37*, 1537-1539; d) Lochmann, L. *Eur. J. Inorg. Chem.* **2000**, 1115-1126; e) Andrews, P. C.; Fallon, G. D.; Maguire, M.; Peatt, A. C. *Angew. Chem., Int. Ed.* **2000**, *39*, 4516-4518. f) Goldfuss, B.; Steigelmann, M.; Rominger, F.; Urtel, H. *Chem. Eur. J.* **2001**, *7*, 4456-4464; g) Mueller, G.; Schaetzle, T. *Z. Naturforsch., B Chem. Sci.* **2004**, *59*, 1400-1410.
- (9) a) W. Gausing, G. Wilke, *Angew. Chem. Int. Ed.* **1978**, *17*, 371-372; b) T. G. Wetzels, S. Dehnen, P. W. Roesky, *Organometallics* **1999**, *18*, 3835-3842; c) T. R. Hoye, B. M. Eklov, M. Voloshin, *Org. Lett.* **2004**, *6*, 2567-2570.
- (10) a) K. R. Metz, M. M. Lam, A. G. Webb, *Concepts Magn. Reson.* **2000**, *12(1)*, 21-42; b) R. Laatikainen, M. Niemitz, W. J. Malaisse, M. Biesemans, R. Willem, *Magn. Reson. Med.* **1996**,

36(3), 359-365; c) G. A. Morris, *J. Magn. Reson.* **1988**, *80*, 547-552; d) A. A. De Graaf, J. E. Van Dijk, W. M. M. J. BoeE, *Magn. Reson. Med.* **1990**, *13*, 343-357; e) A. Gibbs, G. A. Morris, *J. Magn. Reson.* **1991**, *91*, 77-83.

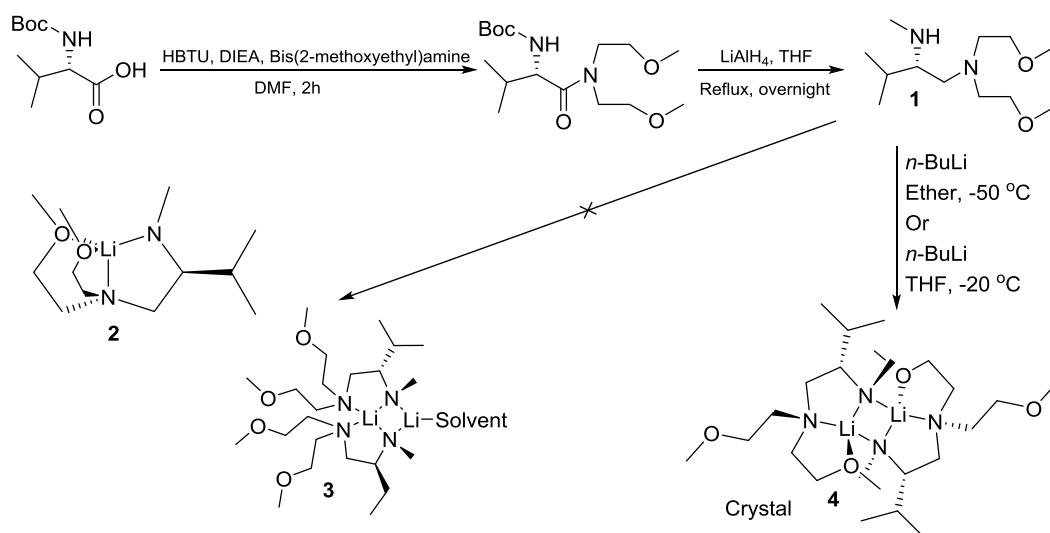
(11) G. T. DeLong, D. K. Pannell, M. T. Clarke, R. D. Thomas, *J. Am. Chem. Soc.*, **1993**, *115*, 7013-7014.

(12) J. F. Allan, R. Nassar, E. Specht, A. Beatty, N. Calin, K. W. Henderson, *J. Am. Chem. Soc.*, **2004**, *126*, 484-485.

(13) a) Li, D.; Sun, C.; Liu, J.; Hopson, R.; Li, W.; Williard, P. G. *J. Org. Chem.* **2008**, *73*, 2373-2381. b) Kagan, G.; Li, W.; Li, D.; Hopson, R.; Williard, P. G. *J. Am. Chem. Soc.* **2011**, *133*, 6596-6602. c) Liu, J.; Li, D.; Sun, C.; Williard, P. G.; *J. Org. Chem.* **2008**, *73*, 4045-4052. d) Li, D.; Hopson, R.; Li, W.; Liu, J.; Williard, P. G. *Org. Lett.* **2008**, *10*, 909-911. e) Li, D.; Sun, C.; Williard, P. G. *J. Am. Chem. Soc.* **2008**, *130*, 11726-11736. f) Kagan, G.; Li, W.; Hopson, R.; Williard, P. G. *Org. Lett.* **2009**, *11*, 4818-4821. g) Kagan, G.; Li, W.; Hopson, R.; Williard, P. G. *Org. Lett.* **2010**, *12*, 520-523. h) Lecachey, B.; Oulyadi, H.; Lameiras, P.; Harrison-Marchand, A.; Gerard, H.; Maddaluno, J. *J. Org. Chem.* **2010**, *75*, 5976-5983.

Chapter 6

Crystal structure and solution state characterization of lithium (*S*)-(1-(Bis(2-methoxyethyl)amino)-3- methylbutan-2-yl)(methyl)amide



6.1 Abstract

The solid state structure of lithiated (*S*)- N^1,N^1 -bis(2-methoxyethyl)- $N^2,3$ -dimethylbutane-1,2-diamine which is a chiral amide base synthesized from (*S*)-valine was determined by single-crystal X-ray diffraction. The complex in solution state is also characterized by a variety of NMR experiments including diffusion-ordered NMR spectroscopy (DOSY) with diffusion coefficient-formula weight correlation analyses and other one- and two-dimensional NMR techniques by dissolving the crystal in toluene- d_8 . The crystallography and NMR results suggest that the chiral amide is dimeric in both solid and solution states.

6.2 Introduction

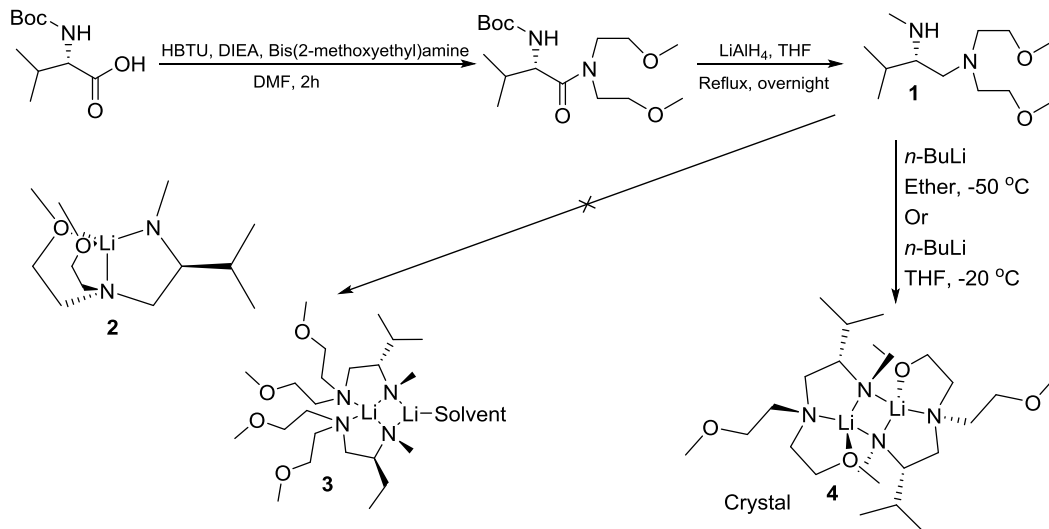
Organolithium reagents are one of the most widely used reagents in the synthesis of organic compounds.¹ Non-nucleophilic organolithium amide bases such as lithium diisopropylamide and lithium hexamethyldisilazide have long been widely employed in the deprotonation of various organic compounds.^{1d,1e,2} Chiral lithium amide bases were also developed for asymmetric addition and deprotonation.³ Moreover, chiral lithium amide bases can also be used in catalytic dynamic resolution in enantioselective synthesis.⁴ Owing to the versatility and stereoselectivity of chiral lithium amides, they have been studied by several groups for more than 20 years.^{3,5} Many studies revealed that the reactivity and stereoselectivity of lithium amides highly depend on the aggregation state of the amides.⁶ Therefore, aggregation state determination of chiral lithium amides is critical in understanding, choosing and designing chiral amines.

6.3 Results and Discussion

In an attempt to generate an internally solvated chiral lithium amide, (*S*)-*N*¹,*N*¹-bis(2-methoxyethyl)-*N*²,3-dimethyl-butane-1,2-diamine (**1**) was synthesized by Boc-protected (*S*)-valine in two steps (Scheme 6.1). Bis(2-methoxyethyl)amine was chosen to be incorporated into the ligand because of its extensive use in internally solvating the lithium atom in several organolithium compounds.⁷ Upon reaction of chiral amine **1** with *n*-BuLi as outlined in Scheme 6.1, we expected to generate either monomeric lithium amide **2** or dimeric lithium amide **3** with a Li₂N₂ core which is the representative dimer for (*S*)-valine derived chiral lithium amide.^{5a,e,8} In lieu of obtaining either **2** or **3**, we crystallized and characterized a dimeric aggregate **4** portrayed in Scheme 6.1 and Figure 6.1. The dimer **4** adopts a ladder-type structure which is similar to the structure of lithiated (*S*)-*N*-isopropyl-*O*-triisopropylsilylvalinol in hydrocarbon solvent that our group characterized two years ago.^{5e} Despite the fact that the crystal was grown in a solution containing significant amount of diethyl ether or THF, there was no ether or even THF coordinating the dimer in the crystal structure. Moreover, only one oxygen from the bis(2-methoxyethyl)amine is chelated to a lithium atom as shown in Figure 6.1.

Characterization of lithiated amine **1** in solution state was also conducted through applying various one- and two-dimensional NMR techniques on the solution of the crystal dissolved in toluene-*d*₈. The sample can either be prepared by dissolving dry crystals of lithium amide **4** which had been washed by anhydrous pentane twice in toluene-*d*₈ or by adding stoichiometric amount of *n*-butyllithium into the solution of chiral amine **1** in toluene-*d*₈. The spectra produced are nearly the same except that there

are some large heptane peaks (from the $n\text{-Bu}^6\text{Li}$ solution) when the latter method was used.



Scheme 6.1. Synthesis and Crystallization of lithium amide **1**

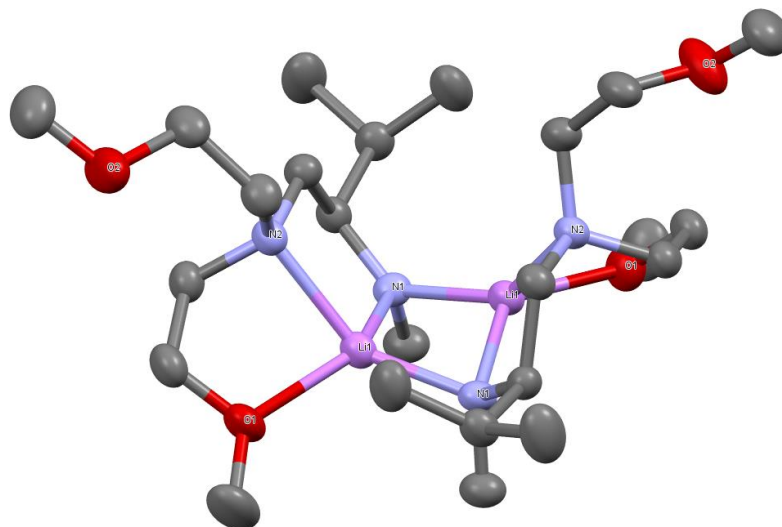


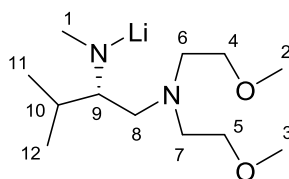
Figure 6.1. Crystal structure of lithiated (S)- N^1,N^1 -bis(2-methoxyethyl)- $N^2,3$ -dimethylbutane-1,2-diamine **4**. Thermal ellipsoid plots are at the 50% probability level. Hydrogen atoms have been omitted for clarity.

A series of ^1H and ^{13}C NMR experiments including ^1H NMR, ^{13}C NMR, COSY,

HSQC, HMBC were carried out in order to assign the ^1H and ^{13}C signals. The result is summarized in Table 6.1.

^6Li NMR was then used to determine the number of different lithium atoms present. The fact that there is only one sharp peak at $-50\text{ }^\circ\text{C}$ indicates that only one kind of lithium is present and is consistent with monomeric amide **2** or dimeric amide **4** but not dimeric amide **3** (Figure 6.2).

Table 6.1. ^1H and ^{13}C signal assignments of lithiated amide **1**



Carbon atom	^{13}C	^1H
1	44.0	3.37
2	59.3	3.04
3	58.9	2.98
4	69.5	3.02, 2.63
5	68.9	3.31, 3.10
6	57.2	2.68, 2.28
7	54.1	3.00, 2.73
8	48.1	2.92, 2.08
9	70.6	2.96
10	26.3	2.60
11	16.2	0.97
12	15.1	1.20

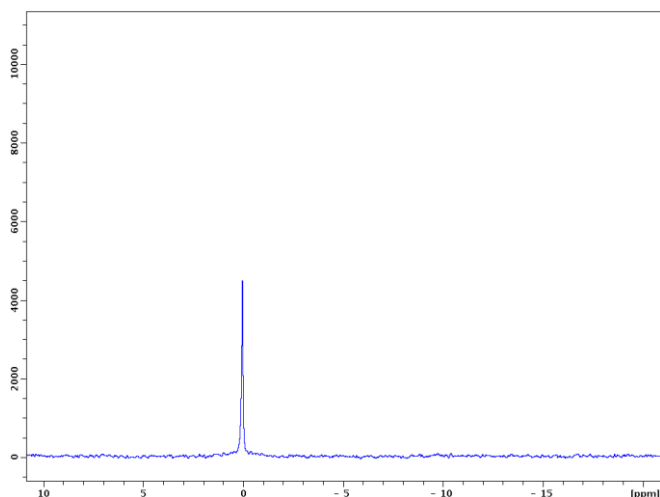


Figure 6.2. ^6Li NMR of [^6Li] Amide **1**.

DOSY techniques were then used to determine the formula weight of the lithiated complex and hence the aggregation state. We first applied DOSY NMR with internal references for the determination of formula weights of reactive complexes by *D-FW* correlation analysis. A linear regression plot of the logarithms of NMR determined diffusion coefficients against the known formula weights of the references is used to deduce the formula weight of unknown complex from its diffusion coefficient.^{5e,f,6f,9} In this proton DOSY, benzene (BEN, 78.11 g/mol), cyclooctene (COE, 110.2 g/mol), 1-tetradecene (TDE, 196.4 g/mol) and squalene (SQU, 410.7 g/mol) were added to the sample solution as our internal references.

After the addition of internal references, the signals of lithiated amine **1** from 1.0 to 2.5 ppm were overlapped with the signals from the internal references; thus, distinct peaks from 2.5 to 7.2 ppm were picked for our *D-FW* analysis. As seen in the DOSY spectrum (Figure 6.3), distinct peaks from lithiated amine **1** have very similar diffusion coefficients.

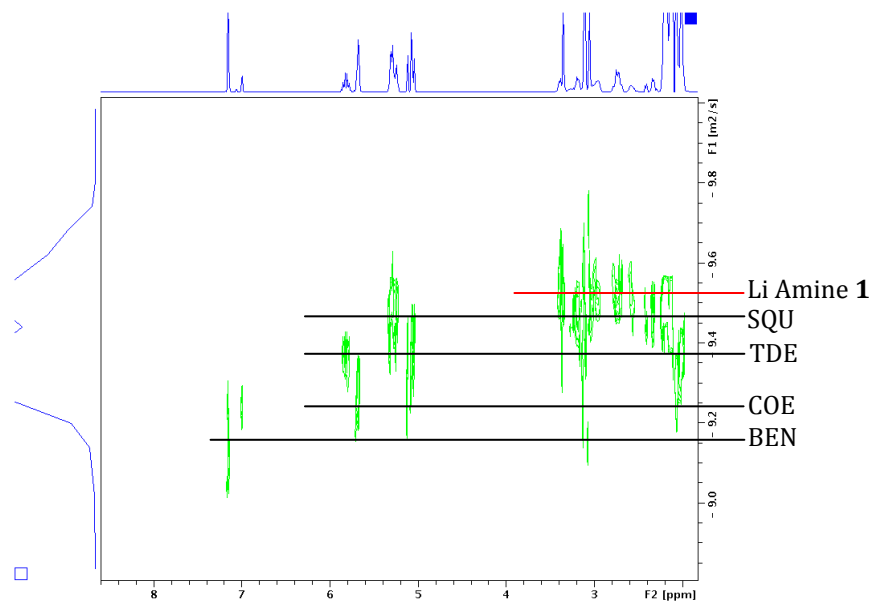


Figure 6.3. ^1H DOSY of lithiated amine **1**.

The correlation between $\log \text{FW}$ and $\log D$ of the linear regression is high ($r^2 > 0.99$) and the average predicted formula weight for the resonances of lithiated amine **1** is 483.8 g/mol which is very close to unsolvated dimer **4** of 476.6 g/mol (Figure 6.4, Table 6.2). Despite the fact that monomer **2** is consistent with our ^6Li NMR, our DOSY result showed that lithiated amine **1** in solution state cannot be monomer **2** which has a formula weight of only 238.3 g/mol and a 103% difference from the result. The possibility of a THF solvated monomer which has a formula weight of 310.4 g/mol can also be ruled out because of the 55.9% difference between the predicted and the actual formula weight. Another possible structure which is consistent with the ^6Li NMR result is the THF disolvated dimer; however, the disolvated dimer has a formula weight of 620.8 g/mol which is a 22.0% difference from our predicted formula weight. Therefore, only a symmetric unsolvated dimer is consistent with our ^6Li and DOSY NMR results.

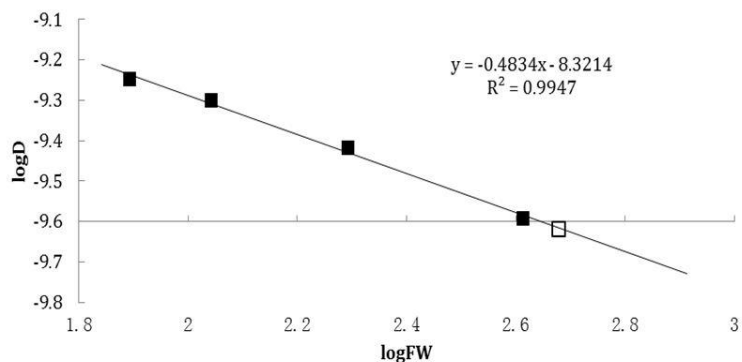


Figure 6.4. *D-FW* analysis of ^1H DOSY data. Internal references are shown as solid squares and lithiated amine **1** is shown as open square.

Table 6.2. *D-FW* analysis of ^1H DOSY data

entry	Compd	FW (g/mol)	$10^{-10}D$ (m^2/s)	Predicted FW (g/mol)	% error
1	BEN	78.11	5.661	82.26	-5.3
2	COE	110.2	4.997	106.5	3.4
3	TDE	196.4	3.818	185.8	5.4
4	SQU	410.7	2.555	426.6	-3.9
5	Li- 1 ^a	476.6 ^b	2.370	498.3	-4.6
6	Li- 1 ^a	476.6 ^b	2.378	494.9	-3.8
7	Li- 1 ^a	476.6 ^b	2.451	464.9	2.5
8	Li- 1 ^a	476.6 ^b	2.418	478.1	-0.3
9 ^c	Li- 1 ^a	476.6 ^b	2.404	483.7	-1.5
	Standard Dev. of Predicted FW of Li- 1			15.5	3.3
10	Li- 1 ^a	238.3 ^d	2.404	483.7	-103
11	Li- 1 ^a	310.4 ^e	2.404	483.7	-55.9
12	Li- 1 ^a	620.8 ^f	2.404	483.7	22.0

^aLi-**1** represents lithiated amine **1** in Tol-d₈. ^b476.6 g/mol is the formula weight of unsolvated dimer **4**. ^cThe average of the above four diffusion coefficients. ^d238.3 g/mol is the formula weight of unsolvated monomer **2**. ^e310.4 g/mol is the formula weight of a THF solvated monomer. ^f620.8 g/mol is the formula weight of a THF solvated dimer with 2 THF.

6.4 Conclusion

In summary, a single crystal of lithium (*S*)-(1-(bis(2-methoxyethyl)amino)-3-methylbutan-2-yl)(methyl)amide can be easily grown in both pentane-ether and pentane-THF solution. The crystal structure is a symmetric dimer shown in Figure 6.1. The solution state study was carried out by various one- and two-dimensional NMR techniques. ^6Li NMR result revealed that only one kind of lithium exists and ruled out the possibility of dimer **3**. After assigning the ^1H and ^{13}C signals, ^1H DOSY was run to evaluate the formula weight of the lithiated amine **1** in toluene- d_8 and the result of *D*-FW analysis suggested that lithium amine **1** existed as a unsolvated dimer in toluene- d_8 . With the crystallography and NMR data, we have definitive evidence that dimeric lithium amide **4** exists in both solid and solution states.

6.5 Experimental Section

6.5.1 Synthesis of (*S*)- N^1, N^1 -bis(2-methoxyethyl)- $\text{N}^2, 3$ -di-methyl butane-1,2-diamine (1**).** To a solution of Boc-(*S*)-valine (3.00 g, 13.8 mmol) dissolved in 50 ml anhydrous dimethyl-formamide and *N,N*-diisopropylethylamine (3.57 g, 27.6 mmol) under N_2 atmosphere was added *O*-(benzotriazol-1-yl)-*N,N,N',N'*-tetramethyluronium hexafluorophosphate (7.80g, 20.6mmol) all at once. After stirring at room temperature for 15 min, bis(2-methoxyethyl)amine (2.02 g, 15.2 mmol) was added dropwise and the reaction mixture was allowed to stir for 2 h before quenching with 80 mL 1 N HCl solution. The mixture was extracted with EtOAc (3 x 80ml) three times and the combined organic phase was washed by 1 N HCl (3 x 25ml) three times, 40 mL brine and dried

over Na₂SO₄. The solvent was first removed by rotary evaporation and then by oil pump yielding a reddish brown viscous liquid. The liquid was used in the next step without further purification.

To a solution of the previous obtained liquid dissolving in 100 ml anhydrous THF at 0 °C was slowly added lithium aluminum hydride (3.84 g, 101 mmol). After the addition, the reaction mixture was allowed to reflux overnight under N₂ atmosphere. The reaction mixture was then cooled down to 0 °C and quenched carefully by adding 0.5 N NaOH slowly upon stirring until all the salts appeared white. The solution was allowed to stir for 5 min before drying over Na₂SO₄. After sitting for 15min, the reaction mixture was then filtered and the white solid salts were washed by EtOAc (4 x 50 mL). The solvent of the filtered organic phase was removed by rotary evaporation and purification was performed by vacuum distillation. Purification (bp = 116 °C, 3 mm Hg) gave a colorless oil (1.71 g, 7.36 mmol, 53.3 %). ¹H NMR (CDCl₃, 400 MHz) δ 3.42 (dt, 4H, *J* = 6.2, 2.4Hz), 3.33 (s, 6H), 2.78-2.59 (m, 4H), 2.49-2.43 (m, 1H), 2.36 (s, 3H), 2.34-2.23 (m, 2H), 2.17-1.92 (br, 1H), 1.92-1.79 (m, 1H), 0.90 (d, 3H, *J* = 7.0Hz), 0.84 (d, 3H, *J* = 7.0Hz); ¹³C NMR (CDCl₃, 100 MHz) δ 71.2, 62.8, 58.7, 55.4, 54.6, 35.2, 27.9, 19.0, 16.9; HRMS-ESI *m/z*: [M + H]⁺ Calcd for C₁₂H₂₉N₂O₂: 233.2229, found: 233.2230.

6.5.2 Synthesis of *n*-Bu⁶Li. The *n*-Bu⁶Li solution was prepared in heptane according to the method that our group has published previously.^{5e}

6.5.3 Preparation of XRD Quality Crystals of Lithium (S)-(1-(bis(2-methoxyethyl)amino)-3-methylbutan-2-yl)(methyl)-amide (4). (I) To a solution of chiral amine **1** (0.10 g, 0.43 mmol) in 1 ml pentane at 0 °C under Ar atmosphere was slowly added 1

equiv *n*-BuLi. The reaction mixture was allowed to stir at 0 °C until white precipitates formed. Anhydrous diethyl ether was then added to the mixture until all the precipitates dissolved into the solution and the solution became clear. XRD quality crystals were grown when the solution was stored at -50 °C overnight. **(II)** To a solution of chiral amine **1** (0.10 g, 0.43 mmol) in 1 ml pentane at 0 °C under Ar atmosphere was slowly added 1 equiv *n*-BuLi. The reaction mixture was allowed to stir at 0 °C until white precipitates formed. Anhydrous tetrahydrofuran was then added to the mixture until all the precipitates dissolved into the solution and the solution became clear (the amount of tetrahydrofuran required is much less than that of diethyl ether). XRD quality crystals were grown over a few days when the solution was stored at a -20 °C freezer.

6.5.4 Procedures for NMR Experiments. NMR samples were prepared in tubes sealed with rubber septa cap purchased from Aldrich and parafilm. NMR tubes were evacuated in vacuo, flame-dried and filled with argon before use. NMR experiments were carried out at -40 °C except the characterization of chiral amine **1** which was done at room temperature and referenced to CDCl₃. ¹H chemical shifts were referenced to toluene-*d*₈ at 7.09 ppm and ¹³C chemical shifts were referenced to toluene-*d*₈ at 137.86 ppm. DOSY experiments were performed on a Bruker DRX400 spectrometer equipped with an Accustar z-axis gradient amplifier and an ATMA BBO probe with a z-axis gradient coil. Maximum gradient strength was 0.214 T/m. ¹H DOSY was performed using the standard Bruker dstebpgp3s program, using double stimulated echo, LED, with bipolar gradient pulses and 3 spoil gradients. Diffusion time was 200 ms, and rectangular gradient pulse duration was 900 μs. Gradient recovery delays were 900 μs. Individual rows of the quasi-2-D diffusion databases were phased and baseline corrected. Actual

diffusion coefficients used for D-FW analysis were obtained in the Bruker Topspin software using the T1/T2 analysis module.

The lithiated amine **1** samples can be prepared by dissolving dry crystals in toluene- d_8 or formed *in situ* by adding $n\text{-Bu}^6\text{Li}$ into a toluene- d_8 solution of chiral amine **1**. Crystals were first prepared by the method described above except $n\text{-Bu}^6\text{Li}$ was used instead. The crystals were kept at $-78\text{ }^\circ\text{C}$ in a cold bath immediately after removing from a $-50\text{ }^\circ\text{C}$ freezer, the solvent was removed by syringe and the crystals were washed twice with anhydrous pentane. After the removal of solution by syringe, the crystals were then kept at a dry ice-acetonitrile bath and evacuated *in vacuo* for 1 h. Toluene- d_8 (0.60 mL) was then added to the crystals under an Ar atmosphere. The solution was allowed to stir at $-40\text{ }^\circ\text{C}$ for 20 min before transferring into a sealed NMR tube via syringe. Alternatively, about 30 mg chiral amine **1** was added via syringe into a sealed NMR tube. Toluene- d_8 (0.60 mL) was then added via syringe to the NMR tube. The solution was then kept at a $-40\text{ }^\circ\text{C}$ bath before the addition of 1 equiv $n\text{-Bu}^6\text{Li}$ solution. After the addition, the NMR tube was shaken vigorously and kept at $-40\text{ }^\circ\text{C}$ for 1h before the signal acquisition. This latter method was not preferred overall since a significant amount of heptane is retained.

6.6 Acknowledgement

The author thanks Dr. Russell Hopson for his help in NMR experiments.

6.7 References

- (1) (a) Rappoport, Z., Marek, I., Eds. *The Chemistry of Organolithium Compounds*; John Wiley & Sons, Ltd.: West Sussex, 2004. (b) Clayden, J. *Organolithiums: Selectivity for Synthesis*; Pergamon: Oxford, 2002. (c) Hodgson, D. *Organo-lithiums in Enantioselective Synthesis*; Springer: New York, 2003. (d) Trost, B. M., Fleming, I., Eds. *Comprehensive Organic Synthesis*; Pergamon: Oxford, 1991. (e) Wu, G.; Huang, M. *Chem. Rev.* **2006**, *106*, 2596–2616.
- (2) (a) Collum, D.; McNeil, A. J.; Ramirez, A. *Angew. Chem. Int. Ed.* **2007**, *46*, 3002–3017. (b) Lucht, B.; Collum, D. *Acc. Chem. Res.* **1999**, *32*, 1035–1042. (c) Snieckus, V. *Chem. Rev.* **1990**, *90*, 879–933.
- (3) (a) Whitesell, J. K.; Felman, S. W. *J. Org. Chem.* **1980**, *45*, 755–756. (b) Eleveld, M. B.; Hogeveen, H. *Tetrahedron Lett.* **1984**, *45*, 5187–5190. (c) Shirai, R.; Tanaka, M.; Koga, K. *J. Am. Chem. Soc.* **1986**, *108*, 543–545. (d) Cain, C. M.; Cousins, R. P. C.; Coumbarides, G.; Simpkins, N. S. *Tetrahedron* **1990**, *46*, 523–544. (e) Bhuniya, D.; DattaGupta, A.; Singh, V. K. *J. Org. Chem.* **1996**, *61*, 6108–6113. (f) Corruble, A.; Valnot, J.-Y.; Maddaluno, J.; Duhamel, P. *Tetrahedron: Asymmetry* **1997**, *8*, 1519–1523. (g) Simpkins, N. S.; Hume, S. C. *J. Org. Chem.* **1998**, *63*, 912–913. (h) Corruble, A.; Valnot, J.-Y.; Maddaluno, J.; Duhamel, P. *J. Org. Chem.* **1998**, *63*, 8266–8275. (i) Matsuo, J.; Odashima, K.; Kobayashi, S. *Org. Lett.* **1999**, *1*, 345–348. (j) Arvidsson, P. I.; Davidsson, O.; Hilmersson, G. *Tetrahedron: Asymmetry* **1999**, *10*, 527–534. (k) De Sousa, S. E.; O'Brien, P.; Pilgram, C. D. *Tetrahedron* **2002**, *58*, 4643–4654. (l) Flinois, K.; Yuan, Y.; Bastide, C.; Harrison-Marchand, A.; Maddaluno, J. *Tetrahedron* **2002**, *58*, 4707–4716. (m) Rodeschini, V.; Simpkins, N. S.; Wilson, C. *J. Org. Chem.* **2007**, *72*, 4265–4267. (n) Stivala, C. E.; Zakarian A. *J. Am. Chem. Soc.* **2011**, *133*, 11936–11939.
- (4) (a) Beng, T. K.; Gawley, R. E. *J. Am. Chem. Soc.* **2010**, *132*, 12216–12217. (b) Beng, T. K.; Tyree, W. S.; Parker, T.; Su, C.; Williard, P. G.; Gawley, R. E. *J. Am. Chem. Soc.* **2012**, *134*, 16845–16855.
- (5) (a) Hilmersson, G.; Davidsson, O. *J. Org. Chem.* **1995**, *60*, 7660–7669. (b) Williard, P. G.; Sun, C. *J. Am. Chem. Soc.* **1997**, *119*, 11693–11694. (c) Sott, R.; Granander, J.; Hilmersson, G. *J. Am. Chem. Soc.* **2004**, *126*, 6798–6805. (d) Li, D.; Sun, C.; Liu, J.; Hopson, R.; Li, W.; Williard, P. G. *J. Org. Chem.* **2008**, *73*, 2373–2381. (e) Kagan, G.; Li, W.; Li, D.; Hopson, R.; Williard, P. G. *J. Am. Chem. Soc.* **2011**, *133*, 6596–6602. (f) Oulyadi, H.; Fressigne, C.; Yuan, Y.; Maddaluno, J.; Harrison-Marchand, A. *Organometallics*, **2012**, *31*, 4801–4809.
- (6) (a) Sato, D.; Kawasaki, H.; Shimada, I.; Arata, Y.; Okamura, K.; Date, T.; Koga, K. *J. Am. Chem. Soc.* **1992**, *114*, 761–763. (b) Arvidsson, P. I.; Hilmersson, G.; Ahlberg, P. *J. Am. Chem. Soc.* **1999**, *121*, 1883–1887. (c) Arvidsson, P. I.; Hilmersson, G.; Davidsson, O. *Chem.—Eur. J.* **1999**, *5*, 2348–2355. (d) Sott, R.; Granander, J.; Hilmersson, G. *Chem.—Eur. J.* **2002**, *8*, 2081–2087. (e) Pate, F.; Duguet, N.; Oulyadi, H.; Harrison-Marchand, A.; Fressigne, C.; Valnot, J.; Lasne, M.; Maddaluno, J. *J. Org. Chem.* **2007**, *72*, 6982–6991. (f) Liu, J.; Li, D.; Sun, C.; Williard, P. G. *J. Org. Chem.* **2008**, *73*, 4045–4052. (g) Lecachey, B.; Duguet, N.; Oulyadi, H.; Fressigne, C.; Harrison-Marchand, A.; Yamamoto, Y.; Tomioka, K.; Maddaluno, J. *Org. Lett.* **2009**, *11*, 1907–1910.
- (7) (a) Fraenkel, G.; Chen, X.; Gallucci, J.; Ren, Y. *J. Am. Chem. Soc.* **2008**, *130*, 4140–4145. (b) Fraenkel, G.; Chen, X.; Chow, A.; Gallucci, J.; Liu, H. *J. Org. Chem.* **2005**, *70*, 9131–9138. (c) Fraenkel, G.; Chow, A.; Fleischer, R.; Liu, H. *J. Am. Chem. Soc.* **2004**, *126*, 3983–3995. (d)

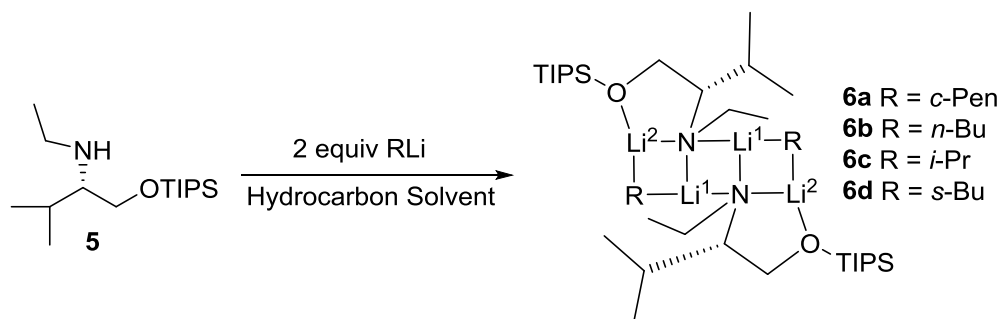
Colquhoun, V. P.; Strohmann, C. *J. Chem. Soc., Dalton Trans.* **2012**, *41*, 1897-1902.

(8) (a) Granander, J.; Sott, R.; Hilmersson, G. *Chem.—Eur. J.* **2006**, *12*, 4191-4197. (b) Hilmersson, G.; Arvidsson, P. I.; Davidsson, O. *Organometallics*, **1997**, *16*, 3352-3362. (c) Hilmersson, G. *Chem.—Eur. J.* **2000**, *6*, 3069-3075. (d) Sott, R.; Granander, J.; Williamson, C.; Hilmersson, G. *Chem.—Eur. J.* **2005**, *11*, 4785-4792.

(9) (a) Li, D.; Hopson, R.; Li, W.; Liu, J.; Williard, P. G. *Org. Lett.* **2008**, *10*, 909-911. (b) Li, D.; Sun, C.; Williard, P. G. *J. Am. Chem. Soc.* **2008**, *130*, 11726-11736. (c) Kagan, G.; Li, W.; Hopson, R.; Williard, P. G. *Org. Lett.* **2009**, *11*, 4818-4821. (d) Kagan, G.; Li, W.; Hopson, R.; Williard, P. G. *Org. Lett.* **2010**, *12*, 520-523. (e) Li, W.; Kagan, G.; Yang, H.; Cai, C.; Hopson, R.; Sweigart, D. A.; Williard, P. G. *Org. Lett.* **2010**, *12*, 2698-2701. (f) Lecachey, B.; Oulyadi, H.; Lameiras, P.; Harrison-Marchand, A.; Gerard, H.; Maddaluno, J. *J. Org. Chem.* **2010**, *75*, 5976-5983.

Chapter 7

Mixed aggregates of an alkyllithium reagent and a chiral lithium amide derived from *N*-ethyl-*O*-triisopropylsilyl valinol



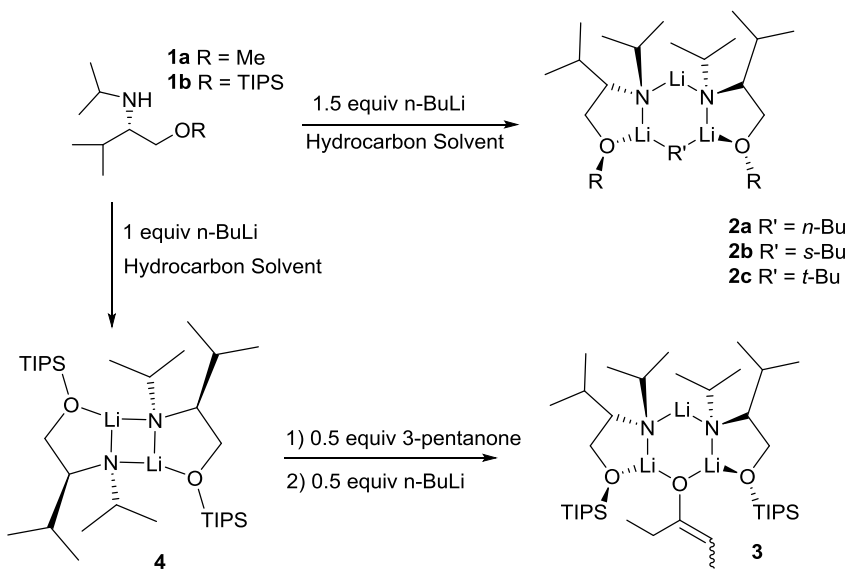
7.1 Abstract

The crystal structure of a mixed aggregate containing lithiated (*S*)-*N*-ethyl-3-methyl-1-(triisopropylsilyloxy)butan-2-amine derived from (*S*)-valinol and cyclopentyllithium is determined by X-ray diffraction. The mixed aggregate adopts a ladder structure in solid state. The ladder-type mixed aggregate is also the major species in a toluene-*d*₈ solution containing approximately 1:1 mole ratio of the lithiated chiral amide to cyclopentyllithium. A variety of NMR experiments including diffusion-ordered NMR spectroscopy (DOSY) with diffusion coefficient-formula (*D*-FW) weight correlation analyses and other one- and two-dimensional NMR techniques allowed us to characterize the complex in solution. Solution state structures of the mixed aggregates of *n*-butyl, *sec*-butyllithium, isopropyllithium with lithiated (*S*)-*N*-ethyl-3-methyl-1-(triisopropyl-silyloxy)butan-2-amine are also reported. Identical dimeric, ladder-type, mixed aggregates are the major species at a stoichiometric ratio of 1:1 lithium chiral amide to alkyllithium in toluene-*d*₈ solution for all of the different alkyllithium reagents.

7.2 Introduction

Organolithium reagents are among the most widely used reagents in organic synthesis.¹ Chiral lithium amide bases were developed for asymmetric addition and deprotonation.² Additionally, Koga reported an intriguing asymmetric aldol reaction in the presence of chiral lithium amide bases implicating the influence of mixed aggregates.³ Recent research indicates that chiral lithium amide bases are also useful for catalytic dynamic resolution in enantioselective synthesis.⁴ Other organolithium reagents

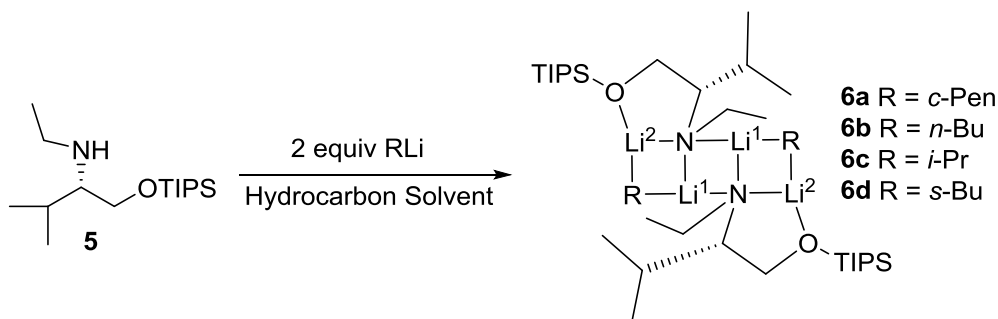
that form mixed aggregates have been reported by several groups including Collum,⁵ Davidsson,⁶ Duhamel,⁷ Hilmersson,⁸ McGarrity,⁹ Maddaluno,¹⁰ Reich,¹¹ Thomas¹² and Strohmann¹³. Many of these studies reveal that the reactivity and stereoselectivity of chiral lithium mixed aggregates depend on the aggregation state of the reagents.^{6a,f,10b,14} Therefore, aggregation state determination of chiral, lithium mixed-aggregates is crucial to the interpretation of the reaction mechanism and the optimization of enantioselectivity in reactions involving chiral lithiated amide reagents.



Scheme 7.1. The trimeric 2:1 complexes **2**, **3** and the homodimer **4**

Previously our group reported solid state structures of mixed trimers consisting of two equiv of the chiral lithium amide derived from *N*-isopropyl valinol **1** and one equivalent of commercially available *n*-butyllithium (*n*-BuLi), or *tert*-butyllithium (*t*-BuLi), or *sec*-butyllithium (*s*-BuLi) depicted as structure **2** in Scheme 7.1.¹⁵ We also reported both the crystal structure and the solution state characterization of a similar trimeric complex

consisting of two equiv of the chiral lithium amide and 3-pentanone lithium enolate complex depicted as complex **3**.¹⁶ We also reported the asymmetric addition of *n*-BuLi from the mixed aggregate **2a** to aldehydes.^{14c} Most recently, we characterized the solution state structure of the pure chiral lithium amide in the absence any additional reagents as the homodimer **4** in hydrocarbon solvent.¹⁷ Moreover, Hilmersson and coworkers reported solution state characterization of a similar chiral lithium amide as a mixed dimer between *n*-BuLi and the chiral lithium amide in diethyl ether.¹⁸ The characterization of yet another structural motif described as the four-rung ladder structures **6a-d** depicted in Scheme 7.2 containing a 2:2 stoichiometric ratio the chiral lithium amide derived from *N*-ethyl-*O*-triisopropylsilyl valinol **5** and either *n*-BuLi, or *s*-BuLi, or *i*-PrLi or cyclopentyllithium is presented in this chapter.



Scheme 7.2. The 2:2 Ladder Structure Mixed Aggregates **6**

7.3 Results and Discussion

7.3.1 Solid state structure of 2:2 mixed aggregate of lithiated (*S*)-*N*-ethyl-3-methyl-1-(triisopropylsilyloxy)butan-2-amine and cyclopentyllithium (**6a**)

Chiral amine **5** was easily synthesized from (*S*)-valine in three steps following the procedure we have used previously to prepare the *N*-isopropyl derivative. Crystals that are suitable for X-ray diffraction were grown by adding two equiv of *c*-PenLi to the toluene solution of chiral amine **5** and keeping the resulting solution at -50 °C for a few days. The X-ray structure determination of the solid material that formed reveals a 2:2 chiral lithium amide to *c*-PenLi mixed aggregate that adopts a ladder-type structure shown in Figure 7.1. The structure contains two chiral lithium amide and two alkyllithium subunits with a Li₂N₂ core. Hilmersson and Davidsson have shown the existence of several 1:1 mixed aggregates of chiral lithium amides and *n*-butyllithium in solution state^{6,8h,18} and Maddaluno has also conducted solution state studies to characterize several 1:1 mixed aggregates of alkyllithium and chiral lithium amides derived from 4-hydroxy-proline.¹⁰ To the best of our knowledge, there is no evidence for the existence of a 2:2 mixed aggregate of a chiral lithium amide and a simple alkyllithium reagent.

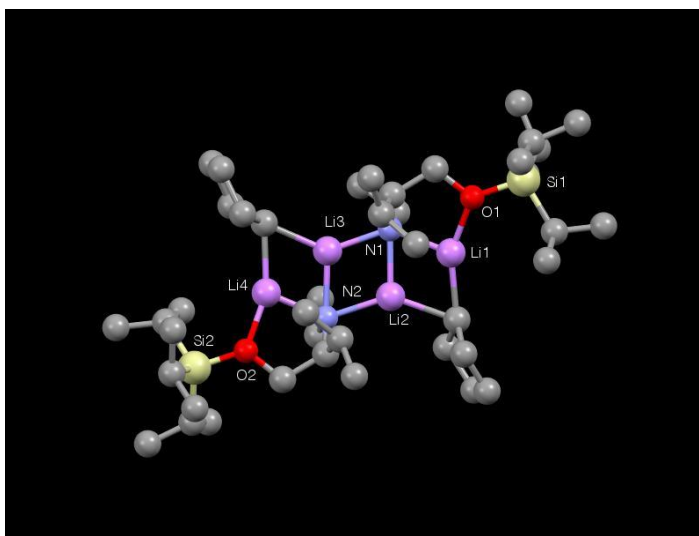


Figure 7.1. Crystal structure of the mixed aggregate of lithiated (*S*)-*N*-ethyl-3-methyl-1-(triisopropylsilyloxy)butan-2-amine and *c*-PenLi **6a**.

7.3.2 Solution state characterization of a 2:2 mixed aggregate of cyclopentyllithium and the chiral lithium amide derived from *N*-ethyl-*O*-triisopropylsilyl valinol (**6a**)

The sample for NMR studies was prepared *in situ* by titrating (*S*)-*N*-ethyl-3-methyl-1-(triisopropylsilyloxy)butan-2-amine into a toluene-*d*₈ solution of ⁶Li labeled cyclopentyllithium at -50 °C. The titration was monitored by ¹H and ⁶Li NMR as depicted in Figures 7.2 and 7.3 respectively.

The methine region of *c*-PenLi was carefully monitored by ¹H NMR. With no amine added, *c*-PenLi exists as a mixture of hexamer (-0.77 ppm) and tetramer (-1.16 ppm).¹⁹ Upon addition of chiral amine **5**, a new peak emerges at -0.59 ppm. As more chiral amine **5** is added to the solution, the intensity of the peak at -0.59 ppm increases significantly simultaneously with a decrease of the peaks due to the tetramer and hexamer of *c*-PenLi. As shown in Figure 7.2, when the mole ratio of lithiated chiral amine **5** to *c*-PenLi equals 1:1, the peak at -0.59 ppm is the major peak in the methine region of *c*-PenLi.

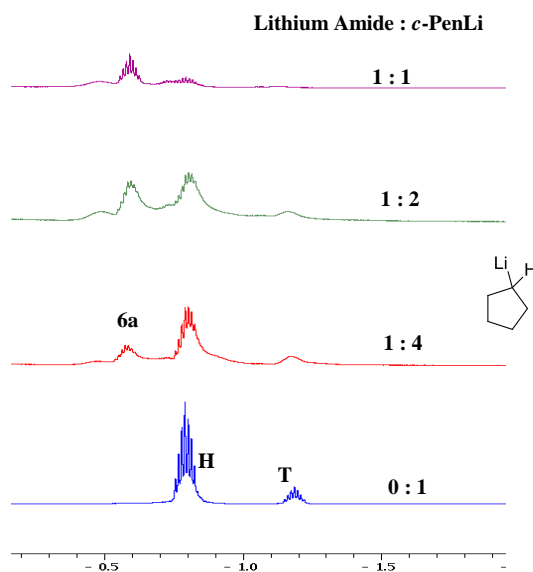


Figure 7.2. ¹H NMR spectra of chiral amine **5** titration of 0.47 M *c*-Pen⁶Li toluene-*d*₈ solution at -50 °C. H represents the resonance of *c*-Pen⁶Li in hexamer; T represents the resonance *c*-Pen⁶Li in tetramer; 6a represents the resonance of the 2:2 mixed aggregate **6a**.

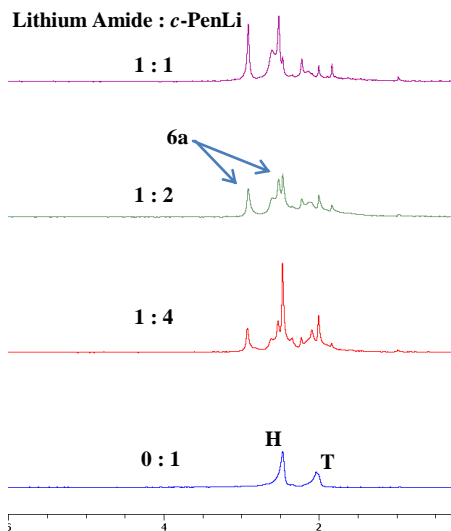


Figure 7.3. ${}^6\text{Li}$ NMR spectra of chiral amine **5** titration of 0.47 M *c*-Pen ${}^6\text{Li}$ toluene- d_8 solution at $-50\text{ }^\circ\text{C}$. H represents the resonance of *c*-Pen ${}^6\text{Li}$ in hexamer; T represents the resonance *c*-Pen ${}^6\text{Li}$ in tetramer; 6a represents the resonances of the 2:2 mixed aggregate **6a**. Smaller peaks are unknown species.

In ${}^6\text{Li}$ NMR in toluene- d_8 , *c*-PenLi exhibits two peaks corresponding to a hexamer and a tetramer. After the addition of chiral amine **5**, several peaks emerge. When the ratio of lithiated chiral amine **5** to *c*-PenLi equals 1:1, there are two peaks with approximately equal intensity that are significantly higher than the other peaks. These spectra are consistent with the 2:2 mixed aggregate.

To confirm that the two major peaks in ${}^6\text{Li}$ spectra represent the 2:2 mixed aggregate, a ${}^1\text{H}\{{}^6\text{Li}\}$ HMBC spectrum was performed. This spectrum is shown in Figure 7.4. The HMBC showed strong correlation from Li(1) to the protons of the methylene (2.95, 3.02 ppm) and methine (2.91 ppm) groups adjacent to nitrogen, as well as the methine peak (-0.59 ppm) of *c*-PenLi. Additionally, Li(2) also showed strong correlation to the methine proton of *c*-PenLi, as well as one of the protons of the methylene (3.51 ppm) group

adjacent to oxygen. This spectrum confirmed the formation of a mixed complex between *c*-PenLi and the lithiated chiral amine **5**.

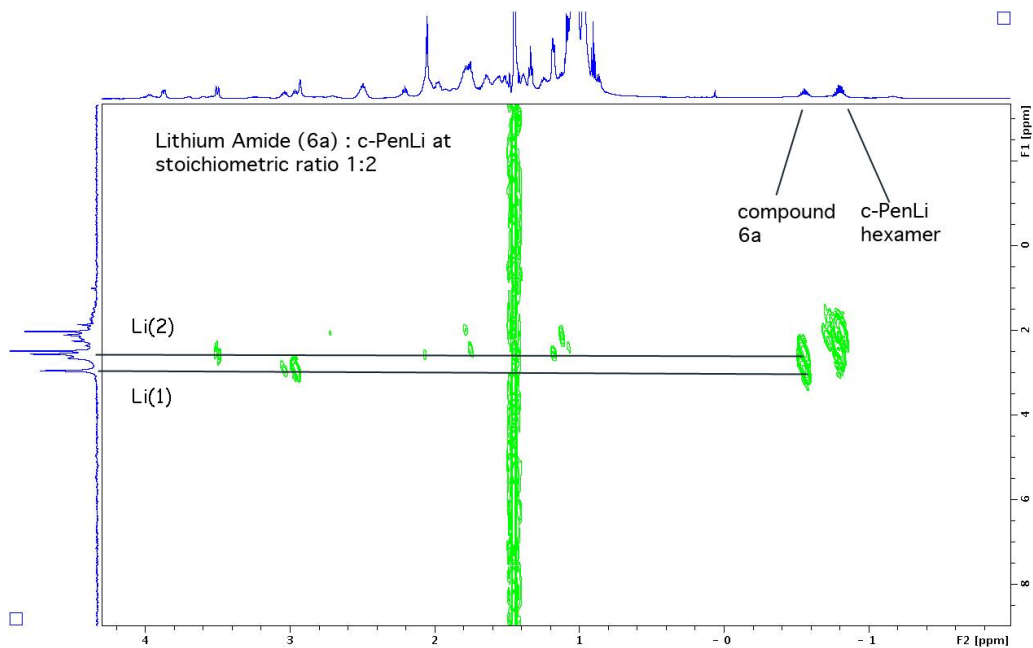
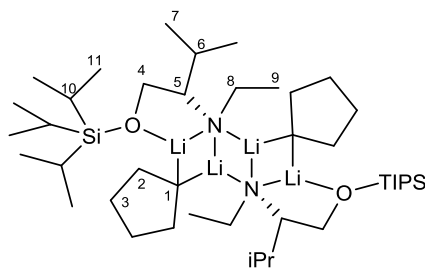


Figure 7.4. $^1\text{H} \{^6\text{Li}\}$ HMBC of **6a** in toluene- d_8 at $-50\text{ }^\circ\text{C}$.

A series of ^1H and ^{13}C NMR experiments including ^1H NMR, ^{13}C NMR, COSY, HSQC, HMBC were performed to confirm ^1H and ^{13}C chemical shift assignments. These results are summarized in Table 7.1. By comparing the integration of the resonance of *c*-PenLi methine proton to the distinctive protons (2.5 – 4.0 ppm) of the chiral lithium amide, the mole ratio of chiral lithium amide to *c*-PenLi is approximately 1:1. The methine carbon (carbon atom 1) of *c*-PenLi within the mixed aggregate **6a** is a quintet ($J = 10.3\text{ Hz}$) at 24.7 ppm (Figure 7.5). This is consistent with with C(1) of *c*-PenLi interacting with two ^6Li atoms. Both the multiplicity and coupling constant comply with the Bauer–Winchester –Schleyer rule.^{7,10e,20}

Table 7.1. ^1H and ^{13}C signal assignments of mixed aggregate **6a**



Carbon atom	^{13}C (ppm)	^1H (ppm)
1	24.7	-0.59
2	36.4	2.46, 1.61
3	29.4	2.03, 1.73
4	62.9	3.88, 3.51
5	65.8	2.91
6	36.2	1.80
7	20.0, 23.0	1.17, 1.08
8	44.0	3.02, 2.95
9	17.1	1.32
10	12.6	0.98
11	18.6, 18.5	1.02, 0.97

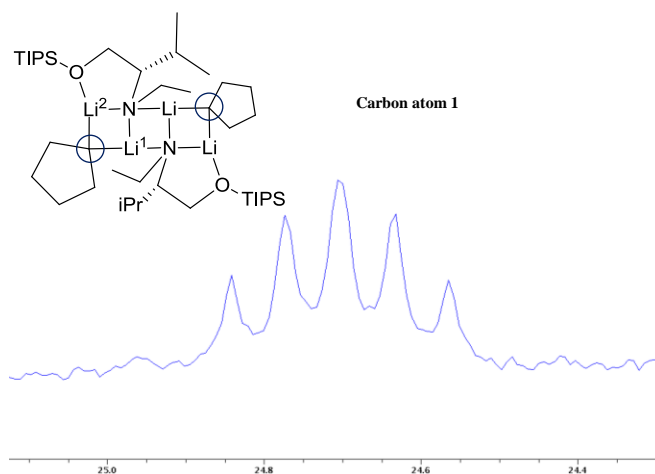


Figure 7.5. ^{13}C NMR of carbon atom 1 of mixed aggregate **6a** in toluene- d_8 at $-50\text{ }^\circ\text{C}$.

To distinguish a 2:2 mixed aggregate from a 1:1 mixed aggregate, the formula weight of the complex must be established. Diffusion-ordered NMR spectroscopy and diffusion coefficient-formula weight (*D-FW*) correlation analysis have been established as an efficient method for the evaluation of formula weight of reactive organolithium complexes in solution.^{15-17,21} Consequently, we add benzene (BEN, 78.11 g/mol), cyclooctene (COE, 110.2 g/mol), 1-tetradecene (TDE, 196.4 g/mol) and squalene (SQU, 410.7 g/mol) as internal references to the sample solution containing the putative complex **6a** to carry out *D-FW* correlation analysis.

After the addition of internal references, the resonances of the complex from 1.0 to 2.5 ppm overlapped with the resonances of the internal references; thus, distinct resonances of the chiral lithium amide from 2.5 to 4.0 ppm, as well as the resonance of the methine proton of *c*-PenLi at -0.59 ppm were utilized for our *D-FW* analysis. As seen in the ¹H DOSY spectrum (Figure 7.6), distinct peaks from lithiated chiral amine **5** and the peak of *c*-PenLi methine proton have very similar diffusion coefficients. The result establishes complexation between the lithiated chiral amine **5** and *c*-PenLi.

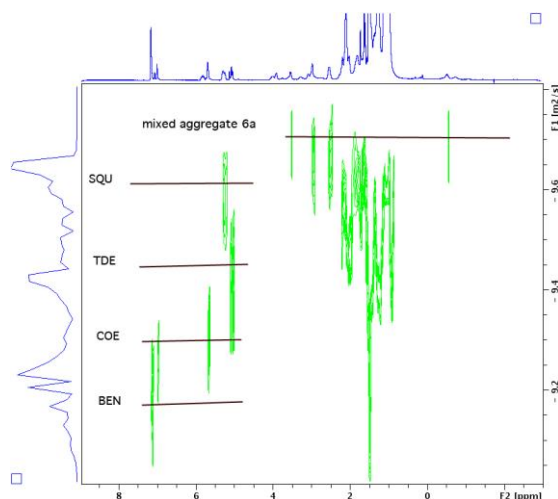


Figure 7.6. ¹H DOSY of mixed aggregate **6a** in toluene-*d*₈ at -50 °C.

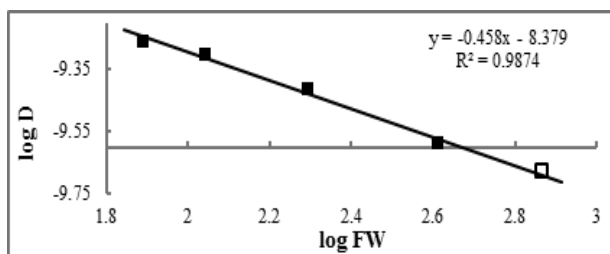


Figure 7.7. *D-FW* analysis of ^1H DOSY data. Internal references are shown as solid squares and mixed aggregate **6a** is shown as open square.

Table 7.2. *D-FW* analysis of ^1H DOSY data of **6a**

entry	Compd	FW (g mol^{-1})	$10^{-10}D$ (m^2/s)	Predicted FW (g mol^{-1})	% error
1	BEN	78.11	5.458	85.07	-8.9
2	COE	110.2	4.997	103.1	6.4
3	TDE	196.4	3.849	182.4	7.1
4	SQU	410.7	2.588	433.9	-5.6
5	6a ^a	735.4 ^b	2.085 ^a	695.5	5.4
6	6a ^a	735.4 ^b	2.092 ^a	690.4	6.1
7	6a ^a	735.4 ^b	2.075 ^a	702.8	4.4
8	6a ^c	735.4 ^b	2.093 ^c	689.7	6.2
9	6a ^d	735.4 ^b	2.086 ^d	694.6	5.5

^aThe measured diffusion coefficients are from the resonances of chiral lithium amide. ^b735.4 g mol^{-1} is the formula weight of 2:2 lithiated chiral amine **5**/*c*-PenLi (^6Li labeled) complex **6a**. ^cThe measured diffusion coefficient is from the methine proton peak (-0.59 ppm) of *c*-PenLi. ^dThe diffusion coefficient is the average of the above four values.

The correlation between $\log \text{FW}$ and $\log D$ of the linear regression is high ($r^2 = 0.987$) and the average predicted formula weight for the resonances of mixed aggregate **6a** is 694.6 g/mol , a 5.5 % difference from the formula weight of mixed aggregate **6a** (735.4 g/mol) (Figure 7.7, Table 7.2). Assuming a 10 % intrinsic error of the *D-FW* analysis,²⁰ our DOSY data are also consistent with a 2:1 mixed trimer (660.3 g/mol , 5.2 % error) that

adopts a structure similar to **2**. However, the 2:1 mixed trimer structure previously reported with the homologous *N*-isopropyl analog of the chiral amide base utilized in this study does not match the ^1H NMR and ^6Li NMR data; therefore, it cannot be the major species in the sample solution. Thus we are forced to conclude that the solution structure is a 2:2 mixed dimer analogous to that determined in the solid state by XRD.

7.3.3 Solution state characterization of a 2:2 mixed aggregate of *n*-butyllithium and the chiral lithium amide derived from *N*-ethyl-*O*-triisopropylsilyl valinol (6b**)**

The sample for NMR studies was also prepared by titrating (*S*)-*N*-ethyl-3-methyl-1-(triisopropylsilyloxy)butan-2-amine into a toluene- d_8 solution of ^6Li labeled *n*-butyllithium at $-50\text{ }^\circ\text{C}$. The titration was also monitored by ^1H and ^6Li NMR (Figures 7.8 and 7.9).

The α -methylene protons of *n*-BuLi were carefully monitored by ^1H NMR. As seen in Figure 7.8, a peak at -0.40 ppm increases in intensity as the amount of lithiated chiral amine **5** increases. It becomes the major peak when the ratio of lithiated chiral amine **5** to *n*-BuLi equals 1:1.3. Moreover, the ^6Li NMR data show very clearly the decrease of the resonance of the unsolvated hexameric *n*-BuLi aggregate and the rise of two sharp peaks with 1:1 ratio upon addition of chiral amine **5**. The two sharp peaks become the dominant peaks when the ratio of lithiated chiral amine **5** to *n*-BuLi equals 1:1.3. These results are consistent with a 2:2 mixed aggregate structure **6b**.

The $^1\text{H}\{^6\text{Li}\}$ HMBC (Figure 7.10) shows strong correlation from Li(1) to the α -methylene protons of *n*-BuLi (-0.40 ppm) and the protons of methylene (3.03 ppm) and

methine (2.98 ppm) groups adjacent to nitrogen. Li(2) also strongly correlates to one of the protons of the methylene group (3.46 ppm) adjacent to oxygen and the α -methylene protons of *n*-BuLi. These spectra support the assignment of a 2:2 mixed complex between *n*-BuLi and the lithiated chiral amine **5**.

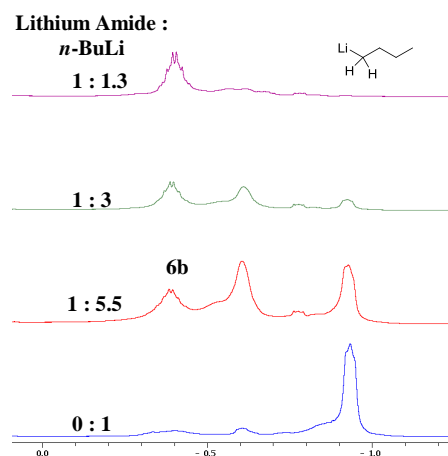


Figure 7.8. ^1H NMR spectra of chiral amine **5** titration of 0.45 M *n*-Bu ^6Li toluene- d_8 solution at $-50\text{ }^\circ\text{C}$. 6b represents the resonance of the 2:2 mixed aggregate **6b**.

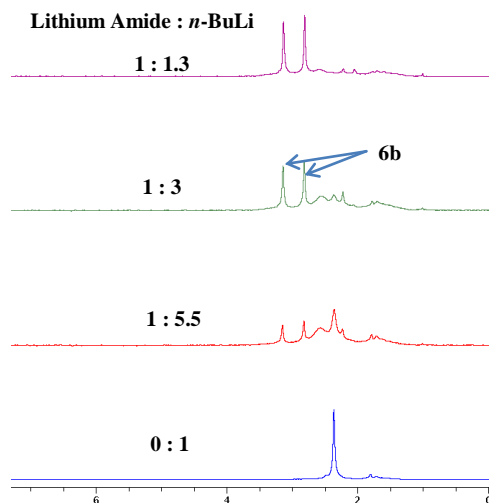


Figure 7.9. ^6Li NMR spectra of chiral amine **5** titration of 0.45 M *n*-Bu ^6Li toluene- d_8 solution at $-50\text{ }^\circ\text{C}$. 6b represents the resonance of the 2:2 mixed aggregate **6b**.

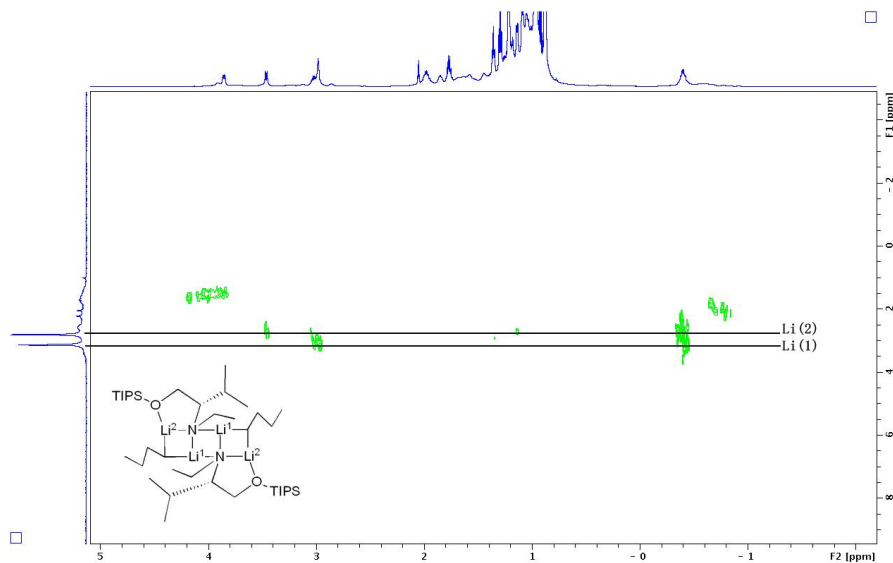


Figure 7.10. $^1\text{H}\{^6\text{Li}\}$ HMBC of **6b** in toluene- d_8 at $-50\text{ }^\circ\text{C}$.

Chemical shift assignments are summarized in Table 7.3 as determined ^1H and ^{13}C NMR experiments. The mole ratio of lithiated chiral amine **5** to $n\text{-BuLi}$ is approximately 1:1 by comparing the integration of the resonances of distinctive protons. Because the α -methylene carbon (carbon atom 1) of $n\text{-BuLi}$ of the mixed aggregate **6b** is a quintet ($J = 10.8\text{ Hz}$) at 10.1 ppm (Figure 7.11), the carbon atom 1 of $n\text{-BuLi}$ is surrounded by two lithium-6 atoms.

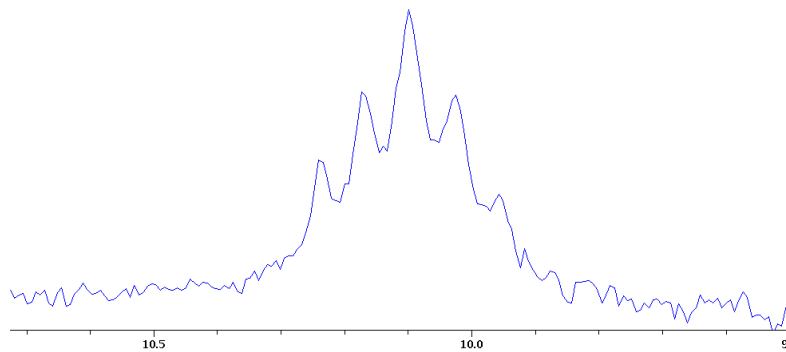
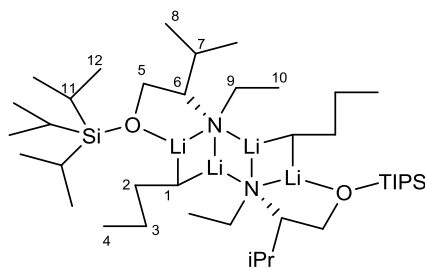


Figure 7.11. ^{13}C NMR of carbon atom 1 of mixed aggregate **6b** in toluene- d_8 at $-50\text{ }^\circ\text{C}$.

Table 7.3. ^1H and ^{13}C signal assignments of mixed aggregate **6b**

Carbon atom	^{13}C (ppm)	^1H (ppm)
1	10.1	-0.40
2	35.4	1.98
3	34.4	1.77
4	15.3	1.29
5	62.7	3.85, 3.46
6	65.3	2.98
7	35.9	1.85
8	22.9, 20.2	1.14, 1.09
9	45.3	3.03
10	16.8	1.36
11	12.5	0.96
12	18.5, 18.4	1.05, 0.97

Diffusion-ordered NMR spectroscopy and *D-FW* analysis were performed. Distinct resonances of the chiral lithium amide from 2.5 to 4.0 ppm and the resonance of the α -methylene protons of *n*-BuLi at -0.40 ppm were utilized for our *D-FW* analysis. The ^1H DOSY spectrum (Figure 7.12) shows that the α -methylene protons of *n*-BuLi and distinct peaks from lithiated chiral amine **5** diffuse at a very similar rate.

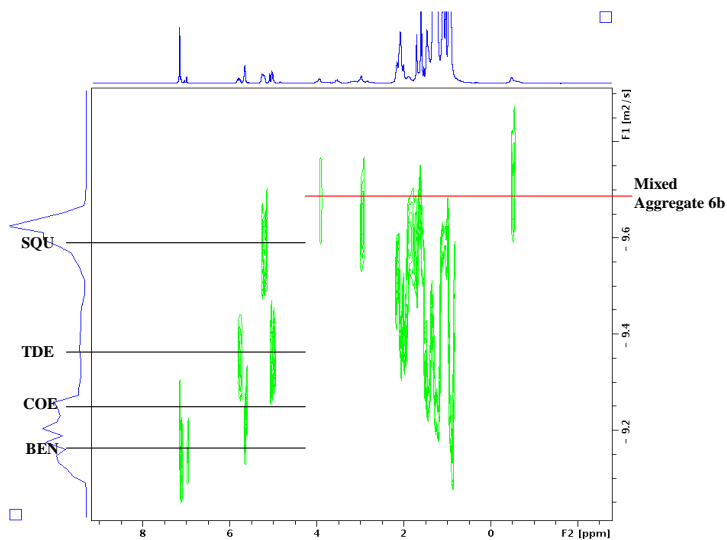


Figure 7.12. ^1H DOSY of mixed aggregate **6b** in toluene- d_8 at $-50\text{ }^\circ\text{C}$.

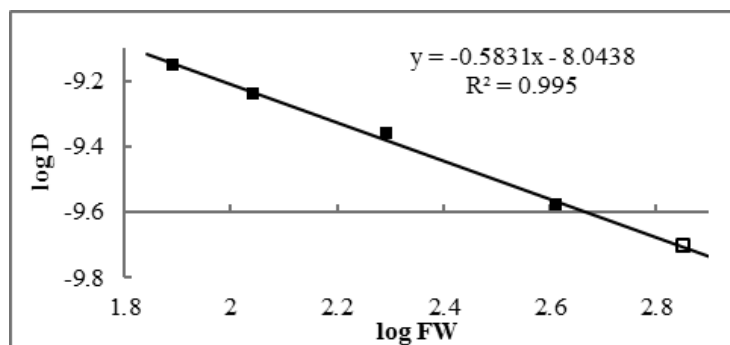


Figure 7.13. D -FW analysis of ^1H DOSY data. Internal references are shown as solid squares and mixed aggregate **6b** is shown as open square.

From correlation between $\log \text{FW}$ and $\log D$, the average predicted formula weight for the mixed aggregate **6b** is 706.9 g/mol. This represents a 0.6 % difference from the formula weight of the 2:2 mixed aggregate **6b** (711.4 g/mol) (Figure 7.13, Table 7.4).

Overall, our NMR data support the formation of the 2:2 mixed aggregate **6b** between lithiated chiral amine **5** and $n\text{-BuLi}$ in toluene when the mole ratio of chiral lithium amide to $n\text{-BuLi}$ is approximately 1:1.

Table 7.4. *D*-FW analysis of ¹H DOSY data of **6b**

entry	Compd	FW (g mol ⁻¹)	10 ⁻¹⁰ D (m ² /s)	Predicted FW (g mol ⁻¹)	% error
1	BEN	78.11	7.064	79.16	-1.3
2	COE	110.2	5.738	113.1	-2.6
3	TDE	196.4	4.347	182.0	7.3
4	SQU	410.7	2.647	426.1	-3.8
5	6b ^a	711.4 ^b	2.018 ^a	678.6	4.6
6	6b ^a	711.4 ^b	1.862 ^a	779.0	-9.5
7	6b ^a	711.4 ^b	2.015 ^a	680.3	4.4
8	6b ^c	711.4 ^b	1.999 ^c	689.7	3.1
9	6b ^d	711.4 ^b	1.974 ^d	706.9	0.6

^aThe measured diffusion coefficients are from the resonances of chiral lithium amide. ^b711.4 g mol⁻¹ is the formula weight of 2:2 lithiated chiral amine **5**/*n*-BuLi (⁶Li labeled) complex **6b**. ^cThe measured diffusion coefficient is from the resonance of α -methylene protons (-0.40 ppm) of *n*-BuLi. ^dThe diffusion coefficient is the average of the above four values.

7.3.4 Solution state characterization of a 2:2 mixed aggregate of isopropyllithium and the chiral lithium amide derived from *N*-ethyl-*O*-triisopropylsilyl valinol (**6c**)

A sample was prepared by titrating (*S*)-*N*-ethyl-3-methyl-1-(triisopropylsilyloxy)-butan-2-amine into a toluene-*d*₈ solution of ⁶Li labeled isopropyllithium at -50 °C. The methine proton of *i*-PrLi was carefully monitored in ¹H NMR. Upon addition of chiral amine **5**, a peak at -0.39 ppm increases in intensity as the amount of lithiated chiral amine **5** increases as shown in Figure 7.14. It becomes the major peak when the mole ratio of lithiated chiral amine **5** to *i*-PrLi equals approximately 1:1. The ⁶Li NMR data, Figure 7.15, shows very clearly the emergence and rise of two sharp peaks with 1:1 intensity upon addition of chiral amine **5** and these two sharp peaks become dominant when the

mole ratio of lithiated chiral amine **5** to *i*-PrLi equals 1:1.1. These results are consistent with a 2:2 mixed aggregate structure **6c**.

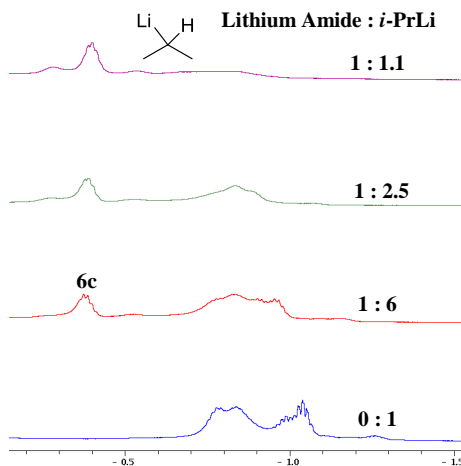


Figure 7.14. ^1H NMR spectra of chiral amine **5** titration of 0.35 M *i*-Pr ^6Li toluene- d_8 solution at $-50\text{ }^\circ\text{C}$. **6c** represents the resonance of the 2:2 mixed aggregate **6c**.

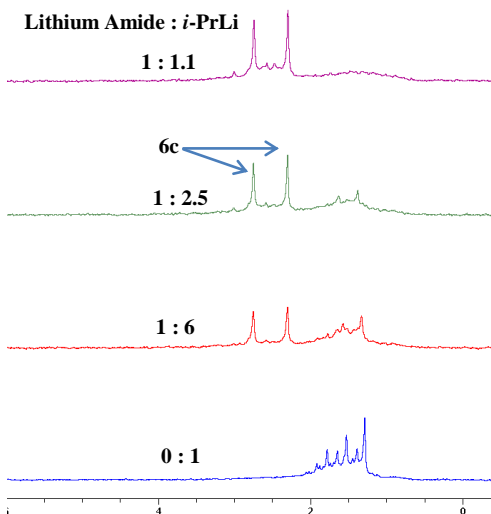


Figure 15. ^6Li NMR spectra of chiral amine **5** titration of 0.35 M *i*-Pr ^6Li toluene- d_8 solution at $-50\text{ }^\circ\text{C}$. **6c** represents the resonance of the 2:2 mixed aggregate **6c**.

The $^1\text{H}\{^6\text{Li}\}$ HMBC (Figure 7.16) shows a strong correlation from Li(1) to the methine proton of *i*-PrLi (-0.39 ppm), to the protons of methylene (3.04, 2.96 ppm) and to the methine (2.98 ppm) groups adjacent to nitrogen. Additionally, Li(2) also shows strong correlation to the methine proton of *i*-PrLi, as well as one of the protons of the methylene (3.46 ppm) group adjacent to oxygen. The result confirms mixed complex formation between *i*-PrLi and the lithiated chiral amine **5**.

Assignments of ^1H and ^{13}C resonances are summarized in Table 7.5. The mole ratio of lithiated chiral amine **5** to *i*-PrLi is approximately 1:1 by comparing the integration of distinctive proton peaks. Moreover, the methine carbon (carbon atom 1) of *i*-PrLi of the mixed aggregate **6c** is a quintet ($J = 10.6$ Hz) at 11.5 ppm (Figure 7.17). This result indicates that carbon atom 2 in *i*-PrLi is surrounded by two lithium-6 atoms.

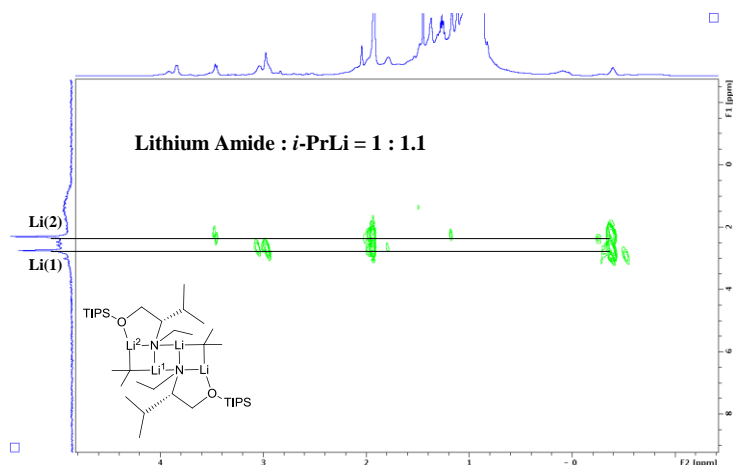


Figure 7.16. $^1\text{H}\{^6\text{Li}\}$ HMBC of **6c** in toluene- d_8 at -50 °C.

Diffusion-ordered NMR spectroscopy (Figure 7.18) and *D*-FW analysis results shows that lithiated chiral amine **5** and isopropyllithium (-0.39 ppm) diffuse at a very similar

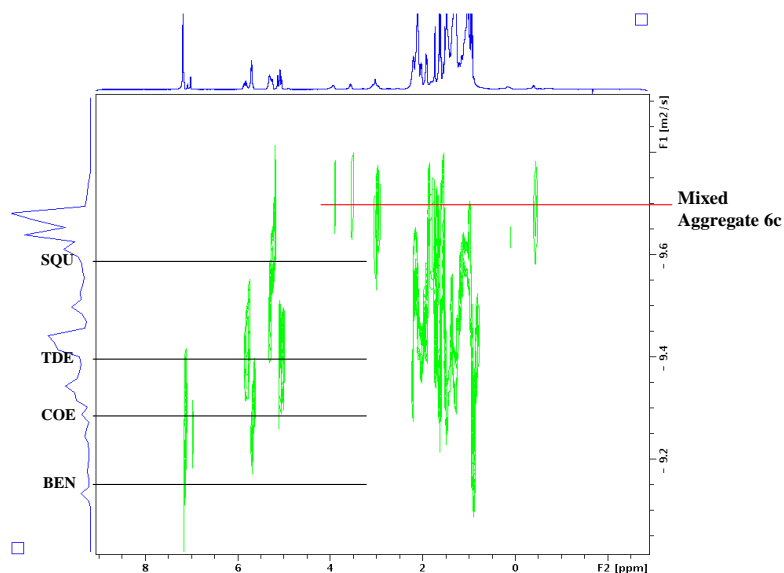


Figure 7.18. ^1H DOSY of mixed aggregate **6c** in toluene- d_8 at $-50\text{ }^\circ\text{C}$.

Table 7.6. D -FW analysis of ^1H DOSY data of **6c**

entry	Compd	FW (g mol^{-1})	$10^{-10}D$ (m^2/s)	Predicted FW (g mol^{-1})	% error
1	BEN	78.11	5.817	77.40	0.9
2	COE	110.2	4.787	114.5	-3.9
3	TDE	196.4	3.748	187.2	4.7
4	SQU	410.7	2.512	418.4	-1.9
5	6c ^a	683.3 ^b	1.946 ^a	698.9	-2.3
6	6c ^a	683.3 ^b	1.986 ^a	670.9	1.8
7	6c ^a	683.3 ^b	2.059 ^a	624.0	8.7
8	6c ^c	683.3 ^b	2.037 ^c	637.6	6.7
9	6c ^d	683.3 ^b	2.036 ^d	656.9	3.9

^aThe measured diffusion coefficients are from the resonances of chiral lithium amide. 683.3 g mol^{-1} is the formula weight of 2:2 lithiated chiral amine **5**/*i*-PrLi (^6Li labeled) complex **6c**. ^cThe measured diffusion coefficient is from the resonance of the methine proton (-0.39 ppm) of *i*-PrLi. ^dThe diffusion coefficient is the average of the above four values.

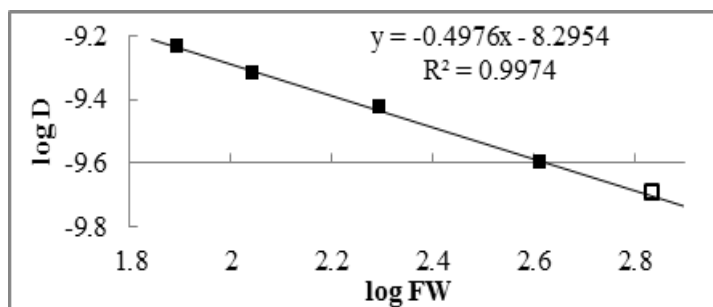


Figure 7.19. *D*-FW analysis of ^1H DOSY data. Internal references are shown as solid squares and mixed aggregate **6c** is shown as open square.

7.3.5 Solution state characterization of a 2:2 mixed aggregate of *s*-butyllithium and the chiral lithium amide derived from *N*-ethyl-*O*-triisopropylsilyl valinol (**6d**)

Upon addition of chiral amine **5** to a solution of *s*-BuLi, a peak at -0.51 ppm due to the methine proton of *s*-BuLi increases in intensity as the amount of lithiated chiral amine **5** increases in the ^1H NMR (Figure 7.20). In the ^6Li NMR spectra (Figure 7.21), the original hexamer, tetramer and *s*-BuLi/*s*-BuOLi mixed aggregate²² peaks disappear when 0.5 equiv of chiral amine **5** was added. A triplet and a singlet with 1:1 intensity emerge and increase in intensity with addition of chiral amine **5**. The two peaks become dominant when the mole ratio of lithiated chiral amine **5** to *s*-BuLi equals 1:1. The spectra of this complex are more complicated than that of **6a-c** because of the additional stereoisomers that are possible by incorporation of an additional stereogenic center from *s*-BuLi. It is noteworthy that the N atoms in all of the complexes **6a-d** are also chiral, stereogenic centers. However, both the NMR spectra and the crystal structure of **6a** indicate that only a single diastereomer is formed. Assuming that the relative stereochemistry between N atoms and the chiral carbon in the valine derived residue in all of the complexes **6a-d** are

similar, then we suggest that three peaks seen for Li(1) in Figure 7.9 are due to diastereomeric complexes that differ in relative stereochemistry of the C-2 of the *s*-BuLi residue.²³ It is noteworthy that only Li(1) is resolved into three peaks and Li(2) remains as a single peak as seen in the Figure 7.21 in the two middle spectra. However, it is also clear that at a 1:1 ratio of Li amide to *s*-BuLi, a distinctly new resonance close to that of Li(1) is apparent and is likely to arise from a diastereomeric complex.

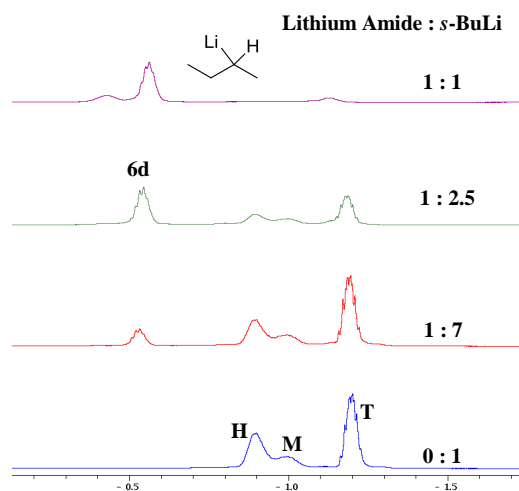


Figure 7.20. ^1H NMR spectra of chiral amine **5** titration of 0.38 M *s*-Bu⁶Li toluene-*d*₈ solution at -50 °C. H represents the resonance of *s*-Bu⁶Li in hexamer; T represents the resonance *s*-Bu⁶Li in tetramer; M represents mixed aggregate of *s*-Bu⁶Li/*s*-BuO⁶Li and **6d** represents the resonance of the 2:2 mixed aggregate **6d**.

The $^1\text{H}\{^6\text{Li}\}$ HMBC (Figure 7.22) spectrum reveals strong correlation from both the Li(1) and Li(2) resonances to the methine proton of *s*-BuLi (-0.51 ppm). The protons on the methylene (3.11, 2.93 ppm) and methine (2.26 ppm) groups adjacent to nitrogen in the valine residue correlate to Li(1). Finally we note that Li(2) also correlates strongly to one of the protons of the methylene group (3.47 ppm) adjacent to oxygen. These results are consistent with a mixed 2:2 complex **5**.

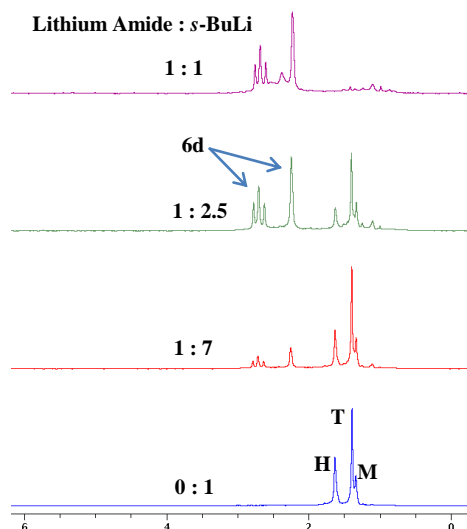


Figure 7.21. ${}^6\text{Li}$ NMR spectra of chiral amine **5** titration of 0.38 M $s\text{-Bu}^6\text{Li}$ in $\text{toluene-}d_8$ solution at -50°C . H represents the resonance of $s\text{-Bu}^6\text{Li}$ in hexamer; T represents the resonance $s\text{-Bu}^6\text{Li}$ in tetramer; M represents mixed aggregate of $s\text{-Bu}^6\text{Li}/s\text{-BuO}^6\text{Li}$ and **6d** represents the resonance of the 2:2 mixed aggregate **6d**.

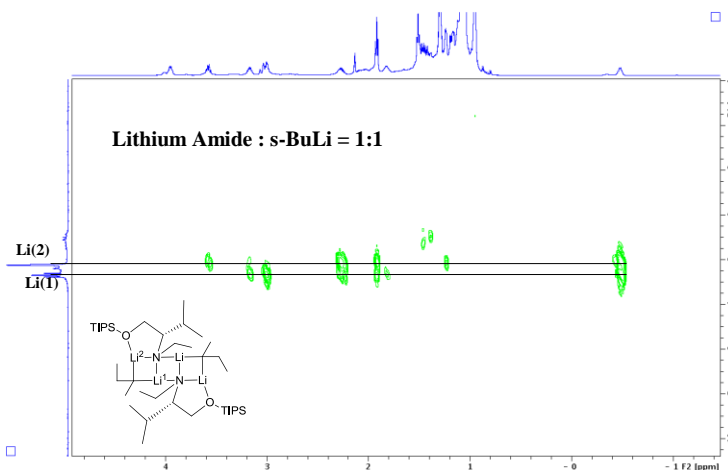
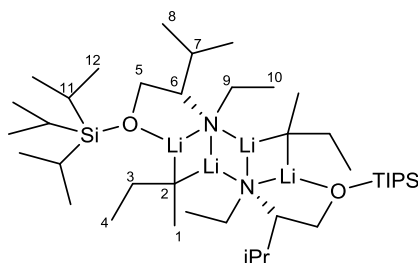


Figure 7.22. ${}^1\text{H} \{ {}^6\text{Li} \}$ HMBC of **6d** in $\text{toluene-}d_8$ at -50°C .

${}^1\text{H}$ and ${}^{13}\text{C}$ assignments are summarized in Table 7.7. The ratio of lithiated chiral amine **5** to $s\text{-BuLi}$ in **6d** is approximately 1:1 by comparing the integration of distinctive proton peaks in the spectrum of the complex containing a 1:1 stoichiometric ration of $s\text{-}$

BuLi to lithium amide. Unfortunately, we were not able to obtain an interpretable ^{13}C methine peak of *s*-BuLi, probably due to the presence of diastereomers.

Table 7.7. ^1H and ^{13}C signal assignments of mixed aggregate **6d**



Carbon atom	^{13}C (ppm)	^1H (ppm)
1	25.0, 25.1, 24.7, 24.5	1.89
2	23.0, 22.9	-0.51
3	36.2, 36.1, 36.0, 35.9	2.26
4	19.4, 19.3, 19.2, 19.1	1.47
5	62.8, 62.7, 62.5	3.85, 3.47
6	66.5, 65.5, 64.5, 64.4	2.96
7	36.3	1.73
8	23.0, 22.9	1.10
9	44.6, 44.0, 43.3	3.11, 2.93
10	17.3, 17.1, 16.9, 16.7	1.37
11	12.6, 12.7	0.96
12	18.5, 18.6, 18.4, 18.5	0.97

The diffusion-ordered NMR spectroscopy (Figure 7.23) and *D*-FW analysis show that lithiated chiral amine **5** and *s*-BuLi (-0.51 ppm) have very similar diffusion coefficients. The average predicted formula weight for the resonances of mixed aggregate **6d** is 685.2 g/mol which is only 3.7 % different from the formula weight of the 2:2 mixed aggregate

6d (711.4 g/mol) (Figure 7.24, Table 7.8).

Overall, the ^1H NMR titration results suggest the formation of a complex with 1:1 mole ratio of chiral lithium amide and *s*-BuLi, while $^1\text{H}\{^6\text{Li}\}$ HMBC confirms the complexation between chiral lithium amide and *s*-BuLi. The ^6Li NMR result is consistent with the 2:2 mixed aggregate **6d** but is not consistent with the 2:1 mixed aggregate. Therefore, our results point to the existence of 2:2 mixed aggregate **6d** as the major species in a toluene solution with 1:1 mole ratio of lithiated chiral amine **5** and *s*-BuLi.

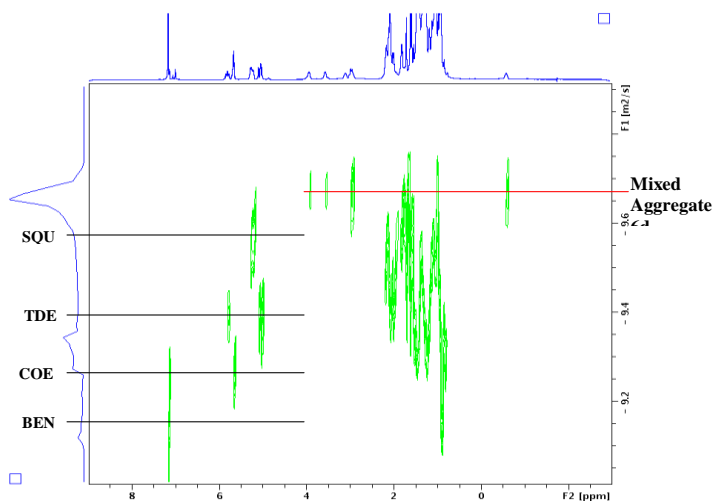


Figure 7.23. ^1H DOSY of mixed aggregate **6d** in toluene- d_8 at $-50\text{ }^\circ\text{C}$.

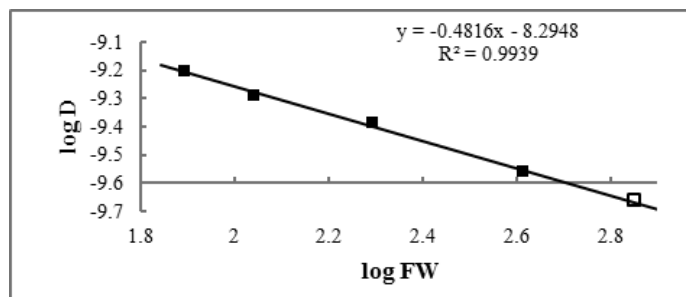


Figure 7.24. *D*-FW analysis of ^1H DOSY data. Internal references are shown as solid squares and mixed aggregate **6d** is shown as open square.

Table 7.8. *D-FW* analysis of ^1H DOSY data of **6d**

entry	Compd	FW (gmol^{-1})	10^{-10}D (m^2/s)	Predicted FW (gmol^{-1})	% error
1	BEN	78.11	6.279	76.56	2.0
2	COE	110.2	5.110	117.4	-6.6
3	TDE	196.4	4.122	183.5	6.6
4	SQU	410.7	2.763	421.0	-2.5
5	6d ^a	711.4 ^b	2.163 ^a	699.9	1.6
6	6d ^a	711.4 ^b	2.174 ^a	692.6	2.6
7	6d ^a	711.4 ^b	2.200 ^a	675.7	5.0
8	6d ^c	711.4 ^b	2.204 ^c	673.1	5.4
9	6d ^d	711.4 ^b	2.185 ^d	685.2	3.7

^aThe measured diffusion coefficients are from the resonances of chiral lithium amide. 711.4 gmol^{-1} is the formula weight of 2:2 lithiated chiral amine **5**/*s*-BuLi (^6Li labeled) complex **6d**. ^cThe measured diffusion coefficient is from the resonance of the methine proton (-0.51 ppm) of *s*-BuLi. ^dThe diffusion coefficient is the average of the above four values.

7.4 Conclusion

The formation of a 2:2 mixed aggregate between lithiated (*S*)-*N*-ethyl-3-methyl-1-(triisopropylsilyloxy)butan-2-amine and cyclopentyllithium, *n*-butyllithium, *sec*-butyllithium or isopropyllithium has been established by X-ray diffraction and various NMR techniques including diffusion-ordered NMR spectroscopy (DOSY) with *D-FW* correlation analyses and other one- and two-dimensional NMR techniques. The 2:2 ladder-type mixed aggregate is found to be the major species in a toluene-*d*₈ solution containing approximately 1:1 mole ratio of the lithium chiral amide to any of the simple alkyllithium reagents.

The complete characterization of the 2:2 mixed aggregates enriches our knowledge of the structural motifs of chiral lithium amide mixed aggregates. It is well established that lithiated *N*-isopropyl-*O*-triisopropylsilyl valinol **1b** forms a 2:1 mixed aggregate with *n*-butyllithium and that this mixed aggregate is responsible for the enantioselectivity of asymmetric addition of *n*-BuLi in the mixed aggregate to aldehydes. These results demonstrate the influence and importance of the *N*-substitute group of the chiral amine ligands since the simple replacement of an *N*-isopropyl group with an *N*-ethyl group leads to completely different mixed aggregates both in the solid state and in solution. These results are relevant to developing a mechanistic picture of the enantioselective reaction mediated by chiral lithium amide.

7.5 Experimental Section

7.5.1 Procedures for NMR Experiments. NMR samples were prepared in tubes sealed with rubber septa cap and parafilm. NMR tubes were evacuated *in vacuo*, flame-dried and filled with argon before use. ¹H chemical shifts were referenced to toluene-*d*₈ at 7.09 ppm and ¹³C chemical shifts were referenced to toluene-*d*₈ at 137.86 ppm. All NMR experiments except DOSY experiments were acquired on a 600 MHz spectrometer. All DOSY experiments were acquired on a 400 MHz spectrometer equipped with a z-axis gradient amplifier with a z-axis gradient coil. Maximum gradient strength was 0.214 T/m. ¹H DOSY was performed using the standard programs, employing a double stimulated echo sequence, bipolar gradient pulses for diffusion, and 3 spoil gradients. Diffusion time was 200 ms, and the rectangular gradient pulse duration was 900 μs (**6b**) and 1000 μs (**6a**,

6c, 6d). Gradient recovery delays were 200 μ s. Individual rows of the quasi-2-D diffusion databases were phased and baseline corrected. Actual diffusion coefficients used for *D*-FW analysis were obtained using the T1/T2 analysis module in commercially available software.

The alkyllithium samples were prepared by laboratory synthesized alkyllithium hydrocarbon (pentane, heptane or cyclohexane) solution. About 150-400 μ L of the alkyllithium hydrocarbon solution was added via syringe to a NMR tube. After the addition, the NMR tube was evacuated in vacuo for 10-30 minutes at 0 °C in order to remove the hydrocarbon solvent. After filling with argon, toluene-*d*₈ was added via syringe to bring the total volume up to 600 μ L.

The internal references (in a ratio of 1:3:3:1 for BEN, COE, TDE, and SQU, respectively) were titrated into the NMR tube and monitored by ¹H NMR. The titration was stopped when the peak intensity of benzene was about the two times as the methine proton peak of *i*-PrLi or *s*-BuLi and about the same as the α -methylene protons of *n*-BuLi or methine proton peak of *c*-PenLi.

7.5.2 Synthesis of (*S*)-*N*-ethyl-3-methyl-1-((triisopropylsilyl)oxy)butan-2-amine.

The synthetic route of chiral amine **5** started from enantiomerically pure (*S*)-valine. The *N*-ethyl (*S*)-valine was prepared according to Ohfuné's method.²⁴ The *N*-ethyl valine was then reduced by lithium aluminum hydride in anhydrous tetrahydrofuran to *N*-ethyl valinol. Chiral amine **5** was prepared as follows: To a solution of *N*-ethyl valinol (2.00 g, 15.2 mmol) and triethylamine (4.25 mL, 30.5 mmol) in 40 mL CH₂Cl₂ was added slowly triisopropylsilyl triflate (5.82 g, 19.0 mmol) at 0 °C. The resulting solution was allowed to stir at room temperature for 4 h before quenching with 15 mL of 2M NaHCO₃. The

mixture was extracted with 20 mL EtOAc three times and the combined organic phase was washed by 10 mL brine and dried over anhydrous Na₂SO₄. The solvent was then removed by rotary evaporation and purification was performed by vacuum distillation. Purification (bp = 129 °C, 3 mmHg) gave a colorless oil (2.03 g, 7.06 mmol, 46.3 %). ¹H NMR (Tol-*d*₈, 400 MHz) δ 3.73-3.55 (m, 2H), 2.70-2.53 (m, 2H), 2.34 (q, 1H, J = 5.0 Hz), 1.89-1.81 (m, 1H), 1.11-1.01 (m, 25H), 0.98 (dd, 6H, J = 9.1, 7.5 Hz); ¹³C NMR (Tol-*d*₈, 100 MHz) δ 65.6, 63.5, 43.3, 29.9, 19.6, 19.5, 18.7, 16.6, 12.8; HRMS-ESI m/z: [M + H]⁺ Calcd for C₁₆H₃₈NOSi: 288.2717, found: 288.2715.

7.5.3 Synthesis of c-Pen⁶Li. About 0.865 g (144 mmol) of finely cut ⁶Li metal was placed into a flame-dried flask with a condenser attached that was flushed with argon. The condenser was fitted with a serum septum and sealed with parafilm. The metal was washed with dry pentane by adding 10 mL of pentane to the flask via syringe. The flask was then placed in an ultrasound bath for 15 minutes. Pentane was then removed via syringe. This was repeated until the washings were clear, with no white solid suspended in the wash (3 times). Dry heptane (10 mL) was added to the flask and the flask was then placed in an oil bath at 50 °C with stirring. A drop of methyl *tert*-butyl ether was added to 6.33 g (60.5 mmol) of chlorocyclopentane and the resulting solution was added via syringe to the hot lithium metal heptane mixture in 2.5 h using a syringe pump. After the addition of chlorocyclopentane, the mixture was stirred overnight at room temperature, after which a purple slurry was obtained. The suspension was transferred via syringe to a clean, flame-dried vial flushed with argon and fitted with a serum septum. The vial was centrifuged until the solid was separated. The supernatant was transferred to a second identical vial and centrifuged again. The supernatant was transferred to a third identical

vial. This cyclopentylolithium solution in heptane was titrated using 2,2-diphenylacetic acid in tetrahydrofuran and found to be 1.4 M.

7.5.4 Synthesis of *n*-Bu⁶Li. The *n*-Bu⁶Li solution was prepared in heptane according to the method that our group has published previously.¹⁶

7.5.5 Synthesis of *s*-Bu⁶Li. About 0.60 g (100 mmol) of finely cut ⁶Li metal was placed into a flame-dried flask with a condenser attached that was flushed with argon. The condenser was fitted with a serum septum and sealed with parafilm. The metal was washed with dry pentane by adding 5 mL of pentane to the flask via syringe. The flask was then placed in an ultrasound bath for 15 minutes. Pentane was then removed via syringe. This was repeated until the washings were clear, with no white solid suspended in the wash (3 times). Dry cyclohexane (6 mL) was added to the flask and the flask was placed in an oil bath at 50 °C with stirring. A drop of methyl *tert*-butyl ether was added to 3.50 g (37.8 mmol) of 2-chlorobutane and the resulting solution was added via syringe to the hot lithium metal cyclohexane mixture in 2.5 h using a syringe pump. After the addition of 2-chlorobutane, the mixture was stirred overnight at room temperature, after which a purple slurry was obtained. The suspension was transferred via syringe to a clean, flame-dried vial flushed with argon and fitted with a serum septum. The vial was centrifuged until the solid was separated. The supernatant was transferred to a second identical vial and centrifuged again. The supernatant was transferred to a third identical vial. This *s*-Bu⁶Li solution in cyclohexane was titrated using 2,2-diphenylacetic acid in tetrahydrofuran and found to be 0.57 M.

7.5.6 Synthesis of *i*-Pr⁶Li. About 0.60 g (100 mmol) of finely cut ⁶Li metal was placed into a flame-dried flask with a condenser attached that was flushed with argon. The condenser was fitted with a serum septum and sealed with parafilm. The metal was washed with dry pentane by adding 5 mL of pentane to the flask via syringe. The flask was then placed in an ultrasound bath for 15 minutes. Pentane was then removed via syringe. This was repeated until the washings were clear, with no white solid suspended in the wash (3 times). Dry pentane (8 mL) was added to the flask and the flask was placed in an oil bath at 40 °C with stirring. A drop of methyl *tert*-butyl ether was added to 3.00 g (38.2 mmol) of 2-chloropropane and the resulting solution was added via syringe to the warm lithium metal pentane mixture in 2.5 h using a syringe pump. After the addition of 2-chloropropane, the mixture was stirred overnight at room temperature, after which a purple slurry was obtained. The suspension was transferred via syringe to a clean, flame-dried vial flushed with argon and fitted with a serum septum. The vial was centrifuged until the solid was separated. The supernatant was transferred to a second identical vial and centrifuged again. The supernatant was transferred to a third identical vial. This *i*-Pr⁶Li solution in pentane was titrated using 2,2-diphenylacetic acid in tetrahydrofuran and found to be 0.52 M.

7.5.7 Preparation of XRD Quality Crystals of the 2:2 Mixed Aggregate of Lithiated (*S*)-*N*-ethyl-3-methyl-1-(triisopropylsilyloxy)butan-2-amine and Cyclopentyllithium **6a.** To a solution of chiral amine **5** (0.050 g, 0.17mmol) in 0.4 mL toluene at 0 °C under Ar atmosphere was slowly added 2 equiv *c*-PenLi. The reaction mixture was shaken vigorously at 0 °C. XRD quality crystals of **6a** were grown when the solution was stored at -50 °C for a few days.

7.6 Acknowledgement

The author wishes to thank Dr. Russell Hopson.

7.7 References

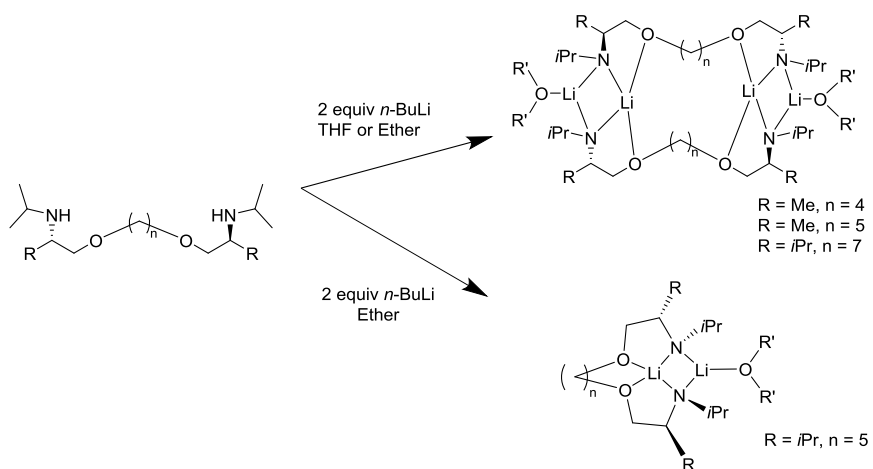
- (1) (a) Trost, B. M., Fleming, I., Eds. *Comprehensive Organic Synthesis*; Pergamon: Oxford, **1991**. (b) Clayden, J. *Organolithiums: Selectivity for Synthesis*; Pergamon: Oxford, **2002**. (c) Hodgson, D. *Organolithiums in Enantioselective Synthesis*; Springer: New York, **2003**. (d) Rappoport, Z., Marek, I., Eds. *The Chemistry of Organolithium Compounds*; John Wiley & Sons, Ltd.: West Sussex, **2004**. (e) Wu, G.; Huang, M. *Chem. Rev.* **2006**, *106*, 2596–2616.
- (2) (a) Whitesell, J. K.; Felman, S. W. *J. Org. Chem.* **1980**, *45*, 755-756. (b) Eleveld, M. B.; Hogeveen, H. *Tetrahedron Lett.* **1984**, *45*, 5187-5190. (c) Shirai, R.; Tanaka, M.; Koga, K. *J. Am. Chem. Soc.* **1986**, *108*, 543-545. (d) Cain, C. M.; Cousins, R. P. C.; Coumbarides, G.; Simpkins, N. S. *Tetrahedron* **1990**, *46*, 523-544. (e) Bhuniya, D.; DattaGupta, A.; Singh, V. K. *J. Org. Chem.* **1996**, *61*, 6108-6113. (f) Corruble, A.; Valnot, J.-Y.; Maddaluno, J.; Duhamel, P. *Tetrahedron: Asymmetry* **1997**, *8*, 1519–1523. (g) Simpkins, N. S.; Hume, S. C. *J. Org. Chem.* **1998**, *63*, 912-913. (h) Corruble, A.; Valnot, J.-Y.; Maddaluno, J.; Duhamel, P. *J. Org. Chem.* **1998**, *63*, 8266–8275. (i) Matsuo, J.; Odashima, K.; Kobayashi, S. *Org. Lett.* **1999**, *1*, 345-348. (j) Arvidsson, P. I.; Davidsson, O.; Hilmersson, G. *Tetrahedron: Asymmetry* **1999**, *10*, 527–534. (k) De Sousa, S. E.; O'Brien, P.; Pilgram, C. D. *Tetrahedron* **2002**, *58*, 4643-4654. (l) Flinois, K.; Yuan, Y.; Bastide, C.; Harrison-Marchand, A.; Maddaluno, J. *Tetrahedron* **2002**, *58*, 4707-4716. (m) Rodeschini, V.; Simpkins, N. S.; Wilson, C. *J. Org. Chem.* **2007**, *72*, 4265-4267. (n) Stivala, C. E.; Zakarian A. J. *Am. Chem. Soc.* **2011**, *133*, 11936-11939.
- (3) Uragami, M.; Tomioka, K.; Koga, K. *Tetrahedron: Asymmetry* **1995**, *6*, 701-704.
- (4) (a) Beng, T. K.; Gawley, R. E. *J. Am. Chem. Soc.* **2010**, *132*, 12216-12217. (b) Beng, T. K.; Tyree, W. S.; Parker, T.; Su, C.; Williard, P. G.; Gawley, R. E. *J. Am. Chem. Soc.* **2012**, *134*, 16845-16855.
- (5) (a) Ma, Y.; Stivala, C. E.; Wright, A. W.; Hayton, T.; Liang, J.; Keresztes, I.; Lobkovsky, E.; Collum, D. B.; Zakarian, A. *J. Am. Chem. Soc.* **2013**, *135*, ASAP. (b) Gruver, J. M.; West, S. P.; Collum, D. B.; Sarpong, R. *J. Am. Chem. Soc.* **2010**, *132*, 13212-13213. (c) Ramirez, A.; Sun, X. F.; Collum, D. B. *J. Am. Chem. Soc.* **2006**, *128*, 10326-10336. (d) Briggs, T. F.; Winemiller, M. D.; Collum, D. B.; Parsons, R. L.; Davulcu, A. H.; Harris, G. D.; Fortunak, J. M.; Confalone, P. N. *J. Am. Chem. Soc.* **2004**, *126*, 5427-5435. (e) Zhao, P. J.; Collum, D. B. *J. Am. Chem. Soc.* **2003**, *125*, 4008-4009. (f) Sun, X. F.; Winemiller, M. D.; Xiang, B. S.; Collum, D. B. *J. Am. Chem. Soc.* **2001**, *123*, 8039-8046. (g) Briggs, T. F.; Winemiller, M. D.; Xiang, B. S.; Collum, D. B. *J. Org. Chem.* **2001**, *66*, 6291-6298. (h) Xu, F.; Reamer, R. A.; Tillyer, R.; Cummins, J. M.; Grabowski, E. J. J.; Reider, P. J.; Collum, D. B.; Huffman, J. C. *J. Am. Chem. Soc.* **2000**, *122*, 11212-11218.

- (6) (a) Arvidsson, P. I.; Hilmersson, G.; Davidsson, O. *Chem. Eur. J.* **1999**, *5*, 2348-2355. (b) Hilmersson, G.; Arvidsson, P. I.; Davidsson, O.; Hakansson, M. *Organometallics* **1997**, *16*, 3352-3362. (c) Hilmersson, G.; Davidsson, O. *J. Org. Chem.* **1995**, *60*, 7660-7669. (d) Hilmersson, G.; Davidsson, O. *J. Organomet. Chem.* **1995**, *489*, 175-179.
- (7) (a) Prigent, Y.; Corruble, A.; Valnot, J. Y.; Maddaluno, J.; Duhamel, P.; Davoust, D. *J. Chim. Phys. Phys.-Chim. Biol.* **1998**, *95*, 401-405. (b) Corruble, A.; Valnot, J.-Y.; Maddaluno, J.; Duhamel, P. *J. Org. Chem.* **1998**, *63*, 8266-8275. (c) Corruble, A.; Valnot, J. Y.; Maddaluno, J.; Prigent, Y.; Davoust, D.; Duhamel, P. *J. Am. Chem. Soc.* **1997**, *119*, 10042-10048.
- (8) (a) Granander, J.; Sott, R.; Hilmersson, G. *Chem. Eur. J.* **2006**, *12*, 4191-4197. (b) Granander, J.; Eriksson, J.; Hilmersson, G. *Tetrahedron: Asymmetry* **2006**, *17*, 2021-2027. (c) Sott, R.; Granander, J.; Williamson, C.; Hilmersson, G. *Chem. Eur. J.* **2005**, *11*, 4785-4792. (d) Sott, R.; Granander, J.; Hilmersson, G. *J. Am. Chem. Soc.* **2004**, *126*, 6798-6805. (e) Sott, R.; Granander, J.; Diner, P.; Hilmersson, G. *Tetrahedron: Asymmetry* **2004**, *15*, 267-274. (f) Sott, R.; Granander, J.; Hilmersson, G. *Chem. Eur. J.* **2002**, *8*, 2081-2087. (g) Granander, J.; Sott, R.; Hilmersson, G. *Tetrahedron* **2002**, *58*, 4717-4725. (h) Arvidsson, P. I.; Ahlberg, P.; Hilmersson, G. *Chem. Eur. J.* **1999**, *5*, 1348-1354.
- (9) J. F. McGarrity, C. A. Ogle, *J. Am. Chem. Soc.*, **1985**, *107*, 1805-1810.
- (10) (a) Oulyadi, H.; Fressigne, C.; Yuan, Y.; Maddaluno, J.; Harrison-Marchand, A. *Organometallics* **2012**, *31*, 4801-4809. (b) Pate, F.; Duguet, N.; Oulyadi, H.; Harrison-Marchand, A.; Fressigne, C.; Valnot, J.-Y.; Lasne, M.-C.; Maddaluno, J. *J. Org. Chem.* **2007**, *72*, 6982-6991. (c) Harrison-Marchand, A.; Valnot, J.-Y.; Corruble, A.; Duguet, N.; Oulyadi, H.; Desjardins, S.; Fressigne, C.; Maddaluno, J. *Pure Appl. Chem.* **2006**, *78*, 321-331. (d) Yuan, Y.; Desjardins, S.; Harrison-Marchand, A.; Oulyadi, H.; Fressigne, C.; Giessner-Prettre, C.; Maddaluno, J. *Tetrahedron* **2005**, *61*, 3325-3334. (e) Corruble, A.; Davoust, D.; Desjardins, S.; Fressigne, C.; Giessner-Prettre, C.; Harrison-Marchand, A.; Houte, H.; Lasne, M.-C.; Maddaluno, J.; Oulyadi, H.; Valnot, J.-Y. *J. Am. Chem. Soc.* **2002**, *124*, 15267-15279.
- (11) Jones, A. C.; Sanders, A. W.; Bevan, M. J.; Reich, H. J. *J. Am. Chem. Soc.* **2007**, *129*, 3492-3493.
- (12) (a) Thomas, R. D.; Huang, H. *J. Am. Chem. Soc.*, **1999**, *121*, 11239-11240. (b) DeLong, G. T.; Hoffmann, D.; Nguyen, H. D.; Thomas, R. D. *J. Am. Chem. Soc.*, **1997**, *119*, 11998-11999. (c) G. T. DeLong, D. K. Pannell, M. T. Clarke, R. D. Thomas, *J. Am. Chem. Soc.*, **1993**, *115*, 7013-7014.
- (13) (a) Strohmman, C.; Dilsky, S.; Strohfeltdt, K. *Organometallics*, **2006**, *25*, 41-44. (b) Strohmman, C.; Abele, B. C. *Organometallics*, **2000**, *19*, 4173-4175.
- (14) (a) Sato, D.; Kawasaki, H.; Shimada, I.; Arata, Y.; Okamura, K.; Date, T.; Koga, K. *J. Am. Chem. Soc.* **1992**, *114*, 761-763. (b) Arvidsson, P. I.; Hilmersson, G.; Ahlberg, P. *J. Am. Chem. Soc.* **1999**, *121*, 1883-1887. (c) Liu, J.; Li, D.; Sun, C.; Williard, P. G.; *J. Org. Chem.* **2008**, *73*, 4045-4052. (d) Lecachey, B.; Duguet, N.; Oulyadi, H.; Fressigne, C.; Harrison-Marchand, A.; Yamamoto, Y.; Tomioka, K.; Maddaluno, J. *Org. Lett.* **2009**, *11*, 1907-1910.
- (15) (a) Li, D.; Sun, C.; Liu, J.; Hopson, R.; Li, W.; Williard, P. G. *J. Org. Chem.* **2008**, *73*, 2373-2381. (b) Williard, P. G.; Sun, C. *J. Am. Chem. Soc.* **1997**, *119*, 11693-11694.

- (16) (a) Li, D.; Sun, C.; Williard, P. G. *J. Am. Chem. Soc.* **2008**, *130*, 11726-11736. (b) Sun, C.; Williard, P. G. *J. Am. Chem. Soc.* **2000**, *122*, 7829-7830.
- (17) Kagan, G.; Li, W.; Li, D.; Hopson, R.; Williard, P. G. *J. Am. Chem. Soc.* **2011**, *133*, 6596-6602.
- (18) Hilmersson, G.; Malmros, B. *Chem. Eur. J.* **2001**, *7*, 337-341.
- (19) Su, C.; Hopson, R.; Williard, P. G. *J. Am. Chem. Soc.* **2013**, *135*, ASAP
- (20) (a) Pi, R.; Bauer, W.; Brix, B.; Schade, C.; Schleyer, P. v. R. *J. Organomet. Chem.* **1986**, *306*, C1-C4. (b) Bauer, W.; Schleyer, P. v. R. Winchester, W. R. *Organometallics* **1987**, *6*, 2371-2379. (c) Bauer, W.; Schleyer, P. v. R. *Adv. Carbanion Chem.* **1992**, *1*, 89-175. (d) Bauer, W. *J. Am. Chem. Soc.* **1996**, *118*, 5450-5455. (e) Parisel, O.; Fressigne, C.; Maddaluno, J.; Giessner-Prettre, C. *J. Org. Chem.* **2003**, *68*, 1290-1294.
- (21) (a) Li, D.; Hopson, R.; Li, W.; Liu, J.; Williard, P. G. *Org. Lett.* **2008**, *10*, 909-911. (b) Li, D.; Kagan, G.; Hopson, R.; Williard, P. G. *J. Am. Chem. Soc.* **2009**, *131*, 5627-5634. (c) Li, D.; Keresztes, I.; Hopson, R.; Williard, P. G. *Acc. Chem. Res.* **2009**, *42*, 270-280. (d) Kagan, G.; Li, W.; Hopson, R.; Williard, P. G. *Org. Lett.* **2009**, *11*, 4818-4821. (e) Kagan, G.; Li, W.; Hopson, R.; Williard, P. G. *Org. Lett.* **2010**, *12*, 520-523. (f) Li, W.; Kagan, G.; Yang, H.; Cai, C.; Hopson, R.; Sweigart, D. A.; Williard, P. G. *Org. Lett.* **2010**, *12*, 2698-2701. (g) Li, W.; Kagan, G.; Yang, H.; Cai, C.; Hopson, R.; Dai, W.; Sweigart, D. A.; Williard, P. G. *Organometallics*. **2010**, *29*, 1309-1311. (h) Socha, A. M.; Kagan, G.; Li, W.; Hopson, R.; Sello, J. K.; Williard, P. G. *Energy Fuels* **2010**, *24*, 4518-4521. (i) Kagan, G.; Li, W.; Sun, C.; Hopson, R.; Williard, P. G. *J. Org. Chem.* **2011**, *76*, 65-70. (j) Lecachey, B.; Oulyadi, H.; Lameiras, P.; Harrison-Marchand, A.; Gerard, H.; Maddaluno, J. *J. Org. Chem.* **2010**, *75*, 5976-5983. (k) Consiglio, G. B.; Queval, P.; Harrison-Marchand, A.; Mordini, A.; Lohier, J.; Delacroix, O.; Gaumont, A.; Gerard, H.; Maddaluno, J.; Oulyadi, H. *J. Am. Chem. Soc.* **2011**, *133*, 6472-6480. (l) Armstrong, D. R.; Garcia-Alvarez, P.; Kennedy, A. R.; Mulvey, R. E.; Robertson, S. D. *Chem. Eur. J.* **2011**, *17*, 6725-6730.
- (22) Su, C.; Hopson, R.; Williard, P. G. *Eur. J. Inorg. Chem.* **2013**, *24*, 4136-4141.
- (23) (a) Fraenkel G.; Henrichs M.; Hewitt M.; Su, B. M. *J. Am. Chem. Soc.*, **1984**, *106*, 255-256. (b) Fraenkel G.; Winchester, W. R. *J. Am. Chem. Soc.*, **1988**, *110*, 8720-8721. (c) Reich, H. J.; Kulicke, K. J. *J. Am. Chem. Soc.*, **1996**, *118*, 273-274.
- (24) Ohfuné, Y.; Kurokawa, N.; Higuchi, N.; Saito, M.; Hashimoto, M.; Tanaka, T. *Chem. Lett.* **1984**, *13*, 441-444.

Chapter 8

Chiral lithium diamides derived from linked *N*-isopropyl valinol or alaninol



8.1 Abstract

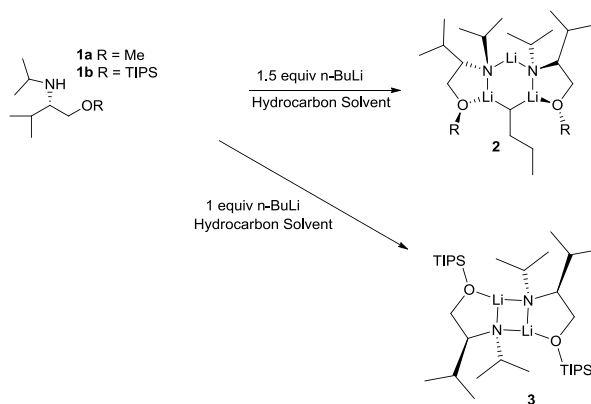
Four different chiral diamino diethers synthesized from *N*-isopropyl valinol or alaninol were lithiated with *n*-butyllithium in tetrahydrofuran or diethyl ether. Crystal structures of the dilithiated diamino diethers are determined by X-ray diffraction. Three dilithiated diamino diethers including (2*S*,2'*S*)-1,1'-(butane-1,4-diylbis(oxy))bis(*N*-isopropylpropan-2-amine) **7**, (2*S*,2'*S*)-1,1'-(pentane-1,5-diylbis(oxy))bis(*N*-isopropylpropan-2-amine) **8** and (2*S*,2'*S*)-1,1'-(heptane-1,7-diylbis(oxy))bis(*N*-isopropyl-3-methylbutan-2-amine) **9** are dimers whereas the structure of dilithiated (2*S*,2'*S*)-1,1'-(pentane-1,5-diylbis(oxy))bis(*N*-isopropyl-3-methylbutan-2-amine) **10** is a monomer. The lithium atoms in all crystal structures adopt a non-equivalent coordination protocol in which these lithium atoms exist in two different environments. One of the lithium atoms is tetra-coordinated while the other one is tri-coordinated.

8.2 Introduction

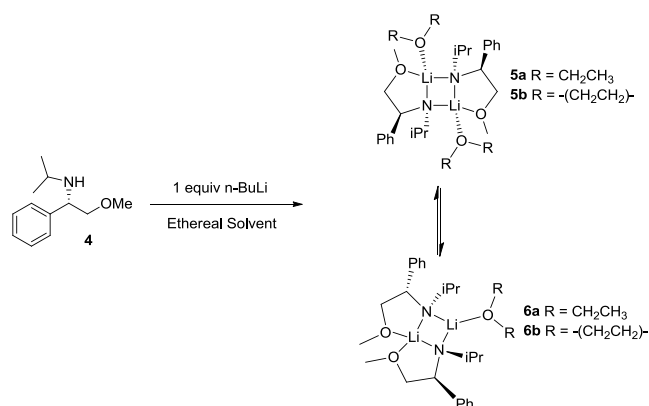
Non-nucleophilic organolithium amide bases such as lithium diisopropylamide and lithium hexamethyldisilazide have long been widely employed in the deprotonation of various organic compounds.¹ Chiral lithium amide bases were also developed for asymmetric addition and deprotonation.² Recently, chiral lithium amide bases have also proven useful in catalytic dynamic resolution in enantioselective synthesis.³ Current research suggests that the aggregation state of a chiral amide base effects its reactivity and stereoselectivity.⁴ Thus, it is crucial to determine the aggregation state of chiral

lithium amides as well as the solvation to reveal a reaction mechanism and to design more efficient chiral amines.

In 1997, our group reported the crystal structures of a mixed trimer containing commercially available butyllithiums with 2 equiv of a lithiated chiral amino ether derived from *N*-isopropyl valinol **1a** (Scheme 8.1).⁵ Later, we carried out solution state characterization of a lithiated chiral amino ether **1b** which is structurally similar to **1a**.⁶ We also reported the asymmetric addition to aldehydes with these reagents.^{4f} The result showed that lithiated chiral amino ether **1b** formed a 2:1 mixed trimer with *n*-butyllithium (*n*-BuLi) in toluene when there was excess *n*-BuLi in the solution.⁶ However, a ladder-type dimer is formed if there is only lithiated chiral amino ether **1b** in the solution without excess *n*-BuLi.⁷ In ethereal solution, lithiated chiral amino ether **4** existed as both a symmetrically solvated dimer **5** and non-equivalently solvated dimer **6** as reported by Hilmersson and his coworkers (Scheme 8.2).⁸ In this chapter, the syntheses and the solid state characterization of four structurally related chiral diamino ethers derived from *N*-isopropyl valinol or alaninol are presented.



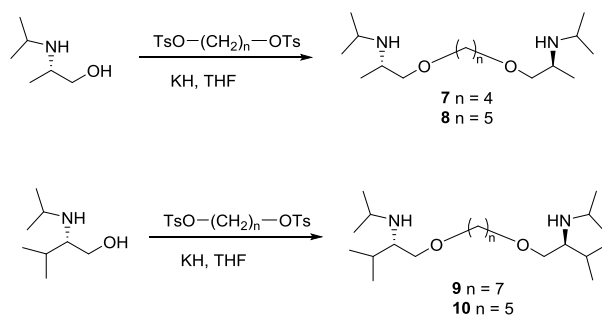
Scheme 8.1. The trimeric complexes **2** and the homodimer **3**



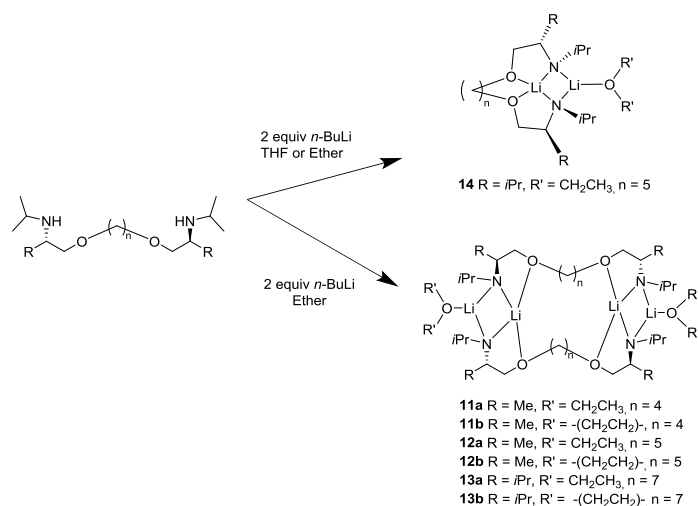
Scheme 8.2. The equivalently solvated dimer **5** and non-equivalently solvated dimer **6**

8.3 Results and Discussion

(2*S*,2'*S*)-1,1'-(butane-1,4-diylbis(oxy))bis(*N*-isopropylpropan-2-amine) **7** and (2*S*,2'*S*)-1,1'-(pentane-1,5-diylbis(oxy))bis(*N*-isopropylpropan-2-amine) **8** were synthesized from *N*-isopropyl alaninol, whereas (2*S*,2'*S*)-1,1'-(heptane-1,7-diylbis(oxy))bis(*N*-isopropyl-3-methylbutan-2-amine) **9** and (2*S*,2'*S*)-1,1'-(pentane-1,5-diylbis(oxy))bis(*N*-isopropyl-3-methylbutan-2-amine) **10** were synthesized from *N*-isopropyl valinol as depicted in Scheme 8.3. In this synthesis, two amino alcohol molecules were linked together with an alkyl chain to form a symmetrical diamino diether. Homologous analogs containing alkyl chains of four, five and seven methylene groups were used to prepare the diamino diethers. Reaction of the chiral diamino diethers **7**, **8**, **9** or **10** with 2 equiv *n*-butyllithium (*n*-BuLi) yielded products whose crystal structures were determined. These structures incorporated tetrahydrofuran (THF) and diethyl ether (DEE). Dilithiated chiral diamino ethers **7**, **8**, and **9** form dimers in solid state, whereas dilithiated chiral diamino ether **10** is a monomer, Scheme 8.4.



Scheme 8.3. Synthesis of chiral diamino ethers **7**, **8**, **9** and **10**



Scheme 8.4. Crystallization of dilithiated chiral diamino ethers **7**, **8**, **9** and **10** in ethereal solvents

8.3.1 Crystal structure of dilithiated (2*S*,2'*S*)-1,1'-(butane-1,4-diylbis(oxy))bis(*N*-isopropylpropan-2-amine) **11a** and **11b**

The crystal structure of THF or DEE coordinated dilithiated chiral diamino diether **7** was generated by reacting the diamino diether with 2 equiv *n*-BuLi in DEE solution. THF was added to the DEE solution to prepare the THF solvated crystal. Crystals grew overnight after storing the lithium amide solutions at $-50\text{ }^\circ\text{C}$. X-ray diffraction analysis

reveals dimeric aggregates for the DEE coordinated and the THF coordinated dilithiated chiral diamino diether **11**. As depicted in Figure 8.1 and 8.2, the crystal structures of the dimeric aggregates adopt the non-equivalent coordination protocol as dimer **6**. Hence within these dimers, there are two differently solvated lithium atoms. One of the lithium atoms is tri-coordinated while the other one is tetra-coordinated. Two subunits that structurally resemble dimer **6** are linked together by two alkyl chains. Within one subunit, there is a Li_2N_2 core and both of the oxygen atoms from the ether groups of the diamides are coordinated to the same lithium atom making it tetra-solvated. The other lithium from the Li_2N_2 core is coordinated to the oxygen atom of diethyl ether (DEE) or tetrahydrofuran (THF), and is tri-solvated. The solid state structures of these alaninol derived lithium diamides solvated by different ethereal solvents (THF or DEE) are very similar to each other. However, THF is more strongly coordinated to the lithium atoms than DEE because the THF solvated crystals are grown from diethyl ether solution. It is noteworthy that the THF solvated dimer has a slightly shorter Li-O distance (1.94 Å) than that of DEE solvated dimer (1.97 Å).

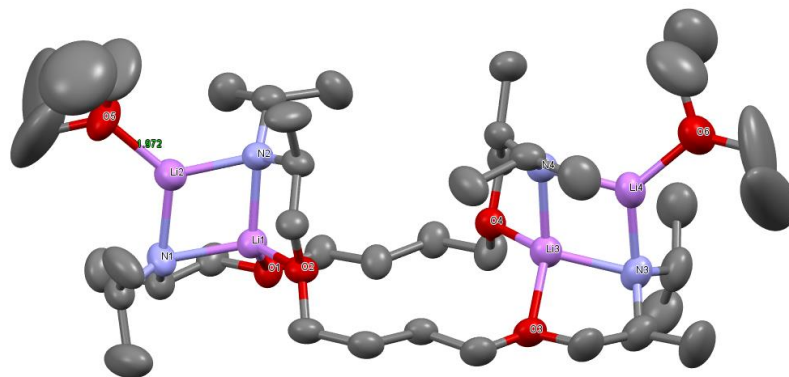


Figure 8.1. Crystal structure of DEE coordinated dilithiated chiral diamino diethers **11a**. Thermal ellipsoid plots are at the 50% probability level. Hydrogen atoms have been omitted for clarity.

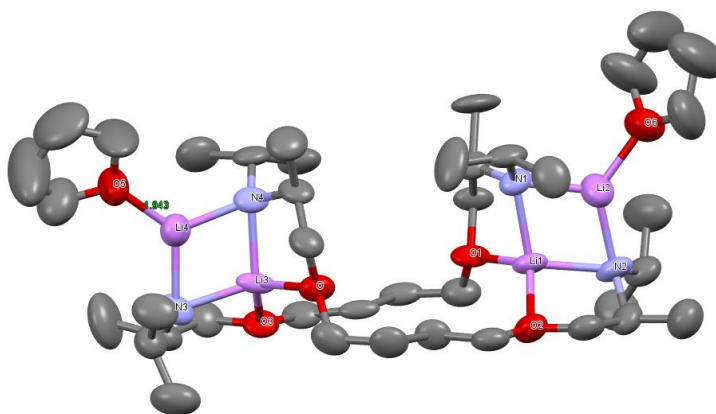


Figure 8.2. Crystal structure of DEE coordinated dilithiated chiral diamino diethers **11b**. Thermal ellipsoid plots are at the 50% probability level. Hydrogen atoms have been omitted for clarity.

8.3.2 Crystal structure of dilithiated (2*S*,2'*S*')-1,1'-(pentane-1,5-diylbis(oxy))bis(*N*-isopropylpropan-2-amine) **12a** and **12b**

The crystal structures of THF and DEE coordinated dilithiated chiral diamino diether **8** were generated using the same method as those of dilithiated chiral diamino diether **7**.

The crystal structures of DEE solvated and THF solvated dilithiated chiral diamino diether **8** are also dimeric and depicted in Figures 8.3 and 8.4. However, the crystal structures of the dilithiated chiral diamino diether **8** are different from the structures of dilithiated chiral diamino diether **7**. The carbon chains of aggregates **11**, which have four carbon linkers, array parallel to each other in a relatively ordered manner as depicted in Figure 8.1 and 8.1. The distances between corresponding carbon atoms in the alkyl linker chains are relatively constant at around 4.6 to 4.9 Å, as illustrated in Figure 8.5a. In contrast, the arrangement of the alkyl chains of aggregates **12** is relatively disordered. The distances between corresponding carbon atoms in the alkyl chains range from 3.9 to 5.3 Å.

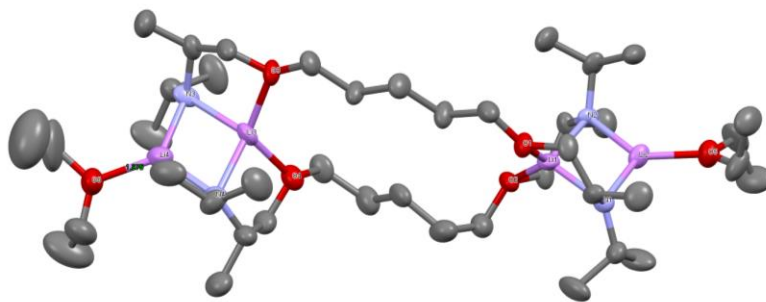


Figure 8.3. Crystal structure of DEE coordinated dilithiated chiral diamino diethers **12a**. Thermal ellipsoid plots are at the 50% probability level. Hydrogen atoms have been omitted for clarity.

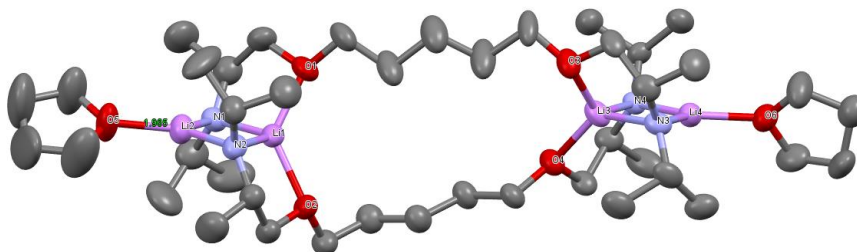


Figure 8.4. Crystal structure of THF coordinated dilithiated chiral diamino diethers **12b**. Thermal ellipsoid plots are at the 50% probability level. Hydrogen atoms have been omitted for clarity.

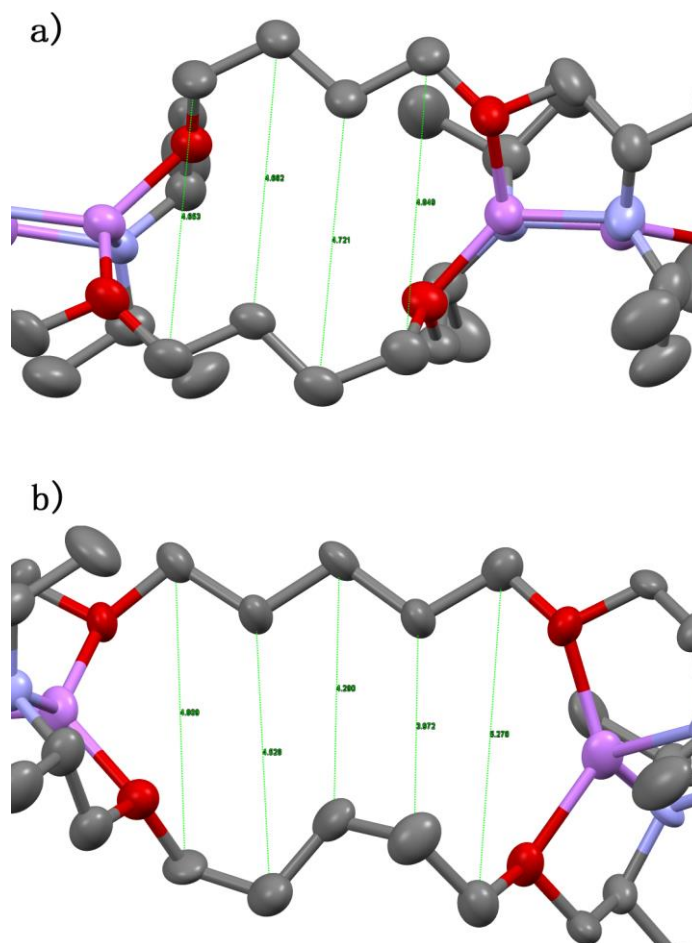


Figure 8.5. (a) Distances between alkyl chains of **11a**. (b) Distances between alkyl chains of **12a**.

8.3.3 Crystal structure of dilithiated (2*S*,2'*S*)-1,1'-(heptane-1,7-diylbis(oxy))bis(*N*-isopropyl-3-methylbutan-2-amine) **13a** and **13b**

The crystal structures of dilithiated (2*S*,2'*S*)-1,1'-(heptane-1,7-diylbis(oxy))bis(*N*-isopropyl-3-methylbutan-2-amine) **9** were formed by adding 2 equiv *n*-BuLi to the diamino diether DEE solution. The solution was then stored at -50 °C for a few days until some white solids formed. After the removal of the solvent at -78 °C, these white solids were

recrystallized by the addition of a small amount of DEE or THF (for the THF coordinated complex) at room temperature. Crystals grew after storing at $-20\text{ }^{\circ}\text{C}$ overnight.

The crystal structures for both of the DEE coordinated and THF coordinated the dilithiated chiral diamino diether **9** are dimers that are structurally similar to those of dilithiated chiral diamino diether **8**. As depicted in Figure 8.6 and 8.7, the chains array in a relatively ordered manner similar to the alkyl chains of crystal structures **11**. The distances between each carbon atom in the alkyl chains are relatively constant at around 4.4 to 4.7 Å as depicted in Figure 8.8. Although the reason for the disordered behavior of **12**, which has a five carbon atoms unit in the alkyl chains, is not known, we did observe a difference in the arrangement of the structures of **12** from **11**. This difference is even pronounced for the lithiated (*S*)-valinol derived diamino diether containing five carbon atom linkers, because its crystal structure is a monomeric instead of dimeric.

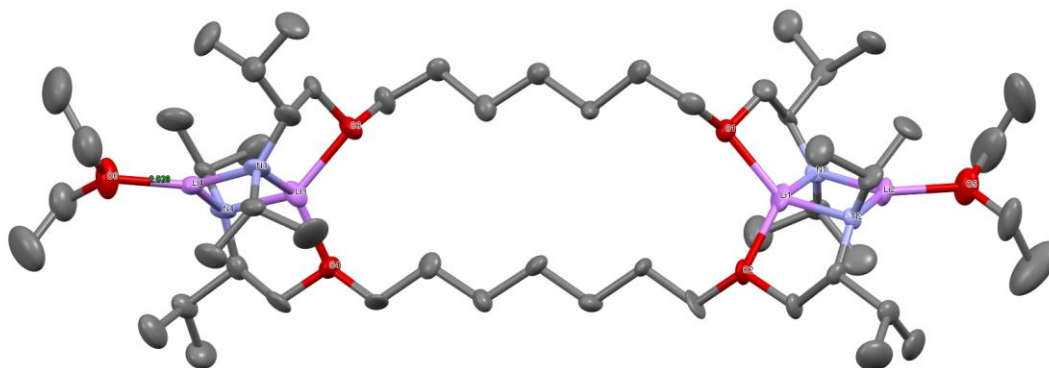


Figure 8.6. Crystal structure of DEE coordinated dilithiated chiral diamino diether **13a**. Thermal ellipsoid plots are at the 50% probability level. Hydrogen atoms have been omitted for clarity.

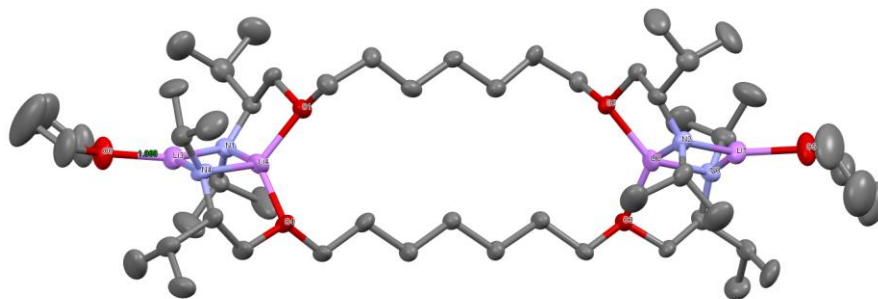


Figure 8.7. Crystal structure of THF coordinated dilithiated chiral diamino diether **13b**. Thermal ellipsoid plots are at the 50% probability level. Hydrogen atoms have been omitted for clarity.

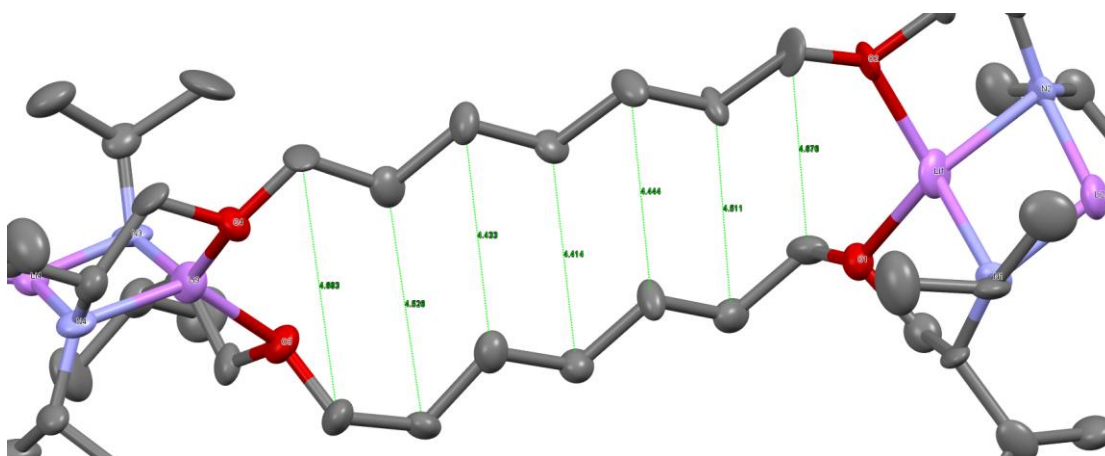


Figure 8.8. Distances between alkyl chains of **13a**.

8.3.4 Crystal Structure of Dilithiated (2*S*,2'*S*)-1,1'-(pentane-1,5-diylbis(oxy))bis(*N*-isopropyl-3-methylbutan-2-amine) **14**

A crystal structure of dilithiated (2*S*,2'*S*)-1,1'-(pentane-1,5-diylbis(oxy))bis(*N*-isopropyl-3-methylbutan-2-amine) **10** was obtained using the same procedure that was used with aggregates **13a,b**.

Unlike the previous six structures, the crystal structure of DEE coordinated dilithiated (2*S*,2'*S*)-1,1'-(pentane-1,5-diylbis(oxy))bis(*N*-isopropyl-3-methylbutan-2-amine) **10** is a monomer with two different types of lithium atoms. As depicted in Figure 8.9, one of the lithium atoms is tri-coordinate while the other one is tetra-coordinate. Both oxygen atoms are coordinated to the same lithium atom making it tetra-coordinate, while the other lithium atom from the Li₂N₂ core is coordinated to the oxygen atom of DEE and is tri-coordinate. The alkyl chain of the monomer bends to form an eight-membered ring incorporating Li1, O1 and O2.

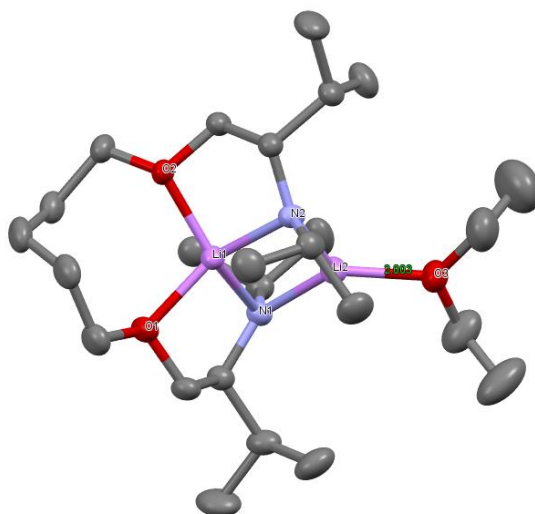


Figure 8.9. Crystal structure of DEE coordinated dilithiated chiral diamino ethers **14**. Thermal ellipsoid plots are at the 50% probability level. Hydrogen atoms have been omitted for clarity.

8.4 Conclusion

Four chiral diamino diether ligands have been synthesized from *N*-isopropyl valinol

or alaninol. Upon lithiation, the crystal structures of the lithium chiral diamido diethers reveal one monomer and six dimeric structures that are solvated by ethereal solvents. X-ray diffraction experiments reveal that the dimers contain two subunits linked together by two alkyl chains. Each subunit adopts a non-equivalent coordination protocol in which one of the lithium atoms is tetra-coordinated while the other one is tri-coordinated. Moreover, the alkyl chain with five carbon atom linker unit is found to array differently from those of four and seven carbon atoms units.

8.5 Experimental Section

8.5.1 Materials and Methods. Tetrahydrofuran (THF), diethyl ether (DEE), dichloromethane (DCM) and pyridine were used from a dry solvent dispensing system. Solvents for extraction and chromatography were technical grade. Unless otherwise stated, purchased chemicals were used as received. All reactions under anhydrous conditions were conducted using flame- or oven-dried glassware and standard syringe techniques under an atmosphere of argon.

NMR spectra were recorded at either 400 MHz or 600 MHz using CDCl_3 or C_6D_6 as the solvent. Chemical shifts are reported in ppm and were referenced to residual protonated solvent for ^1H -NMR (δ 7.27 ppm for CHCl_3 , 7.16 ppm for C_6H_6) and ^{13}C -NMR (δ 77.00 ppm for CDCl_3 , 128.39 ppm for C_6D_6). Data are represented as follows: chemical shift (multiplicity [br = broad, s = singlet, d = doublet, q = quartet, sp = septet, m = multiplet], integration, coupling constants in Hz). Mass spectra were obtained using electrospray ionization method.

8.5.2 General Procedures for the Synthesis of Chiral Diamines **7**, **8**, **9** and **10**.

(*S*)-2-(isopropylamino)propan-1-ol and (*S*)-2-(isopropylamino)-3-methylbutan-1-ol were prepared according to the methods described by Shioiri.⁹ Butane-1,4-diyl bis(4-methylbenzenesulfonate), pentane-1,5-diyl bis(4-methylbenzenesulfonate), and heptane-1,7-diyl bis(4-methylbenzenesulfonate) were prepared according to the methods described by Bulkowski¹⁰ Jackson,¹¹ and Herdering respectively.¹²

Typical Procedure: About 7.36 g (55.1 mmol, 2 equiv) of potassium hydride (30 wt % dispersion in mineral oil) was placed into a flame-dried flask flushed with argon. About 5 mL of dry pentane was added to the flask via syringe and the suspension was stirred for 5 minutes. The mineral oil pentane solution was then removed via syringe. This washing was repeated three times before 80 mL anhydrous THF was added to the flask. A solution of 4.00 g (27.5 mmol, 1 equiv) (*S*)-2-(isopropylamino)-3-methylbutan-1-ol [(*S*)-2-(isopropylamino)propan-1-ol for **9** and **10**] dissolving in 20 mL anhydrous THF was added slowly to the potassium hydride THF suspension stirring at room temperature in 30 minutes using a syringe pump. The yellow suspension was stirred for 4 hours at room temperature. After that, 6.07 g (13.8 mmol, 0.5 equiv) heptane-1,7-diyl bis(4-methylbenzenesulfonate) [butane-1,4-diyl bis(4-methylbenzenesulfonate) was used for **7** and pentane-1,5-diyl bis(4-methylbenzenesulfonate) was used for **8** and **10**] dissolving in 40 mL anhydrous THF was added dropwise using a syringe pump to the suspension. The suspension was allowed to stir overnight at room temperature. The suspension was placed into an ice bath for 10 min before quenching slowly with 30 mL water. The mixture was then extracted with 60 mL ethyl acetate three times and the organic phase was washed with brine and dried over NaSO₄. Evaporation of the solvent and purification of crude

product by flash column chromatography on silica gel (Elution: Hexanes/EtOAc 5:1 with 1% triethyl amine) gave pure (2*S*,2'*S*)-1,1'-(heptane-1,7-diylbis(oxy))bis(*N*-isopropyl-3-methylbutan-2-amine) **9** as light yellow oil (2.87 g, 7.4mmol, 54%). The purification of (2*S*,2'*S*)-1,1'-(butane-1,4-diylbis(oxy))bis(*N*-isopropylpropan-2-amine) **7** and (2*S*,2'*S*)-1,1'-(pentane-1,5-diylbis(oxy))bis(*N*-isopropylpropan-2-amine) **8** and (2*S*,2'*S*)-1,1'-(petane-1,5-diylbis(oxy))bis(*N*-isopropyl-3-methyl-butan-2-amine) **10** was achieved by vacuum distillation after the evaporation of the solvent by a rotavap.

8.5.3 (2*S*,2'*S*)-1,1'-(butane-1,4-diylbis(oxy))bis(*N*-isopropylpropan-2-amine) **7.** (2*S*,2'*S*)-1,1'-(butane-1,4-diylbis(oxy))-bis(*N*-isopropylpropan-2-amine) was obtained from (*S*)-2-(isopropylamino)propan-1-ol (3.00 g, 25.6mmol) as described above. Purification (bp = 137-139° C, 4 mmHg) gave a light yellow oil (2.25 g, 7.8 mmol, 61%). ¹H NMR (CDCl₃, 400 MHz) δ 3.51-3.37 (m, 4H), 3.34-3.21 (m, 4H), 3.00-2.83 (m, 4H), 1.70-1.58 (m, 4H), 1.58-1.38 (br, 2H), 1.13-0.95 (m, 18H); ¹³C NMR (CDCl₃, 100 MHz) δ 75.4, 70.9, 49.4, 45.4, 26.4, 24.0, 22.8, 17.9; HRMS-ESI m/z: [M + H]⁺ Calcd for C₁₆H₃₇N₂O₂: 289.2850, found: 289.2848.

8.5.4 (2*S*,2'*S*)-1,1'-(pentane-1,5-diylbis(oxy))bis(*N*-isopropylpropan-2-amine) **8.** (2*S*,2'*S*)-1,1'-(pentane-1,5-diylbis-(oxy))bis(*N*-isopropylpropan-2-amine) was obtained from (*S*)-2-(isopropylamino)propan-1-ol (3.00 g, 25.6mmol) as described above. Purification (bp = 149-151° C, 4 mmHg) gave a light yellow oil (2.28 g, 7.5 mmol, 59 %). ¹H NMR (C₆D₆, 600 MHz) δ 3.32-3.18 (m, 8H), 3.00-2.94 (m, 2H), 2.86 (sp, 2H, J = 6.2 Hz), 1.57-1.50 (m, 4H), 1.46-1.38 (m, 2H), 1.20-1.11 (br, 2H), 1.06-1.01 (m, 12H), 0.99 (d, 6H, J = 6.2 Hz); ¹³C NMR (C₆D₆, 150 MHz) δ 86.5, 81.6, 60.3, 56.0, 40.4,

34.8, 33.8, 33.5, 28.8; HRMS-ESI m/z : $[M + H]^+$ Calcd for $C_{17}H_{39}N_2O_2$: 303.3006, found: 303.3004.

8.5.5 (2*S*,2'*S*)-1,1'-(heptane-1,7-diylbis(oxy))bis(*N*-isopropyl-3-methylbutan-2-amine) 9. (2*S*,2'*S*)-1,1'-(heptane-1,7-diylbis(oxy))bis(*N*-isopropyl-3-methylbutan-2-amine) (2.87 g, 7.4 mmol, 54%) was obtained from (*S*)-2-(isopropylamino)-3-methylbutan-1-ol (4.00 g, 27.5mmol) as described above. 1H NMR ($CDCl_3$, 400 MHz) δ 3.42-3.34 (m, 6H), 3.32-3.26 (m, 2H), 2.84 (sp, 2H, $J = 6.1$ Hz), 2.52 (q, 2H, $J = 5.4$ Hz), 1.87-1.75 (m, 2H), 1.63-1.46 (m, 4H), 1.40-1.24 (m, 6H), 1.04 (d, 6H, $J = 2.2$ Hz), 1.02 (d, 6H, $J = 2.2$ Hz), 0.91 (d, 6H, $J = 1.6$ Hz), 0.90 (d, 6H, $J = 1.5$ Hz); ^{13}C NMR ($CDCl_3$, 100 MHz) δ 71.3, 71.2, 59.5, 46.6, 29.6, 29.3, 29.3, 26.2, 23.6, 23.5, 18.6, 18.5; HRMS-FAB m/z : $[M + H]^+$ Calcd for $C_{23}H_{51}N_2O_2$: 387.3951, found: 387.3966.

8.5.6 (2*S*,2'*S*)-1,1'-(petane-1,5-diylbis(oxy))bis(*N*-isopropyl-3-methylbutan-2-amine) 10. (2*S*,2'*S*)-1,1'-(petane-1,5-diylbis(oxy))bis(*N*-isopropyl-3-methylbutan-2-amine) was synthesized according to Dr. Weibin Li's method described in his thesis.

8.5.7 General Procedures for the Crystallization of Lithium Chiral Diamides 11a and 12a. To a solution of the chiral diamine **7** or **8** (0.10 g) in 1 mL diethyl ether at 0 °C under Ar atmosphere was slowly added 2 equiv *n*-BuLi. The reaction mixture was allowed to stir at 0 °C for 5 minutes. The clear yellowish solution was then stored at -50 °C freezer and XRD quality crystals were grown at -50 °C overnight.

8.5.8 General Procedures for the Crystallization of Lithium Chiral Diamides 11b and 12b. To a solution of the chiral diamine **7** or **8** (0.10 g) in 0.9 mL diethyl ether at 0 °C under Ar atmosphere was slowly added 2 equiv *n*-BuLi. Anhydrous THF (0.05 mL)

was then added to the solution and the reaction mixture was allowed to stir at 0 °C for 5 minutes. The clear yellowish solution was then stored at -50 °C freezer and XRD quality crystals were grown at -50 °C overnight.

8.5.9 General Procedures for the Crystallization of Lithium Chiral Diamides 13a and 14. To a solution of the chiral diamine **9** or **10** (0.05 g) in 1 mL diethyl ether at 0 °C under Ar atmosphere was slowly added 2 equiv *n*-BuLi. The reaction mixture was allowed to stir at 0 °C until white precipitates formed. Anhydrous diethyl ether was then added slowly to the mixture until all the precipitates dissolved into the solution and the solution became clear. XRD quality crystals were grown when the solution was stored at -20 °C for overnight.

8.5.10 General Procedures for the Crystallization of Lithium Chiral Diamides 13b. To a solution of the chiral diamine **9** (0.05 g) in 1 mL diethyl ether at 0 °C under Ar atmosphere was slowly added 2 equiv *n*-BuLi. The reaction mixture was allowed to stir at 0 °C until white precipitates formed. Anhydrous THF was then added slowly to the mixture until all the precipitates dissolved into the solution and the solution became clear. XRD quality crystals were grown when the solution was stored at -20 °C for overnight.

8.6 Acknowledgement

The author thanks Dr. Weibin Li for his help in the synthesis of the chiral diamino diether.

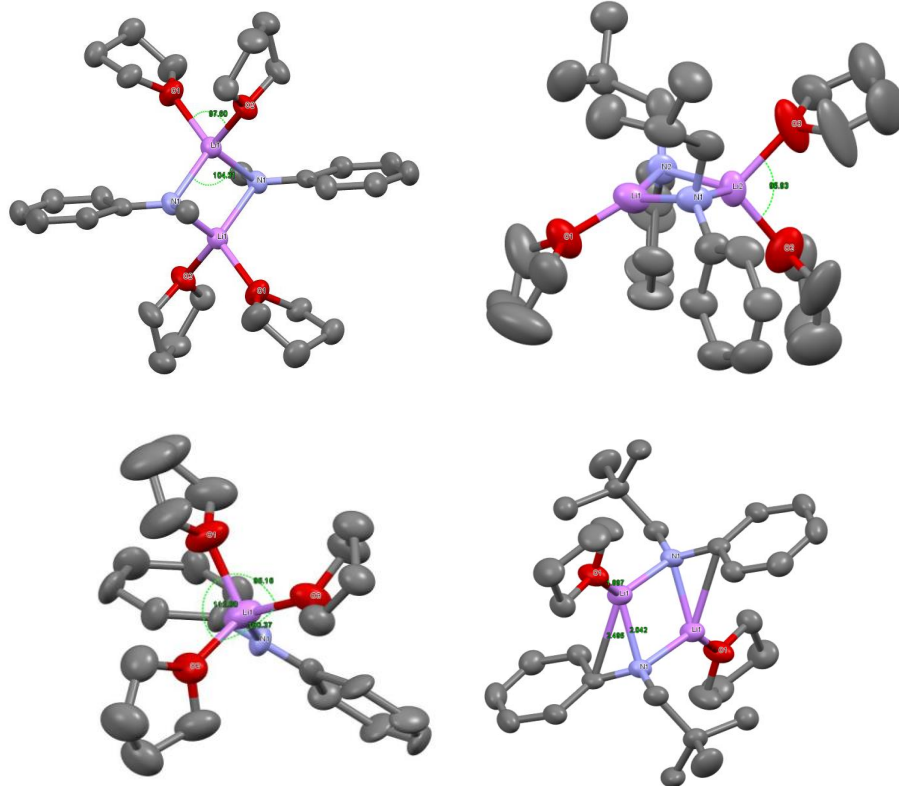
8.7 References

- (1) (a) Collum, D.; McNeil, A. J.; Ramirez, A. *Angew. Chem. Int. Ed.* **2007**, *46*, 3002-3017. (b) Lucht, B.; Collum, D. *Acc. Chem. Res.* **1999**, *32*, 1035-1042. (c) Snieckus, V. *Chem. Rev.* **1990**, *90*, 879-933. (d) Trost, B. M., Fleming, I., Eds. *Comprehensive Organic Synthesis*; Pergamon: Oxford, 1991. (e) Wu, G.; Huang, M. *Chem. Rev.* **2006**, *106*, 2596-2616.
- (2) (a) Whitesell, J. K.; Felman, S. W. *J. Org. Chem.* **1980**, *45*, 755-756. (b) Eleveld, M. B.; Hogeveen, H. *Tetrahedron Lett.* **1984**, *45*, 5187-5190. (c) Shirai, R.; Tanaka, M.; Koga, K. *J. Am. Chem. Soc.* **1986**, *108*, 543-545. (d) Cain, C. M.; Cousins, R. P. C.; Coumbarides, G.; Simpkins, N. S. *Tetrahedron* **1990**, *46*, 523-544. (e) Bhuniya, D.; DattaGupta, A.; Singh, V. K. *J. Org. Chem.* **1996**, *61*, 6108-6113. (f) Corruble, A.; Valnot, J.-Y.; Maddaluno, J.; Duhamel, P. *Tetrahedron: Asymmetry* **1997**, *8*, 1519-1523. (g) Simpkins, N. S.; Hume, S. C. *J. Org. Chem.* **1998**, *63*, 912-913. (h) Corruble, A.; Valnot, J.-Y.; Maddaluno, J.; Duhamel, P. *J. Org. Chem.* **1998**, *63*, 8266-8275. (i) Matsuo, J.; Odashima, K.; Kobayashi, S. *Org. Lett.* **1999**, *1*, 345-348. (j) Arvidsson, P. I.; Davidsson, O.; Hilmersson, G. *Tetrahedron: Asymmetry* **1999**, *10*, 527-534. (k) De Sousa, S. E.; O'Brien, P.; Pilgram, C. D. *Tetrahedron* **2002**, *58*, 4643-4654. (l) Flinois, K.; Yuan, Y.; Bastide, C.; Harrison-Marchand, A.; Maddaluno, J. *Tetrahedron* **2002**, *58*, 4707-4716. (m) Rodeschini, V.; Simpkins, N. S.; Wilson, C. *J. Org. Chem.* **2007**, *72*, 4265-4267. (o) Stivala, C. E.; Zakarian A. *J. Am. Chem. Soc.* **2011**, *133*, 11936-11939.
- (3) (a) Beng, T. K.; Gawley, R. E. *J. Am. Chem. Soc.* **2010**, *132*, 12216-12217. (b) Beng, T. K.; Tyree, W. S.; Parker, T.; Su, C.; Williard, P. G.; Gawley, R. E. *J. Am. Chem. Soc.* **2012**, *134*, 16845-16855.
- (4) (a) Sato, D.; Kawasaki, H.; Shimada, I.; Arata, Y.; Okamura, K.; Date, T.; Koga, K. *J. Am. Chem. Soc.* **1992**, *114*, 761-763. (b) Arvidsson, P. I.; Hilmersson, G.; Ahlberg, P. *J. Am. Chem. Soc.* **1999**, *121*, 1883-1887. (c) Arvidsson, P. I.; Hilmersson, G.; Davidsson, O. *Chem.—Eur. J.* **1999**, *5*, 2348-2355. (d) Sott, R.; Granander, J.; Hilmersson, G. *Chem.—Eur. J.* **2002**, *8*, 2081-2087. (e) Pate, F.; Duguet, N.; Oulyadi, H.; Harrison-Marchand, A.; Fressigne, C.; Valnot, J.; Lasne, M.; Maddaluno, J. *J. Org. Chem.* **2007**, *72*, 6982-6991. (f) Liu, J.; Li, D.; Sun, C.; Williard, P. G.; *J. Org. Chem.* **2008**, *73*, 4045-4052. (g) Lecachey, B.; Duguet, N.; Oulyadi, H.; Fressigne, C.; Harrison-Marchand, A.; Yamamoto, Y.; Tomioka, K.; Maddaluno, J. *Org. Lett.* **2009**, *11*, 1907-1910.
- (5) Williard, P. G.; Sun, C. *J. Am. Chem. Soc.* **1997**, *119*, 11693-11694.
- (6) Li, D.; Sun, C.; Liu, J.; Hopson, R.; Li, W.; Williard, P. G. *J. Org. Chem.* **2008**, *73*, 2373-2381.
- (7) Kagan, G.; Li, W.; Li, D.; Hopson, R.; Williard, P. G. *J. Am. Chem. Soc.* **2011**, *133*, 6596-6602.
- (8) Granander, J.; Sott, R.; Hilmersson, G. *Chem.—Eur. J.* **2006**, *12*, 4191-4197.
- (9) Ando, A.; Shioiri, T. *Tetrahedron* **1989**, *45*, 4969-4988.
- (10) Martin, A. E.; Ford, T. M.; Bulkowski, J. E. *J. Org. Chem.* **1982**, *47*, 412-415.
- (11) Zhou, X.; Day, A. I.; Edwards, A. J.; Willis, A. C.; Jackson, W. G. *Inorg. Chem.* **2005**, *44*, 452-460.

(12) Yu, K. H.; Kim, Y. S.; Kim, S. W.; Park, J. H.; Yang, S. D.; Herdering, W.; Knoechel, A. J. *Label. Compd. Radiopharm.* **2003**, *46*, 1151-1160.

Chapter 9

Crystal structures of lithium *N*-alkylanilides: from tetra-solvated dimer to tri-solvated monomer



9.1 Abstract

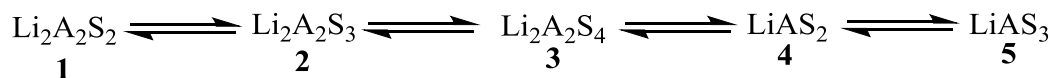
Crystal structure determination of lithiated *N*-methylaniline with a variety of ligands including tetrahydrofuran, methyltetrahydrofuran, dimethyltetrahydrofuran, dimethoxyethane, tetrahydropyran and *N,N*-diethylpropionamide reveals a common four-membered ring dimeric structure motif. A transition from tetrasolvated dimer ($\text{PhNMeLi}_2 \cdot \text{S}_4$) through trisolvated dimer to disolvated dimer ($\text{PhNMeLi} \cdot \text{S}$)₂ was observed by increasing the steric hindrance of the ligand. Solid state structures of several other lithium *N*-alkylanilides solvated by tetrahydrofuran are also reported. When the methyl group of *N*-methylaniline is replaced by an isopropyl or a phenyl group, a trisolvated monomer is formed instead of a dimer. Interestingly, the solid state structure of lithiated *N*-isobutylaniline in tetrahydrofuran is a trisolvated dimer while lithium *N*-neopentylanilide is a disolvated dimer.

9.2 Introduction

Lithium diisopropylamide (LDA), lithium hexamethyldisilazide (LiHMDS) and lithium tetramethylpiperidine (LiTMP) are widely used to abstract protons from various substrates.¹ The reactivity and aggregation state of LDA, LiHMDS and LiTMP have been extensively studied.^{1,2} Although lithiated secondary anilines are also useful in deprotonation reactions,³ knowledge of their reactivity, aggregation and solvation states is not as well established as those of LDA, LiHMDS and LiTMP. More importantly, lithium phenolates display similar behavior as lithium enolates and are often used as the models of enolate.⁴ Analogously lithium anilides are used as the models of lithium enamides

which are important substitutes for enolates.⁵

In 1987, Jackman reported a series of NMR experiments to evaluate the solution structures of several lithium anilides including indolide, 2-methylindolide, methylanilide, tetrahydroquinolide, isopropylanilide and butylanilides in ethereal solvents.⁶ The results suggest that the aggregation state of lithium anilides depends on steric properties. Jackman proposed that different lithium anilide aggregates were in equilibrium as depicted in Scheme 9.1, where A represents anilide and S represents solvent. Depending on the steric hindrance of the anilides, only one or two aggregates co-exist. It is noteworthy that no evidence of the existence of aggregate **2** was proposed by Jackman. Moreover, definitive evidence for the existence of a trisolvated monomer corresponding to aggregate **5** is rare. Collum and coworkers carried out thorough studies of lithium diphenylamide.⁷ These studies led to the conclusion that lithium diphenylamide exists as a dimer and a monomer in equilibrium with each other in tetrahydrofuran (THF). However, the solvation state of the monomeric aggregate remains obscure.



Scheme 9.1. Equilibrium of lithium anilide aggregates (**1-5**)

In an attempt to obtain a greater understanding of the structure of lithium anilides, as well as to augment the previous work done by Jackman and Collum, we synthesized and crystallized a series of lithium *N*-alkylanilides in ethereal solvents. The crystal structures of fourteen lithium anilides were obtained and are reported. These structures reveal that the aggregation and solvation states highly depend on the steric factors of the anilide as

well as those of the solvent. These results not only provide vital details of the structure of previous species observed in solution by Jackman and Collum, but they also offer important solvation information about the lithium anilides.

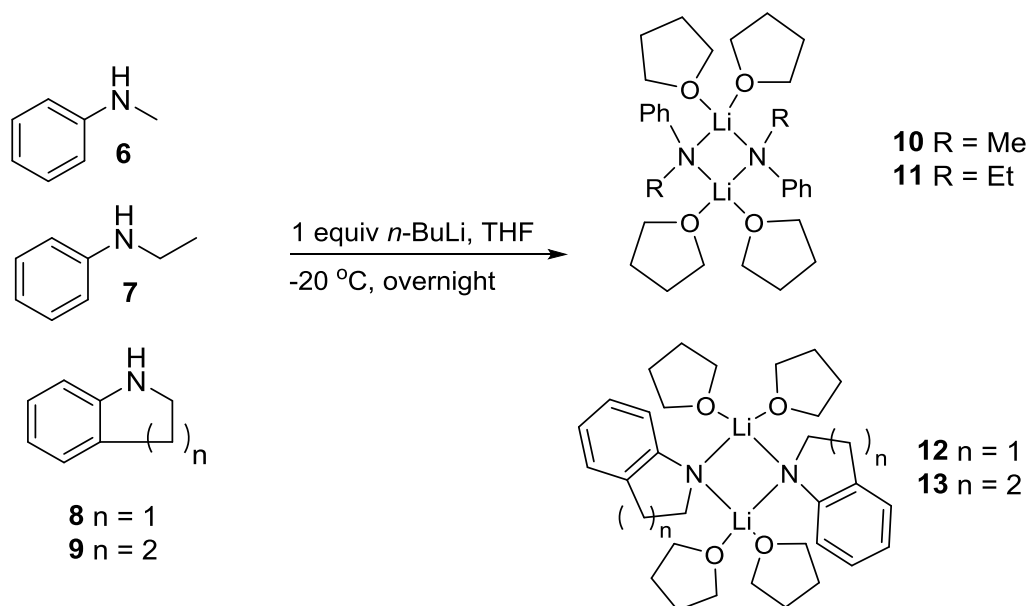
9.3 Results and Discussion

9.3.1 Tetrahydrofuran tetra-solvated dimers of various lithium anilides

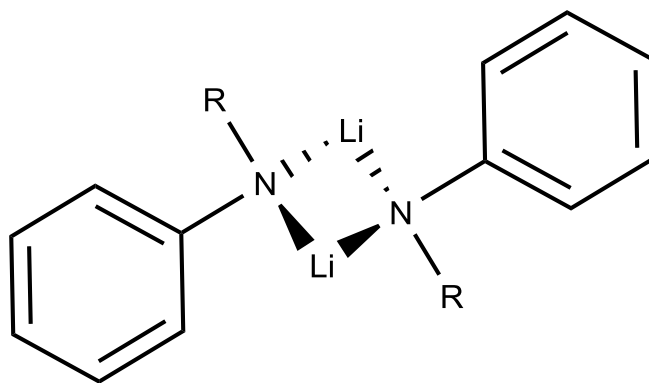
The THF solvates of lithiated *N*-methylaniline **6**, *N*-ethylaniline **7**, indoline **8** and tetrahydroquinoline **9** are tetra-solvated dimers as determined by x-ray diffraction analyses. As depicted in Scheme 9.2, 1 equiv *n*-butyllithium (*n*-BuLi) was added to the anilines dissolved in pentane to generate yellow precipitates. These precipitates dissolved in THF. By storing the resulting solutions at -20 °C overnight, we were able to obtain crystals suitable for x-ray crystallography.

A few crystal structures of tetrasolvated lithium secondary amides are reported.⁸ Newly obtained crystal structures of lithium *N*-methylanilide **10**, *N*-ethylanilide **11**, indolinide **12** and tetrahydroquinolide **13** are depicted in Figures 9.1, 9.2, 9.3 and 9.4, as dimers with a planar Li₂N₂ core with the tetracoordinate lithium atoms. The four lithium anilide dimers all adopt a structure in which the phenyl groups of the anilides are *trans* to each other as illustrated in Scheme 9.3. The N-Li-N angles within the Li₂N₂ core are very similar for all four structures (103.3°-104.3°); however, the O-Li-O angles are significantly different, see figures 1-4. The O-Li-O angles of **10** and **12** are 97.6° and 98.6° respectively. The O-Li-O angle of **13** is 95.3° whereas the corresponding angle of **11** is 92.4° which is significantly smaller than those of **10** and **12**. Since the terminal

methyl group of **11** points away from the plane shared by the phenyl and methylene groups of the *N*-ethylanilides, as seen in Figure 9.2, we ascribe the relatively small O-Li-O angle of **11** to the steric effect of the ethyl group.



Scheme 9.2. Crystallization of THF tetra-solvated lithium anilides **10**, **11**, **12** and **13**



Scheme 9.3. The *trans* structure of lithium anilides **10**, **11**, **12** and **13**

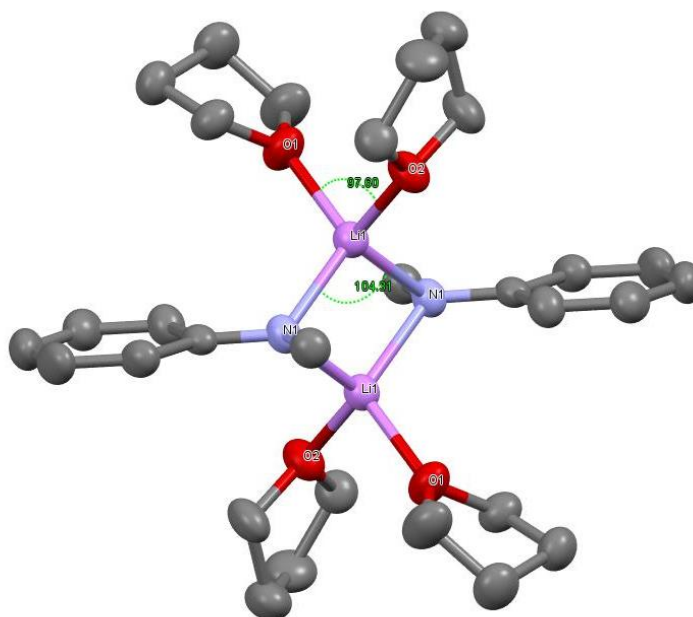


Figure 9.1. Crystal structure of THF solvated lithium *N*-methylanilide **10**. Thermal ellipsoid plots are at the 50% probability level. Hydrogen atoms have been omitted for clarity.

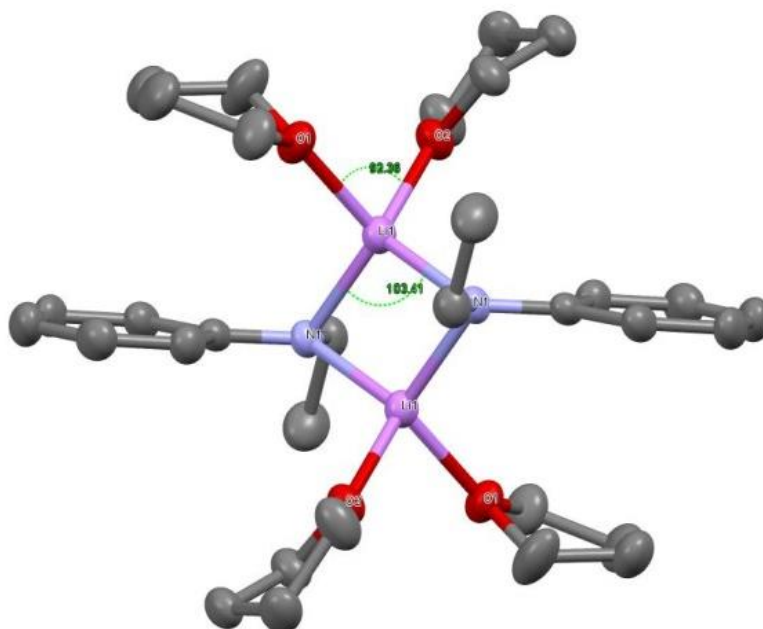


Figure 9.2. Crystal structure of THF solvated lithium *N*-ethylanilide **11**. Thermal ellipsoid plots are at the 50% probability level. Hydrogen atoms have been omitted for clarity.

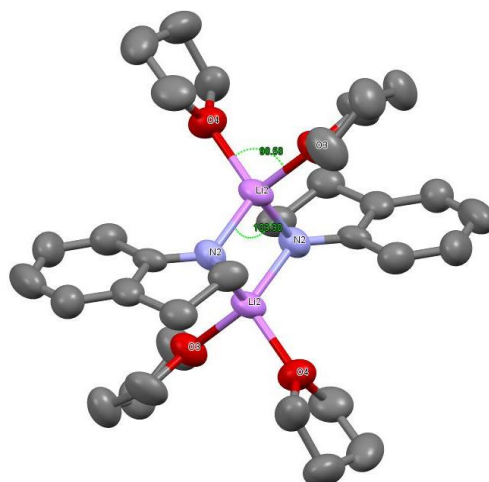


Figure 9.3. Crystal structure of THF solvated lithium indolide **12**. Thermal ellipsoid plots are at the 50% probability level. Hydrogen atoms have been omitted for clarity.

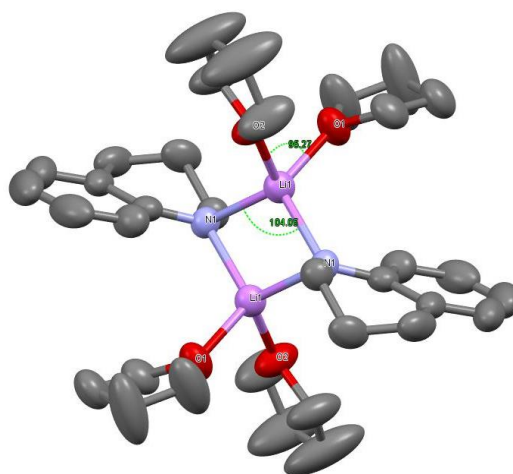


Figure 9.4. Crystal structure of THF solvated lithium tetrahydroquinolide **13**. Thermal ellipsoid plots are at the 50% probability level. Hydrogen atoms have been omitted for clarity.

9.3.2 Tetrahydropyran, methyltetrahydrofuran and *N,N*-diethylpropionamide tetra-solvated dimers of lithium *N*-methylanilide

The crystals of tetrahydropyran (THP), methyltetrahydrofuran and *N,N*-diethylpropionamide solvated lithium *N*-methylanilide were prepared using the same method

previously described. As illustrated in Figures 9.5, 9.6 and 9.7, the solid structures of THP solvated lithium *N*-methylanilide **14**, 2-methyltetrahydrofuran (MeTHF) solvated lithium *N*-methylanilide **15** and *N,N*-diethyl-propionamide (DEPA) solvated lithium *N*-methylanilide **16** are all tetrasolvated dimers. These are similar to the structure of THF tetrasolvated lithium *N*-methylanilide in Figure 9.1. The two *N*-methylanilides nearly lie on the same plane and adopt the *trans* structure same as previously described.

The O-Li-O angle in dimer **15** equals to 92.3°. It is significantly smaller than that of structure **10** and is nearly the same as the O-Li-O angle of structure **11**. We attribute the compression of the O-Li-O angle to the steric interaction the methyl group of MeTHF with the anilide. As illustrated in Figure 9.6, the methyl groups of all four MeTHF molecules point away from the plane shared by two molecules of *N*-methylanilides.

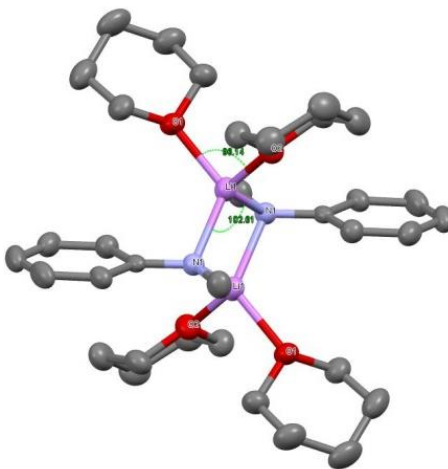


Figure 9.5. Crystal structure of THP solvated lithium *N*-methylanilide **14**. Thermal ellipsoid plots are at the 50% probability level. Hydrogen atoms have been omitted for clarity.

In the crystal structure **16**, the dimeric lithium *N*-methylanilide is solvated by four DEPA molecules. As expected, the oxygen atom coordinates to the lithium instead of the

nitrogen atom of the amide group. The O-Li-O angle equals 104.7° which is significantly larger than that of structure **10** because the steric hindrance around the carbonyl oxygen is less than the hindrance around the ethereal oxygen of THF. Structure **16** also provides some insight into the basicity of lithium *N*-methylanilide in that DEPA appears in this complex unenolized.

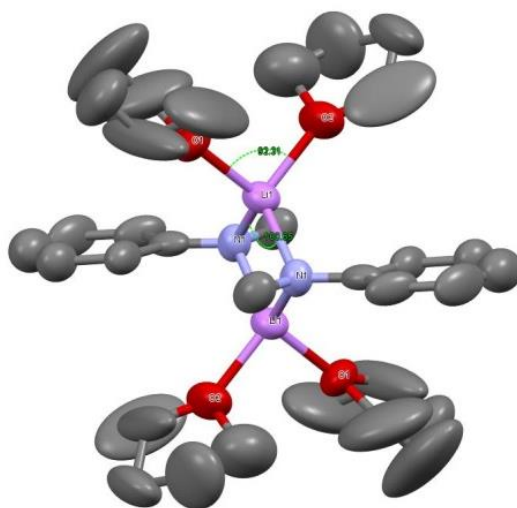


Figure 9.6. Crystal structure of MeTHF solvated lithium *N*-methylanilide **15**. Thermal ellipsoid plots are at the 50% probability level. Hydrogen atoms have been omitted for clarity.

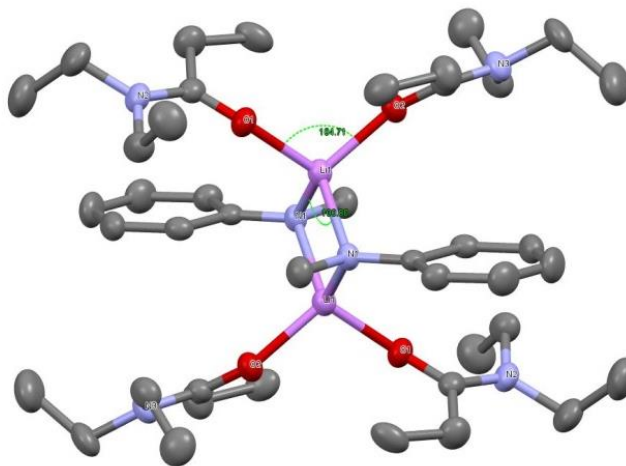


Figure 9.7. Crystal structure of DEPA solvated lithium *N*-methylanilide **16**. Thermal ellipsoid plots are at the 50% probability level. Hydrogen atoms have been omitted for clarity.

9.3.3 Dimethoxymethane tetra-solvated dimers of two lithium *N*-alkylanilides

In 1987, Snaith and coworkers reported the crystal structure of a *N,N,N',N'*-tetramethylethylenediamine (TMEDA) disolvated lithium *N*-methylanilide dimer.⁹ Later, Schleyer and coworkers reported the solid structure of TMEDA disolvated lithium indolate dimer.¹⁰ The TMEDA disolvated lithium *N*-diphenylamide dimer was reported by O'Hara et al. in 2009.¹¹ Since dimethoxymethane (DME) is also a bidentate ligand, we anticipated that the solid structure of DME solvated lithium anilides would adopt the same motif as the TMEDA solvate. However, the solid structure of TMEDA solvated LiHMDS differs from that of DME solvated LiHMDS. The former is a monosolvated monomer while the latter is a η^1 -DME disolvated dimer.¹² Therefore, we attempted to crystallize the DME solvated lithium *N*-methylanilide and *N*-ethylanilide to evaluate the solvation state of the lithium with DME.

As depicted in Figures 9.8 and 9.9, the crystal structures of DME solvated lithium *N*-methylanilide **17** and *N*-ethylanilide **18** adopt the same solvation pattern as the TMEDA solvated lithium *N*-methylanilide. Both are η^2 -DME disolvated dimers with a planar Li_2N_2 core in which the lithium atoms are tetracoordinate. The dimers both adopt the *trans* structure depicted in Scheme 9.3. Similar to structure **11**, the terminal methyl groups in structure **18** also point away from the plane shared by the phenyl and methylene groups of the *N*-ethylanilides. However, the O-Li-O angle of structure **18** is very similar to that of structure **17** because the steric hindrance of one DME molecule is significantly smaller than the hindrance of two THF molecules.

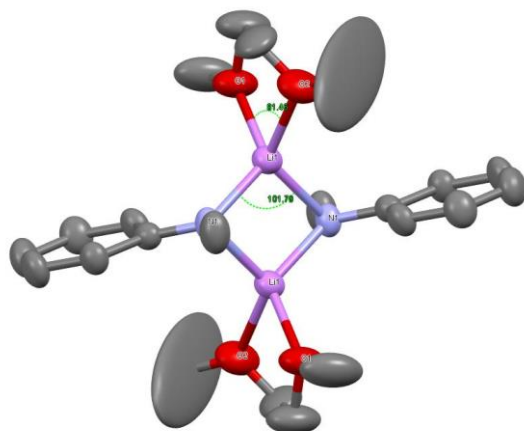


Figure 9.8. Crystal structure of DME solvated lithium *N*-methylanilide **17**. Thermal ellipsoid plots are at the 50% probability level. Hydrogen atoms have been omitted for clarity.

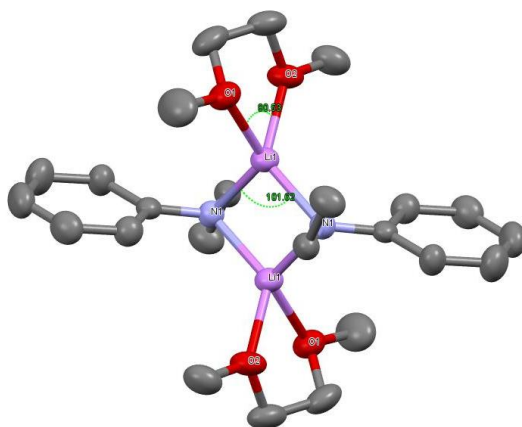


Figure 9.9. Crystal structure of DME solvated lithium *N*-ethylanilide **18**. Thermal ellipsoid plots are at the 50% probability level. Hydrogen atoms have been omitted for clarity.

9.3.4 Dimethyltetrahydrofuran di-solvated dimer of lithium *N*-methylanilide

To assess the effect of steric hindrance of solvent on the aggregation and solvation states of lithium *N*-methylanilide, we crystallized 2,5-dimethyltetrahydrofuran (DMTHF) lithium *N*-methylanilide using the method described previously. The crystal structure is a

DMTHF di-solvated dimer is analogous to numerous bis solvated dimeric lithium amide structures as well as the structures of diethyl ether di-solvated *N*-(2,2-dimethyl-1-methylenepropyl)-*N*-lithiobenzeneamine and THF solvated lithium dipentafluorobenzene amide.¹³ The phenyl groups of the methylanilides are *trans* to each other in a distorted plane. The lithium atoms in the Li₂N₂ core bind to the nitrogen of the anilide and are in close proximity, 2.47 Å, to the *ipso* carbon of the benzene ring. This result suggests the existence of auxiliary π coordination in this complex.

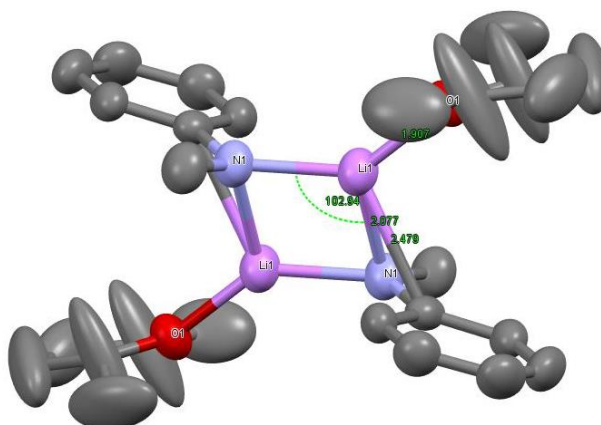


Figure 9.10. Crystal structure of DMTHF solvated lithium *N*-methylanilide **19**. Thermal ellipsoid plots are at the 50% probability level. Hydrogen atoms have been omitted for clarity.

9.3.5 Tetrahydrofuran tri-solvated monomers of lithium *N*-isopropylanilide and *N*-diphenylamide

To assess the effect steric hindrance of the alkyl group on the aggregation and solvation states of lithium *N*-alkylanilide, crystals of THF solvated lithium *N*-isopropylanilide and *N*-diphenylamide were grown. As illustrated in Figures 9.11 and 9.12, the crystal structures are THF trisolvated monomers similar to the solid structure of

THF trisolvated monomer of lithium phenothiazide reported by Cragg-Hine and coworkers.¹⁴ The three O-Li-O angles of structure **20** are 95.2°, 100.4° and 112.8° whereas the three O-Li-O angles of structure **21** are 93.9°, 96.6° and 111.2°. The values suggest that the steric hindrance of isopropyl group is slightly larger than the phenyl group. The THF trisolvated monomers provide an important clue for the solvation state of lithium diphenylamide in THF.^{5b} These structures illustrate that the formation of a THF trisolvated monomer occurs upon addition of a methyl group to the α -carbon of *N*-methylanilide (Scheme 9.4).

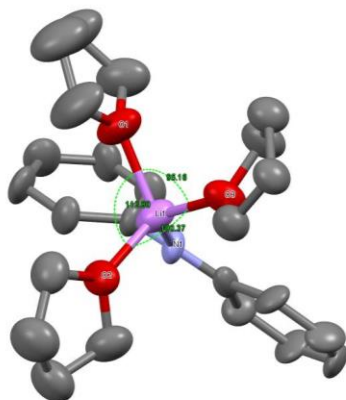


Figure 9.11. Crystal structure of THF solvated lithium *N*-diphenylamide **20**. Thermal ellipsoid plots are at the 50% probability level. Hydrogen atoms have been omitted for clarity.

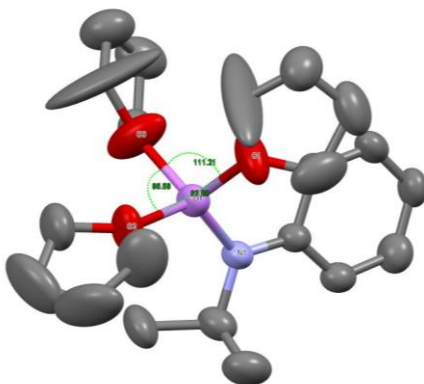
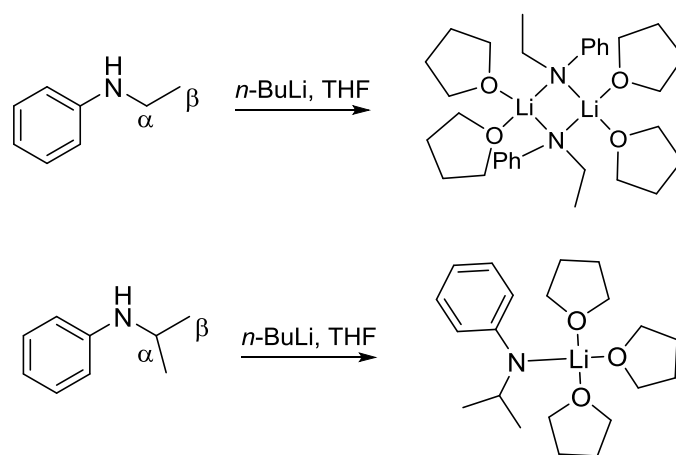


Figure 9.12. Crystal structure of THF solvated lithium *N*-isopropylanilide **21**. Thermal ellipsoid plots are at the 50% probability level. Hydrogen atoms have been omitted for clarity.



Scheme 9.4. Branched chains of *N*-alkylanilines

9.3.6 Tetrahydrofuran tri-solvated dimer of lithium *N*-isobutylanilide and tetrahydrofuran di-solvated dimer of lithium *N*-neopentylanilide

In an attempt to assess how the size of the alkyl group in *N*-alkyl lithium anilides influences the aggregation and solvation states of lithium *N*-alkylanilides, we synthesized and crystallized THF solvated lithium *N*-isobutylanilide and lithium *N*-neopentylanilide as representative exemplars of increasingly larger substrates.

The solid structure of THF solvated *N*-isobutylanilide is an unusual trisolvated dimer as depicted in Figure 9.13. The Li_2N_2 core is not planar and the phenyl groups of the anilides are *cis* to each other. There are two different lithium atoms with one tricoordinate and another one tetracoordinate. Moreover, the two *cis* isobutyl groups bend towards the same direction of tri-coordinate lithium atom and thus, provide enough space for the two THF molecules to bind with the other lithium atom in the opposite direction. This solid structure of trisolvated dimer supports the existence of aggregate **2** proposed by Jackman.^{4a}

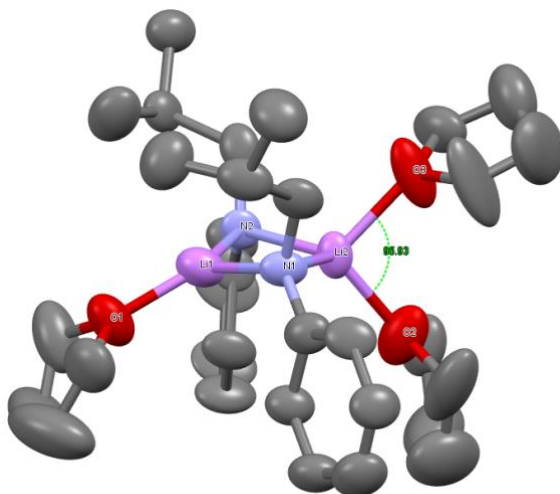


Figure 9.13. Crystal structure of THF solvated lithium *N*-isobutylanilide **22**. Thermal ellipsoid plots are at the 50% probability level. Hydrogen atoms have been omitted for clarity.

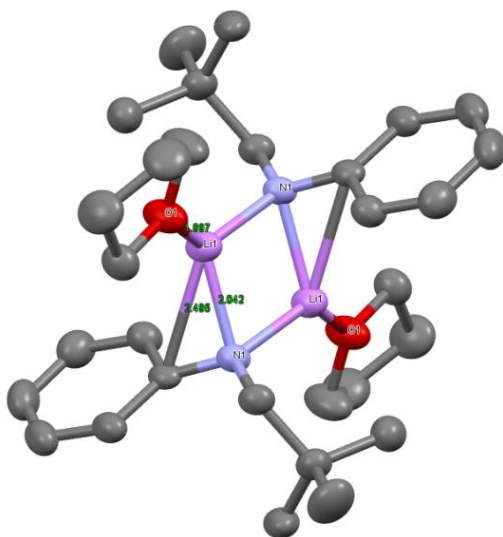


Figure 9.14. Crystal structure of THF solvated lithium *N*-neopentylanilide **23**. Thermal ellipsoid plots are at the 50% probability level. Hydrogen atoms have been omitted for clarity.

Further increase in steric hindrance of the β carbon of the alkyl group leads to the formation of THF disolvated dimer. As depicted in Figure 9.14, the THF solvated lithium *N*-neopentylanilide is a disolvated dimer similar to the DMTHF disolvated dimer of

lithium *N*-methylanilide. In 2001, Lappert and coworkers reported the crystal structure of diethyl ether di-solvated dimer of lithium *N*-neopentylanilide.¹⁵ In the THF disolvated dimer depicted in Figure 9.14 and the Lappert compound, the phenyl groups of the anilides are *trans* to each other in a distorted plane and the two neopentyl groups point in opposite directions. Similar to structure **19**, the lithium atoms in structure **23** and the analogous diethyl ether solvate display a short contact with the *ipso* carbon of the benzene ring (approximately 2.5 Å).

Taken together, these results suggest that the increase in the steric hindrance of β carbon of the alkyl group affects the solvation state significantly. While the lithium anilides in solid structures **11**, **22** and **23** are all dimeric, the solvation state changes from tetra-solvated in structure **11** to disolvated in structure **23** with the increase of the steric hindrance of β carbon of the alkyl group.

9.4 Conclusion

It is clearly evident that the solid structures of lithium *N*-alkylanilides highly depend on the steric factors in both the alkyl group and the solvating solvent. With sterically unhindered alkyl groups, lithium *N*-methylanilide, *N*-ethylanilide, indolide and tetrahydroquinolide crystallize as tetrasolvated dimers in THF. An increase of steric hindrance in the α -carbon of the alkyl group alters the aggregation state to a monomer in THF. This is evident in the solid structures of THF trisolvated monomer of lithium diphenylamide and lithium *N*-isopropylanilide. However, upon increase in steric hindrance of the β -carbon, the solvation state changes instead of the aggregation state.

The crystal structure of THF solvated lithium *N*-isobutylanilide is a trisolvated dimer and supports this conclusion. Moreover, further increase in steric hindrance of the β -carbon leads to the formation of THF disolvated dimer as the THF solvated lithium *N*-neopentylanilide.

The size of coordinating solvent alters the solvation state of the dimeric lithium *N*-methylanilide. With relatively unhindered coordinating solvents, the solid structures of lithium *N*-methylanilide are all tetrasolvated dimers in THF, THP, DEPA and MeTHF. The crystal structures of lithium *N*-methylanilide and *N*-ethylanilide with relatively unhindered coordinating DME, which is a bidentate ligand, are also disolvated dimers; however, the lithium atoms are tetracoordinate, identical to that of the tetra-solvated dimers. When sterically hindered DMTHF is used as the coordinating solvent, the structure motif changes to a disolvated dimer in the solid state.

Most importantly, these results confirm the existence of a trisolvated dimeric aggregate **2**. They also provide proof of the solvation states of these lithium anilides. We believe that these results provide some definitive insight into the relationship between substrate and/or solvent size to both the aggregation and/or solvation state of the corresponding lithiated derivatives in a homologous series of *N*-substituted anilines ranging from trisolvated monomers through di-, tri-, and tetrasolvated tetramers.

9.5 Experimental Section

9.5.1 Synthesis of *N*-neopentylaniline. *N*-neopentylaniline was synthesized by the method described by Lappert.¹⁵

9.5.2 General Procedure for the crystallization of THF solvated lithium *N*-methylanilide 10, *N*-ethylanilide 11, indolide 12, tetrahydroquinolide 13 and *N*-neopentylanilide 23. To a solution of the *N*-alkylaniline (0.9 mmol) in 1 mL anhydrous pentane at 0 °C under Ar atmosphere was slowly added 1 equiv *n*-BuLi. The reaction mixture was allowed to stir at 0 °C until light yellow to orange precipitates formed. Anhydrous THF was then added slowly to the mixture until all the precipitates dissolved into the solution and the solution became clear. XRD quality crystals were grown when the solution was stored at -20 °C for overnight.

9.5.3 General Procedure for the crystallization of THF solvated lithium *N*-isobutylanilide 22. To a solution of the *N*-isopropylaniline (0.9 mmol) in 1 mL anhydrous pentane at 0 °C under Ar atmosphere was slowly added 1 equiv *n*-BuLi. The reaction mixture was allowed to stir at 0 °C until light yellow to orange precipitates formed. Anhydrous THF was then added slowly to the mixture until all the precipitates dissolved into the solution and the solution became clear. Precipitates formed after storing the solution at -78 °C freezer overnight. After re-dissolving the crystals at room temperature, the clear solution was stored at -20 °C freezer. XRD quality crystals were grown at -20 °C for overnight.

9.5.3 General Procedure for the crystallization of DEPA solvated lithium *N*-methylanilide 16 and DME solvated lithium *N*-ethylanilide 18. To a solution of the *N*-alkylaniline (0.9 mmol) in 1 mL anhydrous pentane at 0 °C under Ar atmosphere was slowly added 1 equiv *n*-BuLi. The reaction mixture was allowed to stir at 0 °C until light yellow precipitates formed. DEPA or DME was then added slowly to the mixture until all

the precipitates dissolved into the solution and the solution became clear. XRD quality crystals were grown when the solution was stored at -20 °C for overnight.

9.5.4 General Procedure for the crystallization of MeTHF solvated lithium *N*-methylanilide 15, DMTHF solvated lithium *N*-methylanilide 19 and THF solvated lithium diphenylamide 20. To a solution of the *N*-alkylaniline (0.9 mmol) in 1 mL anhydrous pentane at 0 °C under Ar atmosphere was slowly added 1 equiv *n*-BuLi. The reaction mixture was allowed to stir at 0 °C until light yellow or purple precipitates formed. THF or MeTHF or DMTHF was then added slowly to the mixture until all the precipitates dissolved into the solution and the solution became clear. The clear solution was then stored at -50 °C freezer and XRD quality crystals were grown at -50 °C overnight.

9.5.4 General Procedure for the crystallization of THP solvated lithium *N*-methylanilide 14 and DME solvated lithium *N*-methylanilide 17. To a solution of the *N*-methylaniline (0.05 g) in 2 mL THP or DME at room temperature under Ar atmosphere was added 1 equiv *n*-BuLi. The resulting solution was shaken vigorously and then stored at room temperature and XRD quality crystals were grown overnight.

9.6 Acknowledgement

The author thanks Ms. Jie Guang for the provision of the crystal structure of lithium *N*-isopropylanilide.

9.7 References

- (1) (a) Trost, B. M.; Fleming, I., Eds. *Comprehensive Organic Synthesis*; Pergamon: Oxford, **1991**. (b) Wu, G.; Huang, M. *Chem. Rev.* **2006**, *106*, 2596–2616. (c) Collum, D.; McNeil, A. J.; Ramirez, A. *Angew. Chem. Int. Ed.* **2007**, *46*, 3002-3017. (d) Lucht, B.; Collum, D. *Acc. Chem. Res.* **1999**, *32*, 1035-1042. (e) Snieckus, V. *Chem. Rev.* **1990**, *90*, 879-933.
- (2) (a) Satoh, T. *Chem. Rev.* **1996**, *96*, 3303-3325. (b) Lappert, M. F.; Protchenko, A. V.; Power, P. P.; Seeber, A. *Metal Amide Chemistry*; John Wiley & Sons, Ltd.: Chichester, **2009**.
- (3) (a) Xie, L.; Isenberger, K. M.; Held, G.; Dahl, L. M. *J. Org. Chem.* **1997**, *62*, 7516-7519. (b) Abe, T.; Sato, C.; Ushirogochi, H.; Sato, K.; Takasaki, T.; Isoda, T.; Mihira, A.; Yamamura, I.; Hayashi, K.; Kumagai, T.; Tamai, S.; Shiro, M.; Venkatesan, A. M.; Mansour, T. S. *J. Org. Chem.* **2004**, *69*, 5850-5860. (c) Yan, X.-X.; Liang, C.-G.; Zhang, Y.; Hong, W.; Cao, B.-X.; Dai, L.-X.; Hou, X.-L. *Angew. Chem. Int. Ed.* **2005**, *44*, 6544-6546. (d) Jung, M. E.; Zhang, T.-H. *Org. Lett.* **2008**, *10*, 137-140.
- (4) (a) Jackman, L. M.; Smith, B. D. *J. Am. Chem. Soc.* **1988**, *110*, 3829-3835. (b) Jackman, L. M.; Petrei, M. M.; Smith, B. D. *J. Am. Chem. Soc.* **1991**, *113*, 3451-3458. (c) Jackman, L. M.; Rakiewicz, E. F.; Benesi, A. J. *J. Am. Chem. Soc.* **1991**, *113*, 4101-4109. (d) Jackman, L. M.; Chen, X. *J. Am. Chem. Soc.* **1992**, *114*, 403-411. (e) Jackman, L. M.; Chen, X. *J. Am. Chem. Soc.* **1997**, *119*, 8681-8684. (f) Gruver, J. M.; Liou, L. R.; McNeil, A. J.; Ramirez, A.; Collum, D. B. *J. Org. Chem.* **2008**, *73*, 7743-7747. (g) Tomasevich, L. L.; Collum, D. B. *J. Org. Chem.* **2013**, *78*, 7498-7507.
- (5) (a) Jackman, L. M.; Scarmoutzos, L. M.; Smith, B. D.; Williard, P. G. *J. Am. Chem. Soc.* **1988**, *110*, 6058-6063. (b) Wanat, R. A.; Collum, D. B.; Duyne, G. V.; Clardy, J.; DePue, R. T. *J. Am. Chem. Soc.* **1986**, *108*, 3415-3422.
- (6) Jackman, L. M.; Scarmoutzos, L. M. *J. Am. Chem. Soc.* **1987**, *109*, 5348-5355.
- (7) (a) DePue, J. S.; Collum, D. B. *J. Am. Chem. Soc.* **1988**, *110*, 5518-5524. (b) DePue, J. S.; Collum, D. B. *J. Am. Chem. Soc.* **1988**, *110*, 5524-5533.
- (8) (a) Frenzel A.; Herbst-Irmer, R.; Klingebiel, U.; Noltemeyer, M.; Schafer, M. *Z. Naturforsch. B. Chem. Sci.* **1995**, *50*, 1658-1664. (b) Lutz M. Engelhardt, Geraldine E. Jacobsen, Allan H. White, Colin L. Raston. *Inorg. Chem.* **1991**, *30*, 3978-3980.
- (9) Henderson, K. W.; Dorigo, A. E.; Liu, Q.-Y.; Williard, P. G. *J. Am. Chem. Soc.* **1997**, *119*, 11855-11863.
- (10) Barr, D.; Clegg, W.; Mulvey, R. E.; Snaith, R.; Wright, D. S. *J. Chem. Soc., Chem. Commun.* **1987**, 716-718.
- (11) Gregory, K.; Bremer, M.; Bauer, W.; Schleyer, P. v. R. *Organometallics*, **1990**, *9*, 1485-1492.
- (12) Kennedy, A. R.; Klett, J.; O'Hara, C. T.; Mulvey, R. E.; Robertson, G. M. *Eur. J. Inorg. Chem.* **2009**, 5029-5035.

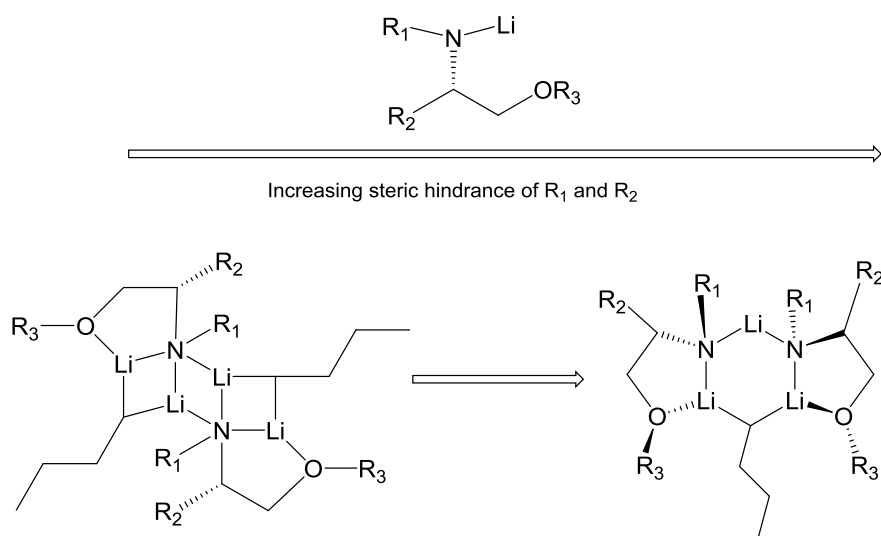
(13) Dietrich, H.; Mahdi, W.; Knorr, R. *J. Am. Chem. Soc.* **1986**, *108*, 2462-2464.

(14) Ball, S. C.; Cragg-Hine, I.; Davidson, M. G.; Davies, R. P.; Edwards, A. J.; Lopez-Solera, I.; Raithby, P. R.; Snaith, R. *Angew. Chem. Int. Ed.* **1995**, *34*, 921-923.

(15) Bezombes, J. P.; Hitchcock, P. B.; Lappert, M. F.; Merle, P. G. *J. Chem. Soc., Dalton Trans.* **2001**, 816-821.

Chapter 10

The Mixed Aggregates of Chiral Lithium Amides



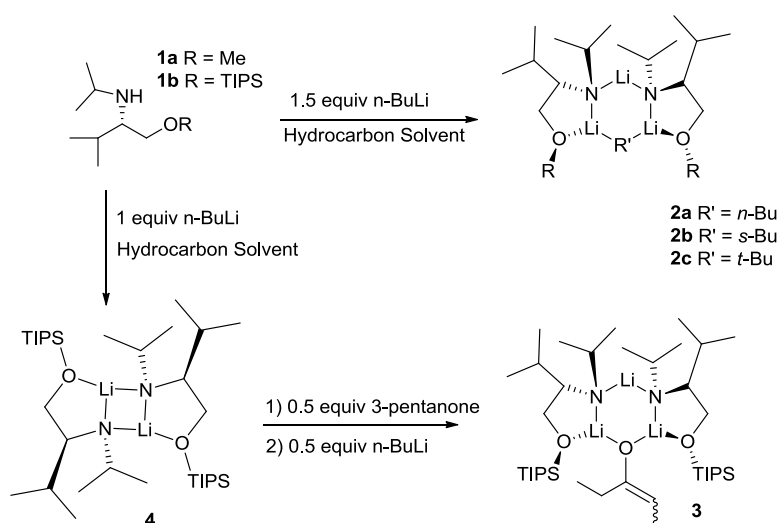
10.1 Abstract

The solution structures of three mixed aggregates consisting of the lithiated amides (*S*)-*N*-isopropyl-1-((triisopropylsilyl)oxy)propan-2-amine, (*R*)-*N*-(1-phenyl-2-((triisopropylsilyl)oxy)ethyl)propan-2-amine, or (*S*)-*N*-isobutyl-3-methyl-1-((triisopropylsilyl)oxy)butan-2-amine and *n*-butyllithium are characterized by various NMR experiments including diffusion-ordered NMR spectroscopy with diffusion coefficient-formula weight correlation analyses and other one- and two-dimensional NMR techniques. We report that steric hindrance of R₁ and R₂ groups of the chiral lithium amide control the aggregation state of the mixed aggregates. With a less hindered R₂ group, lithium (*S*)-*N*-isopropyl-1-((triisopropylsilyl)oxy)propan-2-amine forms mostly a 2:2 ladder-type mixed aggregate with *n*-butyllithium. Increase of steric hindrance of the R₁ and R₂ groups suppresses the formation of the 2:2 mixed aggregate and promotes formation of a 2:1 mixed aggregate. We observe that lithium (*S*)-*N*-isobutyl-3-methyl-1-((triisopropylsilyl)oxy)butan-2-amine forms both a 2:2 mixed aggregate and a 2:1 mixed trimer with *n*-butyllithium. Further increase in the steric hindrance of R₁ and R₂ groups results in the formation of only 2:1 mixed aggregate as observed with lithium (*R*)-*N*-(1-phenyl-2-((triisopropylsilyl)oxy)ethyl)propan-2-amine.

10.2 Introduction

Organolithium amide bases such as lithium diisopropylamide and lithium hexamethyldisilazide are generally used to deprotonate weakly acidic organic compounds such as ketones, esters, etc.¹ Chiral lithium amide bases have also been developed for use

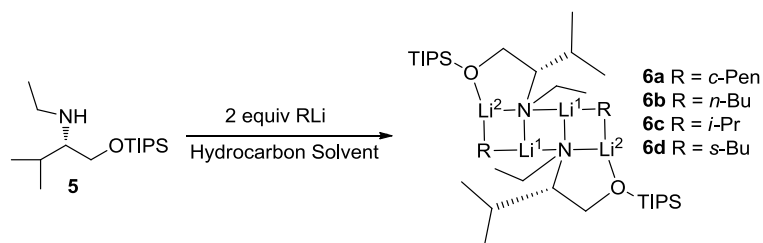
in asymmetric deprotonation and addition reactions.² As a representative example, Koga and coworkers reported a highly enantioselective aldol reaction in the presence of chiral lithium amide bases strongly implicating the influence of mixed aggregates.³ Several groups including Collum,⁴ Davidsson,⁵ Duhamel,⁶ Hilmersson,⁷ McGarrity,⁸ Maddaluno,⁹ Reich,¹⁰ Strohmann,¹¹ and Thomas¹² also reported the formation of mixed aggregates that incorporate lithium amide bases.



Scheme 10.1. The Trimeric 2:1 Complexes **2,3** and the Homodimer **4**

We previously reported the crystal structures of mixed trimers containing two equivalents of the chiral lithium amide derived from *N*-isopropyl valinol **1** and one equivalent of the alkyl lithium reagents depicted as structure **2** in Scheme 10.1.¹³ Later, we also reported both the solid state structure and the solution state characterization of a similar trimeric complex consisting of two equivalents of the chiral lithium amide and 3-pentanone lithium enolate depicted as complex **3**.¹⁴ More recently we reported the homodimeric solution structure **4** of the pure lithiated chiral amine **1** in the absence of

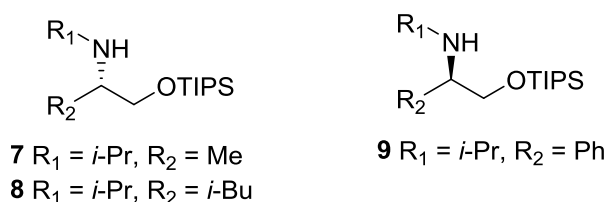
any additional reagents in hydrocarbon solvent.¹⁵ Most recently, we reported the four-rung ladder structures **6a-d** of mixed aggregates consisting of a 2:2 stoichiometric ratio of the chiral lithium amide derived from *N*-ethyl-*O*-triisopropylsilyl valinol **5** and either *n*-butyllithium (*n*-BuLi), *sec*-butyllithium (*s*-BuLi), or isopropyllithium (*i*-PrLi) or cyclopentyllithium.¹⁶ Since the amino acid derived chiral amides are shown to be useful in asymmetric addition and deprotonation reactions,¹⁷ and also since the reactivity and stereoselectivity of chiral lithium mixed aggregates depend on the aggregation state of the reagents,^{6a,f,10b,17} the aggregation state determination of these chiral lithium mixed aggregates is crucial in controlling the mechanism of reactions in which they are employed, and in designing new chiral lithium reagents.



Scheme 10.2. The 2:2 Ladder Structure Mixed Aggregates **6**

In an attempt to rationalize the formation of completely different mixed aggregates, we synthesized chiral amines **7**, **8**, **9** (Scheme 10.3) and characterized the mixed aggregates of lithium amides derived from **7**, **8**, and **9** with *n*-BuLi. We report that the steric factors of R₁ and R₂ group dictate the formation of 2:2 mixed aggregate or 2:1 mixed trimers. With a sterically less hindered methyl group at the R₂ position, lithiated chiral amine **7** forms exclusively 2:2 mixed aggregate with the same motif as aggregates **6**. When the methyl group is replaced by a sterically more hindered isobutyl group at the

R₂ position, lithiated chiral amine **8** forms both 2:2 mixed aggregate and 2:1 mixed trimer similar to the structure of complex **2a**. Further increase in the steric hindrance of R₂ group prevents the formation of 2:2 mixed aggregate, as lithiated chiral amine **9** with a phenyl group at its R₂ position forms 2:1 mixed trimer and only a small amount of homodimer resembling the structure of complex **4**. No 2:2 mixed aggregate is observed with chiral amide derived from **9**.



Scheme 10.3. Chiral amines **7**, **8** and **9**

10.3 Results and Discussion

10.3.1 Solution State Characterization of the 2:2 Mixed Aggregate of Lithiated Chiral Amine **7** and *n*-BuLi (**10**)

Chiral amine **7** was easily synthesized from (*S*)-alanine in three steps following the procedure we have used previously to prepare the *N*-isopropyl-*O*-triisopropylsilyl valinol. The sample for NMR studies was prepared *in situ* by titrating (*S*)-*N*-isopropyl-1-((triisopropylsilyl)oxy)propan-2-amine **7** into a toluene-*d*₈ solution of ⁶Li labeled *n*-BuLi at -40 °C. The titration was monitored by ¹H and ⁶Li NMR as depicted in Figures 10.1 and 10.2 respectively.

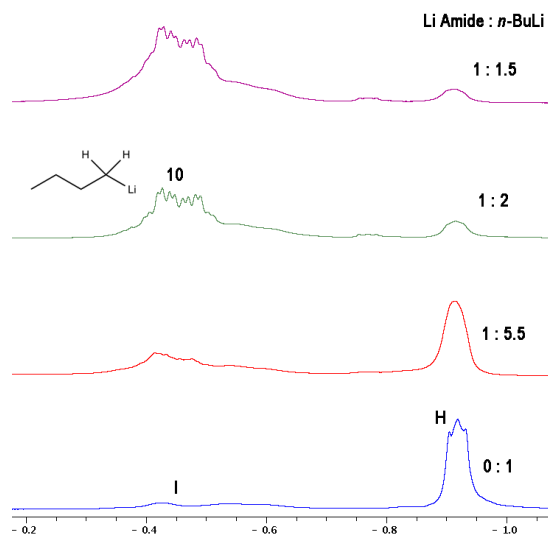


Figure 10.1. ^1H NMR spectra of chiral amine **7** titration of 0.2 M $n\text{-Bu}^6\text{Li}$ toluene- d_8 solution at $-40\text{ }^\circ\text{C}$. H represents the resonance of $n\text{-Bu}^6\text{Li}$ hexamer; I represents the resonances of impurities and mixed aggregates of $n\text{-Bu}^6\text{Li}$ and $n\text{-BuO}^6\text{Li}$; 10 represents the resonances of the 2:2 mixed aggregate **10**.

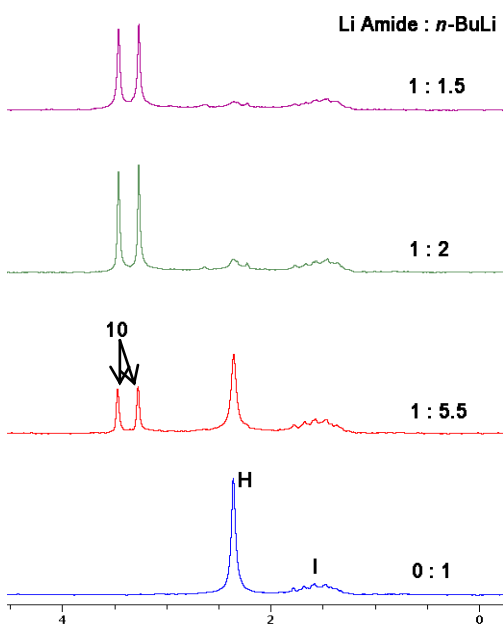
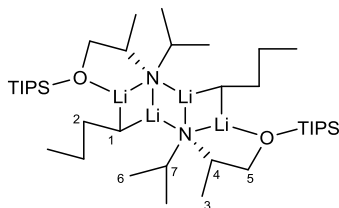


Figure 10.2. ^6Li NMR spectra of chiral amine **7** titration of 0.2 M $n\text{-Bu}^6\text{Li}$ toluene- d_8 solution at $-40\text{ }^\circ\text{C}$. H represents the resonance of $n\text{-Bu}^6\text{Li}$ hexamer; I represents the resonances of impurities and mixed aggregates of $n\text{-Bu}^6\text{Li}$ and $n\text{-BuO}^6\text{Li}$; 10 represents the resonances of the 2:2 mixed aggregate **10**.

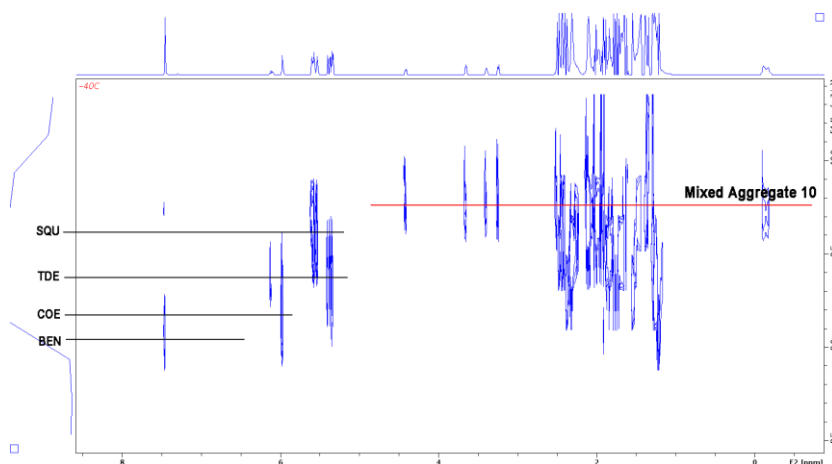
In the ^6Li NMR spectra, *n*-BuLi exhibits one major peak corresponding to a hexamer and a minor broad peak corresponding to some unknown aggregates of *n*-BuLi and *n*-BuOLi. The spectra show clearly the decrease of the resonance of the unsolvated hexameric *n*-BuLi aggregate and the rise of two sharp peaks with 1:1 ratio upon addition of chiral amine **7**. These two sharp peaks dominate when the ratio of lithiated chiral amine **7** to *n*-BuLi equals 1:1.5. These results are consistent with a 2:2 mixed aggregate structure **10** depicted in Table 10.1.

The $^1\text{H}\{^6\text{Li}\}$ HMBC spectrum confirms the formation of a mixed aggregate because both sharp peaks in the ^6Li correlate to the protons of lithiated chiral amine **7** and the α -methylene protons of *n*-BuLi. ^1H and ^{13}C NMR experiments including ^1H NMR, ^{13}C NMR, COSY, HSQC, and HMBC confirm the ^1H and ^{13}C chemical shift assignments. These results are summarized in Table 10.1.²¹ The α -methylene carbon (carbon atom 1) of *n*-BuLi within the mixed aggregate **10** is a quintet ($J = 10.7$ Hz) at 11.9 ppm. This pattern confirms that C (1) of *n*-BuLi interacts with two ^6Li atoms because both the multiplicity and coupling constant comply with the Bauer–Winchester–Schleyer rule.²²

To distinguish a 2:2 mixed aggregate from an 1:1 mixed aggregate, diffusion-ordered NMR spectroscopy and diffusion coefficient-formula weight (D-FW) correlation analysis were performed.^{15,16,17a,23} A linear regression plot of the logarithms of NMR determined diffusion coefficients against the known formula weights of reference standards was used to deduce the formula weight of unknown complexes. In this experiment, benzene (BEN, 78.11 g/mol), cyclooctene (COE, 110.2 g/mol), 1-tetradecene (TDE, 196.4 g/mol) and squalene (SQU, 410.7 g/mol) were added to the sample solution as internal molecular weight references.

Table 10.1. ^1H and ^{13}C signal Assignments of Mixed Aggregate **10**

Carbon atom	^{13}C (ppm)	^1H (ppm)
1	11.9	-0.45
2	35.3	1.94
3	23.8	1.26
4	54.3	3.31
5	66.9	4.06, 2.88
6	26.6	1.39
7	48.5	3.05

**Figure 10.3.** ^1H DOSY of mixed aggregate **10** in toluene- d_8 at $-40\text{ }^\circ\text{C}$.

Distinct resonances of the chiral lithium amide from 2.8 to 4.1 ppm and the resonance of the α -methylene protons of n -BuLi at -0.45 ppm were used for the D-FW analysis because the resonances of the complex from 1.0 to 2.5 ppm overlap with the internal reference resonances. As seen in the ^1H DOSY spectrum (Figure 10.3), the peak of n -BuLi α -methylene protons and distinct peaks from lithiated chiral amine **7** have very similar diffusion coefficients. The result establishes complexation between the lithiated

chiral amine **7** and *n*-BuLi. The average predicted formula weight for the resonances of mixed aggregate **10** is 667 g/mol, a 2.4 % difference from the formula weight of mixed aggregate **10** (683.3 g/mol) (Figure 10.4, Table 10.2).

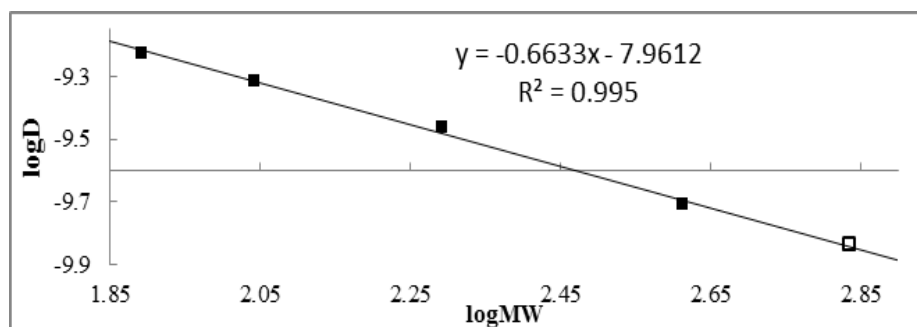


Figure 10.4. D-FW analysis of ^1H DOSY data. Internal references are shown as solid squares and mixed aggregate **10** is shown as open square.

Table 10.2. D-FW Analysis of ^1H DOSY Data of **10**

entry	Compd	FW (gmol $^{-1}$)	10^{-10}D (m 2 /s)	Predicted FW (gmol $^{-1}$)	% error
1	BEN	78.11	5.960	80	-2.9
2	COE	110.2	4.816	110	-0.6
3	TDE	196.4	3.462	182	7.2
4	SQU	410.7	1.967	427	-4.1
5	10 ^a	683.3 ^b	1.480 ^a	656	3.9
6	10 ^a	683.3 ^b	1.466 ^a	666	2.5
7	10 ^a	683.3 ^b	1.413 ^a	704	-3.0
8	10 ^a	683.3 ^b	1.504 ^a	640	6.2
9	10 ^c	683.3 ^b	1.463 ^c	668	2.2
10	10 ^d	683.3 ^b	1.465 ^d	667	2.4

^aThe measured diffusion coefficients are from the resonances of chiral lithium amide. ^b683.3 gmol $^{-1}$ is the formula weight of 2:2 lithiated chiral amine **7**/*n*-BuLi (^6Li labeled) complex **10**. ^cThe measured diffusion coefficient is from the α -methylene protons peak (-0.45 ppm) of *n*-BuLi. ^dThe diffusion coefficient is the average of the above five values.

Overall, our NMR data indicate that when the mole ratio of chiral lithium amide to *n*-BuLi is approximately 1:1, the solution structure of the mixed aggregate between

lithiated, chiral amine **7** and *n*-BuLi in toluene is the 2:2 mixed aggregate **10**. This resembles the structure of mixed aggregate **6b**.

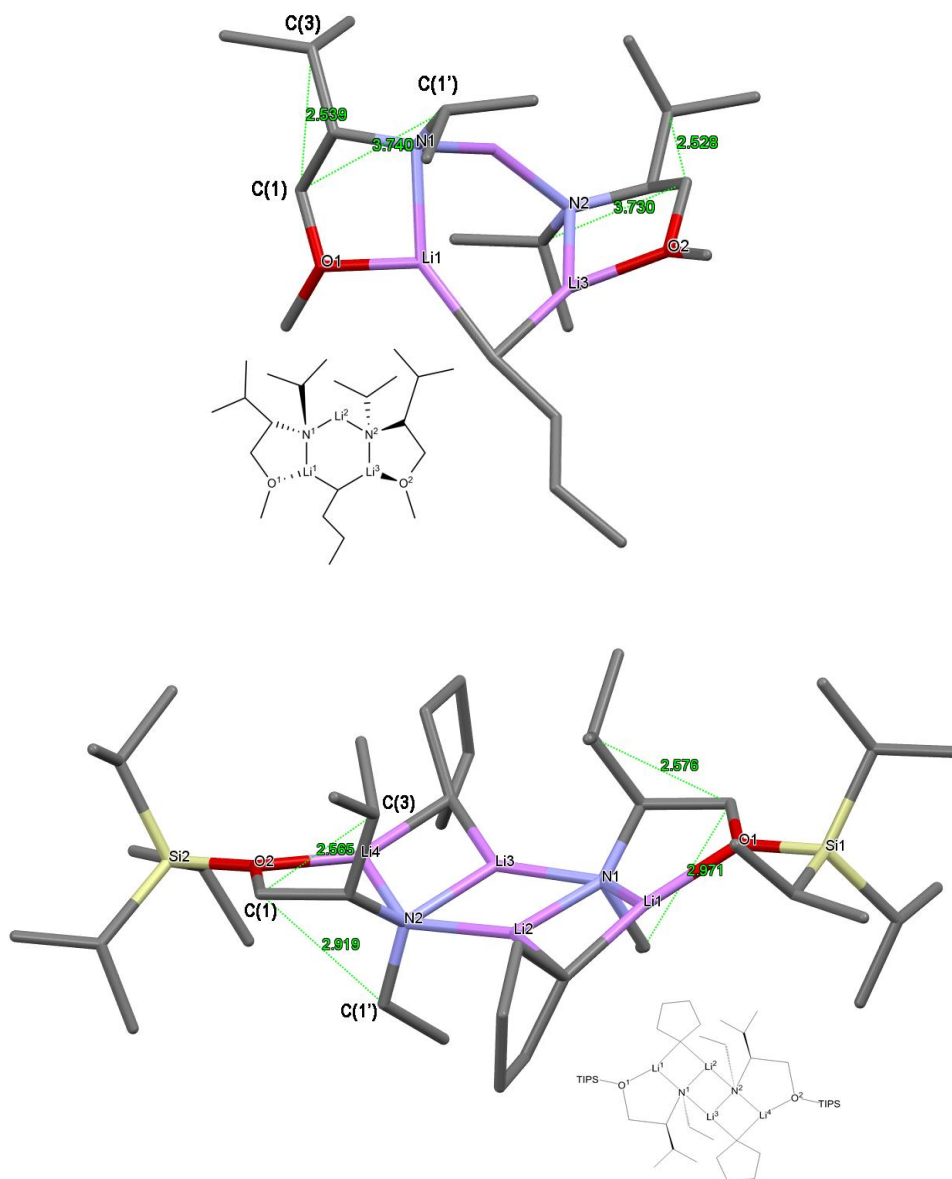
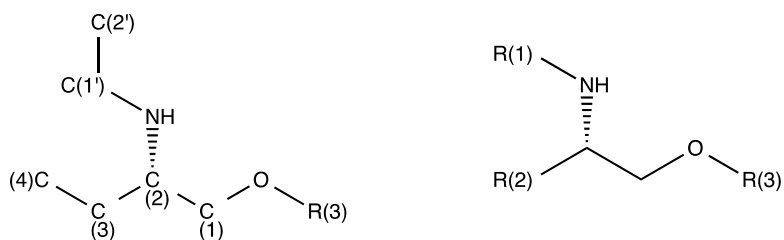


Figure 10.5. Crystal structures of the mixed aggregates **2a** and **6a**.

Previously we reported that lithiated chiral amine **1b** forms the 2:1 mixed trimer **2a** with *n*-BuLi; whereas lithiated chiral amine **5**, with simple replacement of the R₁ group

of **1b** to an ethyl group, forms 2:2 mixed aggregate **6b**. Interestingly, these observations illustrate that lithiated chiral amine **7**, with simple replacement of the R₂ group of **1b** to a methyl group also forms a 2:2 mixed aggregate. This prompted us to compare the crystal structures of **2a**^{13b} and **6a**¹⁶ more carefully. As depicted in Figure 10.5, the distances from C(3) and C(1') carbon to C(1) (Scheme 10.4) in structure **6a** are 2.92 Å and 2.57 Å respectively, while the corresponding distances in structure **2a** are 3.74 Å and 2.54 Å respectively. Therefore, the steric effect between R₁, R₂ groups and C(1) methylene group is significantly reduced when a 2:1 mixed trimer is formed instead of a 2:2 mixed aggregate. Thus we propose that the steric bulk of the R₁ and R₂ groups, especially the hindrance on the C(3) and C(1') carbons, predetermines the formation of 2:2 mixed aggregate or 2:1 mixed trimer. With relatively less hindered R₁ and R₂ groups, lithiated chiral amines **5** and **7** form 2:2 mixed aggregates with *n*-BuLi, while lithiated chiral amines **1a** and **1b** containing relatively hindered R₁ and R₂ groups form 2:1 mixed trimers with *n*-BuLi. To verify our hypothesis, we synthesized and characterized lithiated chiral amine **8**, which has an isobutyl R₂ group and is sterically less hindered than chiral amine **1b** in its C(3) position.



Scheme 10.4. Numbering and labeling scheme of chiral amines

10.3.2 Solution State Characterization of the Mixed Aggregates of Lithiated Chiral Amine **8** and *n*-BuLi (**11** and **12**)

Chiral amine **8** was easily synthesized from (*S*)-leucine in three steps. The sample for NMR studies was prepared by titrating (*S*)-*N*-isobutyl-3-methyl-1-((triisopropylsilyl)-oxy)butan-2-amine **8** into a toluene-*d*₈ solution of ⁶Li labeled *n*-butyllithium at -40 °C. The titration was monitored by ¹H and ⁶Li NMR (Figures 10.6 and 10.7). Upon addition of chiral amine **8**, new peaks around -0.50 to -0.60 ppm emerge and increase in intensity as the amount of lithiated chiral amine **8** increases as shown in Figure 10.6. Moreover, the number of peaks from 2.8 to 4.1 ppm is double the number of peaks of non-lithiated chiral amine **8**, implicating the formation of more than one type of aggregate of lithiated chiral amine **8**. The ⁶Li NMR data, Figure 10.7, shows very clearly the emergence and rise of two downfield sharp peaks with 1:1 intensity upon addition of chiral amine **8**, as well as two sharp peaks with 1:2 intensity slightly upfield of the 1:1 sharp peaks. From the results of our previous findings,^{13,16} we postulate that the 1:1 peaks correspond to 2:2 mixed aggregate **11** and the 1:2 peaks correspond to 2:1 mixed trimer **12** as depicted in Table 10.3.

To verify the existence of the putative mixed aggregates **11** and **12**, we obtained the ¹H {⁶Li} HMBC spectrum. As depicted in Figure 10.8, Li(1) shows a strong correlation to the α -methylene protons of *n*-BuLi (-0.52 ppm) and the proton of the methine (3.16 ppm) group adjacent to nitrogen. Additionally, Li(2) also shows a strong correlation to the α -methylene protons of *n*-BuLi and one of the protons of the methylene (3.42 ppm) group adjacent to oxygen. Moreover, Li(3) shows a strong correlation to the proton of the methine (2.98 ppm) group adjacent to nitrogen while Li(4) shows a strong correlation to

the α -methylene protons of *n*-BuLi (-0.58 ppm) and the proton of the methine (3.12 ppm) group adjacent to nitrogen. These results are consistent with Li(1) and Li(2) representing the 2:2 mixed complex **11** between *n*-BuLi and the lithiated chiral amine **8** and Li(3) and Li(4) representing the 2:1 mixed trimer **12**.

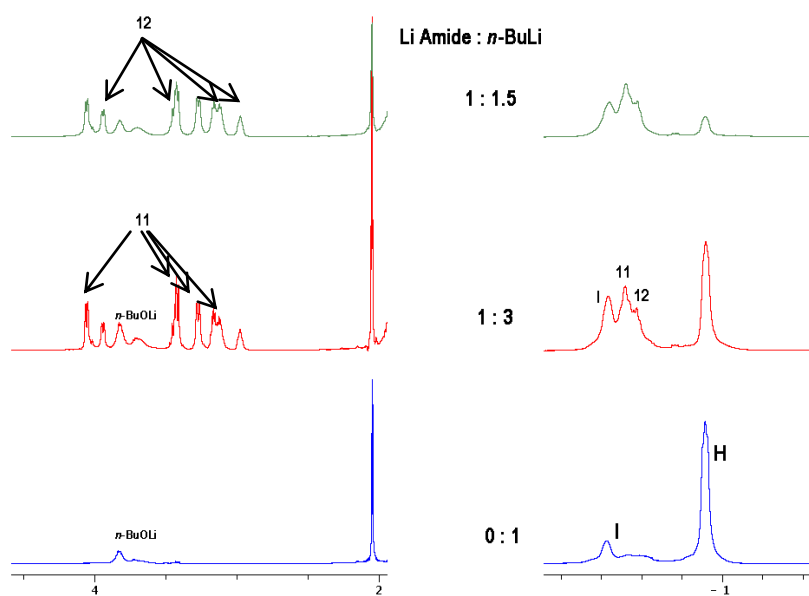


Figure 10.6. ^1H NMR spectra of chiral amine **8** titration of 0.2 M $n\text{-Bu}^6\text{Li}$ toluene- d_8 solution at $-40\text{ }^\circ\text{C}$. H represents the resonance of $n\text{-Bu}^6\text{Li}$ in hexamer; I represents the resonances of impurities and mixed aggregates of $n\text{-Bu}^6\text{Li}$ and $n\text{-BuO}^6\text{Li}$; 11 represents the resonances of the 2:2 mixed aggregate **11**; 12 represents the resonances of the 2:1 mixed trimer **12**.

A series of ^1H and ^{13}C NMR experiments including ^1H NMR, ^{13}C NMR, COSY, HSQC, HMBC confirm the ^1H and ^{13}C chemical shift assignments of complexes **11** and **12**. These experiments are summarized in Table 10.3. The α -methylene carbon (carbon atom 1) of *n*-BuLi within the mixed aggregate **11** is a quintet ($J = 10.2\text{ Hz}$) at 11.7 ppm (Figure 10.9). This suggests that C(1) of *n*-BuLi interacts with two ^6Li atoms. Moreover, as depicted in Figure 10.9, The α -methylene carbon (carbon atom 7) of *n*-BuLi within the

mixed aggregate **12** at 13.7 ppm is also a quintet ($J = 10.4$ Hz) as a consequence of the interaction of C(6) with two equivalent ${}^6\text{Li}$ atoms.

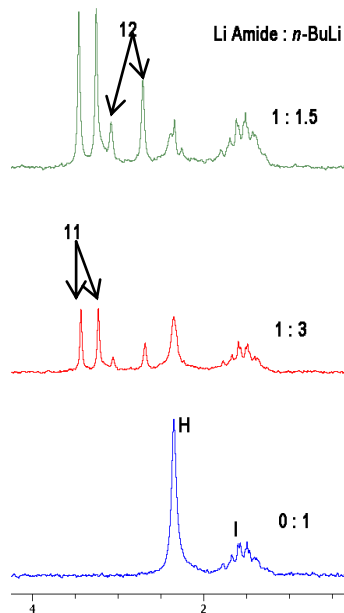


Figure 10.7. ${}^6\text{Li}$ NMR spectra of chiral amine **8** titration of 0.2 M $n\text{-Bu}{}^6\text{Li}$ in toluene- d_8 solution at -40 °C. H represents the resonance of $n\text{-Bu}{}^6\text{Li}$ in hexamer; I represents the resonances of impurities and mixed aggregates of $n\text{-Bu}{}^6\text{Li}$ and $n\text{-BuO}{}^6\text{Li}$; 11 represents the resonances of the 2:2 mixed aggregate **11**; 12 represents the resonances of the 2:1 mixed trimer **12**.

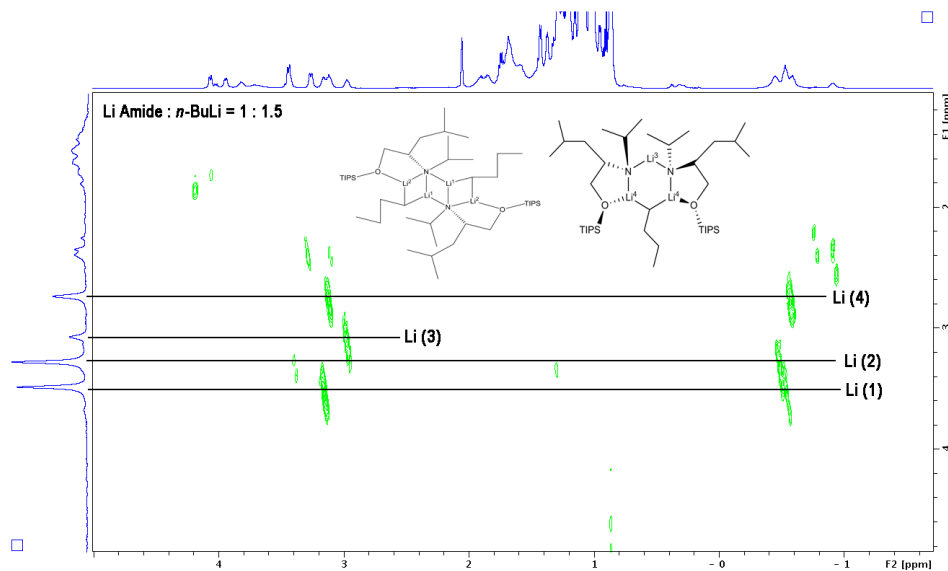
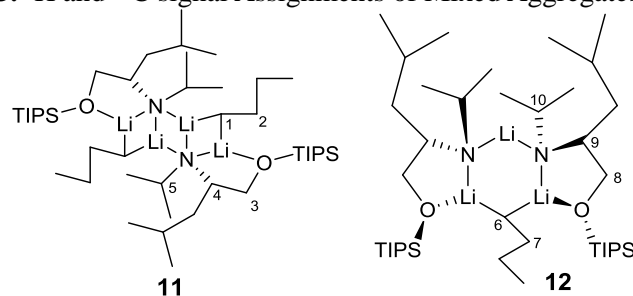


Figure 10.8. ${}^1\text{H}$ $\{{}^6\text{Li}\}$ HMBC of **11** and **12** in toluene- d_8 at -40 °C.

Table 10.3. ^1H and ^{13}C signal Assignments of Mixed Aggregates **11** and **12**



Carbon atom	^{13}C (ppm)	^1H (ppm)
1	11.7	-0.52
2	34.8	1.87
3	63.3	4.05, 3.42
4	57.1	3.28
5	48.7	3.16
6	13.7	-0.58
7	34.4	1.77
8	70.7	3.94, 3.44
9	60.6	2.98
10	51.3	3.12

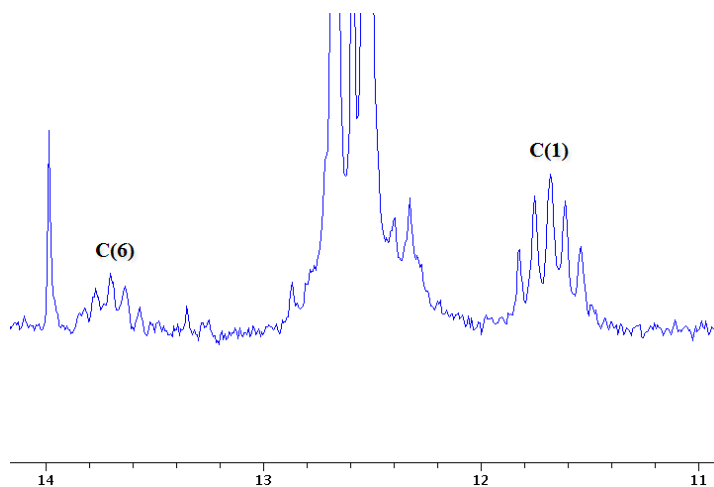


Figure 10.9. ^{13}C NMR of carbon atoms 1 and 7 of mixed aggregates **11** and **12** in toluene- d_8 at $-40\text{ }^\circ\text{C}$.

Diffusion-ordered NMR spectroscopy and D-FW analysis were performed. Four distinct peaks of the two different putative complexes from 2.9 to 4.1 ppm were utilized for our D-FW analysis because other resonances overlapped. The ^1H DOSY spectrum

(Figure 10.10) shows that the putative complexes diffuse considerably slower than squalene, indicating that the formula weights of these complexes are significantly higher than the formula weight of squalene.

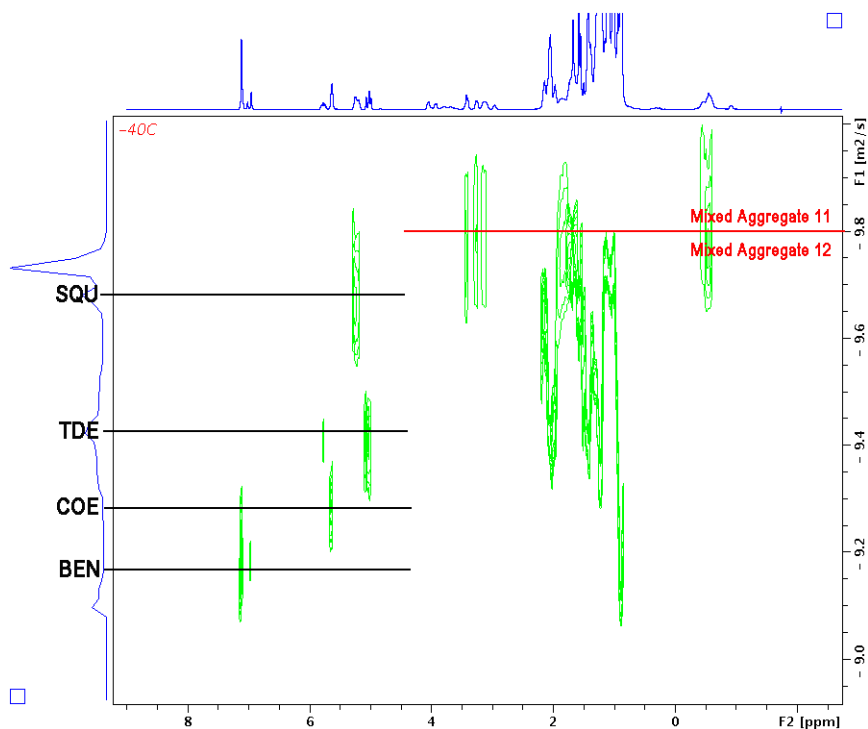


Figure 10.10. ^1H DOSY of mixed aggregates **11** and **12** in toluene- d_8 at $-40\text{ }^\circ\text{C}$.

The D-FW experiment yields a predicted formula weight of 712 g/mol for the 2:2 mixed aggregate **11** and an average predicted formula weight of 758 g/mol for the mixed aggregate **12**. These results differ by 7.2 % from the calculated formula weight of the 2:2 mixed aggregate **11** (765.5 g/mol) and 7.7 % from the calculated formula weight of the 2:1 mixed aggregate **11** (704.4 g/mol). Thus these D-FW experiments unambiguously define the aggregation state of the species in solution with molecular weights in the range of 680-800 g/mol. However, these D-FW results alone cannot distinguish between the

aggregates **11** and **12**.

Taken together, our NMR data support the existence of both 2:2 mixed aggregate **11** and 2:1 mixed trimer **12** between lithiated chiral amine **8** and *n*-BuLi in toluene when the mole ratio of *n*-BuLi to chiral lithium amide **8** is more than 1:1.5.

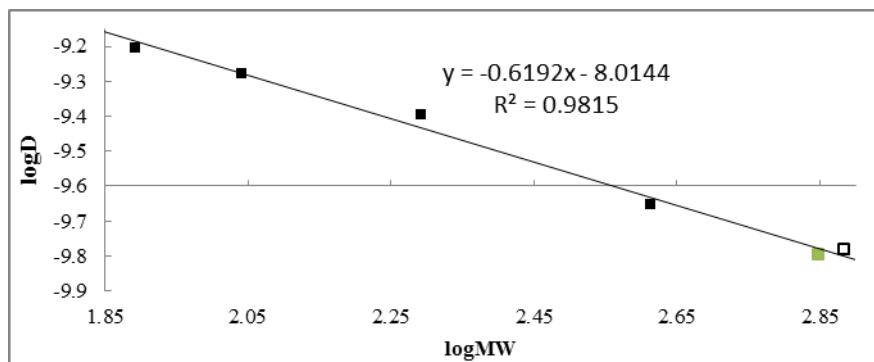


Figure 10.11. D-FW analysis of ^1H DOSY data. Internal references are shown as solid squares and mixed aggregate **11** is shown as green square and mixed trimer **12** is shown as the white square.

Table 10.4. D-FW Analysis of ^1H DOSY Data of **11** and **12**

entry	Compd	FW (g mol^{-1})	10^{-10}D (m^2/s)	Predicted FW (g mol^{-1})	% error
1	BEN	78.11	6.260	83	-6.6
2	COE	110.2	5.268	110	0.2
3	TDE	196.4	4.013	170	13
4	SQU	410.7	2.220	444	-8.1
5	11 ^a	767.5 ^b	1.616 ^a	741	3.4
6	11 ^a	767.5 ^b	1.702 ^a	682	11
7	12 ^a	704.4 ^c	1.541 ^a	800	-14
8	12 ^a	704.4 ^c	1.504 ^a	715	-1.6
9	11 ^d	767.5 ^b	1.659 ^d	711	7.2
10	12 ^d	704.4 ^c	1.596 ^d	758	-7.7

^aThe measured diffusion coefficients are from the resonances of chiral lithium amide. ^b767.5 g mol^{-1} is the formula weight of 2:2 lithiated chiral amine **8**/*n*-BuLi (^6Li labeled) complex **11**. ^c704.4 g mol^{-1} is the formula weight of 2:1 lithiated chiral amine **8**/*n*-BuLi (^6Li labeled) complex **12**. ^dThe diffusion coefficient is the average of the above two values.

10.3.3 Solution State Characterization of the Mixed Aggregate of Lithiated Chiral Amine **9** and *n*-BuLi **13** and Homodimer **14**

Chiral amine **9** was synthesized from (*R*)-phenylglycine in three steps. Compound **9** is more sterically hindered than chiral amine **8** at the C(3) position. An NMR sample was prepared by titrating (*R*)-*N*-(1-phenyl-2-((triisopropylsilyl)oxy)ethyl)propan-2-amine into a toluene-*d*₈ solution of ⁶Li labeled *n*-butyllithium at -40 °C. Upon addition of chiral amine **9**, the ¹H NMR reveals that a peak at -0.54 ppm increases in intensity as the amount of lithiated chiral amine **9** increases (Figure 10.12). The number of peaks in the 2.9 to 4.5 ppm region is double the number of peaks of non-lithiated chiral amine **9**, suggesting that lithiated chiral amine **9** forms more than one type of aggregate. As depicted in Figure 10.13, the ⁶Li NMR shows very clearly the emergence and rise of two sharp peaks with 1:2 intensity upon addition of chiral amine **9**, as well as a minor sharp peak slightly upfield of the 1:2 peaks. These three sharp peaks become dominant when the mole ratio of lithiated chiral amine **9** to *n*-BuLi equals 1:0.9. These results are similar to the titration results of chiral amine **1b** with *n*-BuLi.^{13,15} Thus, we postulate the 1:2 peaks correspond to the 2:1 mixed trimer **13** and the minor upfield peak corresponds to the homodimer **14** depicted in Table 10.5.

The ¹H {⁶Li} HMBC (Figure 10.14) shows a strong correlation from Li(1) to the proton of the methine (4.26 ppm) group adjacent to nitrogen while Li(2) shows a strong correlation to the α -methylene protons of *n*-BuLi and the proton of another methine (2.91 ppm) group adjacent to nitrogen. Meanwhile, Li(3) shows a strong correlation to the proton of methine groups (4.45, 3.07 ppm) adjacent to nitrogen. These results are

consistent with the assignment of Li(1) and Li(2) to the 2:1 mixed trimer **13** between *n*-BuLi and the lithiated chiral amine **9** and Li(3) to the homodimer **14**.

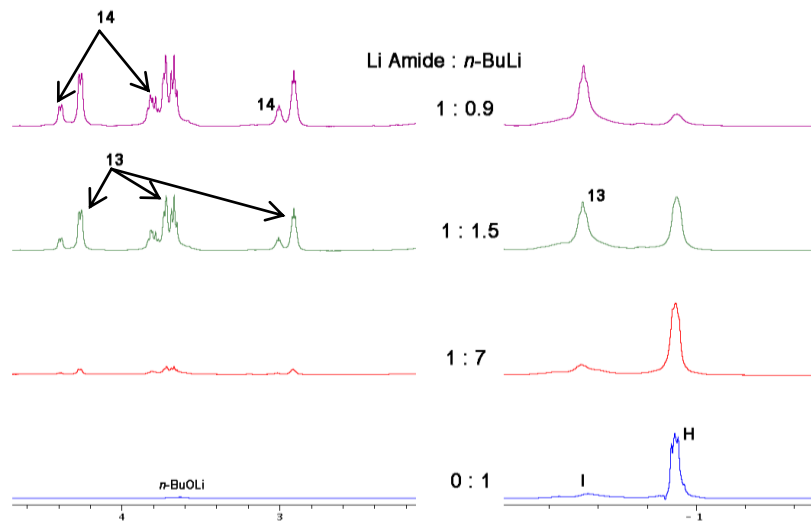


Figure 10.12. ^1H NMR spectra of chiral amine **9** titration of 0.2 M $n\text{-Bu}^6\text{Li}$ toluene- d_8 solution at $-40\text{ }^\circ\text{C}$. H represents the resonance of $n\text{-Bu}^6\text{Li}$ in hexamer; I represents the resonances of impurities and mixed aggregates of $n\text{-Bu}^6\text{Li}$ and $n\text{-BuO}^6\text{Li}$; 13 represents the resonances of the 2:1 mixed trimer **13**; 14 represents the resonances of homodimer **14**.

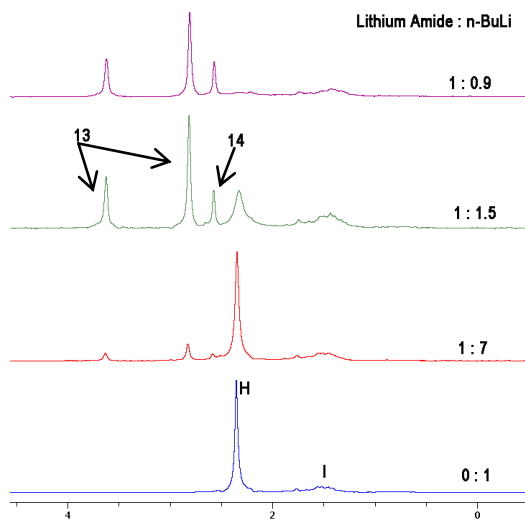


Figure 10.13. ^6Li NMR spectra of chiral amine **9** titration of 0.2 M $n\text{-Bu}^6\text{Li}$ toluene- d_8 solution at $-40\text{ }^\circ\text{C}$. H represents the resonance of $n\text{-Bu}^6\text{Li}$ in hexamer; I represents the resonances of impurities and mixed aggregates of $n\text{-Bu}^6\text{Li}$ and $n\text{-BuO}^6\text{Li}$; 13 represents the resonances of the 2:1 mixed trimer **13**; 14 represents the resonances of homodimer **14**.

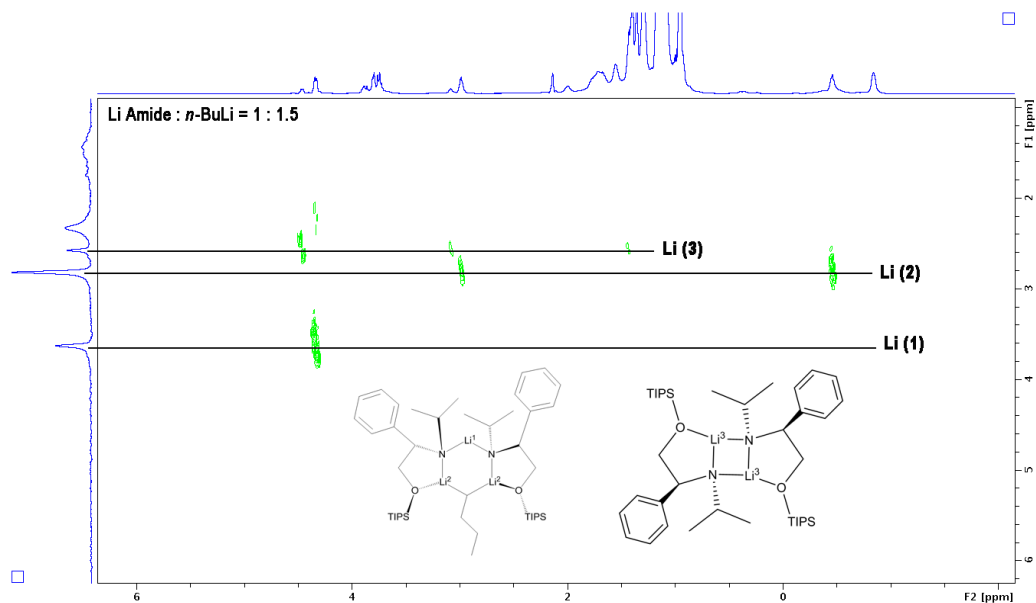


Figure 10.14. $^1\text{H} \{^6\text{Li}\}$ HMBC of **13** and **14** in toluene- d_8 at -40°C .

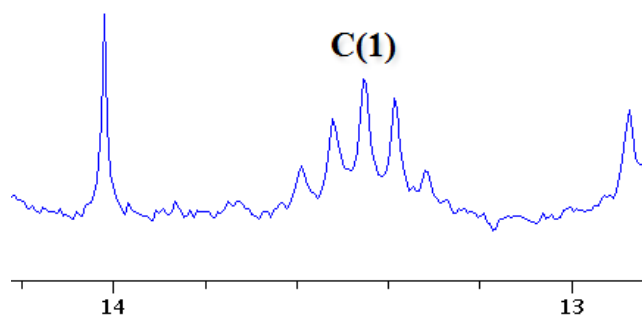


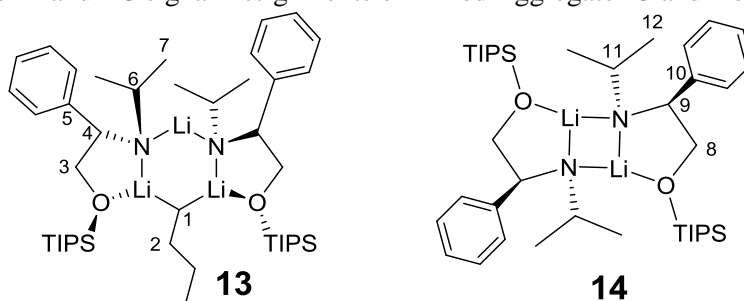
Figure 10.15. ^{13}C NMR of carbon atoms 1 of mixed trimer **13** in toluene- d_8 at -40°C .

Assignments of ^1H and ^{13}C resonances for aggregates **13** and **14** are summarized in Table 10.5. As illustrated in Figure 10.15, the α -methylene carbon (carbon atom 1) of *n*-BuLi of the putative mixed trimer **13** is a quintet ($J = 10.1$ Hz) at 13.5 ppm. This pattern indicates that carbon atom 1 in *n*-BuLi is J-coupled to two ^6Li atoms.

Diffusion-ordered NMR spectroscopy (Figure 10.16) and D-FW analysis results shows that the major peaks of the lithiated chiral amine **9** from 2.9 to 4.3 ppm and *n*-

butyllithium (-0.54 ppm) diffuse at a very similar rate. The average predicted formula weight for the mixed aggregate **13** is 678 g/mol, an 8.8 % difference from the calculated formula weight of the 2:1 mixed aggregate **13** (743.4 g/mol) (Figure 10.17, Table 10.6). Moreover, the average predicted formula weight for the homodimer **14** is 649 g/mol, a 4.7 % difference from the calculated formula weight of homodimer **14** (681.2 g/mol).

Table 10.5. ^1H and ^{13}C signal Assignments of Mixed Aggregate **13** and Homodimer **14**



Carbon atom	^{13}C (ppm)	^1H (ppm)
1	13.5	-0.54
2	35.0	1.63
3	72.4	3.73, 3.67
4	69.7	4.26
5	148.7	N/A
6	50.8	2.91
7	24.8	1.29
8	71.9	3.87
9	68.9	4.45
10	148.2	N/A
11	50.0	3.07
12	28.2	1.41

Overall, the combination of all these NMR experiments support the formation of the 2:1 mixed trimer **13** between lithiated chiral amine **9** and *n*-BuLi, as well as the formation of homodimer **14** in toluene when the mole ratio of *n*-BuLi to chiral lithium amide is more than 1:0.9.

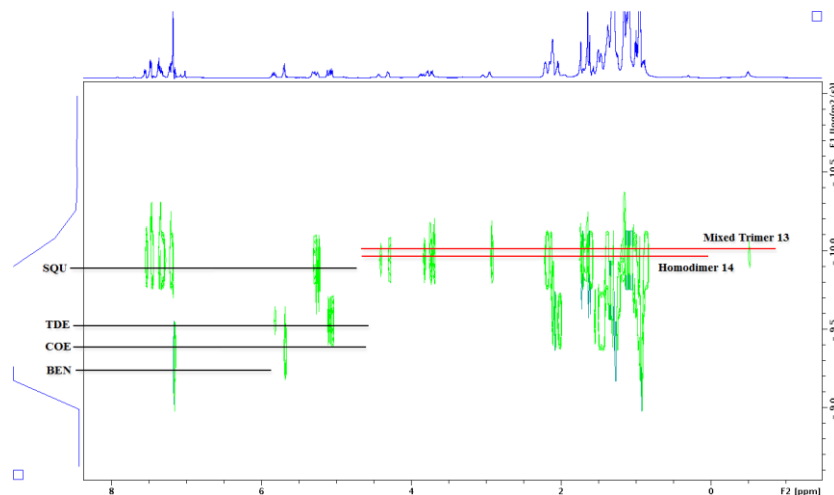


Figure 10.16. ^1H DOSY of mixed trimer **13** and homodimer **14** in toluene- d_8 at $-40\text{ }^\circ\text{C}$.

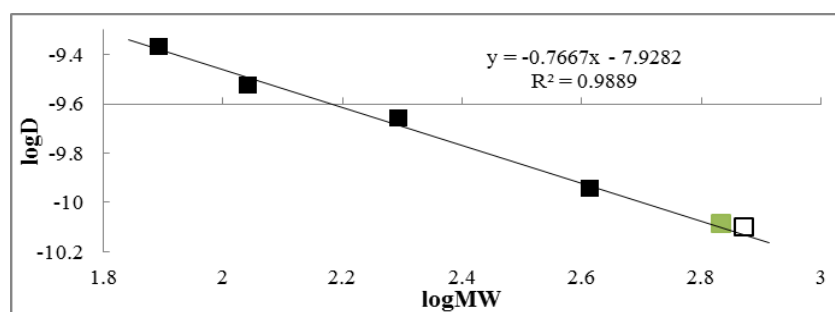


Figure 10.17. D-FW analysis of ^1H DOSY data. Internal references are shown as black squares, mixed trimer **13** is shown as white square and homodimer **14** is shown as the green square.

Table 10.6. D-FW Analysis of ^1H DOSY Data of **13** and **14**

entry	Compd	FW (g mol^{-1})	10^{-10}D (m^2/s)	Predicted FW (g mol^{-1})	% error
1	BEN	78.11	4.296	75	3.6
2	COE	110.2	2.986	121	-9.8
3	TDE	196.4	2.195	180	8.0
4	SQU	410.7	1.146	421	-2.7
5	13 ^a	743.4 ^b	0.811 ^a	662	10.9
6	13 ^a	743.4 ^b	0.821 ^a	651	12.3
7	13 ^c	743.4 ^b	0.757 ^c	724	2.5
8	14	681.2 ^d	0.814	659	3.2
9	14	681.2 ^d	0.834	638	6.2
10	13 ^e	743.4 ^b	0.796 ^e	678	8.8
11	14 ^f	681.2 ^d	0.824 ^f	649	4.7

^aThe measured diffusion coefficients are from the resonances of chiral lithium amide. ^b743.4 g mol^{-1} is the formula weight of 2:1 lithiated chiral amine **9**/*n*-BuLi (⁶Li labeled) complex **13**. ^cThe measured diffusion coefficient is from the α -methylene protons peak (-0.54 ppm) of *n*-BuLi. ^d681.2 g mol^{-1} is the formula weight of homodimer **14**. ^eThe diffusion coefficient is the average of the above three values. ^fThe diffusion coefficient is the average of the above two values.

The aggregation states of the mixed complexes between *n*-butyllithium and different lithium chiral amides with various R₁ and R₂ groups were summarized in Table 10.7. When R₁ and R₂ groups are relatively unhindered, a 2:2 mixed aggregate is the dominant species as with chiral amine **5** and **7**. A 2:1 mixed trimer is observed when the steric hindrance of R₁ and R₂ groups increases. Lithiated chiral amine **8** forms a significant amount of both 2:2 mixed aggregate and 2:1 mixed trimer with *n*-butyllithium. Further increase in the steric hindrance at C(3) position inhibits the formation of 2:2 mixed aggregate; therefore, lithiated chiral amines **1b** and **9** preferably form 2:1 mixed trimers with *n*-butyllithium.

Table 10.7. Aggregation states of different lithium chiral amide/*n*-BuLi complexes

R ₁ group	R ₂ group	Aggregation State
Isopropyl	Methyl	Dominantly 2:2 mixed aggregate
Ethyl	Isopropyl	Dominantly 2:2 mixed aggregate
Isopropyl	Isobutyl	2:2 mixed aggregate & 2:1 mixed trimer
Isopropyl	Phenyl	Majorly 2:1 mixed trimer
Isopropyl	Isopropyl	Majorly 2:1 mixed trimer

10.4 Conclusion

The size of R₁ and R₂ groups significantly influence the aggregation state of the mixed complexes between lithiated chiral amines and *n*-BuLi. When the R₁ and R₂ groups are relatively unhindered, a 2:2 mixed aggregate dominates. Increase in the steric hindrance of R₁ and R₂ groups inhibits the formation of this 2:2 mixed aggregate and promotes the formation of the 2:1 mixed trimer.

It is well established that lithiated *N*-isopropyl-*O*-triisopropylsilyl valinol **1b** forms a 2:1 mixed trimer with *n*-BuLi and that this mixed aggregate is responsible for the enantioselectivity of asymmetric addition of *n*-BuLi in the mixed aggregate to aldehydes.¹⁷ Hence, knowledge of the aggregation state of mixed aggregates is crucial in unveiling the origin of the enantioselectivity of chiral lithium amides. Moreover, the ability to predict the formation of different mixed aggregates enables us to design chiral amines with desired enantioselectivity most efficiently. Extensive work on both enantioselectivity and mechanism of the asymmetric addition of the alkyllithium moiety to electrophiles using these chiral lithium amide/alkyllithium mixed aggregates to various electrophiles is in progress.

10.5 Experimental Section

10.5.1 Procedures for NMR Experiments. NMR samples were prepared in tubes sealed with rubber septa cap and parafilm. NMR tubes were evacuated *in vacuo*, flame-dried and filled with argon before use. ¹H chemical shifts were referenced to toluene-*d*₈ at 7.09 ppm and ¹³C chemical shifts were referenced to toluene-*d*₈ at 137.86 ppm. All NMR experiments except DOSY experiments were acquired on a 600 MHz spectrometer. DOSY experiments were acquired on a 600 MHz or a 400 MHz spectrometer equipped with a z-axis gradient amplifier with a z-axis gradient coil. Maximum gradient strength was 0.5 T/m and 0.214 T/m respectively. ¹H DOSY was performed using the standard programs, employing a double stimulated echo sequence, bipolar gradient pulses for diffusion, and 3 spoil gradients. Diffusion time was 200 ms, and the rectangular gradient

pulse duration was 700 μs (lithiated chiral amine **8**) and 1000 μs (lithiated chiral amine **7** and **9**). Gradient recovery delays were 200 μs . Individual rows of the quasi-2-D diffusion databases were phased and baseline corrected. Actual diffusion coefficients used for D-FW analysis were obtained using the T1/T2 analysis module in commercially available software.

The ^6Li labeled *n*-butyllithium samples were prepared by laboratory synthesized ^6Li labeled *n*-butyllithium heptane solution. About 40 μL of the 2.4 M *n*-butyllithium heptane solution was added via syringe to a NMR tube. After the addition, the NMR tube was evacuated in vacuo for 10-30 minutes at 0 $^\circ\text{C}$ in order to remove the heptane. After filling with argon, toluene-*d*₈ was added via syringe to bring the total volume up to 500 μL .

The internal references (in a ratio of 1:3:3:1 for BEN, COE, TDE, and SQU, respectively) were titrated into the NMR tube and monitored by ^1H NMR. The titration was stopped when the peak intensity of benzene was about the same as the α -methylene protons of *n*-BuLi for lithiated chiral amine **7**, about 0.67 times the intensity as the α -methylene protons of *n*-BuLi for lithiated chiral amine **8** and about 1.5 times the intensity as the α -methylene protons of *n*-BuLi for lithiated chiral amine **9**.

10.5.2 Synthesis of (*S*)-*N*-isopropyl-1-((triisopropylsilyl)oxy)propan-2-amine **7.**

The synthetic route of chiral amine **7** started from enantiomerically pure (*S*)-alanine. The *N*-isopropyl alanine was prepared according to Ohfuné's method.²⁴ The *N*-isopropyl alanine was then reduced by lithium aluminum hydride in anhydrous tetrahydrofuran to *N*-isopropyl alaninol. Chiral amine **7** was prepared as follows: To a solution of *N*-isopropyl alaninol (2.20 g, 18.8 mmol) and triethylamine (10.5 mL, 37.5 mmol) in 60 mL CH_2Cl_2 was added slowly triisopropylsilyl triflate (6.34 g, 23.5 mmol) at 0 $^\circ\text{C}$. The

resulting solution was allowed to stir at room temperature for 4 h before quenching with 25 mL of 2 M NaHCO₃. The mixture was extracted with 30 mL EtOAc three times and the combined organic phase was washed by 20 mL brine and dried over anhydrous Na₂SO₄. The solvent was then removed by rotary evaporation and purification was performed by vacuum distillation. Purification (bp = 115 °C, 5 mmHg) gave a colorless oil (4.12 g, 15.1 mmol, 80.2 %). ¹H NMR (Tol-*d*₈, 400 MHz) δ 3.57-3.45 (m, 2H), 2.91-2.78 (m, 2H), 1.14-1.04 (m, 21H), 1.04-0.97 (m, 10H); ¹³C NMR (Tol-*d*₈, 100 MHz) δ 68.8, 52.5, 46.2, 24.8, 23.7, 18.7, 18.6, 12.8; HRMS-ESI m/z: [M + H]⁺ Calcd for C₁₅H₃₆NOSi: 274.2561, found: 274.2564.

10.5.3 Synthesis of (S)-N-isopropyl-1-((triisopropylsilyl)oxy)propan-2-amine 8. (S)-N-isobutyl-3-methyl-1-((triisopropylsilyl)oxy)butan-2-amine **8** was synthesized using the same method described above from N-isopropyl (S)-leucinol (1.70 g, 10.7 mmol). Purification (bp = 132 °C, 5 mmHg) gave a colorless oil (2.77 g, 8.77 mmol, 82.0 %). ¹H NMR (Tol-*d*₈, 400 MHz) δ 3.65 (dd, 1H, *J* = 4.7, 9.5 Hz), 3.51 (dd, 1H, *J* = 4.4, 9.5 Hz), 2.92 (septet, 1H, *J* = 6.2 Hz), 2.70 (m, 1H), 1.83 (m, 1H), 1.41-1.29 (m, 2H), 1.13-1.00 (m, 28H), 0.99-0.92 (m, 6H); ¹³C NMR (Tol-*d*₈, 100 MHz) δ 66.4, 54.8, 46.1, 43.3, 25.5, 24.7, 24.1, 24.0, 23.4, 18.7, 12.8; HRMS-ESI m/z: [M + H]⁺ Calcd for C₁₈H₄₂NOSi: 316.3036, found: 316.3035.

10.5.4 Synthesis of (R)-N-(1-phenyl-2-((triisopropylsilyl)oxy)ethyl)propan-2-amine 9. (R)-N-(1-phenyl-2-((triisopropylsilyl)oxy)ethyl)propan-2-amine **8** was synthesized using the same method described above from N-isopropyl (R)-phenylglycinol (2.40 g, 13.4 mmol). Purification (bp = 163 °C, 5 mmHg) gave a colorless oil (3.58 g, 10.7 mmol, 79.6 %). ¹H NMR (Tol-*d*₈, 400 MHz) δ 7.44 (d, 2H, *J* = 7.28 Hz), 7.24-7.10

(m, 3H), 3.99 (dd, 1H, $J = 4.1, 8.9$ Hz), 3.74 (dd, 1H, $J = 4.1, 9.6$ Hz), 3.71-3.59 (m, 1H), 2.71 (septet, 1H, $J = 6.28$ Hz), 1.75 (br, 1H), 1.12-0.97 (m, 27H); ^{13}C NMR (Tol- d_8 , 100 MHz) δ 143.1, 128.9, 128.5, 127.9, 70.0, 63.8, 47.0, 25.2, 22.9, 18.6, 12.7; HRMS-ESI m/z : $[\text{M} + \text{H}]^+$ Calcd for $\text{C}_{20}\text{H}_{38}\text{NOSi}$: 336.2723, found: 336.2715.

10.6 Acknowledgement

The author thanks Mr. Chang Liu for synthesizing the chiral amines used in this study and Dr. Russell Hopson for his helpful suggestions.

10.7 References

- (1) (a) Snieckus, V. *Chem. Rev.* **1990**, *90*, 879-933. (b) Trost, B. M., Fleming, I., Eds. *Comprehensive Organic Synthesis*; Pergamon: Oxford, **1991**. (c) Lucht, B.; Collum, D. *Acc. Chem. Res.* **1999**, *32*, 1035-1042. (d) Clayden, J. *Organolithiums: Selectivity for Synthesis*; Pergamon: Oxford, **2002**. (e) Hodgson, D. *Organolithiums in Enantioselective Synthesis*; Springer: New York, **2003**. (f) Rappoport, Z., Marek, I., Eds. *The Chemistry of Organolithium Compounds*; John Wiley & Sons, Ltd.: West Sussex, **2004**. (g) Wu, G.; Huang, M. *Chem. Rev.* **2006**, *106*, 2596-2616. (h) Collum, D.; McNeil, A. J.; Ramirez, A. *Angew. Chem. Int. Ed.* **2007**, *46*, 3002-3017.
- (2) (a) Whitesell, J. K.; Felman, S. W. *J. Org. Chem.* **1980**, *45*, 755-756. (b) Eleveld, M. B.; Hogeveen, H. *Tetrahedron Lett.* **1984**, *45*, 5187-5190. (c) Shirai, R.; Tanaka, M.; Koga, K. *J. Am. Chem. Soc.* **1986**, *108*, 543-545. (d) Cain, C. M.; Cousins, R. P. C.; Coumbarides, G.; Simpkins, N. S. *Tetrahedron* **1990**, *46*, 523-544. (e) Bhuniya, D.; DattaGupta, A.; Singh, V. K. *J. Org. Chem.* **1996**, *61*, 6108-6113. (f) Corruble, A.; Valnot, J.-Y.; Maddaluno, J.; Duhamel, P. *Tetrahedron: Asymmetry* **1997**, *8*, 1519-1523. (g) Simpkins, N. S.; Hume, S. C. *J. Org. Chem.* **1998**, *63*, 912-913. (h) Corruble, A.; Valnot, J.-Y.; Maddaluno, J.; Duhamel, P. *J. Org. Chem.* **1998**, *63*, 8266-8275. (i) Matsuo, J.; Odashima, K.; Kobayashi, S. *Org. Lett.* **1999**, *1*, 345-348. (j) Arvidsson, P. I.; Davidsson, O.; Hilmersson, G. *Tetrahedron: Asymmetry* **1999**, *10*, 527-534. (k) De Sousa, S. E.; O'Brien, P.; Pilgram, C. D. *Tetrahedron* **2002**, *58*, 4643-4654. (l) Flinois, K.; Yuan, Y.; Bastide, C.; Harrison-Marchand, A.; Maddaluno, J. *Tetrahedron* **2002**, *58*, 4707-4716. (m) Rodeschini, V.; Simpkins, N. S.; Wilson, C. *J. Org. Chem.* **2007**, *72*, 4265-4267. (n) Stivala, C. E.; Zakarian A. *J. Am. Chem. Soc.* **2011**, *133*, 11936-11939.
- (3) (a) Muraoka, M.; Kawasaki, H.; Koga, K. *Tetrahedron Lett.* **1988**, *29*, 337-338. (b) Uragami, M.; Tomioka, K.; Koga, K. *Tetrahedron: Asymmetry* **1995**, *6*, 701-704.
- (4) (a) Ma, Y.; Stivala, C. E.; Wright, A. W.; Hayton, T.; Liang, J.; Keresztes, I.; Lobkovsky, E.; Collum, D. B.; Zakarian, A. *J. Am. Chem. Soc.* **2013**, *135*, ASAP. (b) Gruver, J. M.; West, S. P.; Collum, D. B.; Sarpong, R. *J. Am. Chem. Soc.* **2010**, *132*, 13212-13213. (c) Ramirez, A.; Sun, X. F.; Collum, D. B. *J. Am. Chem. Soc.* **2006**, *128*, 10326-10336. (d) Briggs, T. F.; Winemiller, M. D.; Collum, D. B.; Parsons, R. L.; Davulcu, A. H.; Harris, G. D.; Fortunak, J. M.; Confalone, P. N. *J. Am. Chem. Soc.* **2004**, *126*, 5427-5435. (e) Zhao, P. J.; Collum, D. B. *J. Am. Chem. Soc.* **2003**, *125*, 4008-4009. (f) Sun, X. F.; Winemiller, M. D.; Xiang, B. S.; Collum, D. B. *J. Am. Chem. Soc.* **2001**, *123*, 8039-8046. (g) Briggs, T. F.; Winemiller, M. D.; Xiang, B. S.; Collum, D. B. *J. Org. Chem.* **2001**, *66*, 6291-6298. (h) Xu, F.; Reamer, R. A.; Tillyer, R.; Cummins, J. M.; Grabowski, E. J. J.; Reider, P. J.; Collum, D. B.; Huffman, J. C. *J. Am. Chem. Soc.* **2000**, *122*, 11212-11218.
- (5) (a) Arvidsson, P. I.; Hilmersson, G.; Davidsson, O. *Chem. Eur. J.* **1999**, *5*, 2348-2355. (b) Hilmersson, G.; Arvidsson, P. I.; Davidsson, O.; Hakansson, M. *Organometallics* **1997**, *16*, 3352-3362. (c) Hilmersson, G.; Davidsson, O. *J. Org. Chem.* **1995**, *60*, 7660-7669. (d) Hilmersson, G.; Davidsson, O. *J. Organomet. Chem.* **1995**, *489*, 175-179.
- (6) (a) Prigent, Y.; Corruble, A.; Valnot, J. Y.; Maddaluno, J.; Duhamel, P.; Davoust, D. *J. Chim. Phys. Phys.-Chim. Biol.* **1998**, *95*, 401-405. (b) Corruble, A.; Valnot, J.-Y.; Maddaluno, J.; Duhamel, P. *J. Org. Chem.* **1998**, *63*, 8266-8275. (c) Corruble, A.; Valnot, J. Y.; Maddaluno, J.; Prigent, Y.; Davoust, D.; Duhamel, P. *J. Am. Chem. Soc.* **1997**, *119*, 10042-10048.

- (7) (a) Granander, J.; Sott, R.; Hilmersson, G. *Chem. Eur. J.* **2006**, *12*, 4191-4197. (b) Granander, J.; Eriksson, J.; Hilmersson, G. *Tetrahedron: Asymmetry* **2006**, *17*, 2021-2027. (c) Sott, R.; Granander, J.; Williamson, C.; Hilmersson, G. *Chem. Eur. J.* **2005**, *11*, 4785-4792. (d) Sott, R.; Granander, J.; Hilmersson, G. *J. Am. Chem. Soc.* **2004**, *126*, 6798-6805. (e) Sott, R.; Granander, J.; Diner, P.; Hilmersson, G. *Tetrahedron: Asymmetry* **2004**, *15*, 267-274. (f) Sott, R.; Granander, J.; Hilmersson, G. *Chem. Eur. J.* **2002**, *8*, 2081-2087. (g) Granander, J.; Sott, R.; Hilmersson, G. *Tetrahedron* **2002**, *58*, 4717-4725. (h) Arvidsson, P. I.; Ahlberg, P.; Hilmersson, G. *Chem. Eur. J.* **1999**, *5*, 1348-1354.
- (8) J. F. McGarrity, C. A. Ogle, *J. Am. Chem. Soc.*, **1985**, *107*, 1805-1810.
- (9) (a) Oulyadi, H.; Fressigne, C.; Yuan, Y.; Maddaluno, J.; Harrison-Marchand, A. *Organometallics* **2012**, *31*, 4801-4809. (b) Pate, F.; Duguet, N.; Oulyadi, H.; Harrison-Marchand, A.; Fressigne, C.; Valnot, J.-Y.; Lasne, M.-C.; Maddaluno, J. *J. Org. Chem.* **2007**, *72*, 6982-6991. (c) Harrison-Marchand, A.; Valnot, J.-Y.; Corruble, A.; Duguet, N.; Oulyadi, H.; Desjardins, S.; Fressigne, C.; Maddaluno, J. *Pure Appl. Chem.* **2006**, *78*, 321-331. (d) Yuan, Y.; Desjardins, S.; Harrison-Marchand, A.; Oulyadi, H.; Fressigne, C.; Giessner-Prettre, C.; Maddaluno, J. *Tetrahedron* **2005**, *61*, 3325-3334. (e) Corruble, A.; Davoust, D.; Desjardins, S.; Fressigne, C.; Giessner-Prettre, C.; Harrison-Marchand, A.; Houte, H.; Lasne, M.-C.; Maddaluno, J.; Oulyadi, H.; Valnot, J.-Y. *J. Am. Chem. Soc.* **2002**, *124*, 15267-15279.
- (10) Jones, A. C.; Sanders, A. W.; Bevan, M. J.; Reich, H. J. *J. Am. Chem. Soc.* **2007**, *129*, 3492-3493.
- (11) (a) Strohmam, C.; Dilsky, S.; Strohmam, K. *Organometallics*, **2006**, *25*, 41-44. (b) Strohmam, C.; Abele, B. C. *Organometallics*, **2000**, *19*, 4173-4175.
- (12) (a) Thomas, R. D.; Huang, H. *J. Am. Chem. Soc.*, **1999**, *121*, 11239-11240. (b) DeLong, G. T.; Hoffmann, D.; Nguyen, H. D.; Thomas, R. D. *J. Am. Chem. Soc.*, **1997**, *119*, 11998-11999. (c) G. T. DeLong, D. K. Pannell, M. T. Clarke, R. D. Thomas, *J. Am. Chem. Soc.*, **1993**, *115*, 7013-7014.
- (13) (a) Li, D.; Sun, C.; Liu, J.; Hopson, R.; Li, W.; Williard, P. G. *J. Org. Chem.* **2008**, *73*, 2373-2381. (b) Williard, P. G.; Sun, C. *J. Am. Chem. Soc.* **1997**, *119*, 11693-11694.
- (14) (a) Li, D.; Sun, C.; Williard, P. G. *J. Am. Chem. Soc.* **2008**, *130*, 11726-11736. (b) Sun, C.; Williard, P. G. *J. Am. Chem. Soc.* **2000**, *122*, 7829-7830.
- (15) Kagan, G.; Li, W.; Li, D.; Hopson, R.; Williard, P. G. *J. Am. Chem. Soc.* **2011**, *133*, 6596-6602.
- (16) Su, C.; Hopson, R.; Williard, P. G. *J. Am. Chem. Soc.* **2013**, *135*, 14367-14379.
- (17) (a) Liu, J.; Li, D.; Sun, C.; Williard, P. G.; *J. Org. Chem.* **2008**, *73*, 4045-4052. (b) Granander, J.; Sott, R.; Hilmersson, G. *Tetrahedron* **2002**, *58*, 4717-4725. (c) Granander, J.; Eriksson, J.; Hilmersson, G. *Tetrahedron: Asymmetry* **2006**, *17*, 2021-2027. (d) Arvidsson, P. I.; Hilmersson, G.; Davidsson, O. *Chem – Eur. J.* **1999**, *5*, 2348-2355. (e) Ronnholm, P.; Sodergren, M.; Hilmersson, G. *Org. Lett.* **2007**, *9*, 3781-3783. (f) Sott, R.; Granander, J.; Williamson, C.; Hilmersson, G. *Chem – Eur. J.*, **2005**, *11*, 4785-4792. (g) Sott, R.; Granander, J.; Hilmersson, G. *Chem – Eur. J.*, **2002**, *8*, 2081-2087.

(18) (a) Sato, D.; Kawasaki, H.; Shimada, I.; Arata, Y.; Okamura, K.; Date, T.; Koga, K. . *J. Am. Chem. Soc.* **1992**, *114*, 761-763. (b) Arvidsson, P. I.; Hilmersson, G.; Ahlberg, P. *J. Am. Chem. Soc.* **1999**, *121*, 1883-1887. (c) Lecachey, B.; Duguet, N.; Oulyadi, H.; Fressigne, C.; Harrison-Marchand, A.; Yamamoto, Y.; Tomioka, K.; Maddaluno, J. *Org. Lett.* **2009**, *11*, 1907-1910.

(19) Lewis, H. L.; Brown, T. L. *J. Am. Chem. Soc.* **1970**, *92*, 4664-4670.

(20) Su, C.; Hopson, R.; Williard, P. G. *Eur. J. Inorg. Chem.* **2013**, *24*, 4136-4141.

(21) For miscellaneous NMR spectra including ^1H NMR, ^6Li NMR, ^{13}C NMR, COSY, HSQC, $^1\text{H}\{^6\text{Li}\}$ HMBC and $^1\text{H}\{^{13}\text{C}\}$ HMBC. Please see supporting information.

(22) (a) Pi, R.; Bauer, W.; Brix, B.; Schade, C.; Schleyer, P. v. R. *J. Organomet. Chem.* **1986**, *306*, C1-C4. (b) Bauer, W.; Schleyer, P. v. R. Winchester, W. R. *Organometallics* **1987**, *6*, 2371-2379. (c) Bauer, W.; Schleyer, P. v. R. *Adv. Carbanion Chem.* **1992**, *1*, 89-175. (d) Bauer, W. *J. Am. Chem. Soc.* **1996**, *118*, 5450-5455. (e) Parisel, O.; Fressigne, C.; Maddaluno, J.; Giessner-Prettre, C. *J. Org. Chem.* **2003**, *68*, 1290-1294.

(23) (a) Li, D.; Hopson, R.; Li, W.; Liu, J.; Williard, P. G. *Org. Lett.* **2008**, *10*, 909-911. (b) Li, D.; Kagan, G.; Hopson, R.; Williard, P. G. *J. Am. Chem. Soc.* **2009**, *131*, 5627-5634. (c) Li, D.; Keresztes, I.; Hopson, R.; Williard, P. G. *Acc. Chem. Res.* **2009**, *42*, 270-280. (d) Kagan, G.; Li, W.; Hopson, R.; Williard, P. G. *Org. Lett.* **2009**, *11*, 4818-4821. (e) Kagan, G.; Li, W.; Hopson, R.; Williard, P. G. *Org. Lett.* **2010**, *12*, 520-523. (f) Li, W.; Kagan, G.; Yang, H.; Cai, C.; Hopson, R.; Sweigart, D. A.; Williard, P. G. *Org. Lett.* **2010**, *12*, 2698-2701. (g) Li, W.; Kagan, G.; Yang, H.; Cai, C.; Hopson, R.; Dai, W.; Sweigart, D. A.; Williard, P. G. *Organometallics* **2010**, *29*, 1309-1311. (h) Socha, A. M.; Kagan, G.; Li, W.; Hopson, R.; Sello, J. K.; Williard, P. G. *Energy Fuels* **2010**, *24*, 4518-4521. (i) Kagan, G.; Li, W.; Sun, C.; Hopson, R.; Williard, P. G. *J. Org. Chem.* **2011**, *76*, 65-70. (j) Lecachey, B.; Oulyadi, H.; Lameiras, P.; Harrison-Marchand, A.; Gerard, H.; Maddaluno, J. *J. Org. Chem.* **2010**, *75*, 5976-5983. (k) Consiglio, G. B.; Queval, P.; Harrison-Marchand, A.; Mordini, A.; Lohier, J.; Delacroix, O.; Gaumont, A.; Gerard, H.; Maddaluno, J.; Oulyadi, H. *J. Am. Chem. Soc.* **2011**, *133*, 6472-6480. (l) Armstrong, D. R.; Garcia-Alvarez, P.; Kennedy, A. R.; Mulvey, R. E.; Robertson, S. D. *Chem. Eur. J.* **2011**, *17*, 6725-6730.

(24) Ohfuné, Y.; Kurokawa, N.; Higuchi, N.; Saito, M.; Hashimoto, M.; Tanaka, T. *Chem. Lett.* **1984**, *13*, 441-444.

Appendix A

CCDC numbers for all crystal structures

Entry	Crystal Structure	Figure Number	CCDC Number
1	<i>c</i> -PenLi Hexamer	4.1	944702
2	<i>c</i> -PenLi/THF Tetramer	4.7	944703
3	Lithiated (<i>S</i>)- <i>N</i> ¹ , <i>N</i> ¹ -bis(2-methoxyethyl)- <i>N</i> ² ,3-dimethylbutane-1,2-diamine	6.1	934643
4	Lithiated (<i>S</i>)- <i>N</i> -ethyl-3-methyl-1-(triisopropylsilyloxy)butan-2-amine/ <i>c</i> -PenLi	7.1	948999
5	Dilithiated (2 <i>S</i> ,2' <i>S</i>)-1,1'-(butane-1,4-diylbis(oxy))bis(<i>N</i> -isopropylpropan-2-amine)/DEE	8.1	961338
6	Dilithiated (2 <i>S</i> ,2' <i>S</i>)-1,1'-(butane-1,4-diylbis(oxy))bis(<i>N</i> -isopropylpropan-2-amine)/THF	8.2	961339
7	Dilithiated (2 <i>S</i> ,2' <i>S</i>)-1,1'-(pentane-1,5-diylbis(oxy))bis(<i>N</i> -isopropylpropan-2-amine)/DEE	8.3	961340
8	Dilithiated (2 <i>S</i> ,2' <i>S</i>)-1,1'-(pentane-1,5-diylbis(oxy))bis(<i>N</i> -isopropylpropan-2-amine)/THF	8.4	961341
9	Dilithiated (2 <i>S</i> ,2' <i>S</i>)-1,1'-(heptane-1,7-diylbis(oxy))bis(<i>N</i> -isopropyl-3-methylbutan-2-amine)/DEE	8.6	961342
10	Dilithiated (2 <i>S</i> ,2' <i>S</i>)-1,1'-(heptane-1,7-diylbis(oxy))bis(<i>N</i> -isopropyl-3-methylbutan-2-amine)/THF	8.7	961343
11	Dilithiated (2 <i>S</i> ,2' <i>S</i>)-1,1'-(pentane-1,5-diylbis(oxy))bis(<i>N</i> -isopropyl-3-methylbutan-2-amine)/DEE	8.9	961344
12	Lithium <i>N</i> -methylanilide/THF	9.1	958136
13	Lithium <i>N</i> -ethylanilide/THF	9.2	958137
14	Lithium indolide/THF	9.3	958138
15	Lithium tetrahydroquinolide/THF	9.4	958139

16	Lithium <i>N</i> -methylanilide/THP	9.5	958140
17	Lithium <i>N</i> -methylanilide/MeTHF	9.6	958141
18	Lithium <i>N</i> -methylanilide/DEPA	9.7	958142
19	Lithium <i>N</i> -methylanilide/DME	9.8	958143
20	Lithium <i>N</i> -ethylanilide/DME	9.9	958144
21	Lithium <i>N</i> -methylanilide/DMTHF	9.10	958145
22	Lithium diphenylamide/THF	9.11	958146
23	Lithium <i>N</i> -isopropylanilide/THF	9.12	958151
24	Lithium <i>N</i> -isobutylanilide/THF	9.13	958152
25	Lithium <i>N</i> -neopentylanilide/THF	9.14	958153

Complete crystallographic data can be obtained free of charge from The Cambridge Crystallographic Data Centre via www.ccdc.cam.ac.uk/data_request/cif.

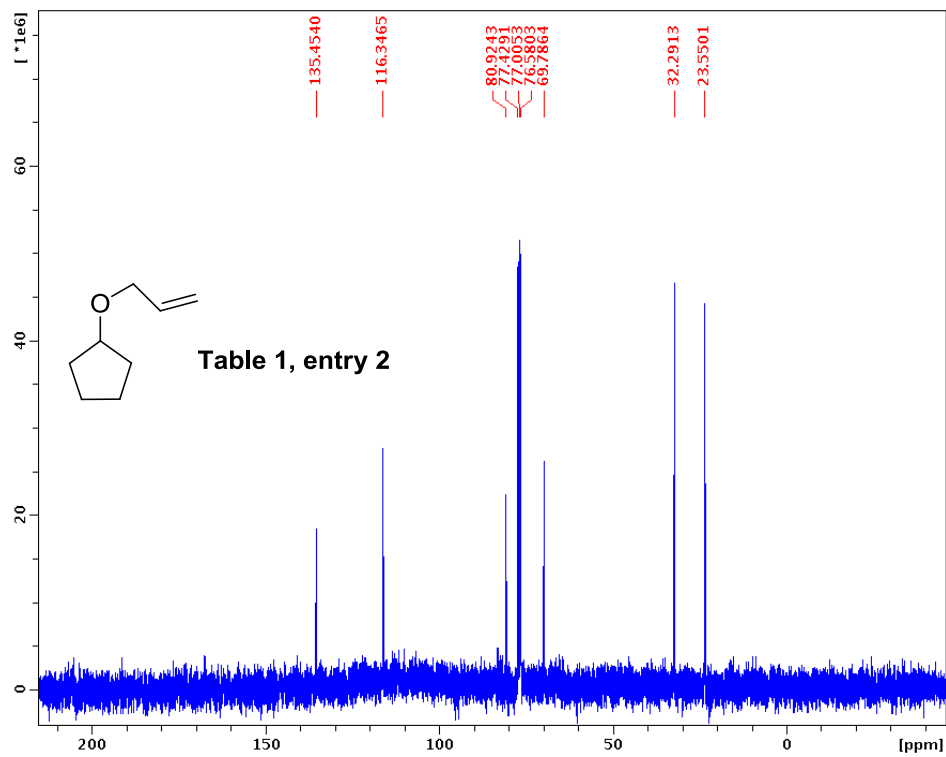
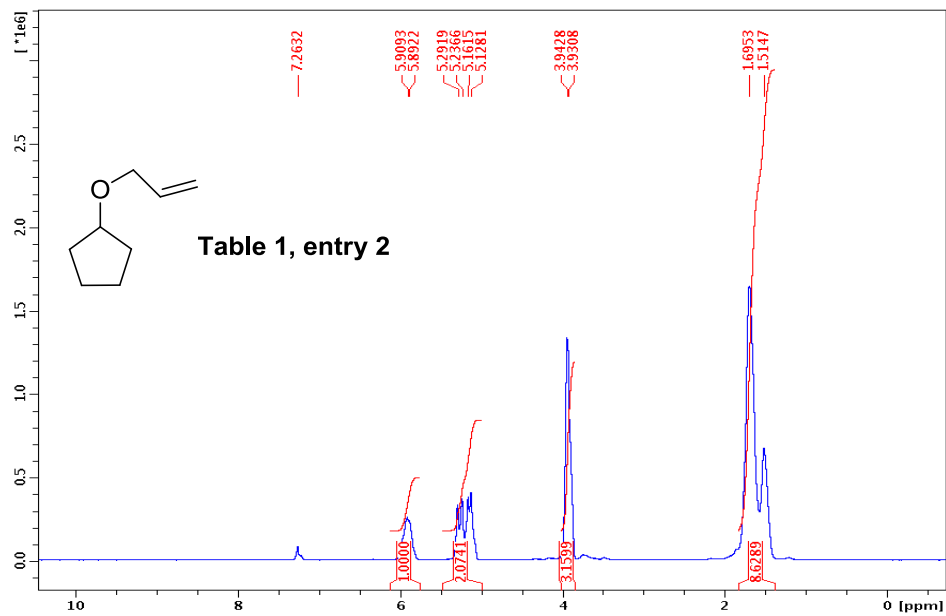
Appendix B

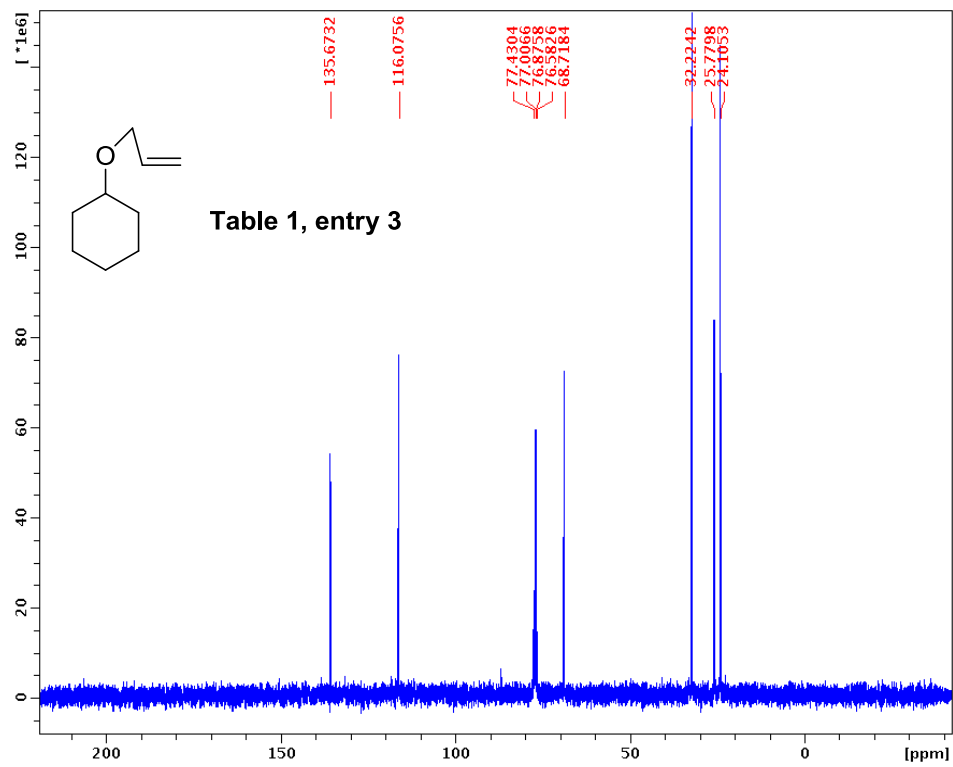
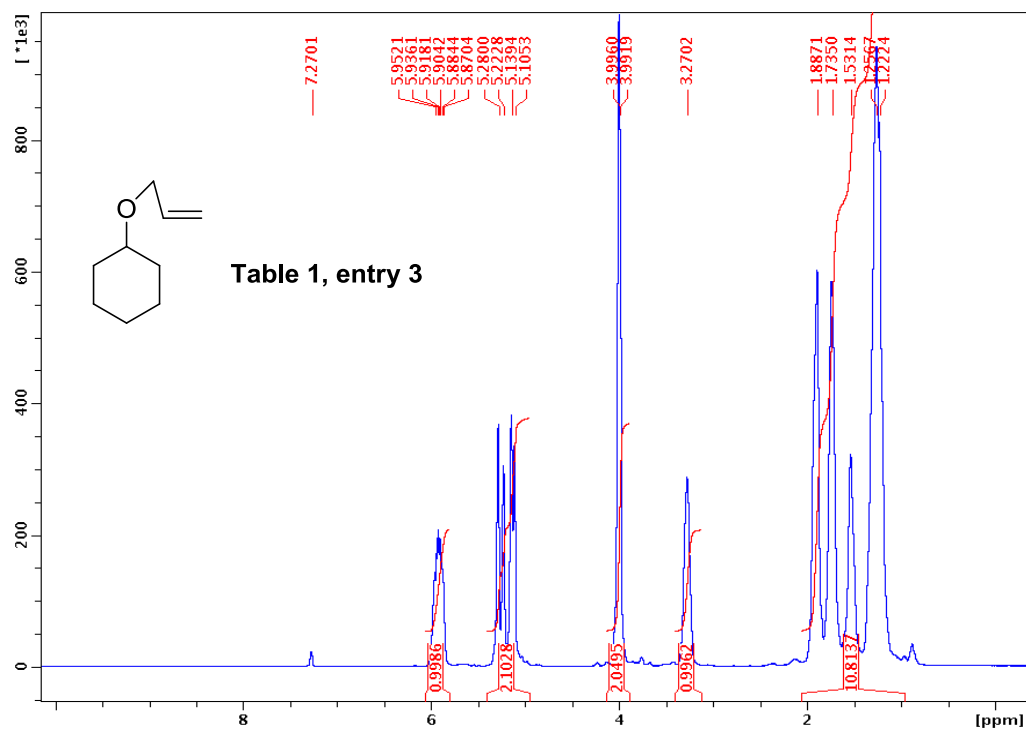
Supporting information for Chapter 2

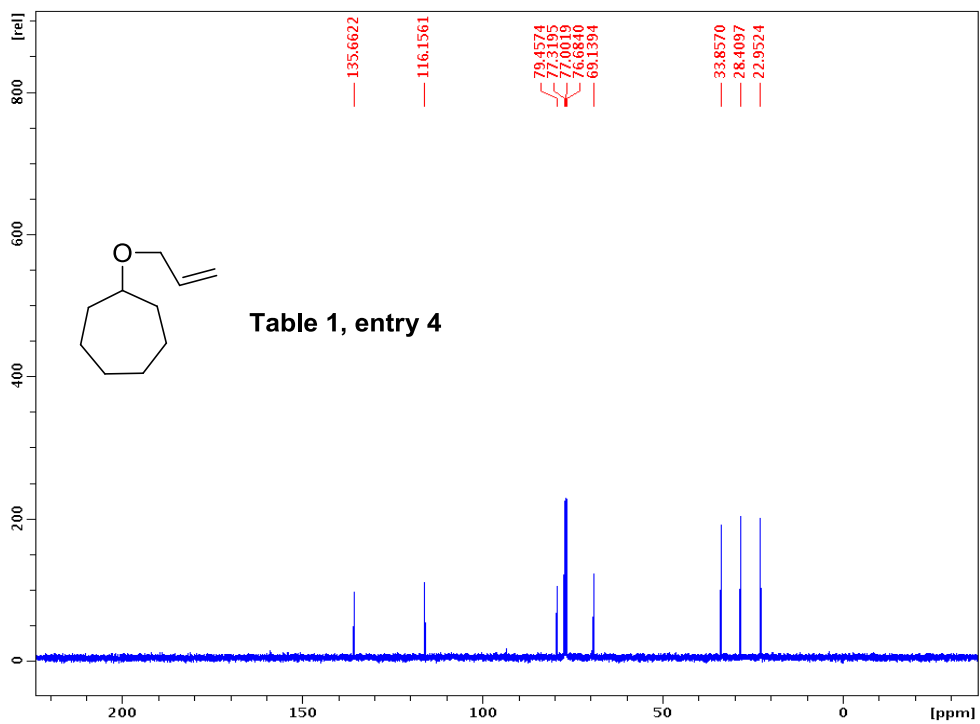
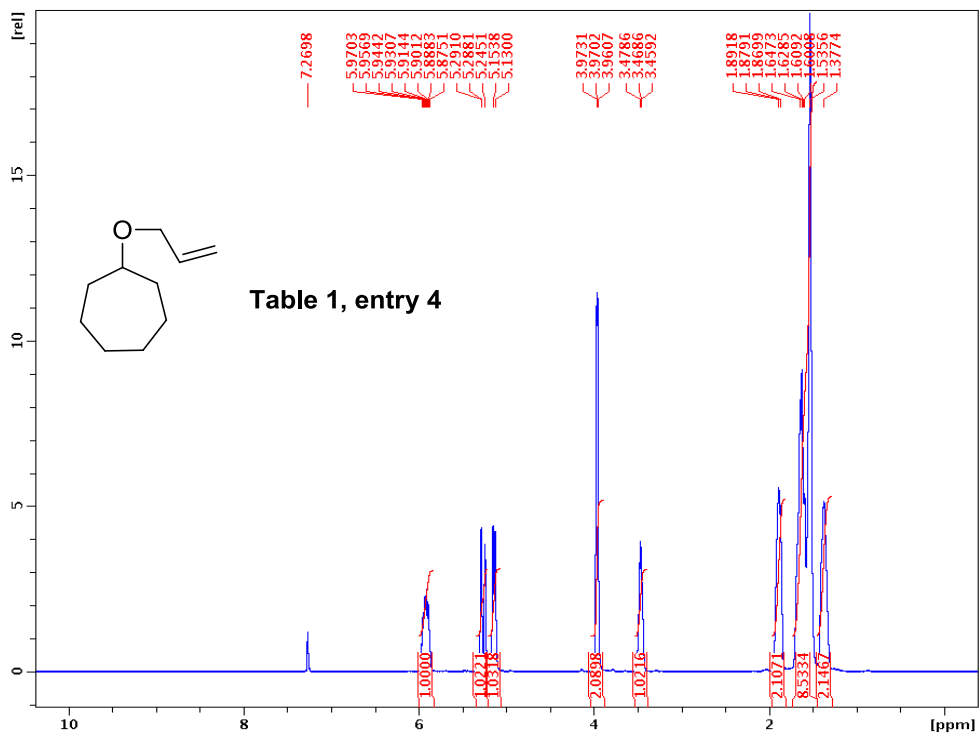
Table of Contents

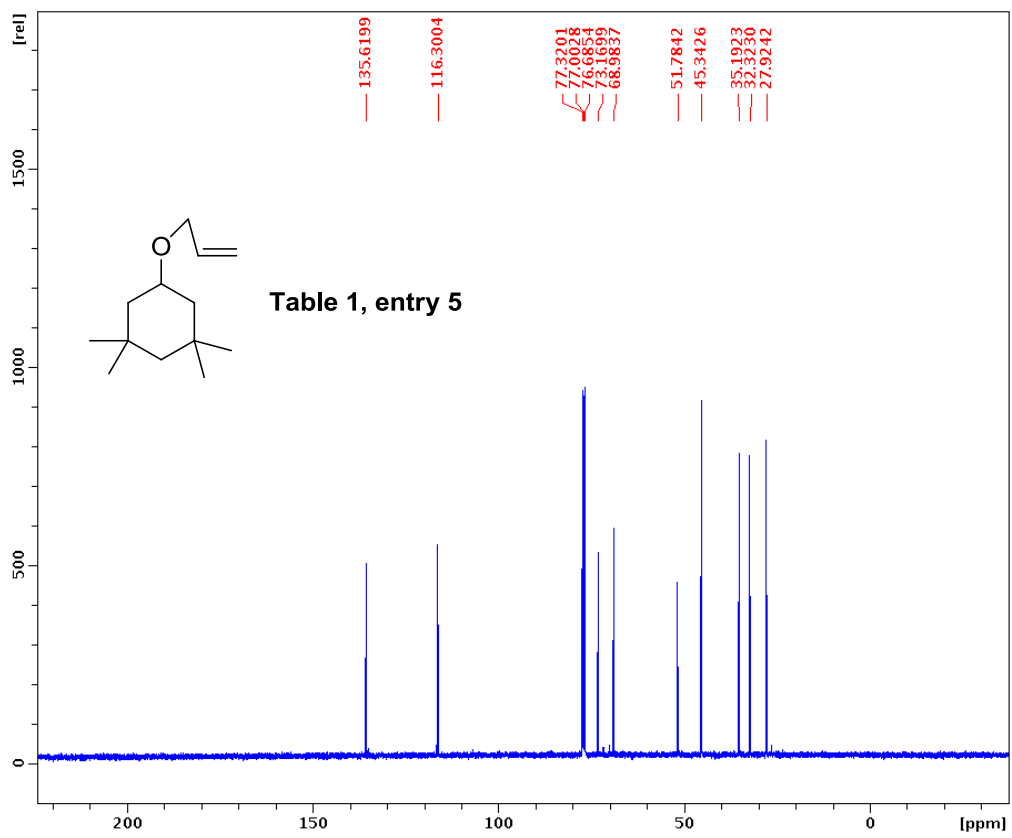
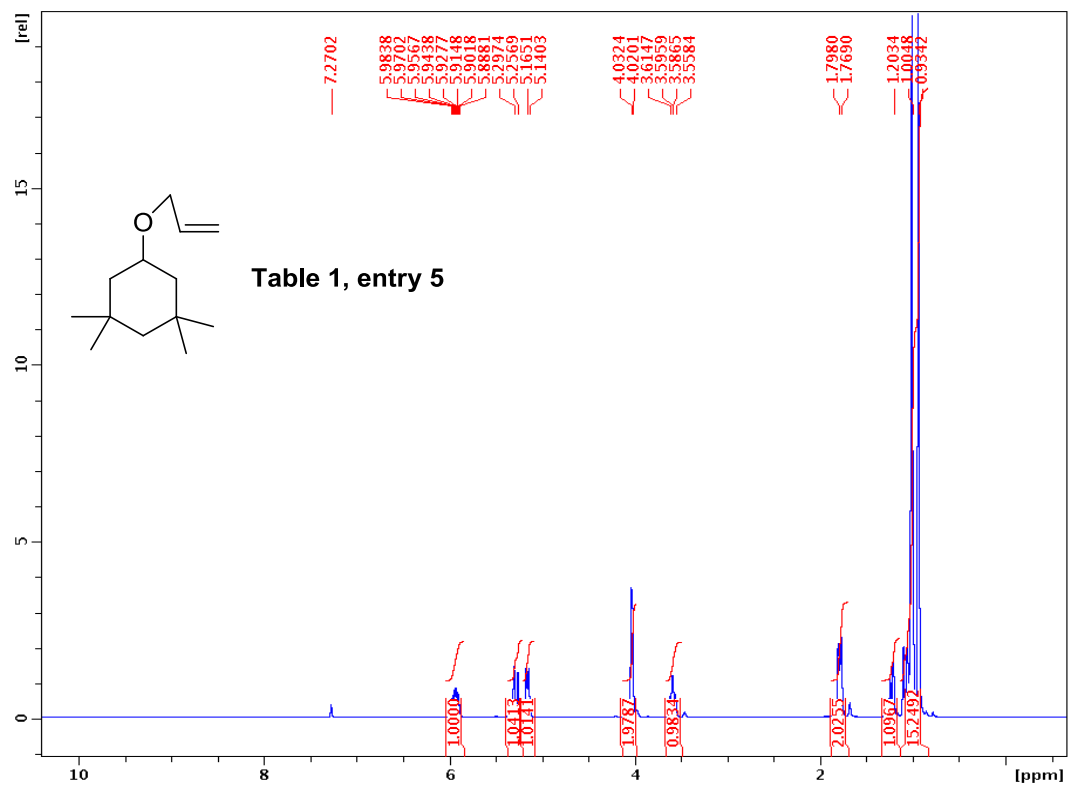
^1H and ^{13}C NMR Spectra for the Allyl Ethers	242
^1H and ^{13}C NMR Spectra for the Vinyl Ethers	257

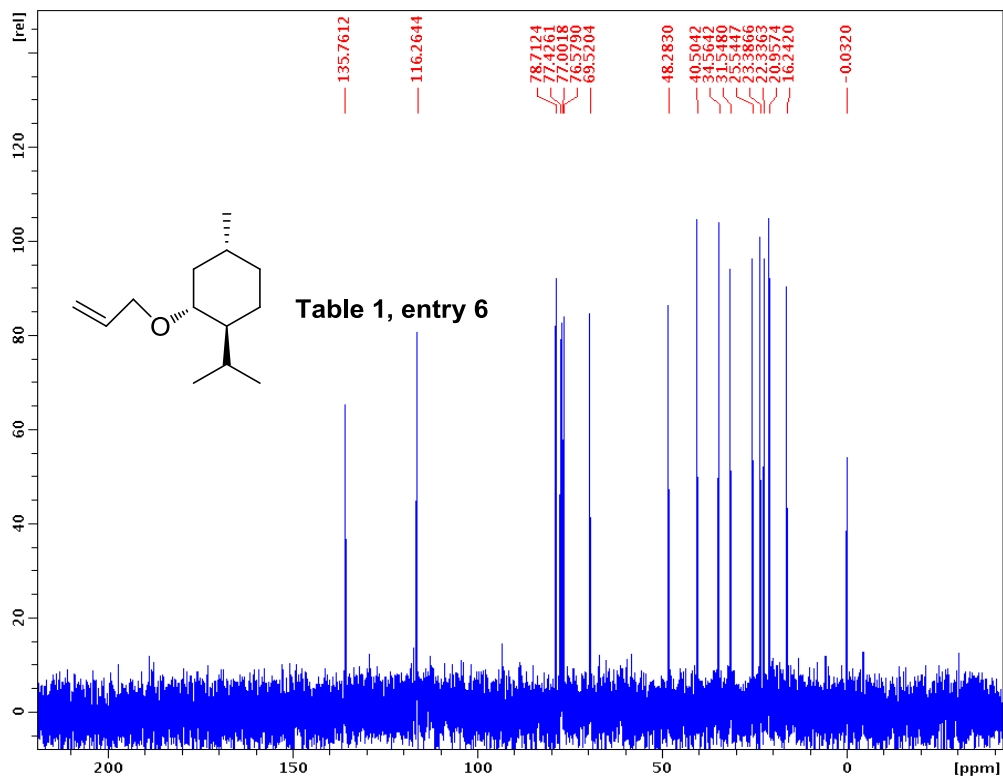
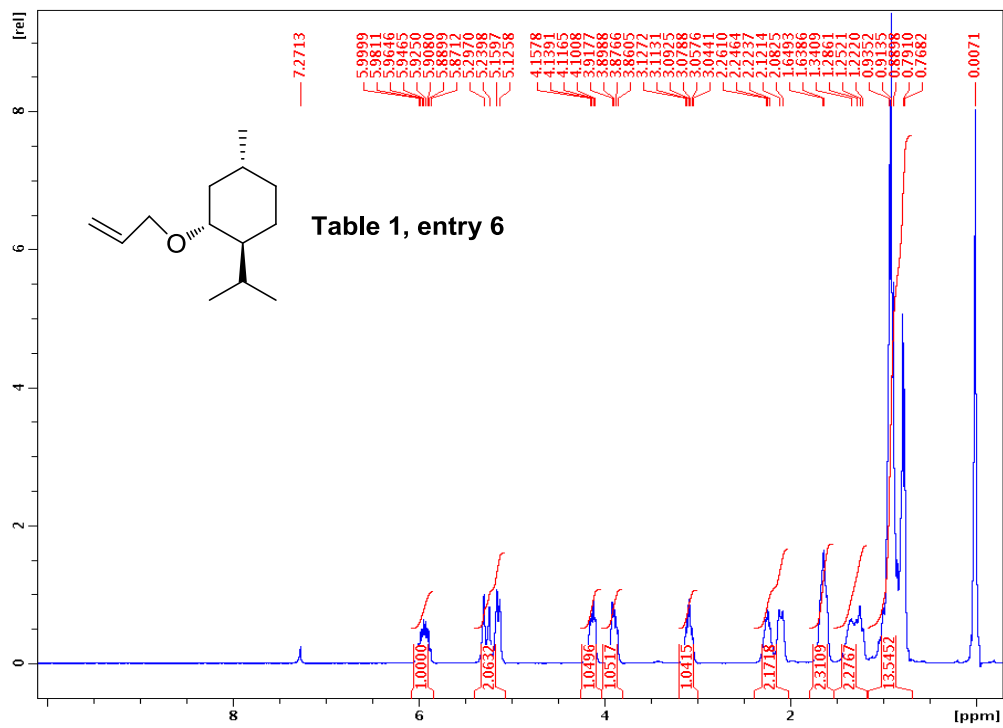
^1H and ^{13}C NMR Spectra for the Allyl Ethers

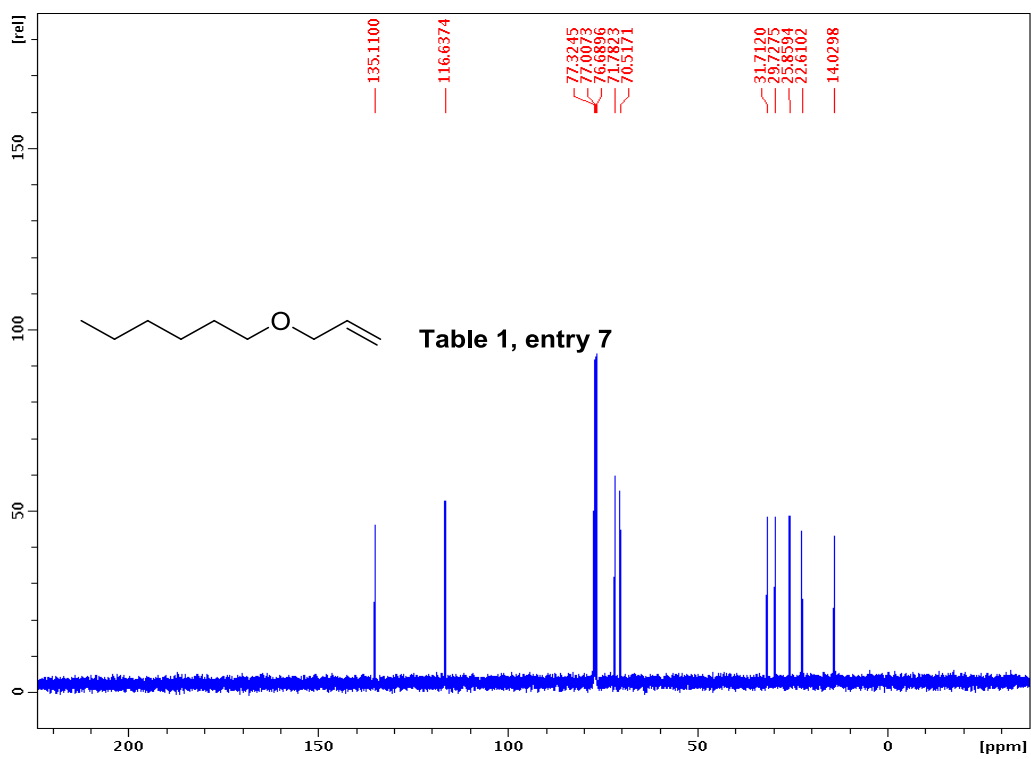
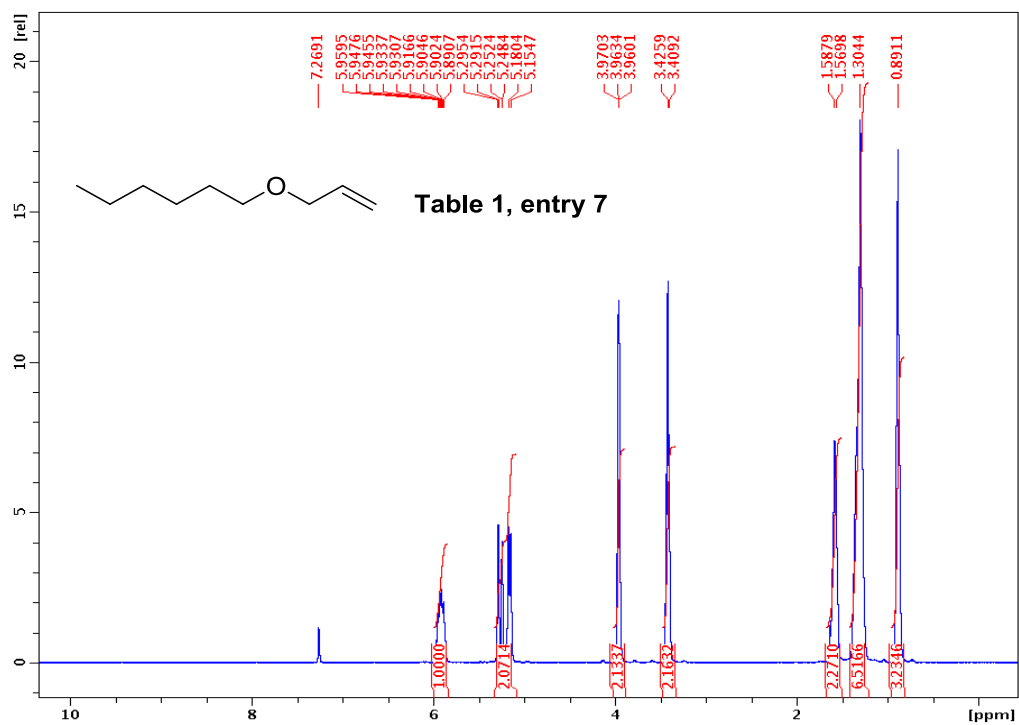


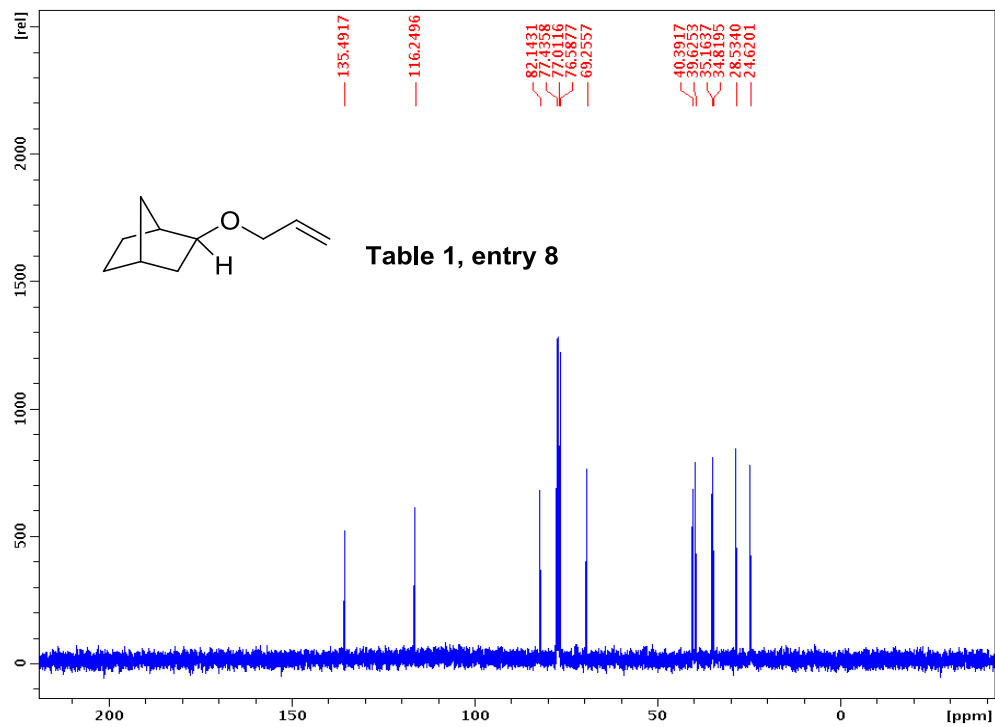
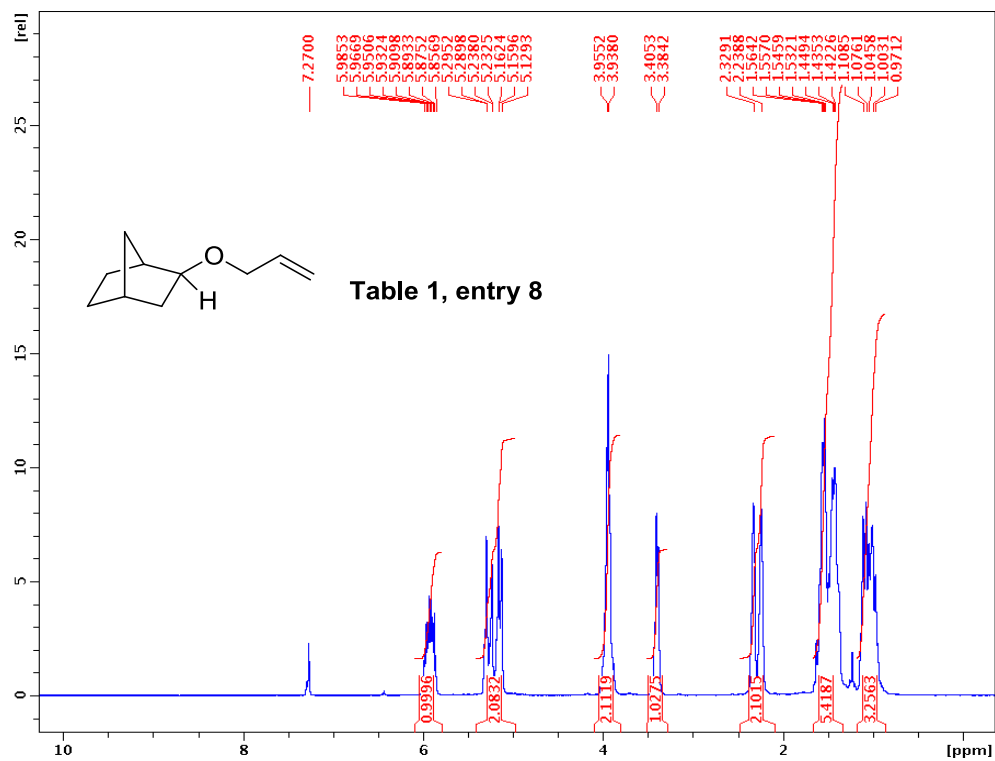


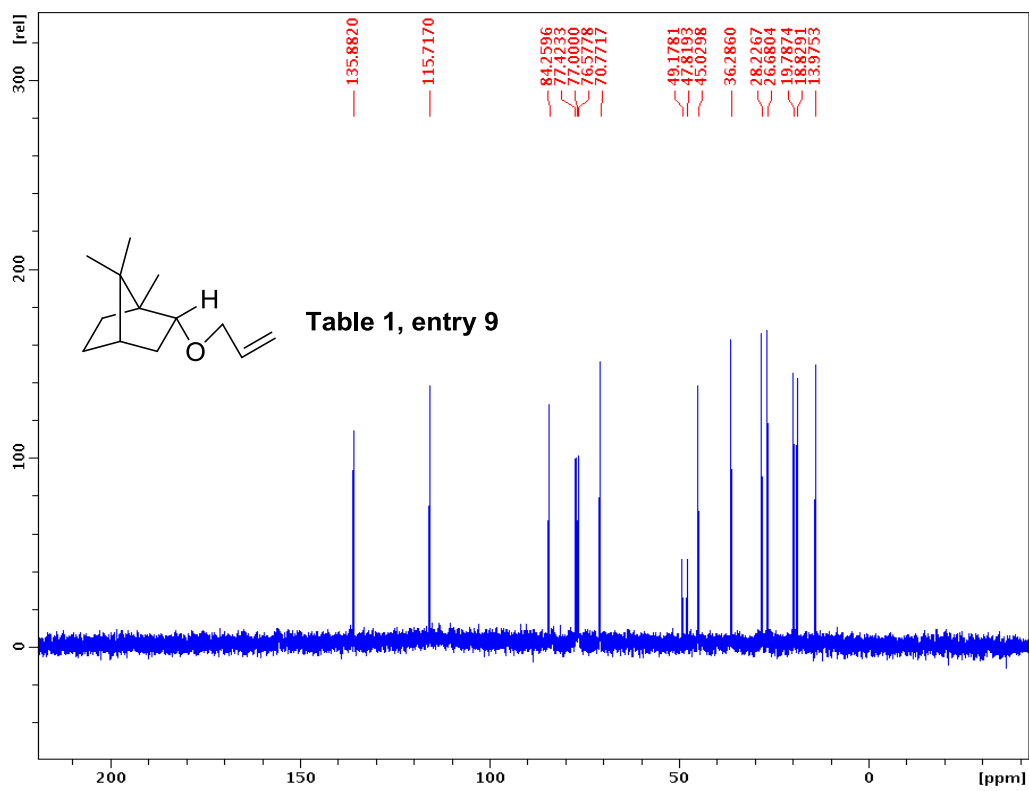
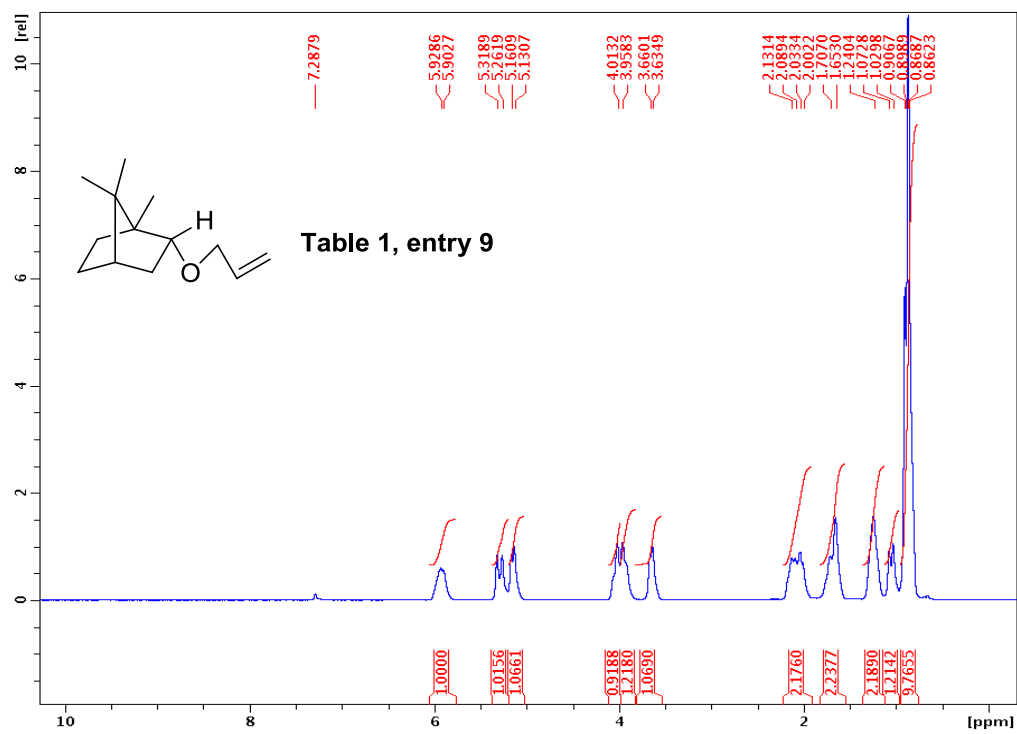


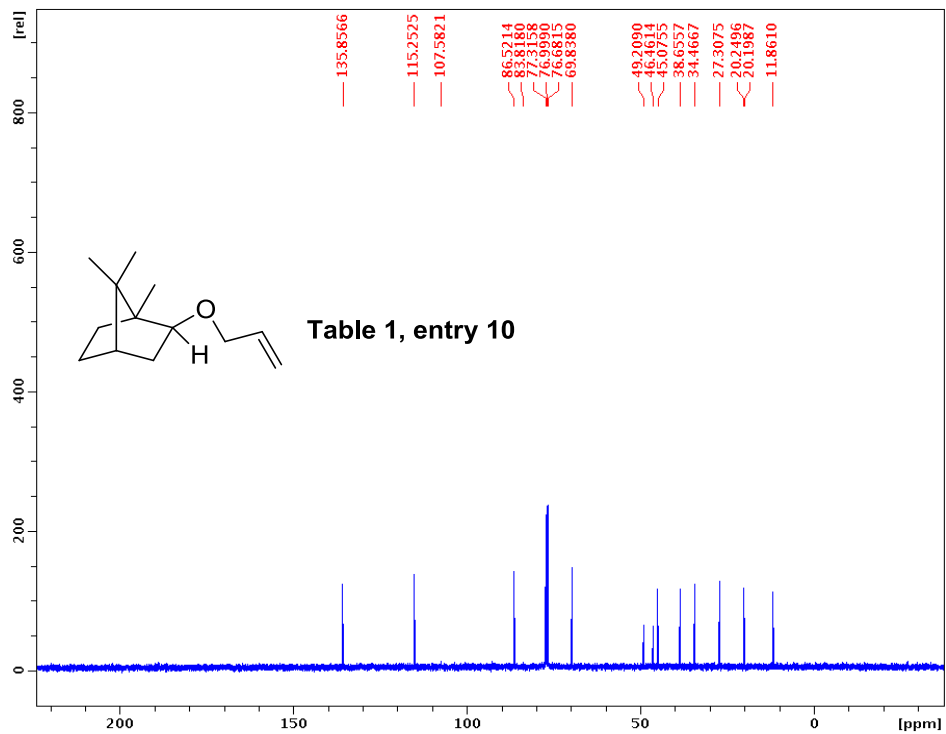
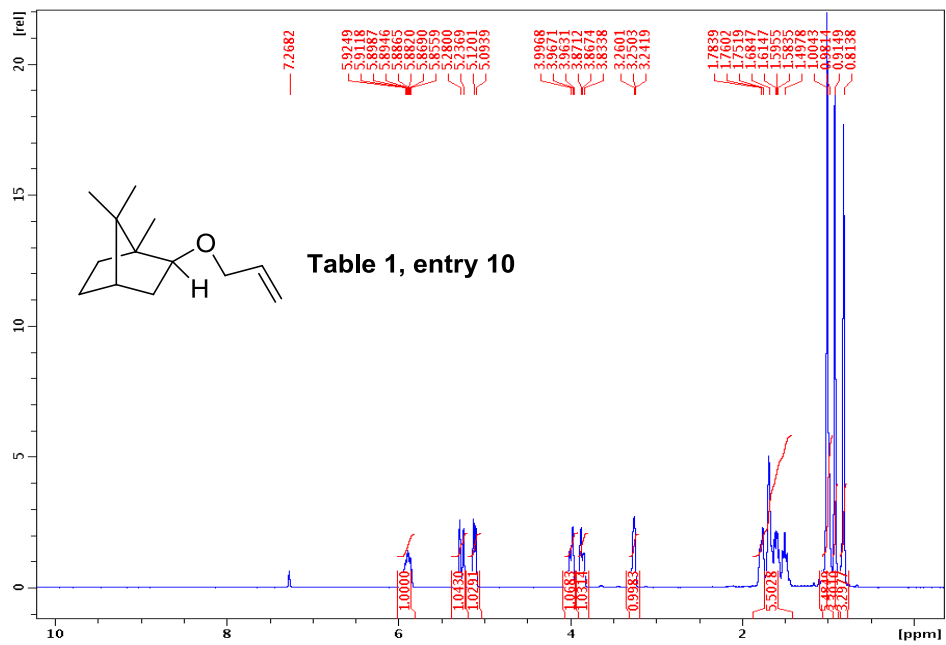


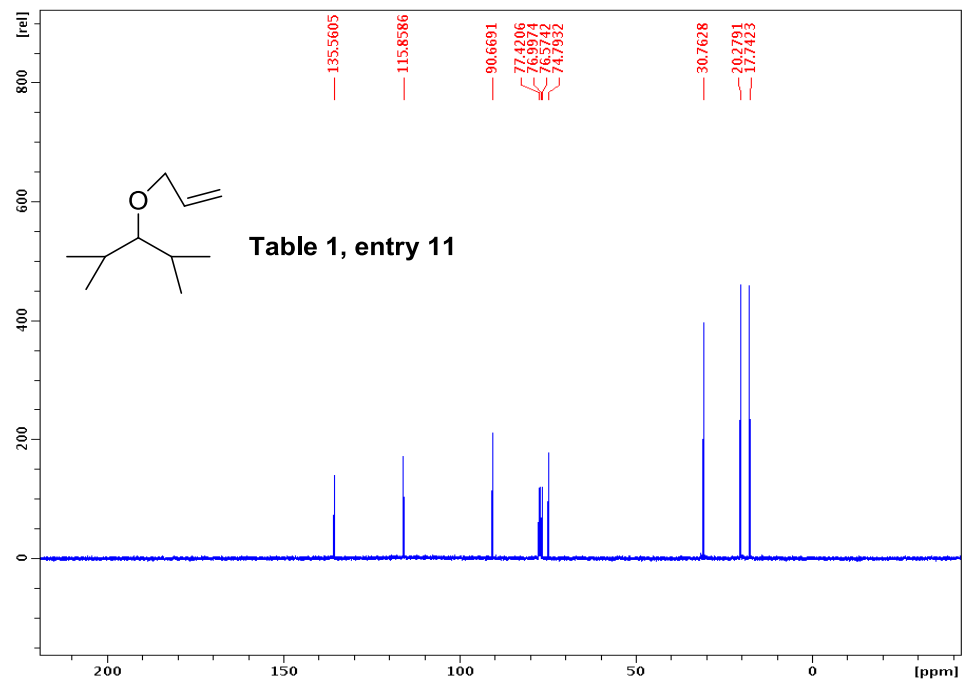
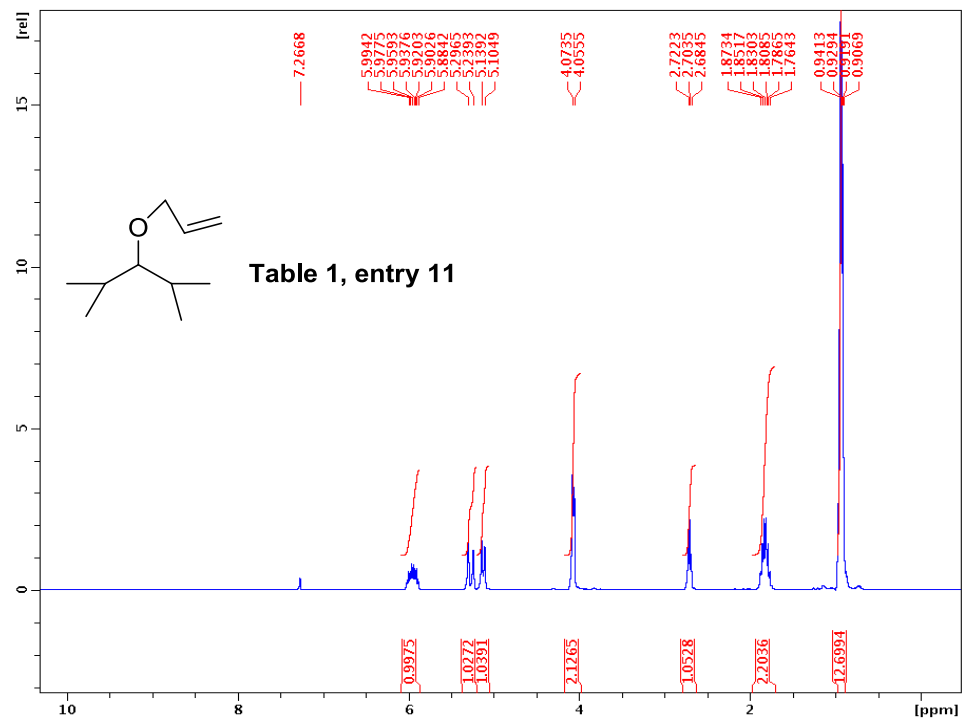


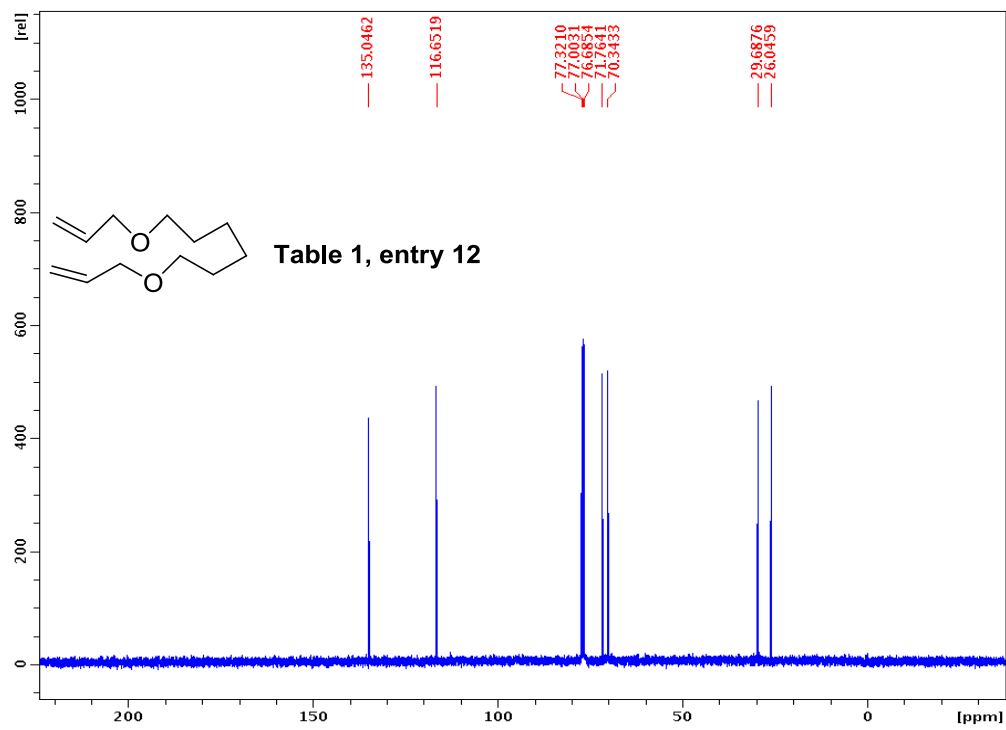
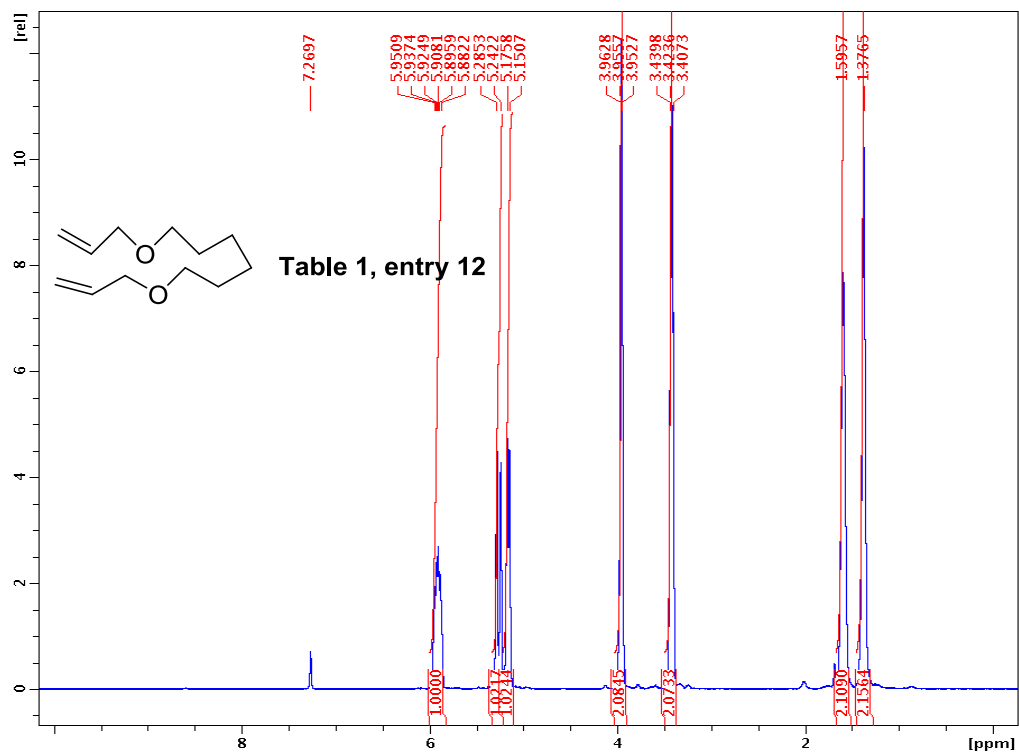


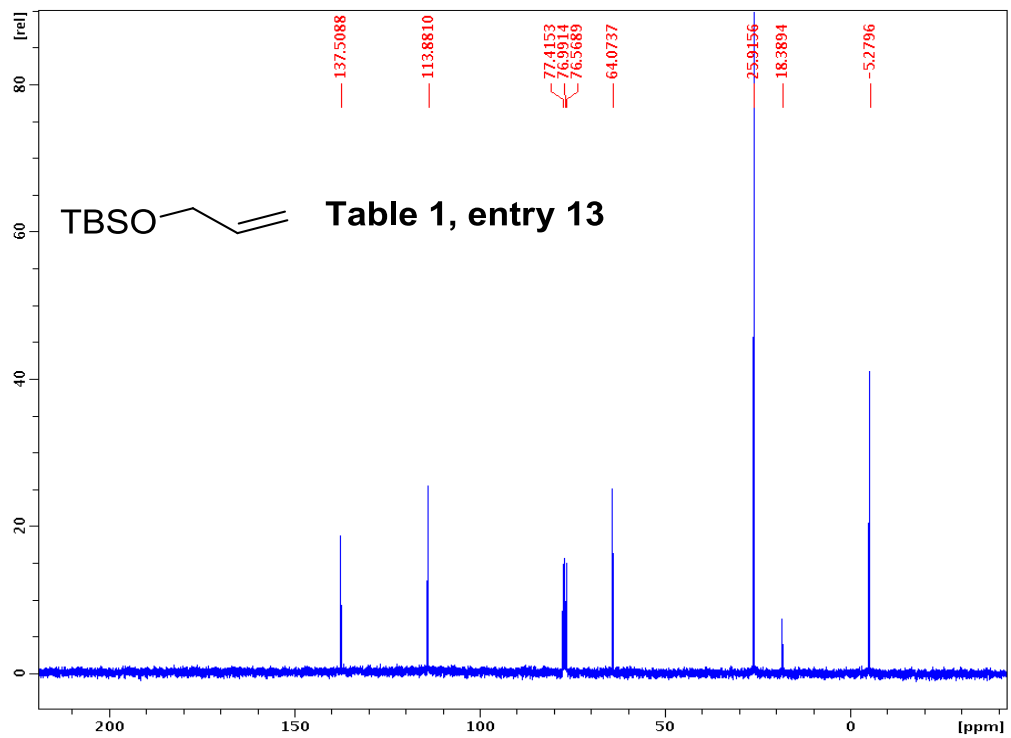
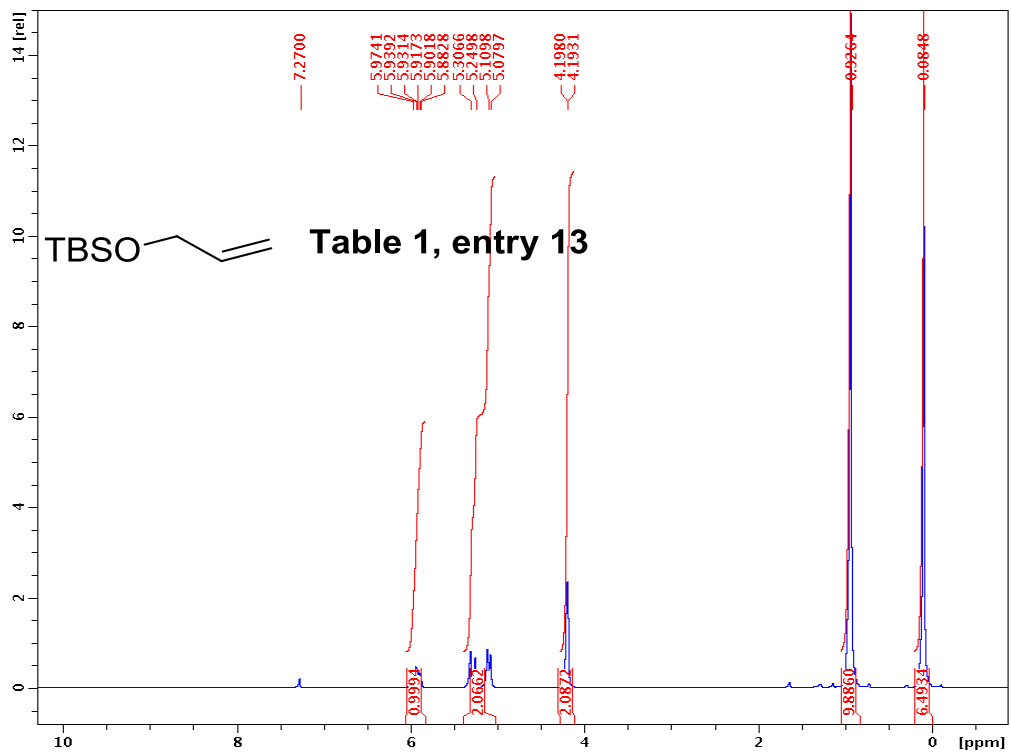


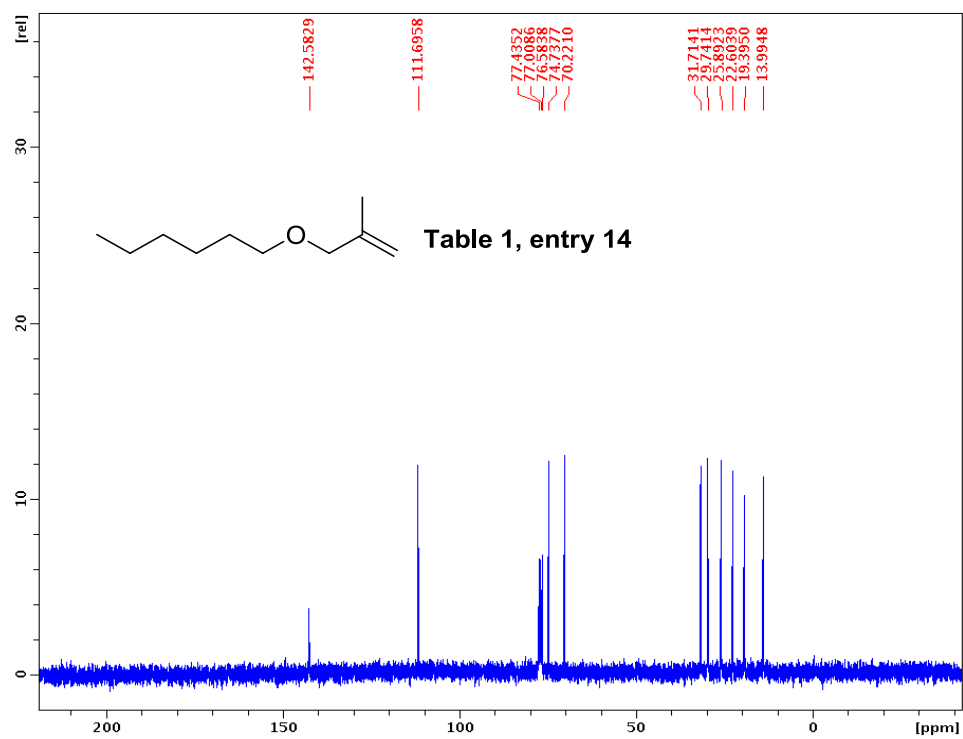
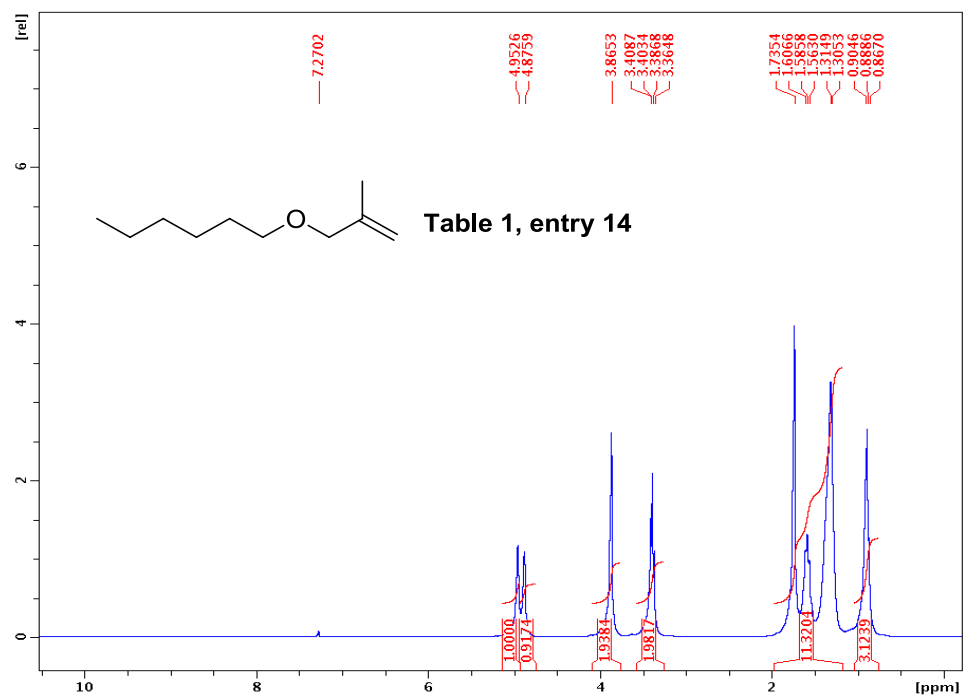


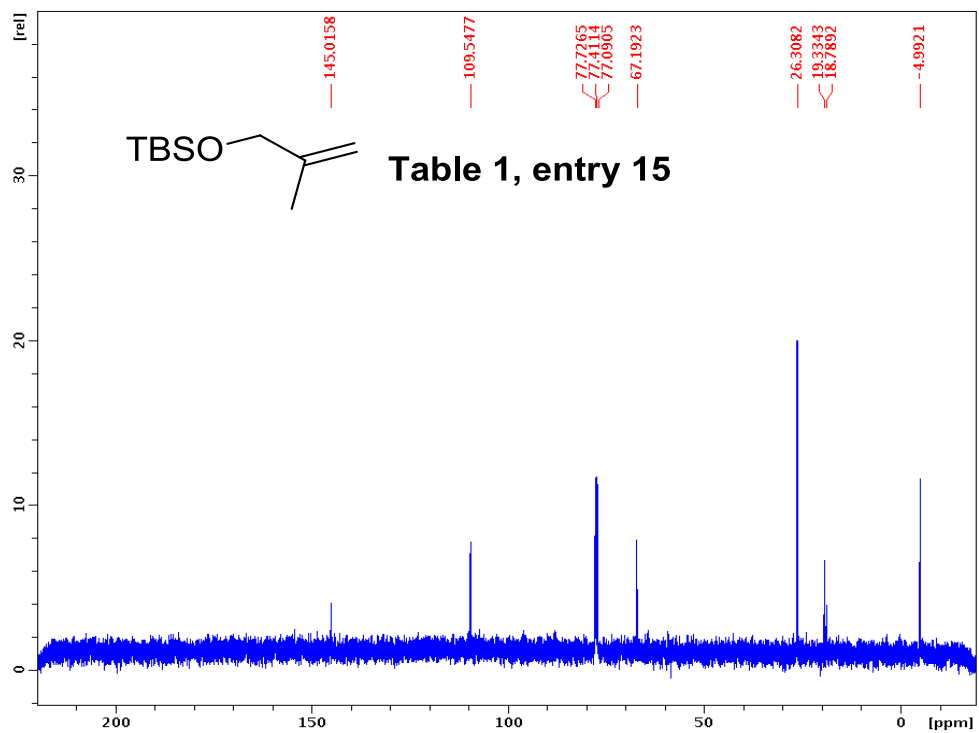
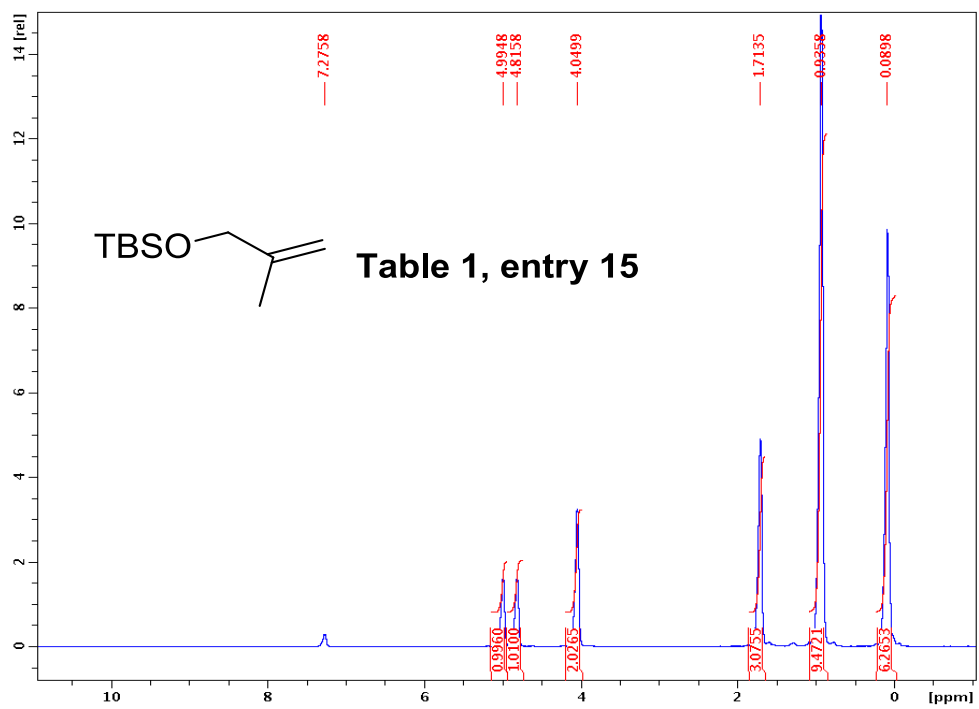


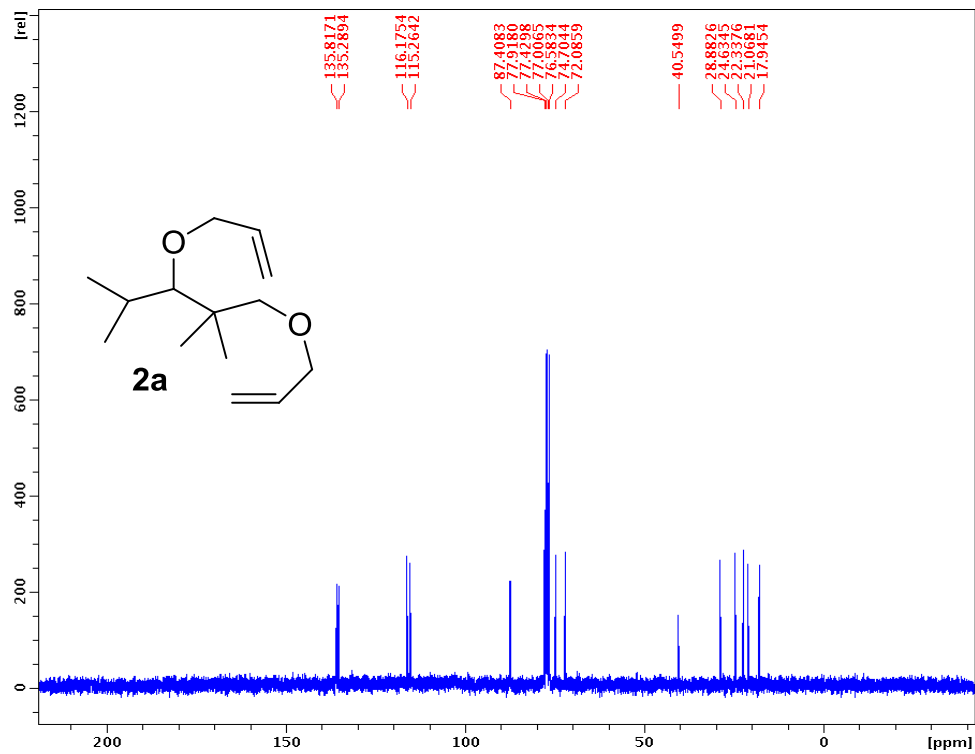
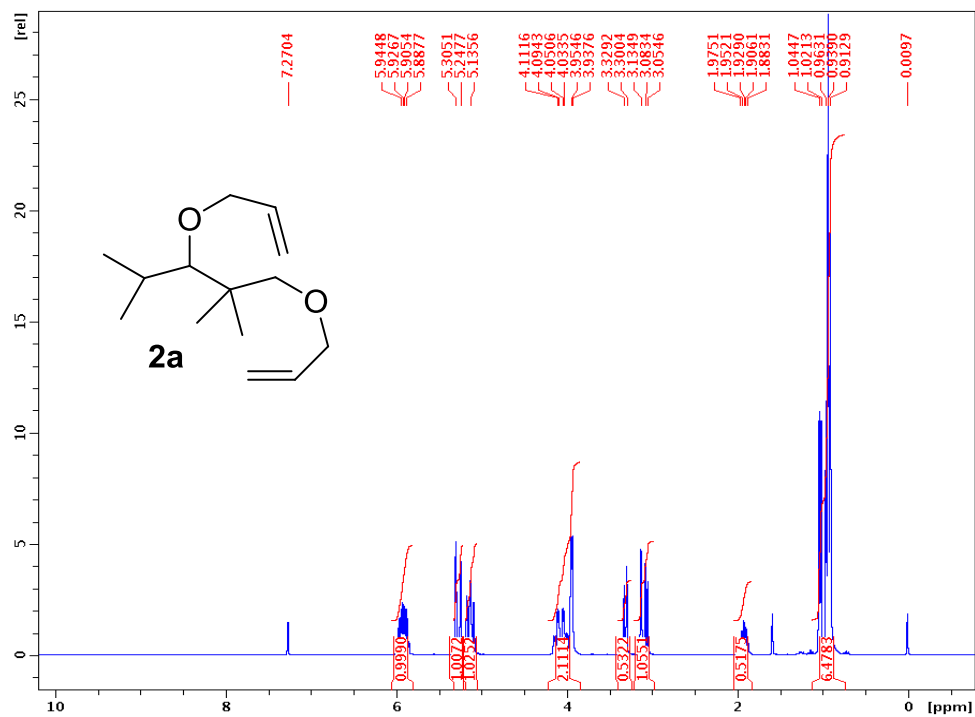




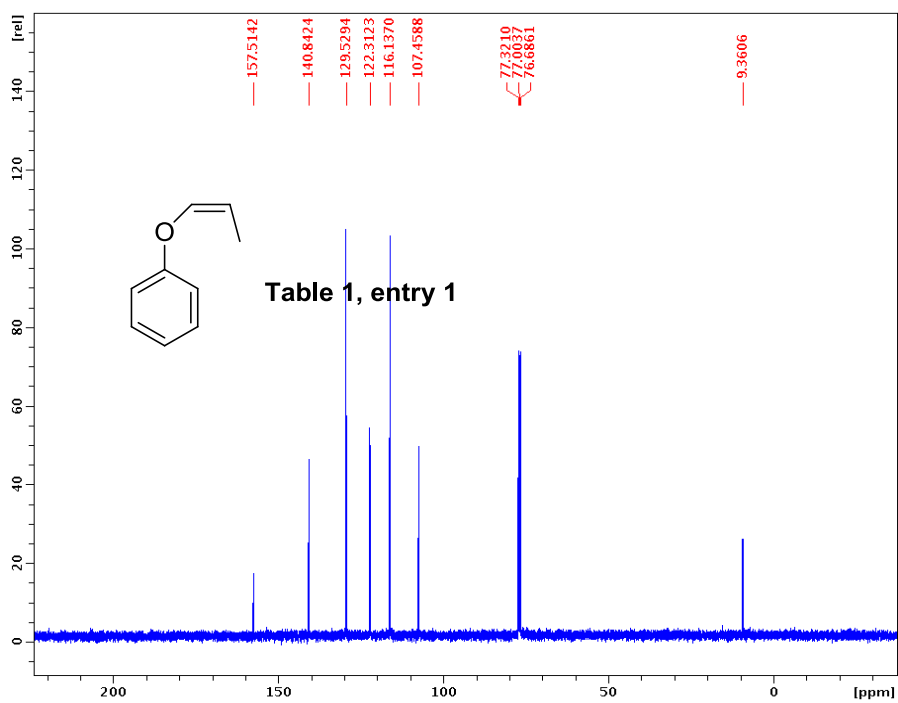
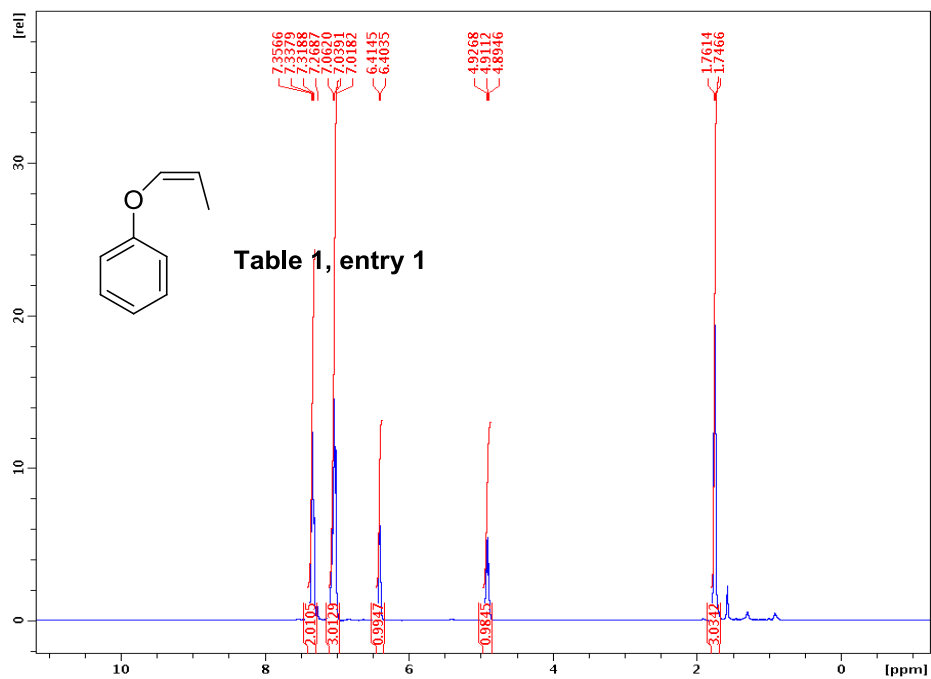


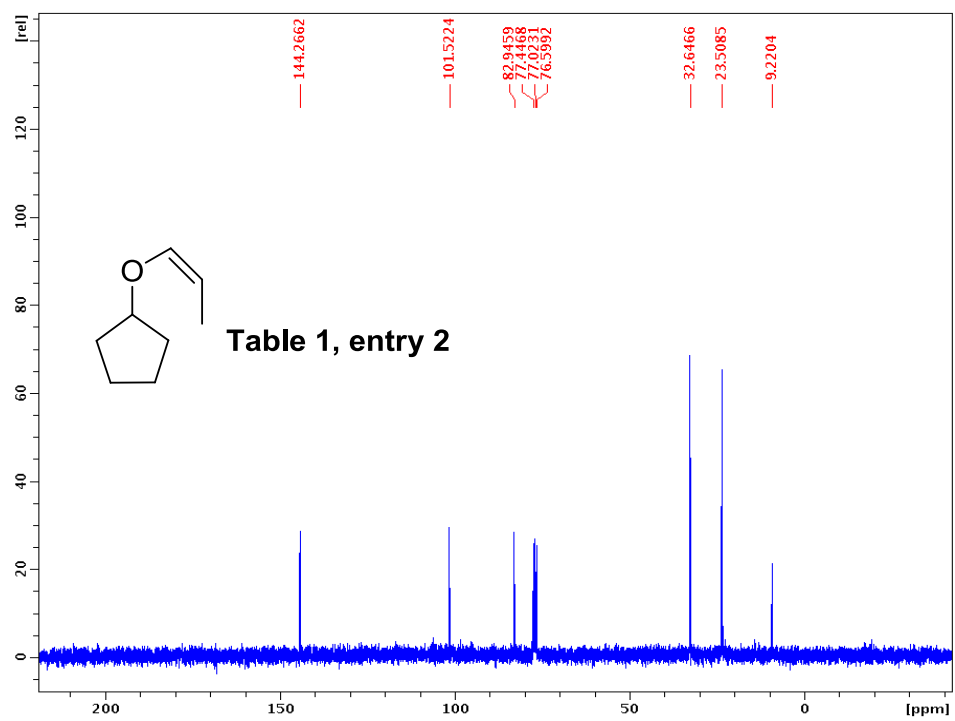
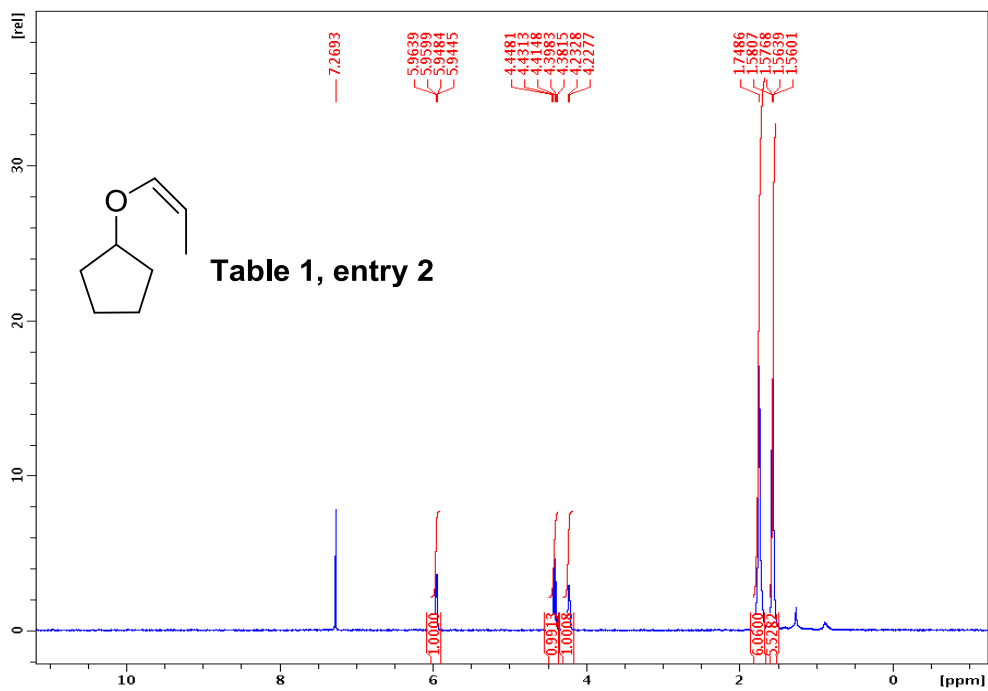


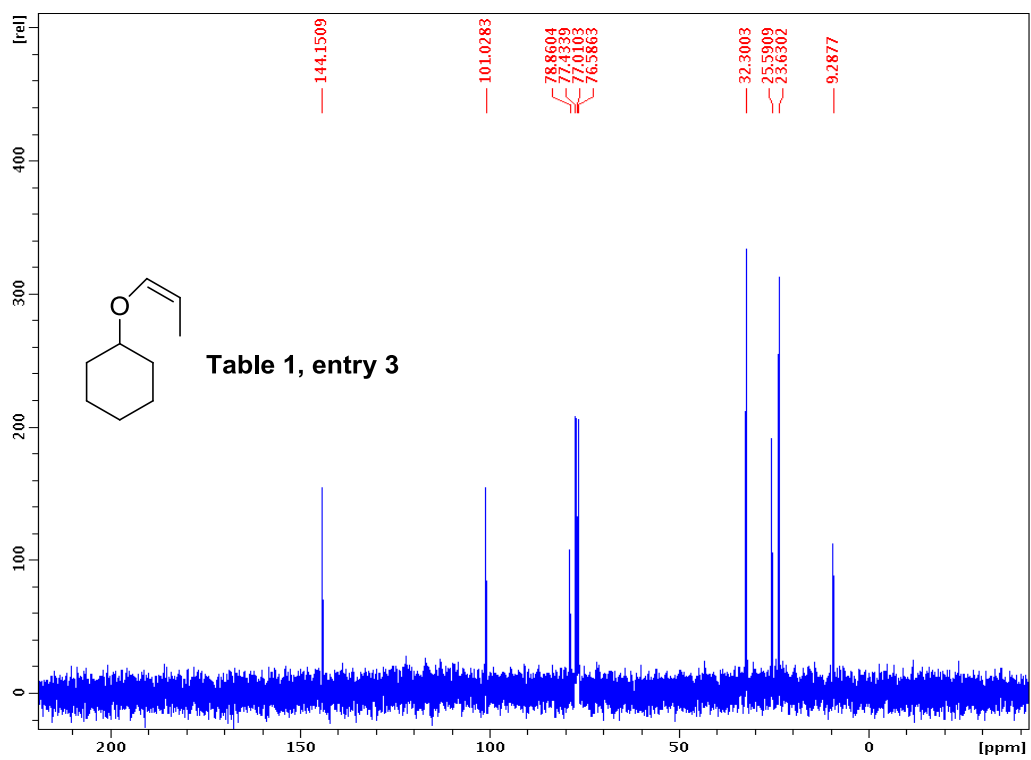
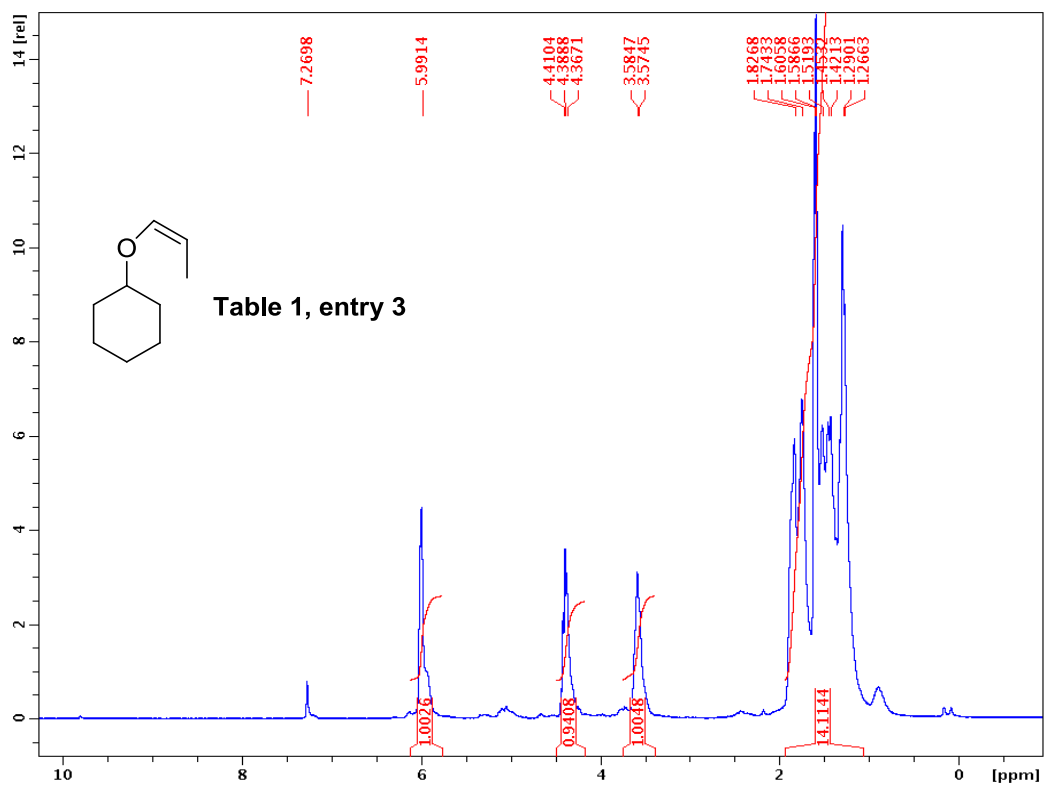


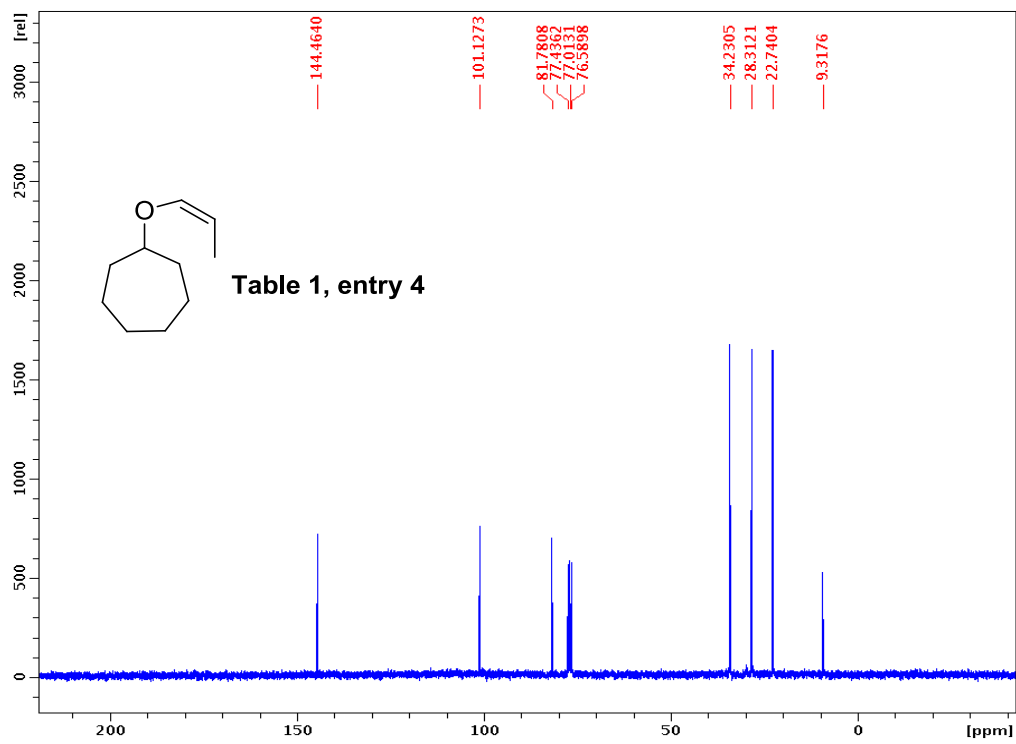
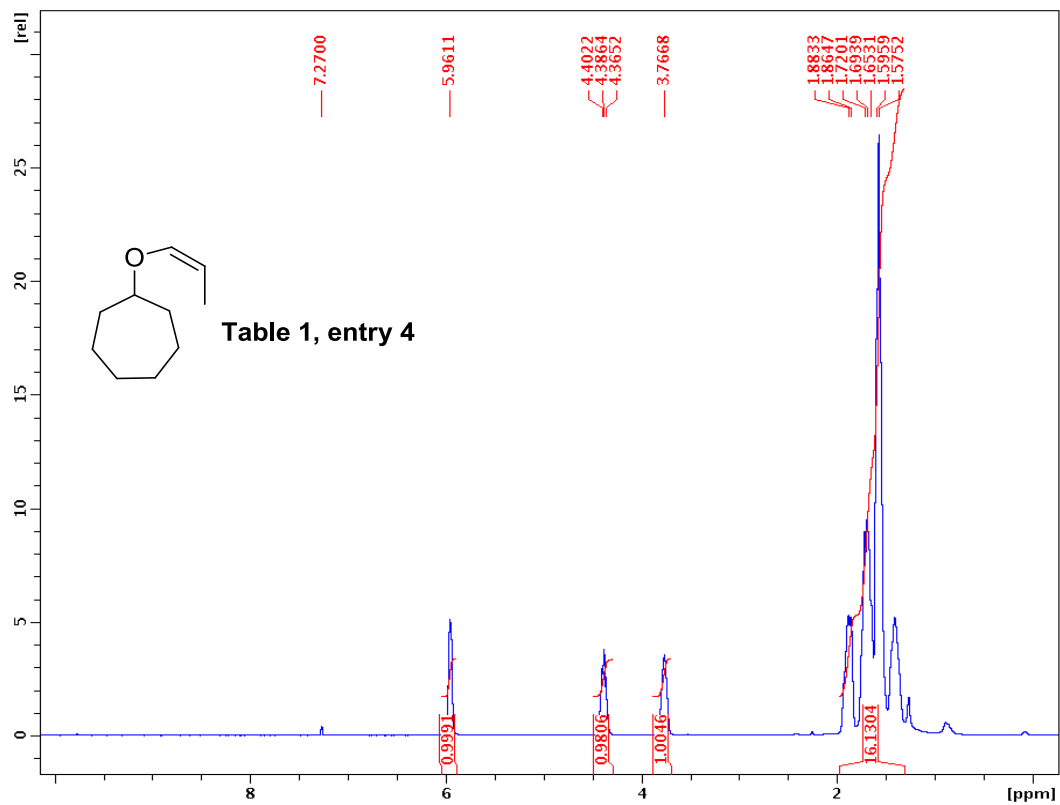


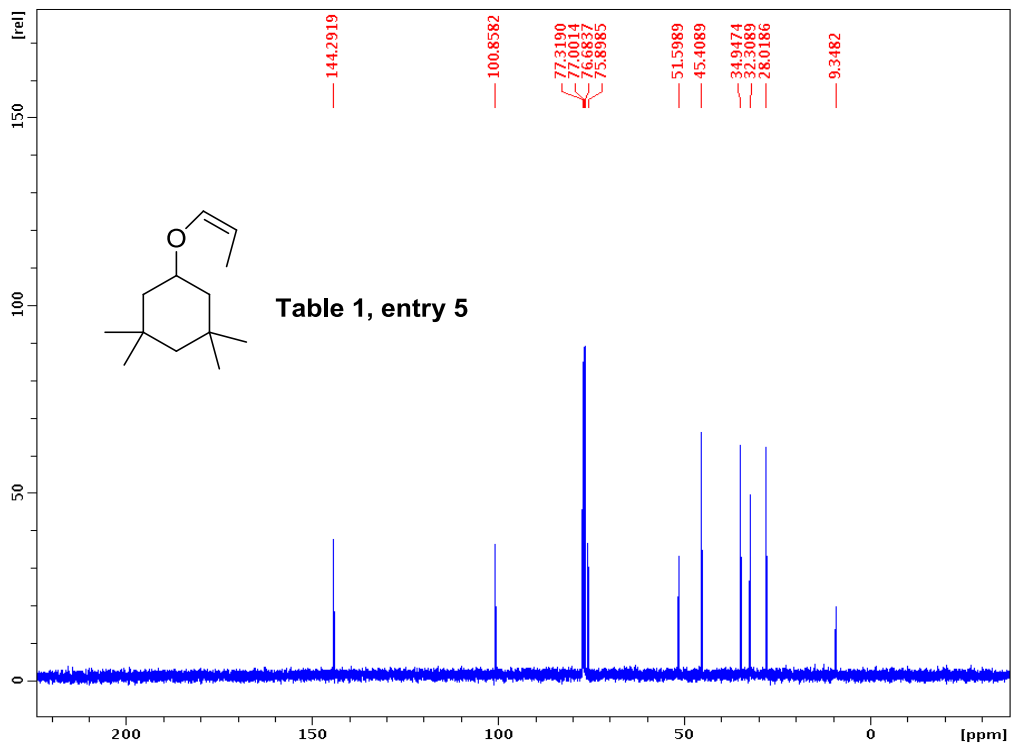
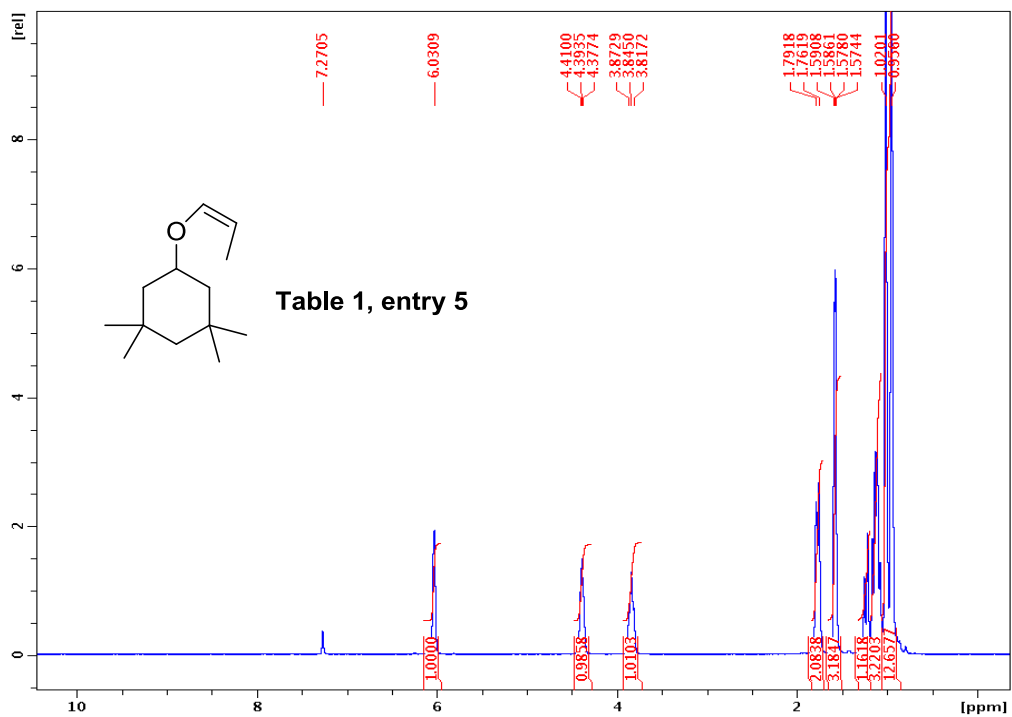
^1H and ^{13}C NMR Spectra for the Vinyl Ethers

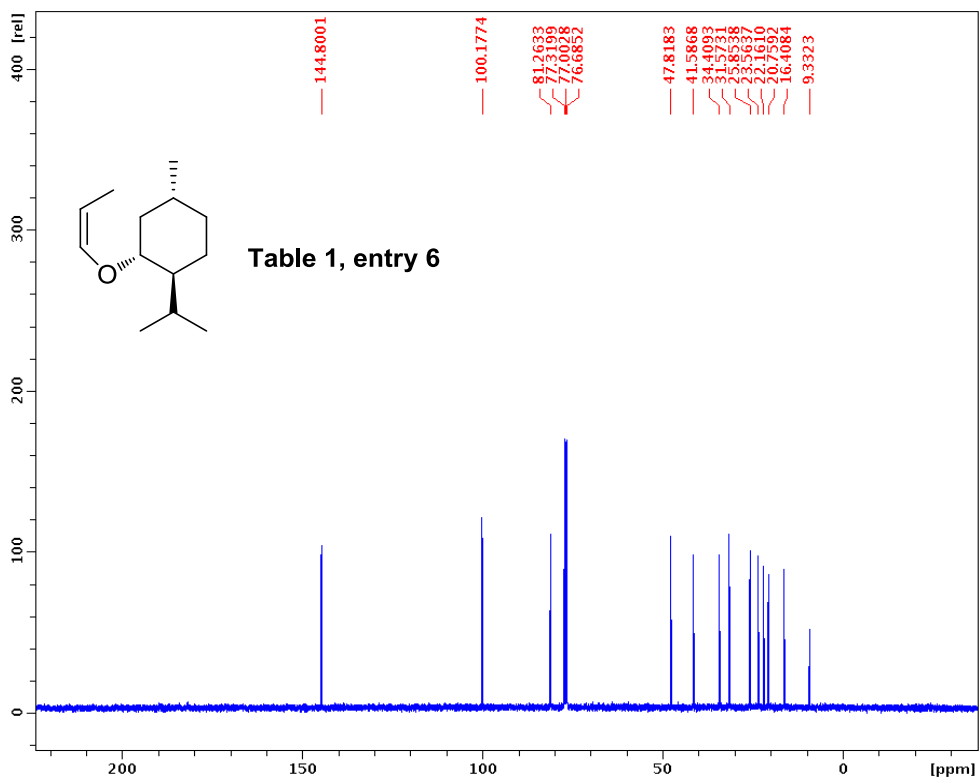
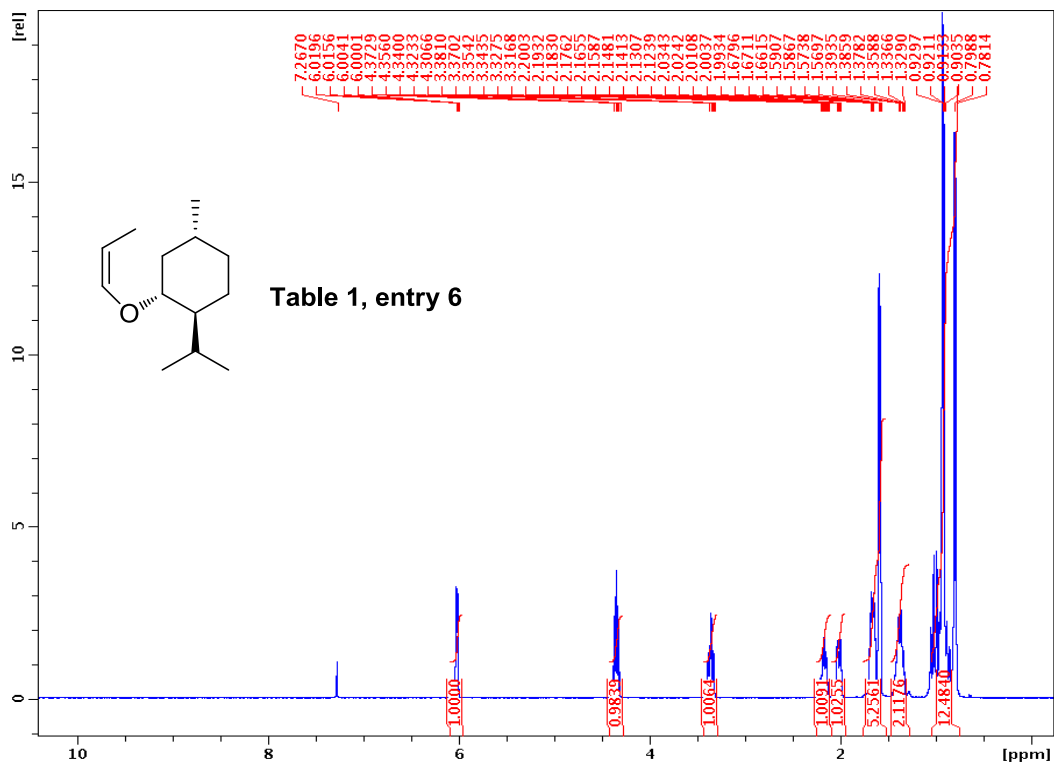


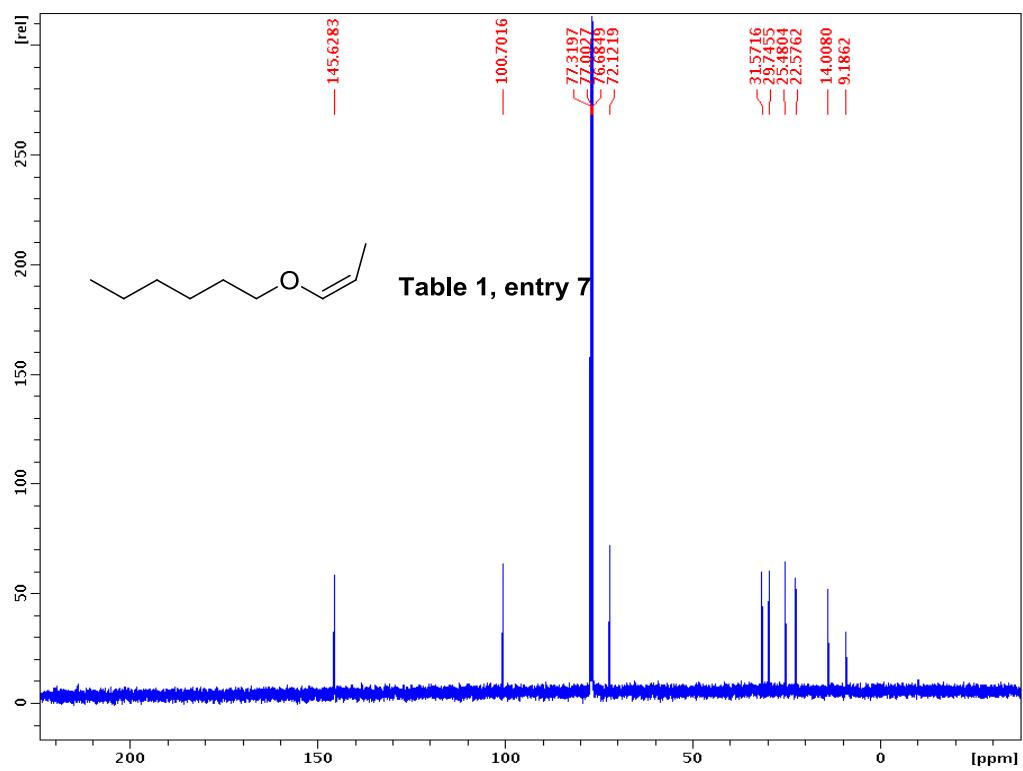
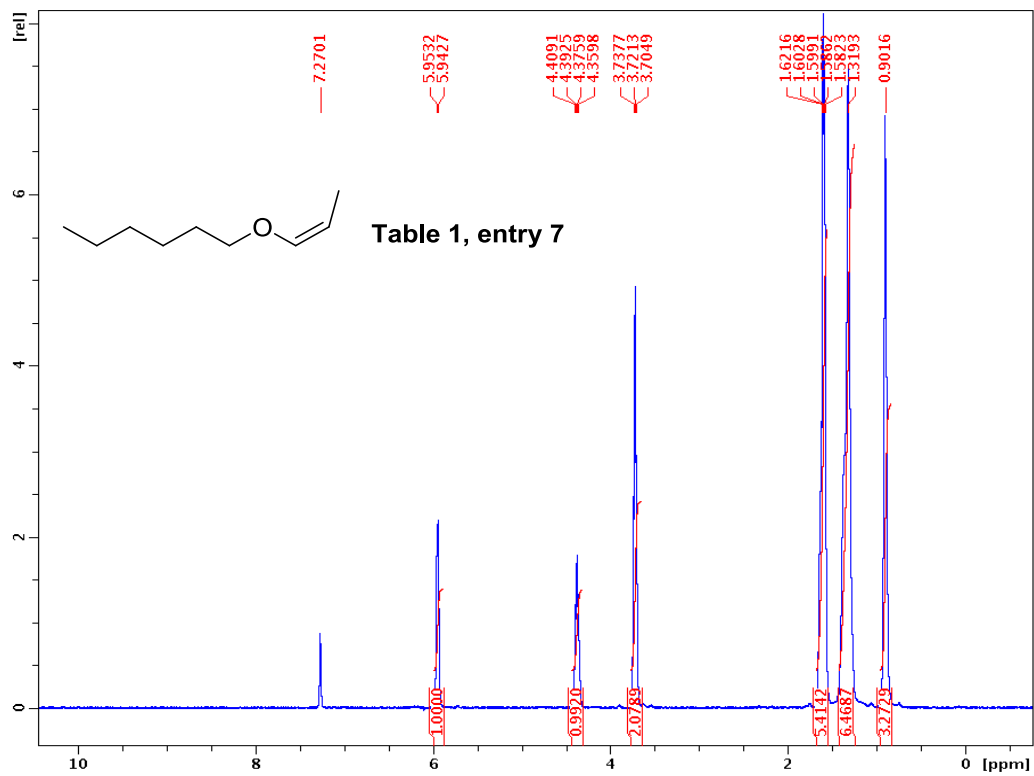


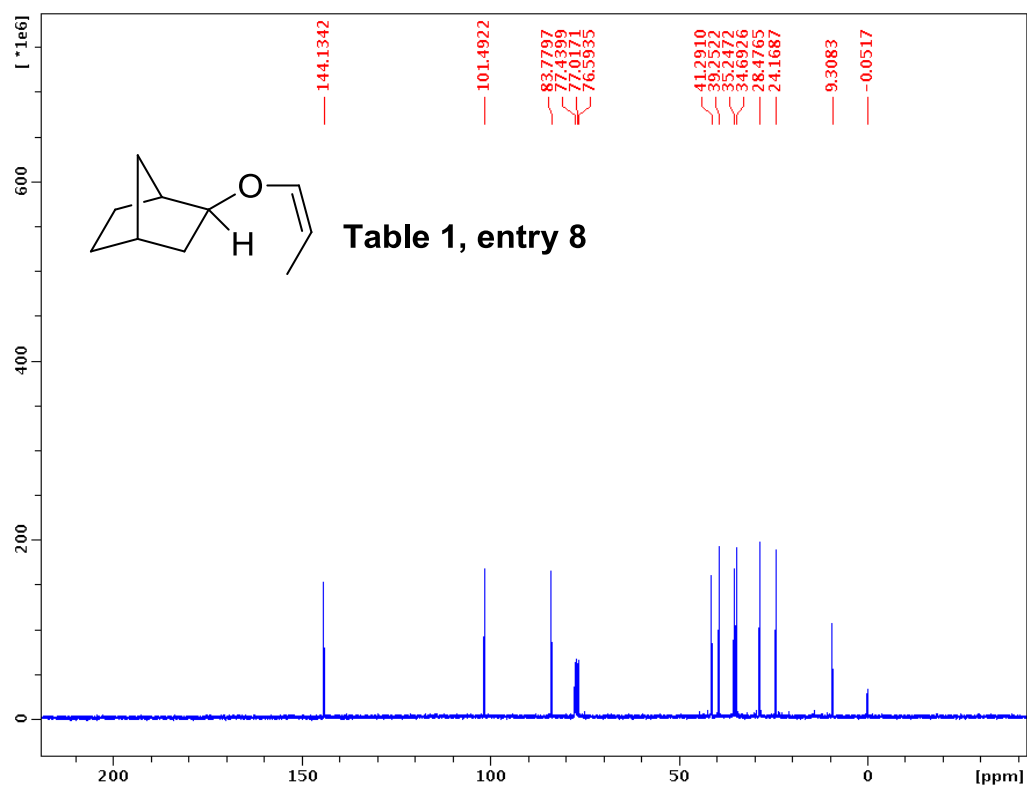
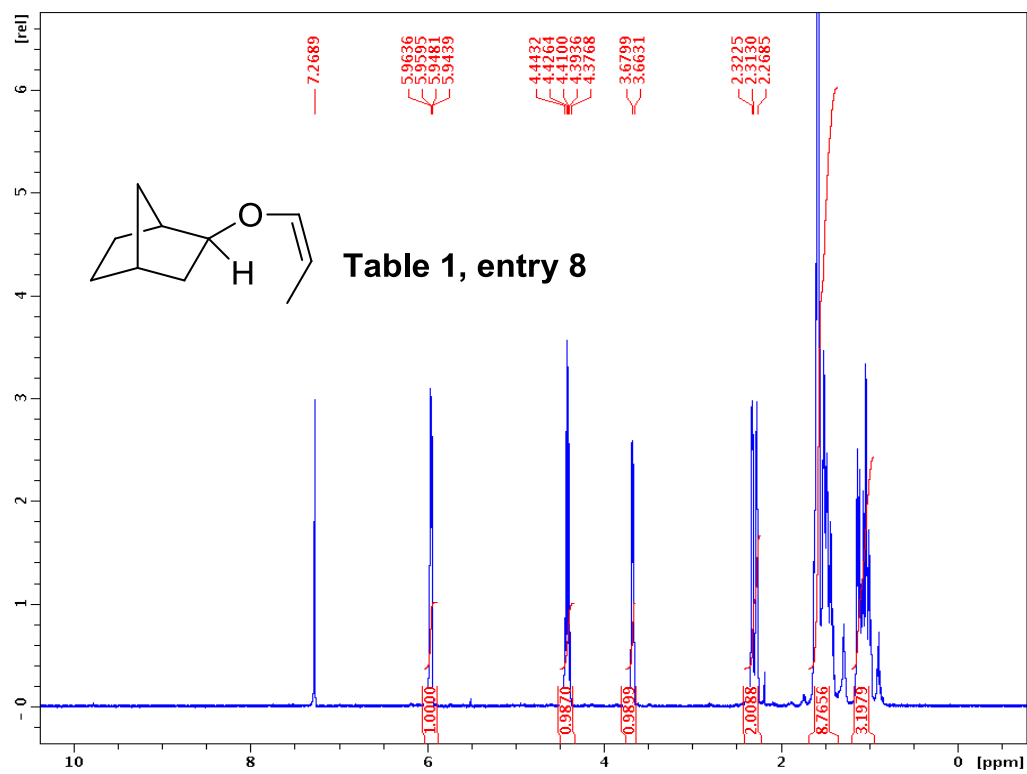


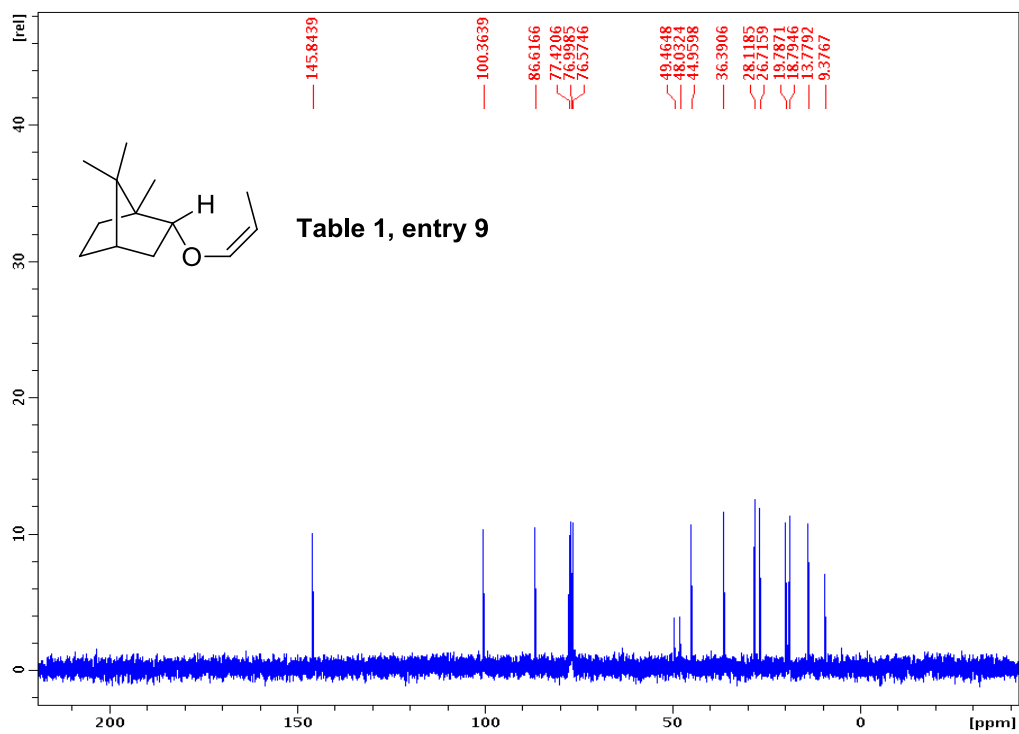
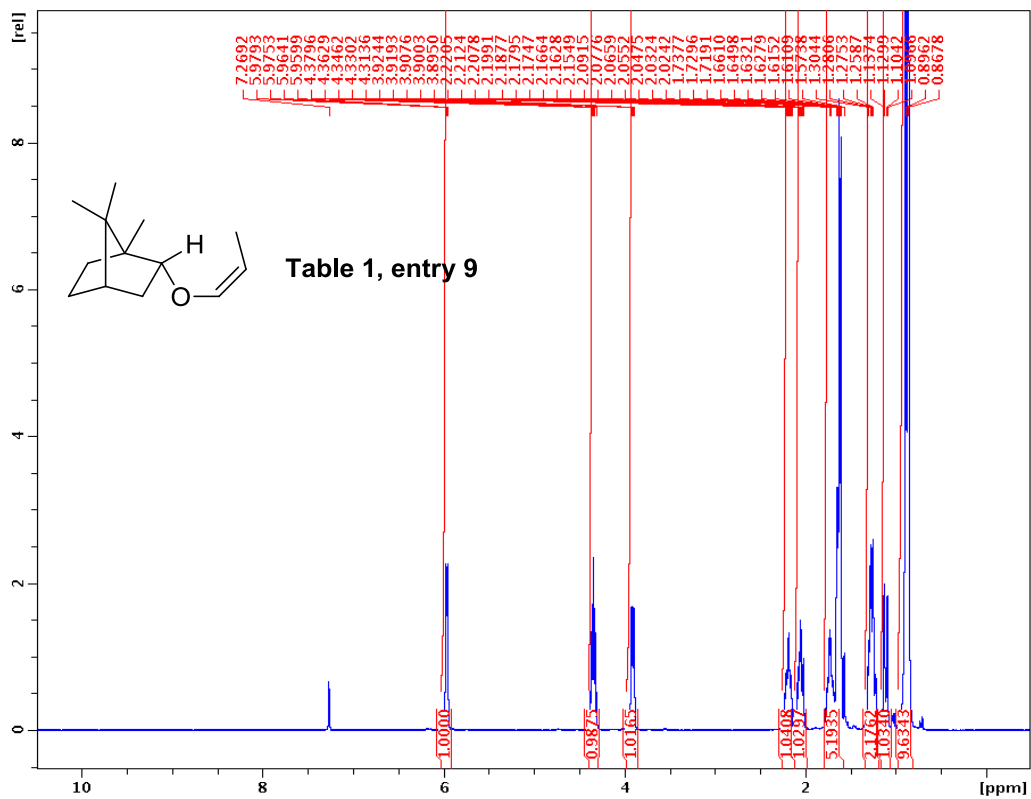


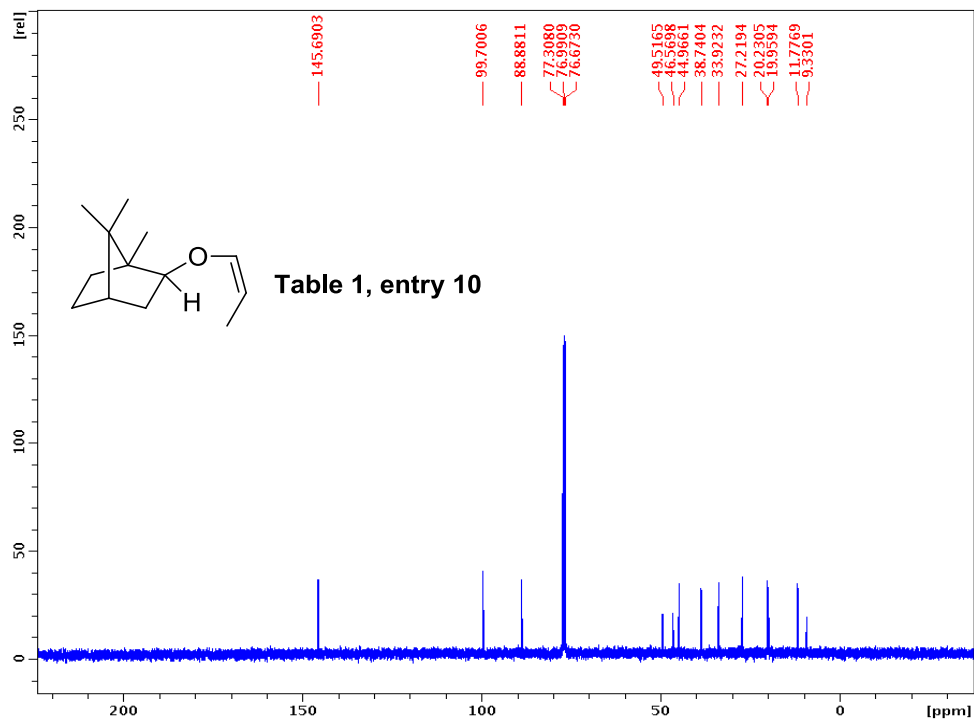
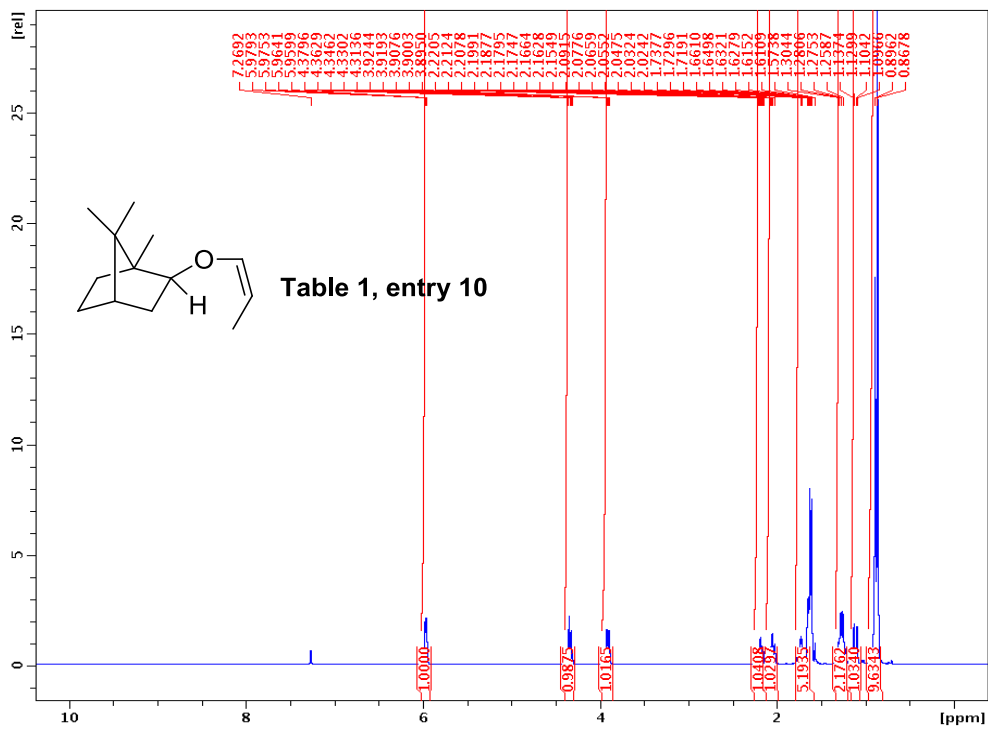


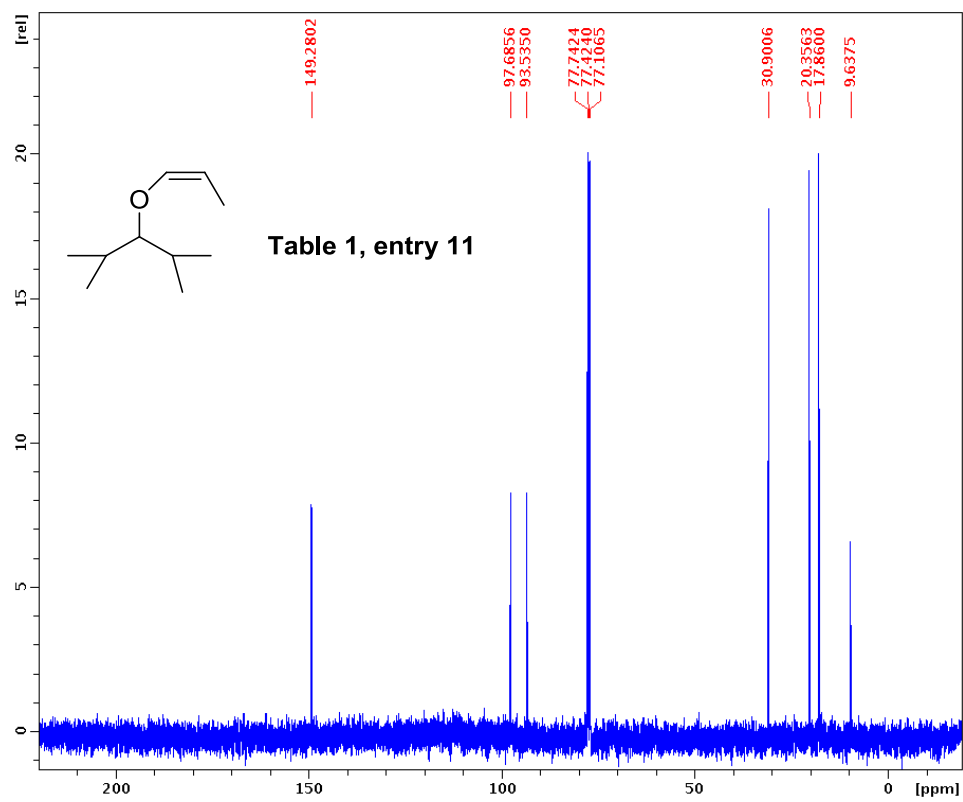
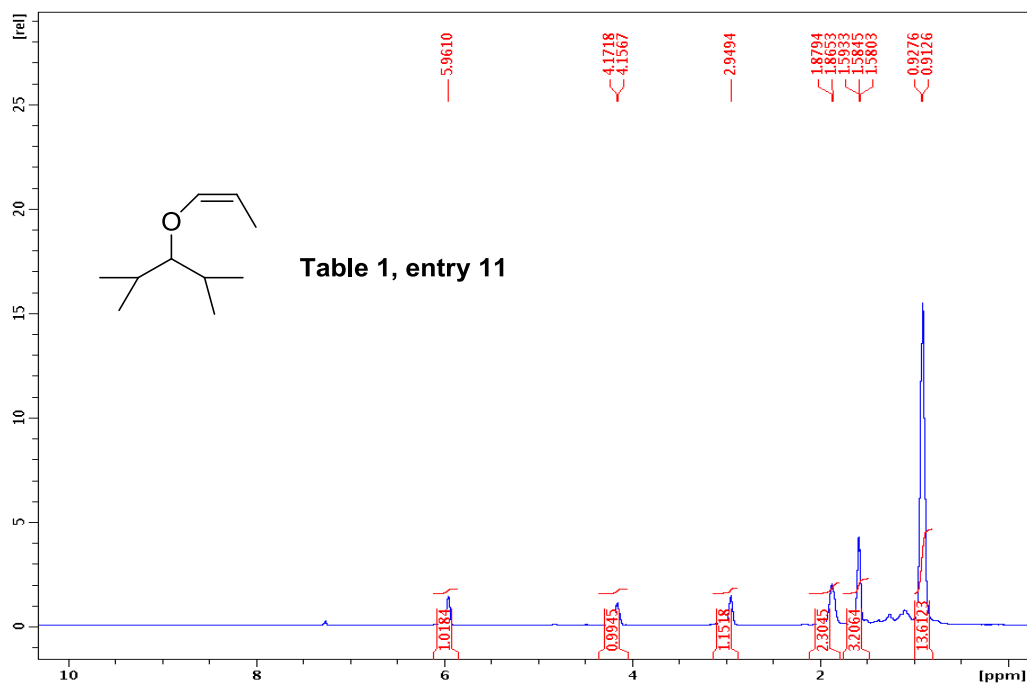


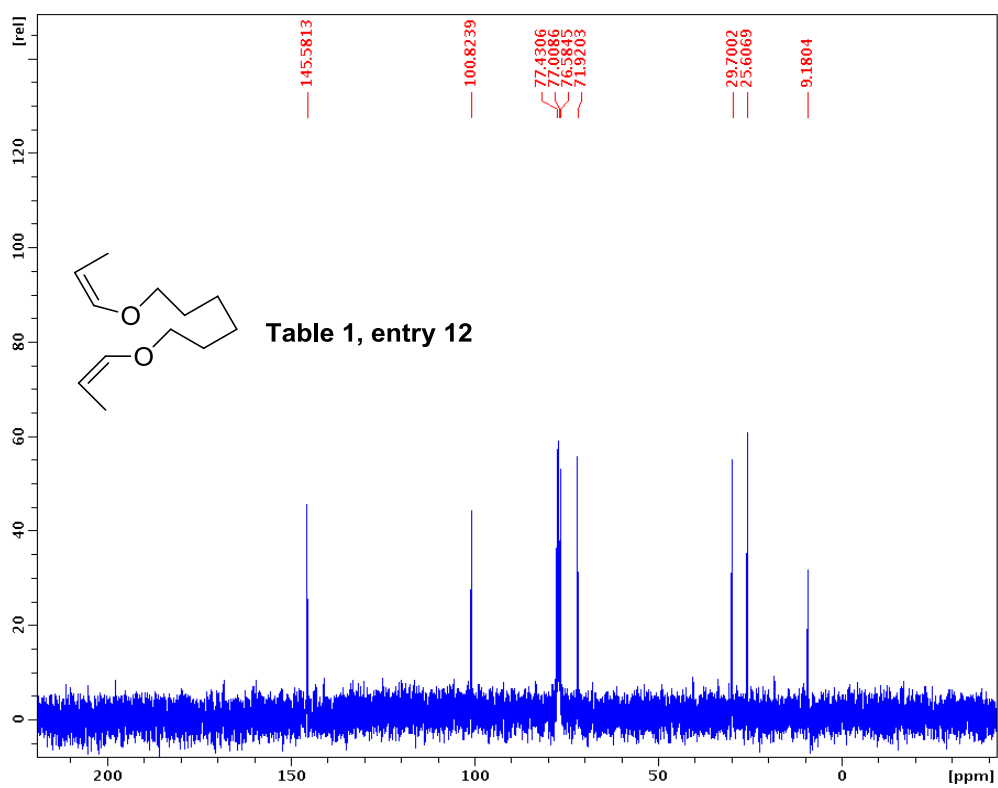
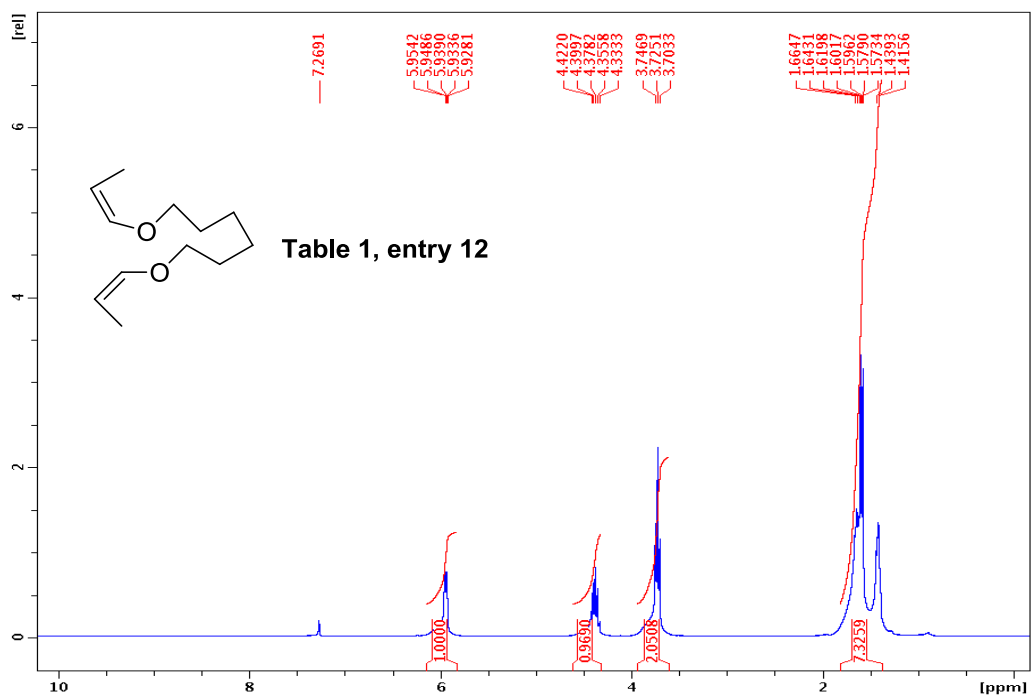


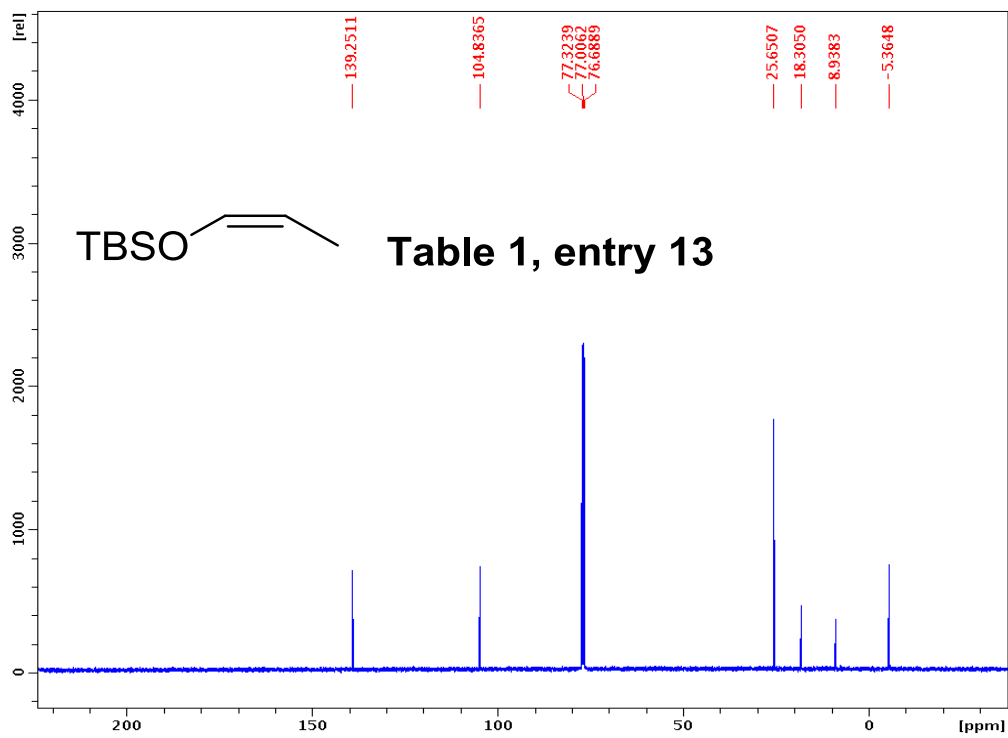
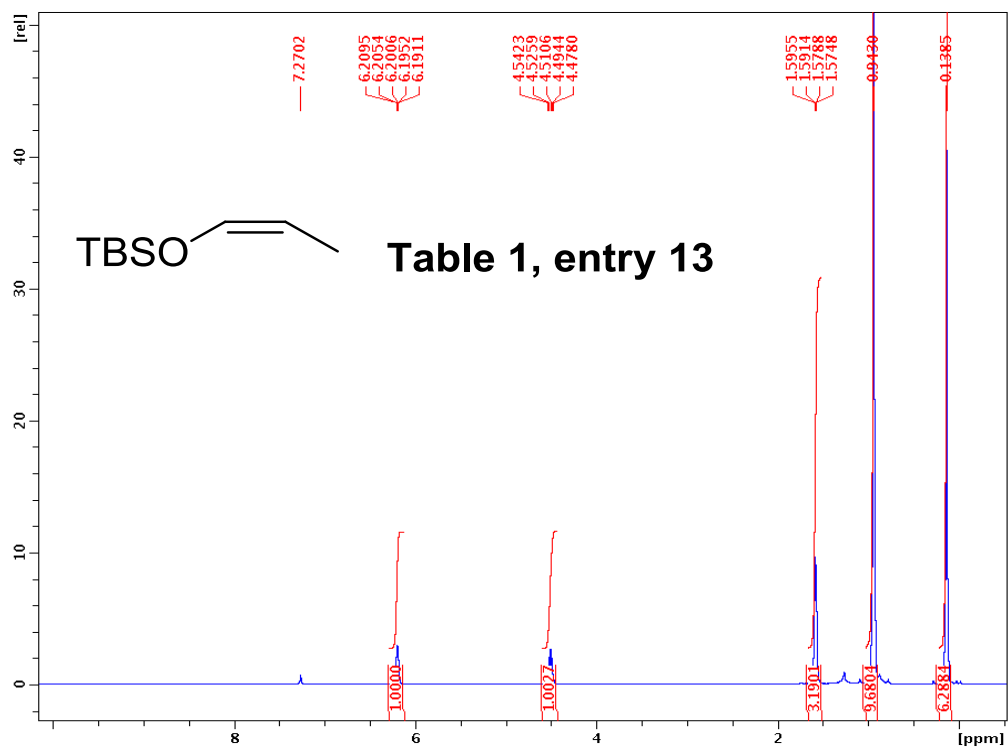


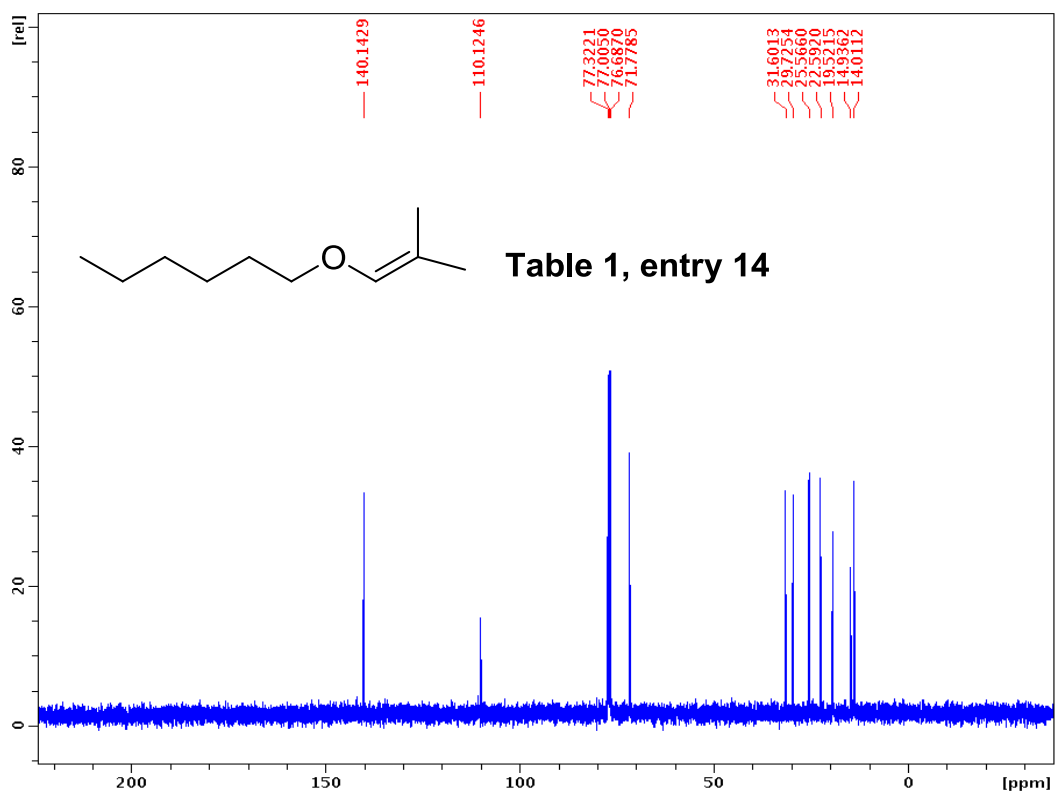
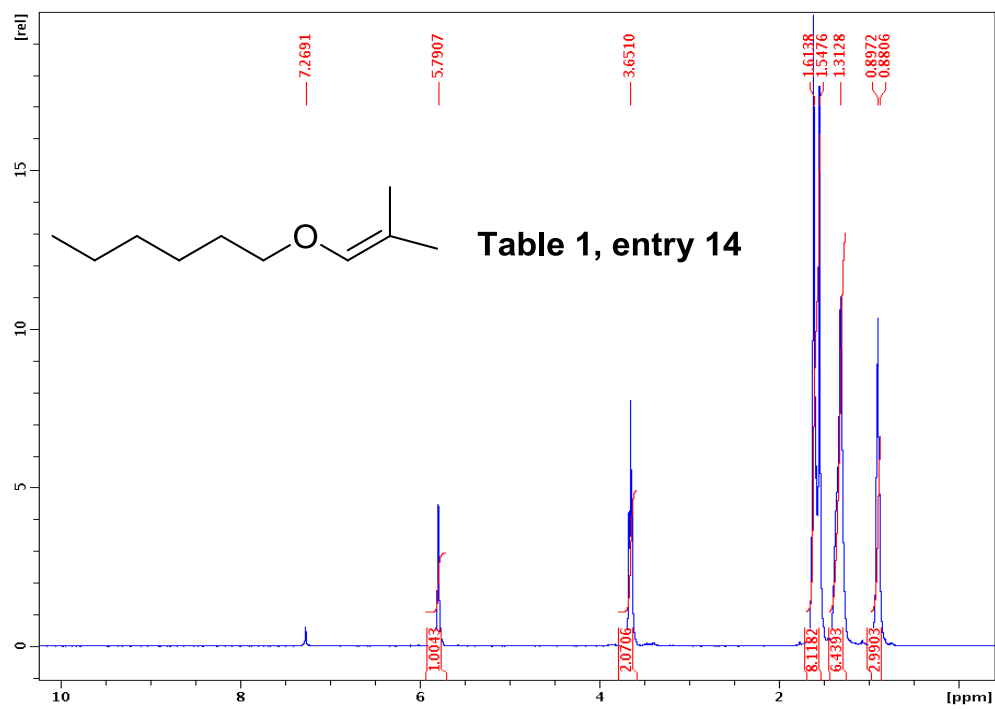


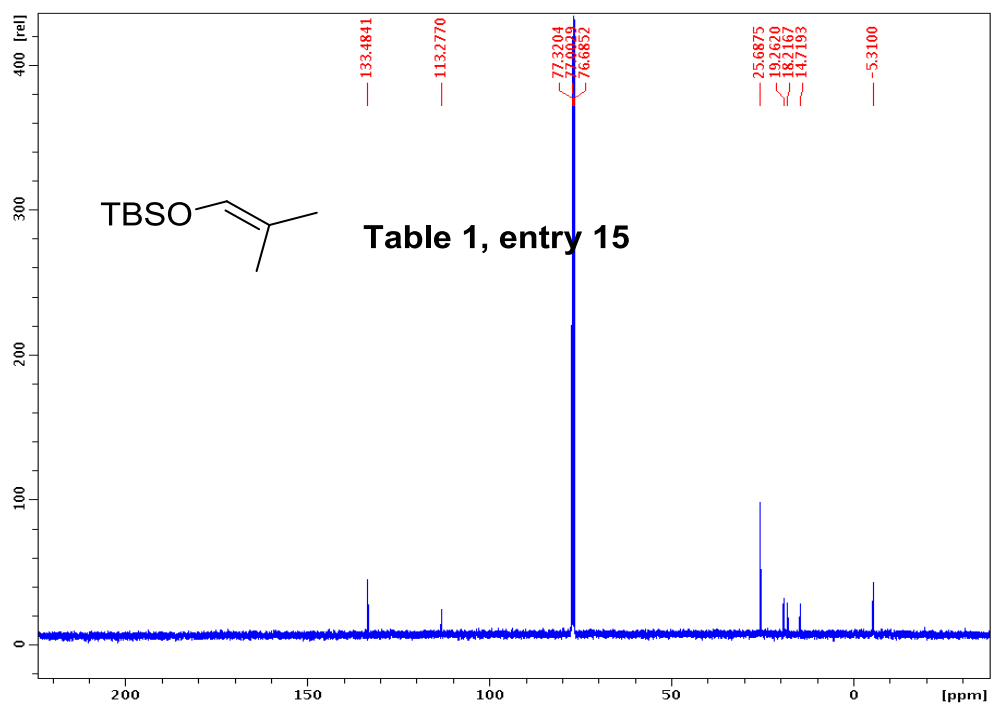
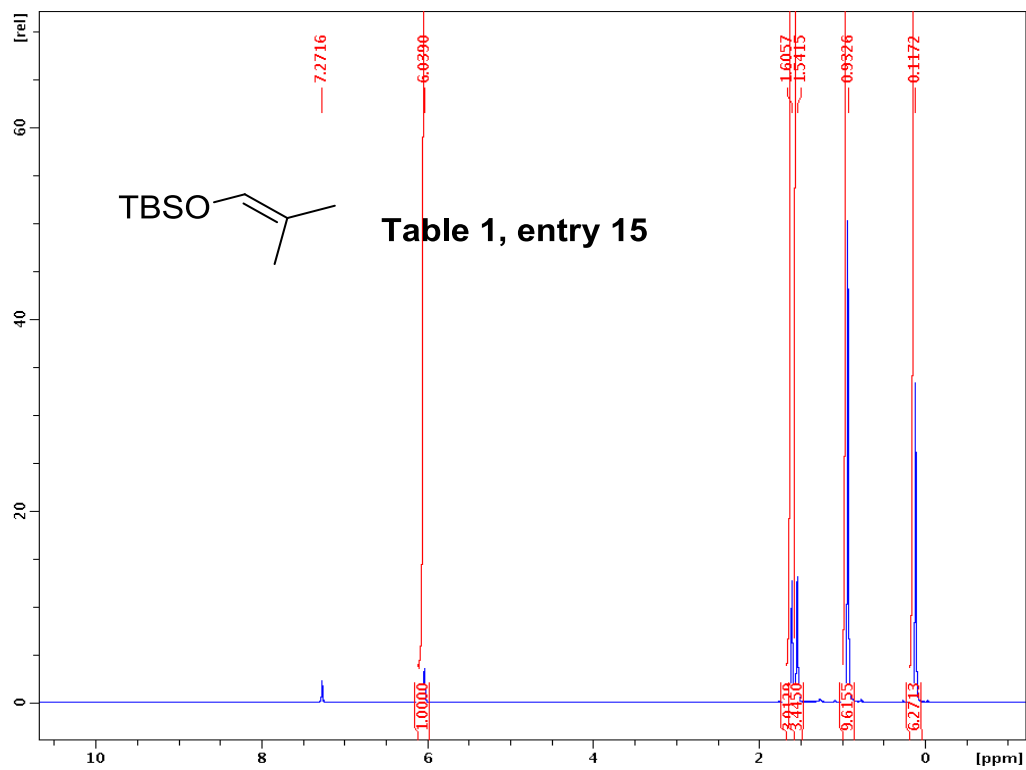


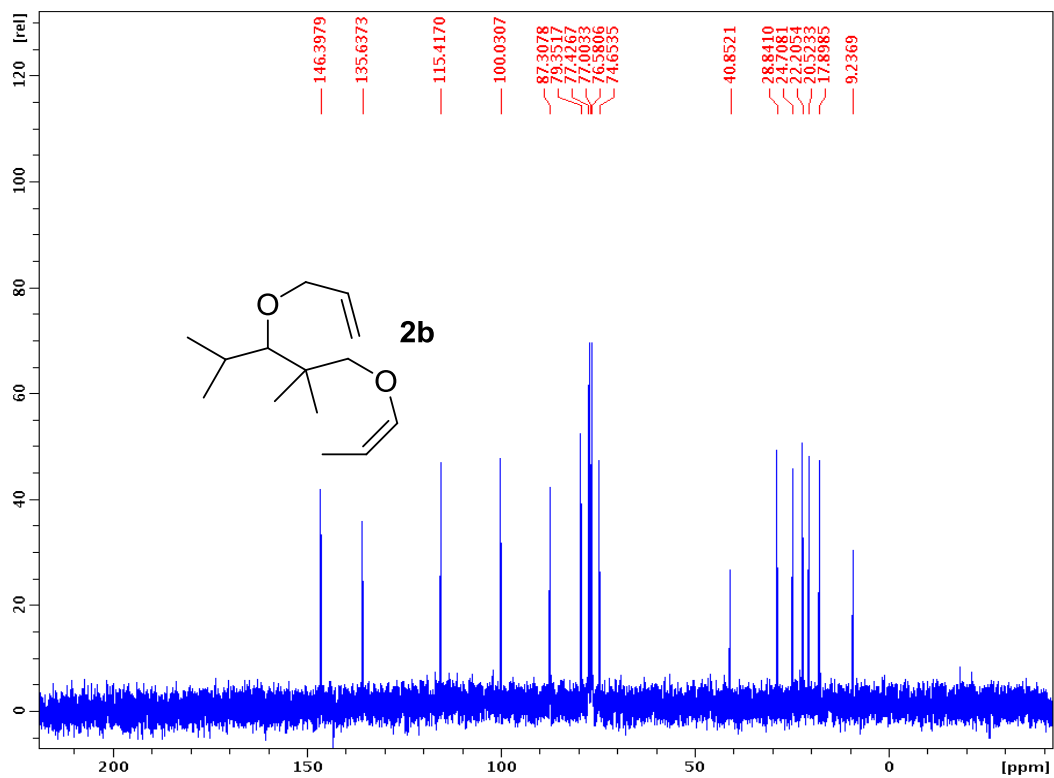
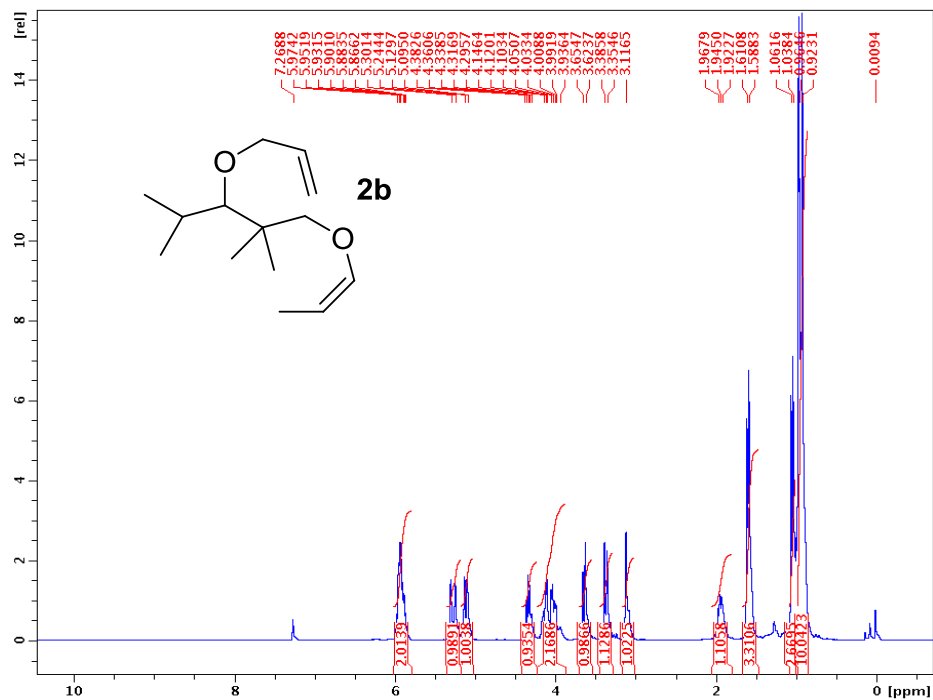


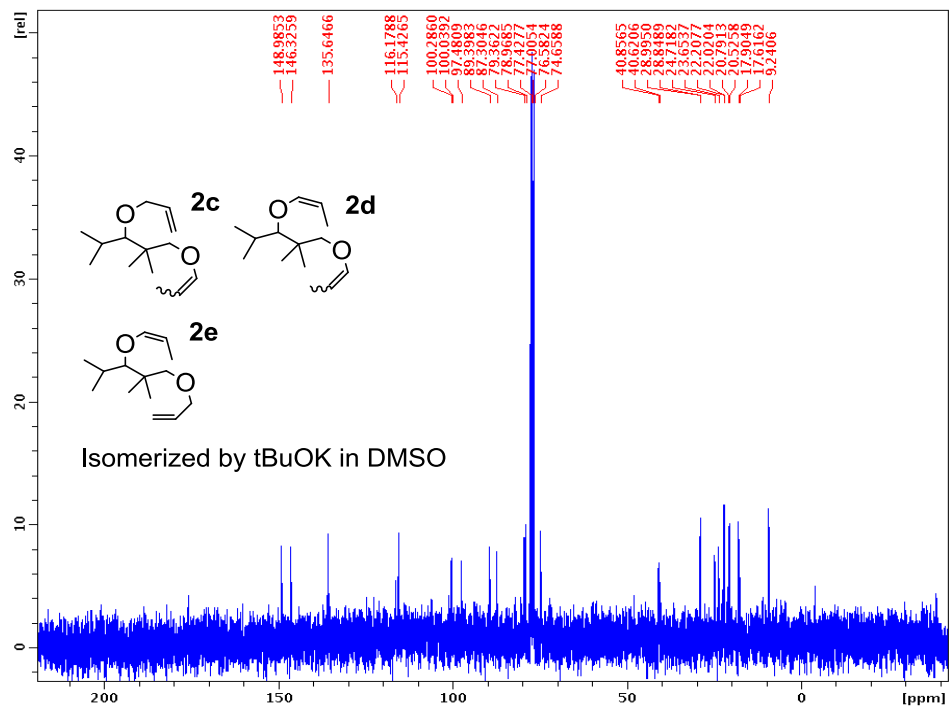
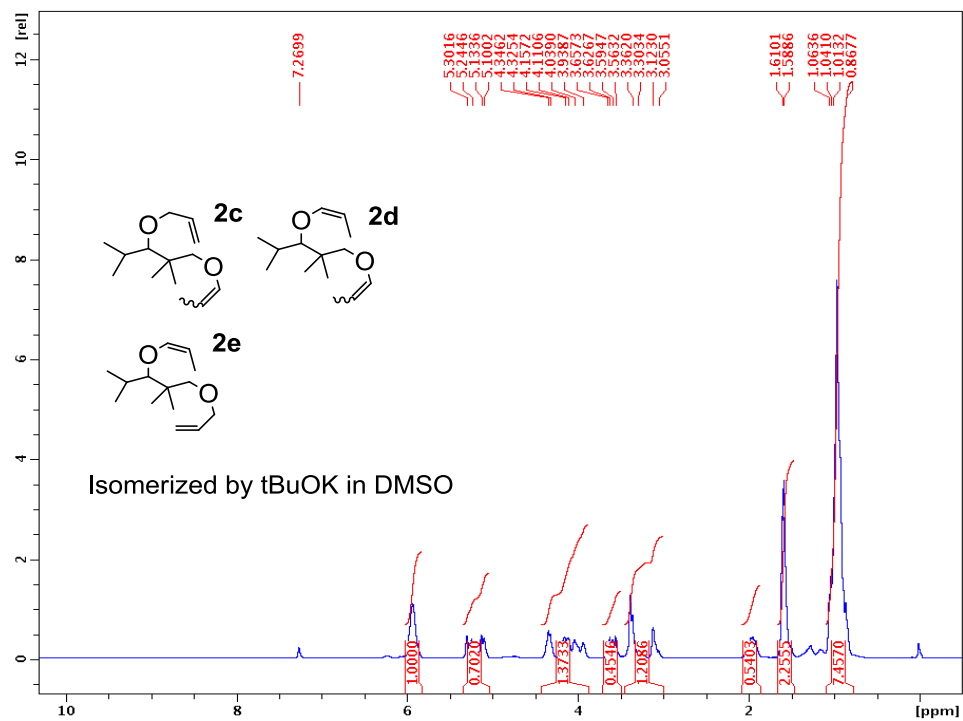


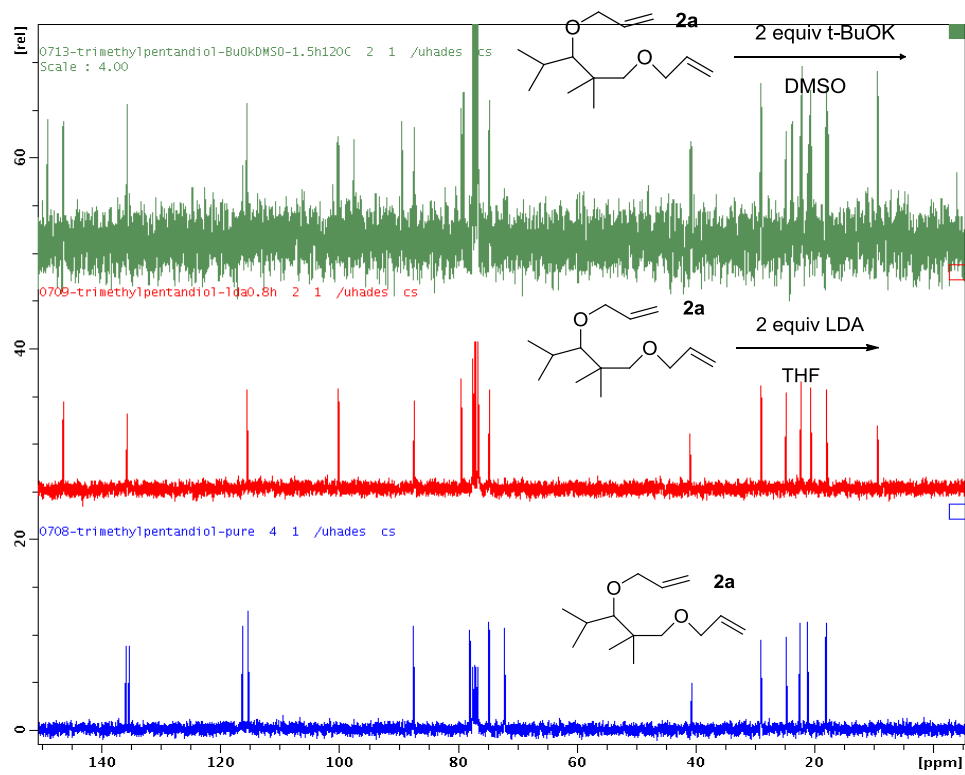
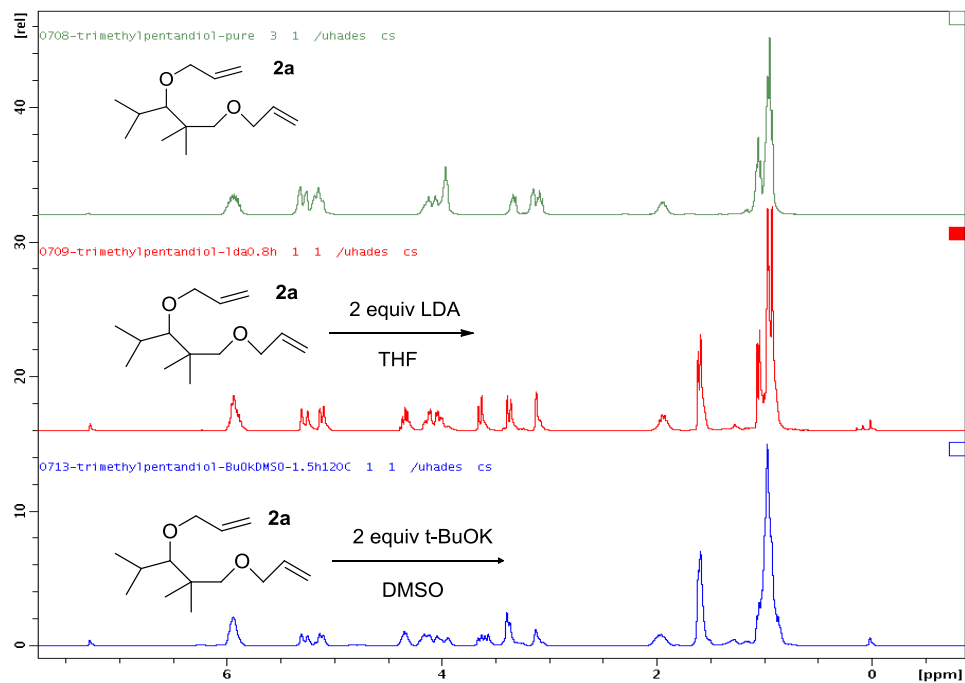












Appendix C

Supporting information for Chapter 3

Table of Contents

Figure S3.1. ^1H NMR of 2-methoxy-2-methyloctane-1- ^{13}C IR1 in CDCl_3	278
Figure S3.2. ^{13}C NMR of (2-methoxy-2-methyloctane-1- ^{13}C IR1 in CDCl_3	278
Figure S3.3. ^1H NMR of (Z)-heptadec-2-ene-1- ^{13}C IR2 in CDCl_3	279
Figure S3.4. ^{13}C NMR of (Z)-heptadec-2-ene-1- ^{13}C IR2 in CDCl_3	279
Figure S3.5. ^1H NMR of 2-(methoxy- ^{13}C)-2-methyltricosane IR3 in benzene- d_6	280
Figure S3.6. ^{13}C NMR of 2-(methoxy- ^{13}C)-2-methyltricosane IR3 in benzene- d_6	280
Figure S3.7. ^1H NMR of IR4 in CDCl_3	281
Figure S3.8. ^{13}C NMR of IR4 in CDCl_3	281
Figure S3.9. ^1H NMR of 2-methylpropan-2-yl-1- ^{13}C 1 in CDCl_3	282
Figure S3.10. ^{13}C NMR of 2-methylpropan-2-yl-1- ^{13}C 1 in CDCl_3	282
Figure S3.11. ^{13}C NMR of 1 in DEE with BEN, IR1 , IR2 , IR3 at 20 °C	283
Figure S3.12. ^{13}C DOSY Decay Curves for 2-methylpropan-2-yl-1- ^{13}C 1	283
Figure S3.13. ^{13}C DOSY Decay Curves for Internal References.....	284
Figure S3.14. ^{13}C NMR of 1 in DEE with BEN, IR1 , IR2 , IR4 at 20 °C	286
Figure S3.15. ^{13}C DOSY Decay Curves for 2-methylpropan-2-yl-1- ^{13}C 1	286
Figure S3.16. ^{13}C DOSY Decay Curves for Internal References.....	287
Figure S3.17. ^{13}C NMR of $^{13}\text{CH}_3^6\text{Li}$ in DEE with BEN, IR1 , IR2 , IR4 at -40 °C.....	289
Figure S3.18. ^{13}C DOSY Decay Curves for Solvated Tetramer 3 and 4	289

Figure S3.19. ^{13}C DOSY Decay Curves for Internal References.....	290
Figure S3.20. ^{13}C NMR of $^{13}\text{CH}_3^6\text{Li}$ in DEE with TMEDA and BEN, IR1 , IR2 , IR4 at $-50\text{ }^\circ\text{C}$	292
Figure S3.21. ^{13}C DOSY Decay Curves for Dimer 7	292
Figure S3.22. ^{13}C DOSY Decay Curves for Internal References.....	293
Figure S3.23. ^{13}C NMR of $^{13}\text{CH}_3^6\text{Li}$ in DEE with TMCDA and BEN, IR1 , IR2 , IR4 at $-40\text{ }^\circ\text{C}$	295
Figure S3.24. ^{13}C DOSY Decay Curves for Dimer 10	295
Figure S3.25. ^{13}C DOSY Decay Curves for Internal References.....	296
Figure S3.26. ^{13}C NMR of $^{13}\text{CH}_3^6\text{Li}$ in DEE with DMB and BEN, IR1 , IR2 , IR4 at $-40\text{ }^\circ\text{C}$	297
Figure S3.27. ^{13}C DOSY of $^{13}\text{CH}_3^6\text{Li}$ in DEE with DMB and BEN, IR1 , IR2 , IR4 at $-40\text{ }^\circ\text{C}$...	298
Figure S3.28. ^{13}C DOSY Decay Curves for Homodimer 12 and Heterodimer 13	298
Figure S3.29. ^{13}C DOSY Decay Curves for Internal References.....	299
Figure S3.30. ^{13}C NMR of $^{13}\text{CH}_3^6\text{Li}$ in DEE with PMDTA and BEN, IR1 , IR2 , IR4 at $-40\text{ }^\circ\text{C}$	300
Figure S3.31. ^{13}C DOSY of $^{13}\text{CH}_3^6\text{Li}$ in DEE with PMDTA and BEN, IR1 , IR2 , IR4 at $-40\text{ }^\circ\text{C}$	301
Figure S3.32. ^{13}C DOSY Decay Curves for Dimer 14	301
Figure S3.33. ^{13}C DOSY Decay Curves for Internal References.....	302
Figure S3.34. ^{13}C NMR of $^{13}\text{CH}_3^6\text{Li}$ in DEE with (-)-SP and BEN, IR1 , IR2 , IR4 at $-40\text{ }^\circ\text{C}$	303
Figure S3.35. ^{13}C DOSY of $^{13}\text{CH}_3^6\text{Li}$ in DEE with (-)-SP and BEN, IR1 , IR2 , IR4 at $-40\text{ }^\circ\text{C}$...	304
Figure S3.36. ^{13}C DOSY Decay Curves for Dimer 15	304
Figure S3.37. ^{13}C DOSY Decay Curves for Internal References.....	305
Table S3.1. <i>D</i> -FW analysis of ^{13}C DOSY data of 1 in DEE with BEN, IR1 , IR2 , IR3 at $20\text{ }^\circ\text{C}$	285

Table S3.2. <i>D-FW</i> analysis of ^{13}C DOSY data of 1 in DEE with BEN, IR1 , IR2 , IR4 at 20 °C	288
Table S3.3. <i>D-FW</i> analysis of ^{13}C DOSY data of $^{13}\text{CH}_3^6\text{Li}$ in DEE at -40 °C.....	291
Table S3.4. <i>D-FW</i> analysis of ^{13}C DOSY data of $^{13}\text{CH}_3^6\text{Li}$ in DEE with TMEDA at -50 °C	294
Table S3.5. <i>D-FW</i> analysis of ^{13}C DOSY data of $^{13}\text{CH}_3^6\text{Li}$ in DEE with TMCDA at -40 °C.	297
Table S3.6. <i>D-FW</i> analysis of ^{13}C DOSY data of $^{13}\text{CH}_3^6\text{Li}$ in DEE with DMB at -40 °C.....	300
Table S3.7. <i>D-FW</i> analysis of ^{13}C DOSY data of $^{13}\text{CH}_3^6\text{Li}$ in DEE with PMDTA at -40 °C.....	303
Table S3.8. <i>D-FW</i> analysis of ^{13}C DOSY data of $^{13}\text{CH}_3^6\text{Li}$ in DEE with (-)-SP at -40 °C.....	306

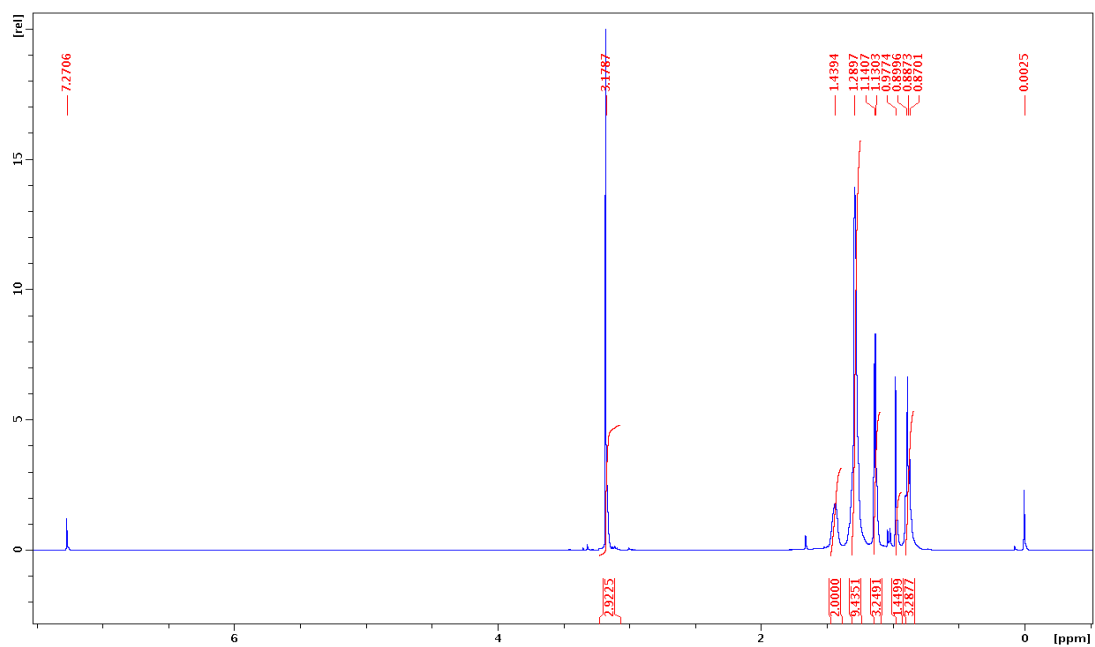


Figure S3.1. ^1H NMR of 2-methoxy-2-methyloctane-1- ^{13}C **IR1** in CDCl_3

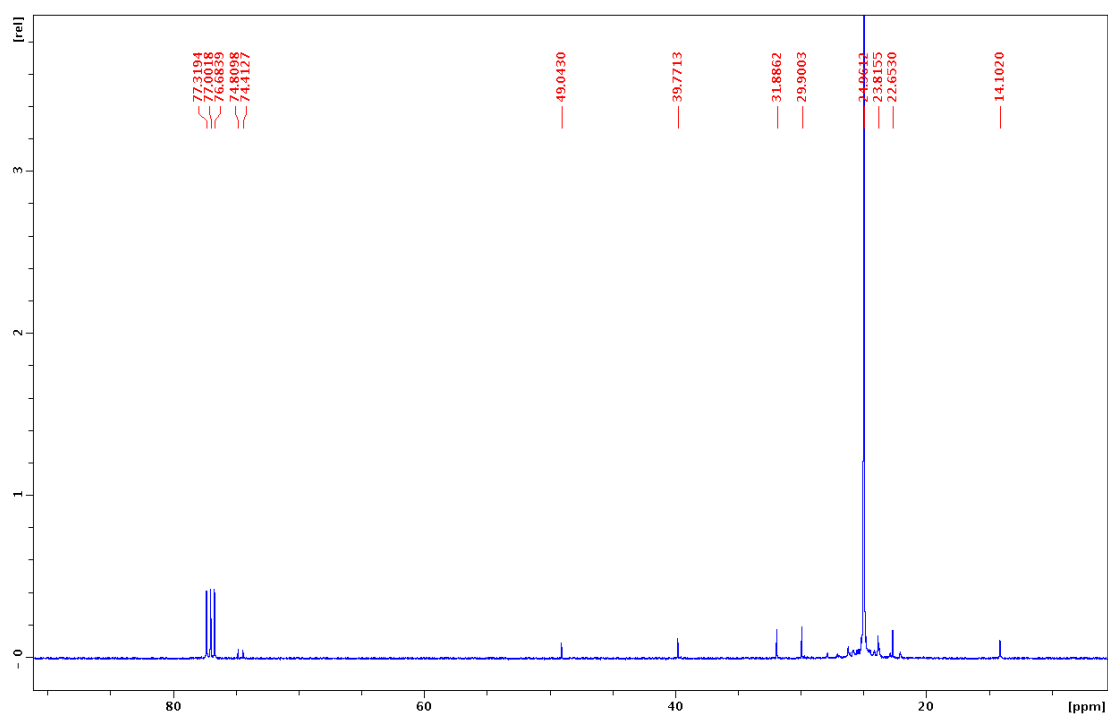


Figure S3.2. ^{13}C NMR of (2-methoxy-2-methyloctane-1- ^{13}C **IR1** in CDCl_3

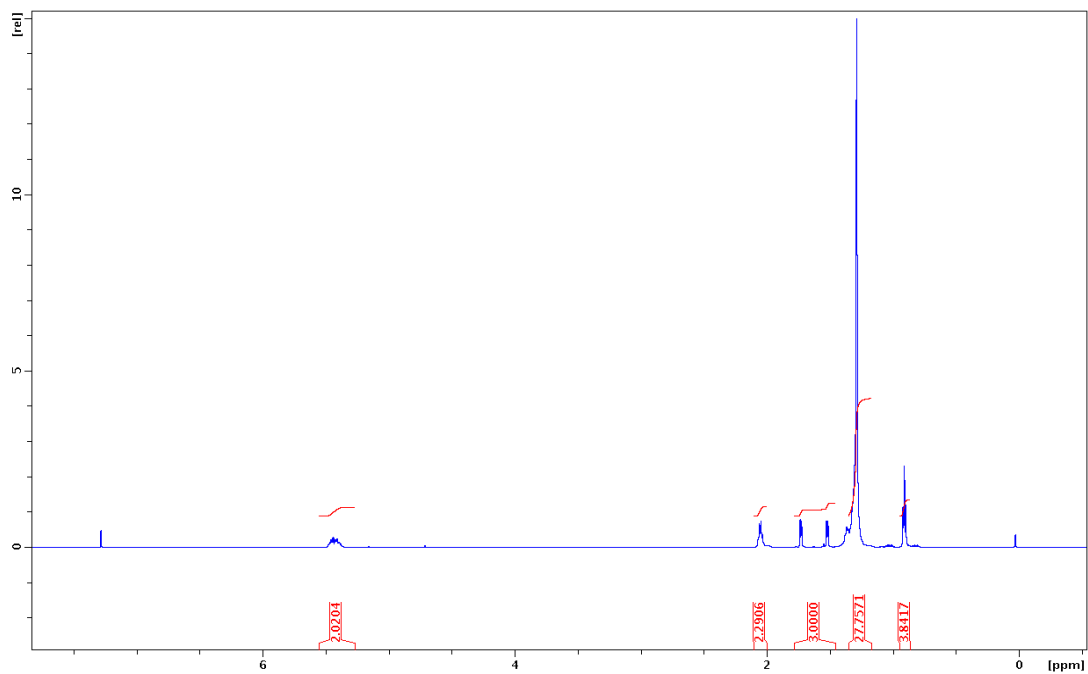


Figure S3.3. ^1H NMR of (Z)-heptadec-2-ene-1- ^{13}C IR2 in CDCl_3

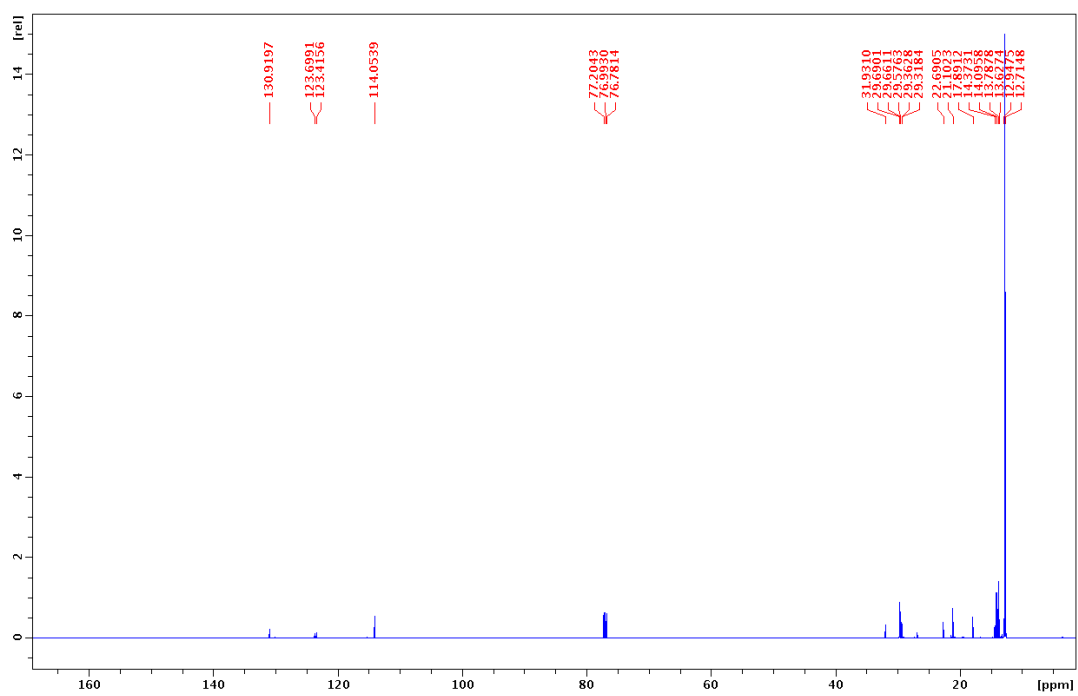


Figure S3.4. ^{13}C NMR of (Z)-heptadec-2-ene-1- ^{13}C IR2 in CDCl_3

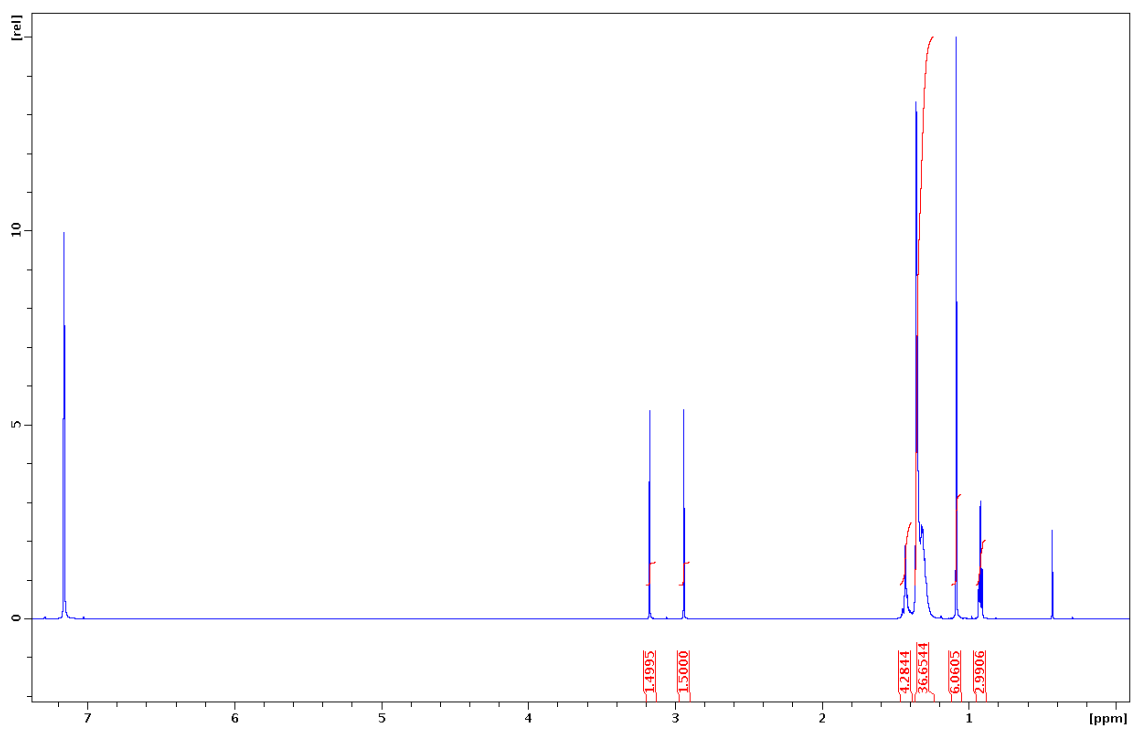


Figure S3.5. ^1H NMR of 2-(methoxy- ^{13}C)-2-methyltricosane **IR3** in benzene- d_6

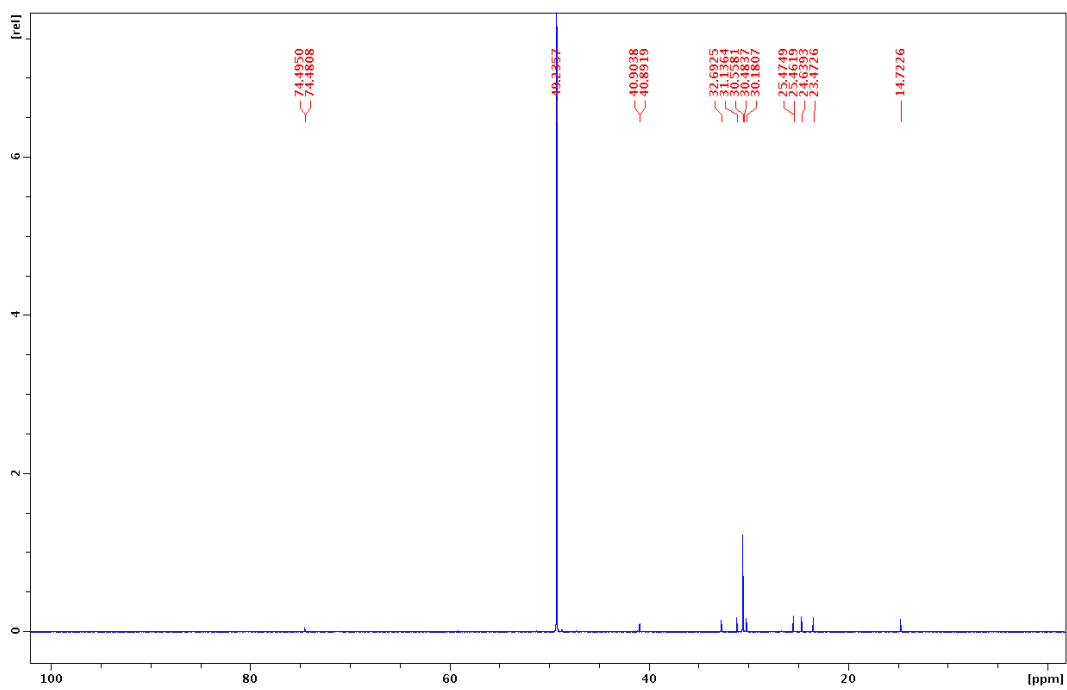


Figure S3.6. ^{13}C NMR of 2-(methoxy- ^{13}C)-2-methyltricosane **IR3** in benzene- d_6

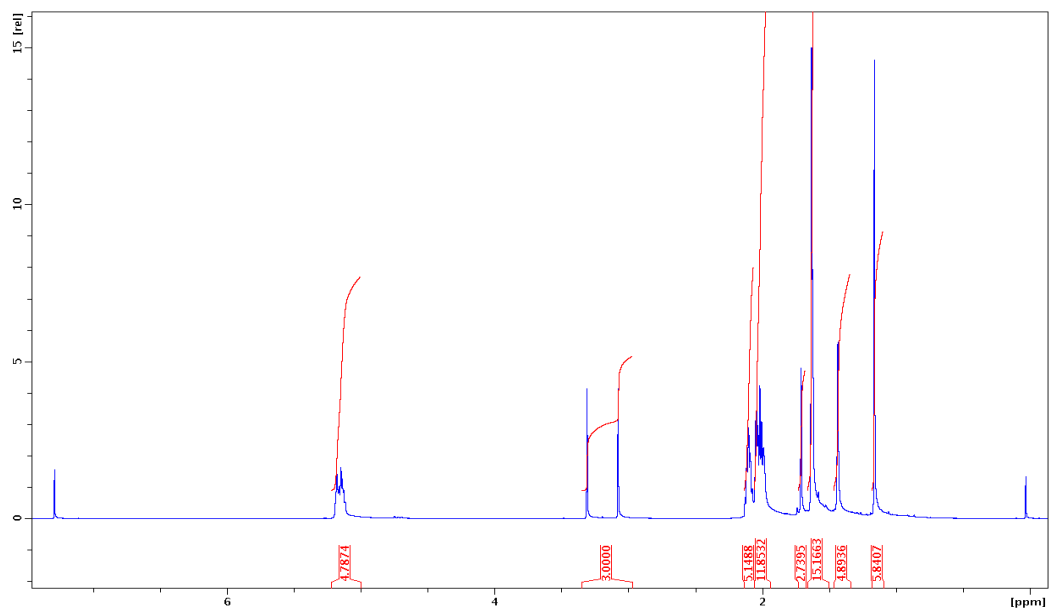


Figure S3.7. ^1H NMR of **IR4** in CDCl_3

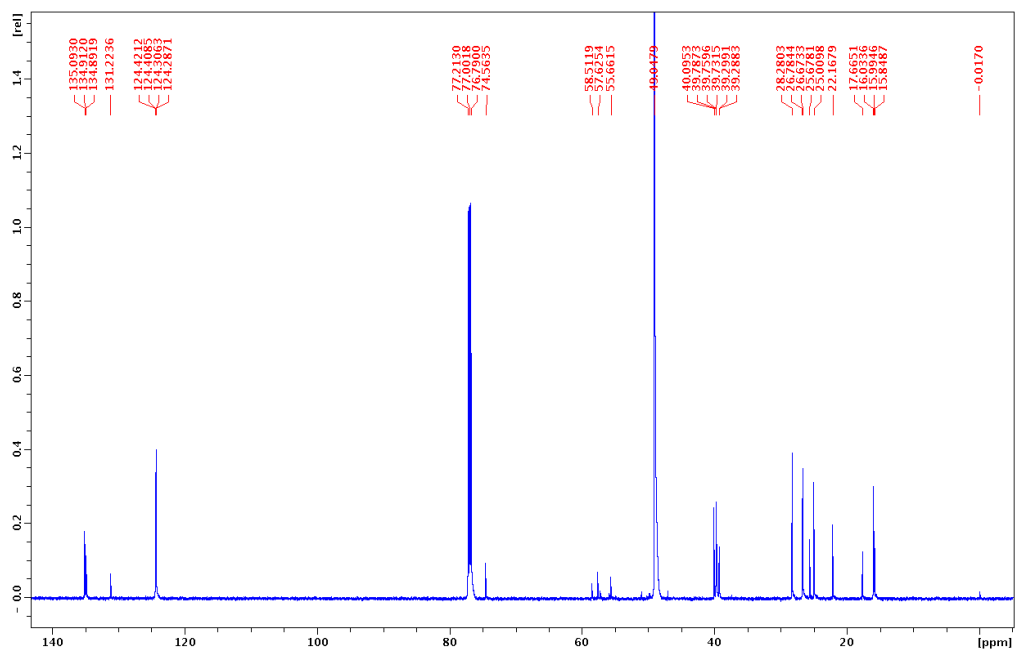


Figure S3.8. ^{13}C NMR of **IR4** in CDCl_3

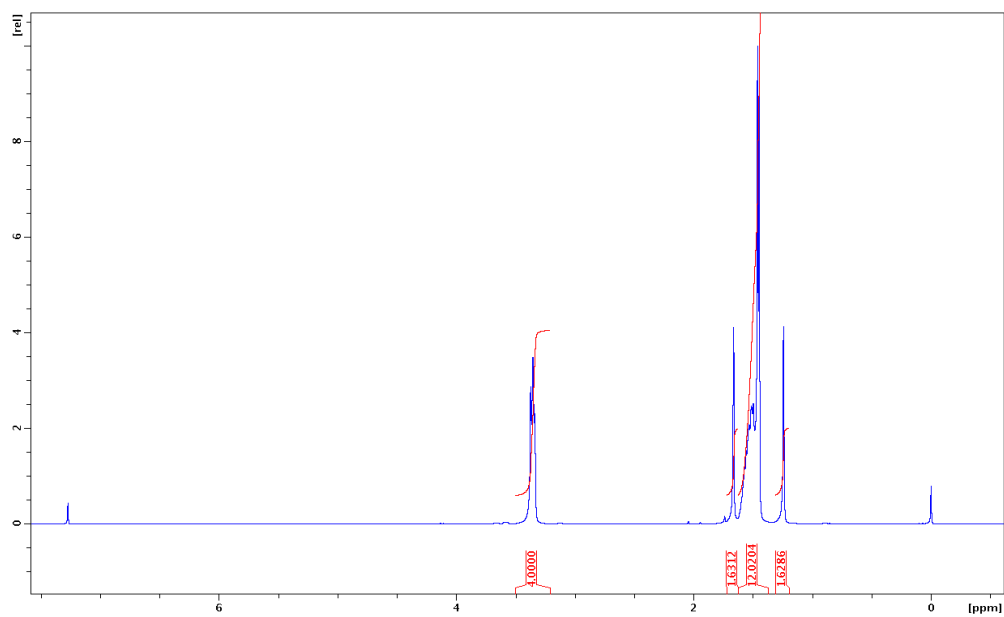


Figure S3.9. ^1H NMR of 2-methylpropan-2-yl- ^{13}C **1** in CDCl_3

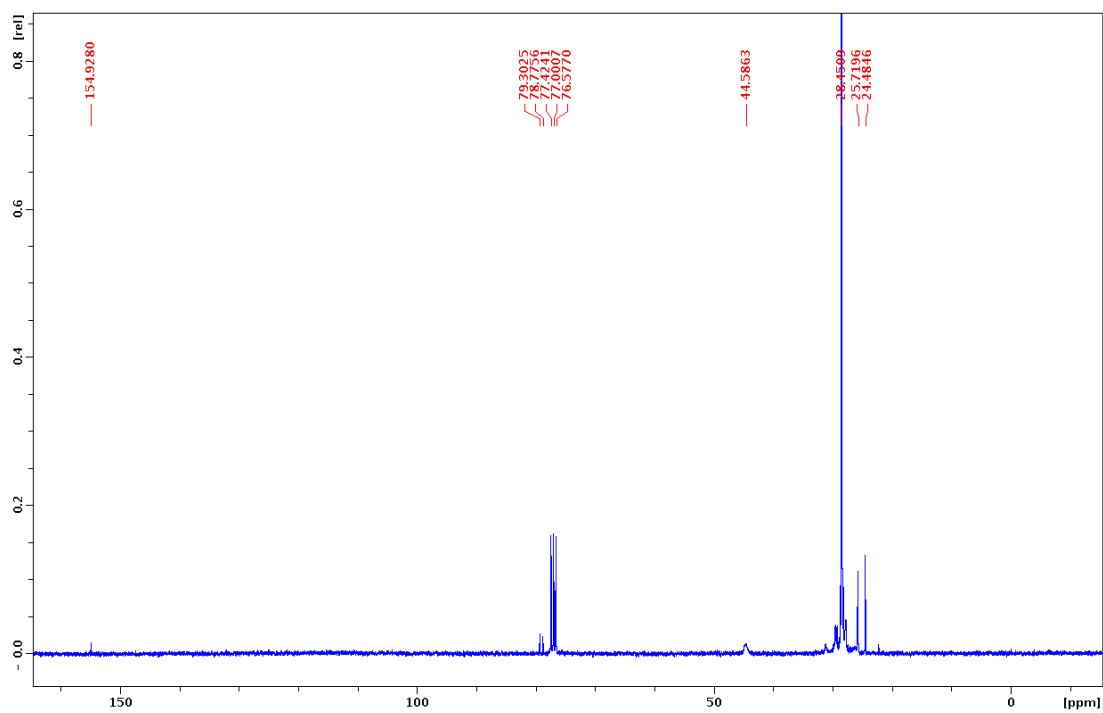


Figure S3.10. ^{13}C NMR of 2-methylpropan-2-yl- ^{13}C **1** in CDCl_3

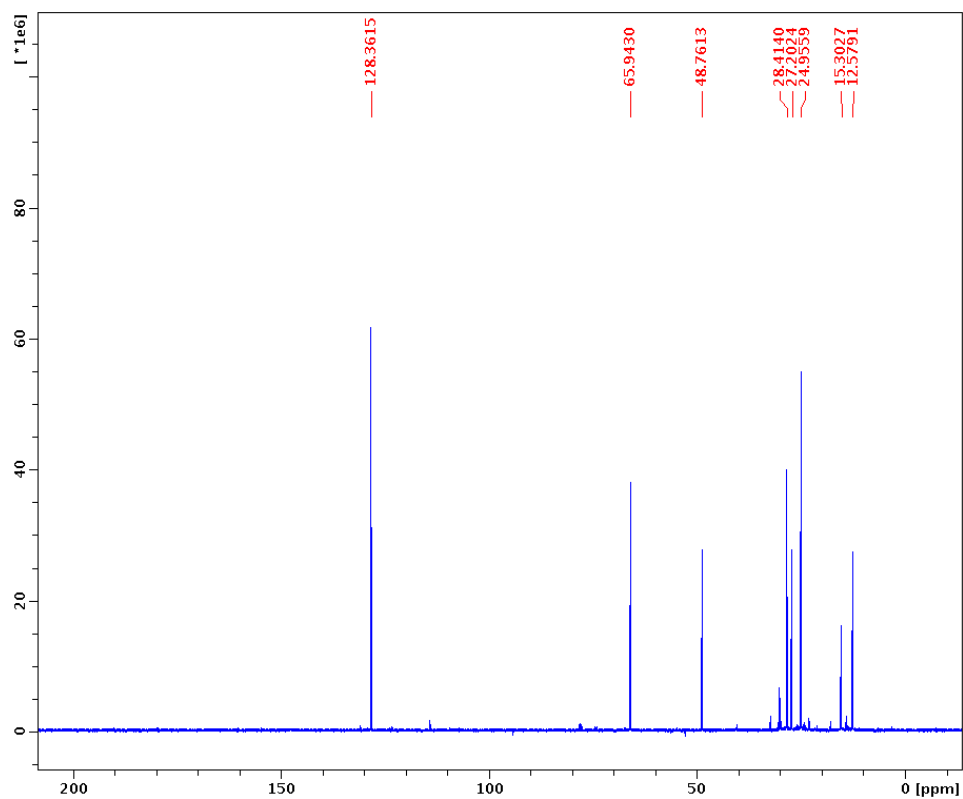


Figure S3.11. ^{13}C NMR of **1** in DEE with BEN, IR1, IR2, IR3 at 20 °C

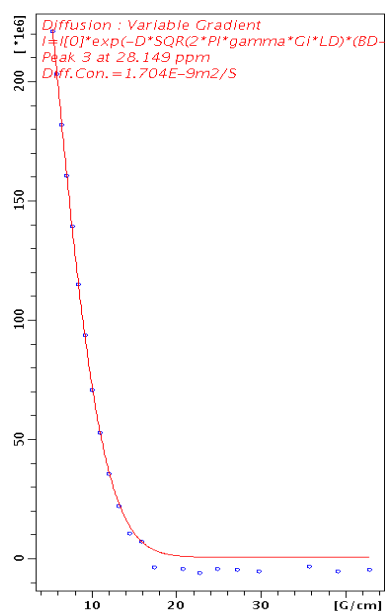


Figure S3.12. ^{13}C DOSY Decay Curves for 2-methylpropan-2-yl- ^{13}C **1**

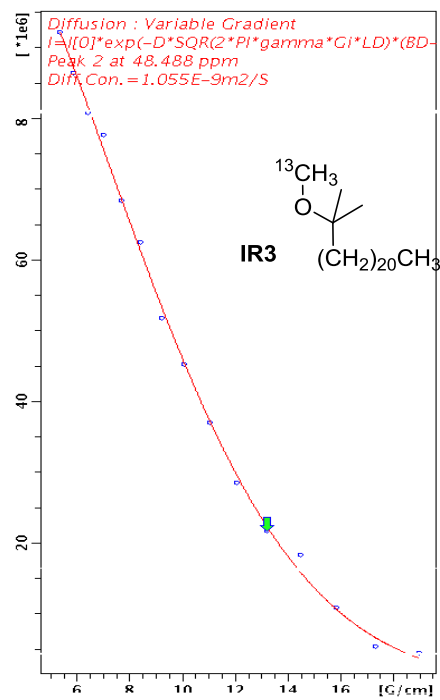
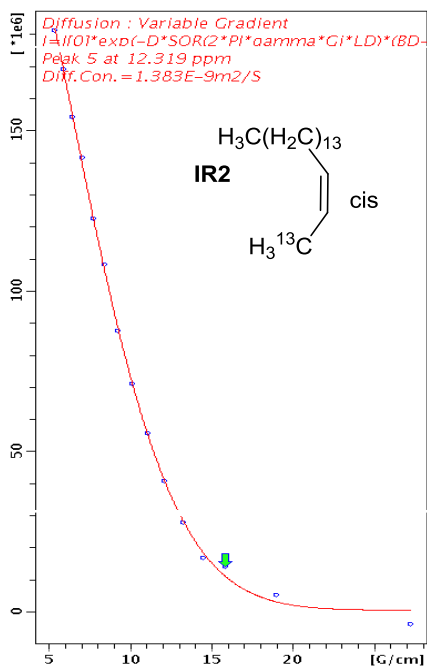
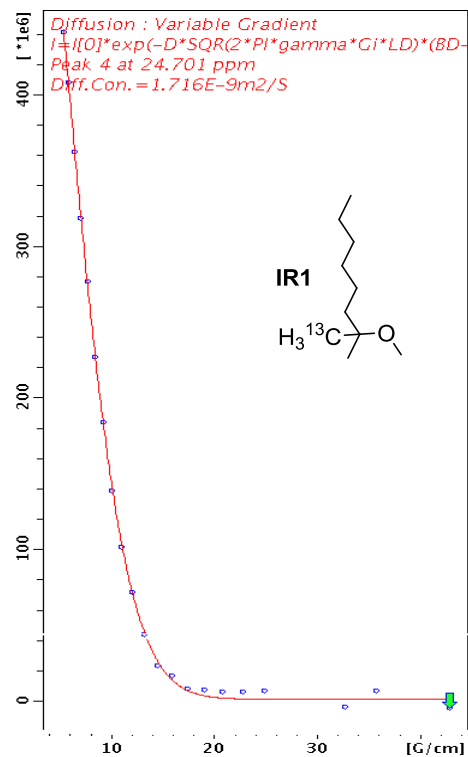
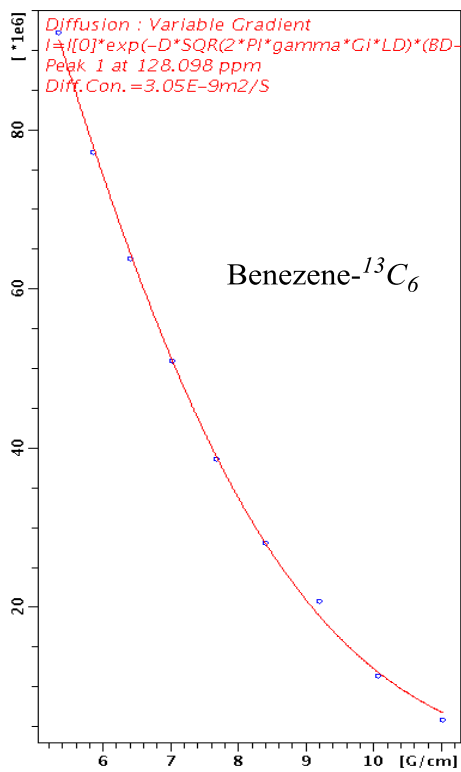


Figure S3.13. ^{13}C DOSY Decay Curves for Internal References

Table S3.1. *D*-FW Analysis of ^{13}C DOSY data of **1** in DEE with BEN, **IR1**, **IR2**, **IR3** at 20 °C

Compound	FW (g/mol)	$10^{-10}D$ (m^2/s)	log FW	log <i>D</i>	Predicted FW (g/mol)	% error
BEN- $^{13}\text{C}_6$	84.07	3.050	1.925	-8.516	78.98	6.1
IR1	159.3	1.716	2.202	-8.765	177.4	-11.4
IR2	239.4	1.383	2.379	-8.859	240.4	-0.4
IR3	369.7	1.055	2.567	-8.977	351.9	4.8
1	186.3	1.704	2.270	-8.769	179.2	3.8

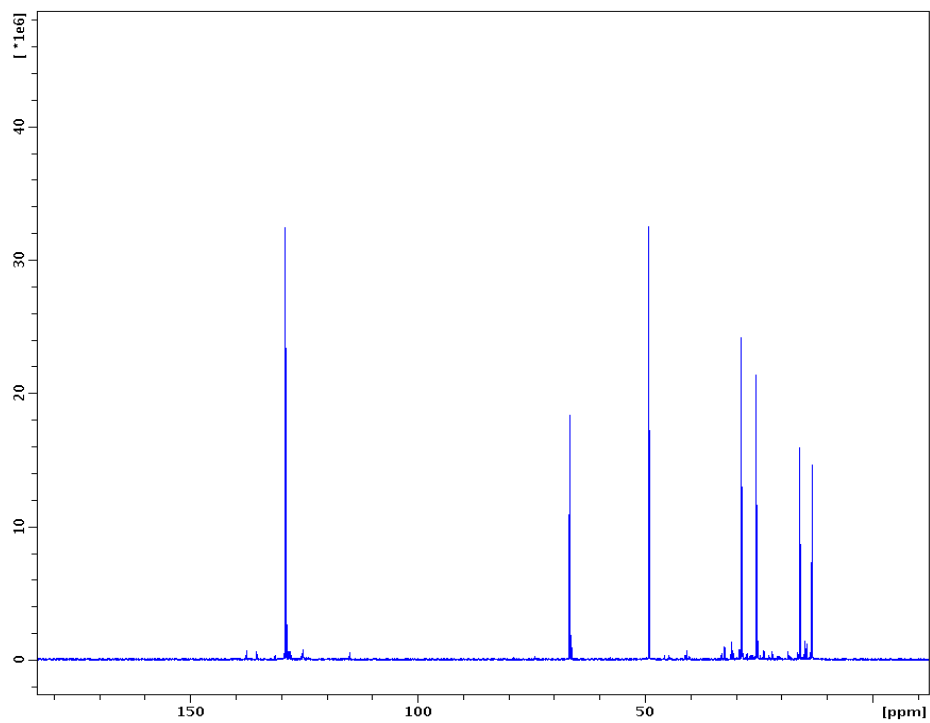


Figure S3.14. ^{13}C NMR of **1** in DEE with BEN, **IR1**, **IR2**, **IR4** at 20 °C

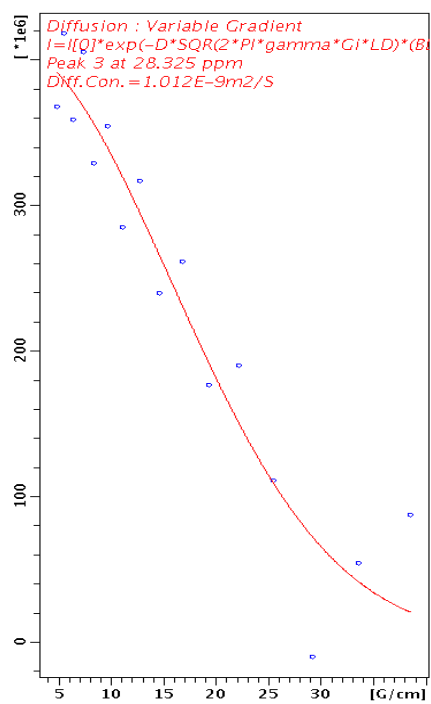


Figure S3.15. ^{13}C DOSY Decay Curves for 2-methylpropan-2-yl- ^{13}C **1**

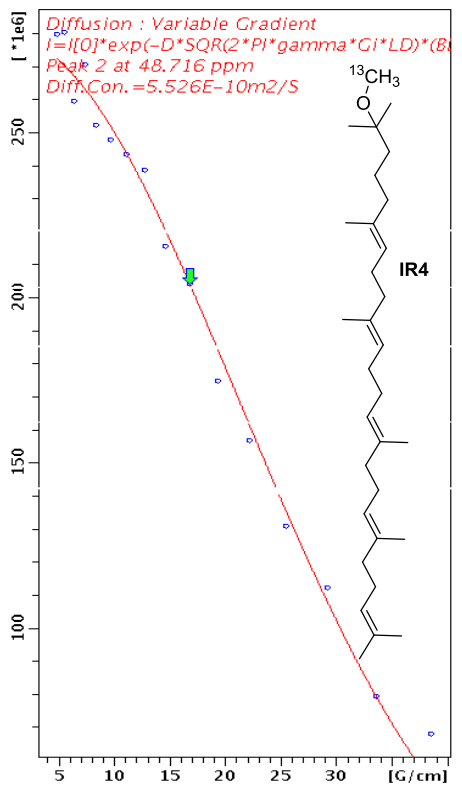
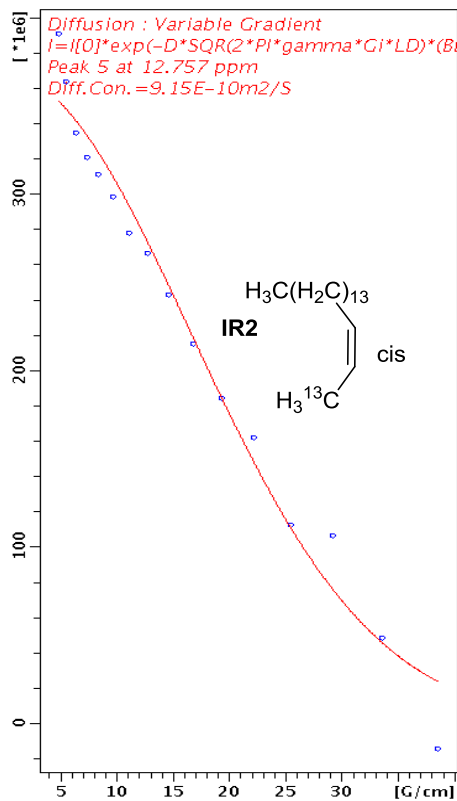
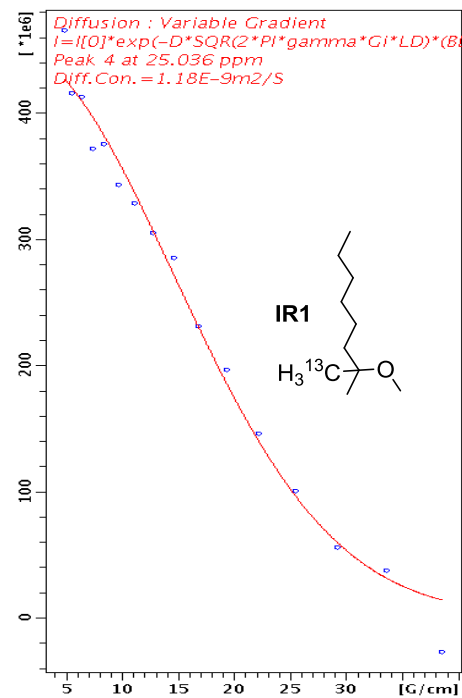
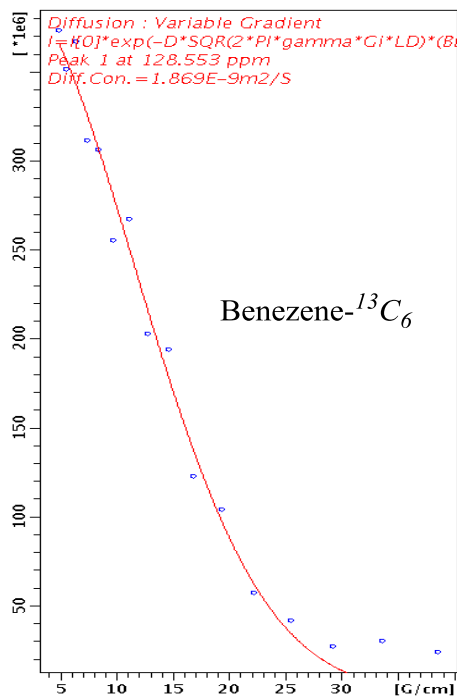


Figure S3.16. ^{13}C DOSY Decay Curves for Internal References

Table S3.2. *D*-FW analysis of ^{13}C DOSY data of **1** in DEE with BEN, **IR1**, **IR2**, **IR4** at 20 °C

Compound	FW (g/mol)	10^{-10}D (m^2/s)	log FW	log D	Predicted FW (g/mol)	% error
BEN- $^{13}\text{C}_6$	84.07	18.69	1.925	-8.728	85.21	-1.4
IR1	159.3	11.80	2.202	-8.928	160.5	-0.8
IR2	239.4	9.150	2.379	-9.039	227.9	4.8
IR4	443.8	5.526	2.647	-9.258	456.4	-2.8
1	186.3	10.12	2.270	-8.995	198.4	-6.5

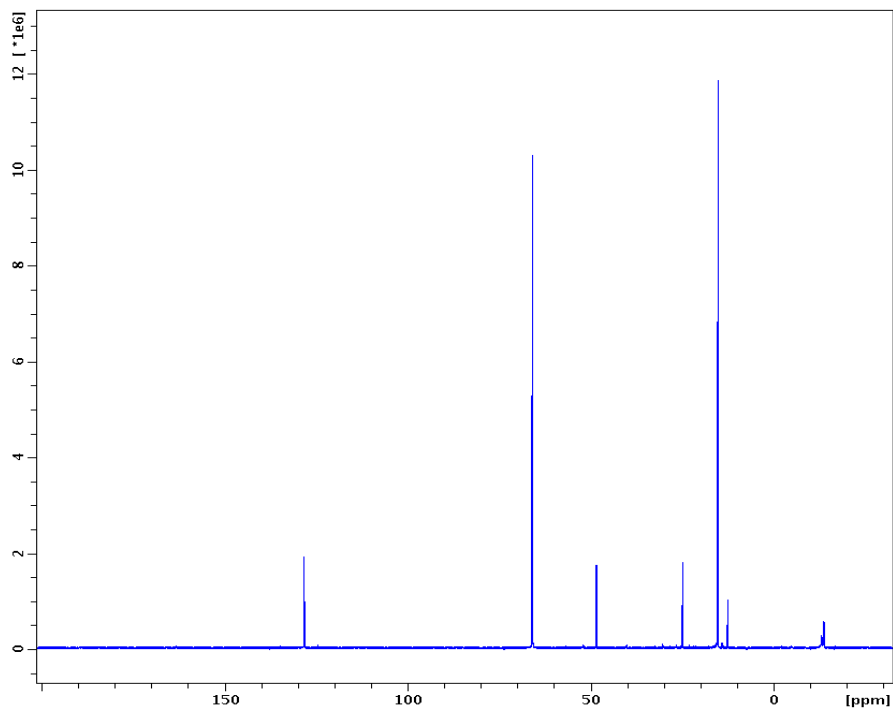


Figure S3.17. ^{13}C NMR of $^{13}\text{CH}_3^6\text{Li}$ in DEE with BEN, **IR1**, **IR2**, **IR4** at $-40\text{ }^\circ\text{C}$

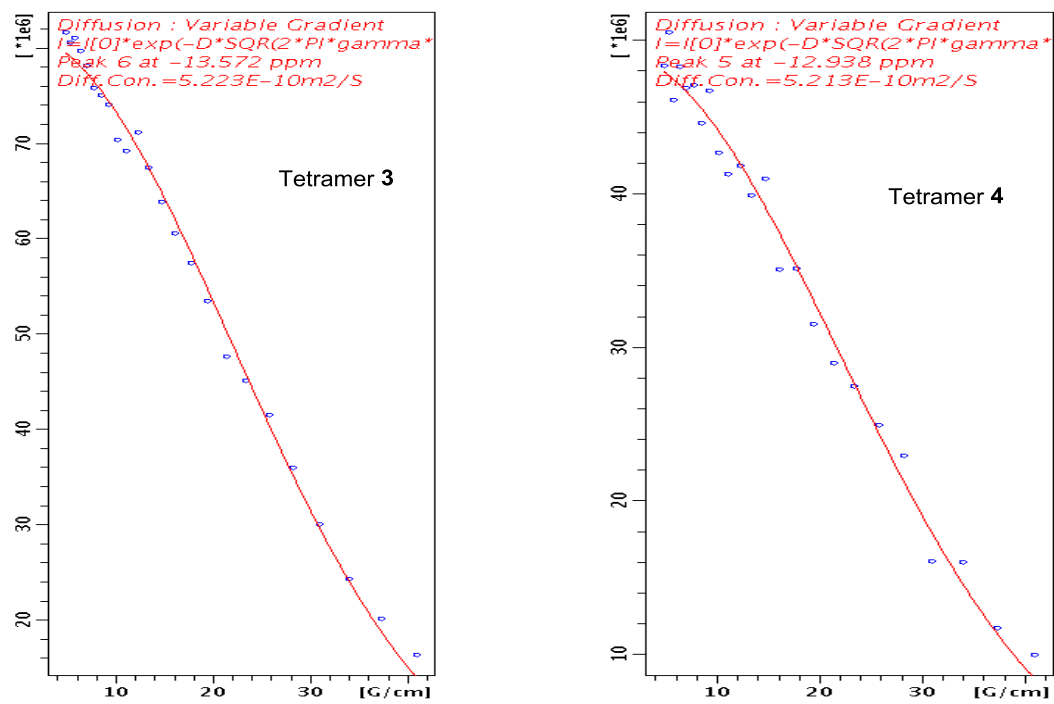


Figure S3.18. ^{13}C DOSY Decay Curves for Solvated Tetramer **3** and **4**

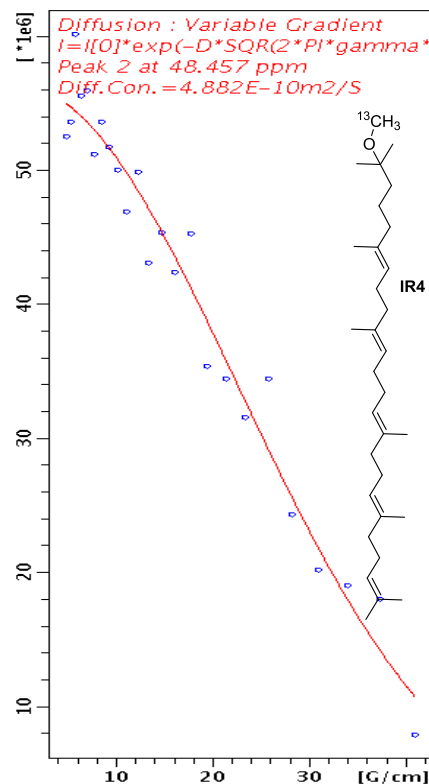
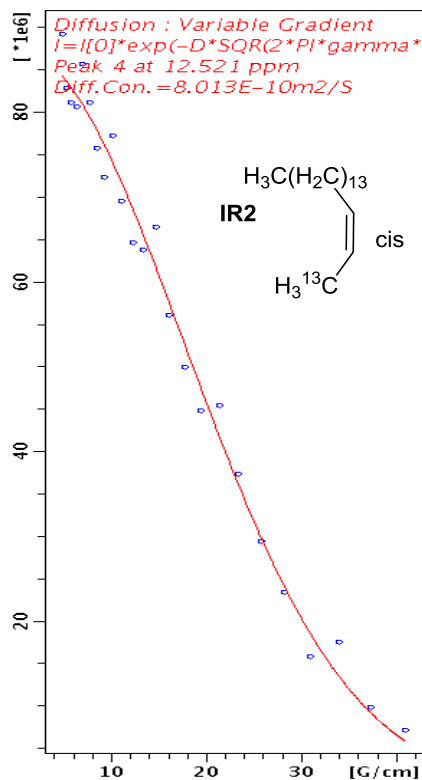
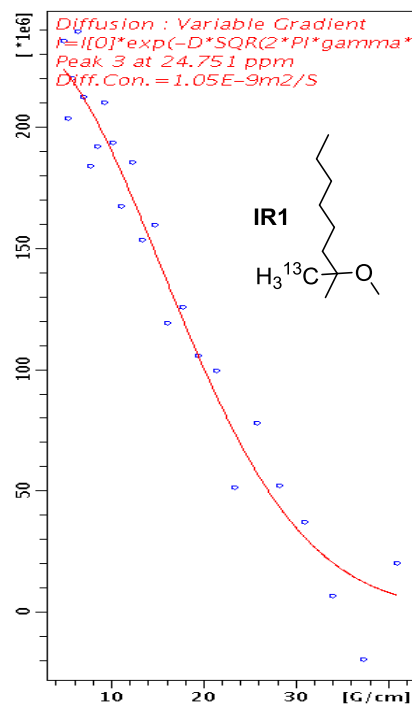
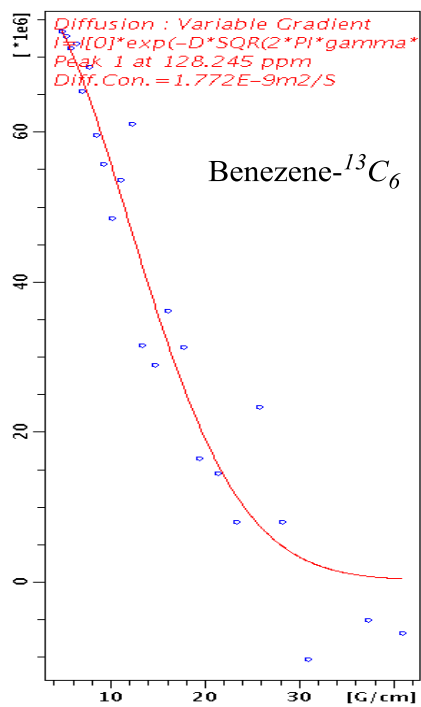


Figure S3.19. ^{13}C DOSY Decay Curves for Internal References

Table S3.3. *D*-FW analysis of ^{13}C DOSY data of $^{13}\text{CH}_3^6\text{Li}$ in DEE at $-40\text{ }^\circ\text{C}$

Compound	FW (g/mol)	10^{-10}D (m^2/s)	log FW	log D	Predicted FW (g/mol)	% error
BEN- $^{13}\text{C}_6$	84.07	17.72	1.925	-8.752	83.21	1.0
IR1	159.3	10.50	2.202	-8.979	164.4	-3.2
IR2	239.4	8.013	2.379	-9.096	233.7	2.4
IR4	443.8	4.882	2.647	-9.311	445.2	-0.3
3 ^a	384.7 ^a	5.223	2.585	-9.282	407.8	-6.0
4 ^b	495.5 ^b	5.213	2.695	-9.283	408.8	17.5

^a384.7 g mol^{-1} is the formula weight of $(^{13}\text{CH}_3^6\text{Li})_4(\text{DEE})_4$ complex. ^b495.5 g mol^{-1} is the formula weight of $(^{13}\text{CH}_3^6\text{Li})_3\text{I}(\text{DEE})_4$ complex.

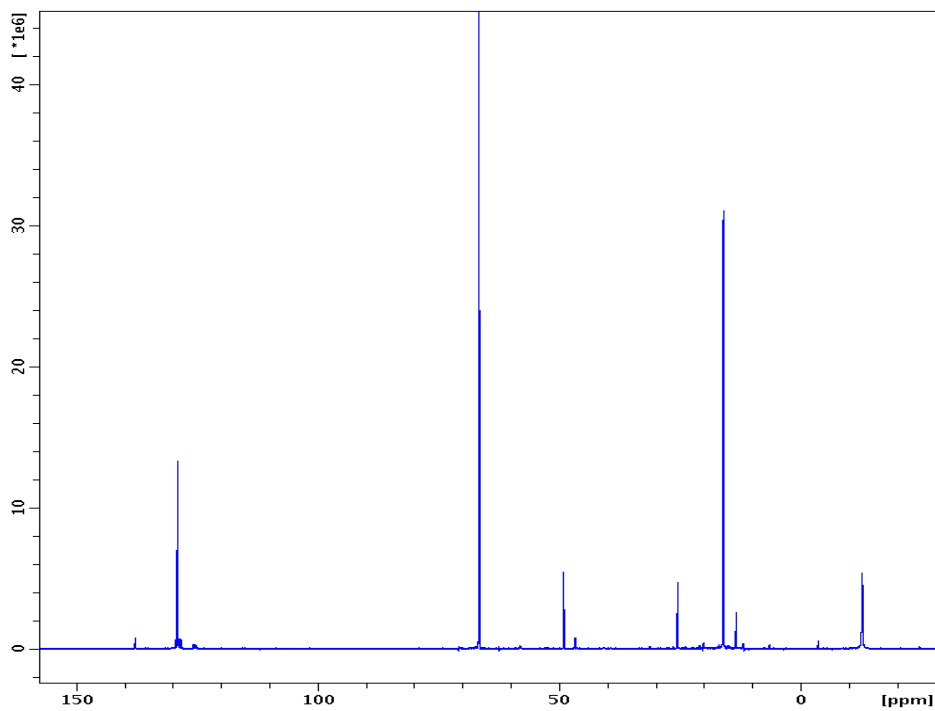


Figure S3.20. ^{13}C NMR of $^{13}\text{CH}_3^6\text{Li}$ in DEE with TMEDA and BEN, **IR1**, **IR2**, **IR4** at $-50\text{ }^\circ\text{C}$

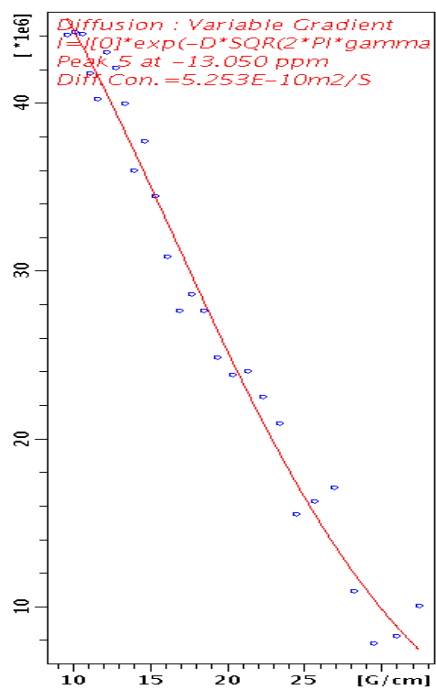


Figure S3.21. ^{13}C DOSY Decay Curves for Dimer **7**

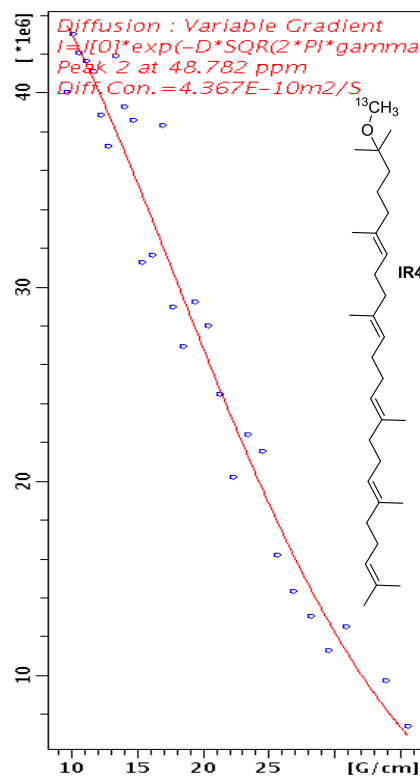
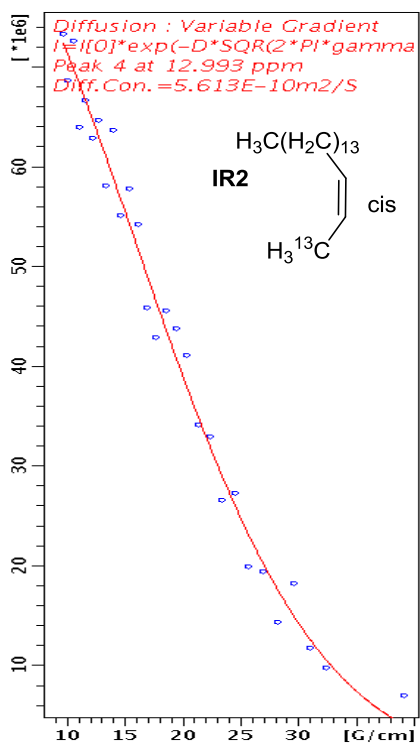
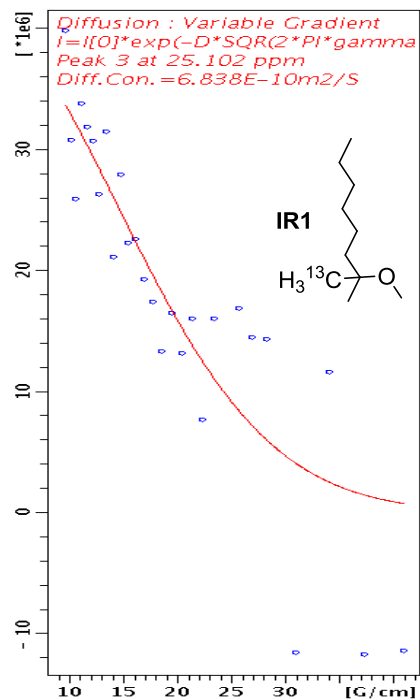
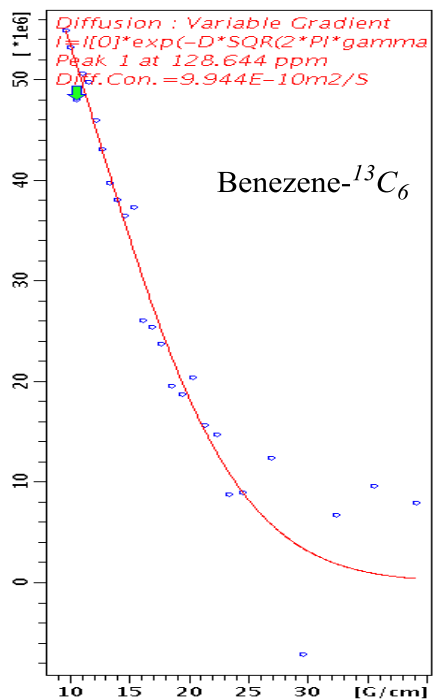


Figure S3.22. ^{13}C DOSY Decay Curves for Internal References

Table S3.4. *D*-FW analysis of ^{13}C DOSY data of $^{13}\text{CH}_3^6\text{Li}$ in DEE with TMEDA at $-50\text{ }^\circ\text{C}$

Compound	FW (g/mol)	10^{-10}D (m^2/s)	log FW	log D	Predicted FW (g/mol)	% error
BEN- $^{13}\text{C}_6$	84.07	9.944	1.925	-9.002	79.40	5.6
IR1	159.3	6.838	2.202	-9.165	169.3	-6.3
IR2	239.4	5.613	2.379	-9.251	233.7	-5.4
IR4	443.8	4.367	2.647	-9.360	445.2	5.5
7 ^a	276.5 ^a	5.253	2.442	-9.278	288.6	-4.4
8 ^b	414.8 ^b	5.253	2.618	-9.278	288.6	30.4

^a276.5 g mol^{-1} is the formula weight of dimer ($^{13}\text{CH}_3^6\text{Li}$)₂(TMEDA)₂ **7**. ^b414.8 g mol^{-1} is the formula weight of trimer ($^{13}\text{CH}_3^6\text{Li}$)₃(TMEDA)₃ **8**.

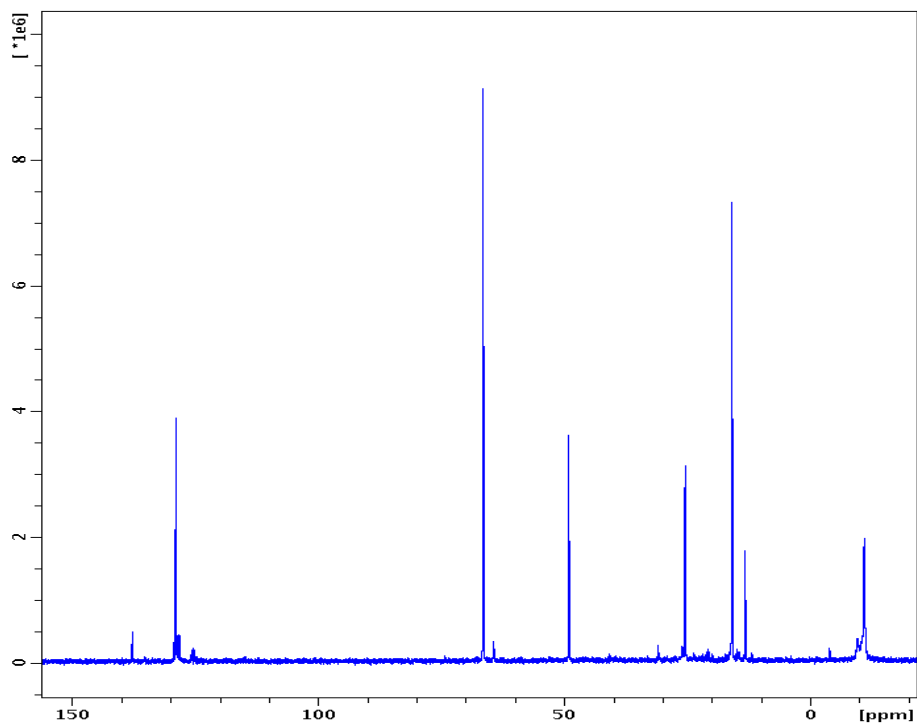


Figure S3.23. ^{13}C NMR of $^{13}\text{CH}_3^6\text{Li}$ in DEE with TMCDA and BEN, **IR1**, **IR2**, **IR4** at $-40\text{ }^\circ\text{C}$

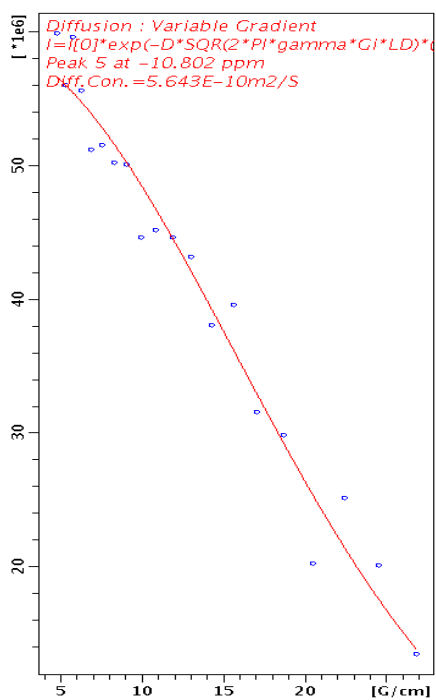


Figure S3.24. ^{13}C DOSY Decay Curves for Dimer **10**

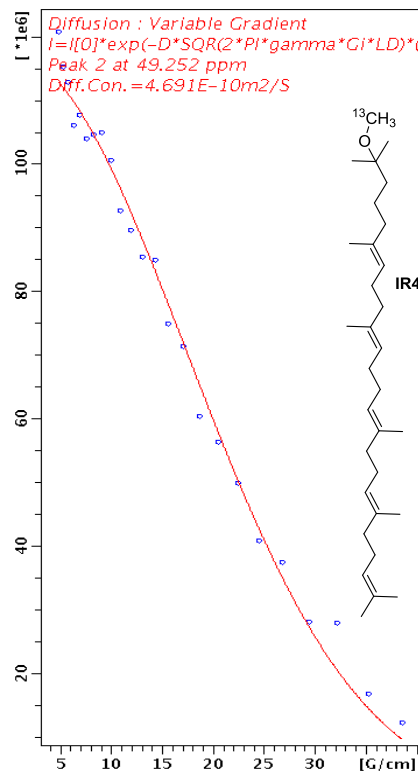
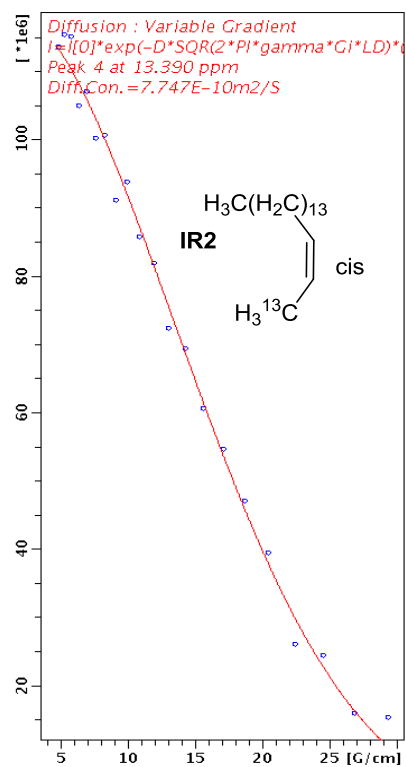
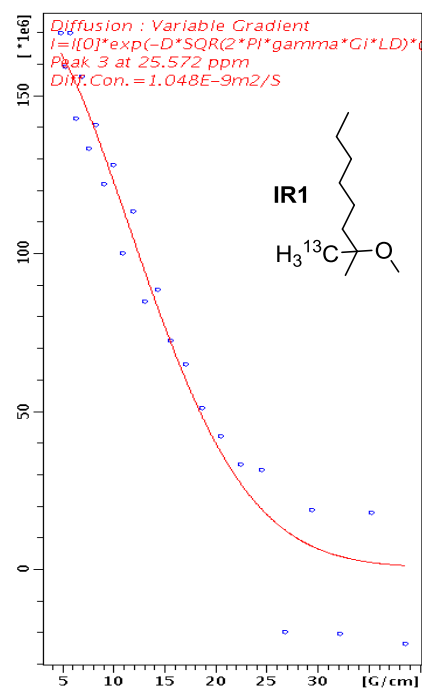
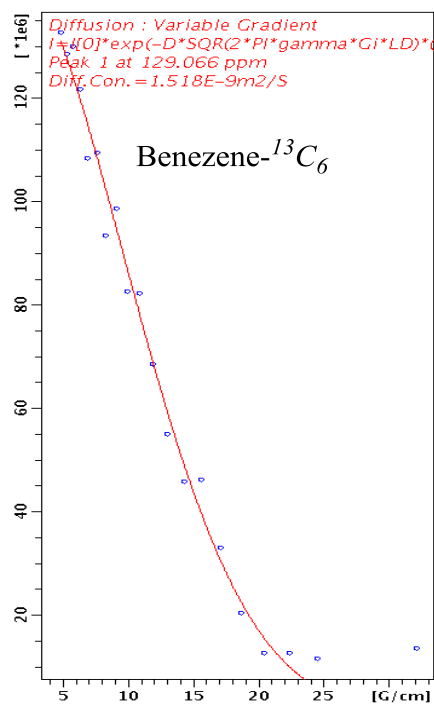


Figure S3.25. ^{13}C DOSY Decay Curves for Internal References

Table S3.5. *D*-FW Analysis of ^{13}C DOSY data of $^{13}\text{CH}_3^6\text{Li}$ in DEE with TMCDA at $-40\text{ }^\circ\text{C}$

Compound	FW (g/mol)	10^{-10}D (m^2/s)	log FW	log D	Predicted FW (g/mol)	% error
BEN- $^{13}\text{C}_6$	84.07	15.18	1.925	-8.819	88.70	-5.5
IR1	159.3	10.48	2.202	-8.980	169.3	6.0
IR2	239.4	7.747	2.379	-9.111	233.7	4.1
IR4	443.8	4.691	2.647	-9.329	445.2	-5.1
10^a	384.7 ^a	5.643	2.585	-9.278	359.3	6.6

^a384.7 g mol^{-1} is the formula weight of dimer $(^{13}\text{CH}_3^6\text{Li})_2(\text{TMCDA})_2$ **10**.

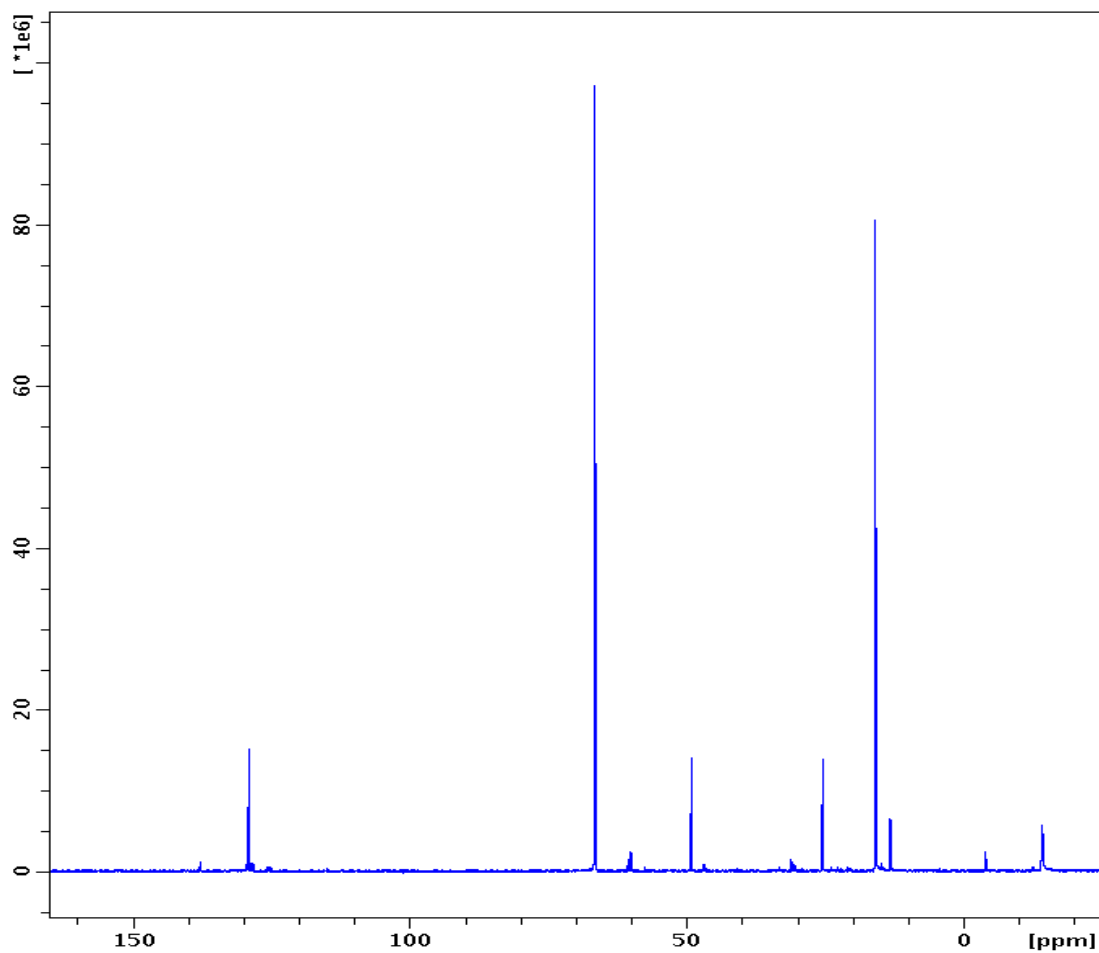


Figure S3.26. ^{13}C NMR of $^{13}\text{CH}_3^6\text{Li}$ in DEE with DMB and BEN, **IR1**, **IR2**, **IR4** at $-40\text{ }^\circ\text{C}$

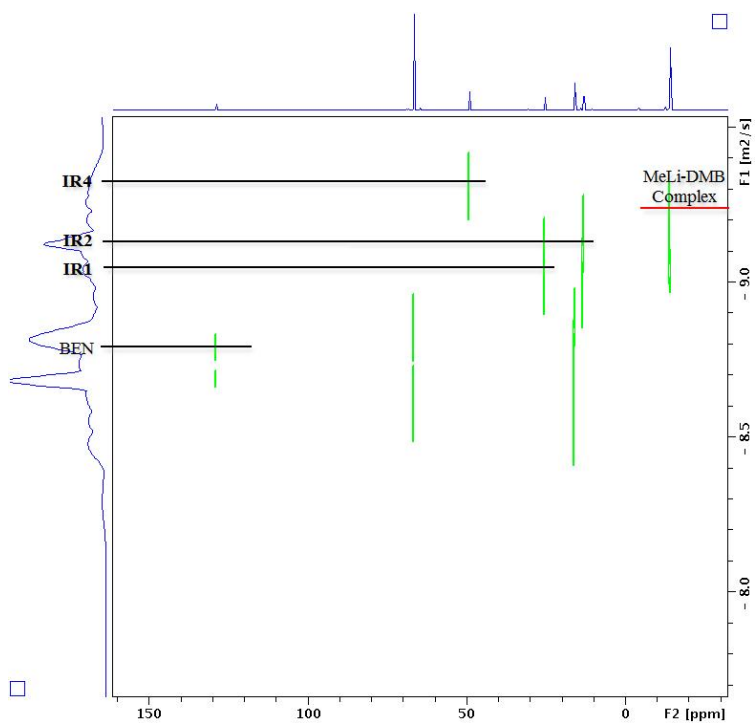


Figure S3.27. ¹³C DOSY of ¹³CH₃⁶Li in DEE with DMB and BEN, **IR1**, **IR2**, **IR4** at -40 °C

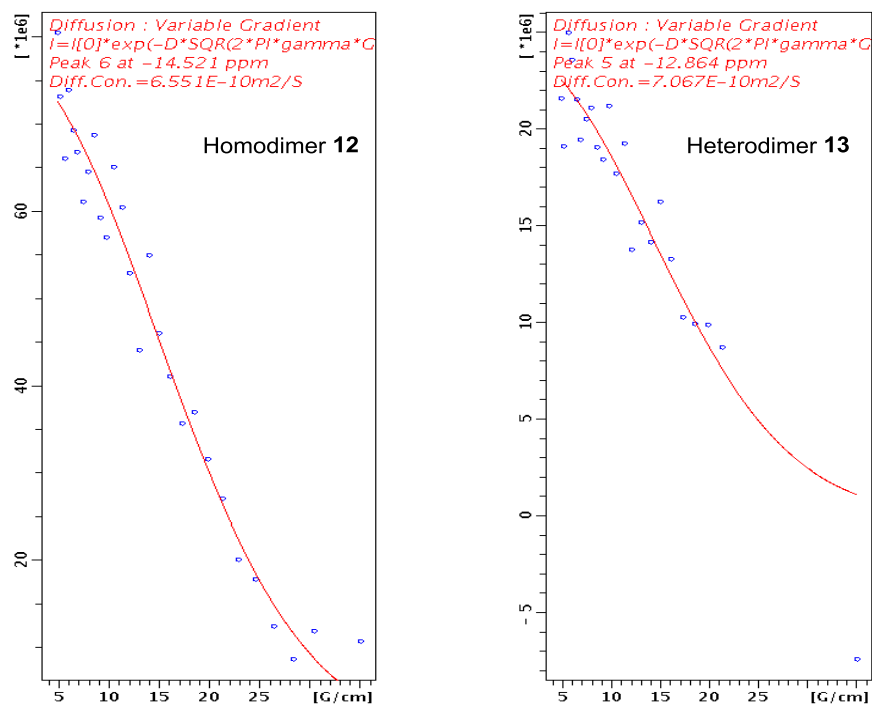


Figure S3.28. ¹³C DOSY Decay Curves for Homodimer **12** and Heterodimer **13**

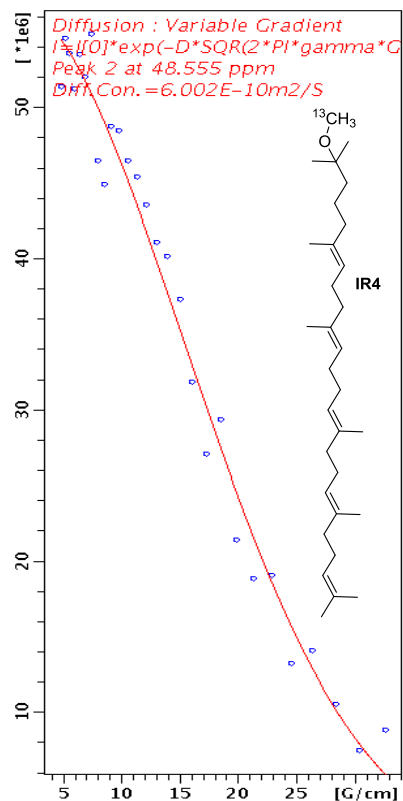
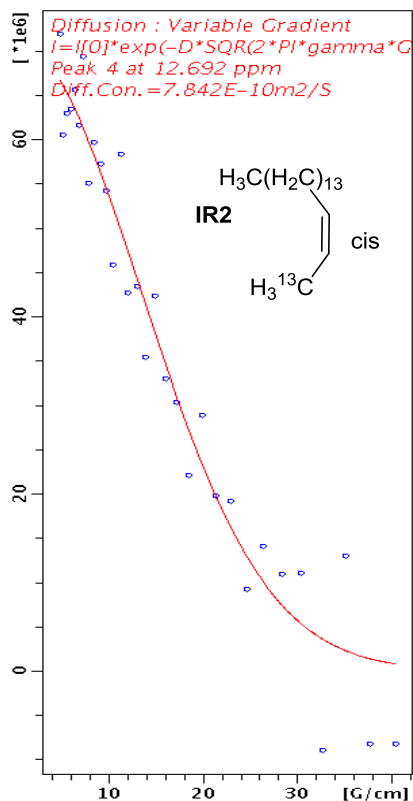
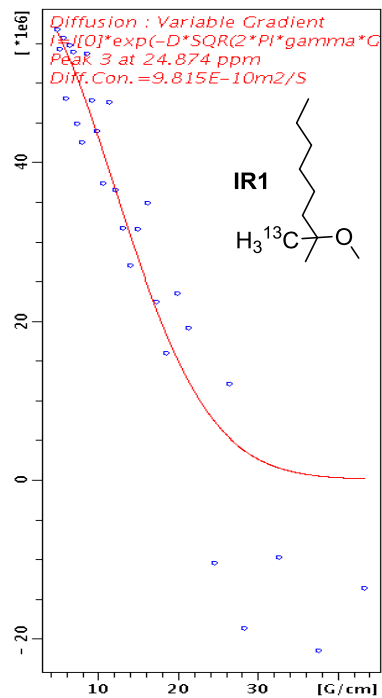
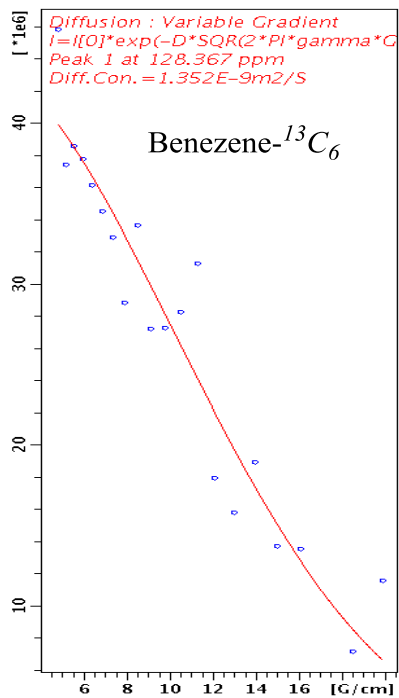


Figure S3.29. ^{13}C DOSY Decay Curves for Internal References

Table S3.6. *D*-FW analysis of ^{13}C DOSY data of $^{13}\text{CH}_3^6\text{Li}$ in DEE with DMB at $-40\text{ }^\circ\text{C}$

Compound	FW (g/mol)	10^{-10}D (m^2/s)	log FW	log D	Predicted FW (g/mol)	% error
BEN- $^{13}\text{C}_6$	84.07	13.52	1.925	-8.869	82.81	1.5
IR1	159.3	9.815	2.202	-9.008	158.8	0.3
IR2	239.4	7.842	2.379	-9.106	250.6	-4.7
IR4	443.8	6.002	2.647	-9.222	431.7	2.7
12^a	352.6 ^a	6.551	2.547	-9.184	361.3	-2.5
13^b	463.5 ^b	7.067	2.666	-9.151	309.7	33.2

^a352.6 $\text{g}\cdot\text{mol}^{-1}$ is the formula weight of homodimer ($^{13}\text{CH}_3^6\text{Li}$)₂(DMB)₂ **12**. ^b463.5 $\text{g}\cdot\text{mol}^{-1}$ is the formula weight of heterodimer ($^{13}\text{CH}_3^6\text{Li}$)I(DMB)₂ **13**.

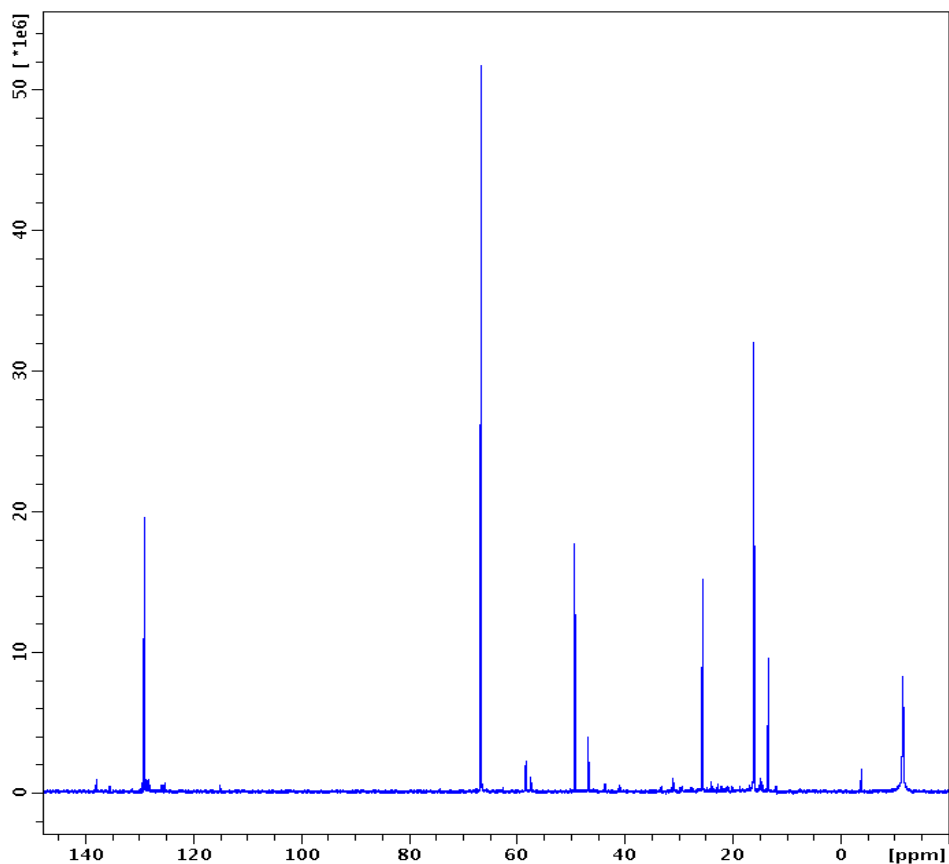


Figure S3.30. ^{13}C NMR of $^{13}\text{CH}_3^6\text{Li}$ in DEE with PMDTA and BEN, **IR1**, **IR2**, **IR4** at $-40\text{ }^\circ\text{C}$

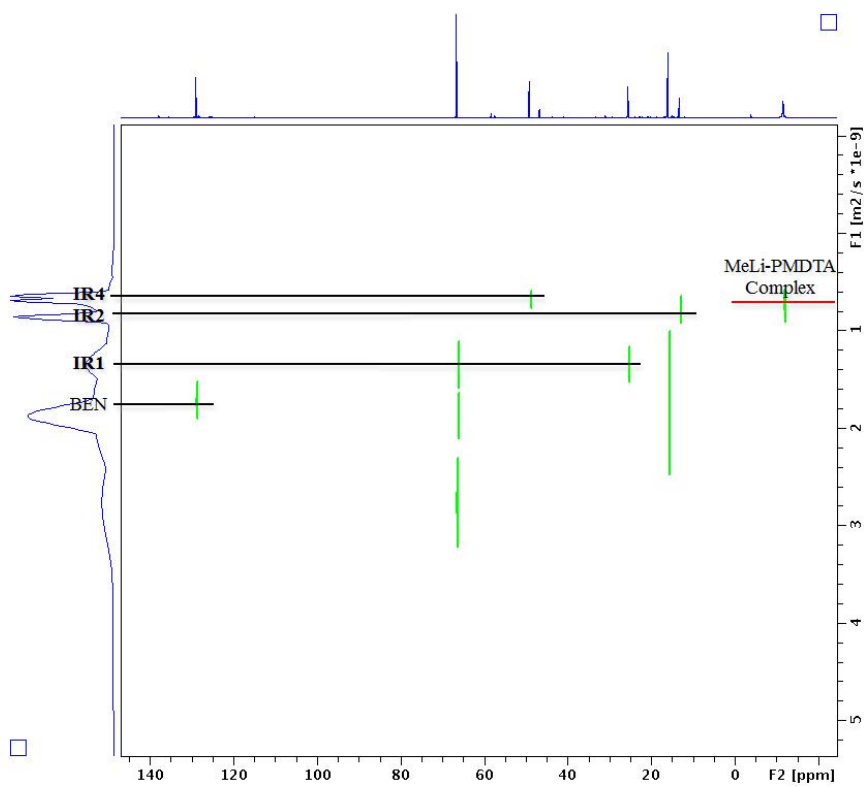


Figure S3.31. ¹³C DOSY of ¹³CH₃⁶Li in DEE with PMDTA and BEN, **IR1**, **IR2**, **IR4** at -40 °C

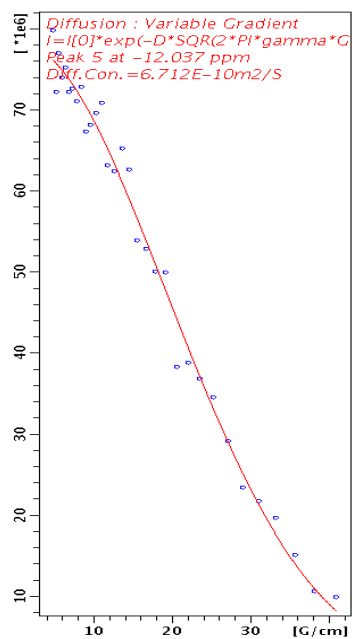


Figure S3.32. ¹³C DOSY Decay Curves for Dimer **14**

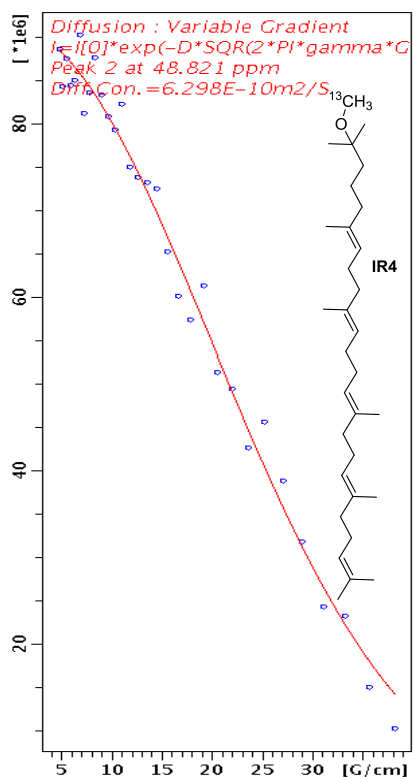
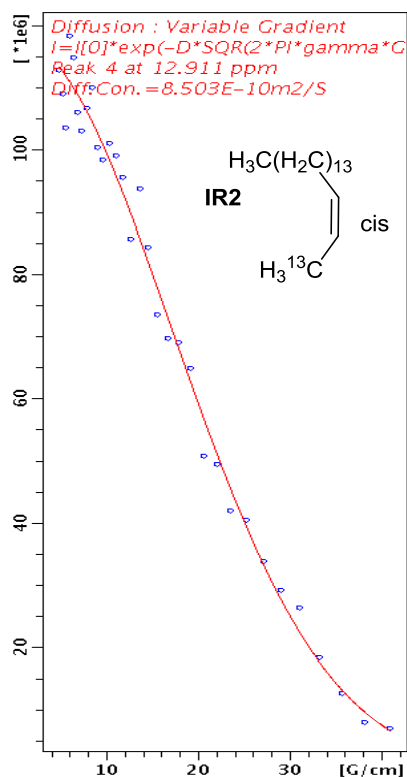
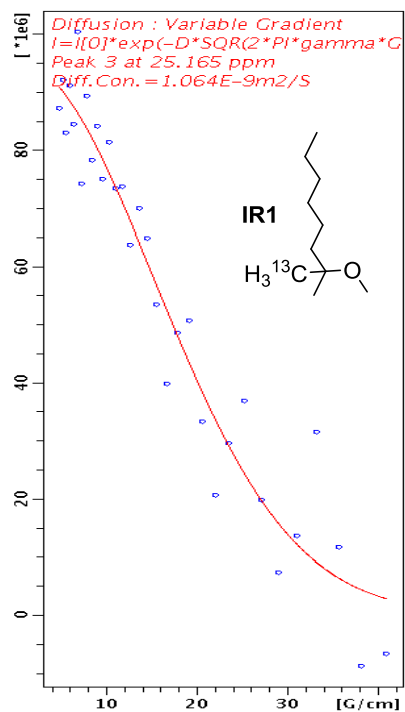
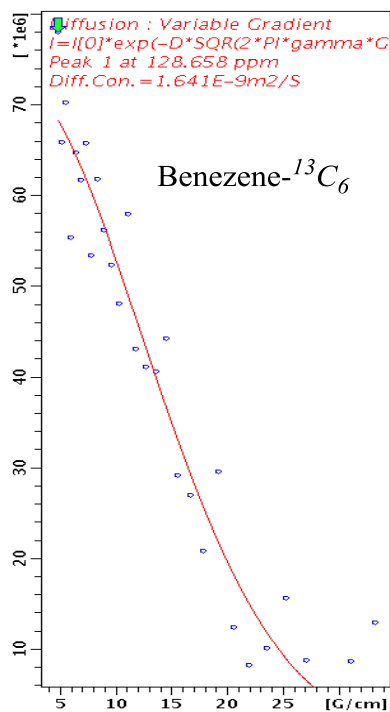


Figure S3.33. ^{13}C DOSY Decay Curves for Internal References

Table S3.7. *D*-FW analysis of ^{13}C DOSY data of $^{13}\text{CH}_3^6\text{Li}$ in DEE with PMDTA at $-40\text{ }^\circ\text{C}$

Compound	FW (g/mol)	10^{-10}D (m^2/s)	log FW	log D	Predicted FW (g/mol)	% error
BEN- $^{13}\text{C}_6$	84.07	16.41	1.925	-8.785	79.66	5.2
IR1	159.3	10.64	2.202	-8.973	169.3	-6.3
IR2	239.4	8.503	2.379	-9.070	250.1	-4.5
IR4	443.8	6.298	2.647	-9.201	421.7	5.0
14^a	390.7 ^a	6.712	2.592	-9.173	377.5	3.4

^a390.7 g mol^{-1} is the formula weight of homodimer ($^{13}\text{CH}_3^6\text{Li}$)₂(PMDTA)₂ **14a** or **14b**.

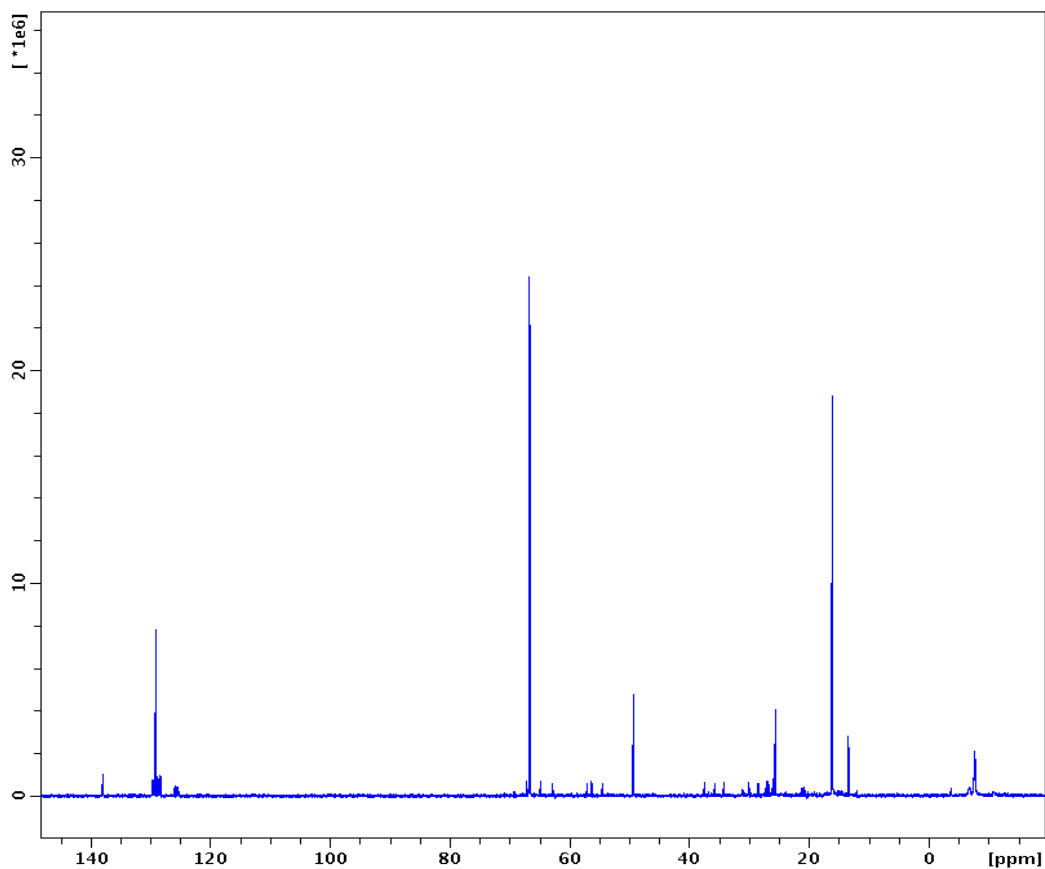


Figure S3.34. ^{13}C NMR of $^{13}\text{CH}_3^6\text{Li}$ in DEE with (-)-SP and BEN, **IR1**, **IR2**, **IR4** at $-40\text{ }^\circ\text{C}$

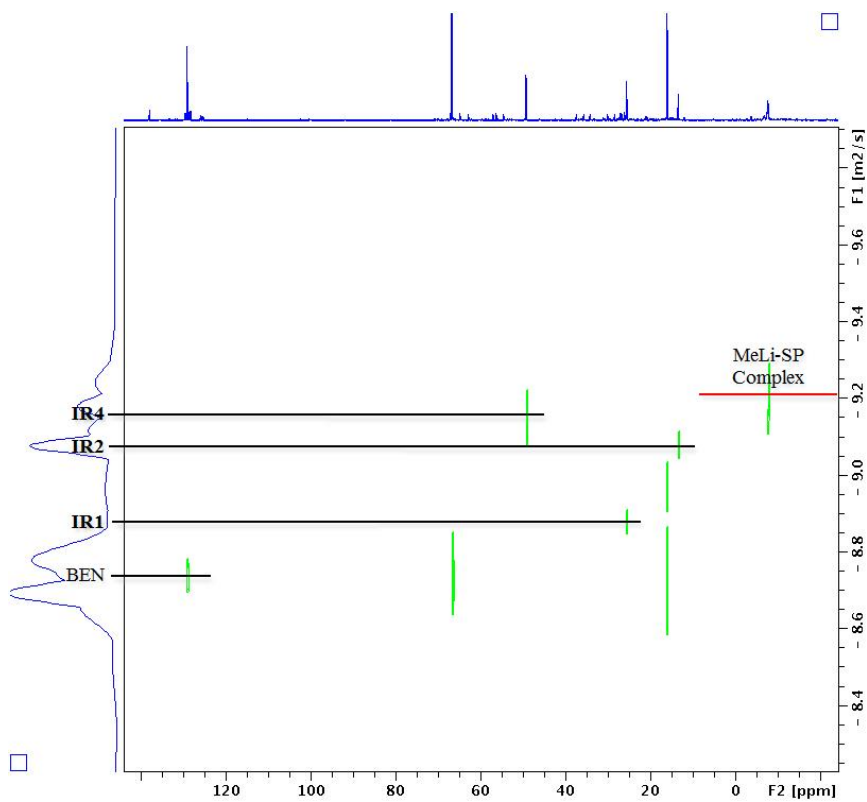


Figure S3.35. ¹³C DOSY of ¹³CH₃⁶Li in DEE with (-)-SP and BEN, **IR1**, **IR2**, **IR4** at -40 °C

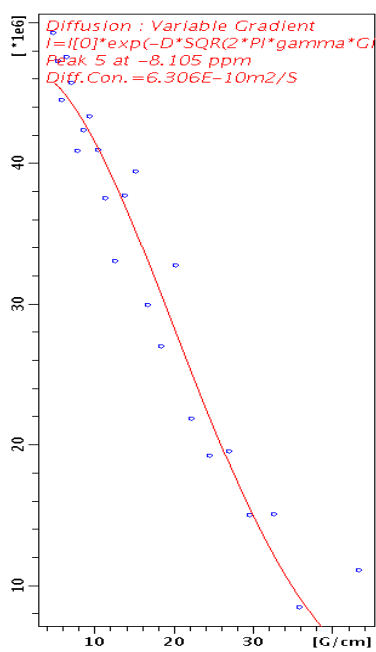


Figure S3.36. ¹³C DOSY Decay Curves for Dimer **15**

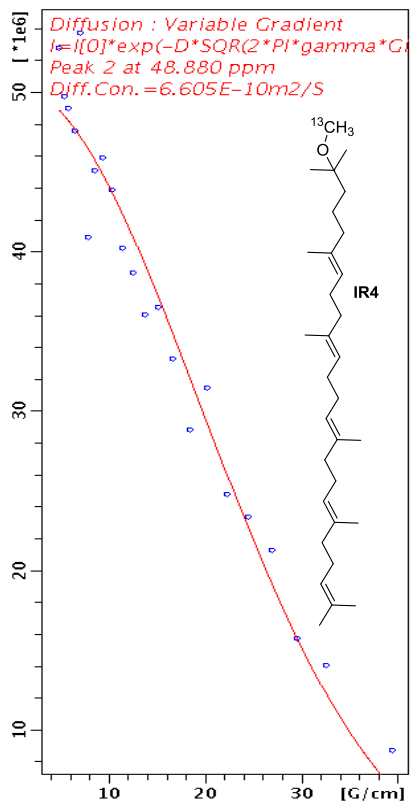
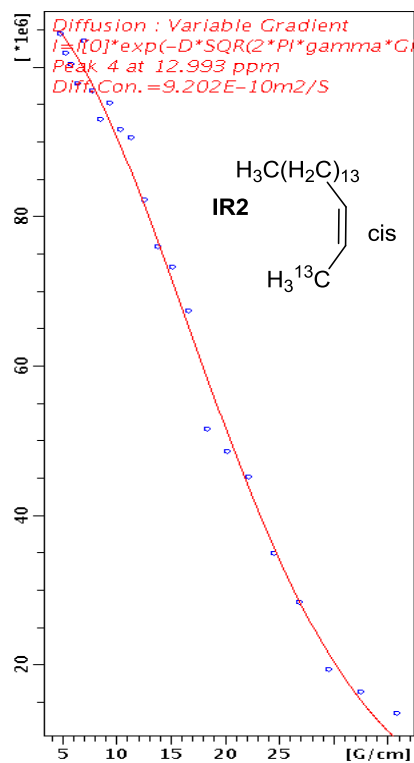
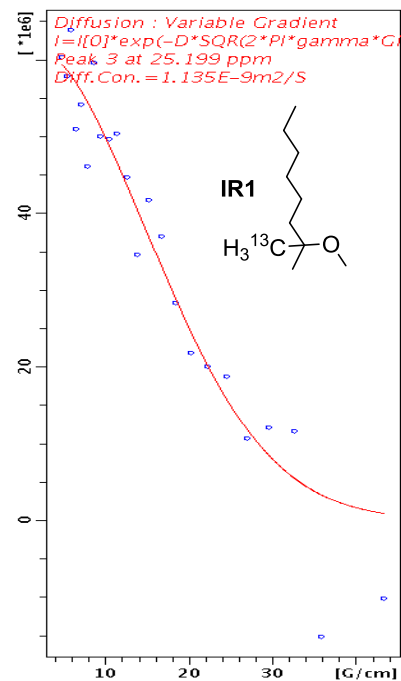
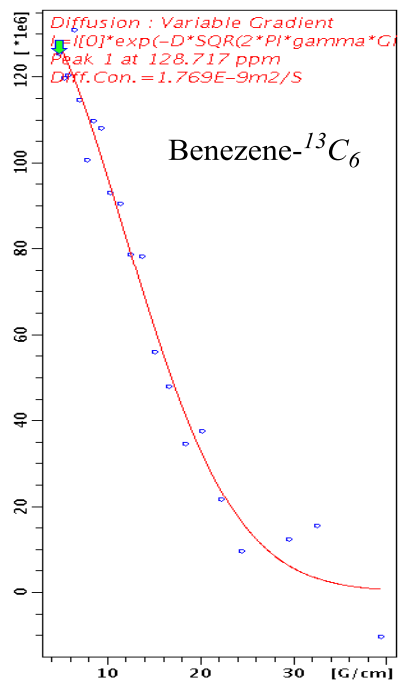


Figure S3.37. ^{13}C DOSY Decay Curves for Internal References

Table S3.8. *D*-FW Analysis of ^{13}C DOSY data of $^{13}\text{CH}_3^6\text{Li}$ in DEE with (-)-SP at $-40\text{ }^\circ\text{C}$

Compound	FW (g/mol)	10^{-10}D (m^2/s)	log FW	log D	Predicted FW (g/mol)	% error
BEN- $^{13}\text{C}_6$	84.07	17.69	1.925	-8.752	80.14	4.7
IR1	159.3	11.35	2.202	-8.945	170.4	-7.0
IR2	239.4	9.202	2.379	-9.036	243.5	-1.7
IR4	443.8	6.605	2.647	-9.180	427.9	3.6
15^a	512.9 ^a	6.306	2.710	-9.200	462.9	9.7

^a512.9 g mol^{-1} is the formula weight of homodimer ($^{13}\text{CH}_3^6\text{Li}$)₂(SP)₂ **15**.

Appendix D

Supporting information for Chapter 4

Table of Contents

Figure S4.1. ¹ H NMR of 650 μL <i>c</i> -PenLi toluene- <i>d</i> ₈ solution with 0.0511g 1-dodecene at -10°C	309
Figure S4.2. ¹ H NMR of 650 μL <i>c</i> -PenLi toluene- <i>d</i> ₈ solution with 0.0511g 1-dodecene at -5°C	309
Figure S4.3. ¹ H NMR of 650 μL <i>c</i> -PenLi toluene- <i>d</i> ₈ solution with 0.0511g 1-dodecene at 0°C.....	310
Figure S4.4. ¹ H NMR of 650 μL <i>c</i> -PenLi toluene- <i>d</i> ₈ solution with 0.0511g 1-dodecene at 5°C.....	310
Figure S4.5. ¹ H NMR of 650 μL <i>c</i> -PenLi toluene- <i>d</i> ₈ solution with 0.0511g 1-dodecene at 10°C.....	311
Figure S4.6. ¹ H NMR of 650 μL <i>c</i> -PenLi toluene- <i>d</i> ₈ solution with 0.0511g 1-dodecene at 15°C.....	311
Figure S4.7. ¹ H NMR of 650 μL <i>c</i> -PenLi toluene- <i>d</i> ₈ solution with 0.0511g 1-dodecene at 20°C.....	312
Figure S4.8. ¹ H NMR of 650 μL <i>c</i> -PenLi toluene- <i>d</i> ₈ solution with 0.0511g 1-dodecene at 25°C.....	312
Figure S4.9. ¹ H NMR of 950 μL <i>c</i> -PenLi toluene- <i>d</i> ₈ solution with 0.0511g 1-dodecene at 15°C.....	313
Figure S4.10. ¹ H NMR of 1.25 mL <i>c</i> -PenLi toluene- <i>d</i> ₈ solution with 0.0511 g 1-dodecene at 15 °C.....	313
Figure S4.11. van 't Hoff Plot and Thermodynamic Data of Reaction (1)	315
Figure S4.12. ¹ H NMR of <i>c</i> -PenLi toluene- <i>d</i> ₈ solution at -25 °C	316
Figure S4.13. ¹³ C NMR of <i>c</i> -PenLi toluene- <i>d</i> ₈ solution at -25 °C.....	316
Figure S4.14. ¹ H COSY of <i>c</i> -PenLi toluene- <i>d</i> ₈ solution at -25 °C.....	317
Figure S4.15. ¹ H- ¹³ C HSQC of <i>c</i> -PenLi toluene- <i>d</i> ₈ solution at -25 °C	317
Figure S4.16. ¹ H- ¹³ C HMBC of <i>c</i> -PenLi toluene- <i>d</i> ₈ solution at -25 °C	318
Figure S4.17. ¹ H NMR of <i>c</i> -PenLi toluene- <i>d</i> ₈ solution with internal references at -25 °C.....	318
Figure S4.18. ¹ H DOSY decay curves for internal references.....	319

Figure S4.19. ^1H DOSY decay curves for <i>c</i> -PenLi aggregates.....	320
Figure S4.20. ^1H NMR of <i>c</i> -PenLi/THF complex toluene- d_8 solution at $-30\text{ }^\circ\text{C}$	321
Figure S4.21. ^{13}C NMR of <i>c</i> -PenLi/THF complex toluene- d_8 solution at $-30\text{ }^\circ\text{C}$	321
Figure S4.22. ^1H COSY of <i>c</i> -PenLi/THF complex toluene- d_8 solution at $-30\text{ }^\circ\text{C}$	322
Figure S4.23. ^1H - ^{13}C HSQC of <i>c</i> -PenLi/THF complex toluene- d_8 solution at $-30\text{ }^\circ\text{C}$	322
Figure S4.24. ^1H - ^{13}C HMBC of <i>c</i> -PenLi/THF complex toluene- d_8 solution at $-30\text{ }^\circ\text{C}$	323
Figure S4.25. ^1H NMR of <i>c</i> -PenLi/THF complex toluene- d_8 solution with internal references at $-35\text{ }^\circ\text{C}$..	323
Figure S4.26. ^1H DOSY decay curves for internal references.....	324
Figure S4.27. ^1H DOSY decay curves for <i>c</i> -PenLi/THF complex	325
Table S4.1. Equilibrium Constant (K) of Reaction (1) in toluene- d_8 at $15\text{ }^\circ\text{C}$	314
Table S4.2. Ratio of Different <i>c</i> -PenLi Aggregates as a Function of Temperature.....	314
Table S4.3. Concentration of Different <i>c</i> -PenLi Aggregates as a Function of Temperature.....	315
Table S4.4. <i>D</i> -FW analysis of ^1H DOSY data of <i>c</i> -PenLi toluene- d_8 solution at $-25\text{ }^\circ\text{C}$	320
Table S4.5. <i>D</i> -FW analysis of ^1H DOSY data of <i>c</i> -PenLi/THF complex toluene- d_8 solution at $-35\text{ }^\circ\text{C}$	325

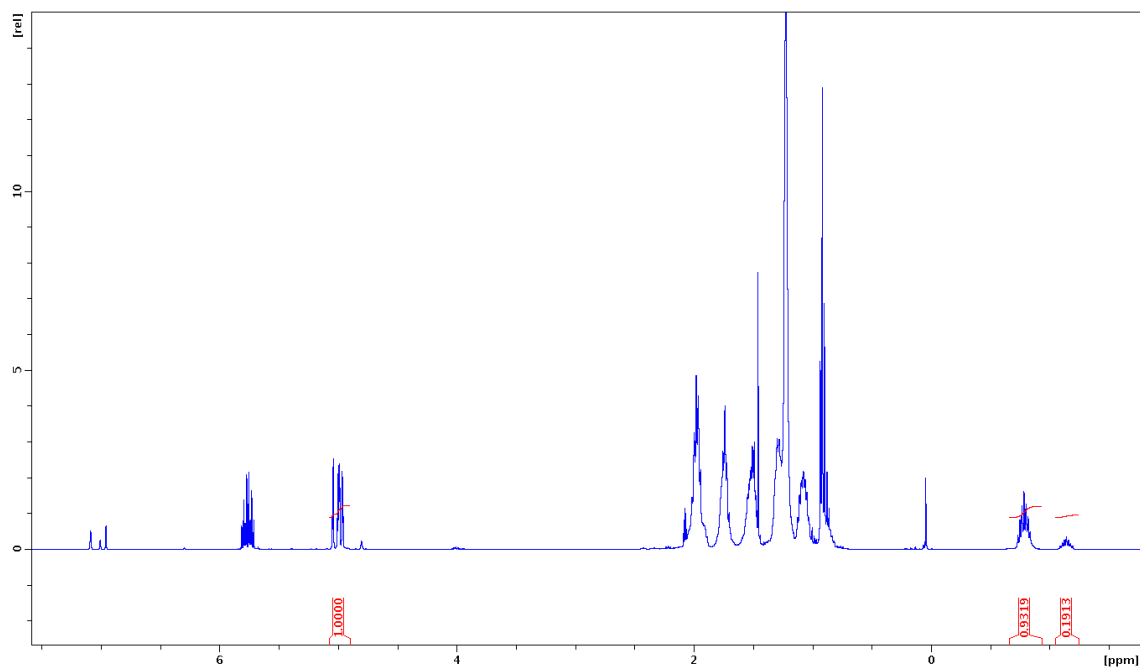


Figure S4.1. ¹H NMR of 650 μL *c*-PenLi toluene-*d*₈ solution with 0.0511 g 1-dodecene at -10 °C

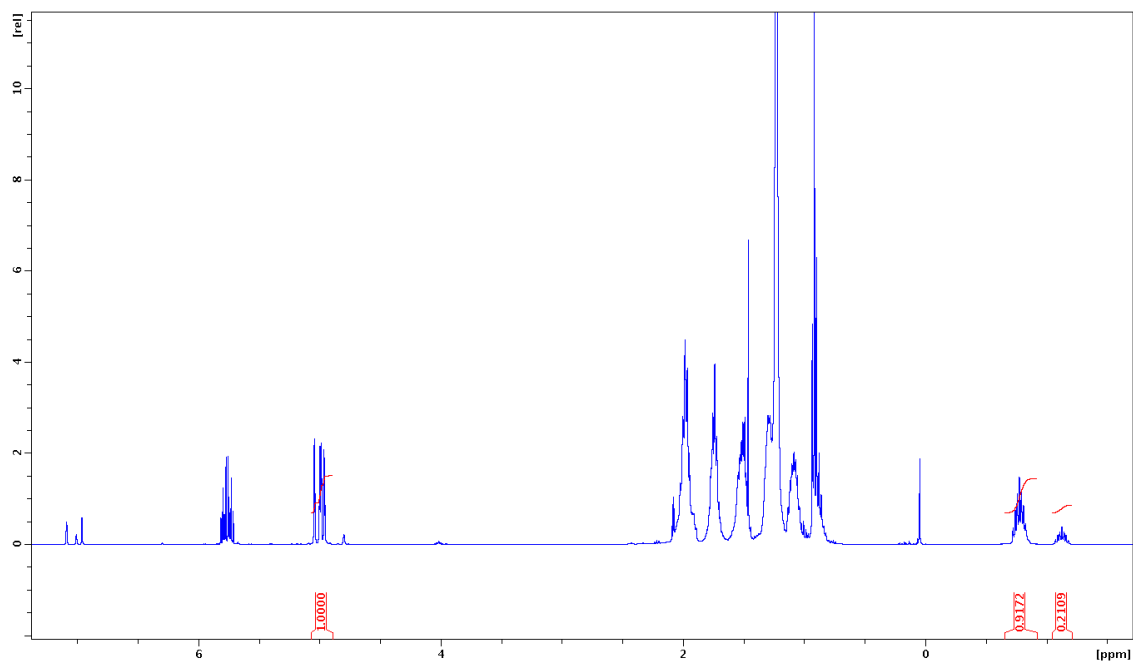


Figure S4.2. ¹H NMR of 650 μL *c*-PenLi toluene-*d*₈ solution with 0.0511 g 1-dodecene at -5 °C

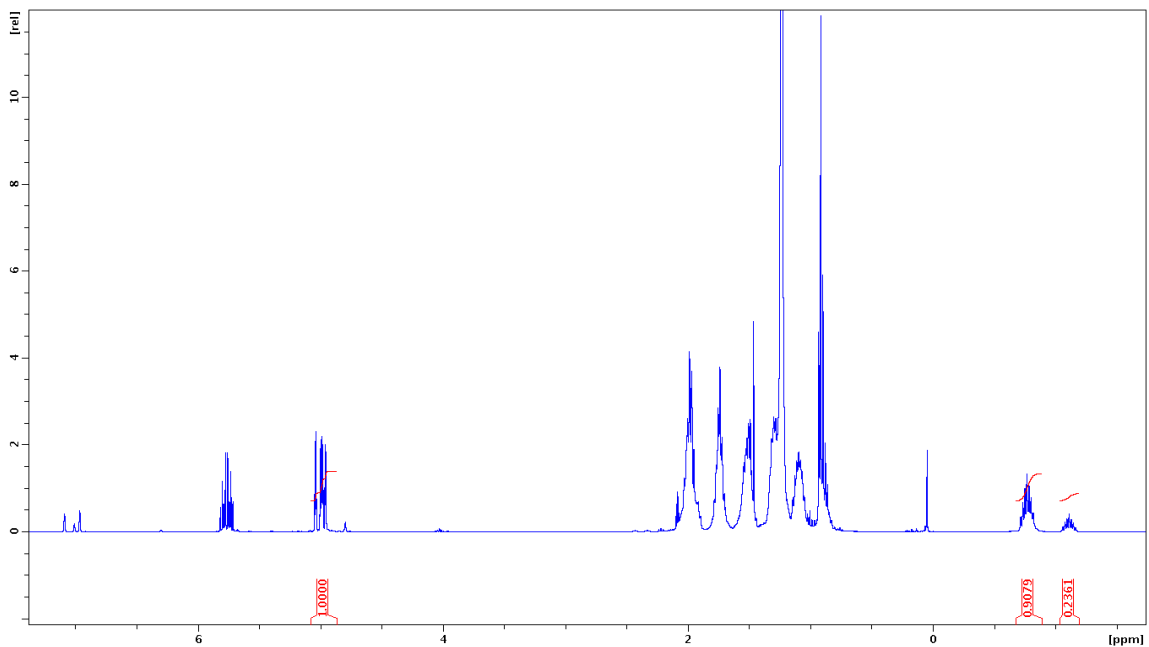


Figure S4.3. ^1H NMR of 650 μL *c*-PenLi toluene- d_8 solution with 0.0511 g 1-dodecene at 0 $^\circ\text{C}$

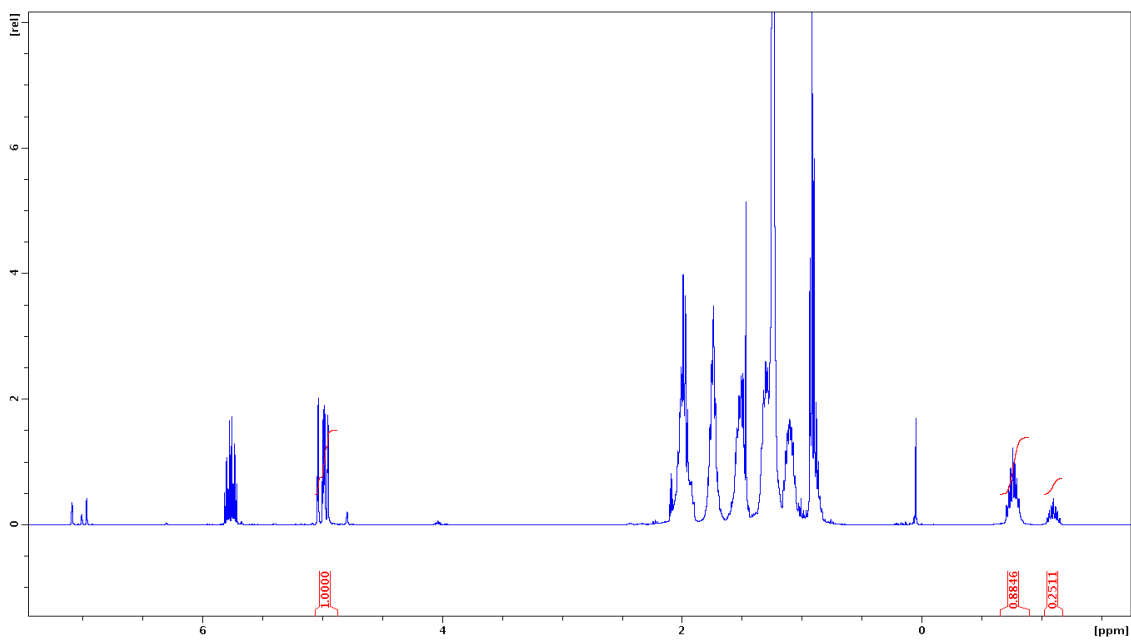


Figure S4.4. ^1H NMR of 650 μL *c*-PenLi toluene- d_8 solution with 0.0511 g 1-dodecene at 5 $^\circ\text{C}$

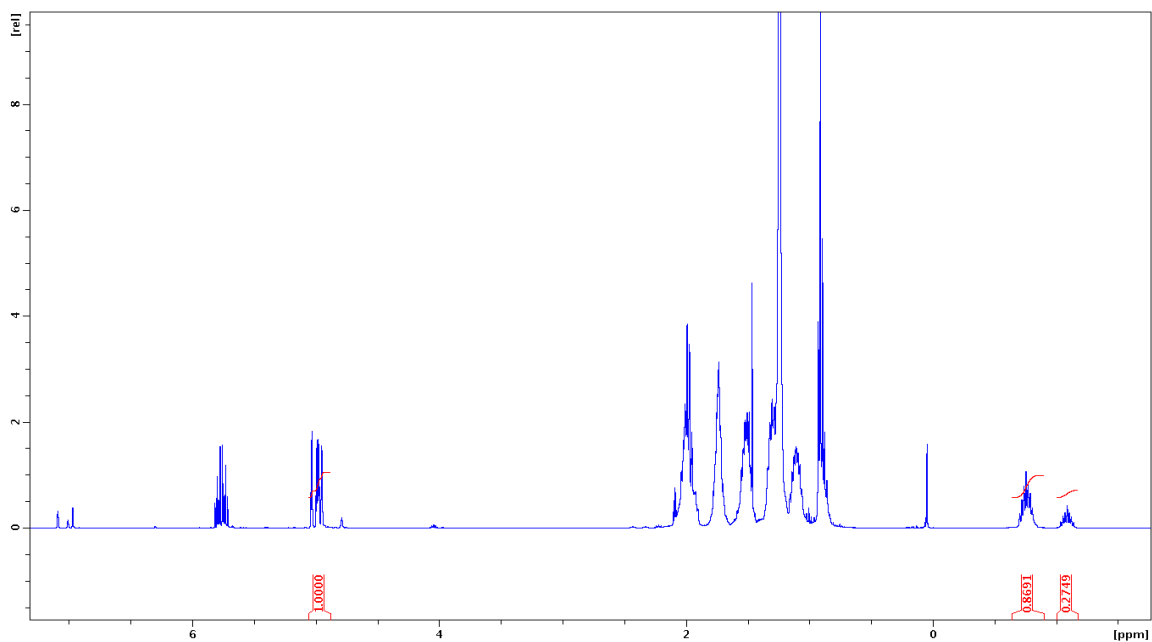


Figure S4.5. ¹H NMR of 650 μ L *c*-PenLi toluene-*d*₈ solution with 0.0511 g 1-dodecene at 10 °C

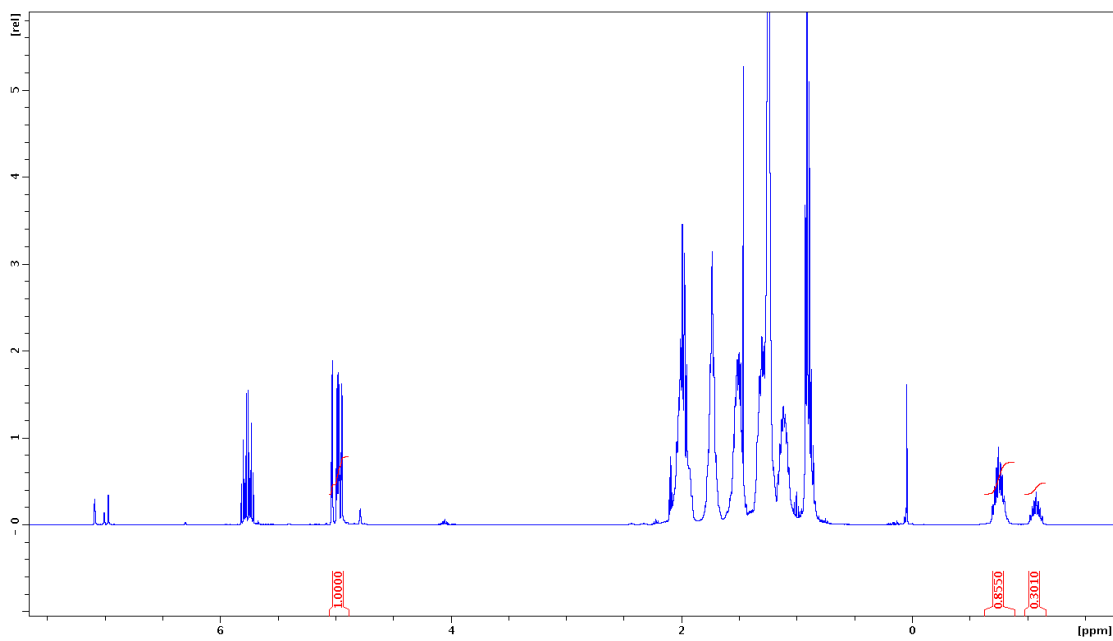


Figure S4.6. ¹H NMR of 650 μ L *c*-PenLi toluene-*d*₈ solution with 0.0511 g 1-dodecene at 15 °C

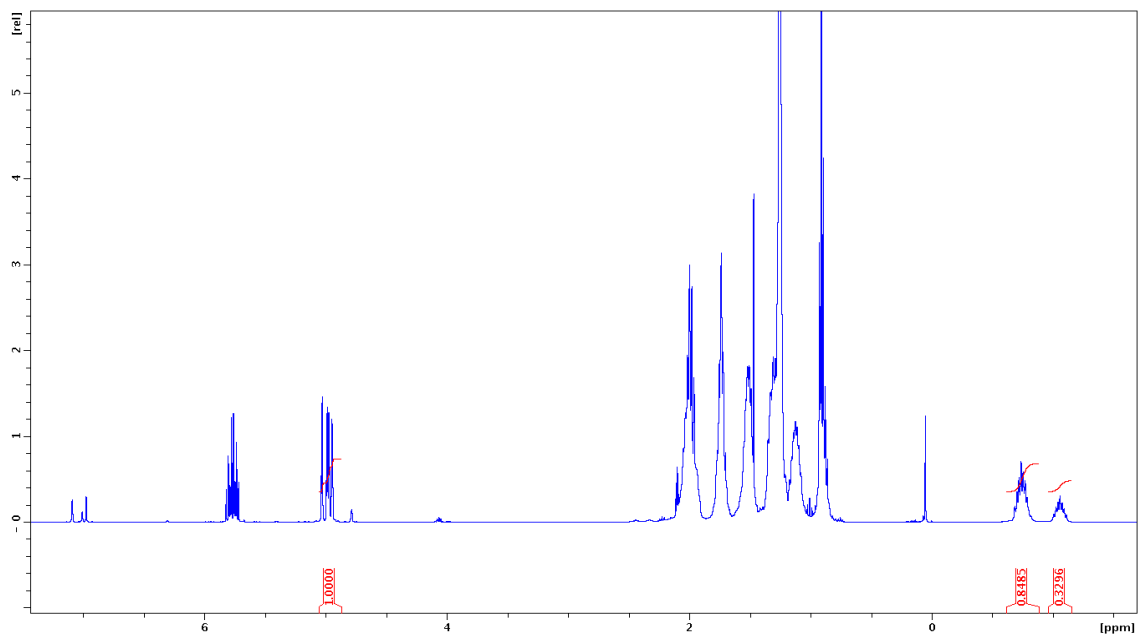


Figure S4.7. ^1H NMR of 650 μL *c*-PenLi toluene- d_8 solution with 0.0511 g 1-dodecene at 20 $^\circ\text{C}$

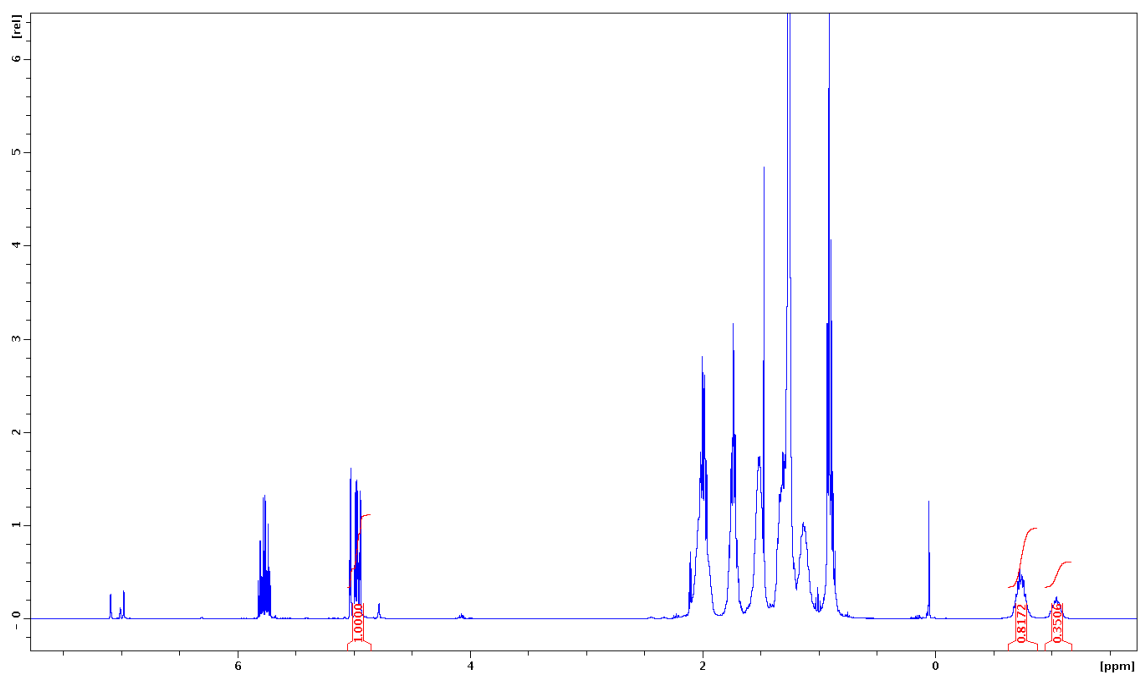


Figure S4.8. ^1H NMR of 650 μL *c*-PenLi toluene- d_8 solution with 0.0511 g 1-dodecene at 25 $^\circ\text{C}$

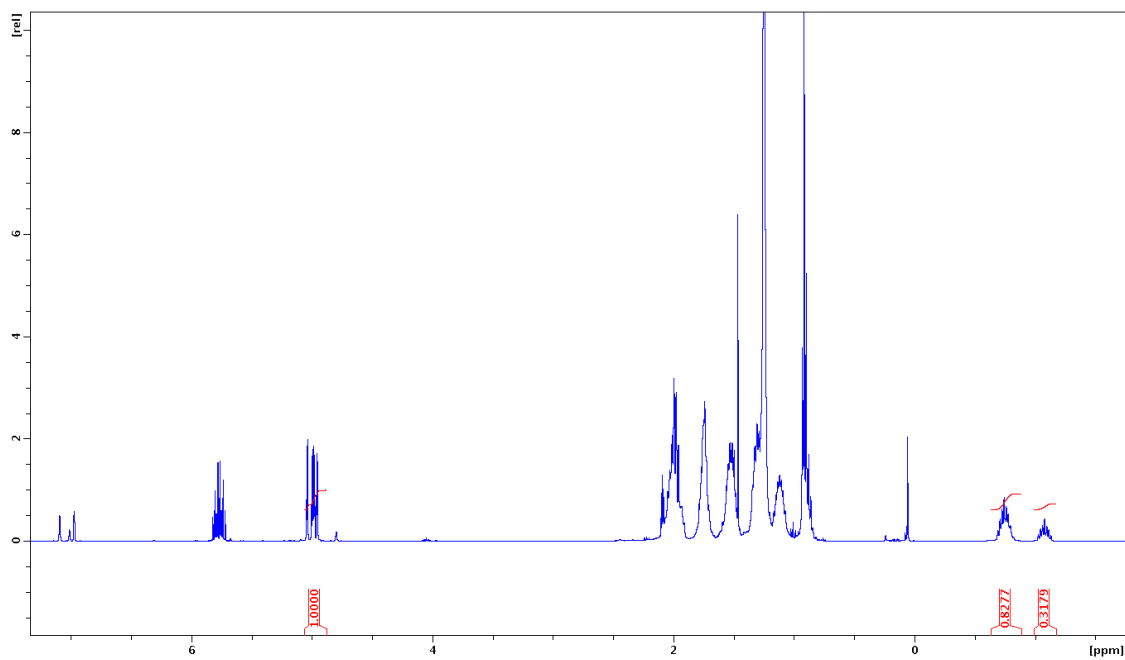


Figure S4.9. ^1H NMR of 950 μL *c*-PenLi toluene- d_8 solution with 0.0511 g 1-dodecene at 15 $^\circ\text{C}$

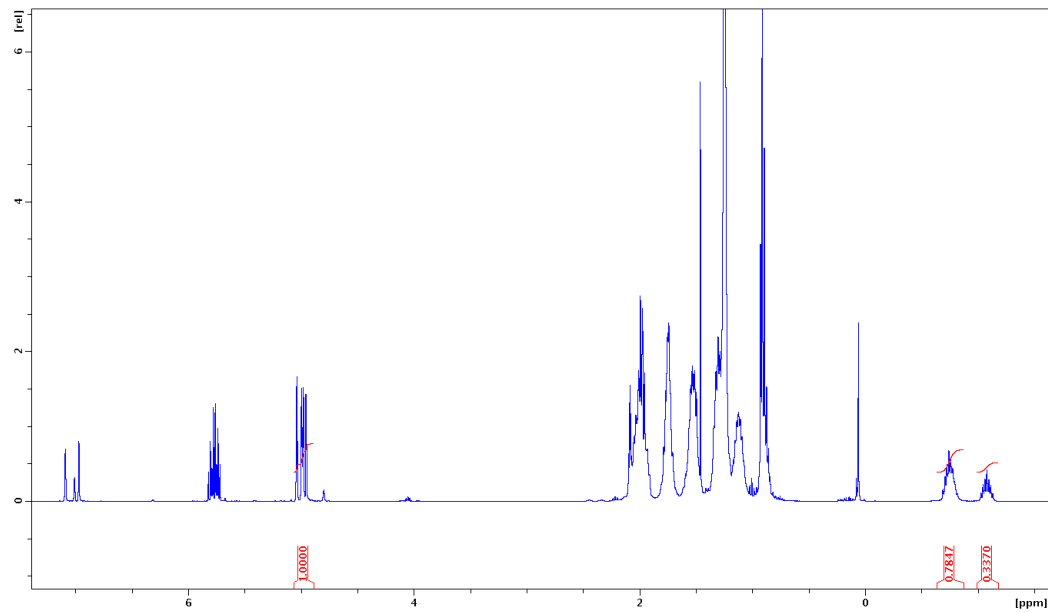


Figure S4.10. ^1H NMR of 1.25 mL *c*-PenLi toluene- d_8 solution with 0.0511 g 1-dodecene at 15 $^\circ\text{C}$

Table S4.1. Equilibrium Constant (K) of Reaction (1) in toluene-*d*₈ at 15 °C

Vol. (mL)	Conc. of 1-dodecene ^a (M)	Area ^b of Peak at -0.77 ppm to 1-dodecene	Area ^b of Peak at -1.14 ppm to 1-dodecene	Conc. of <i>c</i> -PenLi ^c at -0.77 ppm, C ₁ (M)	Conc. of <i>c</i> -PenLi ^d at -1.14 ppm, C ₂ (M)	Conc. of Tetramer = C ₂ /4, C _T (M)	Conc. of Hexamer = C ₁ /6, C _H (M)	K = C _T ³ /C _H ² (M ⁻¹)
0.650	0.467	0.854	0.291	0.798	0.272	0.068	0.133	0.018
0.950	0.320	0.828	0.318	0.529	0.203	0.051	0.088	0.017
1.250	0.243	0.785	0.337	0.381	0.164	0.041	0.064	0.017

^aThe concentration of 1-dodecene was measured by weighing exactly 0.0511 g 1-dodecene which was then injected into the toluene-*d*₈ solution. ^bThe area of the two terminal olefinic protons was calibrated to 1.000 and the area of the peaks at -0.77 ppm and -1.14 ppm are the methine peaks of *c*-PenLi different aggregates. Therefore, the ratio of *c*-PenLi to 1-dodecene should be the ratio of area multiplied by 2. ^cThe concentration was expressed as monomer units and calculated by multiplying the concentration of 1-dodecene to the proportion of the peak to the 1-dodecene peak. For example, 0.854/1 x 0.467 x 2 = 0.798 M. ^dThe concentration was expressed as monomer units and calculated by multiplying the concentration of 1-dodecene to the proportion of the peak to the 1-dodecene peak.

Table S4.2. Ratio of Different *c*-PenLi Aggregates as a Function of Temperature

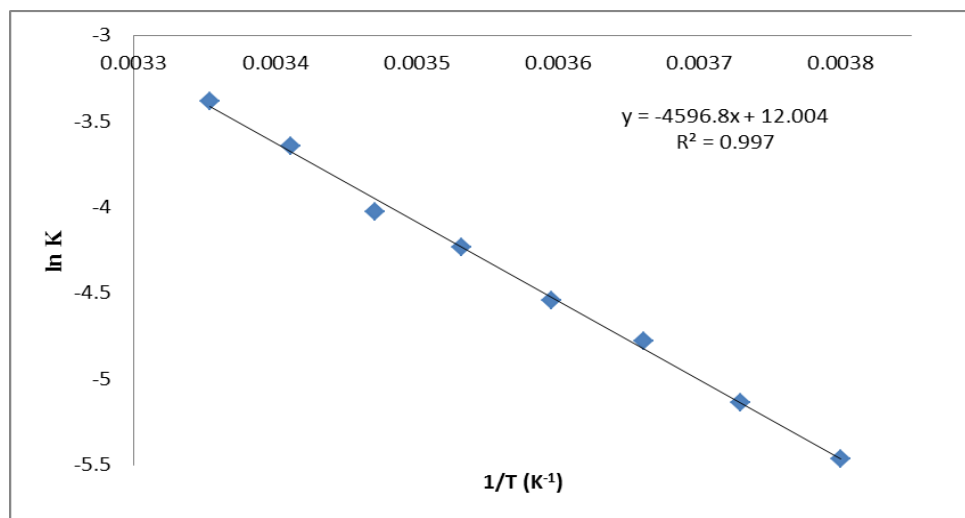
Temperature / °C	Area of terminal olefinic protons of 1-dodecene Peak	Area of Peak at -0.77 ppm	Area of Peak at -1.14 ppm	Ratio ^a of <i>c</i> -PenLi aggregate 1 (-0.77 ppm) to 1-dodecene	Ratio ^a of <i>c</i> -PenLi aggregate 2 (-1.14 ppm) to 1-dodecene
-10.0	1.000	0.932	0.191	1.864	0.383
-5.0	1.000	0.917	0.211	1.834	0.422
0.0	1.000	0.908	0.236	1.816	0.472
5.0	1.000	0.885	0.251	1.769	0.502
10.0	1.000	0.869	0.275	1.738	0.550
15.0	1.000	0.855	0.291	1.709	0.583
20.0	1.000	0.849	0.330	1.697	0.659
25.0	1.000	0.817	0.351	1.634	0.701

^aThe area of the two terminal olefinic protons was calibrated to 1.000 and the area of the peaks at -0.77 ppm and -1.14 ppm are the methine peaks of different *c*-PenLi aggregates. Therefore, the ratio of *c*-PenLi to 1-dodecene should be the ratio of area multiplied by 2.

Table S4.3. Concentration of Different *c*-PenLi Aggregates as a Function of Temperature

Temp. (°C)	1/Temp. (K ⁻¹)	Conc. of <i>c</i> -PenLi ^a at -0.77 ppm, C ₁ (M)	Conc. of <i>c</i> -PenLi ^a at -1.14 ppm, C ₂ (M)	Conc. of Hexamer = C ₁ /6, C _H (M)	Conc. of Tetramer = C ₂ /4, C _T (M)	K = C _T ³ /C _H ² (M ⁻¹)	ln K
-10.0	0.00380	0.871	0.179	0.145	0.0447	0.00424	-5.46
-5.0	0.00373	0.857	0.197	0.143	0.0493	0.00586	-5.14
0.0	0.00366	0.848	0.221	0.141	0.0551	0.00839	-4.78
5.0	0.00360	0.826	0.235	0.138	0.0586	0.01063	-4.54
10.0	0.00353	0.812	0.257	0.135	0.0642	0.01445	-4.24
15.0	0.00347	0.798	0.272	0.133	0.0681	0.01780	-4.03
20.0	0.00341	0.793	0.308	0.132	0.0770	0.02613	-3.64
25.0	0.00335	0.763	0.328	0.127	0.0819	0.03391	-3.38

^aThe concentration was expressed as monomer units and calculated by multiplying the ratio obtained above to the concentration of 1-dodecene (0.467 M).



$$\Delta H = 4596.8 \times 8.314 \text{ Jmol}^{-1} = 38.2 \text{ kJmol}^{-1}$$

$$\Delta S = 12.004 \times 8.314 \text{ Jmol}^{-1}\text{K}^{-1} = 99.8 \text{ Jmol}^{-1}\text{K}^{-1}$$

Figure S4.11. van 't Hoff Plot and Thermodynamic Data of Reaction (1)

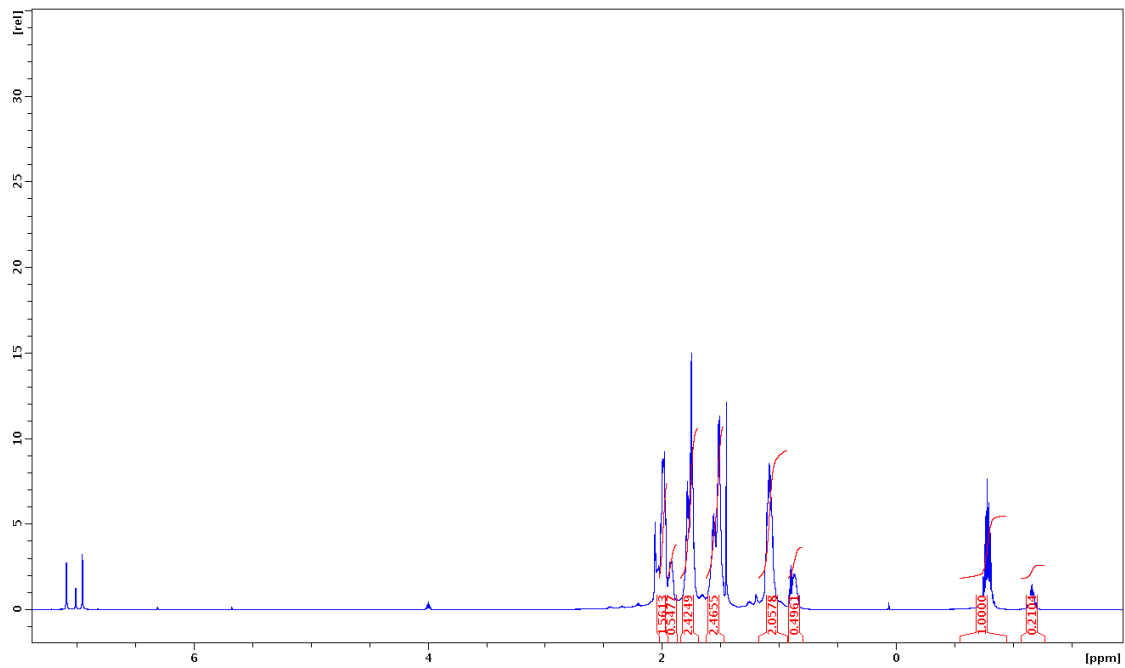


Figure S4.12. ^1H NMR of *c*-PenLi toluene- d_8 solution at $-25\text{ }^\circ\text{C}$

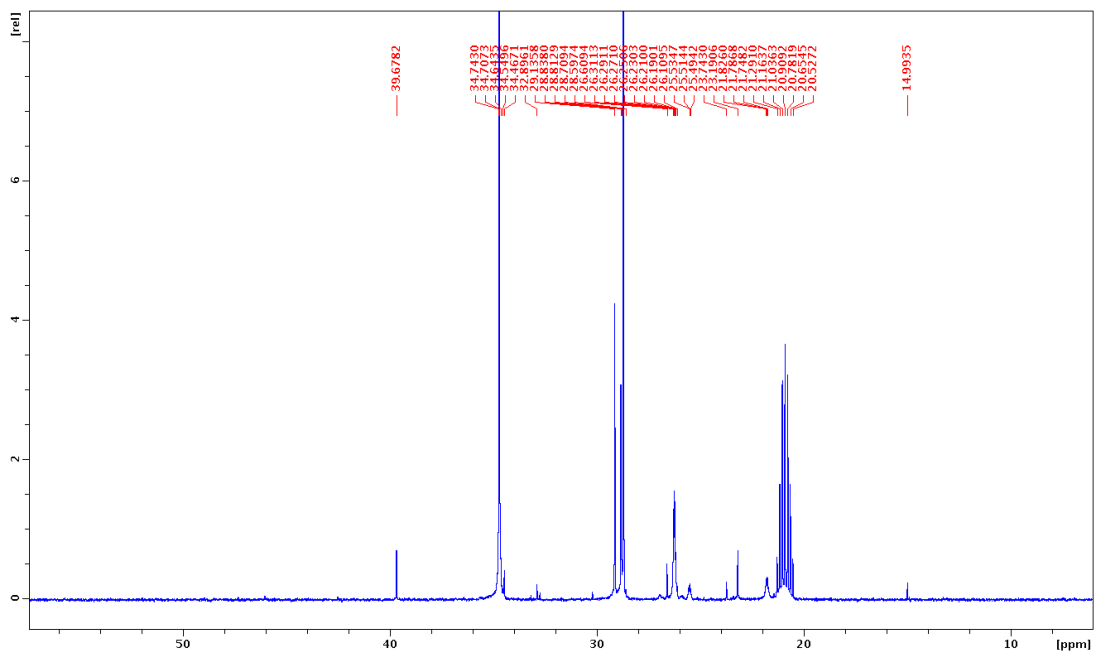


Figure S4.13. ^{13}C NMR of *c*-PenLi toluene- d_8 solution at $-25\text{ }^\circ\text{C}$

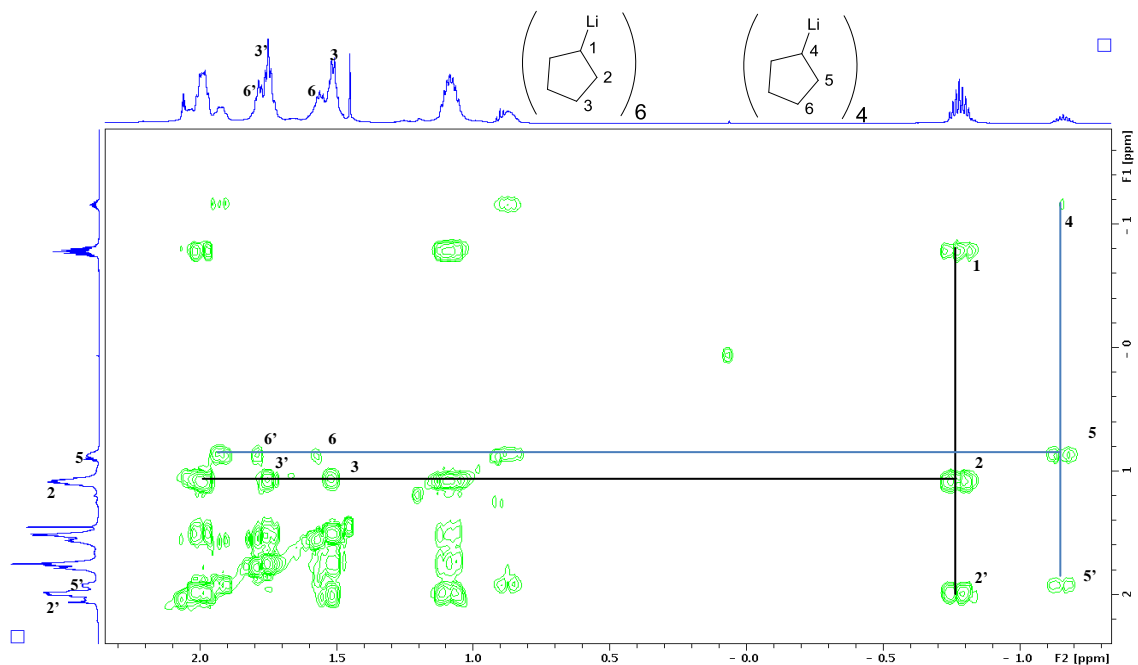


Figure S4.14. ^1H COSY of *c*-PenLi toluene- d_8 solution at $-25\text{ }^\circ\text{C}$

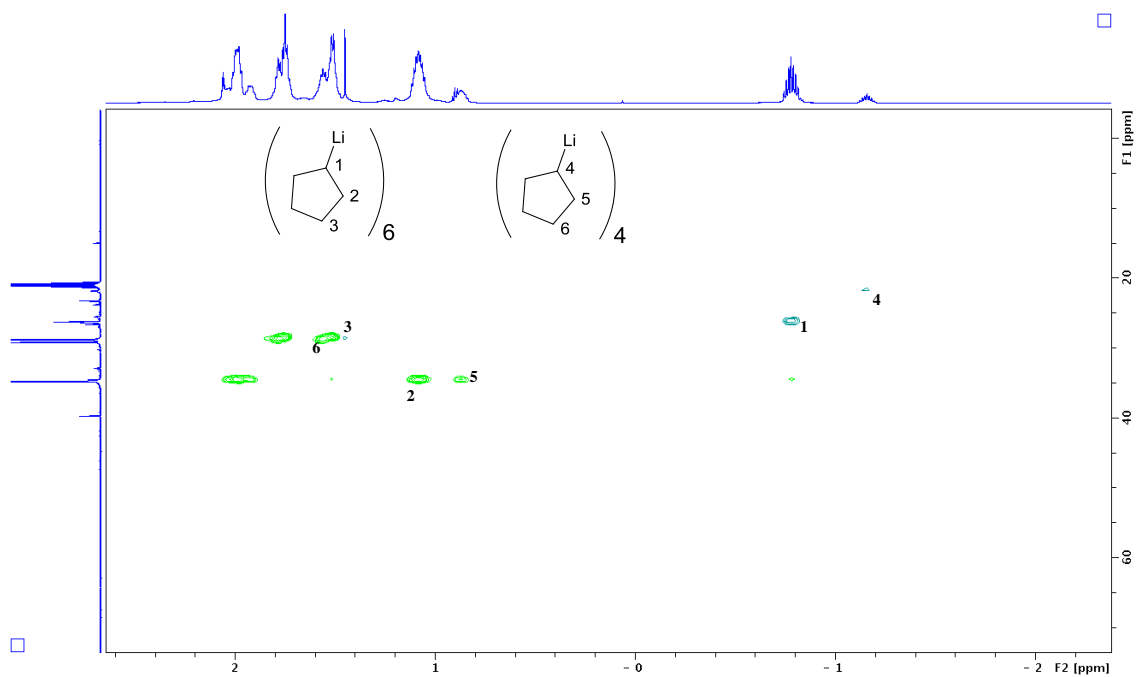


Figure S4.15. ^1H - ^{13}C HSQC of *c*-PenLi toluene- d_8 solution at $-25\text{ }^\circ\text{C}$

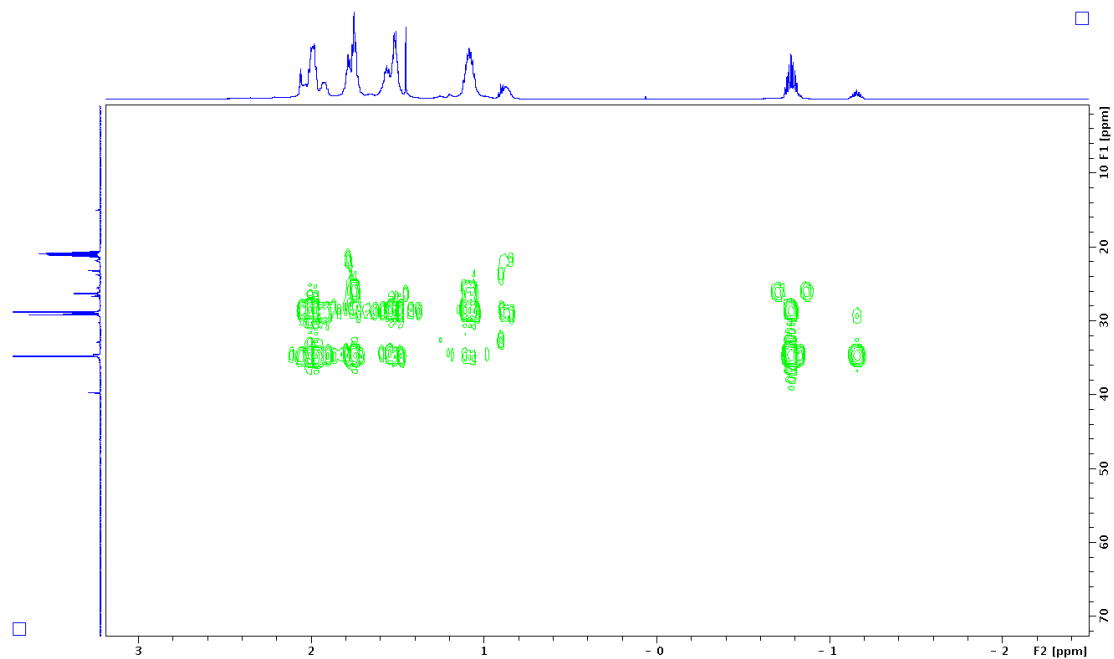


Figure S4.16. ^1H - ^{13}C HMBC of *c*-PenLi toluene- d_8 solution at $-25\text{ }^\circ\text{C}$

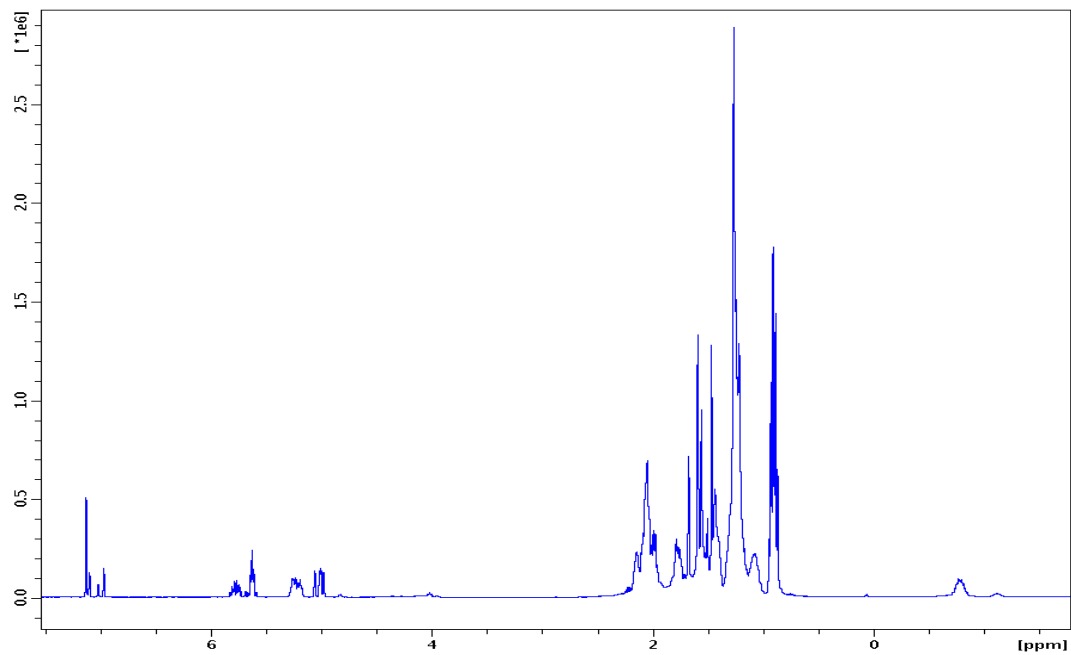


Figure S4.17. ^1H NMR of *c*-PenLi toluene- d_8 solution with Internal References at $-25\text{ }^\circ\text{C}$

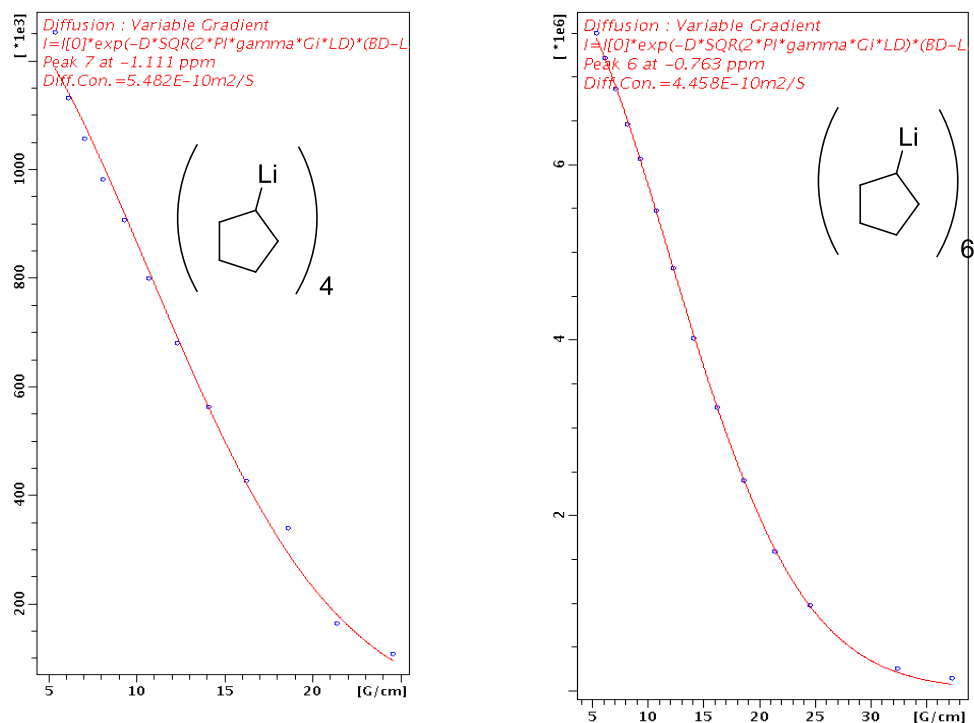


Figure S4.19. ¹H DOSY decay curves for *c*-PenLi aggregates

Table S4.4. *D*-FW analysis of ¹H DOSY data of *c*-PenLi toluene-*d*₈ solution at -25°C

Compound	FW (g/mol)	10 ⁻¹⁰ <i>D</i> (m ² /s)	log FW	log <i>D</i>	Predicted FW (g/mol)	% error
BEN	78.11	11.73	1.893	-8.931	81.84	-4.8
COE	110.2	10.07	2.042	-8.997	106.8	3.1
TDE	196.4	7.311	2.293	-9.136	186.9	4.8
SQU	410.7	4.569	2.614	-9.340	424.9	-3.5
<i>c</i> -PenLi ^a (resonance at -0.77 ppm)	456.4 ^a	4.458	2.659	-9.351	443.5	2.8
<i>c</i> -PenLi ^b (resonance at -1.14 ppm)	304.3 ^b	5.482	2.483	-9.261	309.1	-1.6

^aThe formula weight 456.4 gmol⁻¹ was calculated as *c*-PenLi hexamer.. ^bThe formula weight 384.4 gmol⁻¹ was calculated as *c*-PenLi tetramer.

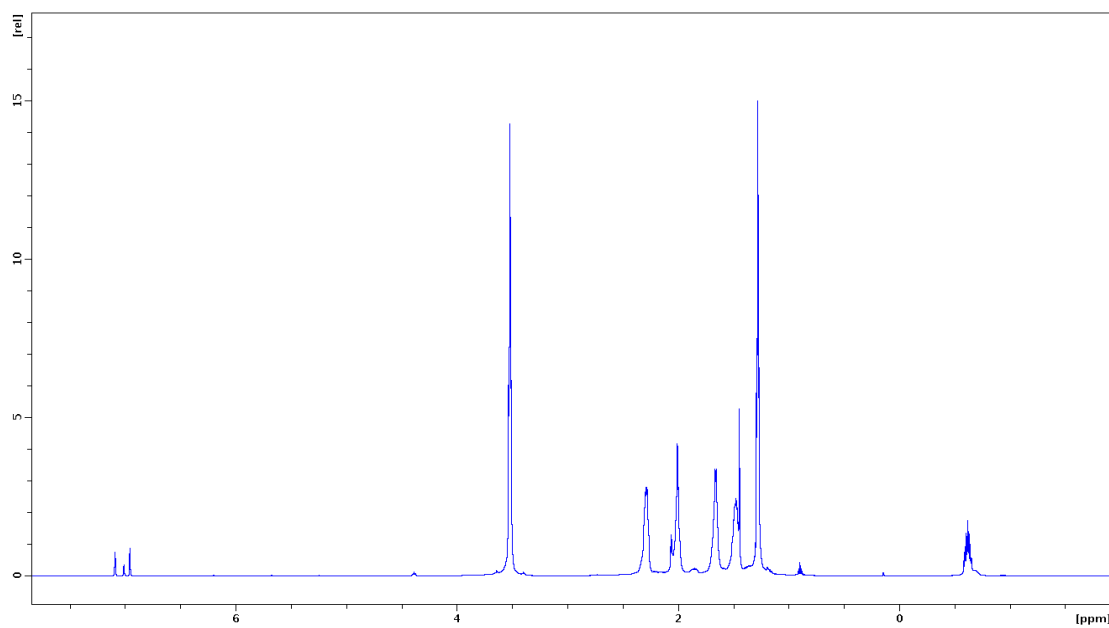


Figure S4.20. ^1H NMR of *c*-PenLi/THF complex toluene- d_8 solution at $-30\text{ }^\circ\text{C}$

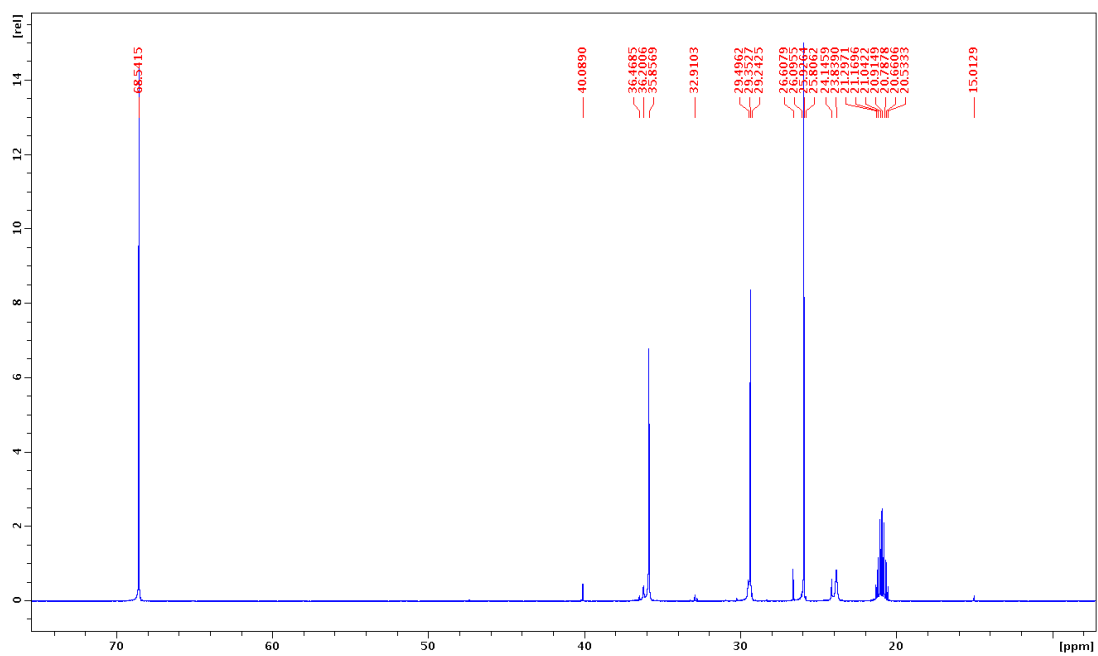


Figure S4.21. ^{13}C NMR of *c*-PenLi/THF complex toluene- d_8 solution at $-30\text{ }^\circ\text{C}$

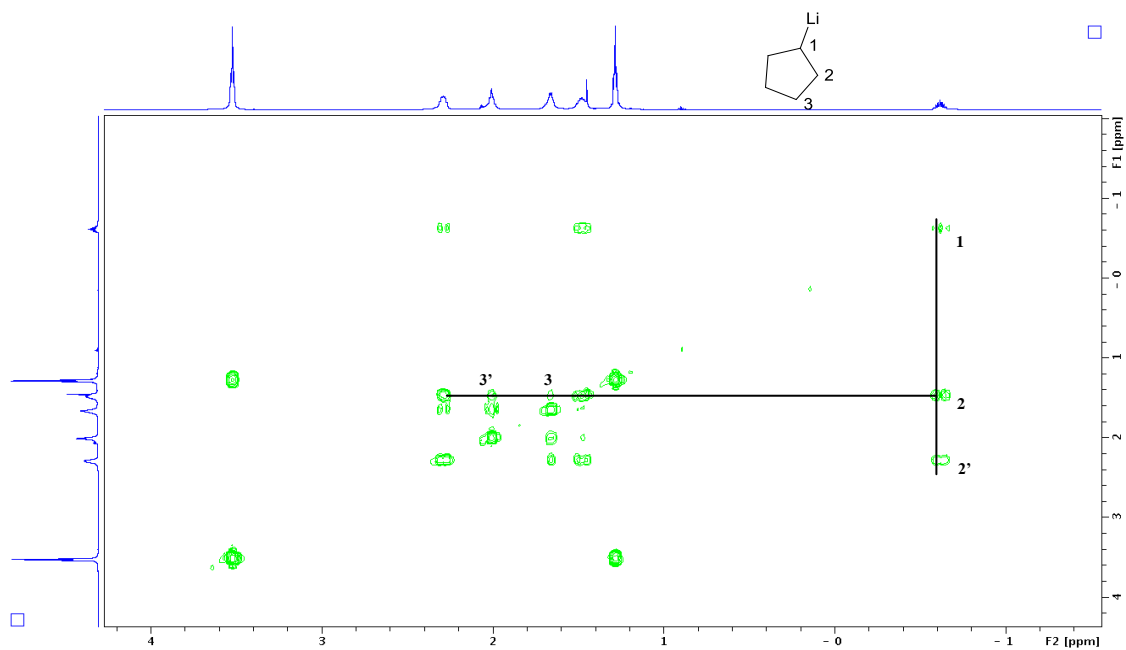


Figure S4.22. ^1H COSY of *c*-PenLi/THF complex toluene- d_8 solution at -30°C

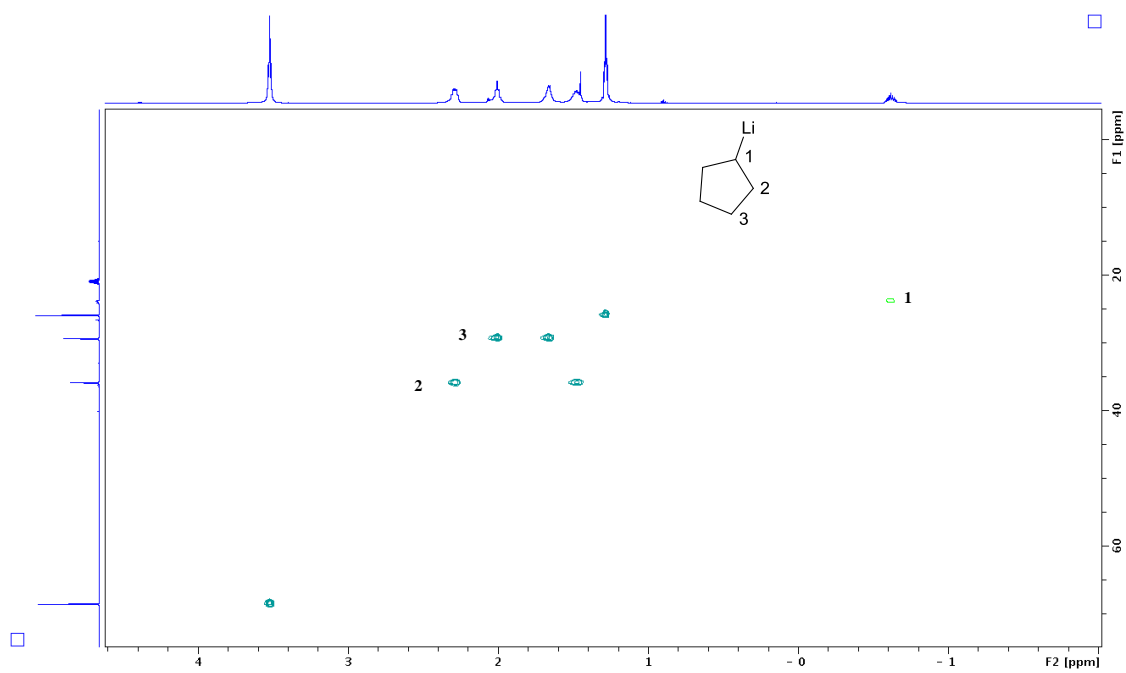


Figure S4.23. ^1H - ^{13}C HSQC of *c*-PenLi/THF complex toluene- d_8 solution at -30°C

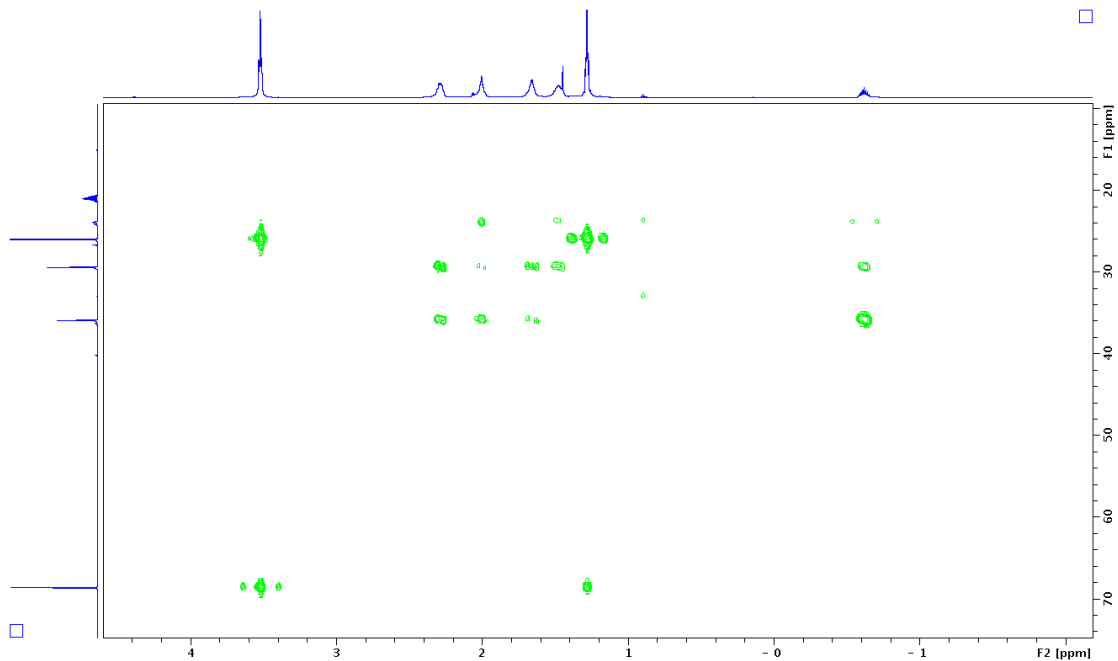


Figure S4.24. ^1H - ^{13}C HMBC of *c*-PenLi/THF complex toluene- d_8 solution at -30°C

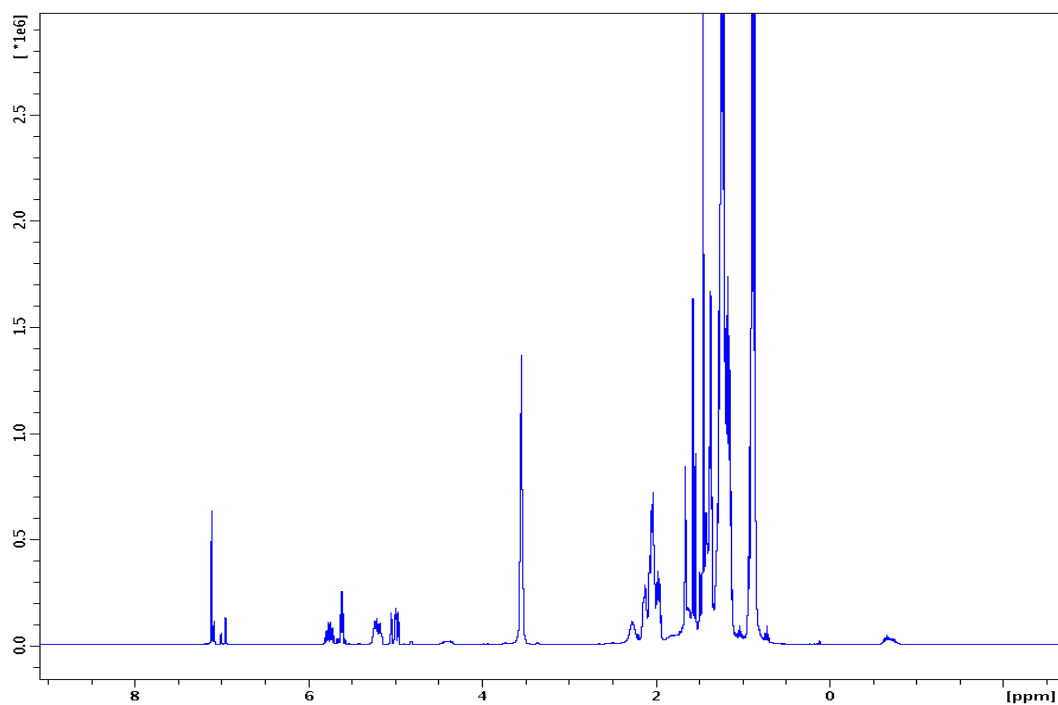


Figure S4.25. ^1H NMR of *c*-PenLi/THF complex toluene- d_8 solution with internal references at -35°C

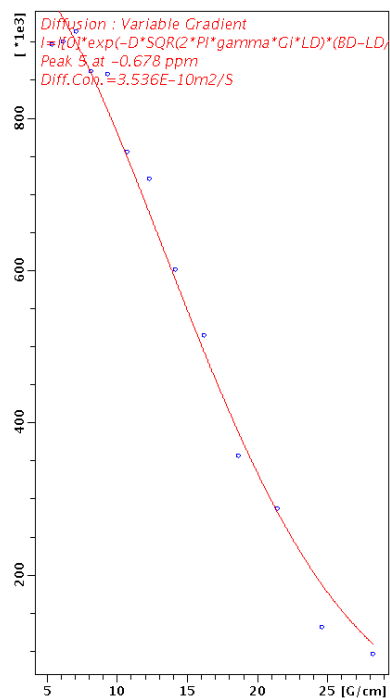


Figure S4.27. ¹H DOSY decay curves for *c*-PenLi/THF complex

Table S4.5. *D*-FW analysis of ¹H DOSY data of *c*-PenLi/THF complex toluene-*d*₈ solution at -35 °C

Compound	FW (g/mol)	10 ⁻¹⁰ <i>D</i> (m ² /s)	log FW	log <i>D</i>	Predicted FW (g/mol)	% error
BEN	78.11	12.41	1.893	-8.906	77.33	1.0
COE	110.2	9.54	2.042	-9.020	116.1	-5.3
TDE	196.4	7.10	2.293	-9.149	183.1	6.8
SQU	410.7	4.14	2.614	-9.383	422.4	-2.8
<i>c</i> -PenLi ^a	592.7 ^a	3.54	2.773	-9.451	539.6	9.2

^a592.7 gmol⁻¹ is the formula weight of (c-PenLi)₄(THF)₄ complex.

Appendix E

Supporting information for Chapter 5

Table of Contents

Figure S5.1. ¹ H NMR of <i>s</i> -BuLi toluene- <i>d</i> ₈ solution at -20 °C.....	329
Figure S5.2. ¹ H NMR of 650 μL <i>s</i> -BuLi toluene- <i>d</i> ₈ solution with 0.0263 g 1-dodecene at -15 °C.....	330
Figure S5.3. ¹ H NMR Simulated Spectrum by Lorentzian Deconvolution of 650 μL <i>s</i> -BuLi solution at -15 °C.....	330
Figure S5.4. ¹ H NMR of 650 μL <i>s</i> -BuLi toluene- <i>d</i> ₈ solution with 0.0263 g 1-dodecene at -20 °C.....	331
Figure S5.5. ¹ H NMR Simulated Spectrum by Lorentzian Deconvolution of 650 μL <i>s</i> -BuLi solution at -20 °C.....	331
Figure S5.6. ¹ H NMR of 650 μL <i>s</i> -BuLi toluene- <i>d</i> ₈ solution with 0.0263 g 1-dodecene at -25 °C.....	332
Figure S5.7. ¹ H NMR Simulated Spectrum by Lorentzian Deconvolution of 650 μL <i>s</i> -BuLi solution at -25 °C.....	332
Figure S5.8. ¹ H NMR of 650 μL <i>s</i> -BuLi toluene- <i>d</i> ₈ solution with 0.0263 g 1-dodecene at -30 °C.....	333
Figure S5.9. ¹ H NMR Simulated Spectrum by Lorentzian Deconvolution of 650 μL <i>s</i> -BuLi solution at -30 °C.....	333
Figure S5.10. ¹ H NMR of 650 μL <i>s</i> -BuLi toluene- <i>d</i> ₈ solution with 0.0263 g 1-dodecene at -35 °C.....	334
Figure S5.11. ¹ H NMR Simulated Spectrum by Lorentzian Deconvolution of 650 μL <i>s</i> -BuLi solution at -35 °C.....	334
Figure S5.12. ¹ H NMR of 650 μL <i>s</i> -BuLi toluene- <i>d</i> ₈ solution with 0.0263 g 1-dodecene at -40 °C.....	335
Figure S5.13. ¹ H NMR Simulated Spectrum by Lorentzian Deconvolution of 650 μL <i>s</i> -BuLi solution at -40 °C.....	335

°C.....	335
Figure S5.14. ¹ H NMR of 950 μL <i>s</i> -BuLi toluene- <i>d</i> ₈ solution with 0.0263 g 1-dodecene at -30 °C.....	336
Figure S5.15. ¹ H NMR Simulated Spectrum by Lorentzian Deconvolution of 950 μL <i>s</i> -BuLi solution at -30 °C.....	336
Figure S5.16. ¹ H NMR of 1.25 mL <i>s</i> -BuLi toluene- <i>d</i> ₈ solution with 0.0263 g 1-dodecene at -30 °C.....	337
Figure S5.17. ¹ H NMR Simulated Spectrum by Lorentzian Deconvolution of 1.25 mL <i>s</i> -BuLi solution at -30 °C.....	337
Figure S5.18. van 't Hoff Plot and Thermodynamic Data of Reaction (1)	340
Figure S5.19. ¹ H NMR of <i>s</i> -BuLi exposing in dioxygen atmosphere for 10 minutes at -20 °C.....	340
Figure S5.20. ¹ H NMR of 0.49 M <i>s</i> -BuLi solution with 2 μL <i>s</i> -BuOH was added at -20 °C.....	341
Figure S5.21. ¹ H NMR of 0.49 M <i>s</i> -BuLi solution with Internal References at -20 °C	341
Figure S5.22. ¹ H DOSY NMR of <i>s</i> -BuLi solution with Internal References at -20 °C	342
Figure S5.23. <i>D</i> -FW Analysis of ¹ H DOSY Data of <i>s</i> BuLi toluene- <i>d</i> ₈ solution at -20 °C	342
Figure S5.24. ¹ H DOSY Decay Curves for Internal References	343
Figure S5.25. ¹ H DOSY Decay Curves for <i>s</i> -BuLi and <i>s</i> -BuOLi.....	344
Figure S5.26. ¹ H NMR of <i>s</i> -BuLi toluene- <i>d</i> ₈ solution with 0.038 equivalent <i>s</i> -BuOLi at -20 °C.....	345
Figure S5.27. ¹ H NMR of <i>s</i> -BuLi toluene- <i>d</i> ₈ solution with 0.054 equivalent <i>s</i> -BuOLi at -20 °C.....	346
Figure S5.28. ¹ H NMR of <i>s</i> -BuLi toluene- <i>d</i> ₈ solution with 0.067 equivalent <i>s</i> -BuOLi at -20 °C.....	346
Figure S5.29. ¹ H NMR of <i>s</i> -BuLi toluene- <i>d</i> ₈ solution with 0.078 equivalent <i>s</i> -BuOLi at -20 °C.....	347
Figure S5.30. ¹ H NMR of <i>s</i> -BuOH Titration of <i>s</i> BuLi toluene- <i>d</i> ₈ solution at -20 °C.....	348
Figure S5.31. ¹ H NMR of <i>s</i> -BuOH Titration of <i>s</i> BuLi toluene- <i>d</i> ₈ solution at -20 °C (Enlarged).....	349
Figure S5.32. Variable temperature ¹ H NMR of 2:7 <i>s</i> -BuOLi to <i>s</i> -BuLi toluene- <i>d</i> ₈ solution at -20 °C.....	350
Figure S5.33. Variable temperature ¹ H NMR of 2:7 <i>s</i> -BuOLi to <i>s</i> -BuLi toluene- <i>d</i> ₈ solution at -20 °C.....	

(Enlarged).....	350
Figure S5.34. ¹ H NMR of 2:7 <i>s</i> -BuOLi to <i>s</i> -BuLi solution with Internal References at -20 °C.....	351
Figure S5.35. ¹ H DOSY NMR of 2:7 <i>s</i> -BuOLi to <i>s</i> -BuLi solution with Internal References at -20 °C.....	351
Figure S5.36. D-FW Analysis of ¹ H DOSY Data of <i>s</i> -BuLi toluene- <i>d</i> ₈ solution at -20 °C.....	352
Figure S5.37. ¹ H DOSY Decay Curves for Internal References.....	353
Figure S5.38. ¹ H DOSY Decay Curves for <i>s</i> -BuLi and <i>s</i> -BuOLi.....	354
Figure S5.39. ¹ H NMR of 0.49 M <i>s</i> -BuLi solution with Internal References at -20 °C.....	355
Figure S5.40. ¹ H DOSY NMR of <i>s</i> -BuLi solution with Internal References at -20 °C.....	355
Figure S5.41. D-FW Analysis of ¹ H DOSY Data of <i>s</i> -BuLi toluene- <i>d</i> ₈ solution at -20 °C.....	356
Figure S5.42. ¹ H DOSY Decay Curves for Internal References.....	357
Figure S5.43. ¹ H DOSY Decay Curves for <i>s</i> -BuLi and <i>s</i> -BuOLi.....	358
Table S5.1. Concentration <i>s</i> -BuLi in the 650 μL toluene- <i>d</i> ₈ solution with 0.0263 g 1-dodecene.....	338
Table S5.2. Ratio of Different Aggregates of <i>s</i> -BuLi in toluene- <i>d</i> ₈ at -30 °C.....	338
Table S5.3. Equilibrium Constant (K) of Reaction (1) in toluene- <i>d</i> ₈ at -30 °C.....	338
Table S5.4. Ratio of Different <i>s</i> -BuLi Aggregates as a Function of Temperature.....	339
Table S5.5. Concentration of Different <i>s</i> -BuLi Aggregates as a Function of Temperature.....	339
Table S5.6. D-FW Analysis of ¹ H DOSY data of <i>s</i> -BuLi toluene- <i>d</i> ₈ solution at -20 °C.....	345
Table S5.7. Determination of the Ratio of <i>s</i> -BuOLi to <i>s</i> -BuLi in the Mixed Hexamer.....	347
Table S5.8. D-FW Analysis of ¹ H DOSY data of <i>s</i> -BuLi toluene- <i>d</i> ₈ solution at -20 °C.....	352
Table S5.9. D-FW Analysis of ¹ H DOSY data of <i>s</i> -BuLi toluene- <i>d</i> ₈ solution at -20 °C.....	356

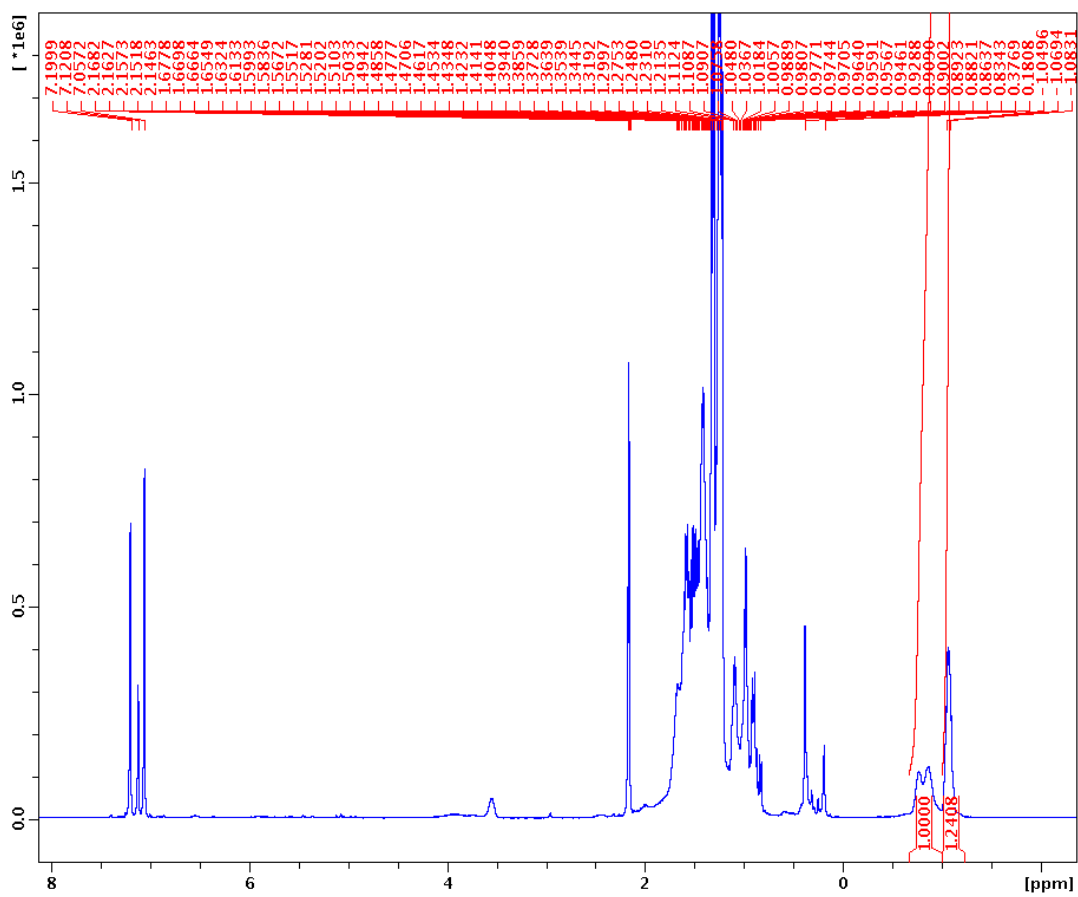
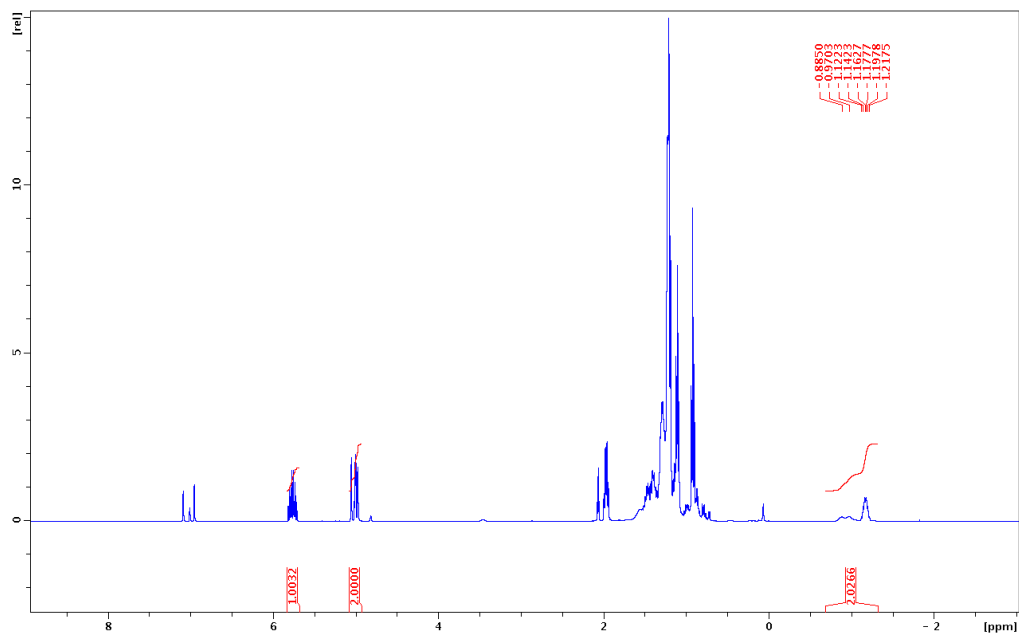


Figure S5.1. ^1H NMR of *s*-BuLi $\text{toluene-}d_8$ solution at $-20\text{ }^\circ\text{C}$



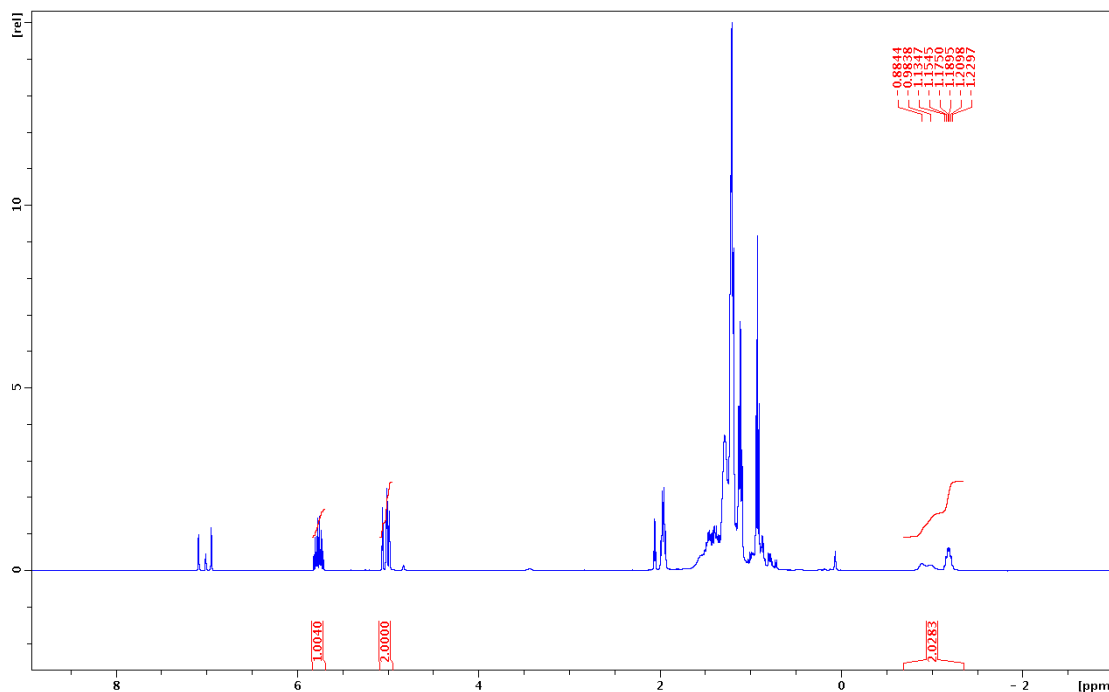


Figure S5.6. ^1H NMR of 650 μL *s*-BuLi toluene- d_8 solution with 0.0263 g 1-dodecene at $-25\text{ }^\circ\text{C}$

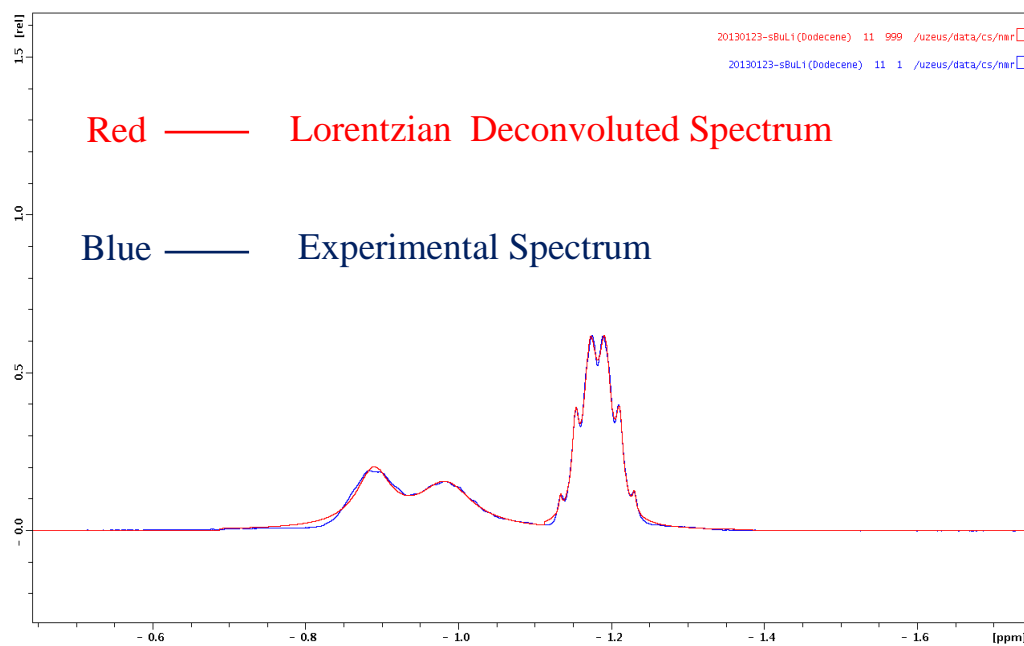


Figure S5.7. ^1H NMR Simulated Spectrum by Lorentz Deconvolution of 650 μL *s*-BuLi solution at $-25\text{ }^\circ\text{C}$

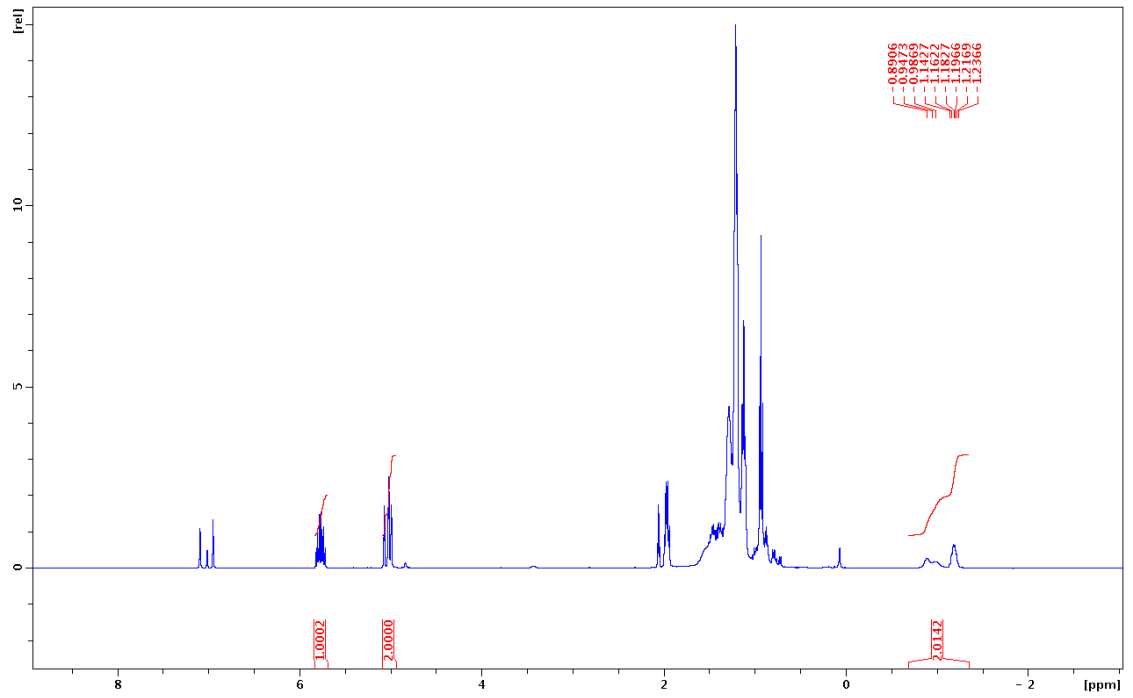


Figure S5.8. ^1H NMR of 650 μL *s*-BuLi toluene- d_8 solution with 0.0263 g 1-dodecene at $-30\text{ }^\circ\text{C}$

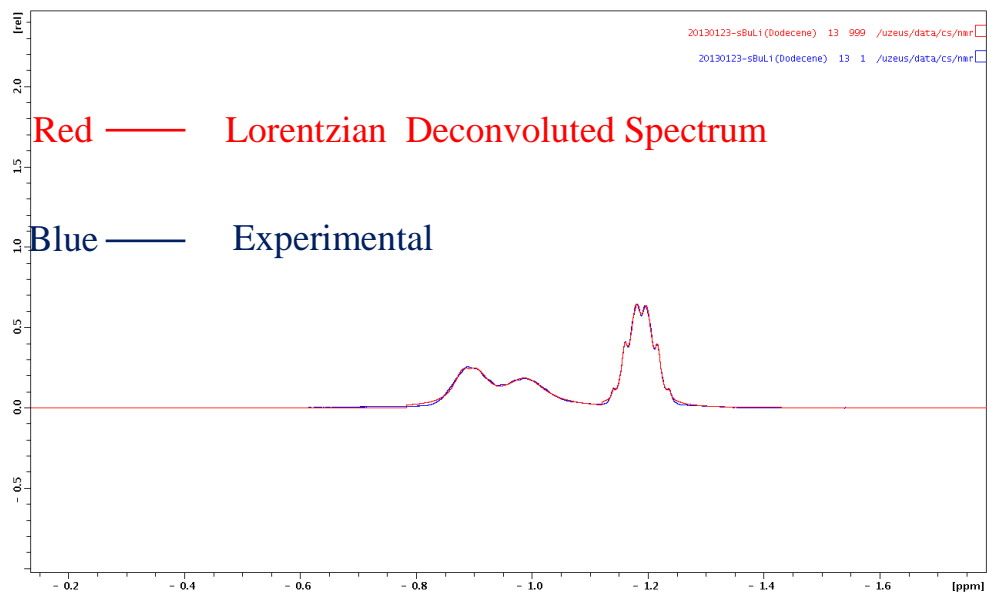


Figure S5.9. ^1H NMR Simulated Spectrum by Lorentz Deconvolution of 650 μL *s*-BuLi solution at $-30\text{ }^\circ\text{C}$

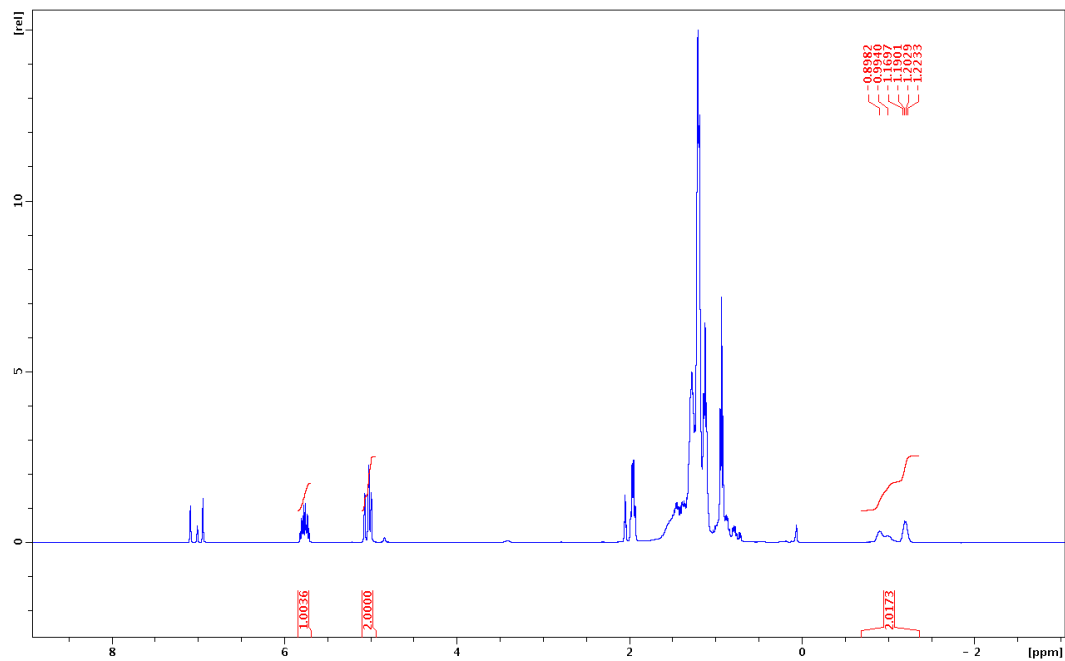


Figure S5.10. ^1H NMR of 650 μL *s*-BuLi toluene- d_8 solution with 0.0263 g 1-dodecene at $-35\text{ }^\circ\text{C}$

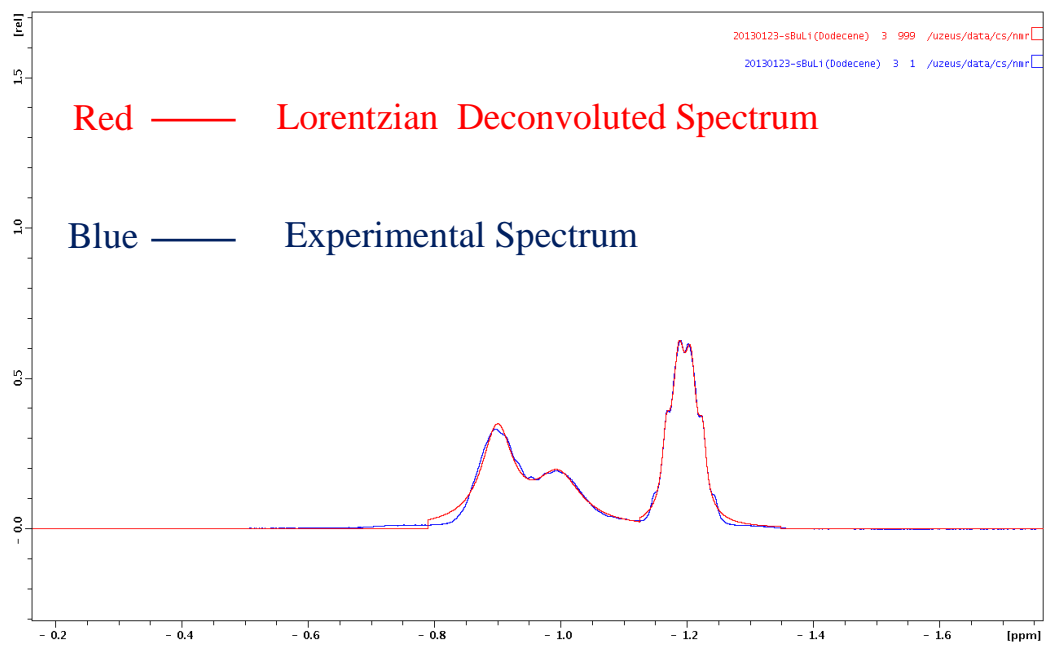


Figure S5.11. ^1H NMR Simulated Spectrum by Lorentz Deconvolution of 650 μL *s*-BuLi solution at $-35\text{ }^\circ\text{C}$

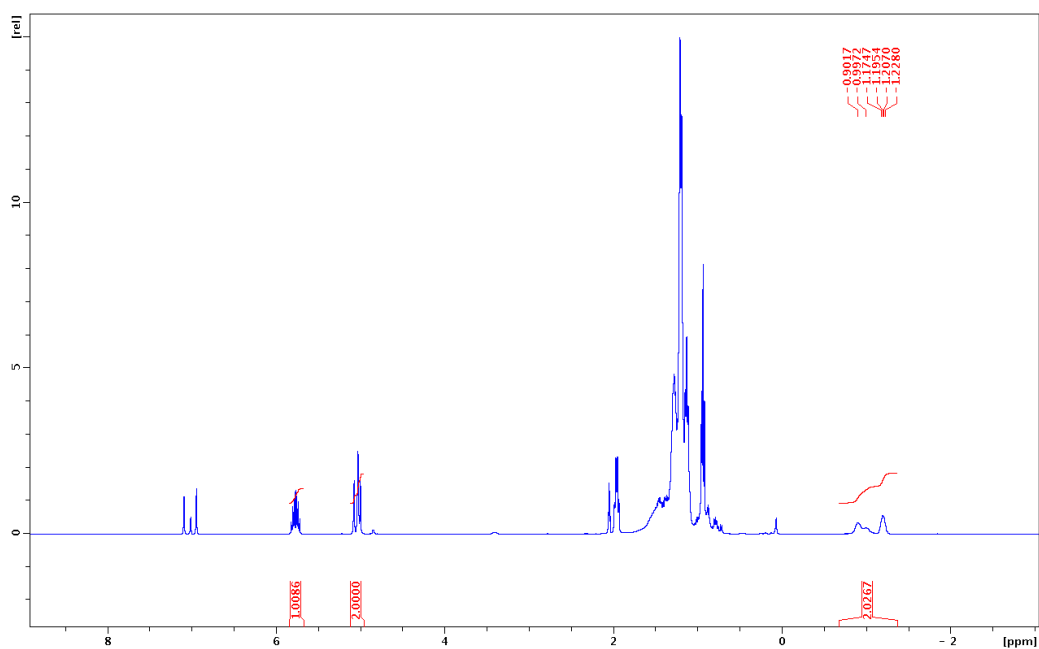


Figure S5.12. ^1H NMR of 650 μL *s*-BuLi toluene- d_8 solution with 0.0263 g 1-dodecene at $-40\text{ }^\circ\text{C}$

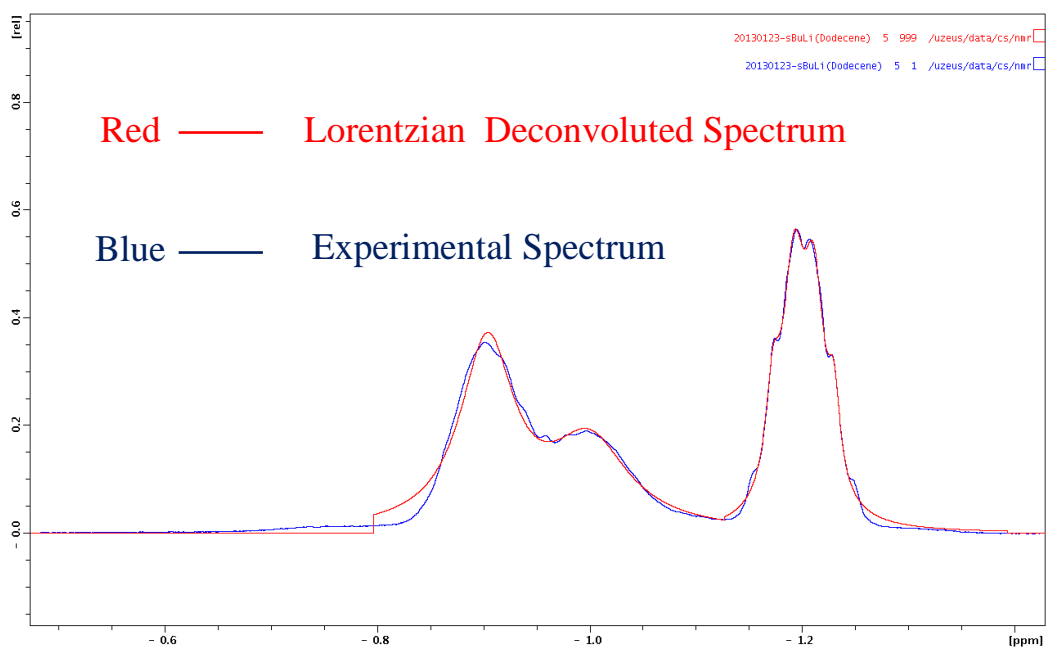


Figure S5.13. ^1H NMR Simulated Spectrum by Lorentz Deconvolution of 650 μL *s*-BuLi solution at $-40\text{ }^\circ\text{C}$

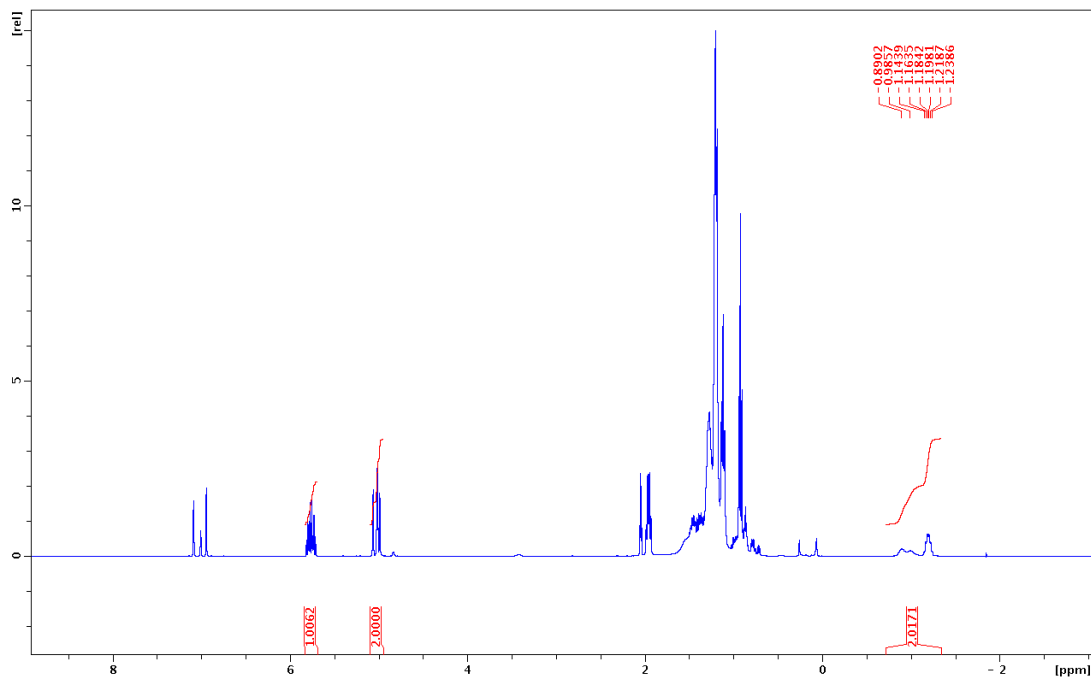


Figure S5.14. ^1H NMR of 950 μL *s*-BuLi toluene- d_8 solution with 0.0263 g 1-dodecene at $-30\text{ }^\circ\text{C}$

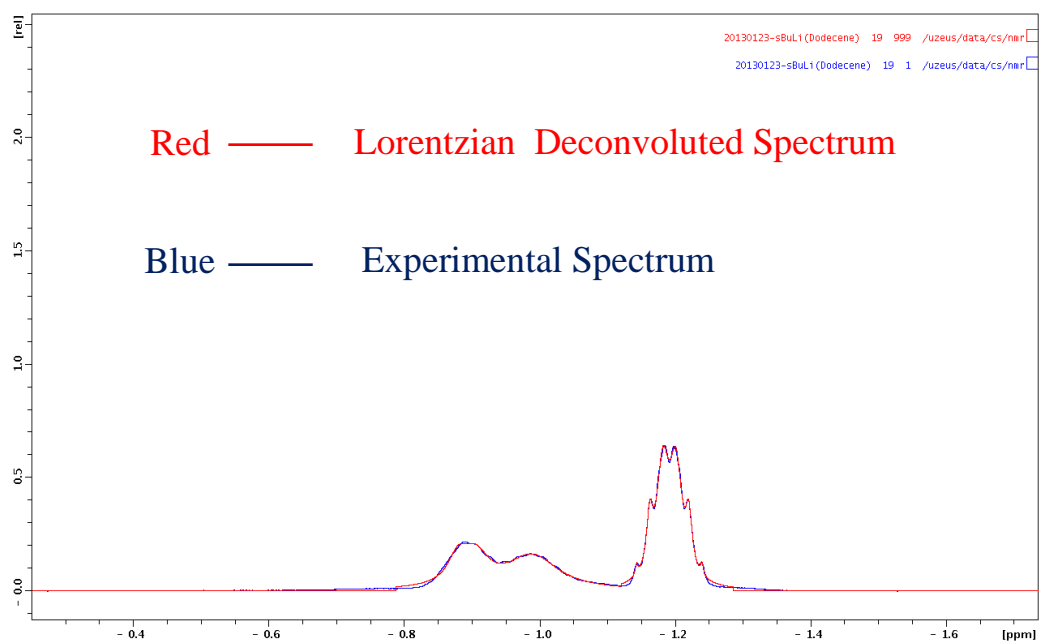


Figure S5.15. ^1H NMR Simulated Spectrum by Lorentz Deconvolution of 950 μL *s*-BuLi solution at $-30\text{ }^\circ\text{C}$

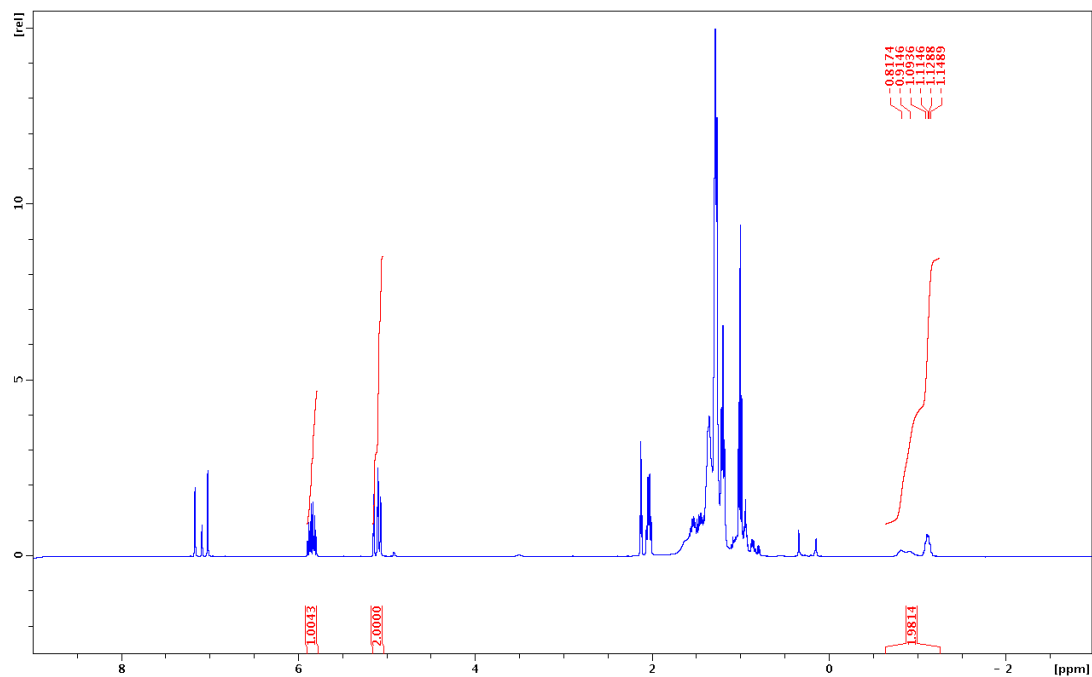


Figure S5.16. ^1H NMR of 1.25 mL *s*-BuLi toluene- d_8 solution with 0.0263 g 1-dodecene at $-30\text{ }^\circ\text{C}$

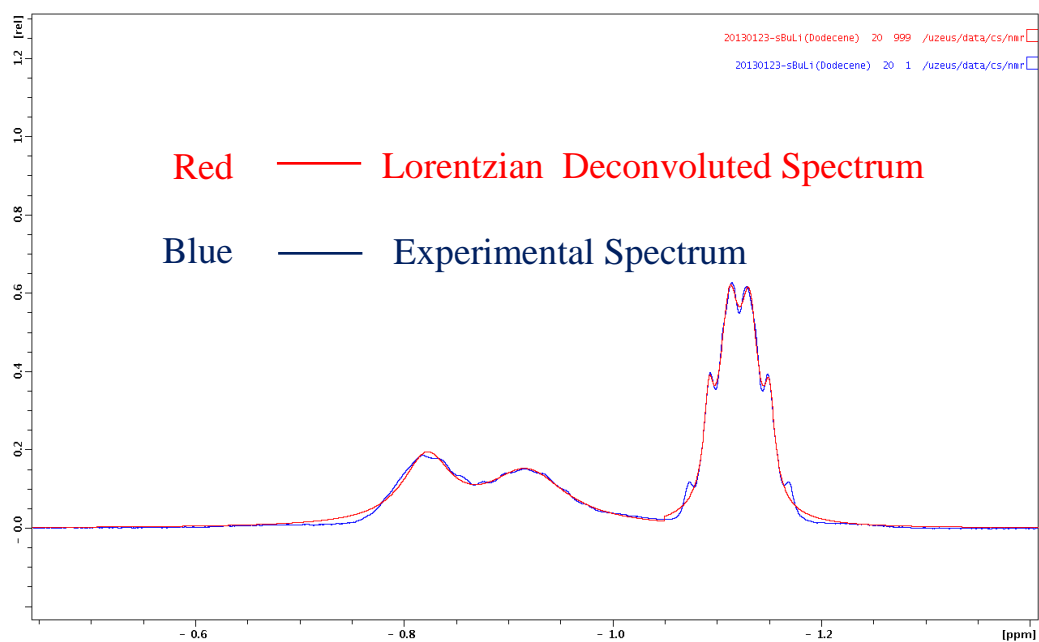


Figure S5.17. ^1H NMR Simulated Spectrum by Lorentz Deconvolution of 1.25 mL *s*-BuLi solution at $-30\text{ }^\circ\text{C}$

Table S5.1. Concentration *s*-BuLi in the 650 μ L toluene- d_8 solution with 0.0263 g 1-dodecene

Temperature / $^{\circ}$ C	Concentration of 1- dodecene ^a , C_1 / M	Ratio of <i>s</i> -BuLi to 1-dodecene (R)	Concentration of <i>s</i> -BuLi ^b , (R x C_1) / M
-15	0.240	2.0266	0.487166
-20	0.240	2.0451	0.491613
-25	0.240	2.0283	0.487575
-30	0.240	2.0142	0.484186
-35	0.240	2.0173	0.484931
-40	0.240	2.0267	0.48719
Average Concentration of <i>s</i> -BuLi / M			0.487
Standard Deviation of Concentration of <i>s</i> -BuLi / M			0.003

^aThe molar mass of 1-dodecene is 168.319 g mol^{-1} . ^bThe total concentration of *s*-BuLi was expressed as monomer units.

Table S5.2. Ratio of Different Aggregates of *s*-BuLi in toluene- d_8 at -30 $^{\circ}$ C

Volume / mL	Area of Peak ^a at - 0.88 ppm	Area of Peak ^a at - 0.97 ppm	Area of Peak ^a at - 1.16 ppm	Total Area	Proportion of Peak at -0.88 ppm	Proportion of Peak at -0.97 ppm	Proportion of Peak at - 1.16 ppm
0.650	55.7	62.0	120.4	238.1	0.234	0.260	0.506
0.950	45.5	59.3	119.0	223.8	0.203	0.265	0.532
1.250	41.4	55.4	115.2	212.1	0.195	0.261	0.543

^aThe area was determined by Lorentz deconvolution.

Table S5.3. Equilibrium Constant (K) of Reaction (1) in toluene- d_8 at -30 $^{\circ}$ C

Vol. (mL)	Conc. of <i>s</i> -BuLi ^a , C_s (M)	Conc. of <i>s</i> - BuLi ^b at - 0.88 ppm, C_1 (M)	Conc. of <i>s</i> - BuLi ^b at - 0.97 ppm, C_2 (M)	Conc. of <i>s</i> - BuLi ^b at - 1.16 ppm, C_3 (M)	Conc. of Hexamer = $C_1/6$, C_H (M)	Conc. of Tetramer = $C_2/4$, C_T (M)	K = C_H^2/C_T^3 (M^{-1})
0.650	0.487	0.114	0.127	0.246	0.019	0.062	1.54
0.950	0.332	0.067	0.088	0.176	0.011	0.044	1.47
1.250	0.278	0.048	0.065	0.135	0.008	0.034	1.71

^aThe total concentration of *s*-BuLi was calculated by comparing the integrations of *s*-BuLi and 1-dodecene and was expressed as monomer units. ^bThe concentration was expressed as monomer units and calculated by multiplying proportion of the peak by total concentration.

Table S5.4. Ratio of Different *s*BuLi Aggregates as a Function of Temperature

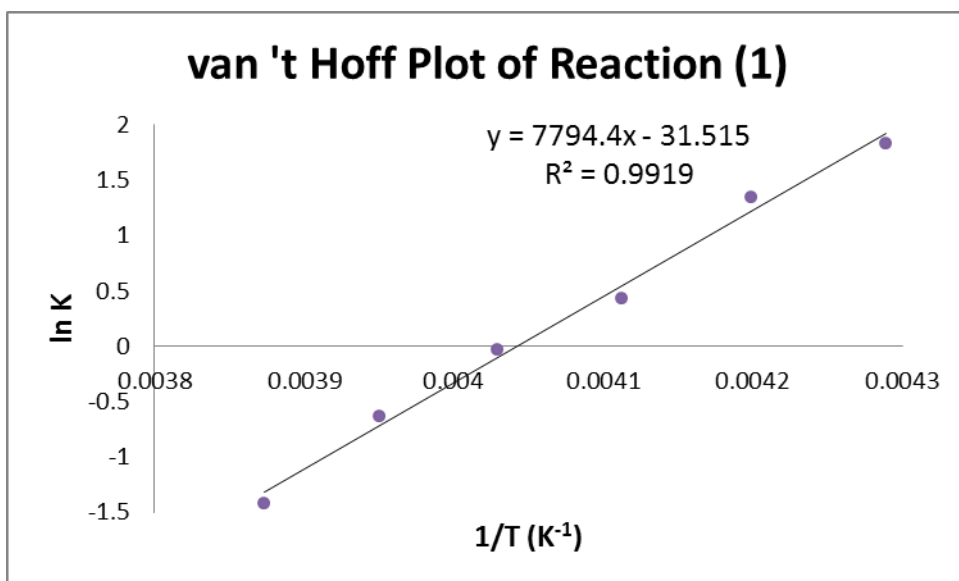
Temp. / °C	Area of Peak ^a at -0.88 ppm	Area of Peak ^a at -0.97 ppm	Area of Peak ^a at -1.16 ppm	Total Area	Proportion of Peak at -0.88 ppm	Proportion of Peak at -0.97 ppm	Proportion of Peak at -1.16 ppm
-15	25.0	55.7	124.8	205.4	0.122	0.271	0.607
-20	34.2	53.7	118.7	206.6	0.166	0.260	0.575
-25	42.6	52.2	112.1	206.9	0.206	0.252	0.542
-30	55.7	62.0	120.4	238.1	0.234	0.260	0.506
-35	82.9	63.0	120.3	266.3	0.311	0.237	0.451
-40	91.5	61.8	108.7	262.0	0.349	0.236	0.415

^aThe area was determined by Lorentz deconvolution.

Table S5.5. Concentration of Different *s*-BuLi Aggregates as a Function of Temperature

Temp. (°C)	1/T (K ⁻¹)	Conc. of <i>s</i> -BuLi ^a at -0.88 ppm, C ₁ (M)	Conc. of <i>s</i> -BuLi ^a at -0.97 ppm, C ₂ (M)	Conc. of <i>s</i> -BuLi ^a at -1.16 ppm, C ₃ (M)	Conc. of Hexamer = C ₁ /6, C _H (M)	Conc. of Tetramer = C ₂ /4, C _T (M)	K = C _H ² /C _T ³ (M ⁻¹)	ln K
-15	0.00387	0.059	0.132	0.296	0.0099	0.0740	0.241	-1.422
-20	0.00395	0.081	0.127	0.280	0.0135	0.0700	0.528	-0.638
-25	0.00403	0.100	0.123	0.264	0.0167	0.0660	0.972	-0.028
-30	0.00411	0.114	0.127	0.246	0.0190	0.0616	1.543	0.434
-35	0.00420	0.152	0.115	0.220	0.0253	0.0550	3.841	1.346
-40	0.00429	0.170	0.115	0.202	0.0283	0.0505	6.234	1.830

^aThe concentration was expressed as monomer units and calculated by multiplying proportion of the peak by total concentration (0.487 M).



$$\Delta H = -7794.4 \times 8.314 \text{ Jmol}^{-1} = -64.8 \text{ kJmol}^{-1}$$

$$\Delta S = -31.515 \times 8.314 \text{ Jmol}^{-1}\text{K}^{-1} = -262 \text{ Jmol}^{-1}\text{K}^{-1}$$

Figure S5.18. van 't Hoff Plot and Thermodynamic Data of Reaction (1)

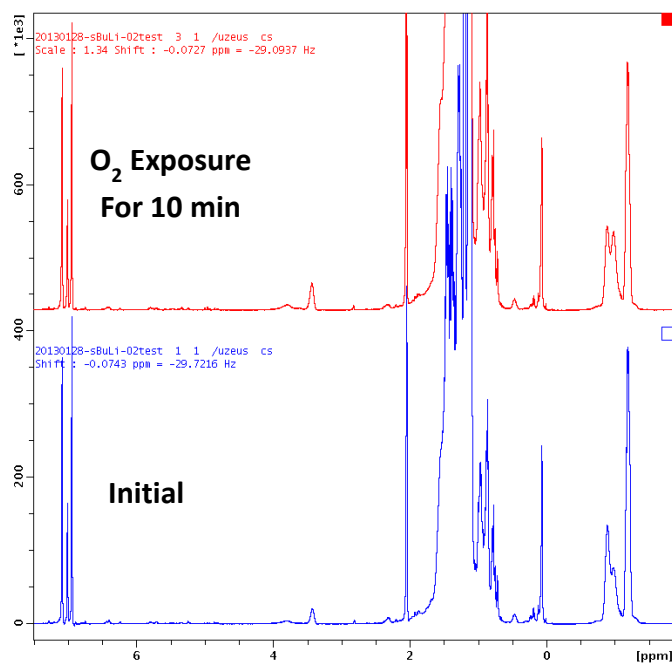


Figure S5.19. ¹H NMR of *s*-BuLi exposing in dioxygen atmosphere for 10 minutes at -20 °C

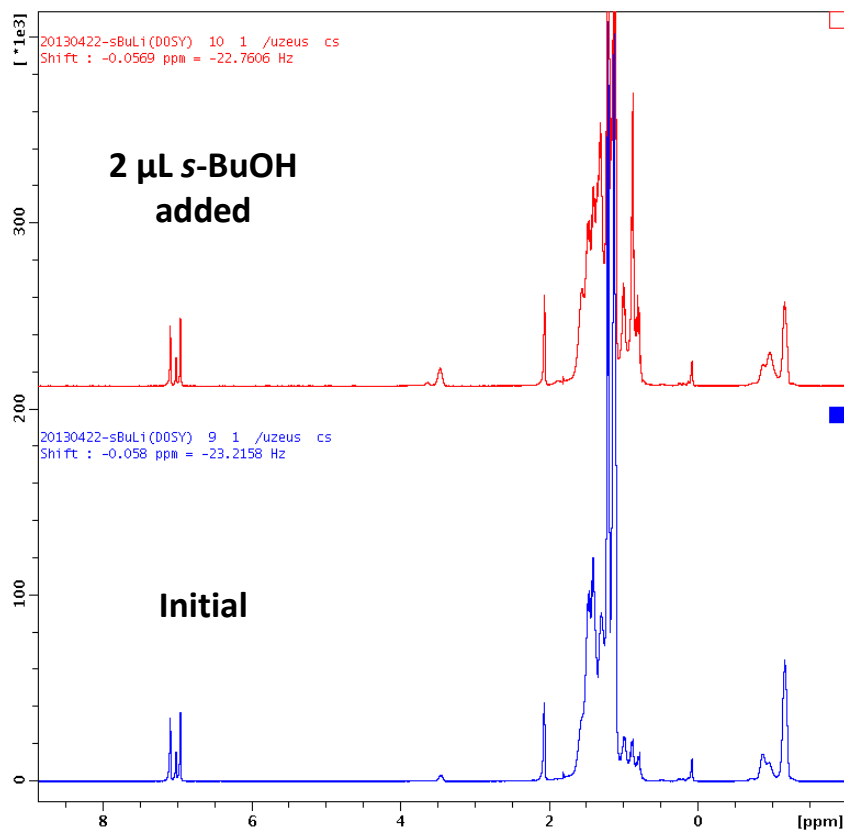


Figure S5.20. ^1H NMR of 0.49 M *s*-BuLi solution with 2 μL *s*-BuOH was added at $-20\text{ }^\circ\text{C}$

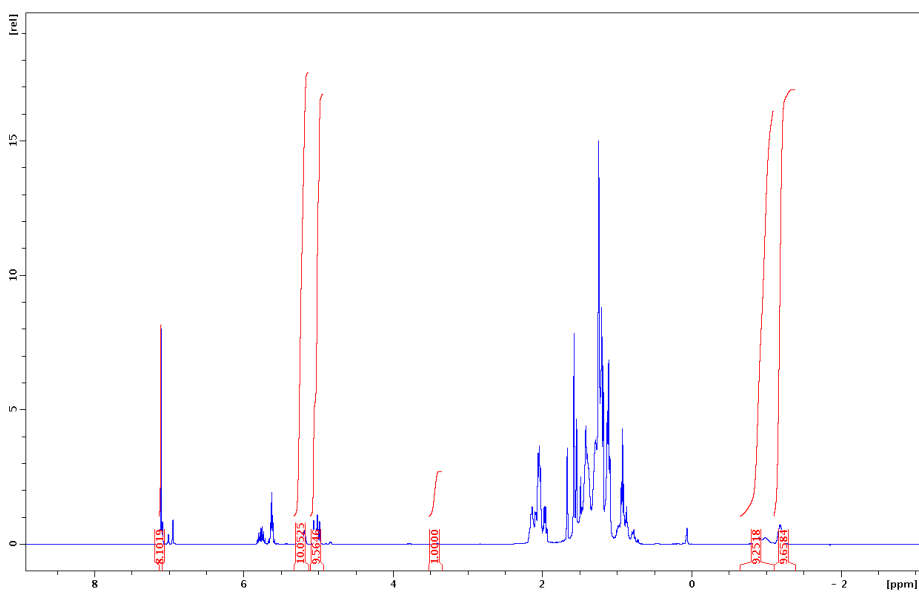


Figure S5.21. ^1H NMR of 0.49 M *s*-BuLi solution with Internal References at $-20\text{ }^\circ\text{C}$

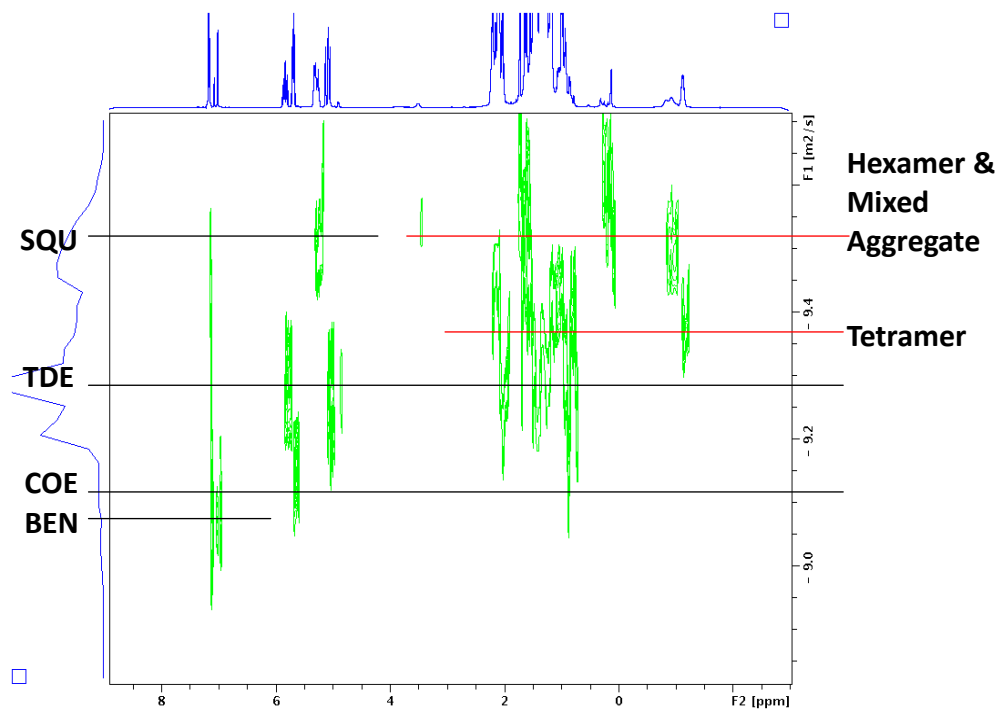


Figure S5.22. ¹H DOSY NMR of *s*-BuLi solution with Internal References at -20 °C

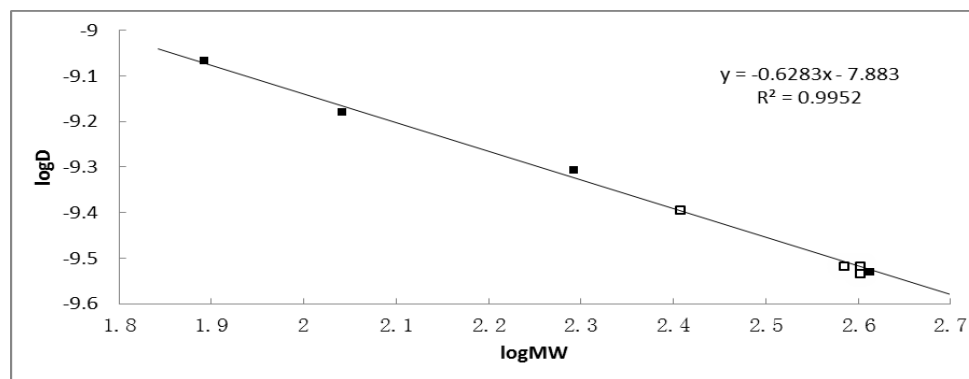


Figure S5.23. D-FW Analysis of ¹H DOSY Data of *s*-BuLi toluene-*d*₈ solution at -20 °C, Reference Compounds are Shown as Solid Squares, *s*-BuLi and *s*-BuOLi are Shown as Open Squares

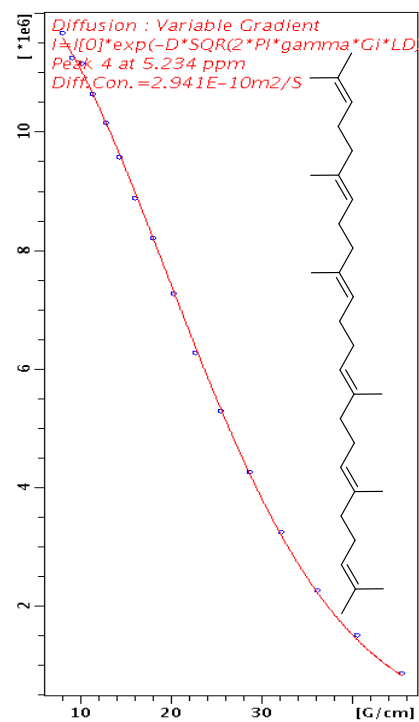
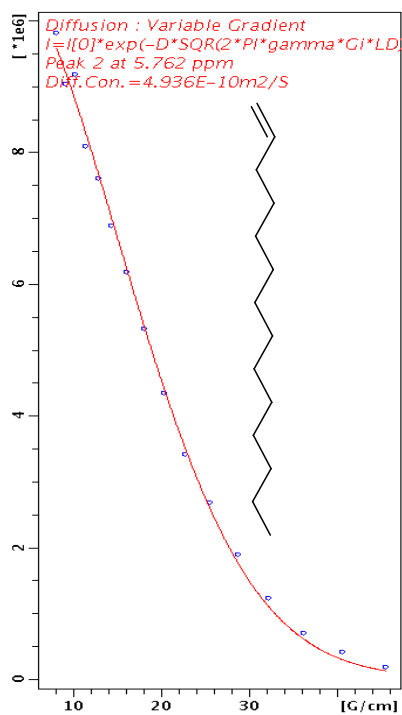
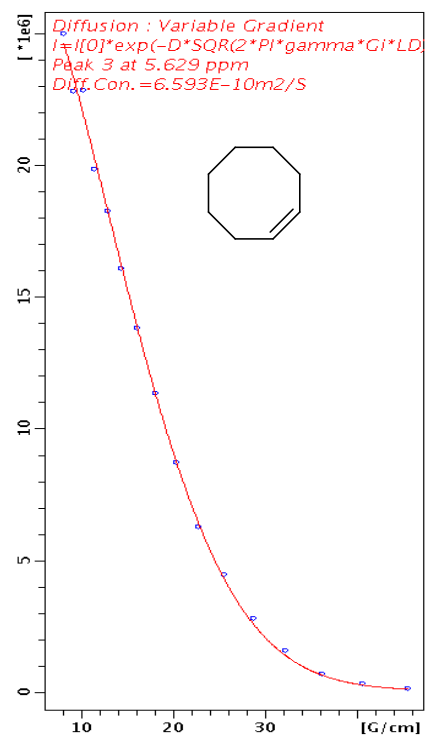
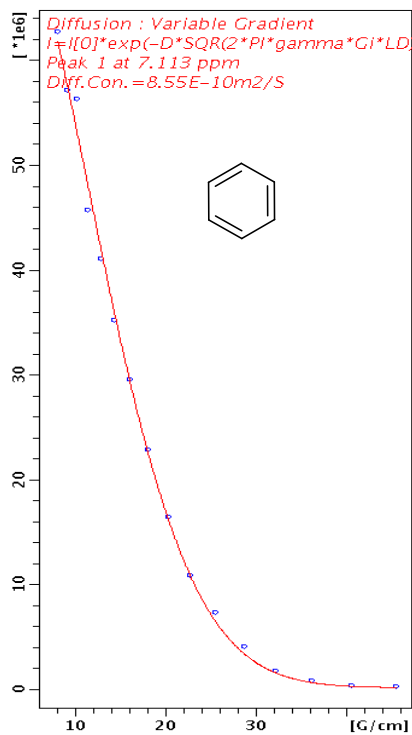


Figure S5.24. ^1H DOSY Decay Curves for Internal References (BEN, COE, TDE, SQU)

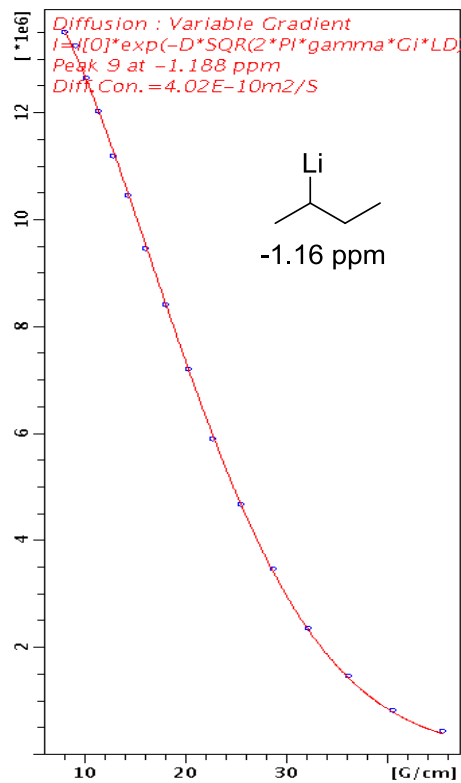
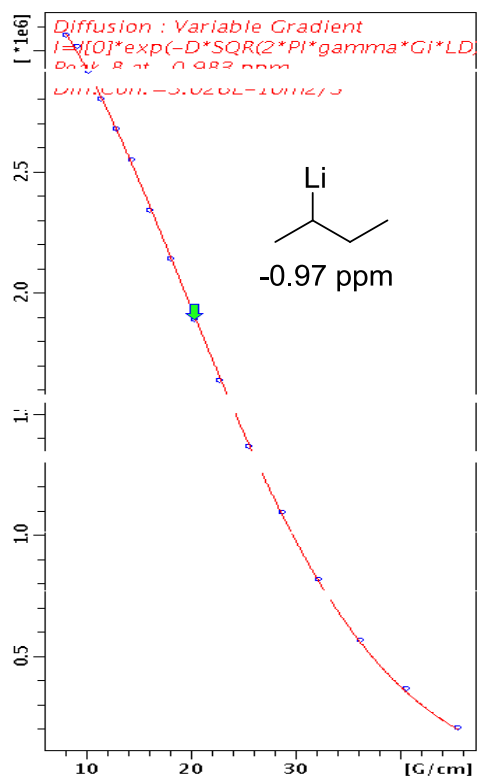
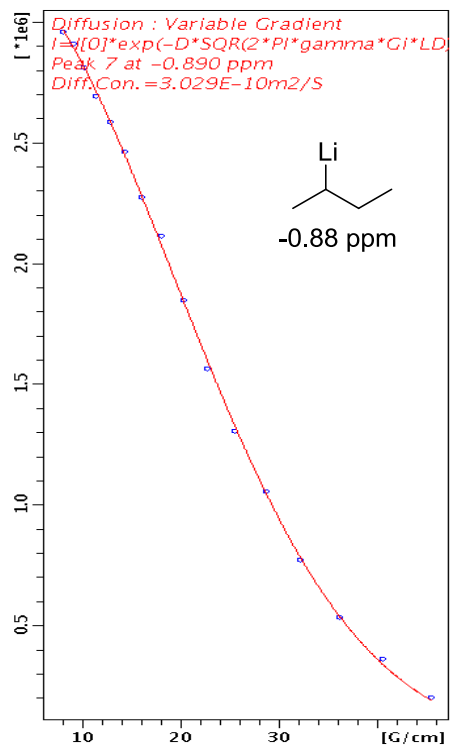
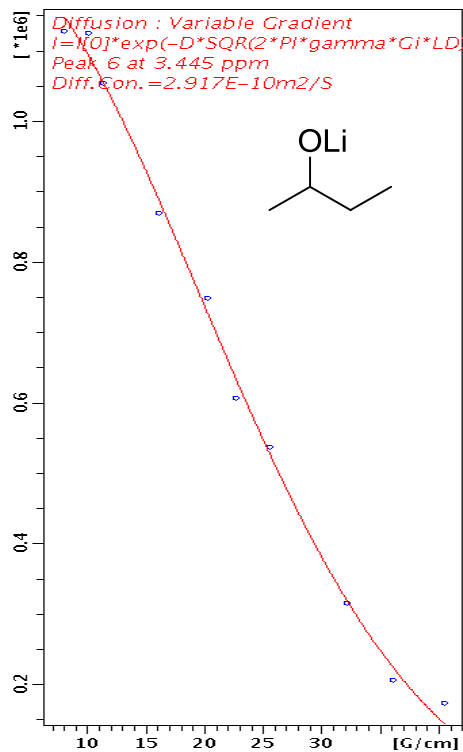


Figure S5.25. ¹H DOSY Decay Curves for *s*-BuLi and *s*-BuOLi

Table S5.6. *D*-FW Analysis of ^1H DOSY data of *s*-BuLi toluene- d_8 solution at $-20\text{ }^\circ\text{C}$

Compound	FW (g/mol)	$10^{-10}D$ (m^2/s)	log FW	log <i>D</i>	Predicted FW (g/mol)	% error
BEN	78.11	8.550	1.893	-9.068	76.93	1.5
COE	110.2	6.593	2.042	-9.181	116.4	-5.6
TDE	196.4	4.936	2.293	-9.307	184.4	6.1
SQU	410.7	2.941	2.614	-9.532	420.5	-2.4
<i>s</i> -BuOLi ^a (resonance at 3.44 ppm)	400.3 ^a	2.917	2.602	-9.535	426.0	-6.4
<i>s</i> -BuLi ^b (resonance at - 0.88 ppm)	384.4 ^b	3.029	2.585	-9.519	401.2	-4.4
<i>s</i> -BuLi ^a (resonance at - 0.97 ppm)	400.3 ^a	3.026	2.602	-9.519	401.9	-0.39
<i>s</i> -BuLi ^c (resonance at - 1.16 ppm)	256.2 ^c	4.020	2.409	-9.396	255.7	0.2

^aThe formula weight 400.3 gmol^{-1} was calculated as 1 : 5 *s*BuOLi to *s*BuLi mixed hexamer.. ^bThe formula weight 384.4 gmol^{-1} was calculated as *s*BuLi hexamer. ^cThe formula weight 256.2 gmol^{-1} was calculated as *s*BuLi tetramer.

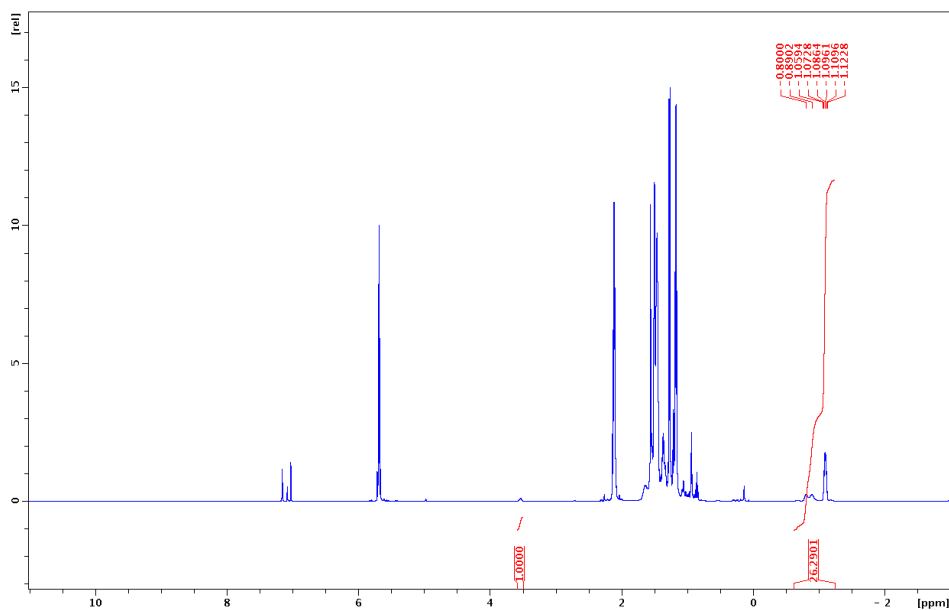


Figure S5.26. ^1H NMR of *s*-BuLi toluene- d_8 solution with 0.038 equivalent *s*-BuOLi at $-20\text{ }^\circ\text{C}$

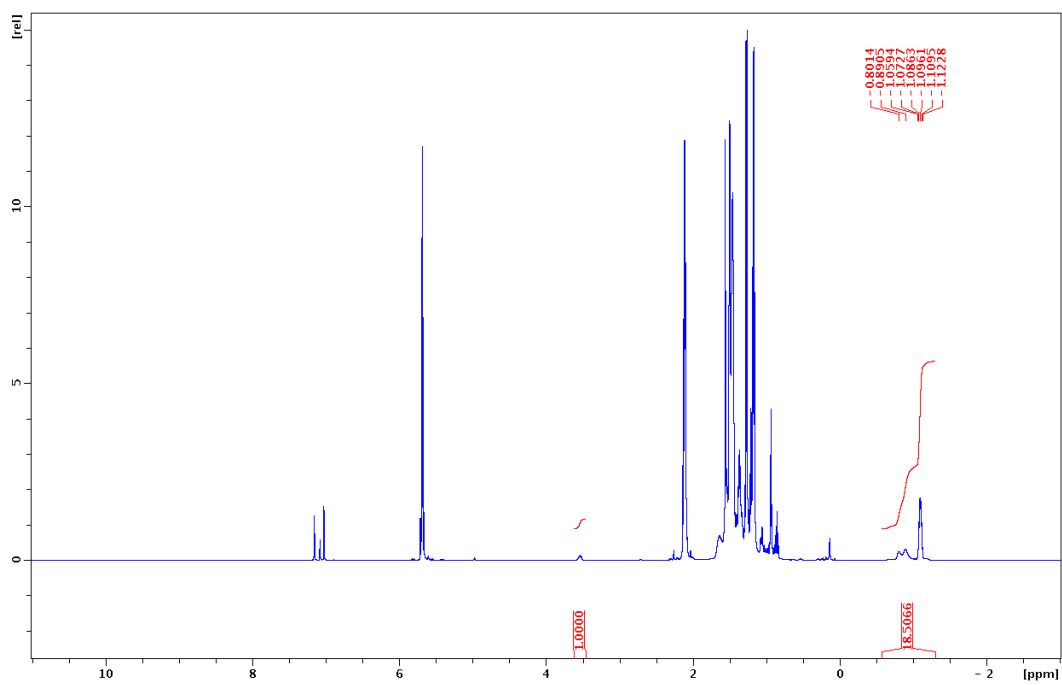


Figure S5.27. ^1H NMR of *s*-BuLi $\text{toluene-}d_8$ solution with 0.054 equivalent *s*-BuOLi at $-20\text{ }^\circ\text{C}$

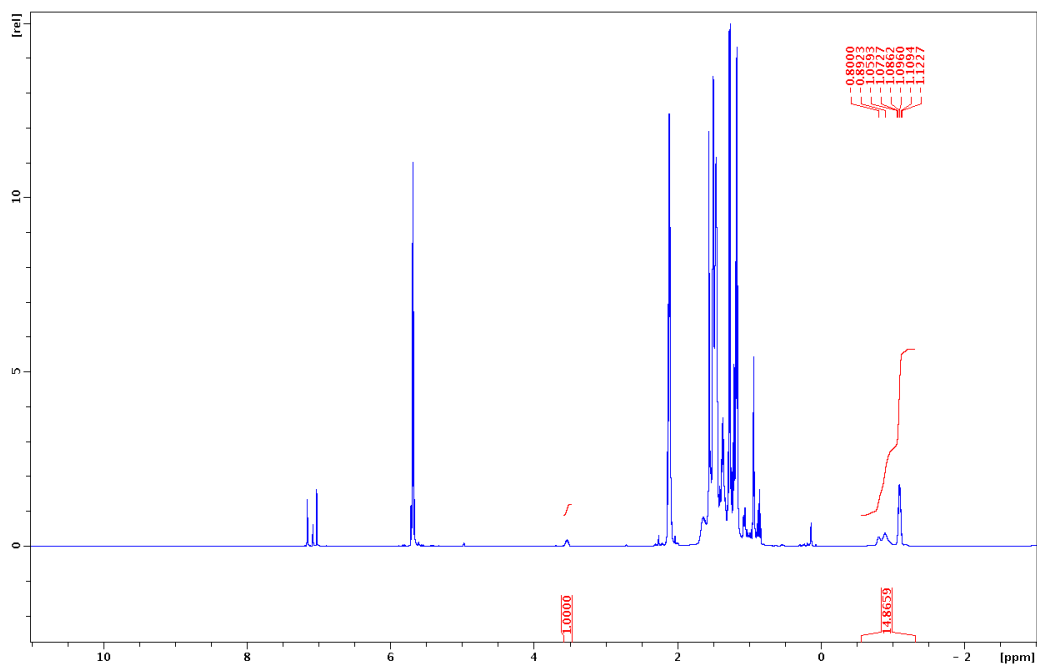


Figure S5.28. ^1H NMR of *s*-BuLi $\text{toluene-}d_8$ solution with 0.067 equivalent *s*-BuOLi at $-20\text{ }^\circ\text{C}$

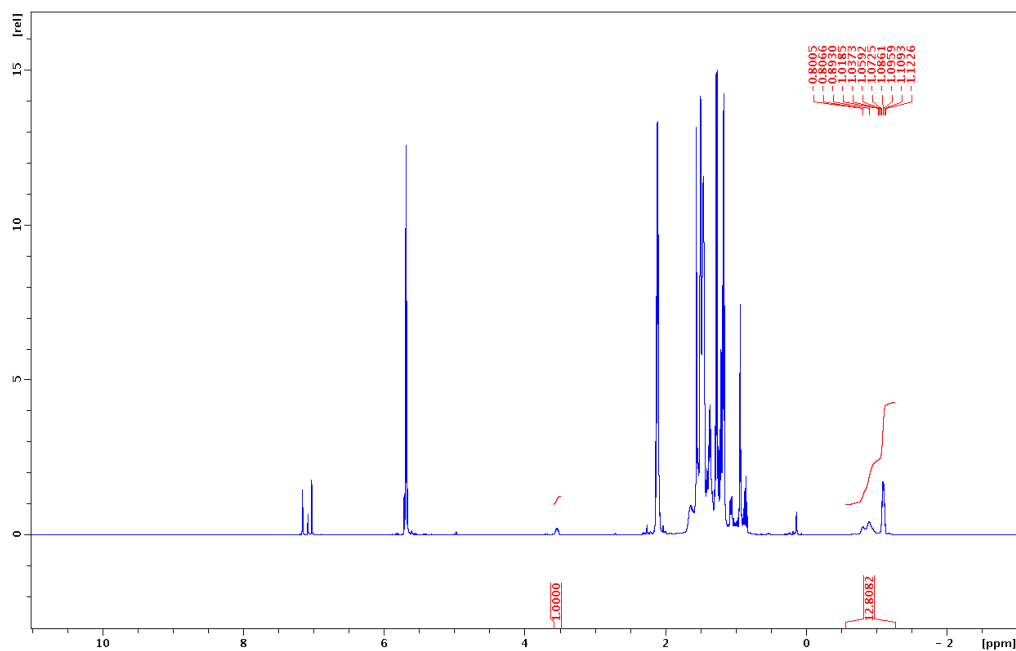


Figure S5.29. ^1H NMR of *s*-BuLi toluene- d_8 solution with 0.078 equivalent *s*-BuOLi at $-20\text{ }^\circ\text{C}$

Table S5.7. Determination of the Ratio of *s*-BuOLi to *s*-BuLi in the Mixed Hexamer

<i>s</i> -BuOLi : <i>s</i> -BuLi (total) ^a	Area of Peak ^b at -0.88 ppm	Area of Peak ^b at -0.97 ppm	Area of Peak ^b at -1.16 ppm	Total Area	Proportion of <i>s</i> -BuLi in the mixed hexamer	<i>s</i> -BuOLi : <i>s</i> -BuLi ^c in the mixed hexamer
1 : 26.29	72.34	118.5	360.7	551.6	0.215	1 : 5.65
1 : 18.51	65.81	162.7	358.6	587.1	0.277	1 : 5.13
1 : 14.87	60.39	211.6	361.5	633.4	0.334	1 : 4.97
1 : 12.81	48.04	252.5	350.2	650.7	0.388	1 : 4.97

^aThe ratio of *s*-BuOLi (monomer units) to all the *s*-BuLi (monomer units) in the solution. ^bThe area was determined by Lorentz deconvolution. ^cThe ratio of *s*-BuOLi (monomer units) to *s*-BuLi (monomer units) in the mixed hexamer only.

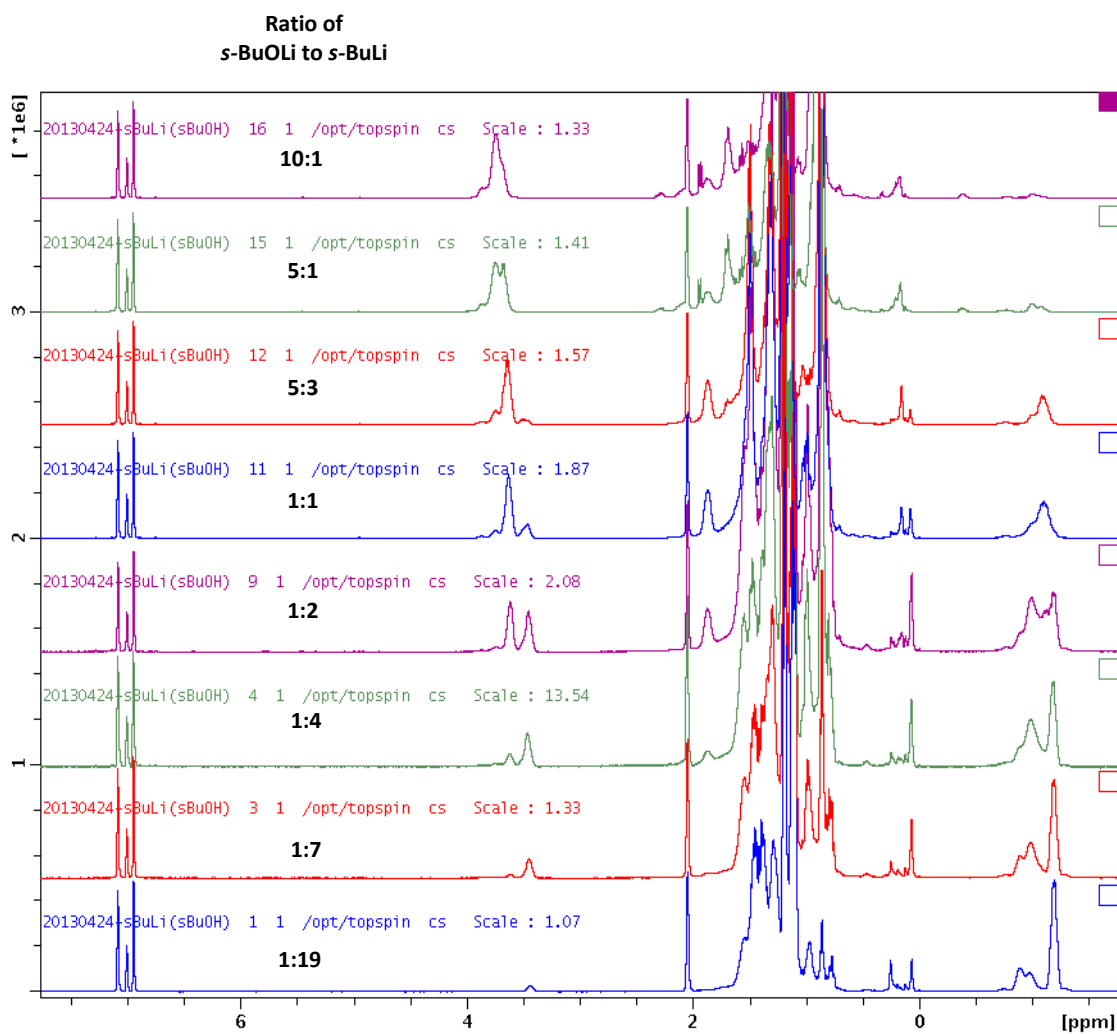


Figure S5.30. ^1H NMR of *s*-BuOH Titration of *s*-BuLi toluene- d_8 solution at $-20\text{ }^\circ\text{C}$

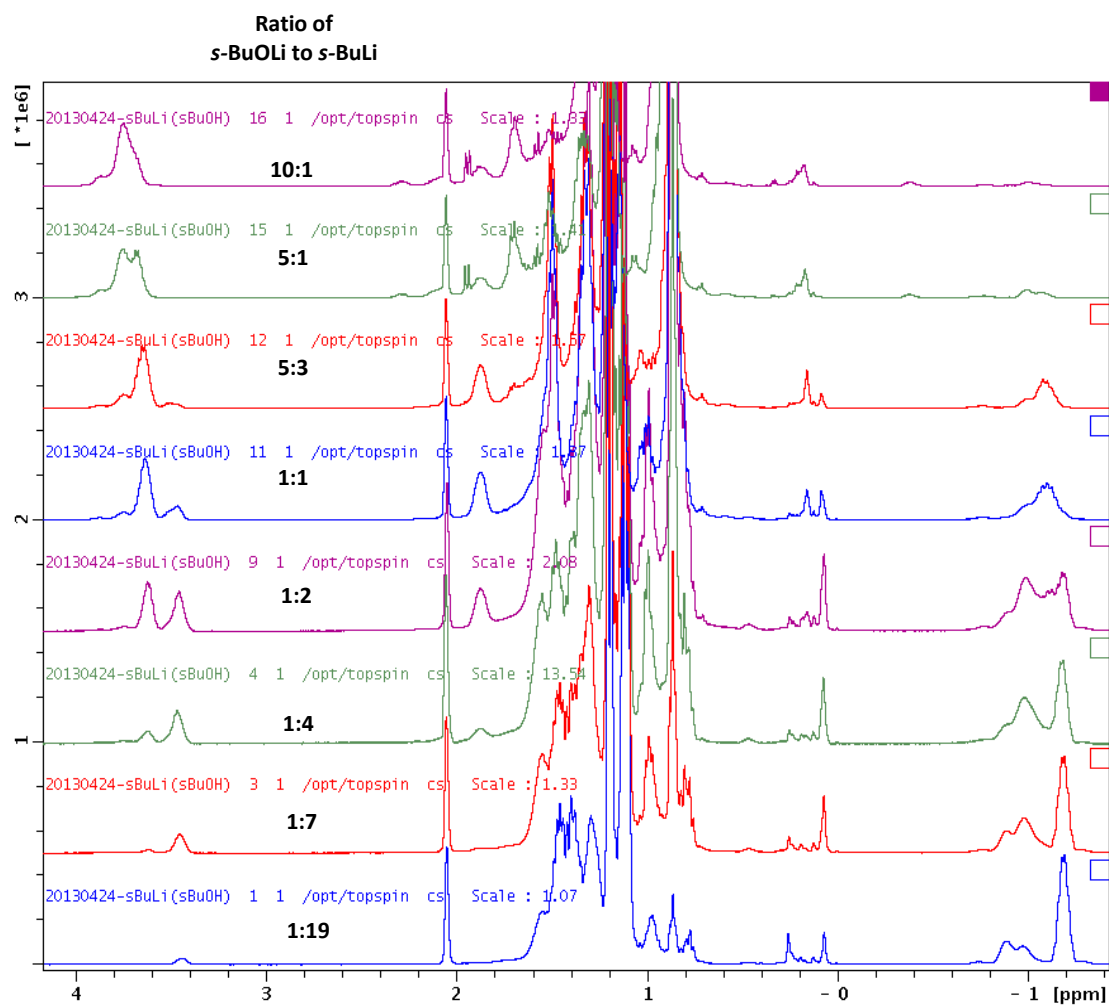


Figure S5.31. ^1H NMR of *s*-BuOH Titration of *s*-BuLi toluene- d_8 solution at $-20\text{ }^\circ\text{C}$ (Enlarged Region)

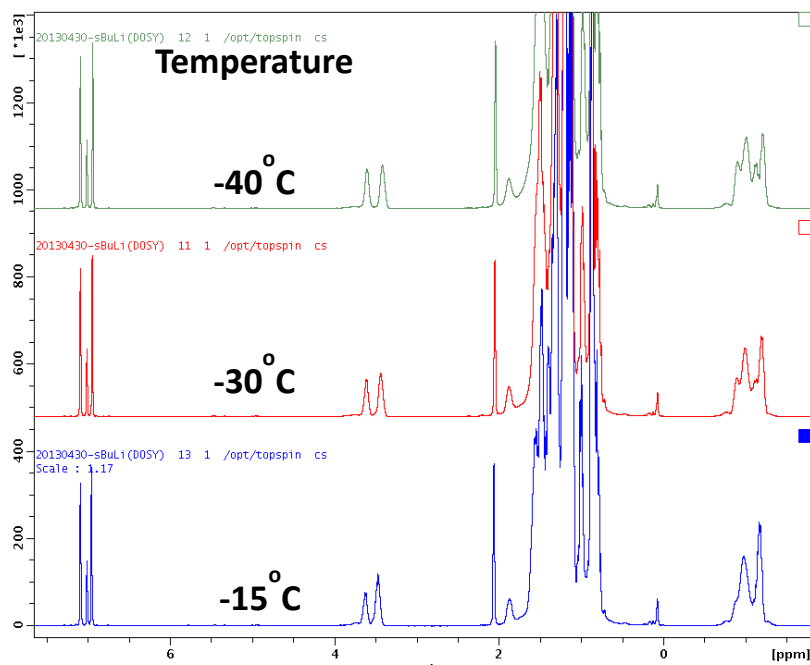


Figure S5.32. Variable temperature ¹H NMR of 2:7 *s*-BuOLi to *s*-BuLi toluene-*d*₈ solution at -20 °C

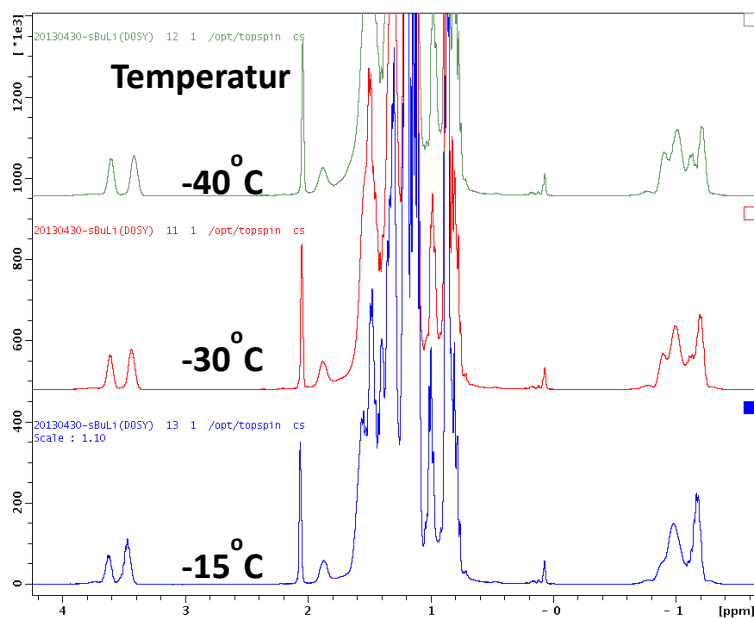


Figure S5.33. Variable temperature ¹H NMR of 2:7 *s*-BuOLi to *s*-BuLi toluene-*d*₈ solution at -20 °C (Enlarged Region)

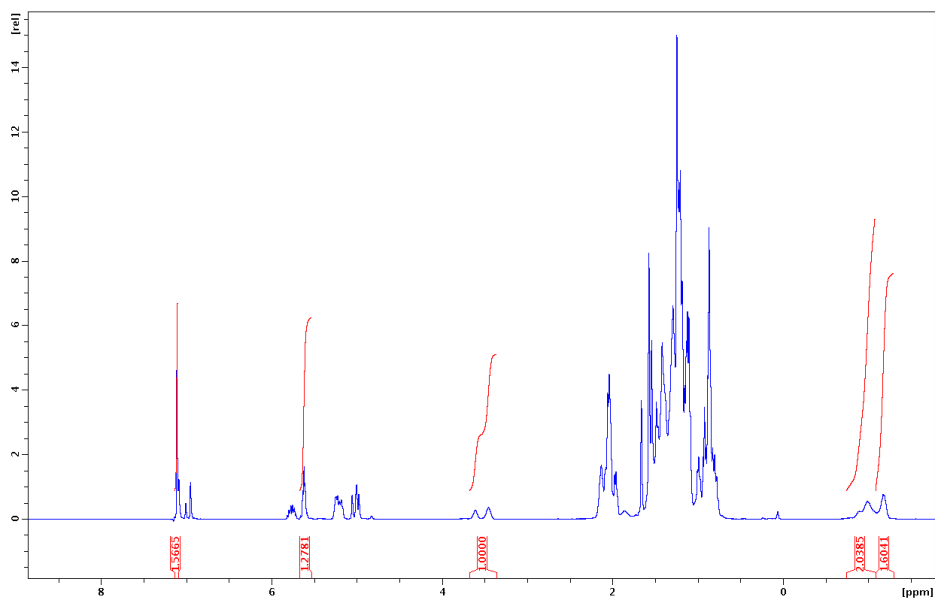


Figure S5.34. ^1H NMR of 2 : 7 *s*-BuOLi to *s*-BuLi solution with Internal References at $-20\text{ }^\circ\text{C}$

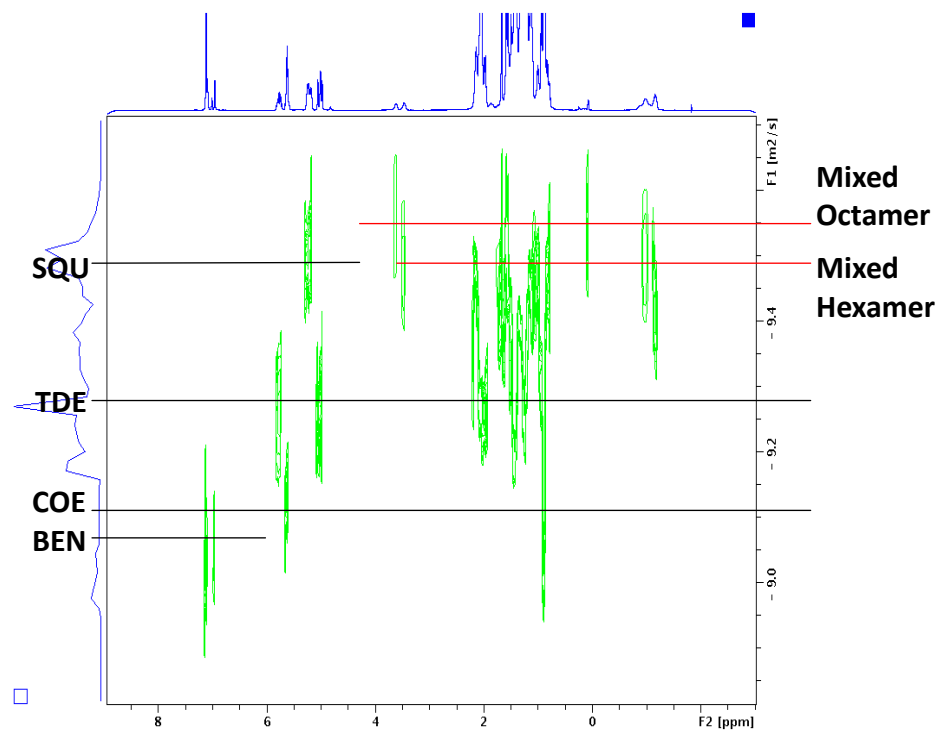


Figure S5.35. ^1H DOSY NMR of 2:7 *s*-BuOLi to *s*-BuLi solution with Internal References at $-20\text{ }^\circ\text{C}$

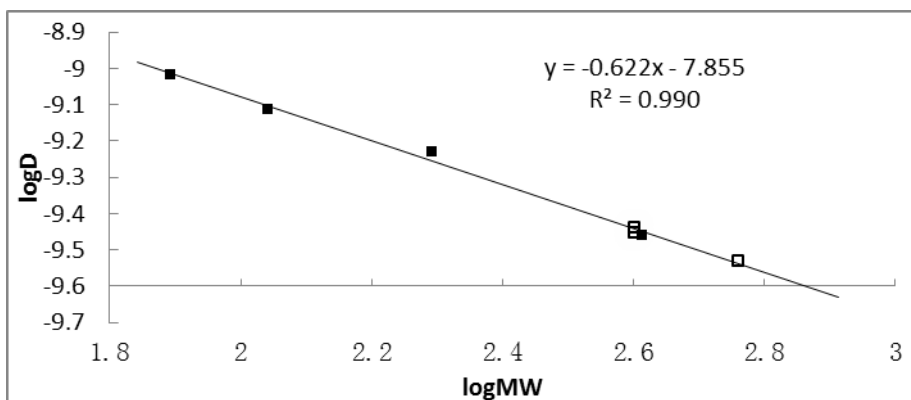


Figure S5.36. *D*-FW Analysis of ^1H DOSY Data of 2:7 *s*-BuOLi to *s*-BuLi solution at $-20\text{ }^\circ\text{C}$, Reference Compounds are Shown as Solid Squares, *s*-BuLi and *s*-BuOLi are Shown as Open Squares

Table S5.8. *D*-FW Analysis of ^1H DOSY data of *s*-BuLi toluene- d_8 solution at $-20\text{ }^\circ\text{C}$

Compound	FW (g/mol)	$10^{-10}D$ (m^2/s)	log FW	log <i>D</i>	Predicted FW (g/mol)	% error
BEN	78.11	9.622	1.893	-9.016	79.05	-1.2
COE	110.2	7.701	2.042	-9.113	114.3	-3.7
TDE	196.4	5.866	2.293	-9.232	179.2	8.7
SQU	410.7	3.462	2.614	-9.461	428.9	-4.4
<i>s</i> -BuOLi (resonance at 3.63 ppm)	576.4 ^a 544.4 ^b	2.942	2.761 ^a 2.736 ^b	-9.531	561.4	2.6 ^a -3.1 ^b
<i>s</i> -BuOLi ^c (resonance at 3.44 ppm)	400.3 ^c	3.029	2.602	-9.452	415.1	-3.7
<i>s</i> -BuLi ^c (resonance at -0.97 ppm)	400.3 ^c	3.026	2.602	-9.440	396.3	1.0

^aThe formula weight 576.4 gmol^{-1} was calculated as 4:4 *s*-BuOLi to *s*-BuLi mixed octamer. ^bThe formula weight 544.4 gmol^{-1} was calculated as 2:6 *s*-BuOLi to *s*-BuLi mixed octamer. ^cThe formula weight 400.3 gmol^{-1} was calculated as 1:5 *s*-BuOLi to *s*-BuLi mixed hexamer.

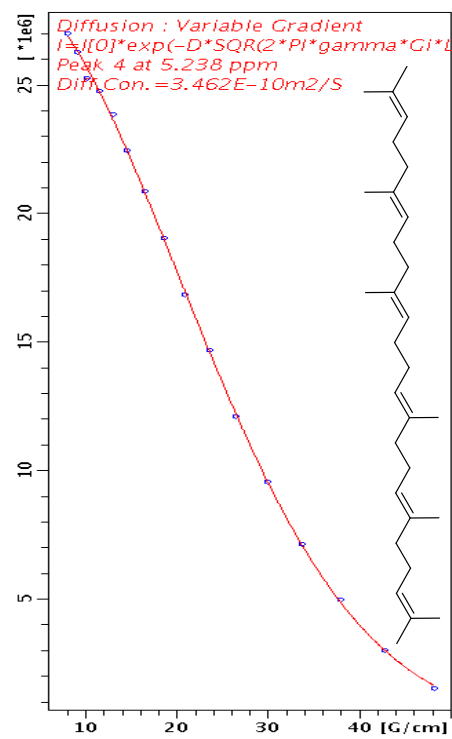
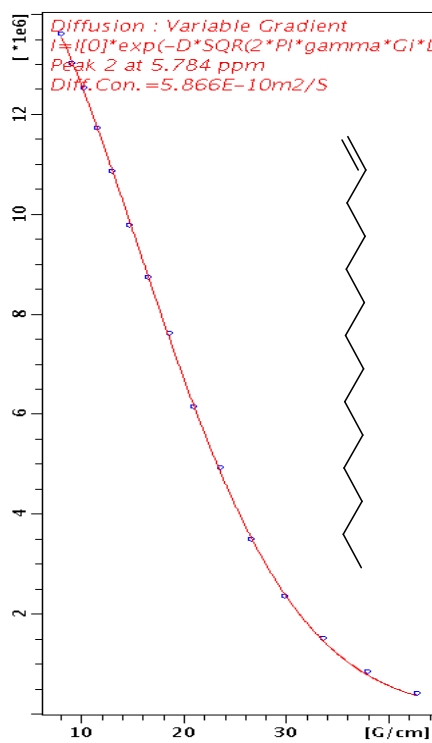
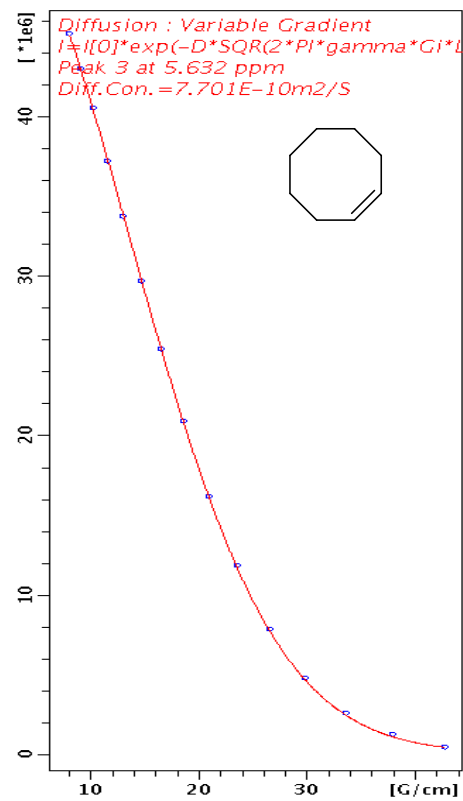
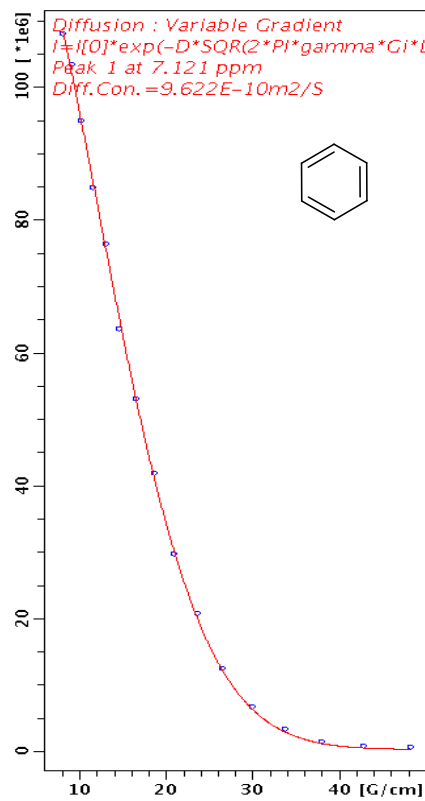


Figure S5.37. ^1H DOSY Decay Curves for Internal References (BEN, COE, TDE, SQU)

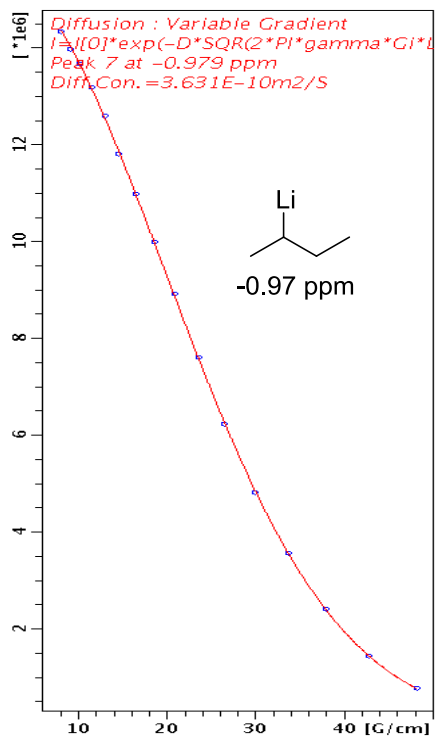
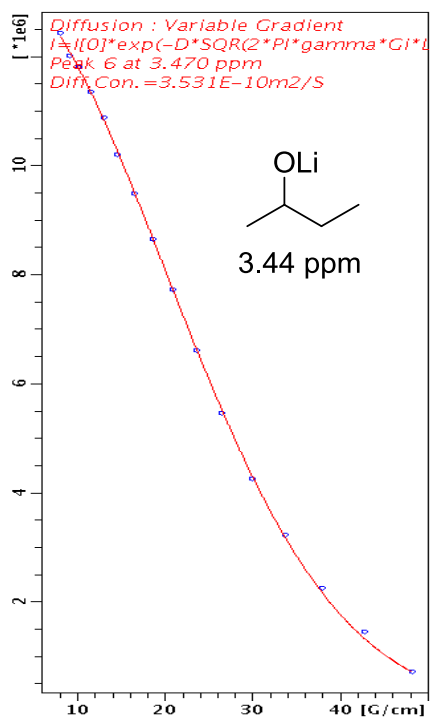
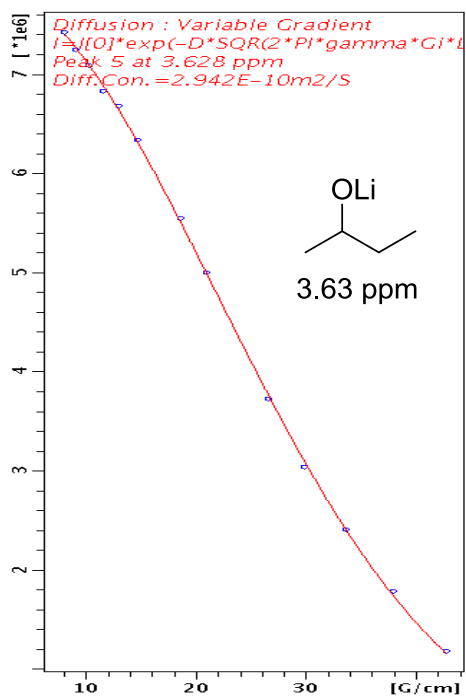


Figure S5.38. ^1H DOSY Decay Curves for *s*-BuLi and *s*-BuOLi

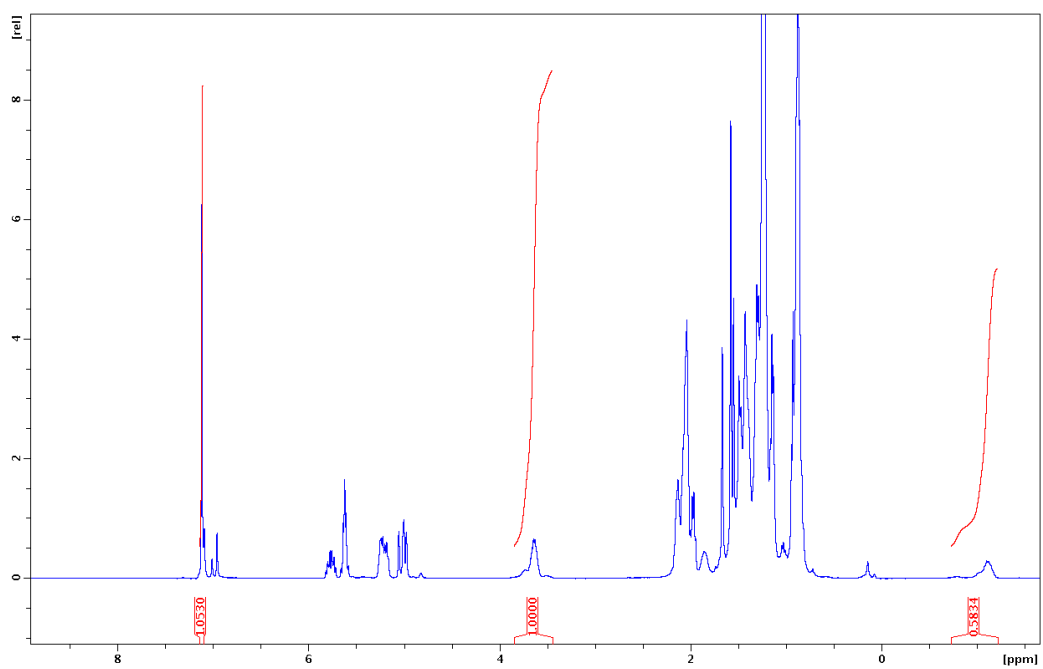


Figure S5.39. ^1H NMR of 5:3 *s*-BuOLi to *s*-BuLi solution with Internal References at $-20\text{ }^\circ\text{C}$

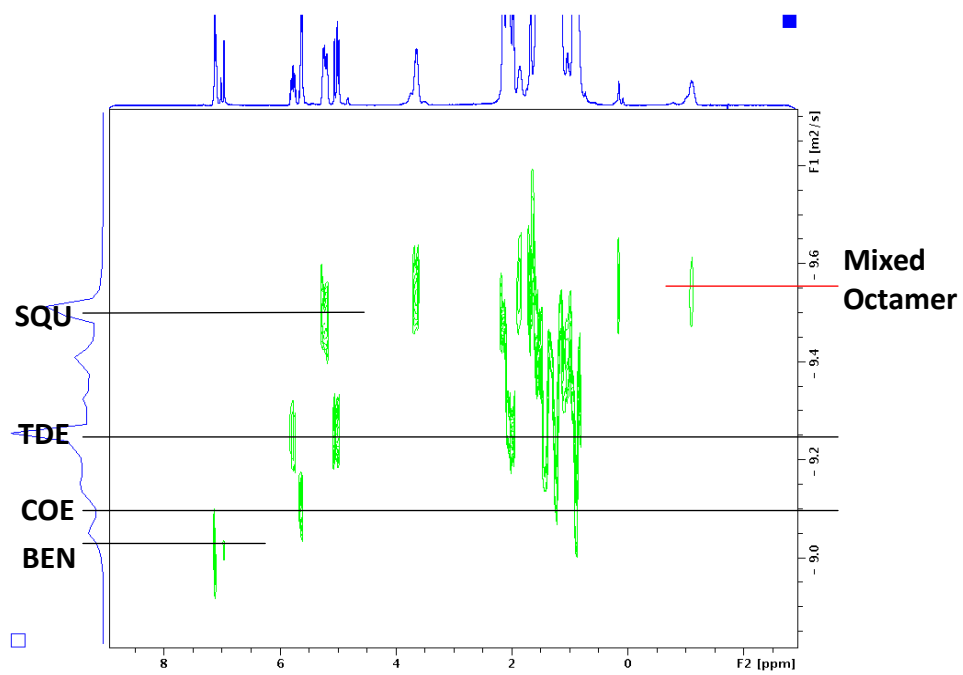


Figure S5.40. ^1H DOSY NMR of 5:3 *s*-BuOLi to *s*-BuLi solution with Internal References at $-20\text{ }^\circ\text{C}$

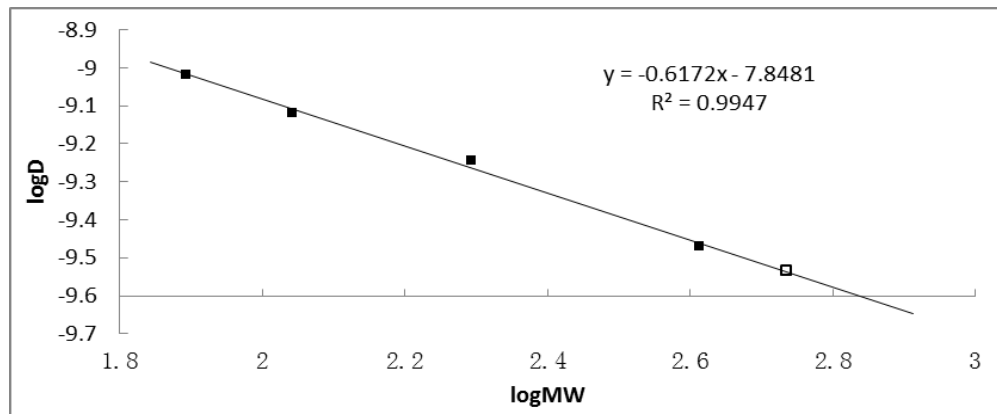


Figure S5.41. *D*-FW Analysis of ^1H DOSY Data of 5:3 *s*-BuOLi to *s*-BuLi solution at $-20\text{ }^\circ\text{C}$, Reference Compounds are Shown as Solid Squares, *s*-BuLi (Octamer) is Shown as Open Square

Table S5.9. *D*-FW Analysis of ^1H DOSY data of *s*-BuLi toluene- d_8 solution at $-20\text{ }^\circ\text{C}$

Compound	FW (g/mol)	$10^{-10}D$ (m^2/s)	log FW	log <i>D</i>	Predicted FW (g/mol)	% error
BEN	78.11	9.595	1.893	-9.018	78.59	-0.6
COE	110.2	7.620	2.042	-9.118	114.2	-3.6
TDE	196.4	5.716	2.293	-9.243	181.9	7.4
SQU	410.7	3.383	2.614	-9.471	425.5	-3.6
<i>s</i> -BuLi (resonance at - 1.12 ppm)	576.4 ^a	2.933	2.761 ^a	-9.533	536.2	7.0 ^a
	544.4 ^b	2.933	2.736 ^b	-9.533	536.2	1.5 ^b

^aThe formula weight 576.4 gmol^{-1} was calculated as 4:4 *s*-BuOLi to *s*-BuLi mixed octamer. ^bThe formula weight 544.4 gmol^{-1} was calculated as 2:6 *s*-BuOLi to *s*-BuLi mixed octamer.

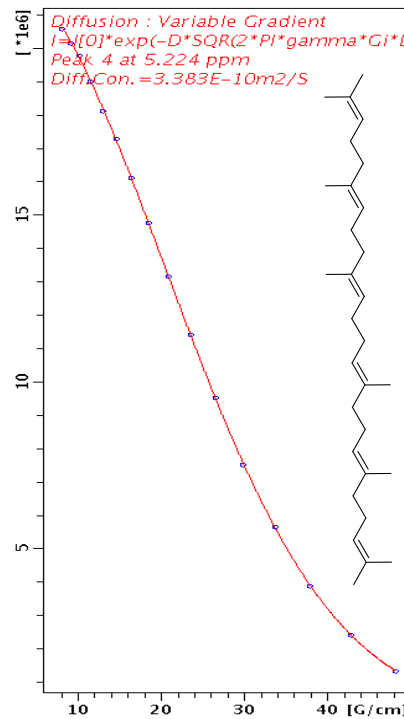
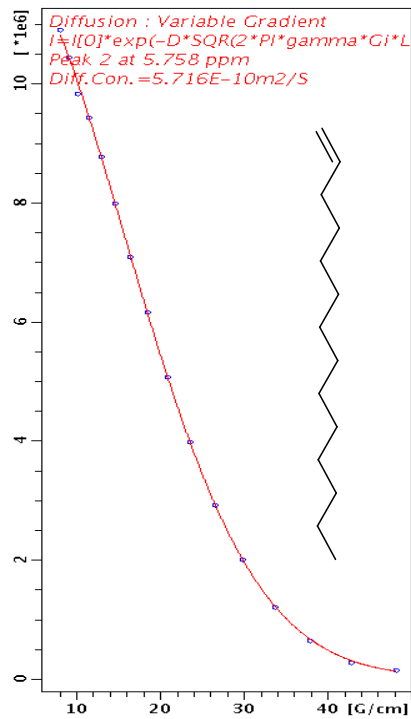
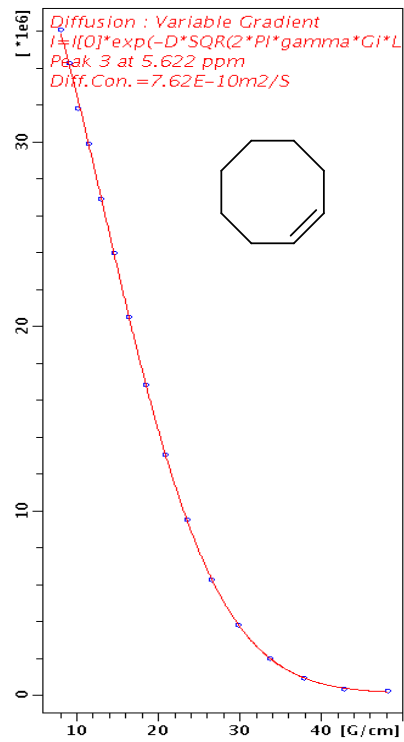
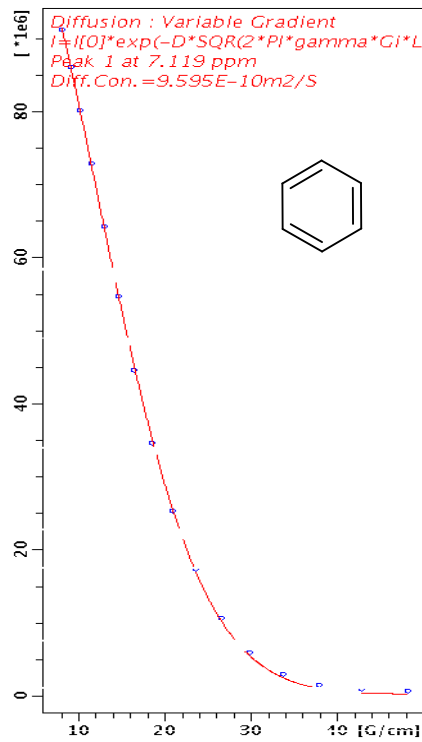


Figure S5.42. ¹H DOSY Decay Curves for Internal References (BEN, COE, TDE, SQU)

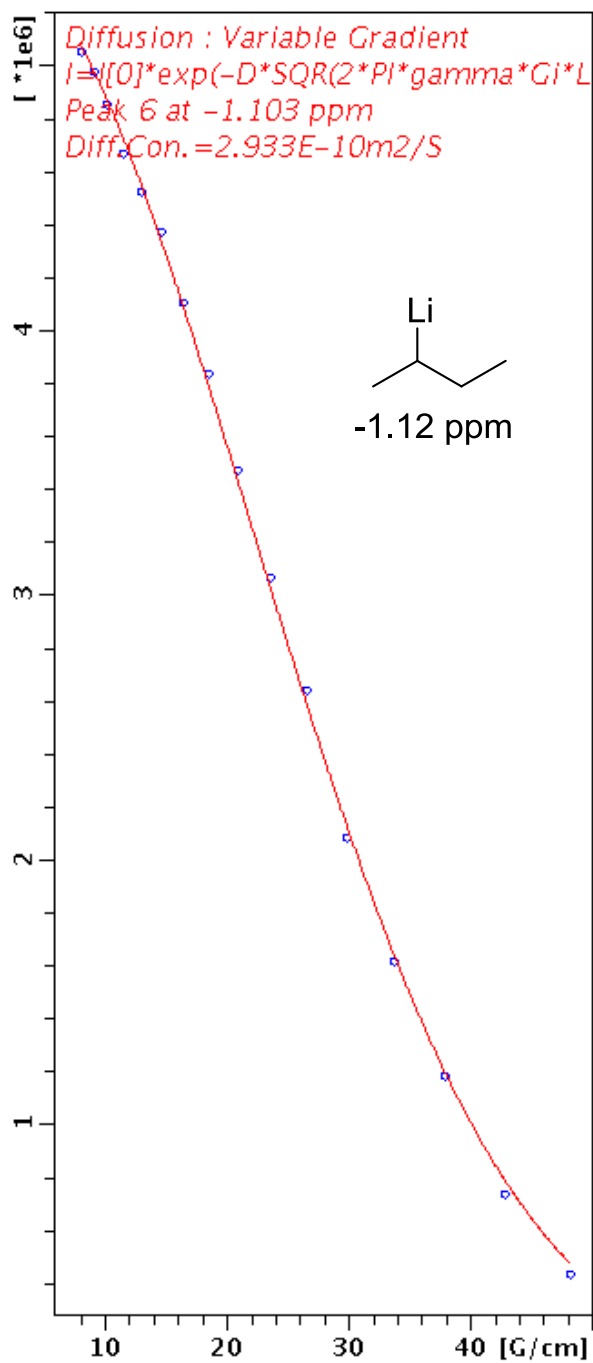


Figure S5.43. ¹H DOSY Decay Curves for s-BuLi

Appendix F

Supporting information for Chapter 6

Table of Contents

Figure S6.1. ^1H NMR of Chiral Amine 1	360
Figure S6.2. ^{13}C NMR of Chiral Amine 1	360
Figure S6.3. ^1H COSY NMR of Chiral Amine 1	361
Figure S6.4. $^1\text{H}\{^{13}\text{C}\}$ HSQC NMR of Chiral Amine 1	362
Figure S6.5. ^6Li NMR of Lithiated Amine 1	363
Figure S6.6. ^1H NMR of Lithiated Amine 1	363
Figure S6.7. ^{13}C NMR of Lithiated Amine 1	364
Figure S6.8. $^1\text{H}\{^{13}\text{C}\}$ HSQC NMR of Lithiated Amine 1	365
Figure S6.9. $^1\text{H}\{^{13}\text{C}\}$ HMBC NMR of Lithiated Amine 1	366
Figure S6.10. ^1H COSY NMR of Lithiated Amine 1	367
Figure S6.11. $^1\text{H}\{^6\text{Li}\}$ HMBC NMR of Lithiated Amine 1	368
Figure S6.12. <i>D</i> -FW Analysis of ^1H DOSY Data of Lithiated Amine 1 . Reference Compounds are Shown as Solid Squares, Lithiated Amine 1 is Shown as Open Square	368
Figure S6.13. ^1H DOSY Decay Curves for Internal References	370
Figure S6.14. ^1H DOSY Decay Curves for Lithiated Amine 1	371
Table S6.1. <i>D</i> -FW analysis of ^1H DOSY data of Lithiated Amine 1	369

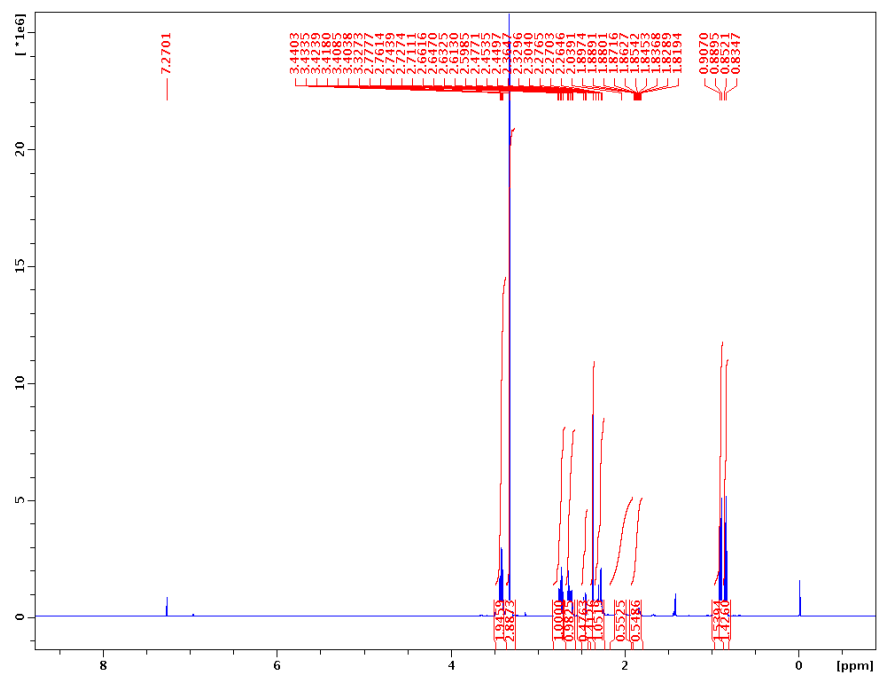


Figure S6.1. ^1H NMR of Chiral Amine **1**

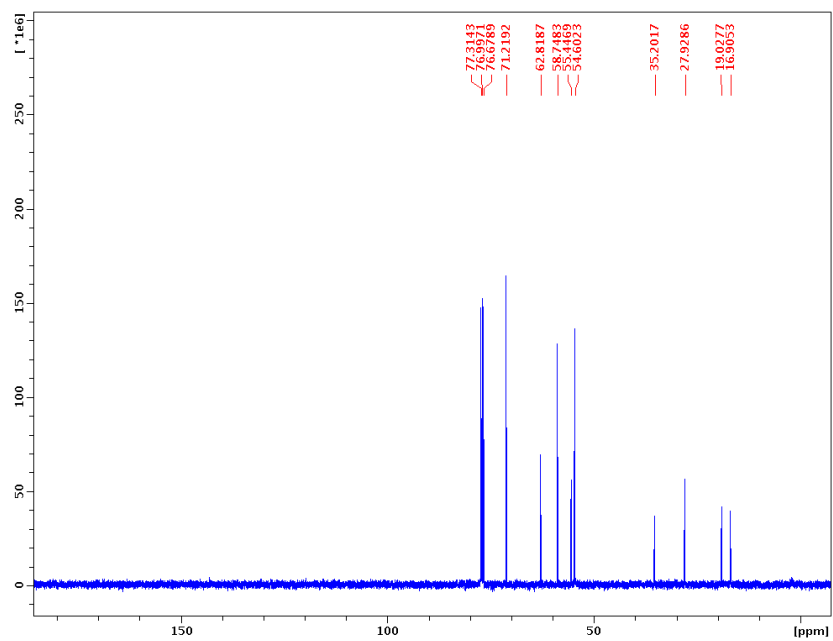


Figure S6.2. ^{13}C NMR of Chiral Amine **1**

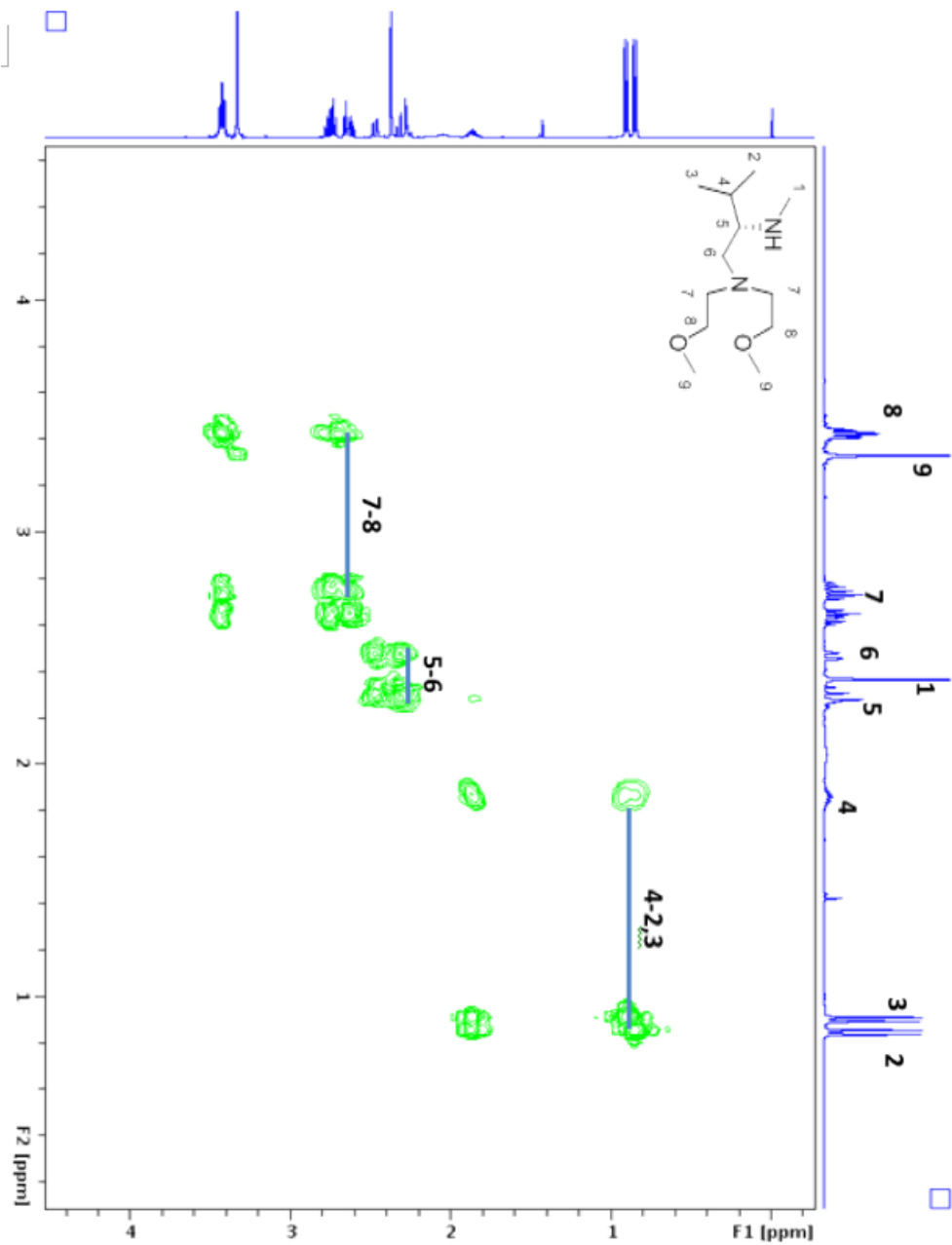


Figure S6.3. ^1H COSY NMR of Chiral Amine **1**

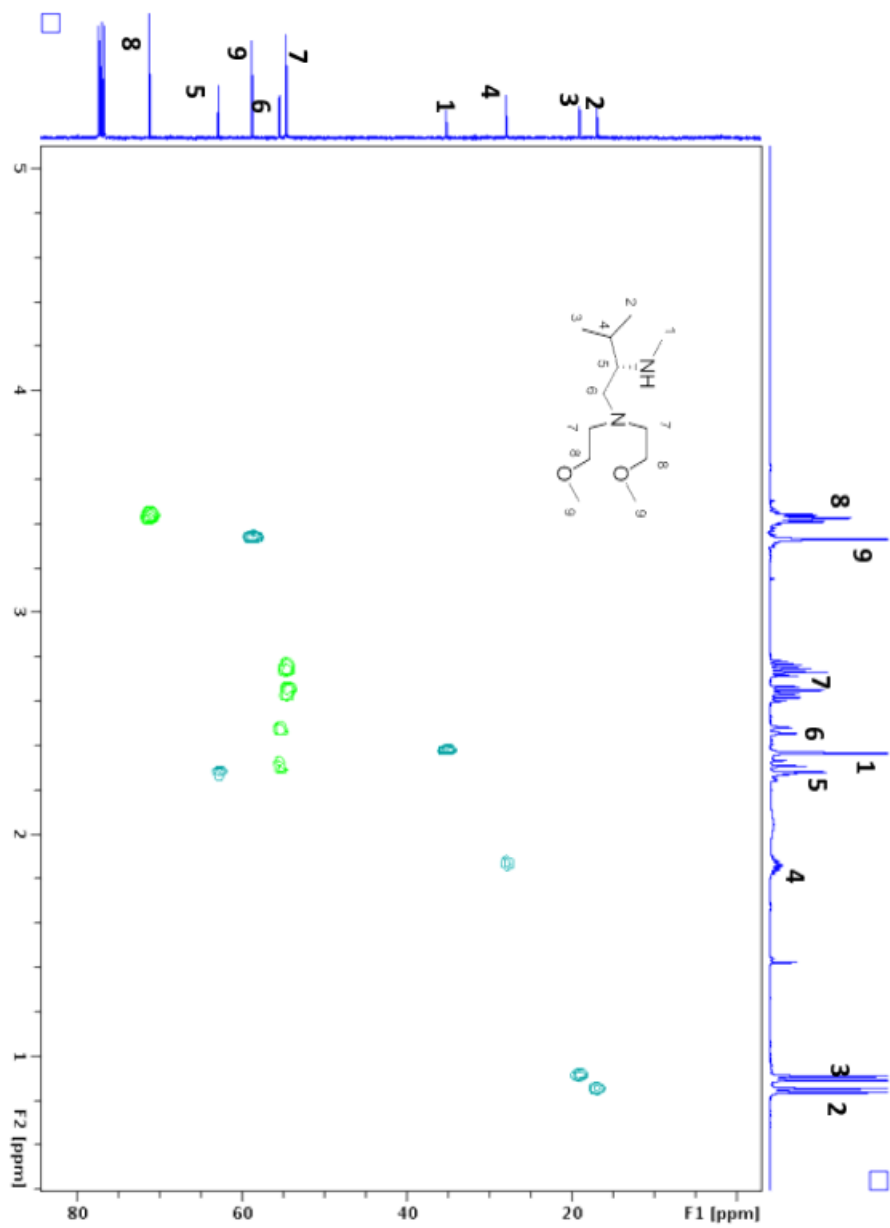


Figure S6.4. $^1\text{H}\{^{13}\text{C}\}$ HSQC NMR of Chiral Amine **1**

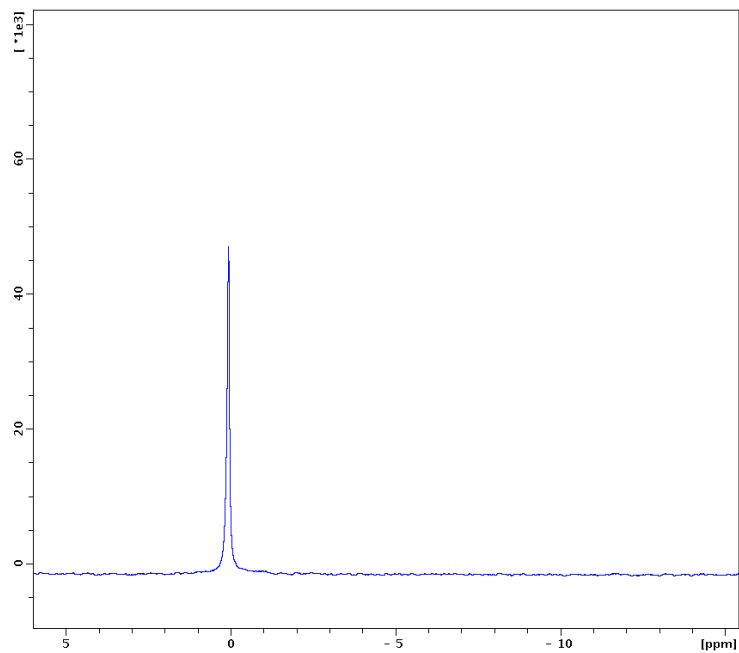


Figure S6.5. ^6Li NMR of Lithiated Amine **1**

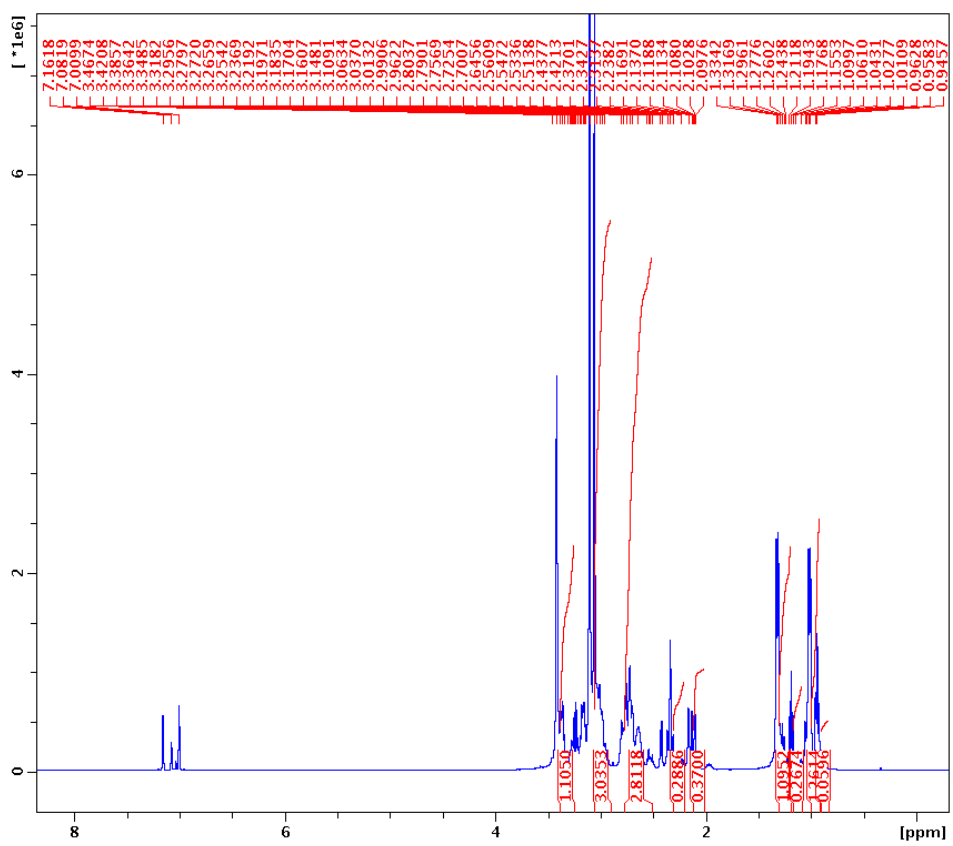


Figure S6.6. ^1H NMR of Lithiated Amine **1**

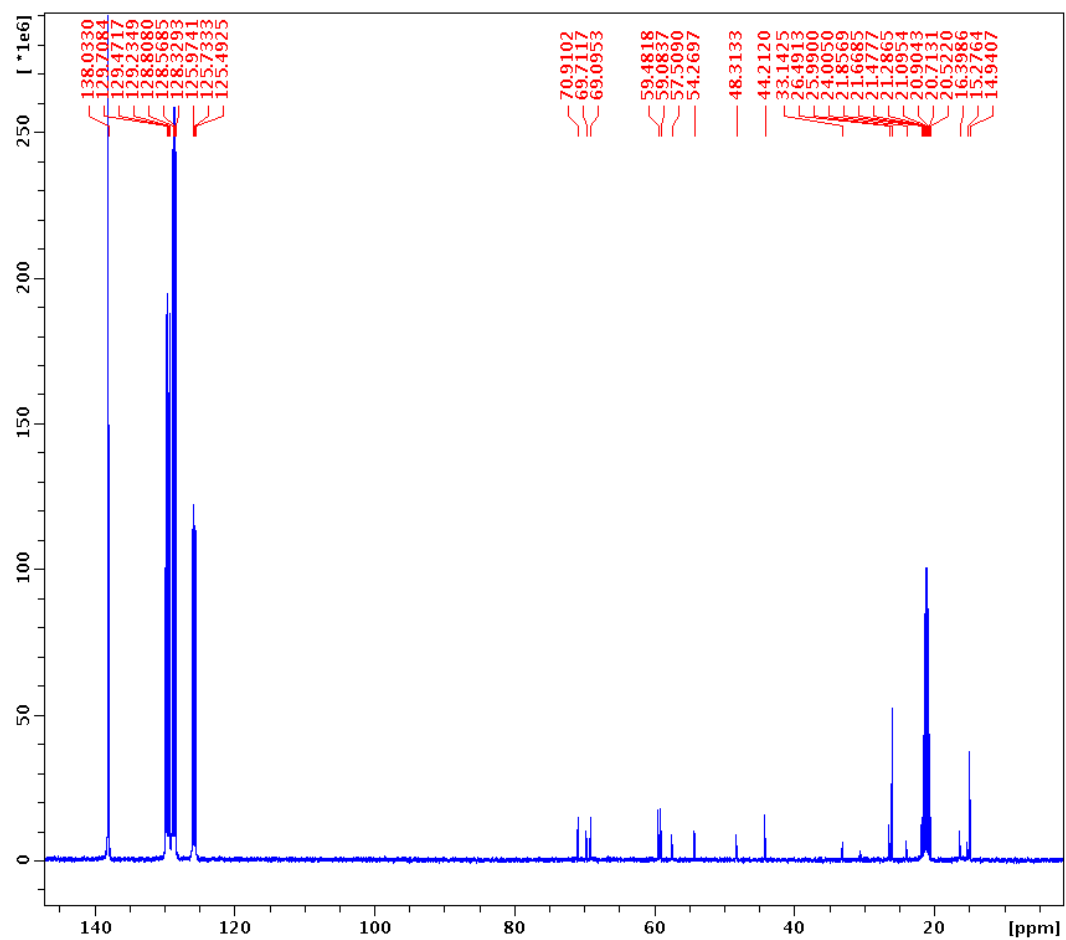


Figure S6.7. ^{13}C NMR of Lithiated Amine **1**

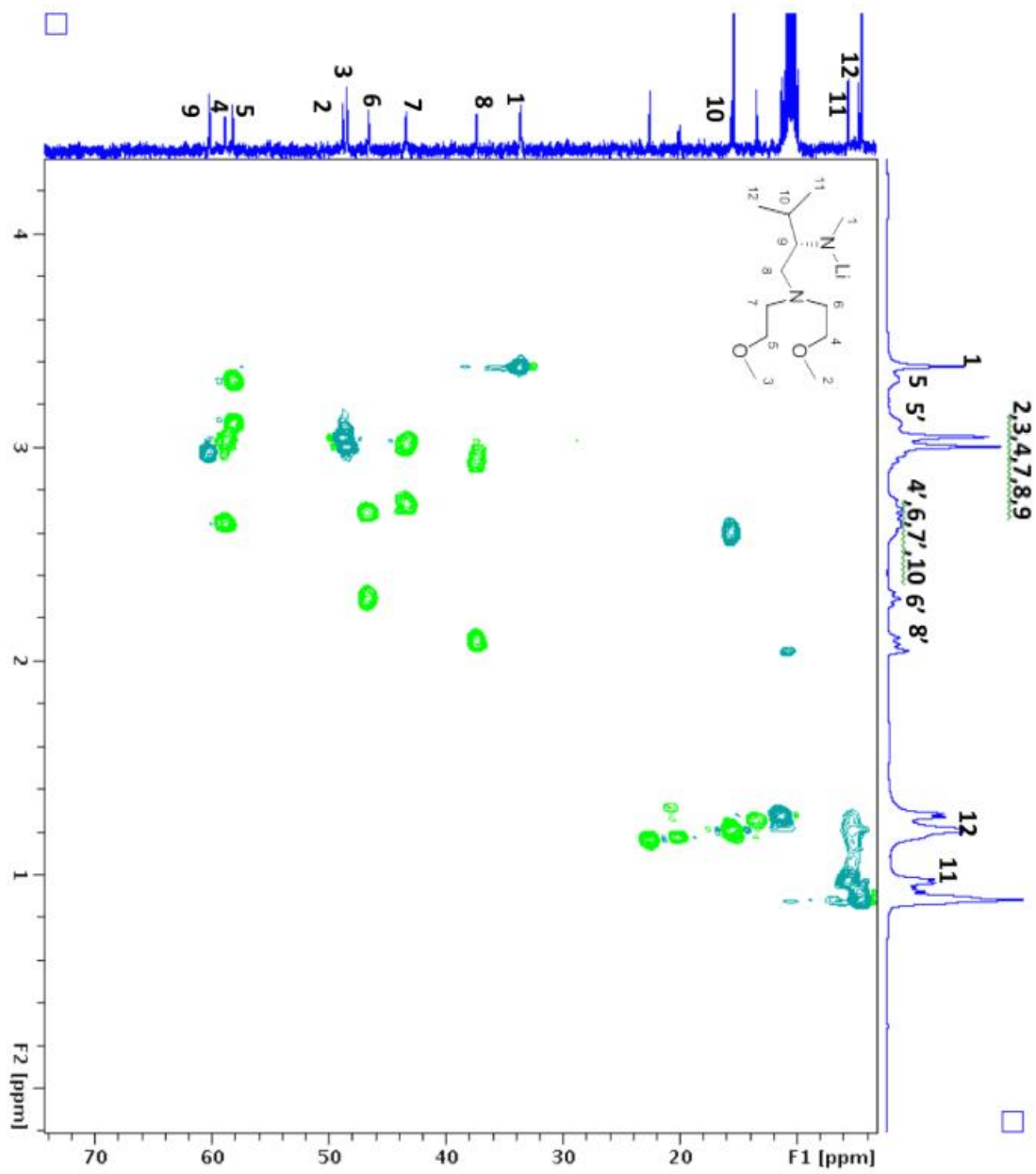


Figure S6.8. $^1\text{H}\{^{13}\text{C}\}$ HSQC NMR of Lithiated Amine **1**

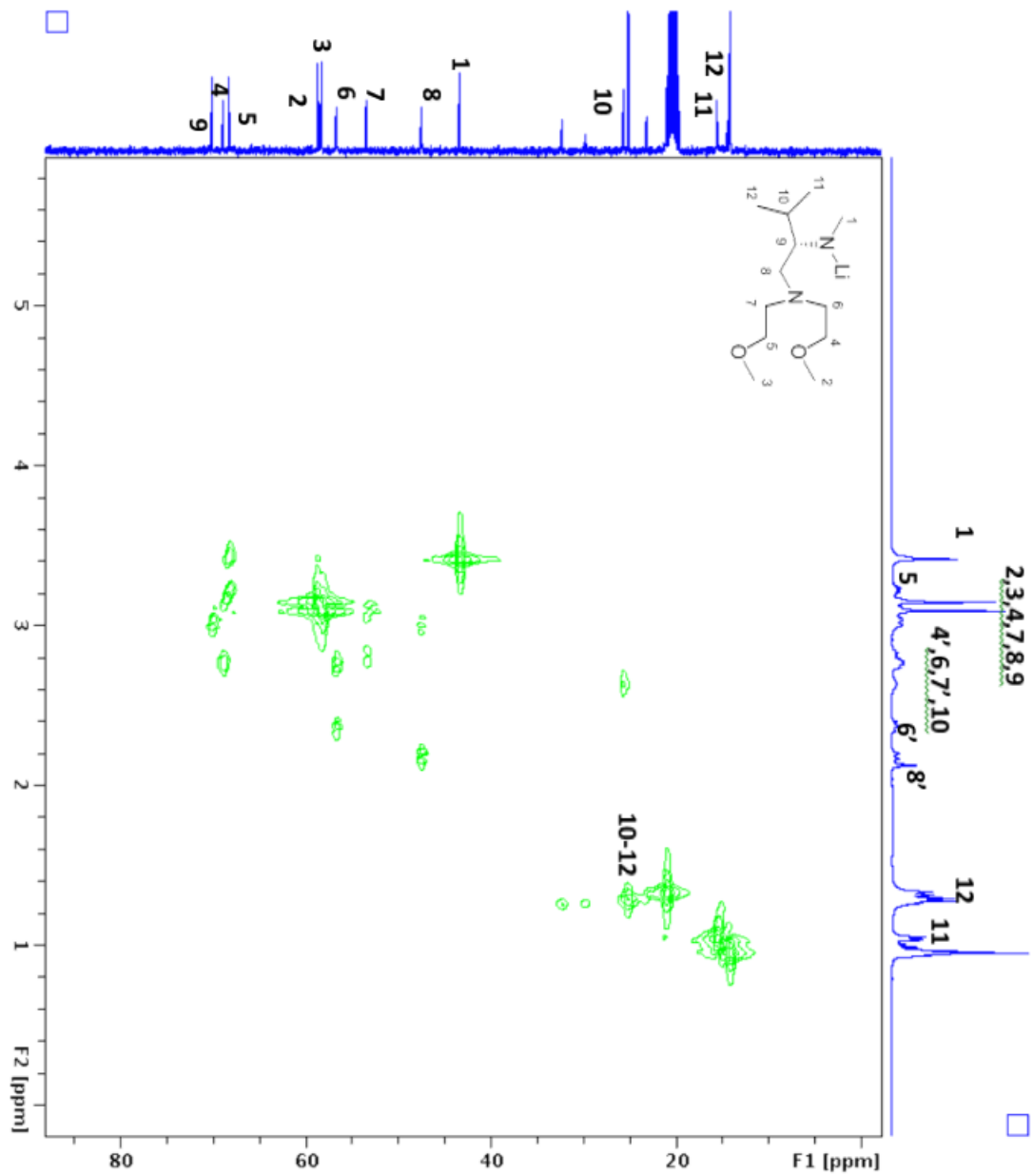


Figure S6.9. $^1\text{H}\{^{13}\text{C}\}$ HMBC NMR of Lithiated Amine **1**

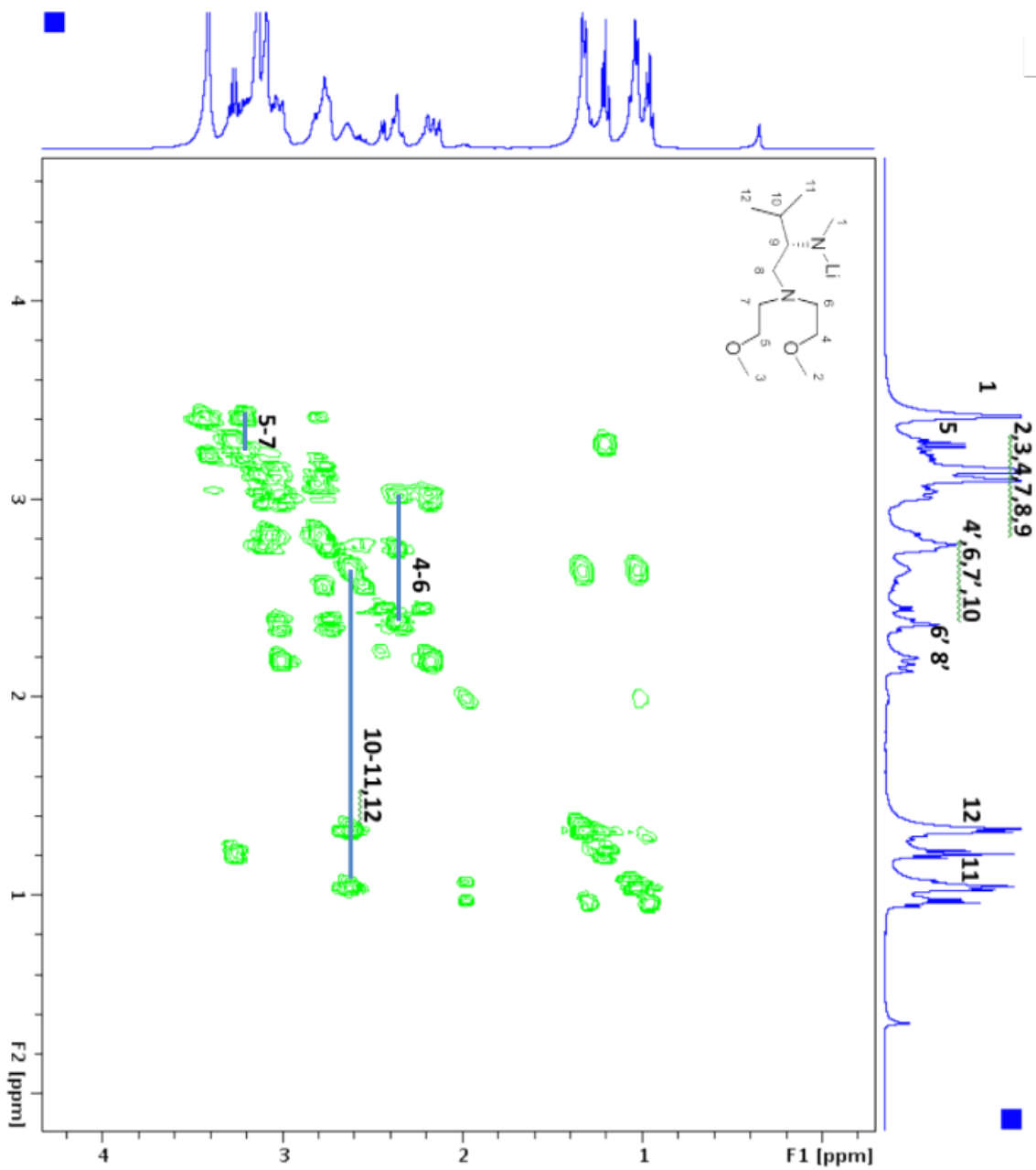


Figure S6.10. ^1H COSY NMR of Lithiated Amine **1**

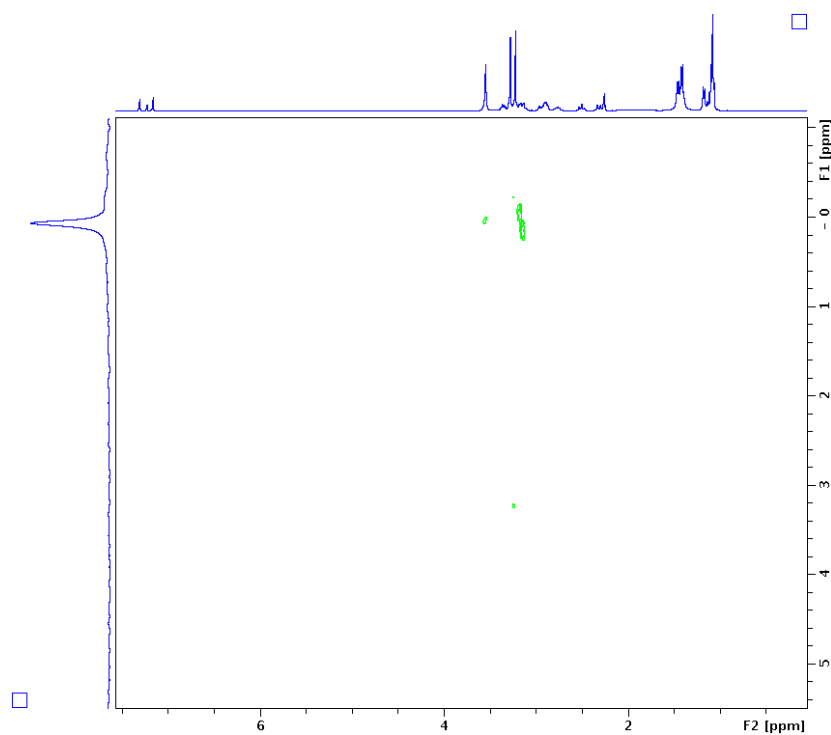


Figure S6.11. $^1\text{H}\{^6\text{Li}\}$ HMBC NMR of Lithiated Amine **1**

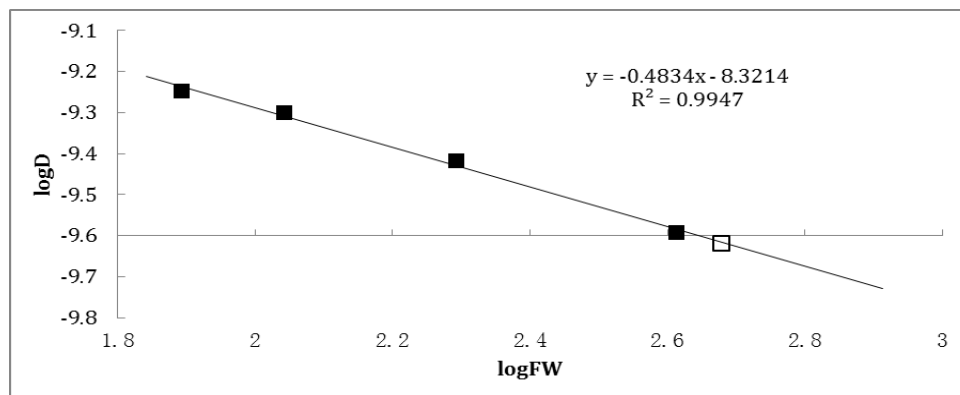


Figure S6.12. *D*-FW Analysis of ^1H DOSY Data of Lithiated Amine **1**. Reference Compounds are Shown as Solid Squares, Lithiated Amine **1** is Shown as Open Square

Table S6.1. *D*-FW analysis of ¹H DOSY data of Lithiated Amine **1**

Compd	FW (g/mol)	10 ⁻¹⁰ D (m ² /s)	log FW	log D	Predicted FW (g/mol)	% error
BEN	78.11	5.661	1.893	-9.247	82.26	-5.3
COE	110.2	4.997	2.042	-9.301	106.5	3.4
TDE	196.4	3.818	2.293	-9.418	185.8	5.4
SQU	410.7	2.555	2.614	-9.593	426.6	-3.9
Li- 1 ^a	476.6 ^b	2.370	2.678	-9.625	498.3	-4.6
Li- 1 ^a	476.6 ^b	2.378	2.678	-9.624	494.9	-3.8
Li- 1 ^a	476.6 ^b	2.451	2.678	-9.611	464.9	2.5
Li- 1 ^a	476.6 ^b	2.418	2.678	-9.612	478.1	-0.3
Li- 1 ^a	476.6 ^b	2.404 ^c	2.678	-9.619	483.7	-1.5
		Standard Dev. of Predicted FW of Li- 1			15.5	3.3
Li- 1 ^a	238.3 ^d	2.404	2.377	-9.619	483.7	-103
Li- 1 ^a	310.4 ^e	2.404	2.492	-9.619	483.7	-55.9
Li- 1 ^a	620.8 ^f	2.404	2.793	-9.619	483.7	22.0

^aLi-**1** represents lithiated amine **1** in Tol-*d*₈. ^b476.6 g/mol is the formula weight of unsolvated dimer **4**. ^cThe average of the above four diffusion coefficients. ^d238.3 g/mol is the formula weight of unsolvated monomer **2**. ^e310.4 g/mol is the formula weight of a THF solvated monomer. ^f620.8 g/mol is the formula weight of a THF solvated dimer with 2 THF.

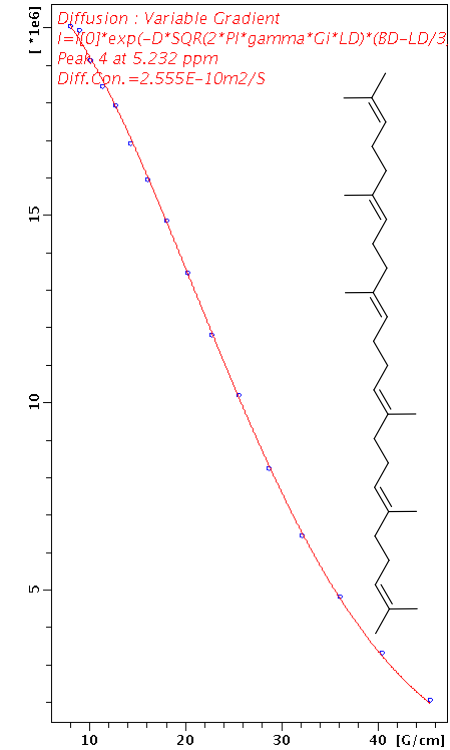
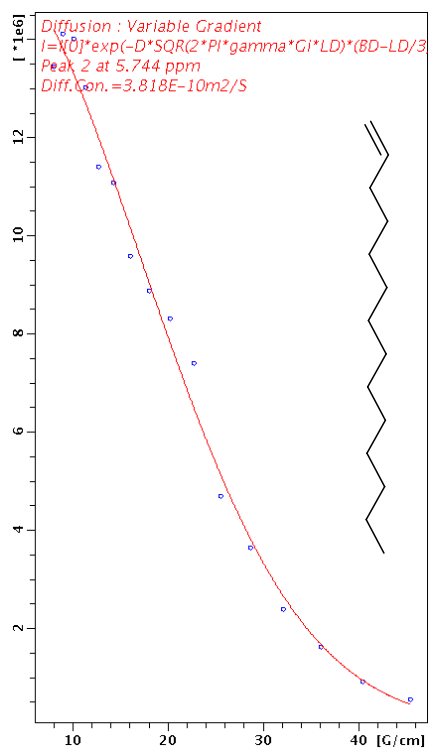
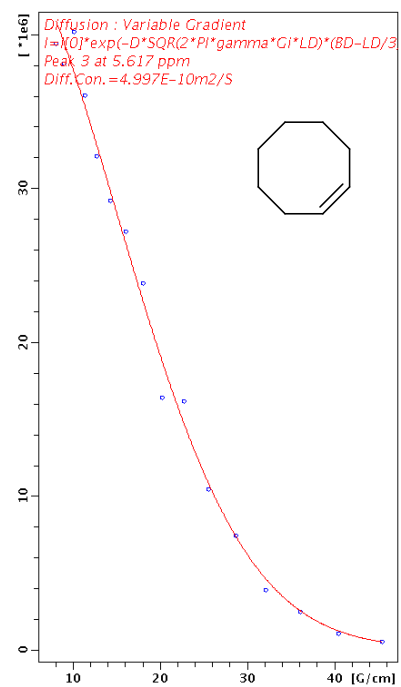
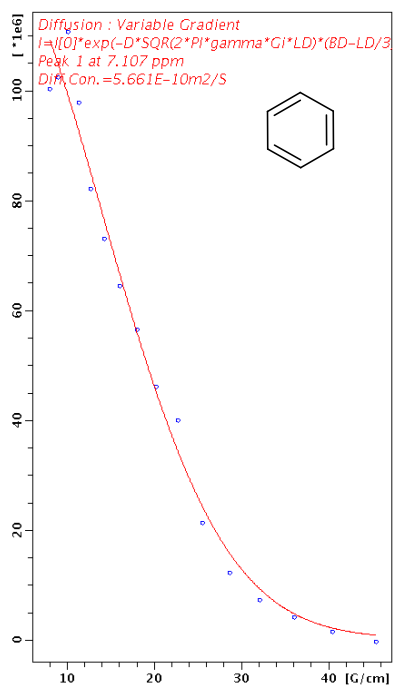


Figure S6.13. ¹H DOSY Decay Curves for Internal References (BEN, COE, TDE, SQU)

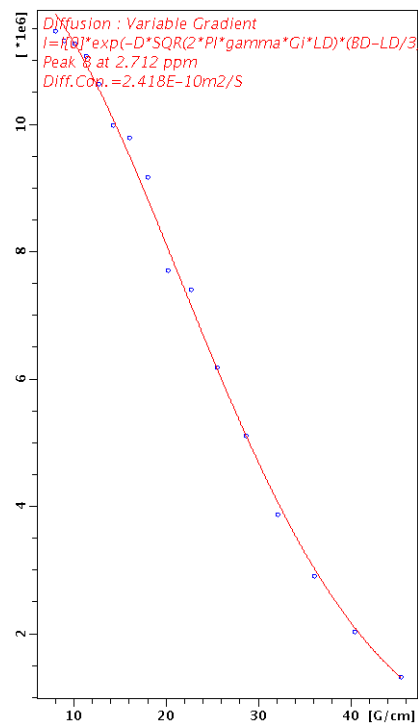
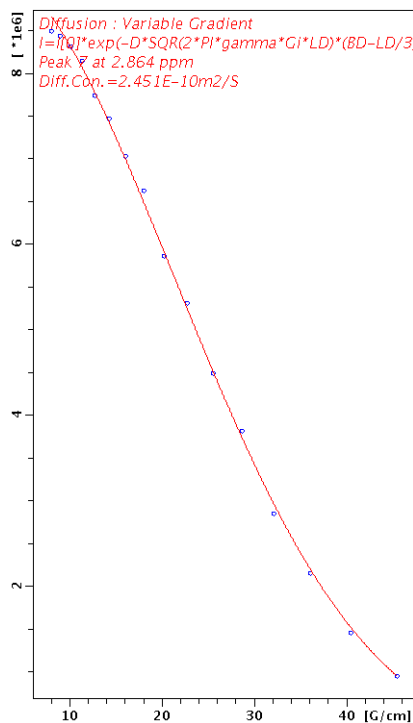
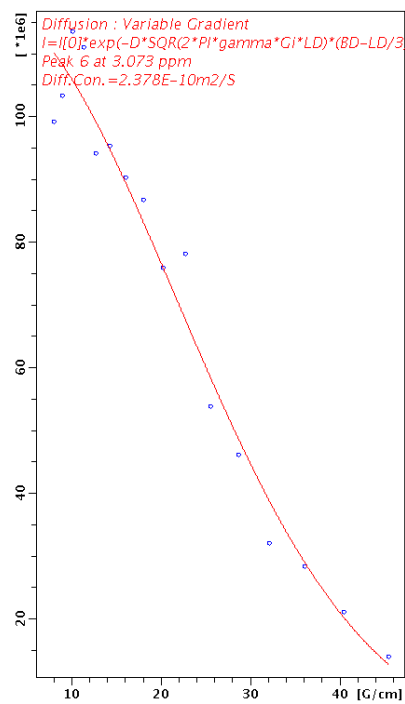
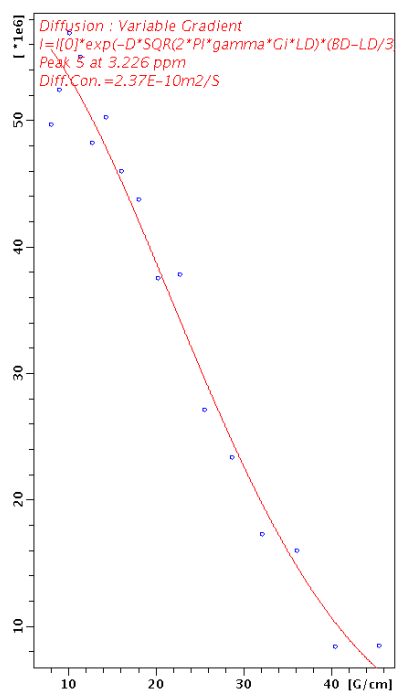


Figure S6.14. ^1H DOSY Decay Curves for Lithiated Amine **1** (Four Distinct Peaks)

Appendix G

Supporting information for Chapter 7

Table of Contents

Figure S7.1. ¹ H NMR of (<i>S</i>)- <i>N</i> -ethyl-3-methyl-1-(triisopropylsilyloxy)butan-2-amine in toluene- <i>d</i> ₈	375
Figure S7.2. ¹³ C NMR of (<i>S</i>)- <i>N</i> -ethyl-3-methyl-1-(triisopropylsilyloxy)butan-2-amine in toluene- <i>d</i> ₈	375
Figure S7.3. ¹ H COSY of (<i>S</i>)- <i>N</i> -ethyl-3-methyl-1-(triisopropylsilyloxy)butan-2-amine in toluene- <i>d</i> ₈	376
Figure S7.4. ¹ H- ¹³ C HSQC (<i>S</i>)- <i>N</i> -ethyl-3-methyl-1-(triisopropylsilyloxy)butan-2-amine in toluene- <i>d</i> ₈	376
Figure S7.5. ¹ H NMR of Mixed Aggregate 6a in toluene- <i>d</i> ₈ at -50° C.....	377
Figure S7.6. ¹³ C NMR of Mixed Aggregate 6a in toluene- <i>d</i> ₈ at -50° C.....	377
Figure S7.7. ⁶ Li NMR of Mixed Aggregate 6a in toluene- <i>d</i> ₈ at -50° C.....	378
Figure S7.8. ¹ H COSY of Mixed Aggregate 6a in toluene- <i>d</i> ₈ at -50° C.....	378
Figure S7.9. ¹ H- ¹³ C HSQC of Mixed Aggregate 6a in toluene- <i>d</i> ₈ at -50° C.....	379
Figure S7.10. ¹ H- ¹³ C HMBC of Mixed Aggregate 6a in toluene- <i>d</i> ₈ at -50° C.....	379
Figure S7.11. ¹ H NMR of Mixed Aggregate 6a in toluene- <i>d</i> ₈ with Internal References at -50° C.....	380
Figure S7.12. ¹ H DOSY Decay Curves for Internal References.....	381
Figure S7.13. ¹ H DOSY Decay Curves for Mixed Aggregate 6a	382
Figure S7.14. ¹ H NMR of Mixed Aggregate 6b in toluene- <i>d</i> ₈ at -50° C.....	383
Figure S7.15. ¹³ C NMR of Mixed Aggregate 6b in toluene- <i>d</i> ₈ at -50° C.....	384
Figure S7.16. ⁶ Li NMR of Mixed Aggregate 6b in toluene- <i>d</i> ₈ at -50° C.....	384
Figure S7.17. ¹ H COSY of Mixed Aggregate 6b in toluene- <i>d</i> ₈ at -50° C.....	385
Figure S7.18. ¹ H- ¹³ C HSQC of Mixed Aggregate 6b in toluene- <i>d</i> ₈ at -50° C.....	385
Figure S7.19. ¹ H- ¹³ C HMBC of Mixed Aggregate 6b in toluene- <i>d</i> ₈ at -50° C.....	386

Figure S7.20. ^1H NMR of Mixed Aggregate 6b in toluene- d_8 with Internal References at -50°C	386
Figure S7.21. ^1H DOSY Decay Curves for Internal References	387
Figure S7.22. ^1H DOSY Decay Curves for Mixed Aggregate 6b	388
Figure S7.23. ^1H NMR of Mixed Aggregate 6c in toluene- d_8 at -50°C	389
Figure S7.24. ^{13}C NMR of Mixed Aggregate 6c in toluene- d_8 at -50°C	390
Figure S7.25. ^6Li NMR of Mixed Aggregate 6c in toluene- d_8 at -50°C	390
Figure S7.26. ^1H COSY of Mixed Aggregate 6c in toluene- d_8 at -50°C	391
Figure S7.27. ^1H - ^{13}C HSQC of Mixed Aggregate 6c in toluene- d_8 at -50°C	391
Figure S7.28. ^1H - ^{13}C HMBC of Mixed Aggregate 6c in toluene- d_8 at -50°C	392
Figure S7.29. ^1H NMR of Mixed Aggregate 6c in toluene- d_8 with Internal References at -50°C	392
Figure S7.30. ^1H DOSY Decay Curves for Internal References	393
Figure S7.31. ^1H DOSY Decay Curves for Mixed Aggregate 6c	394
Figure S7.32. ^1H NMR of Mixed Aggregate 6d in toluene- d_8 at -50°C	395
Figure S7.33. ^{13}C NMR of Mixed Aggregate 6d in toluene- d_8 at -50°C	396
Figure S7.34. ^6Li NMR of Mixed Aggregate 6d in toluene- d_8 at -50°C	396
Figure S7.35. ^1H COSY of Mixed Aggregate 6d in toluene- d_8 at -50°C	397
Figure S7.36. ^1H - ^{13}C HSQC of Mixed Aggregate 6d in toluene- d_8 at -50°C	397
Figure S7.37. ^1H - ^{13}C HSQC of Mixed Aggregate 6d in toluene- d_8 at -50°C (Enlarged).....	398
Figure S7.38. ^1H - ^{13}C HMBC of Mixed Aggregate 6d in toluene- d_8 at -50°C	398
Figure S7.39. ^1H NMR of Mixed Aggregate 6d in toluene- d_8 with Internal References at -50°C	399
Figure S7.40. ^1H DOSY Decay Curves for Internal References	400
Figure S7.41. ^1H DOSY Decay Curves for Mixed Aggregate 6d	401

Table S7.1. <i>D</i> -FW Analysis of ^1H DOSY data of Mixed Aggregate 6a toluene- d_8 solution at -50°C	383
Table S7.2. <i>D</i> -FW Analysis of ^1H DOSY data of Mixed Aggregate 6b toluene- d_8 solution at -50°C	389
Table S7.3. <i>D</i> -FW Analysis of ^1H DOSY data of Mixed Aggregate 6c toluene- d_8 solution at -50°C	395
Table S7.4. <i>D</i> -FW Analysis of ^1H DOSY data of Mixed Aggregate 6d toluene- d_8 solution at -50°C	402

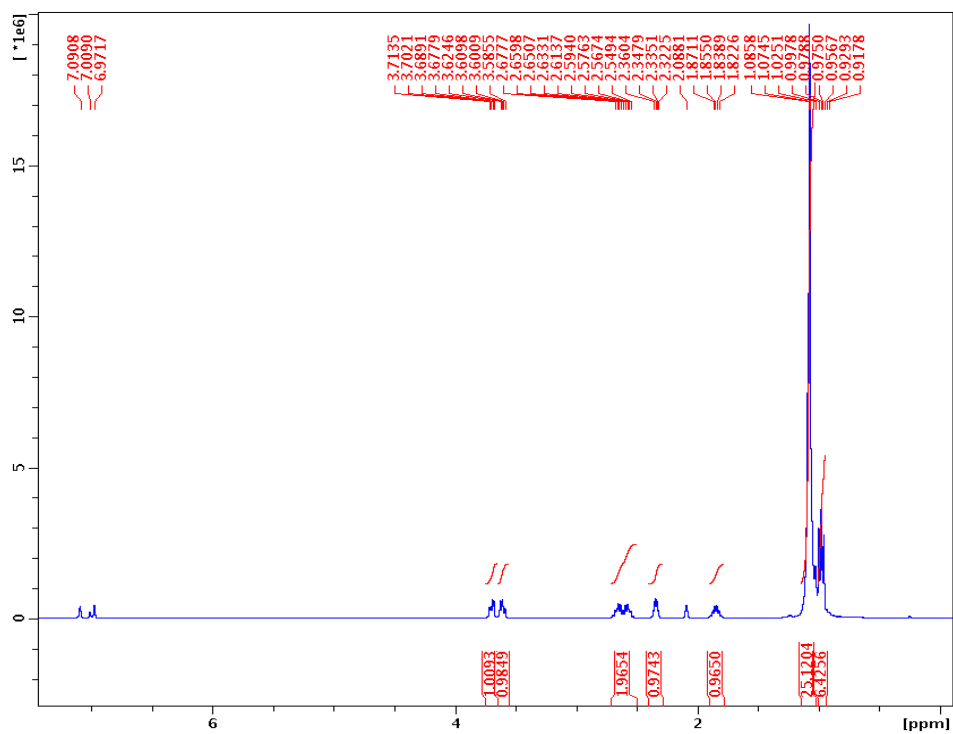


Figure S7.1. ^1H NMR of (*S*)-*N*-ethyl-3-methyl-1-(triisopropylsilyloxy)butan-2-amine in toluene- d_8

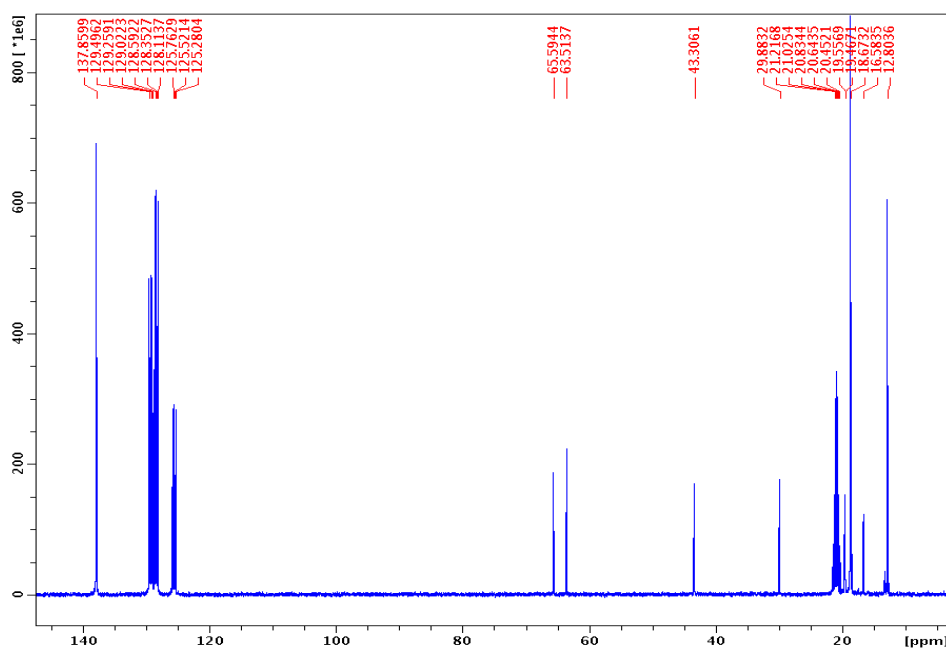


Figure S7.2. ^{13}C NMR of (*S*)-*N*-ethyl-3-methyl-1-(triisopropylsilyloxy)butan-2-amine in toluene- d_8

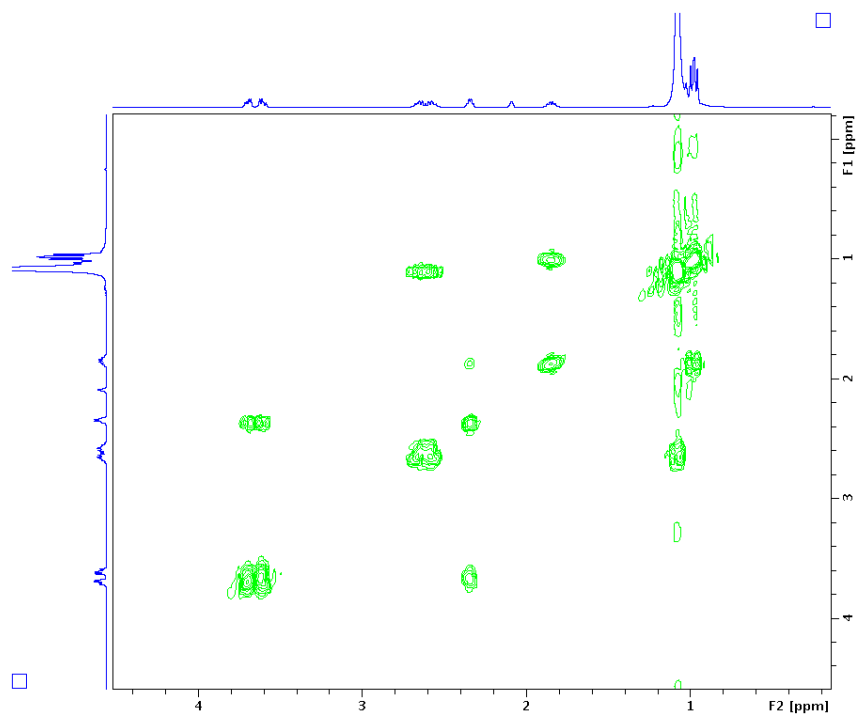


Figure S7.3. ^1H COSY of (*S*)-*N*-ethyl-3-methyl-1-(triisopropylsilyloxy)butan-2-amine in toluene- d_8

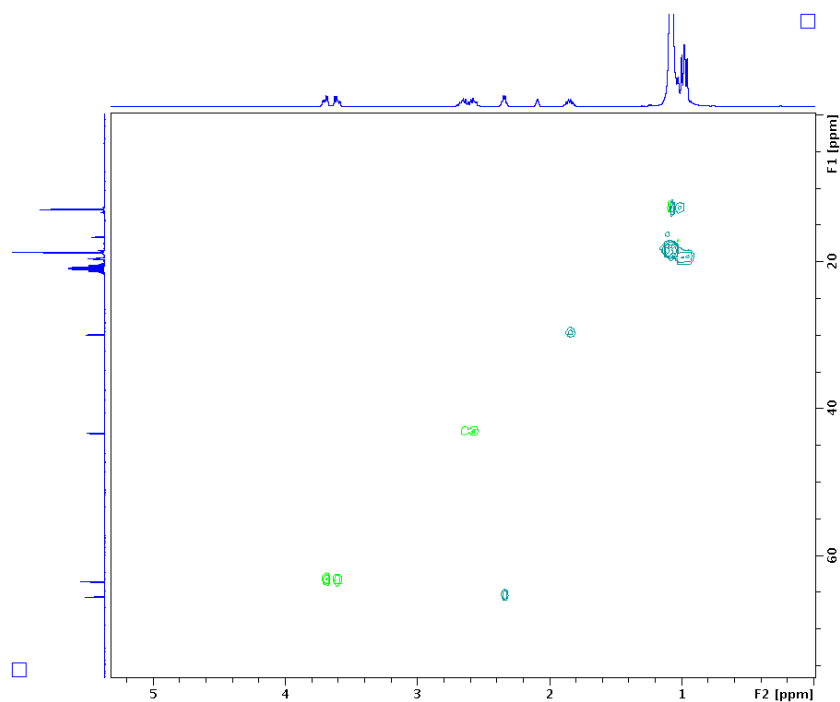


Figure S7.4. ^1H - ^{13}C HSQC (*S*)-*N*-ethyl-3-methyl-1-(triisopropylsilyloxy)butan-2-amine in toluene- d_8

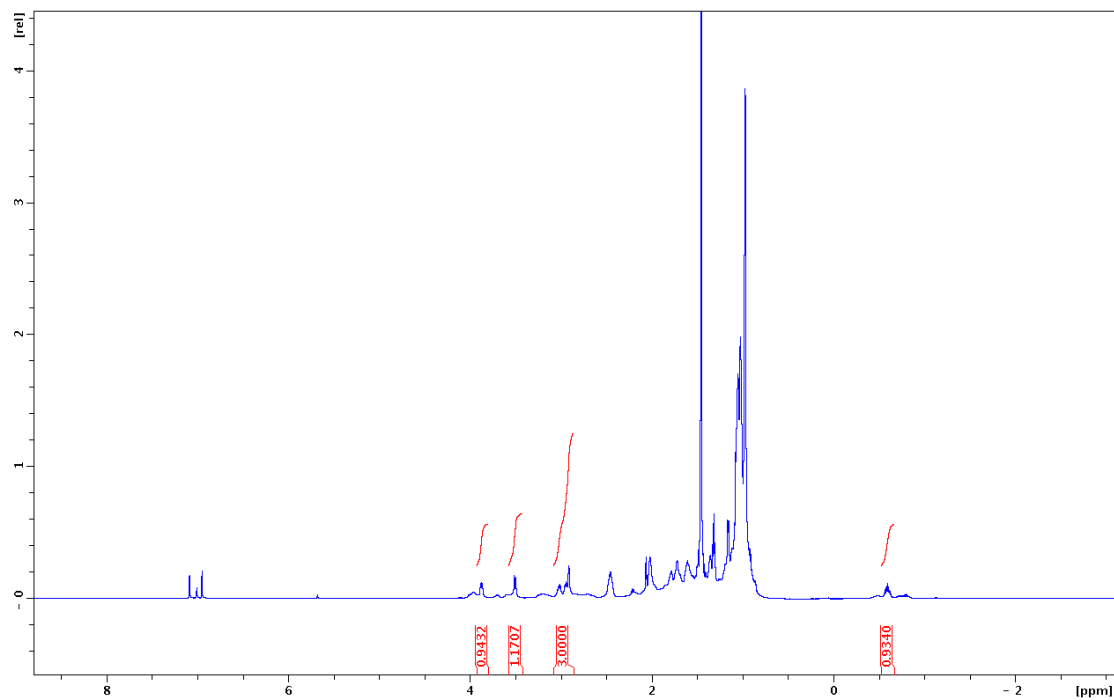


Figure S7.5. ^1H NMR of Mixed Aggregate **6a** in $\text{toluene-}d_8$ at -50°C

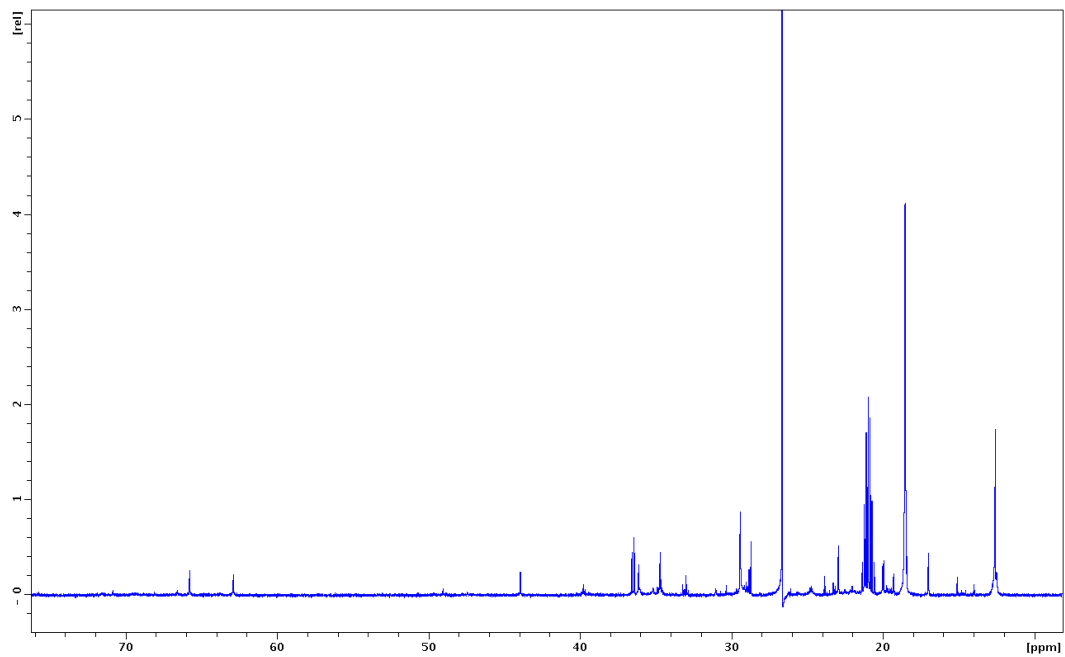


Figure S7.6. ^{13}C NMR of Mixed Aggregate **6a** in $\text{toluene-}d_8$ at -50°C

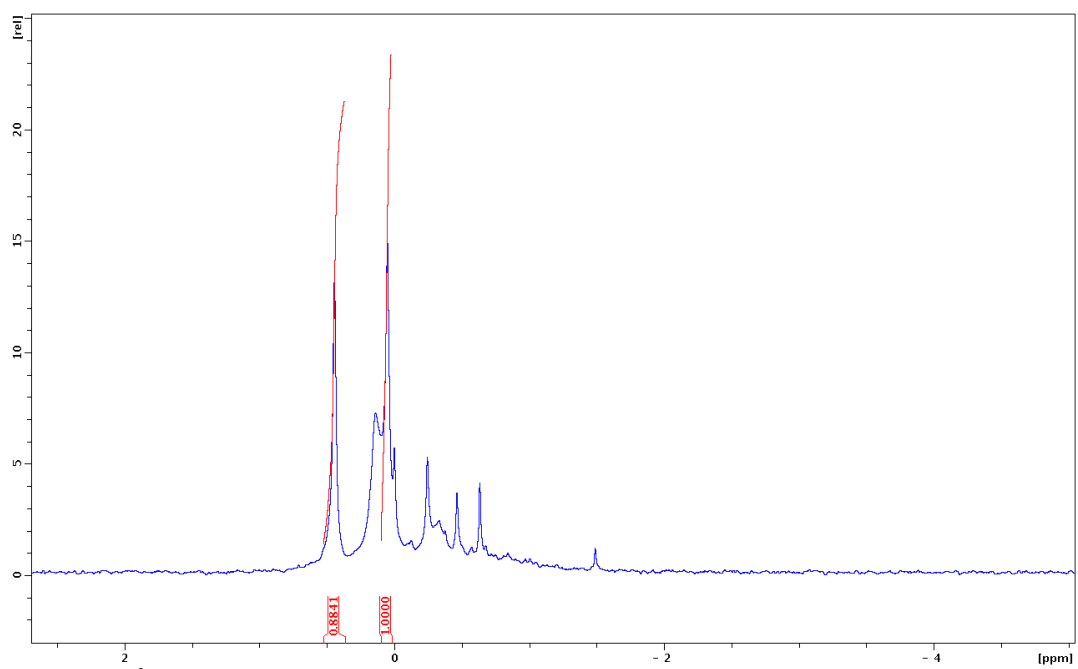


Figure S7.7. ^6Li NMR of Mixed Aggregate **6a** in toluene- d_8 at -50°C

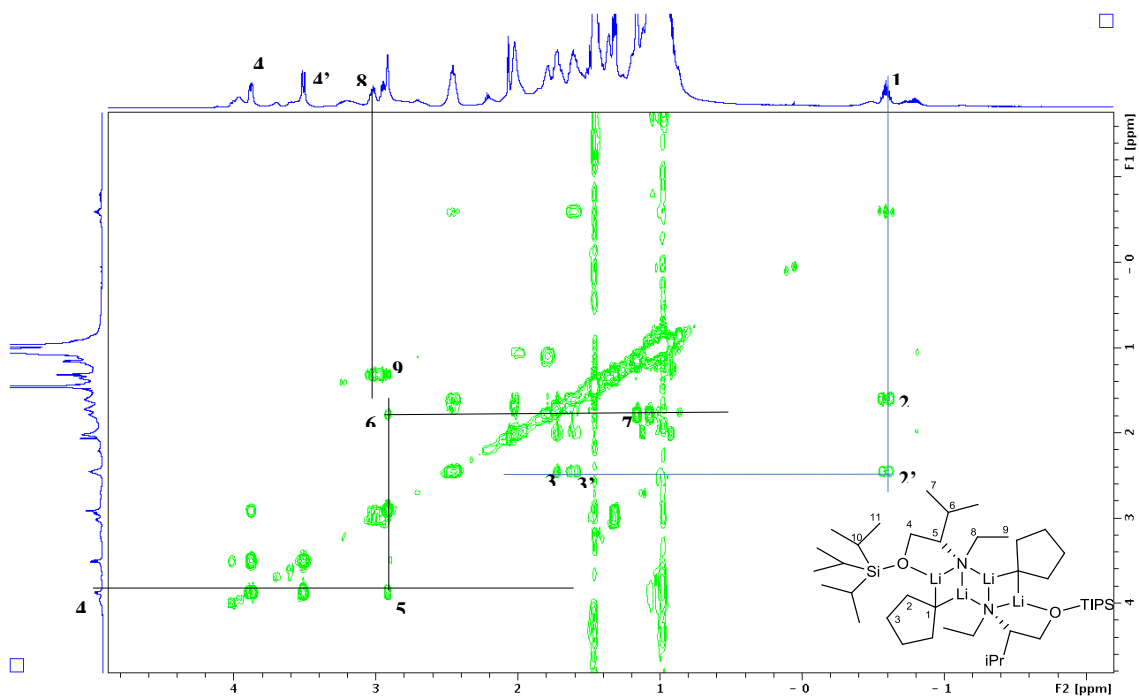


Figure S7.8. ^1H COSY of Mixed Aggregate **6a** in toluene- d_8 at -50°C

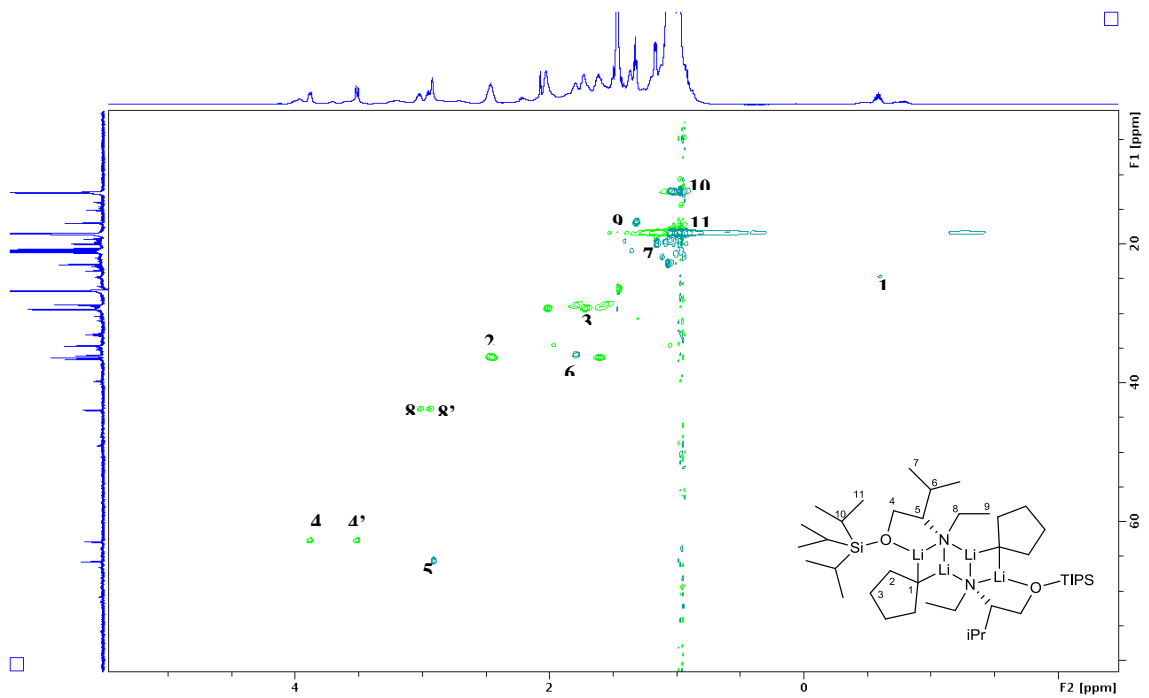


Figure S7.9. ^1H - ^{13}C HSQC of Mixed Aggregate **6a** in toluene- d_8 at -50°C

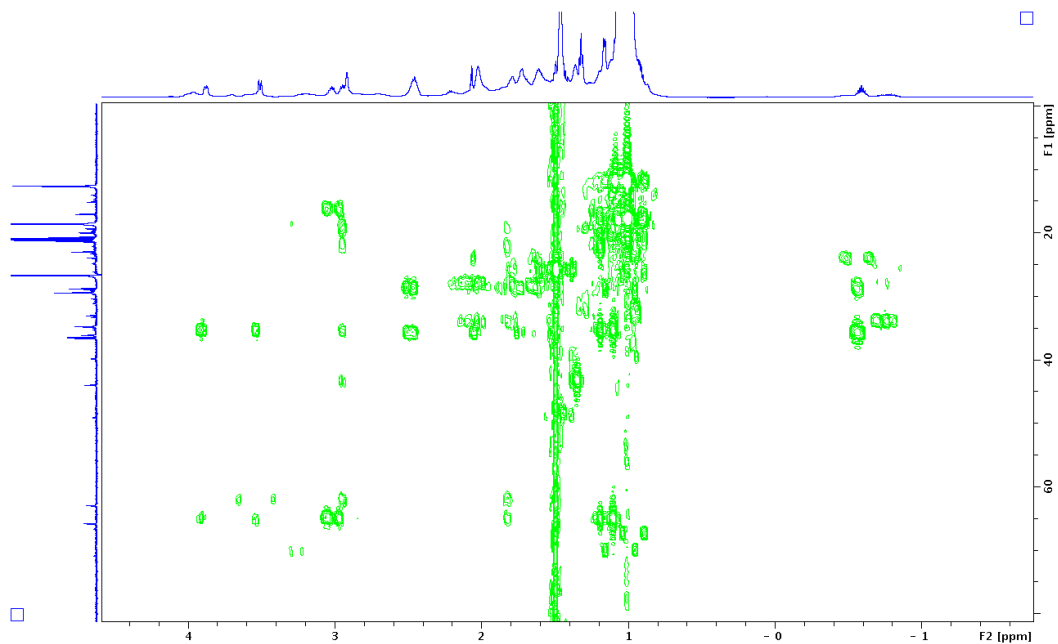


Figure S7.10. ^1H - ^{13}C HMBC of Mixed Aggregate **6a** in toluene- d_8 at -50°C

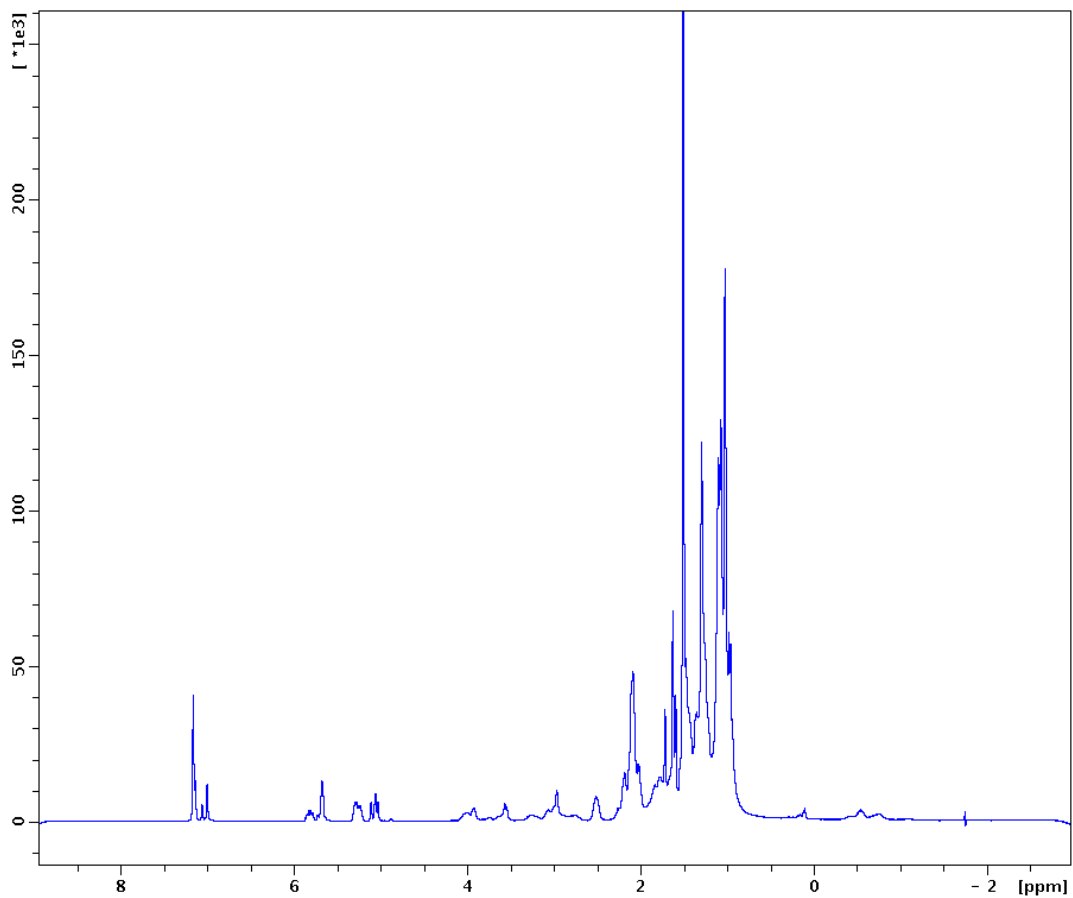


Figure S7.11. ^1H NMR of Mixed Aggregate **6a** in toluene- d_8 with Internal References at -50°C

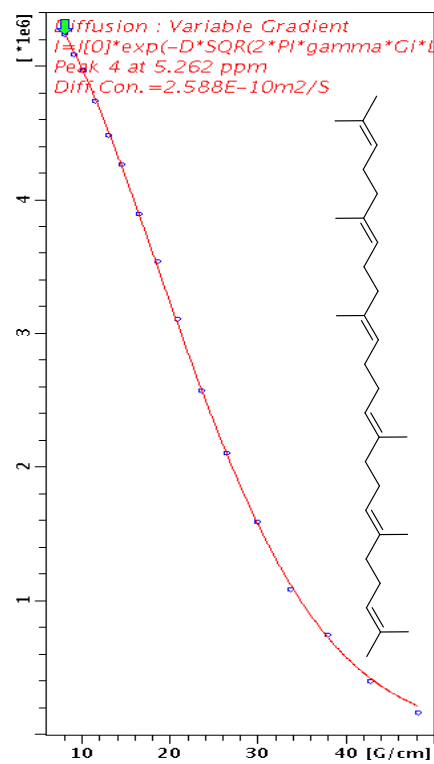
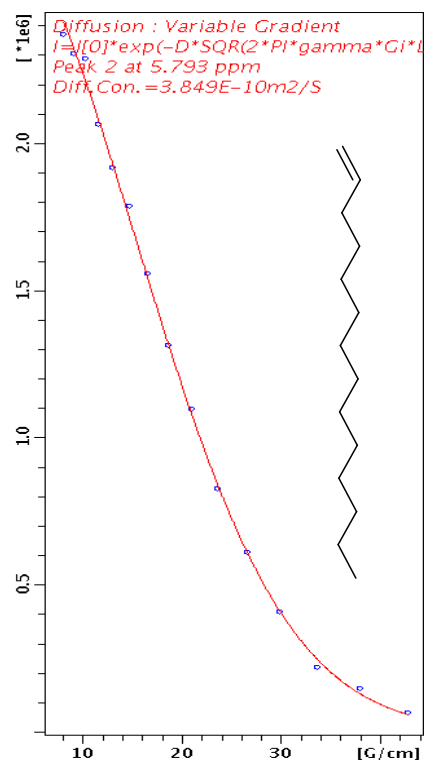
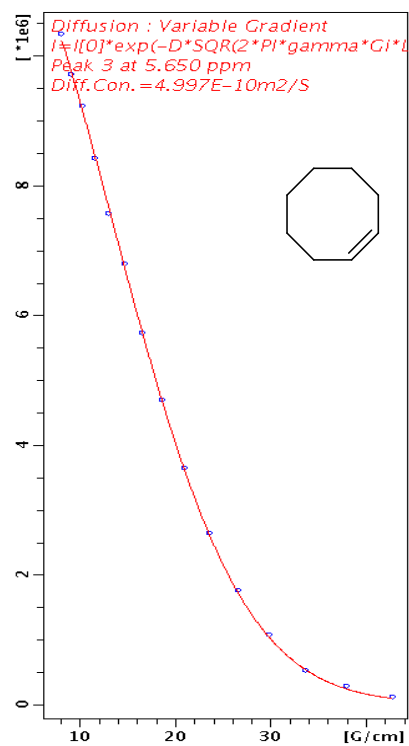
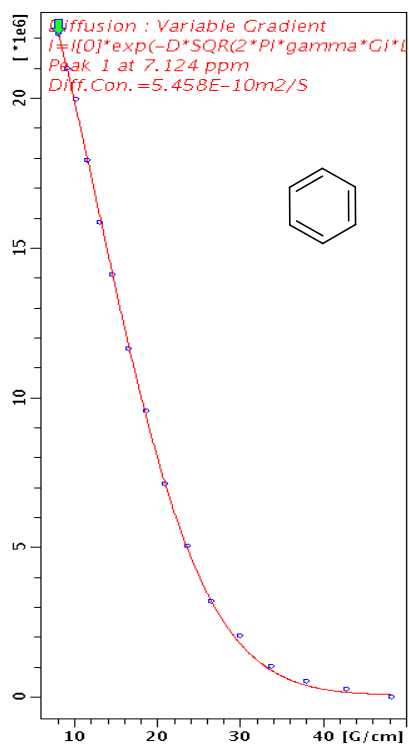


Figure S7.12. ¹H DOSY Decay Curves for Internal References

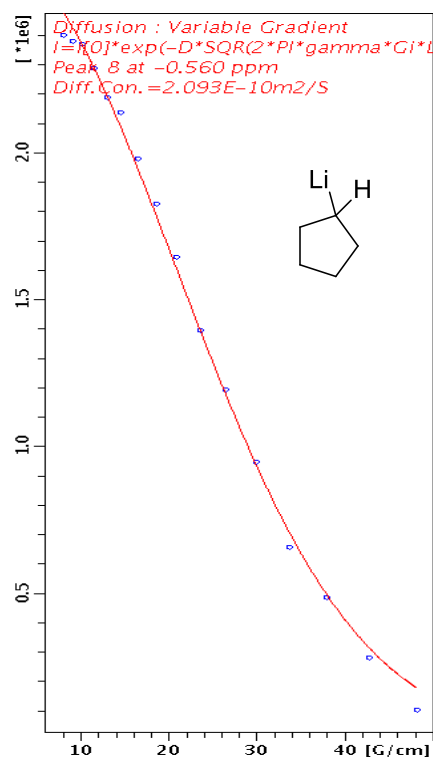
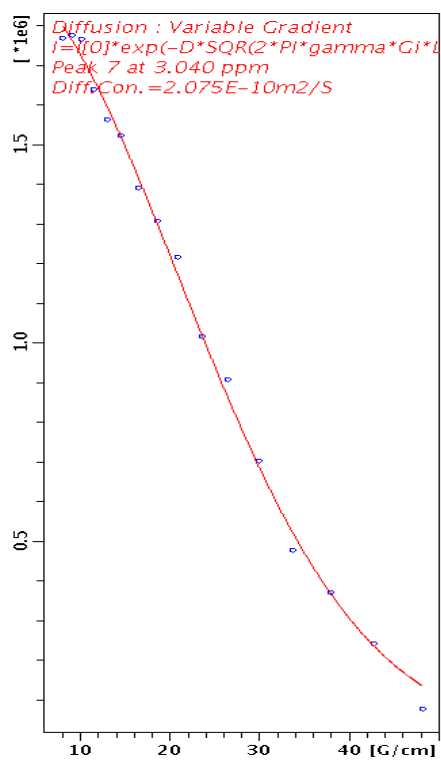
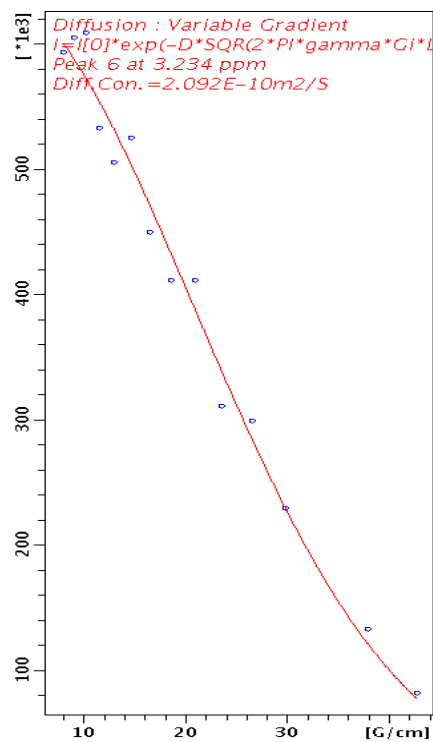
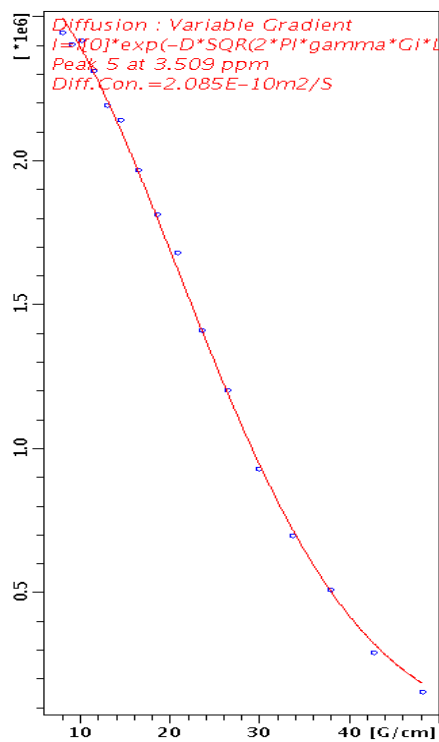


Figure S7.13. ¹H DOSY Decay Curves for Mixed Aggregate **6a**

Table S7.1. *D*-FW analysis of ^1H DOSY data of mixed aggregate **6a** toluene- d_8 solution at -50°C

Compound	FW (g/mol)	$10^{-10}D$ (m^2/s)	log FW	log D	Predicted FW (g/mol)	% error
BEN	78.11	5.458	1.893	-9.263	85.07	-8.9
COE	110.2	4.997	2.042	-9.301	103.1	6.4
TDE	196.4	3.849	2.293	-9.415	182.4	7.1
SQU	410.7	2.588	2.614	-9.587	433.9	-5.6
6a ^a	735.4 ^b	2.085 ^a	2.867	-9.681	695.5	5.4
6a ^a	735.4 ^b	2.092 ^a	2.867	-9.679	690.4	6.1
6a ^a	735.4 ^b	2.075 ^a	2.867	-9.683	702.8	4.4
6a ^c	735.4 ^b	2.093 ^b	2.867	-9.679	689.7	6.2
6a ^d	735.4 ^b	2.086 ^d	2.867	-9.681	694.6	5.5
Standard Dev. of Predicted FW of 6a					6.1	0.8

^aThe measured diffusion coefficients are from the resonances of chiral lithium amide. ^b735.4 g mol^{-1} is the formula weight of 2:2 lithiated chiral amine **5**/*c*-PenLi (^6Li labeled) complex **6a**. ^cThe measured diffusion coefficient is from the methine proton peak (-0.59 ppm) of *c*-PenLi. ^dThe diffusion coefficient is the average of the above four values.

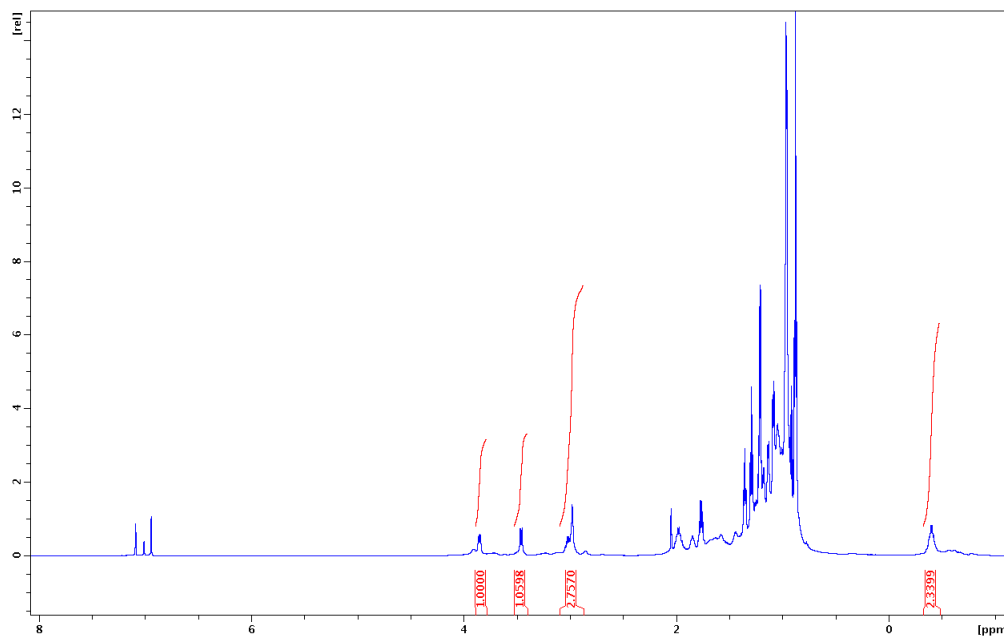


Figure S7.14. ^1H NMR of Mixed Aggregate **6b** in toluene- d_8 at -50°C

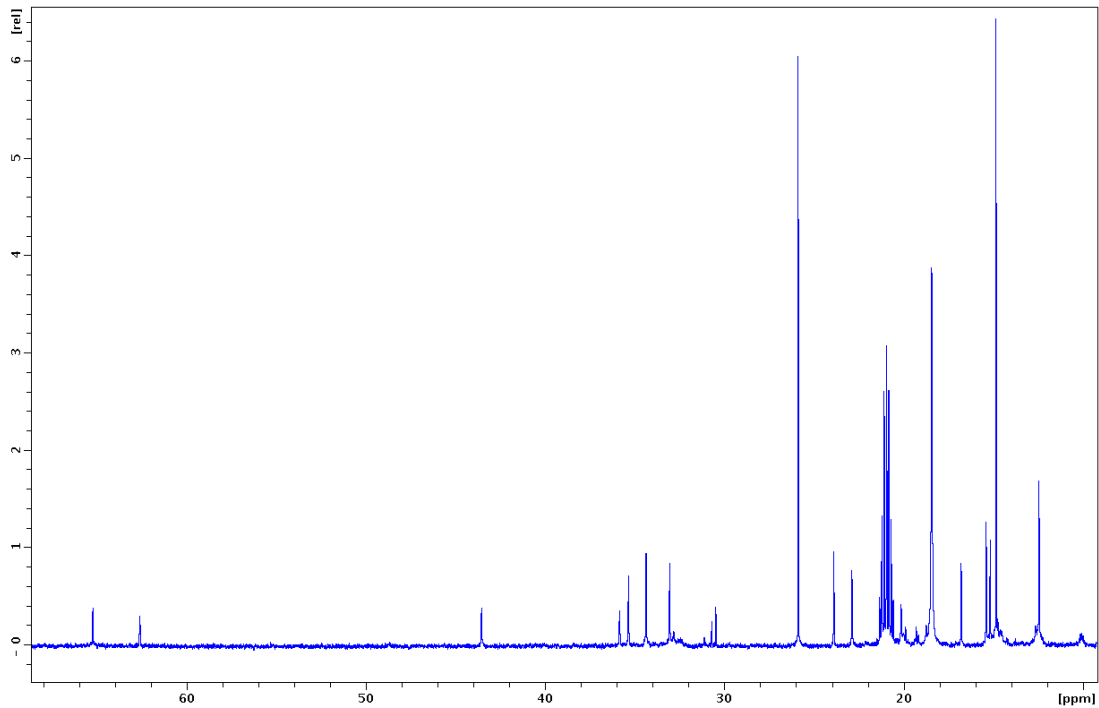


Figure S7.15. ^{13}C NMR of Mixed Aggregate **6b** in toluene- d_8 at $-50\text{ }^\circ\text{C}$

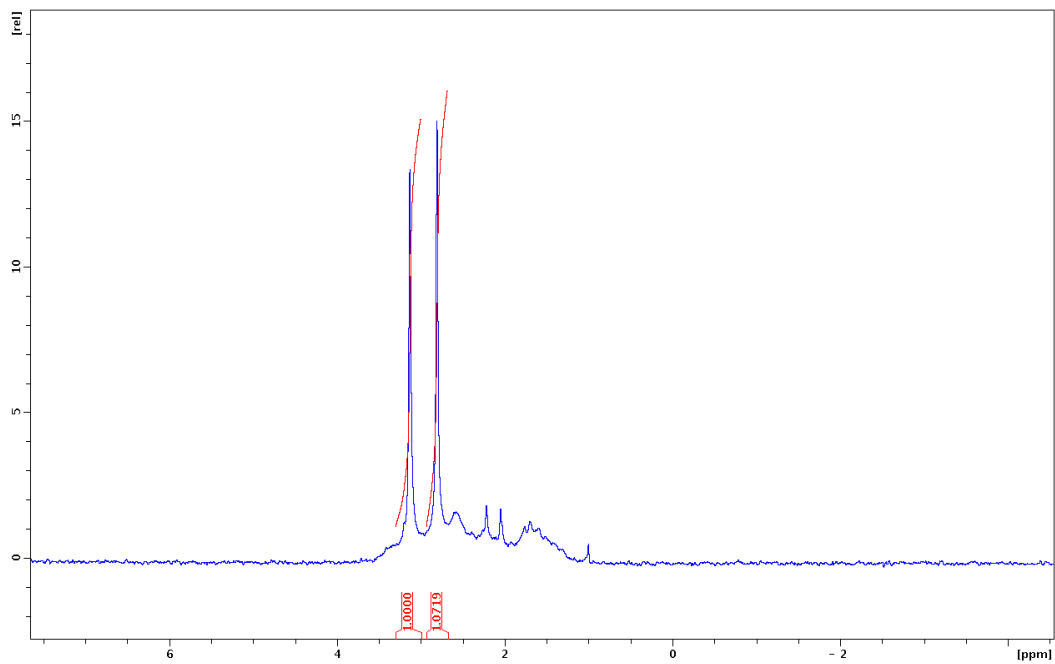


Figure S7.16. ^6Li NMR of Mixed Aggregate **6b** in toluene- d_8 at $-50\text{ }^\circ\text{C}$

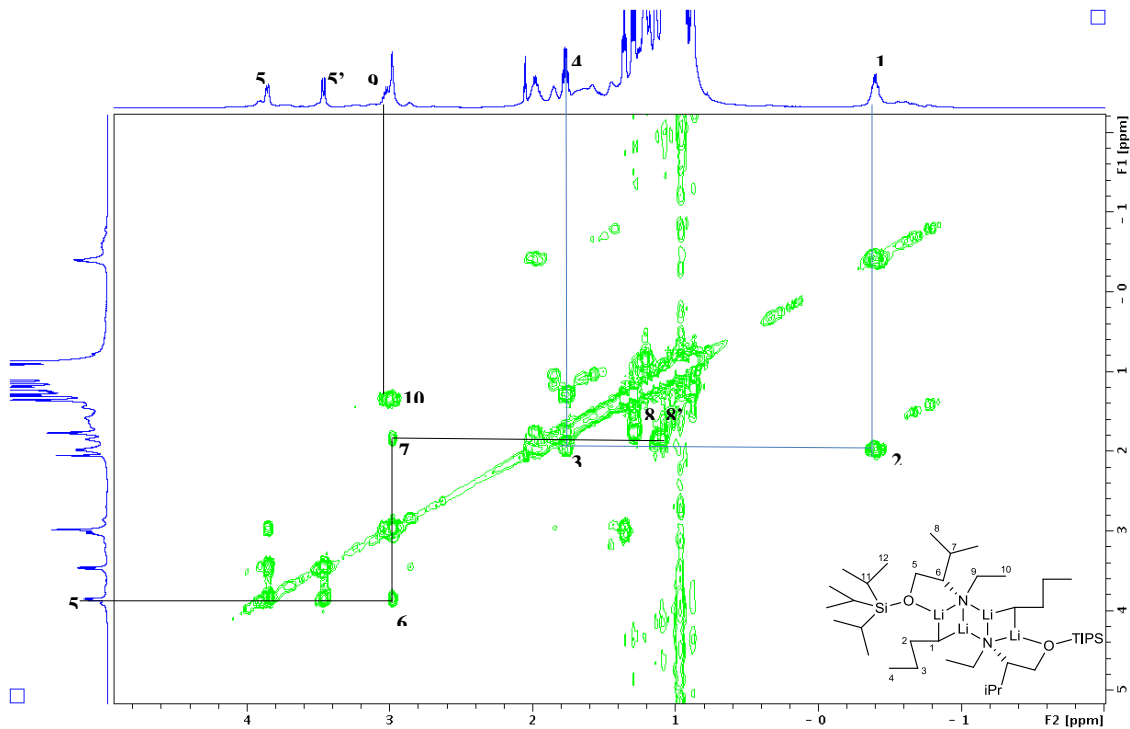


Figure S7.17. ^1H COSY of Mixed Aggregate **6b** in $\text{toluene-}d_8$ at -50°C

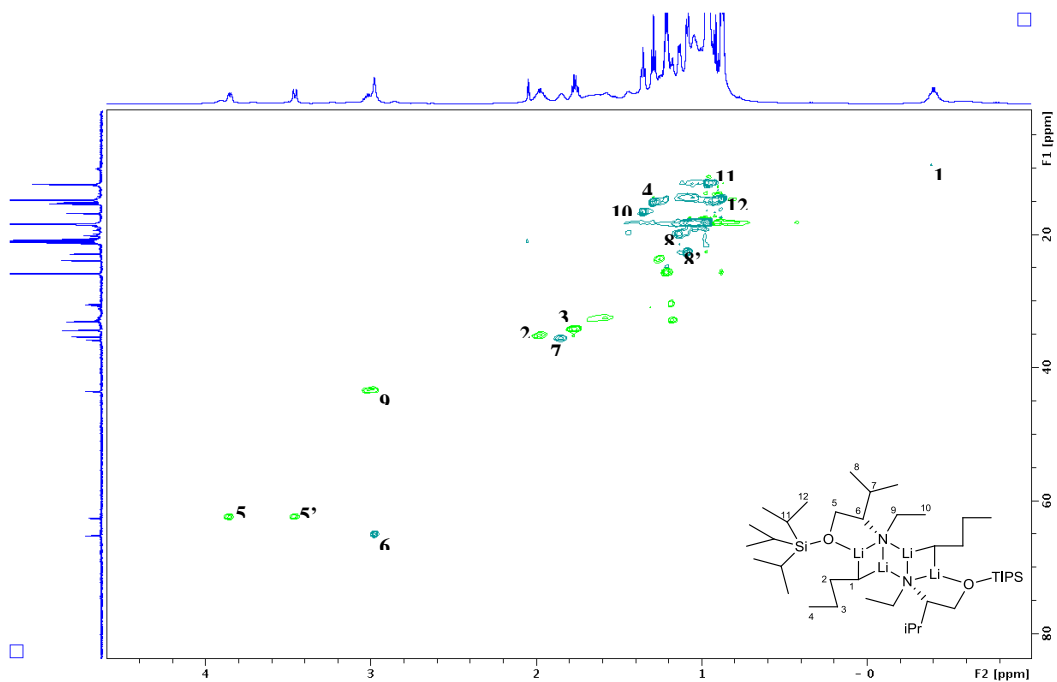


Figure S7.18. ^1H - ^{13}C HSQC of Mixed Aggregate **6b** in $\text{toluene-}d_8$ at -50°C

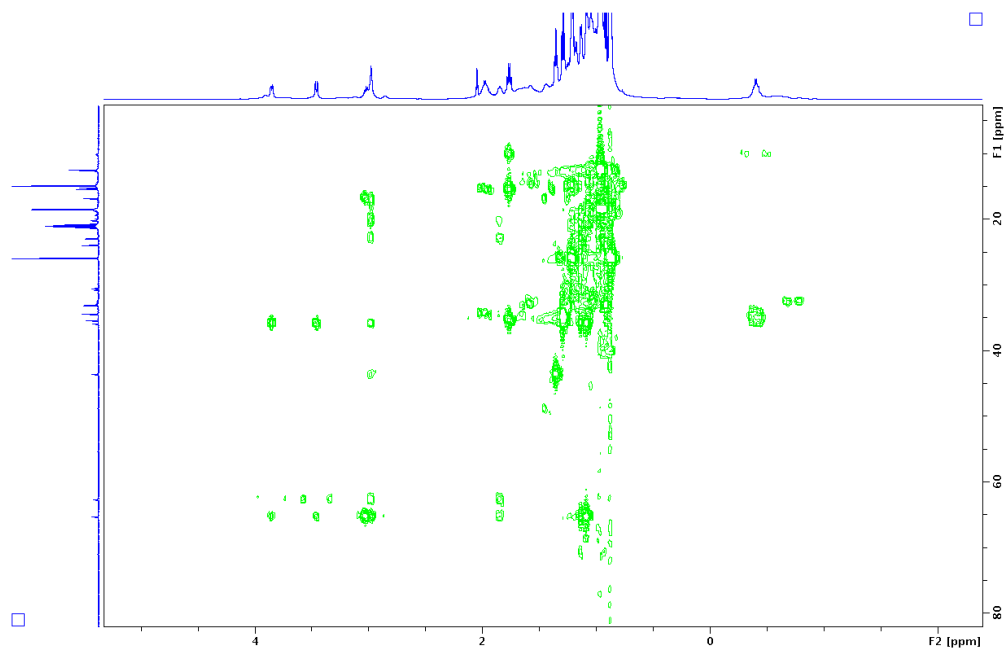


Figure S7.19. ^1H - ^{13}C HMBC of Mixed Aggregate **6b** in toluene- d_8 at $-50\text{ }^\circ\text{C}$

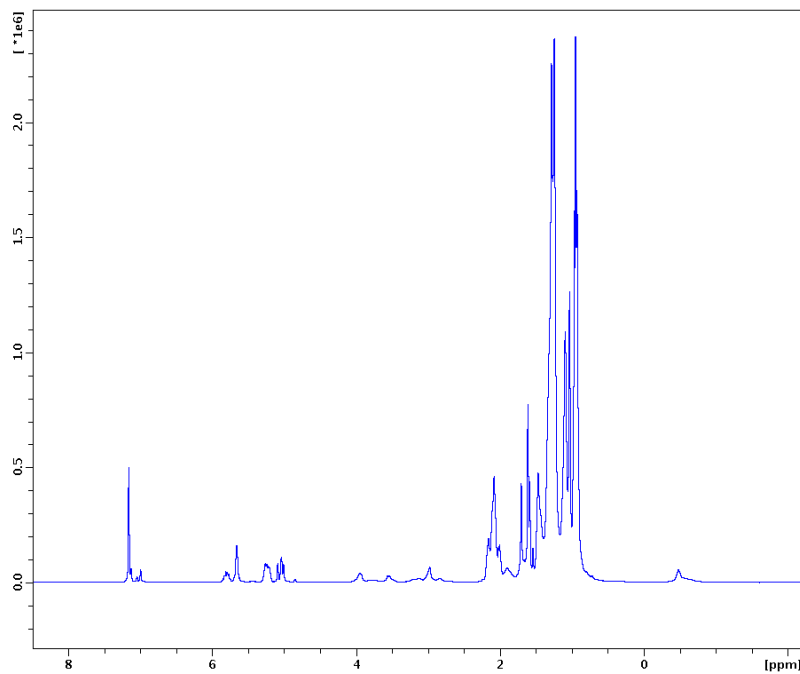


Figure S7.20. ^1H NMR of Mixed Aggregate **6b** in toluene- d_8 with Internal References at $-50\text{ }^\circ\text{C}$

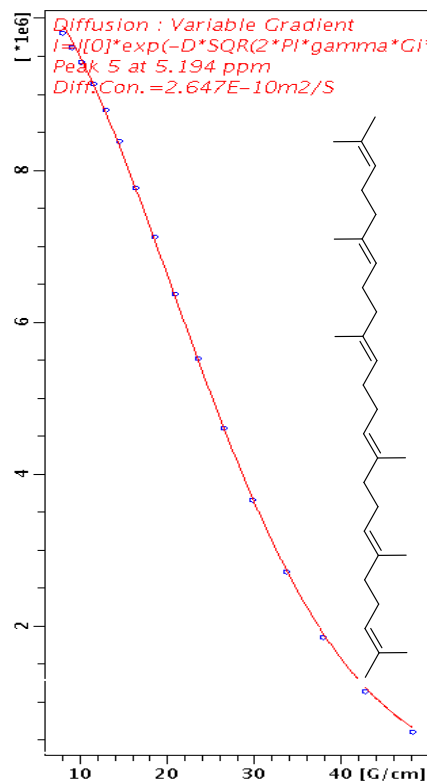
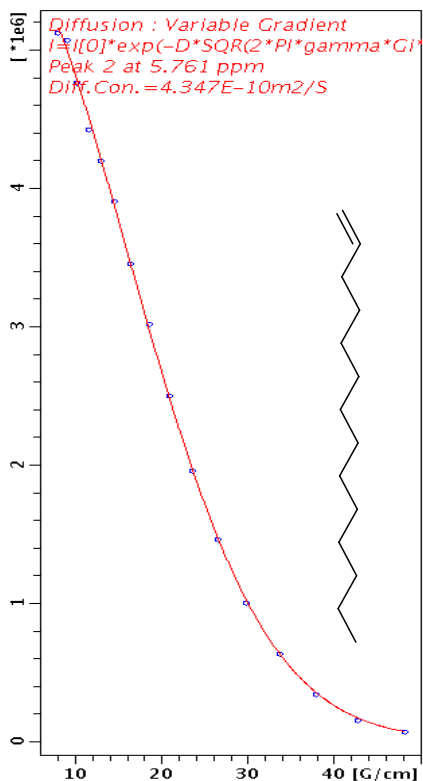
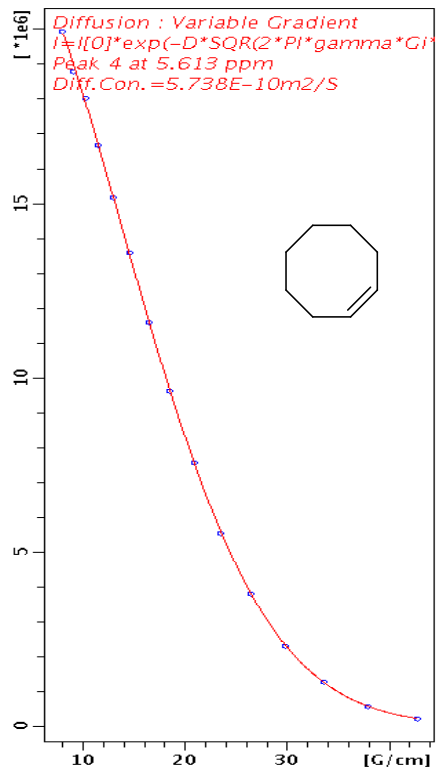
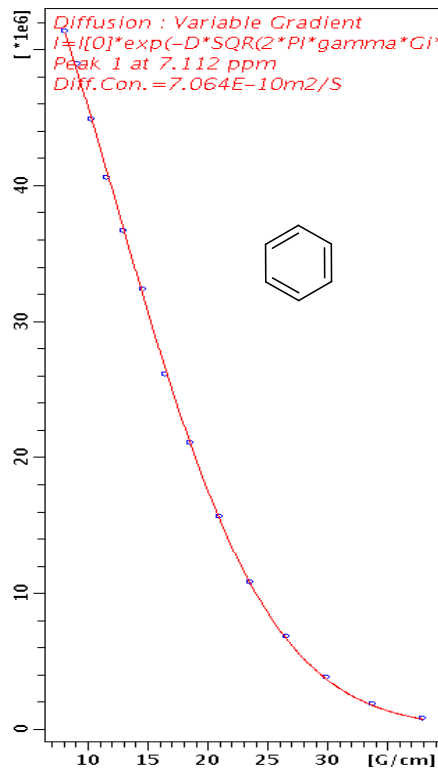


Figure S7.21. ¹H DOSY Decay Curves for Internal References

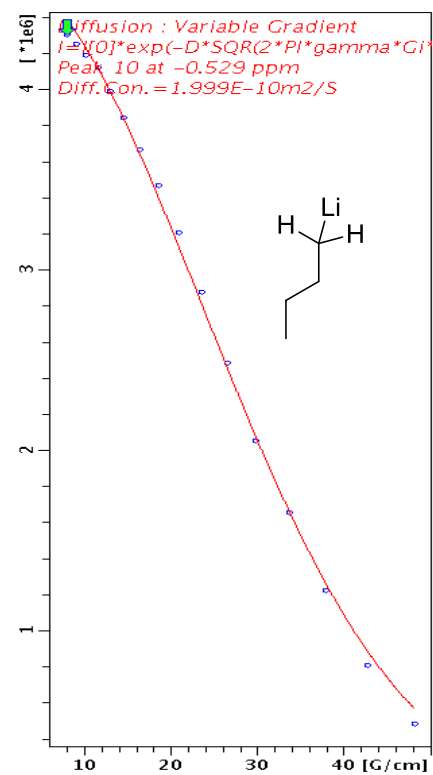
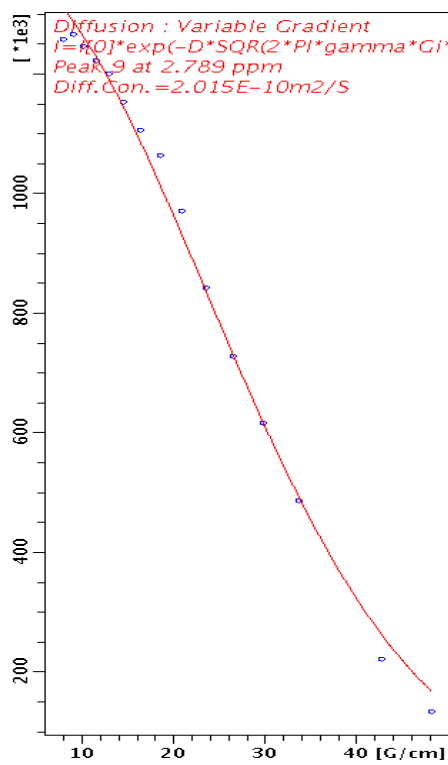
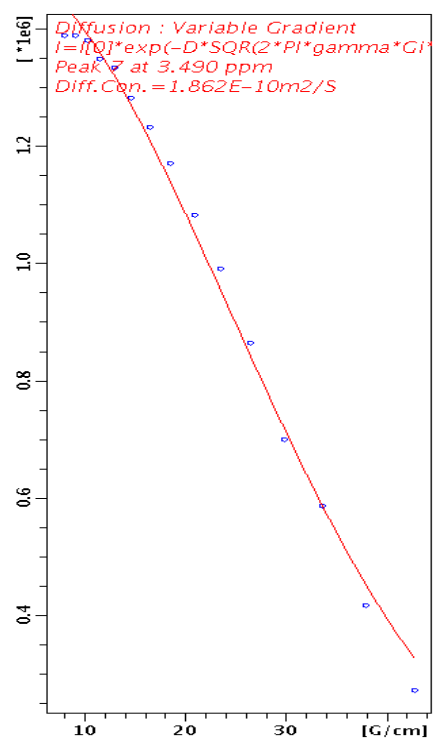
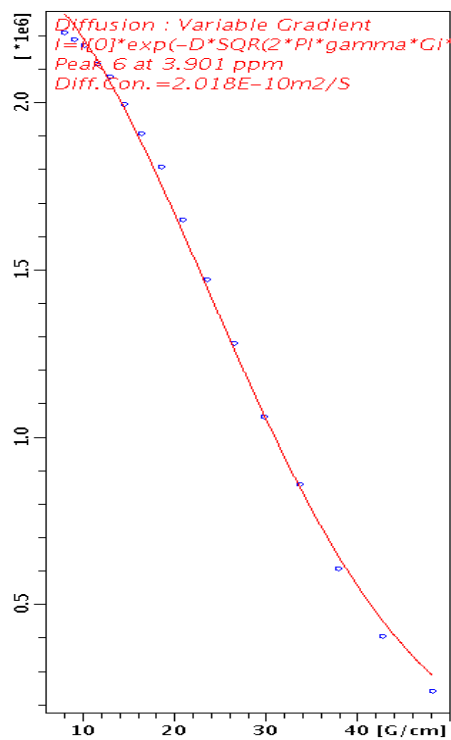


Figure S7.22. ¹H DOSY Decay Curves for Mixed Aggregate **6b**

Table S7.2. *D*-FW analysis of ¹H DOSY data of mixed aggregate **6b** toluene-*d*₈ solution at -50 °C

Compound	FW (g/mol)	10 ⁻¹⁰ <i>D</i> (m ² /s)	log FW	log <i>D</i>	Predicted FW (g/mol)	% error
BEN	78.11	7.064	1.893	-9.151	79.16	-1.3
COE	110.2	5.738	2.042	-9.241	113.1	-2.6
TDE	196.4	4.347	2.293	-9.362	182.0	7.3
SQU	410.7	2.647	2.614	-9.577	426.1	-3.8
6b ^a	711.4 ^b	2.018 ^a	2.852	-9.695	678.6	4.6
6b ^a	711.4 ^b	1.862 ^a	2.852	-9.730	779.0	-9.5
6b ^a	711.4 ^b	2.015 ^a	2.852	-9.696	680.3	4.4
6b ^c	711.4 ^b	1.999 ^b	2.852	-9.699	689.7	3.1
6b ^d	711.4 ^b	1.974 ^d	2.852	-9.705	706.9	0.6
Standard Dev. of Predicted FW of 6b					48.3	6.8

^aThe measured diffusion coefficients are from the resonances of chiral lithium amide. ^b711.4 gmol⁻¹ is the formula weight of 2:2 lithiated chiral amine **5**/*n*-BuLi (⁶Li labeled) complex **6b**. ^cThe measured diffusion coefficient is from the resonance of α -methylene protons (-0.40 ppm) of *n*-BuLi. ^dThe diffusion coefficient is the average of the above four values.

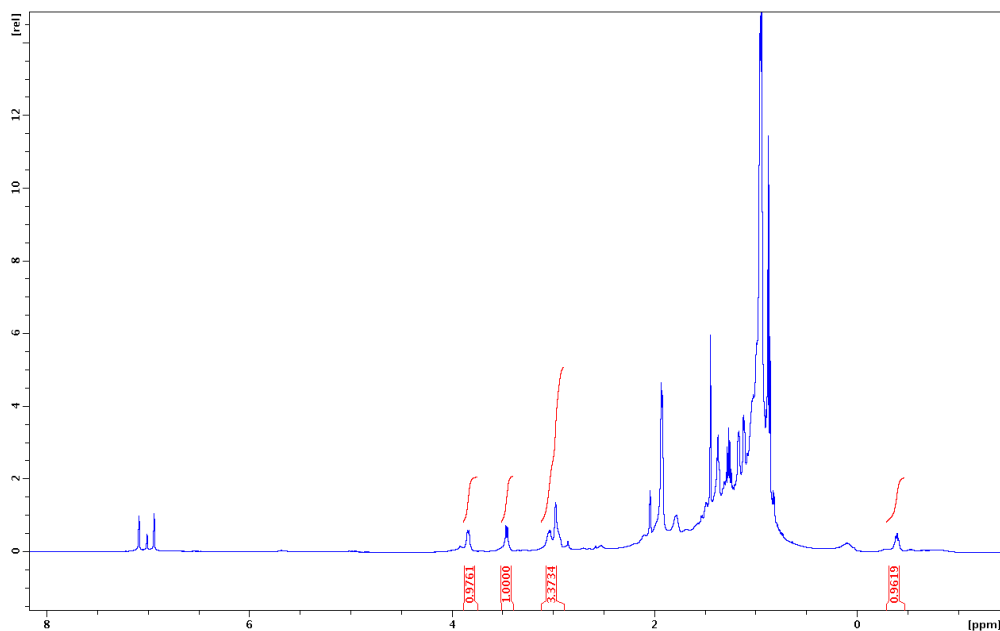


Figure S7.23. ¹H NMR of Mixed Aggregate **6c** in toluene-*d*₈ at -50 °C

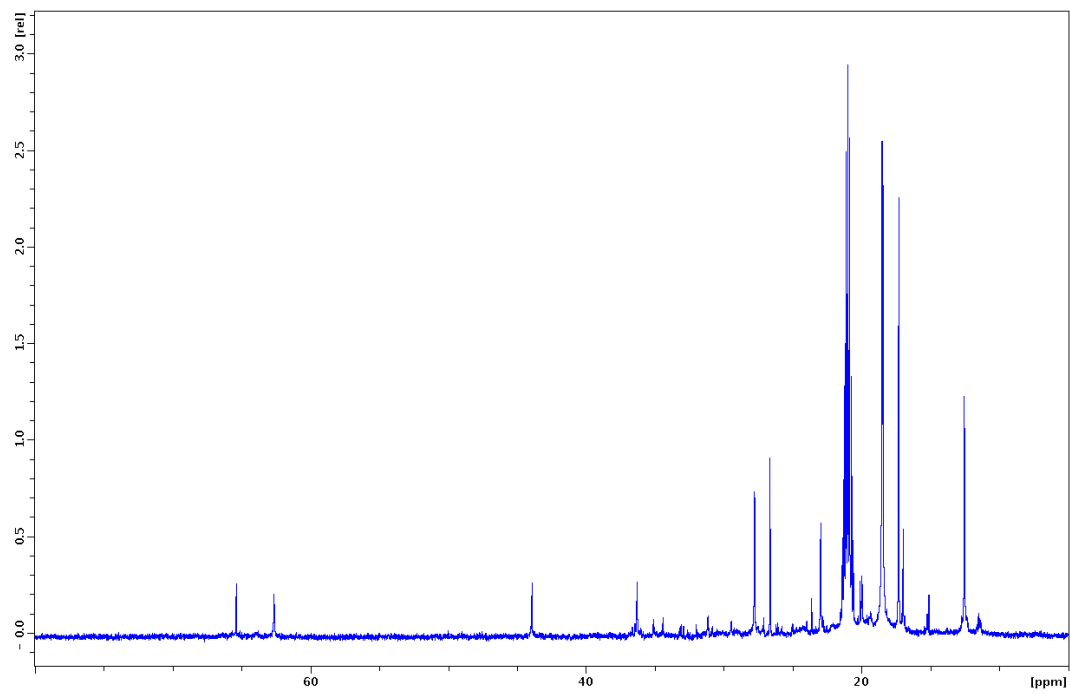


Figure S7.24. ^{13}C NMR of Mixed Aggregate **6c** in toluene- d_8 at $-50\text{ }^\circ\text{C}$

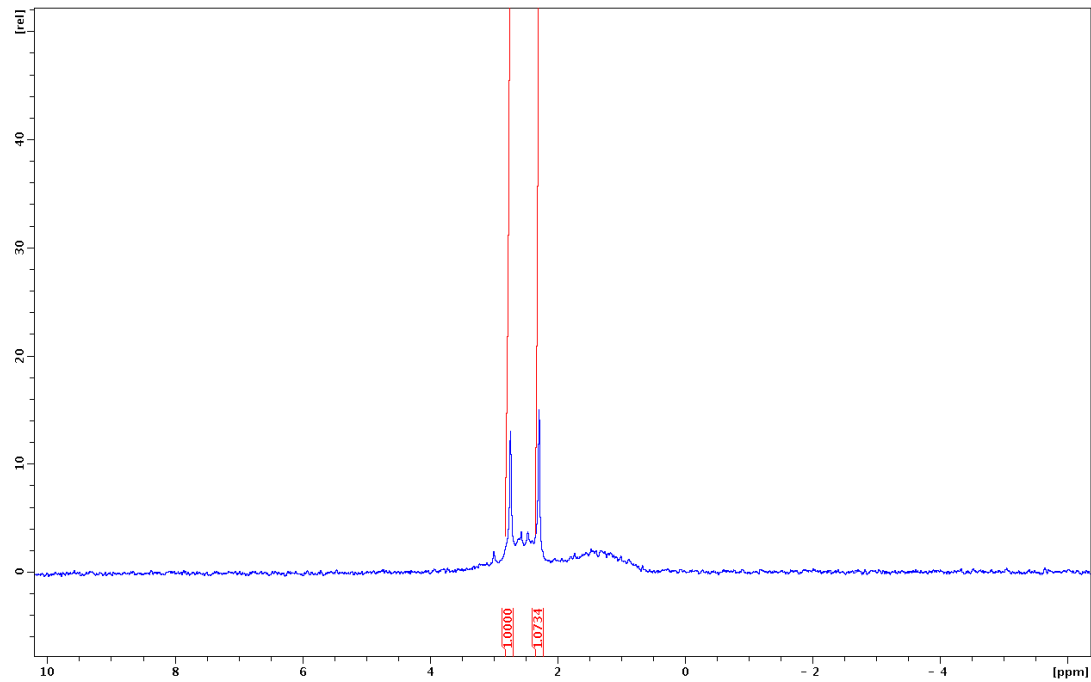


Figure S7.25. ^6Li NMR of Mixed Aggregate **6c** in toluene- d_8 at $-50\text{ }^\circ\text{C}$

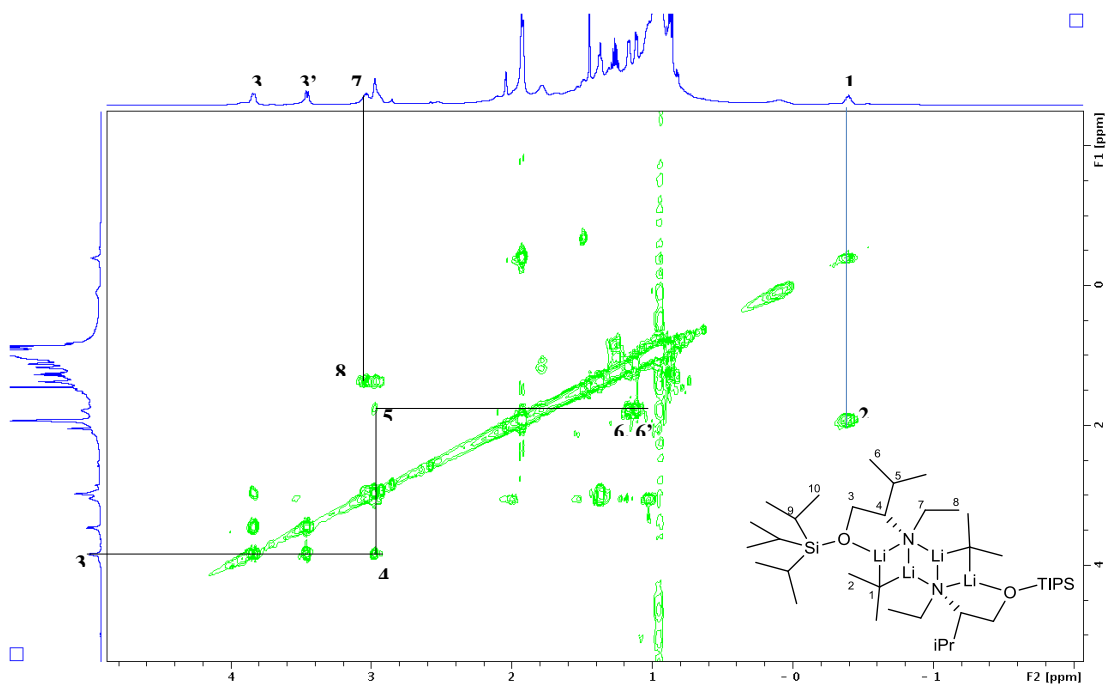


Figure S7.26. ^1H COSY of Mixed Aggregate **6c** in toluene- d_8 at $-50\text{ }^\circ\text{C}$

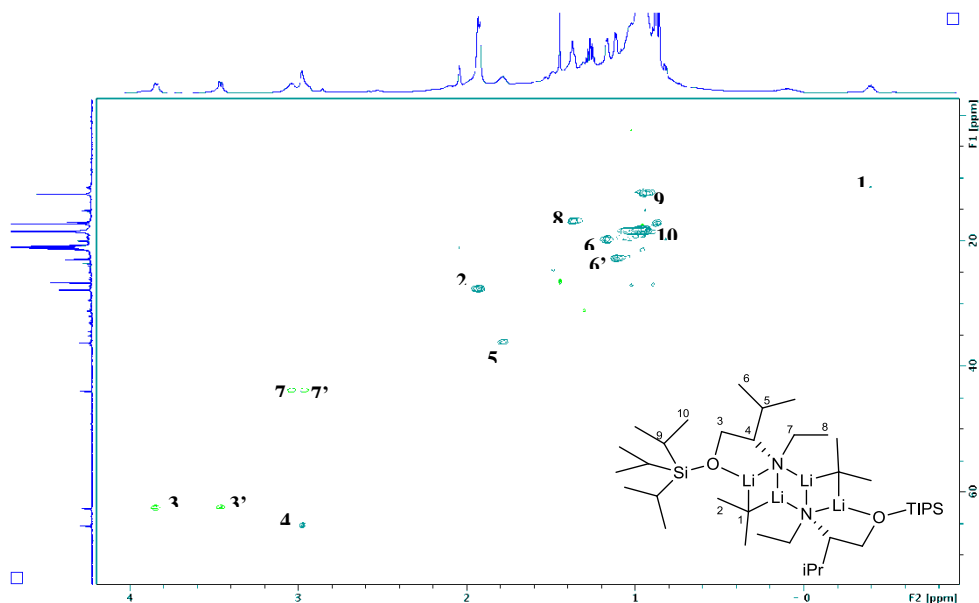


Figure S7.27. ^1H - ^{13}C HSQC of Mixed Aggregate **6c** in toluene- d_8 at $-50\text{ }^\circ\text{C}$

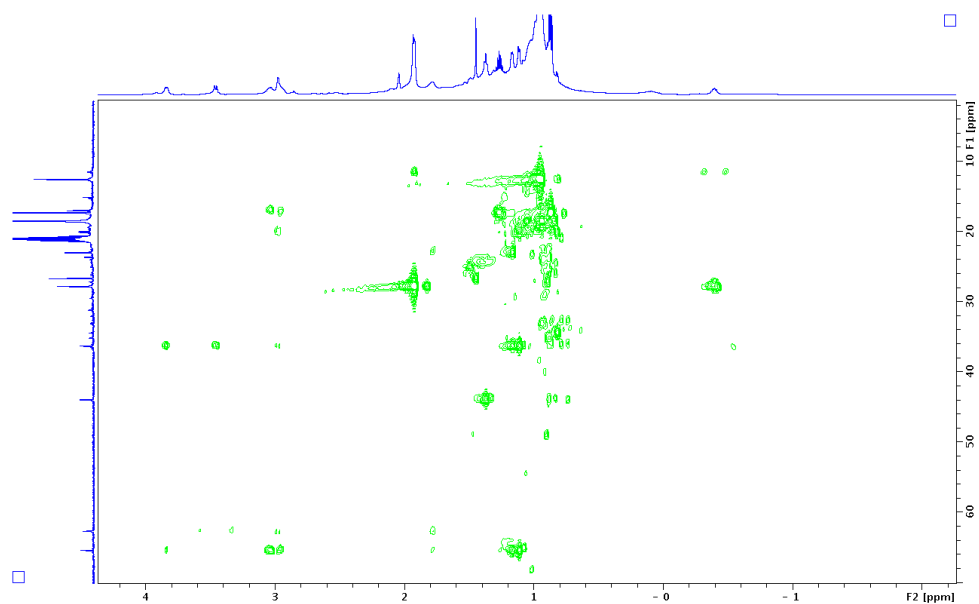


Figure S7.28. ^1H - ^{13}C HMBC of Mixed Aggregate **6c** in toluene- d_8 at $-50\text{ }^\circ\text{C}$

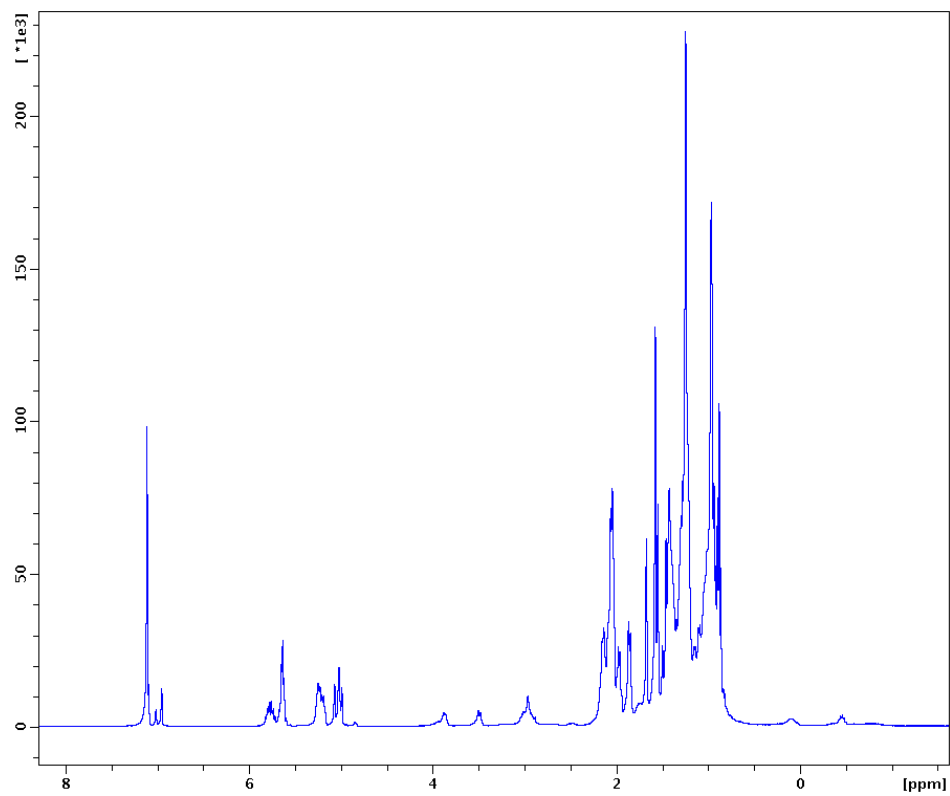


Figure S7.29. ^1H NMR of Mixed Aggregate **6c** in toluene- d_8 with Internal References at $-50\text{ }^\circ\text{C}$

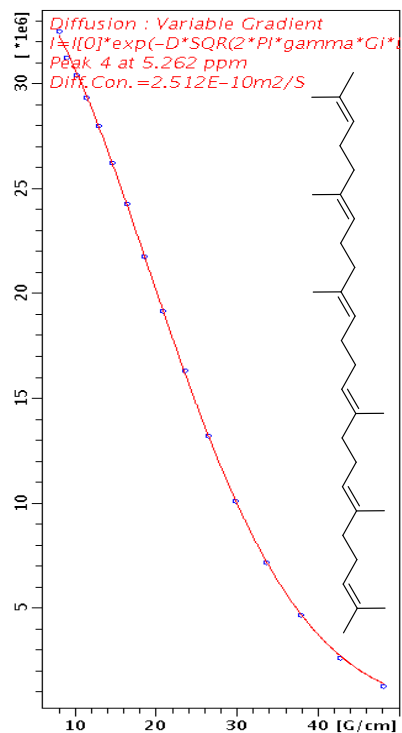
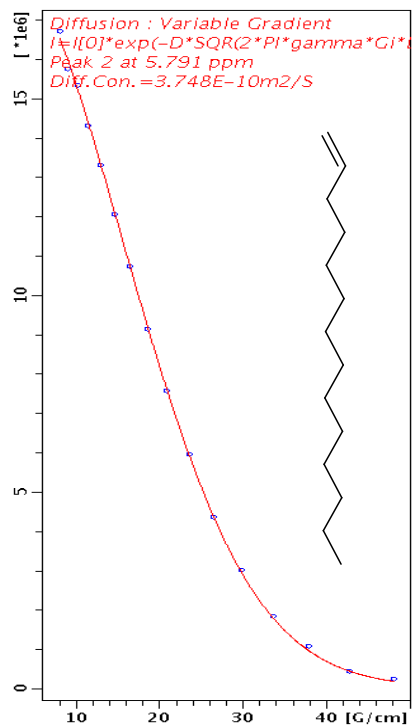
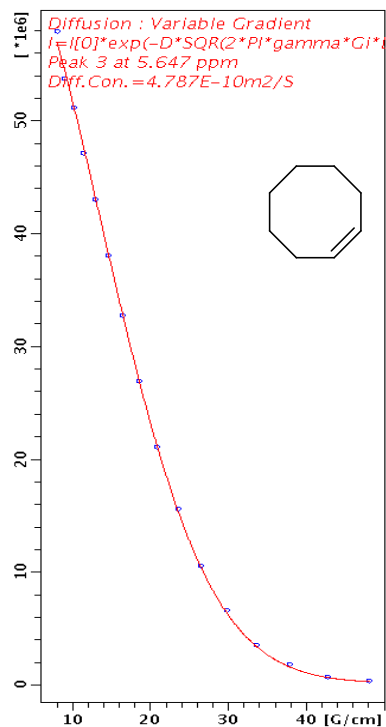
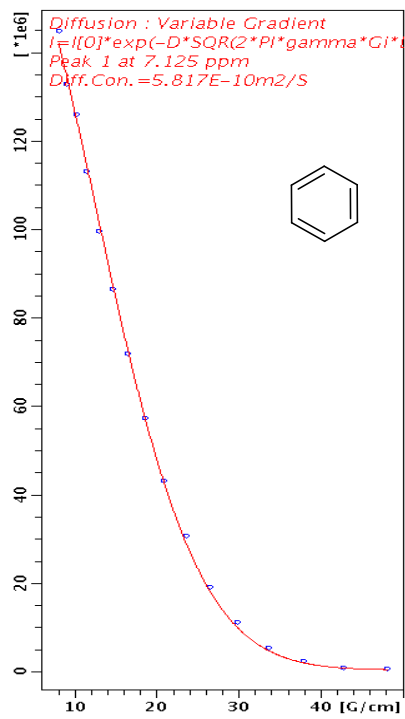


Figure S7.30. ¹H DOSY Decay Curves for Internal References

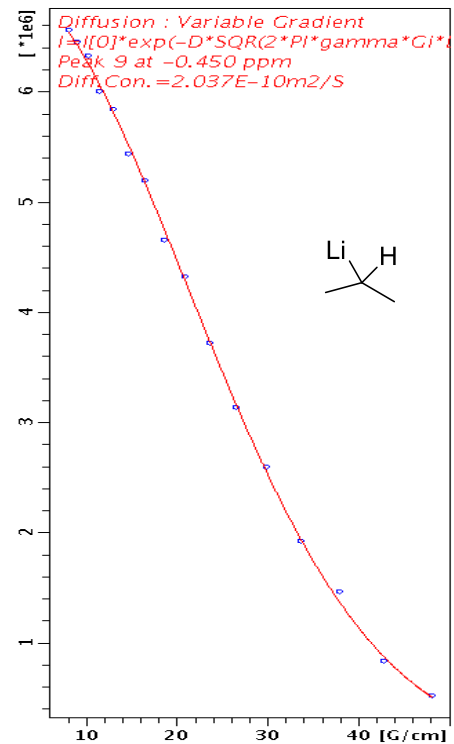
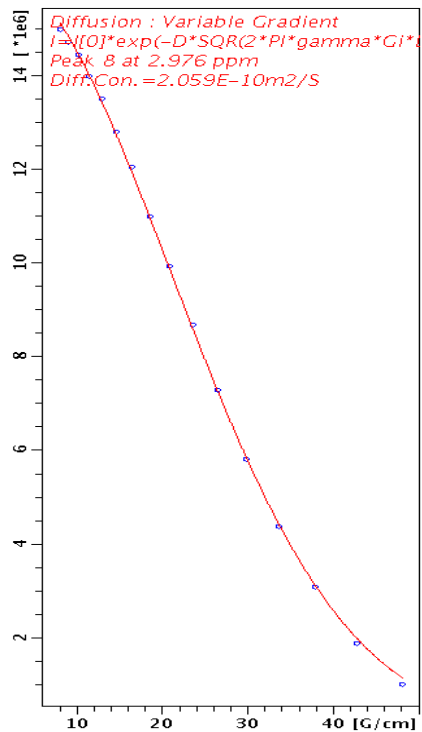
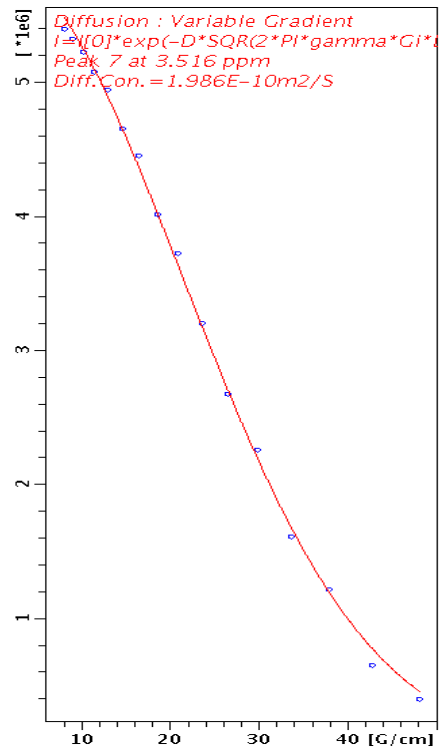
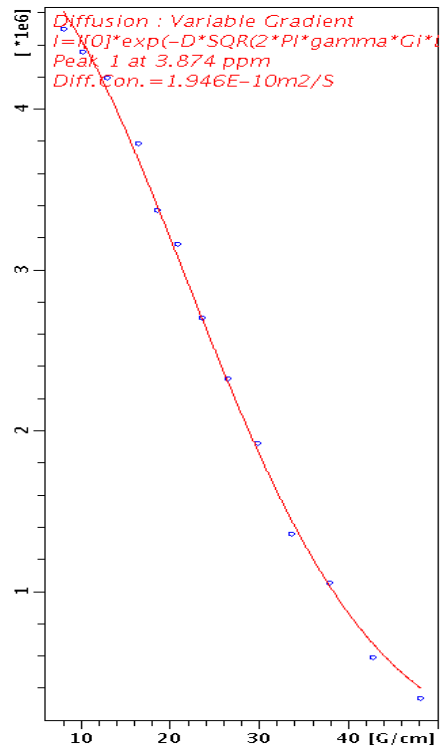


Figure S7.31. ¹H DOSY Decay Curves for Mixed Aggregate **6c**

Table S7.3. *D*-FW analysis of ^1H DOSY data of mixed aggregate **6c** toluene- d_8 solution at $-50\text{ }^\circ\text{C}$

Compound	FW (g/mol)	$10^{-10}D$ (m^2/s)	log FW	log D	Predicted FW (g/mol)	% error
BEN	78.11	5.817	1.893	-9.235	77.40	0.9
COE	110.2	4.787	2.042	-9.320	114.5	-3.9
TDE	196.4	3.748	2.293	-9.426	187.2	4.7
SQU	410.7	2.512	2.614	-9.600	418.4	-1.9
6c ^a	711.4 ^b	1.946 ^a	2.852	-9.711	698.9	-2.3
6c ^a	711.4 ^b	1.986 ^a	2.852	-9.702	670.9	1.8
6c ^a	711.4 ^b	2.059 ^a	2.852	-9.686	624.0	8.7
6c ^c	711.4 ^b	2.037 ^c	2.852	-9.691	637.6	6.7
6c ^d	711.4 ^b	2.036 ^d	2.852	-9.697	656.9	3.9
Standard Dev. of Predicted FW of 6c					33.7	4.9

^aThe measured diffusion coefficients are from the resonances of chiral lithium amide. 683.3 gmol^{-1} is the formula weight of 2:2 lithiated chiral amine **5**/*i*-PrLi (^6Li labeled) complex **6c**. ^cThe measured diffusion coefficient is from the resonance of the methine proton (-0.39 ppm) of *i*-PrLi. ^dThe diffusion coefficient is the average of the above four values.

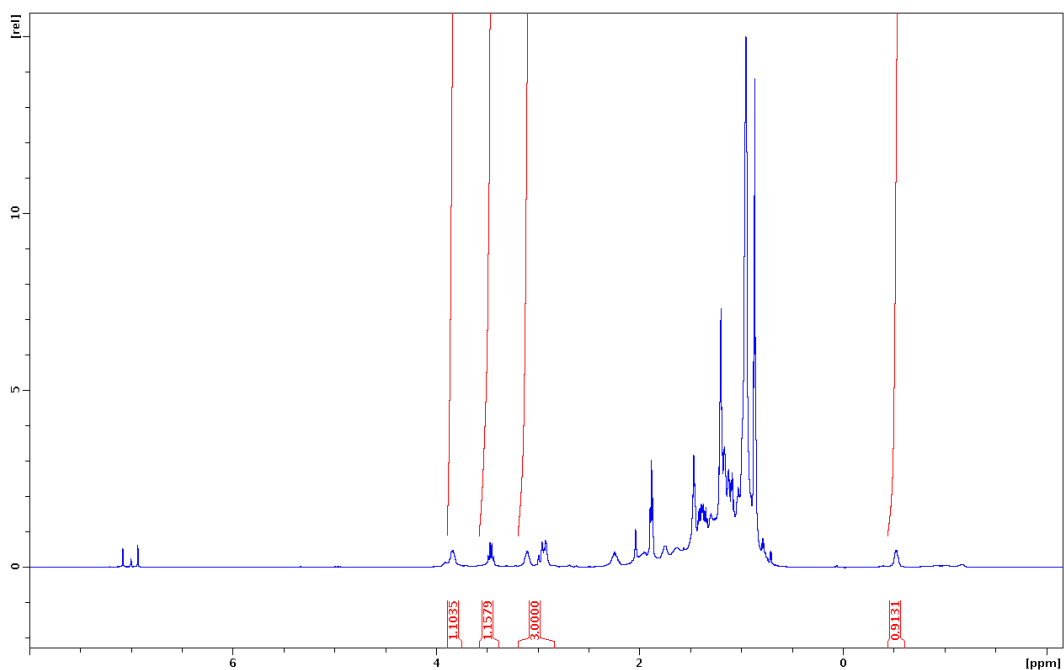


Figure S7.32. ^1H NMR of Mixed Aggregate **6d** in toluene- d_8 at $-50\text{ }^\circ\text{C}$

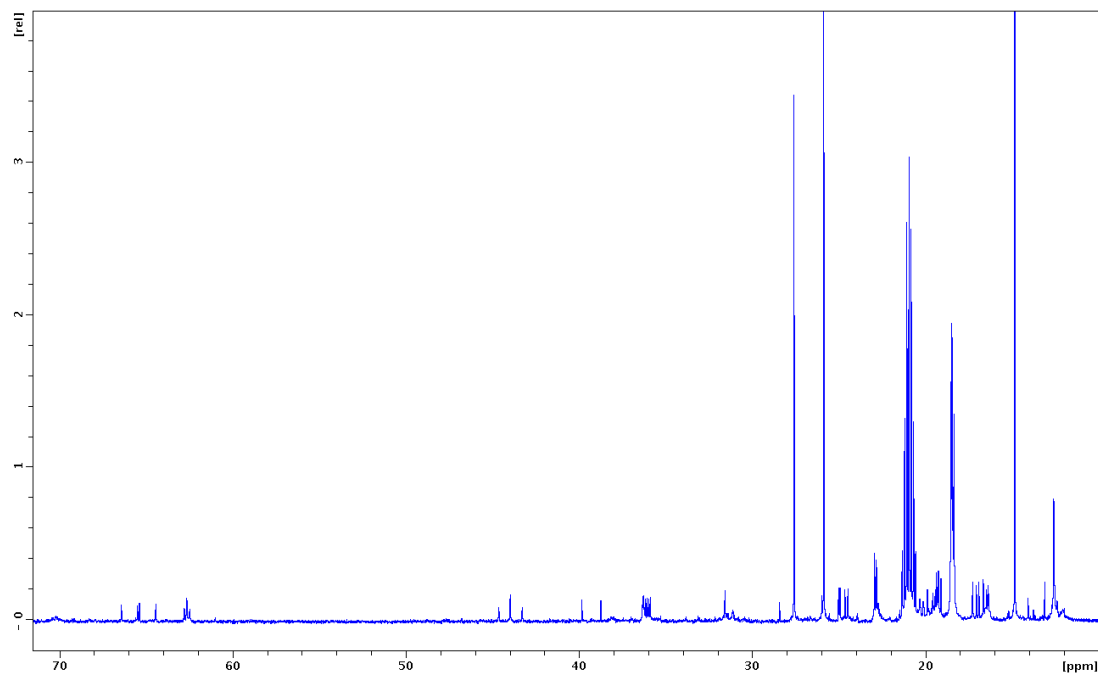


Figure S7.33. ^{13}C NMR of Mixed Aggregate **6d** in toluene- d_8 at $-50\text{ }^\circ\text{C}$

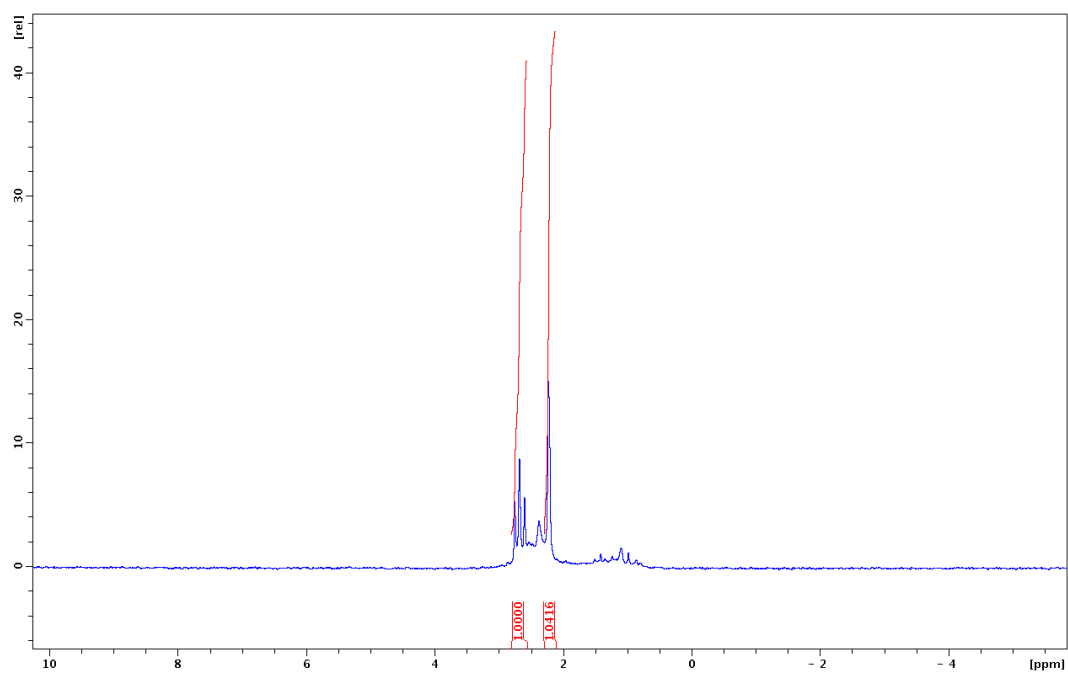


Figure S7.34. ^6Li NMR of Mixed Aggregate **6d** in toluene- d_8 at $-50\text{ }^\circ\text{C}$

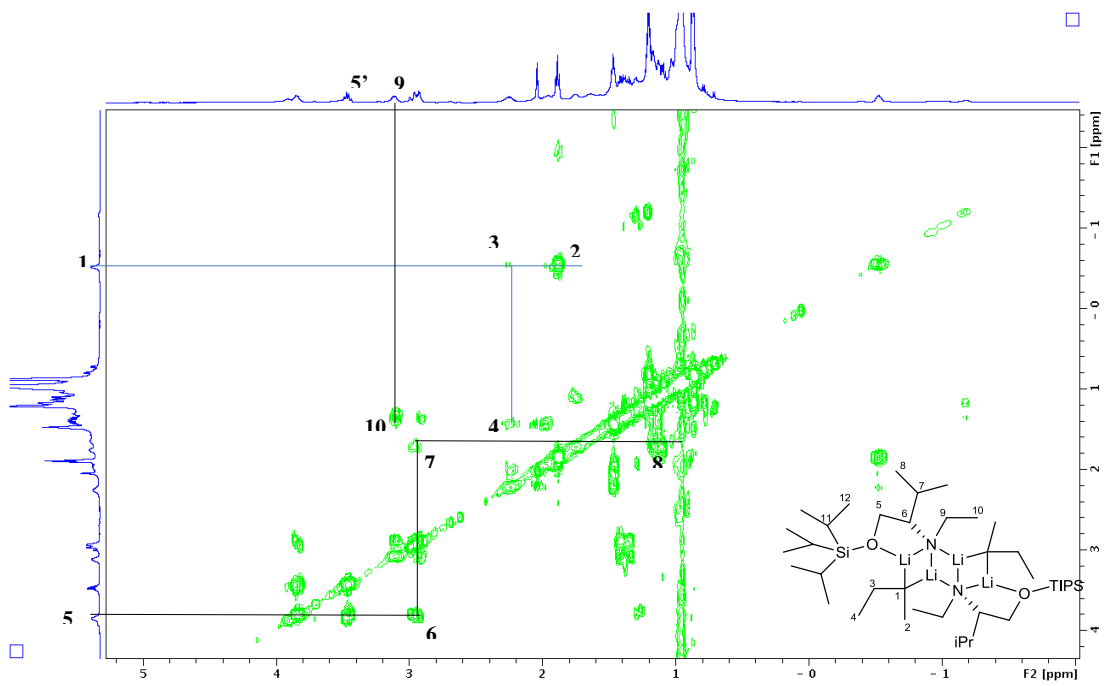


Figure S7.35. ^1H COSY of Mixed Aggregate **6d** in toluene- d_8 at $-50\text{ }^\circ\text{C}$

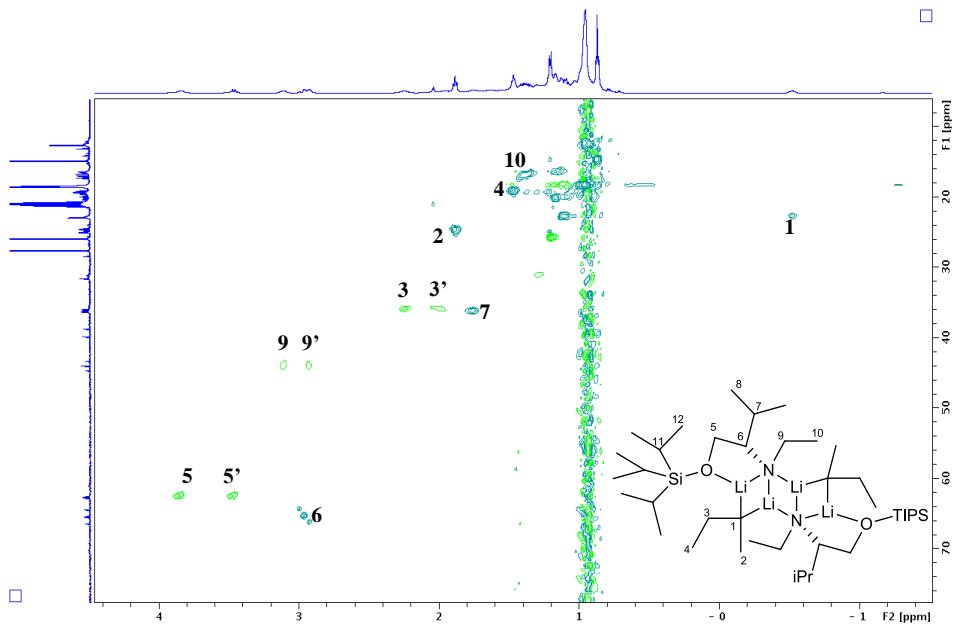


Figure S7.36. ^1H - ^{13}C HSQC of Mixed Aggregate **6d** in toluene- d_8 at $-50\text{ }^\circ\text{C}$

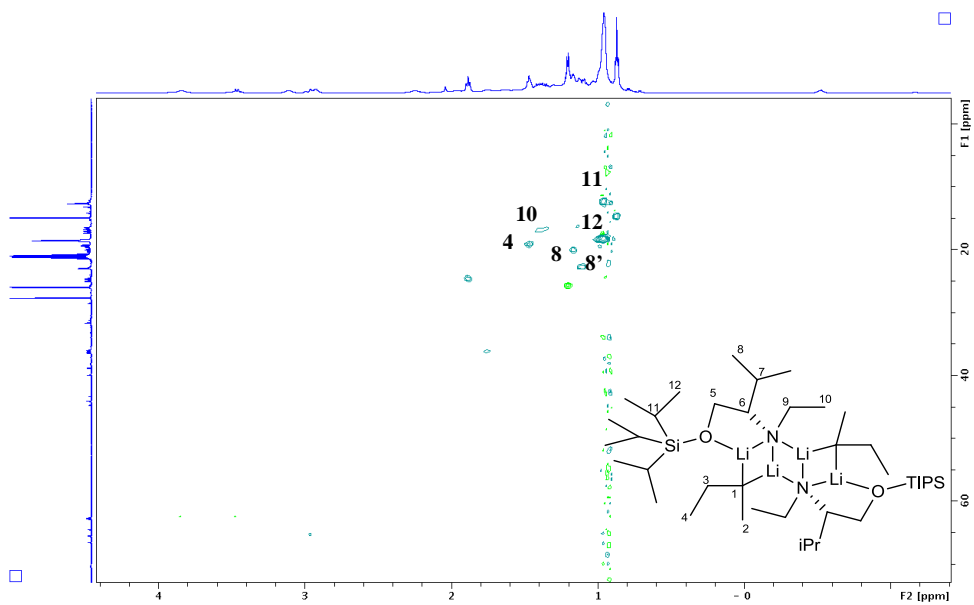


Figure S7.37. ^1H - ^{13}C HSQC of Mixed Aggregate **6d** in toluene- d_8 at $-50\text{ }^\circ\text{C}$ (Enlarged)

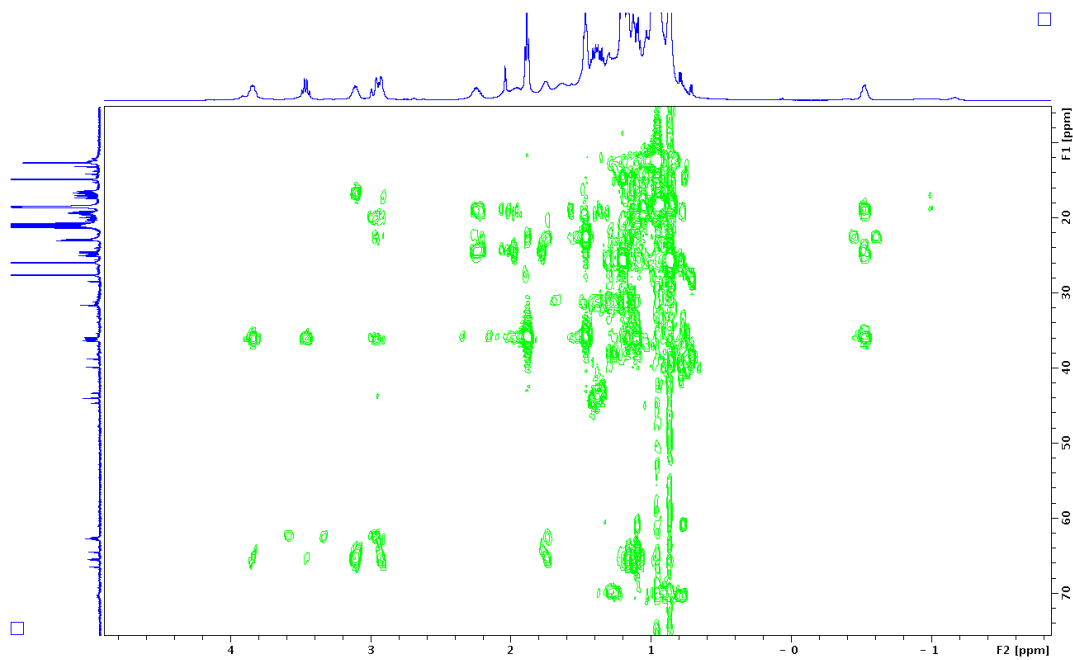


Figure S7.38. ^1H - ^{13}C HMBC of Mixed Aggregate **6d** in toluene- d_8 at $-50\text{ }^\circ\text{C}$

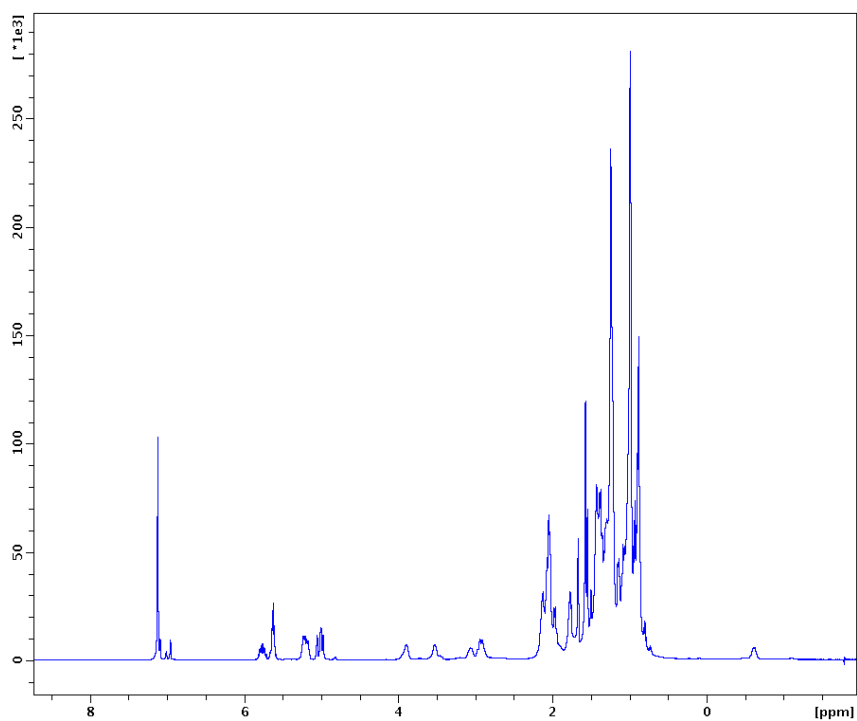


Figure S7.39. ^1H NMR of Mixed Aggregate **6d** in $\text{toluene-}d_8$ with Internal References at $-50\text{ }^\circ\text{C}$

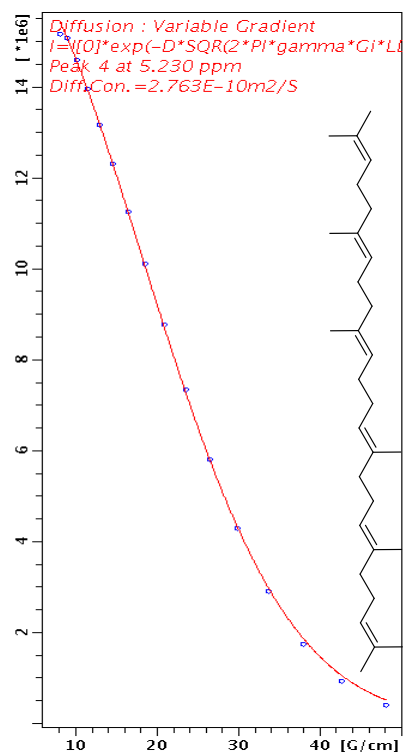
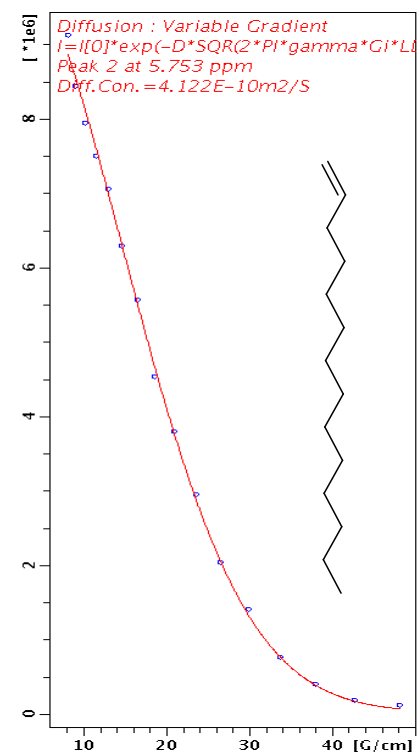
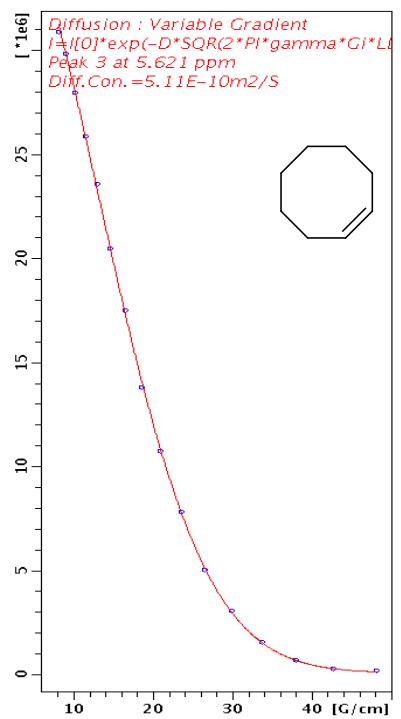
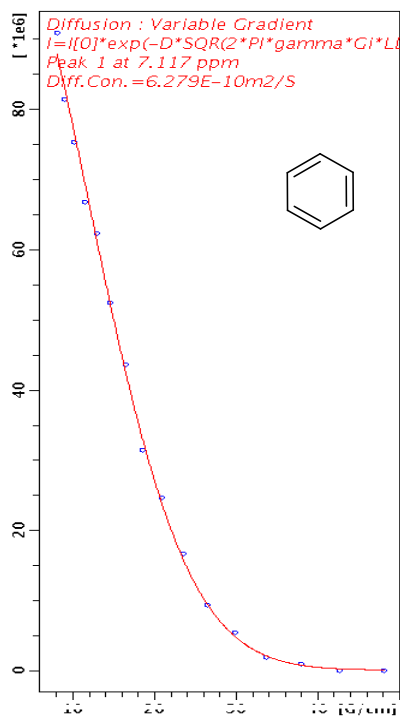


Figure S7.40. ¹H DOSY Decay Curves for Internal References

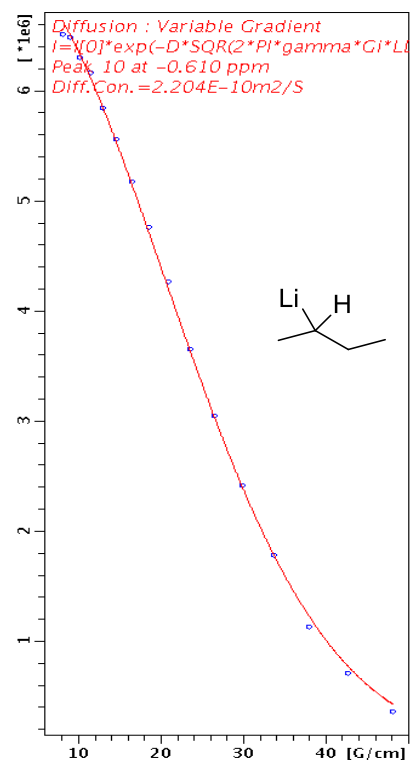
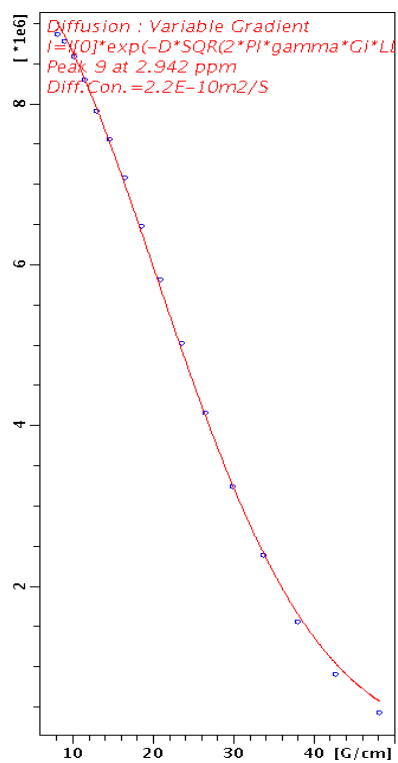
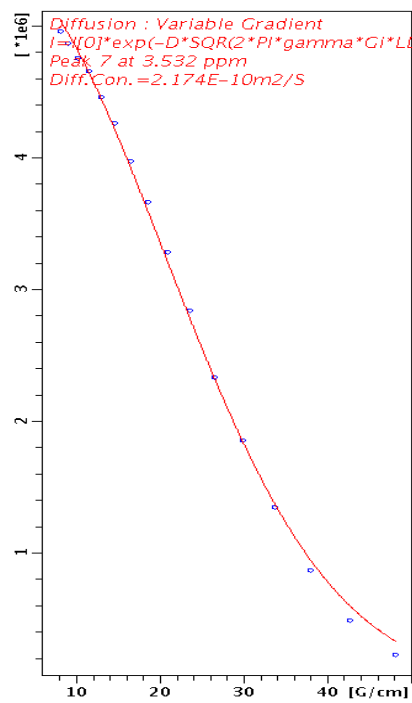
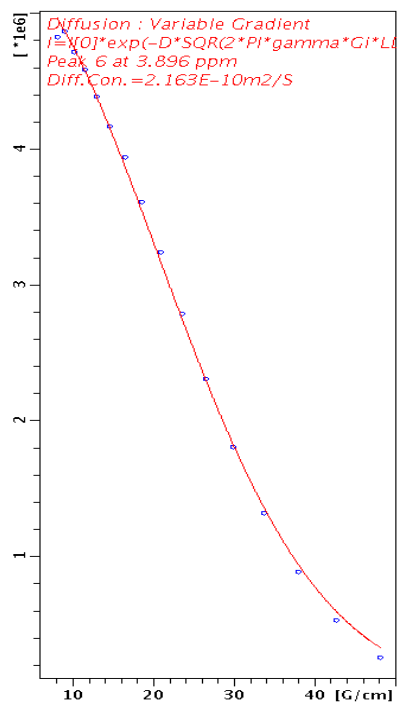


Figure S7.41. ^1H DOSY Decay Curves for Mixed Aggregate **6d**

Table S7.4. *D*-FW analysis of ¹H DOSY data of mixed aggregate **6d** toluene-*d*₈ solution at -50° C

Compound	FW (g/mol)	10 ⁻¹⁰ <i>D</i> (m ² /s)	log FW	log <i>D</i>	Predicted FW (g/mol)	% error
BEN	78.11	6.279	1.893	-9.202	76.56	2.0
COE	110.2	5.110	2.042	-9.292	117.4	-6.6
TDE	196.4	4.122	2.293	-9.3852	183.5	6.6
SQU	410.7	2.763	2.614	-9.559	421.0	-2.5
6d ^a	711.4 ^b	2.163 ^a	2.852	-9.665	699.9	1.6
6d ^a	711.4 ^b	2.174 ^a	2.852	-9.663	692.6	2.6
6d ^a	711.4 ^b	2.200 ^a	2.852	-9.658	675.7	5.0
6d ^c	711.4 ^b	2.204 ^c	2.852	-9.657	673.1	5.4
6d ^d	711.4 ^b	2.185 ^d	2.852	-9.661	685.2	3.7
Standard Dev. of Predicted FW of 6d					13.0	1.8

^aThe measured diffusion coefficients are from the resonances of chiral lithium amide. 711.4 gmol⁻¹ is the formula weight of 2:2 lithiated chiral amine **5**/*s*-BuLi (⁶Li labeled) complex **6d**. ^cThe measured diffusion coefficient is from the resonance of the methine proton (-0.51 ppm) of *s*-BuLi. ^dThe diffusion coefficient is the average of the above four values.

Appendix H

Supporting information for Chapter 8

Table of Contents

Figure S8.1. ^1H NMR of Chiral Diamines 7 in CDCl_3	404
Figure S8.2. ^{13}C NMR Chiral Diamines 7 in CDCl_3	404
Figure S8.3. ^1H NMR of Chiral Diamines 8 in C_6D_6	405
Figure S8.4. ^{13}C NMR Chiral Diamines 8 in C_6D_6	405
Figure S8.5. ^1H NMR of Chiral Diamines 9 in CDCl_3	406
Figure S8.6. ^{13}C NMR Chiral Diamines 9 in CDCl_3	406

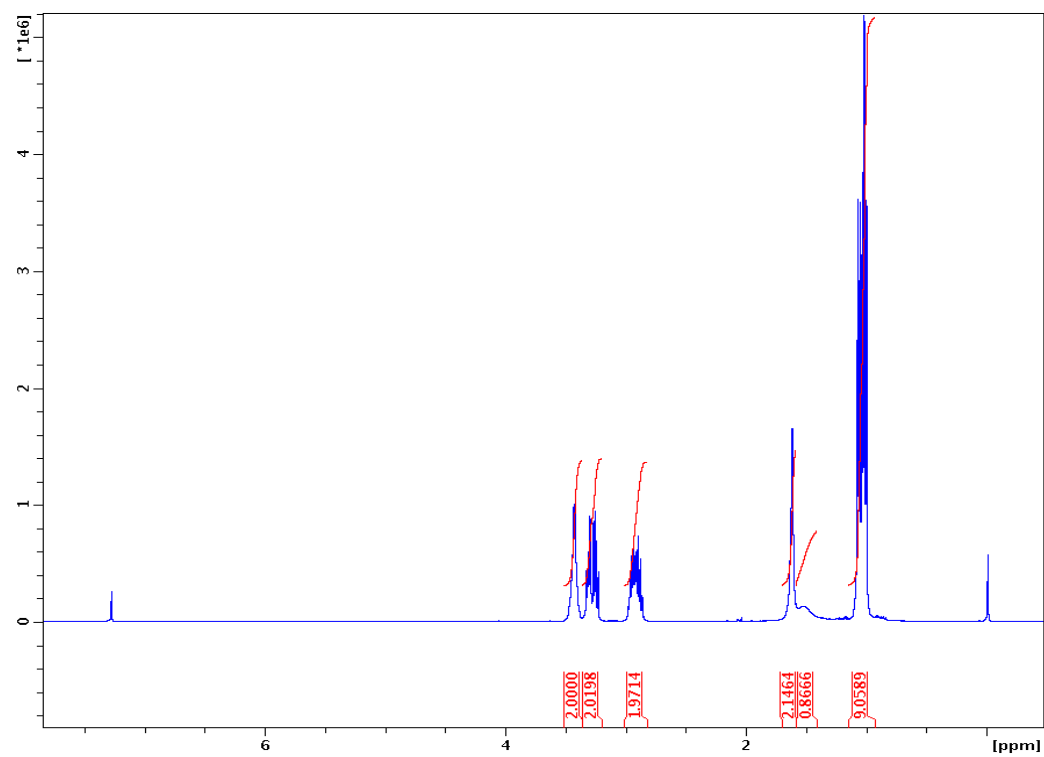


Figure S8.1. ^1H NMR of Chiral Diamines **7** in CDCl_3

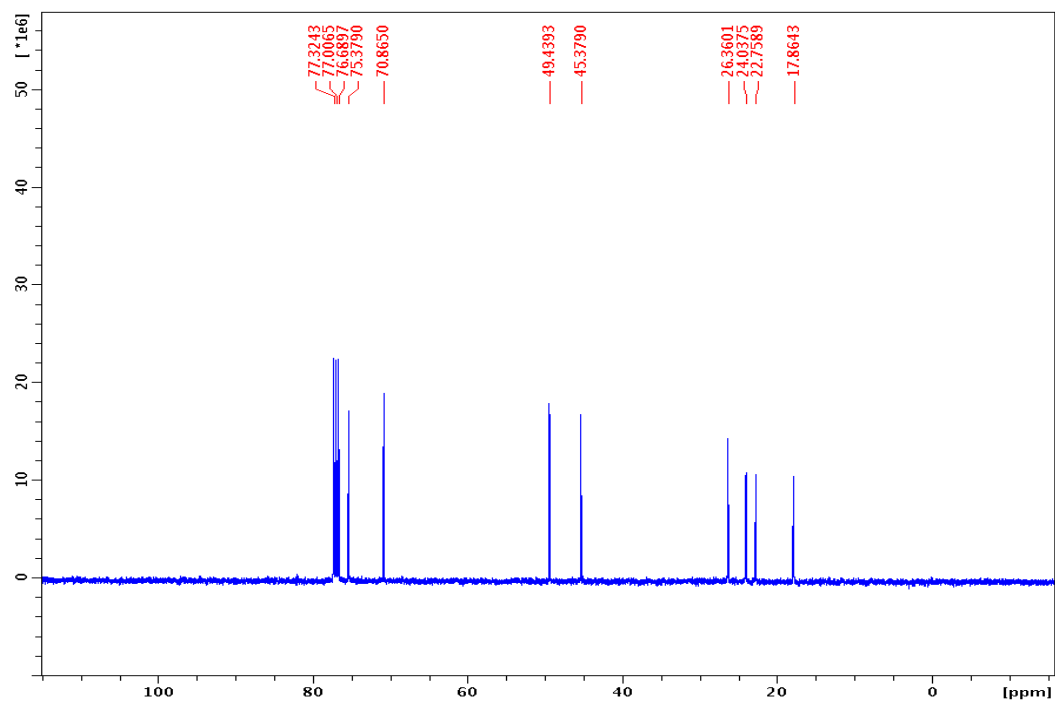


Figure S8.2. ^{13}C NMR of Chiral Diamines **7** in CDCl_3

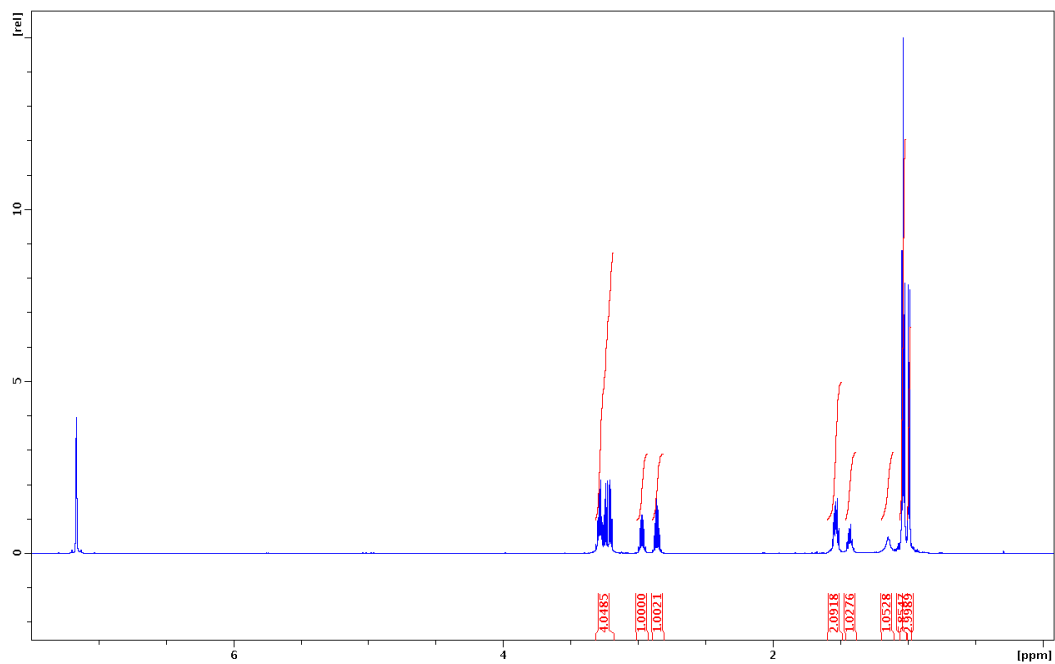


Figure S8.3. ^1H NMR of Chiral Diamines **8** in C_6D_6

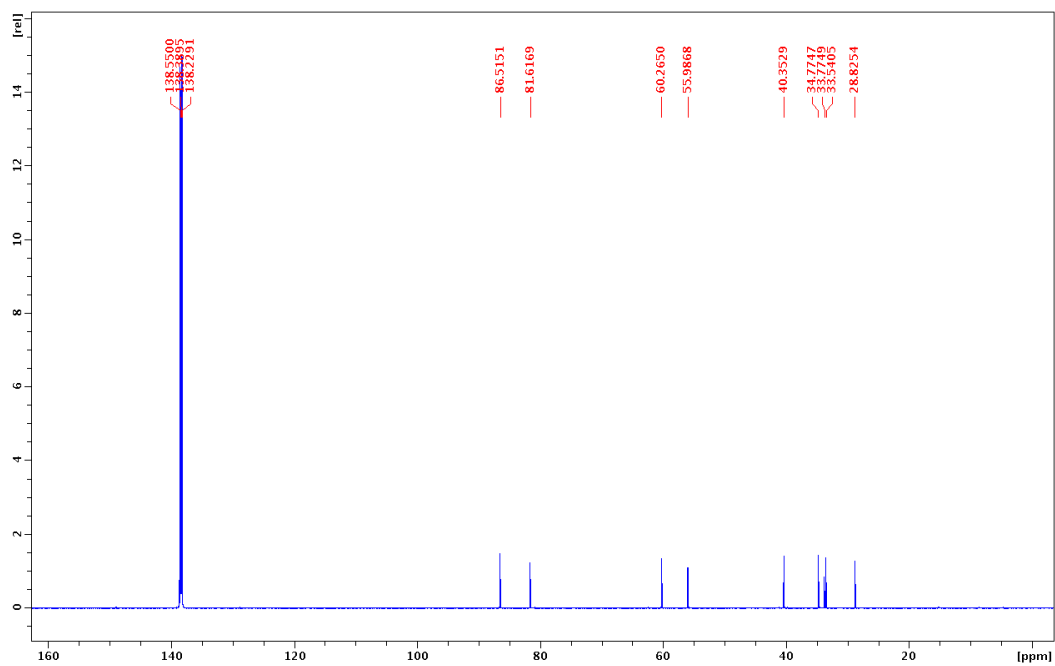


Figure S8.4. ^{13}C NMR of Chiral Diamines **8** in C_6D_6

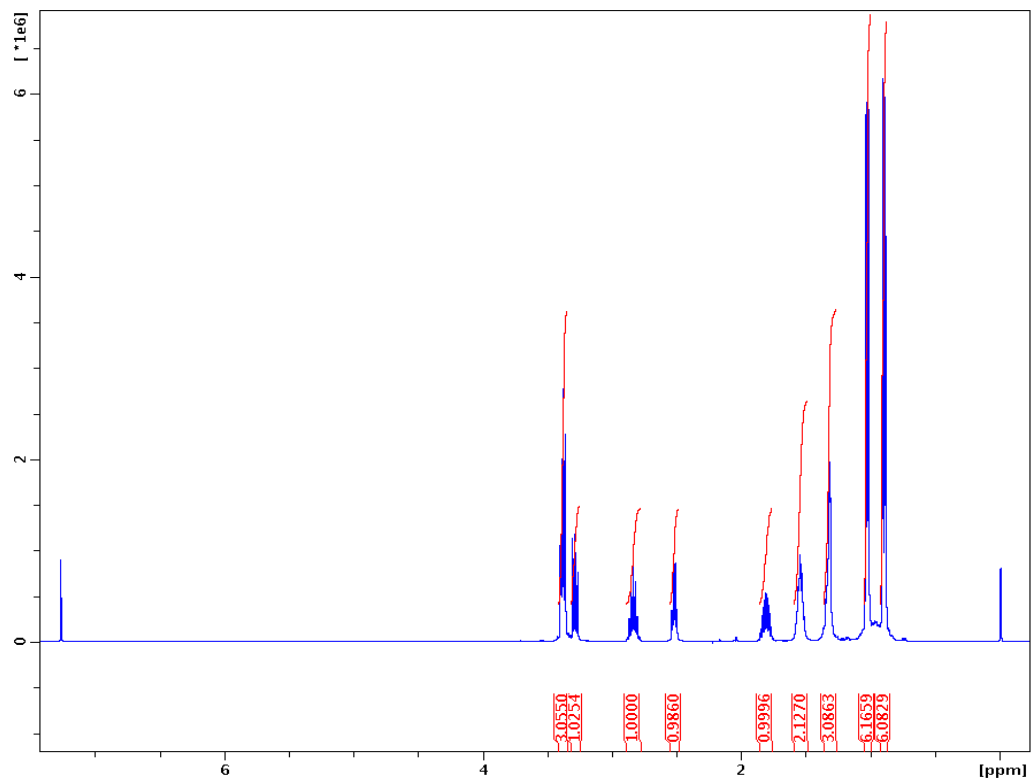


Figure S8.5. ^1H NMR of Chiral Diamines **9** in CDCl_3

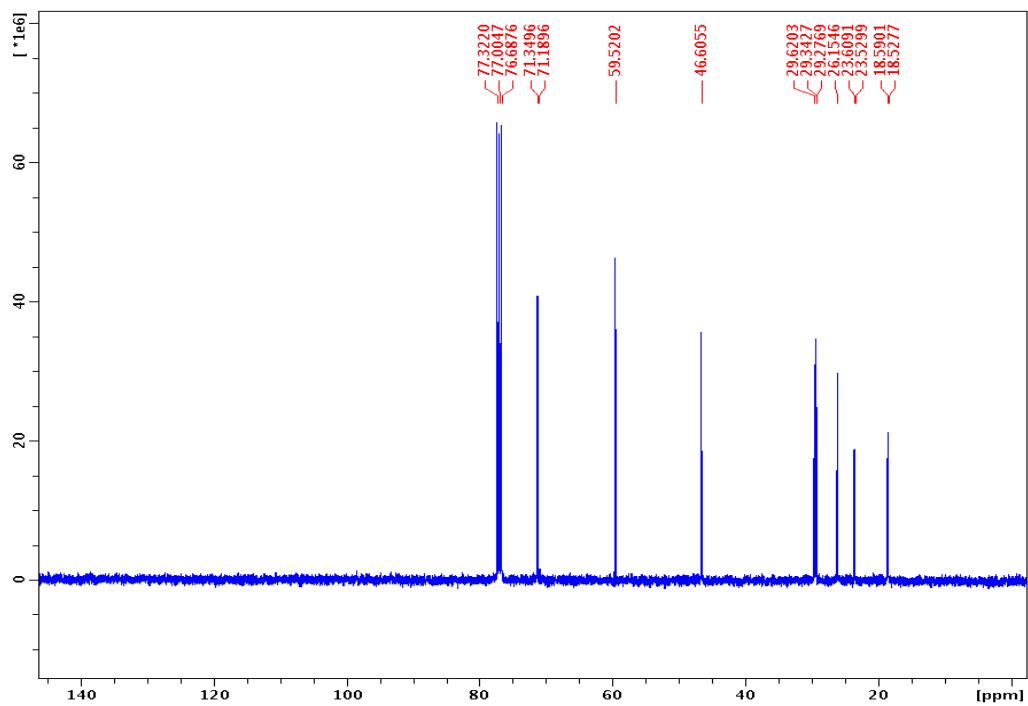


Figure S8.6. ^{13}C NMR of Chiral Diamines **9** in CDCl_3

Appendix I
Supporting information for Chapter 10

Table of Contents

Figure S10.1. ^1H NMR of chiral amine 7 in toluene- d_8	410
Figure S10.2. ^{13}C NMR of chiral amine 7 in toluene- d_8	410
Figure S10.3. ^1H NMR of chiral amine 8 in toluene- d_8	411
Figure S10.4. ^{13}C NMR of chiral amine 8 in toluene- d_8	411
Figure S10.5. ^1H NMR of chiral amine 9 in toluene- d_8	412
Figure S10.6. ^{13}C NMR of chiral amine 9 in toluene- d_8	412
Figure S10.7. ^1H NMR of Mixed Aggregate 10 in toluene- d_8 at $-40\text{ }^\circ\text{C}$	413
Figure S10.8. ^{13}C NMR of Mixed Aggregate 10 in toluene- d_8 at $-40\text{ }^\circ\text{C}$	413
Figure S10.9. ^6Li NMR of Mixed Aggregate 10 in toluene- d_8 at $-40\text{ }^\circ\text{C}$	414
Figure S10.10. ^1H - ^6Li HMBC of Mixed Aggregate 10 in toluene- d_8 at $-40\text{ }^\circ\text{C}$	414
Figure S10.11. ^1H COSY of Mixed Aggregate 10 in toluene- d_8 at $-40\text{ }^\circ\text{C}$	415
Figure S10.12. ^1H - ^{13}C HSQC of Mixed Aggregate 10 in toluene- d_8 at $-40\text{ }^\circ\text{C}$	415
Figure S10.13. ^1H - ^{13}C HMBC of Mixed Aggregate 10 in toluene- d_8 at $-40\text{ }^\circ\text{C}$	416
Figure S10.14. ^1H NMR of Mixed Aggregate 10 in toluene- d_8 with Internal References at $-40\text{ }^\circ\text{C}$	416
Figure S10.15. ^1H DOSY Decay Curves for Internal References.....	417
Figure S10.16. ^1H DOSY Decay Curves for Mixed Aggregate 10	419
Figure S10.17. ^1H NMR of Mixed Aggregates 11 and 12 in toluene- d_8 at $-40\text{ }^\circ\text{C}$	420
Figure S10.18. ^{13}C NMR of Mixed Aggregates 11 and 12 in toluene- d_8 at $-40\text{ }^\circ\text{C}$	420

Figure S10.19. ^6Li NMR of Mixed Aggregates 11 and 12 in toluene- d_8 at $-40\text{ }^\circ\text{C}$	421
Figure S10.20. ^1H COSY of Mixed Aggregates 11 and 12 in toluene- d_8 at $-40\text{ }^\circ\text{C}$	421
Figure S10.21. ^1H - ^{13}C HSQC of Mixed Aggregates 11 and 12 in toluene- d_8 at $-40\text{ }^\circ\text{C}$	422
Figure S10.22. ^1H - ^{13}C HMBC of Mixed Aggregates 11 and 12 in toluene- d_8 at $-40\text{ }^\circ\text{C}$	422
Figure S10.23. ^1H NMR of Mixed Aggregates 11 and 12 in toluene- d_8 with Internal References at $-40\text{ }^\circ\text{C}$	423
Figure S10.24. ^1H DOSY Decay Curves for Internal References.....	424
Figure S10.25. ^1H DOSY Decay Curves for Mixed Aggregate 11	424
Figure S10.26. ^1H DOSY Decay Curves for Mixed Aggregate 12	425
Figure S10.27. ^1H NMR of Complexes 13 and 14 in toluene- d_8 at $-40\text{ }^\circ\text{C}$	426
Figure S10.28. ^{13}C NMR of Complexes 13 and 14 in toluene- d_8 at $-40\text{ }^\circ\text{C}$	426
Figure S10.29. ^6Li NMR of Complexes 13 and 14 in toluene- d_8 at $-40\text{ }^\circ\text{C}$	427
Figure S10.30. ^1H COSY of Complexes 13 and 14 in toluene- d_8 at $-40\text{ }^\circ\text{C}$	427
Figure S10.31. ^1H - ^{13}C HSQC of Complexes 13 and 14 in toluene- d_8 at $-40\text{ }^\circ\text{C}$	428
Figure S10.32. ^1H - ^{13}C HMBC of Complexes 13 and 14 in toluene- d_8 at $-40\text{ }^\circ\text{C}$	428
Figure S10.33. ^1H - ^{13}C HMBC of Complexes 13 and 14 in toluene- d_8 at $-40\text{ }^\circ\text{C}$ (Enlarged).....	429
Figure S10.34. ^1H NMR of Complexes 13 and 14 in toluene- d_8 with Internal References at $-40\text{ }^\circ\text{C}$	429
Figure S10.35. ^1H DOSY Decay Curves for Internal References.....	430
Figure S10.36. ^1H DOSY Decay Curves for Mixed Aggregate 13	431
Figure S10.37. ^1H DOSY Decay Curves for Homodimer 14	431

Table S10.1. D-FW Analysis of ^1H DOSY data of Mixed Aggregate 10 toluene- d_8 solution at -40 °C.....	419
Table S10.2. D-FW Analysis of ^1H DOSY data of Mixed Aggregates 11 and 12 toluene- d_8 solution at -40 °C.....	425
Table S10.3. D-FW Analysis of ^1H DOSY data of Complexes 13 and 14 in toluene- d_8 solution at -40 °C.....	432

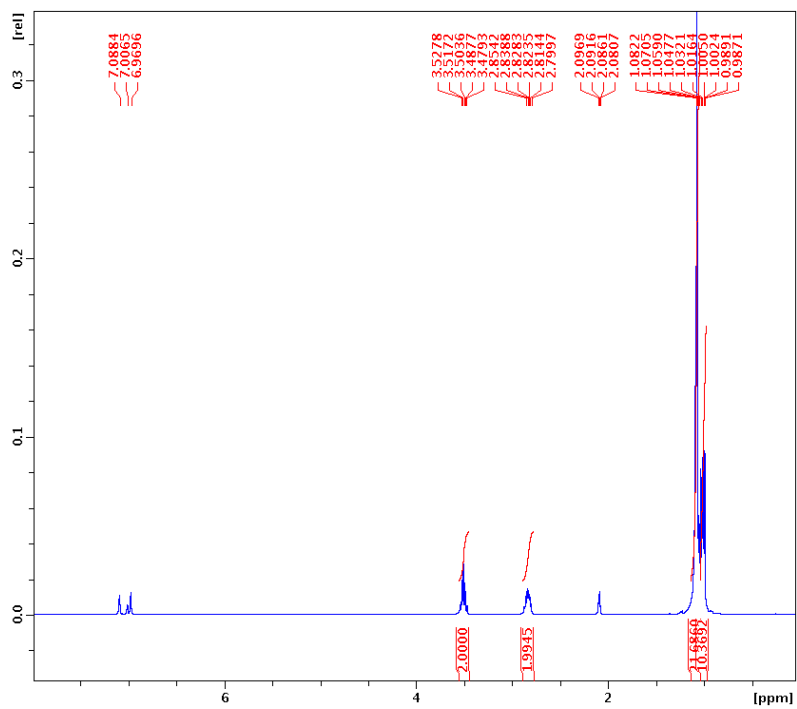


Figure S10.1. ^1H NMR of chiral amine **7** in toluene- d_8

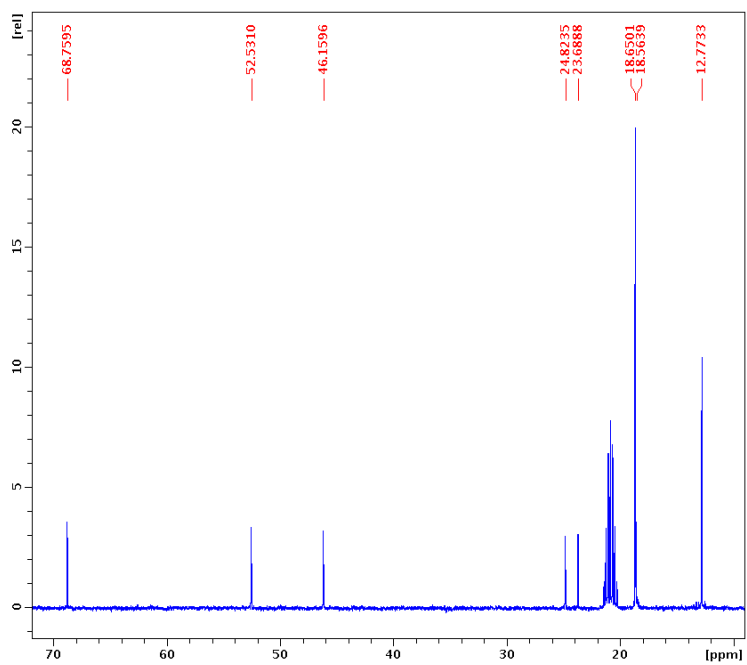


Figure S10.2. ^{13}C NMR of chiral amine **7** in toluene- d_8

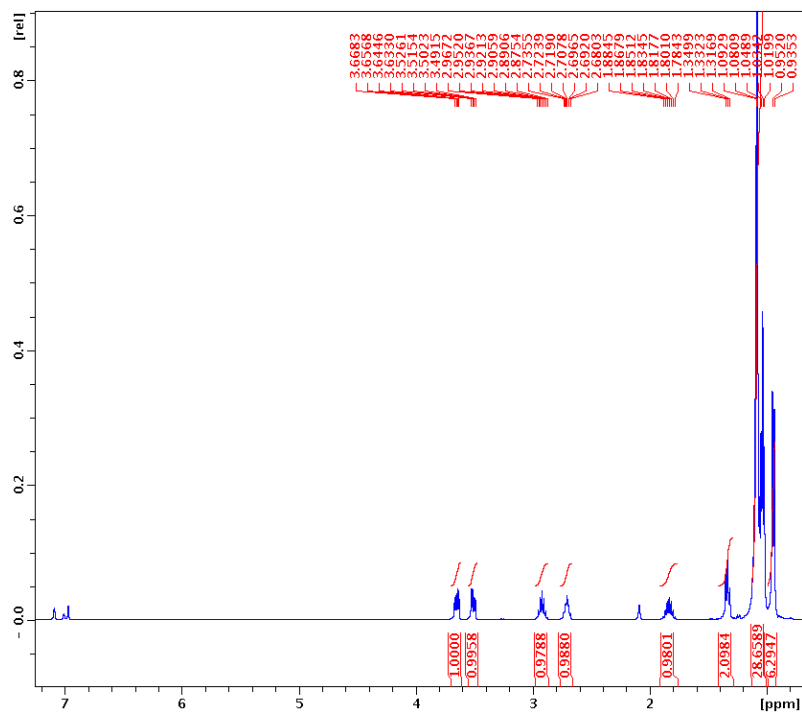


Figure S10.3. ^1H NMR of chiral amine **8** in toluene- d_8

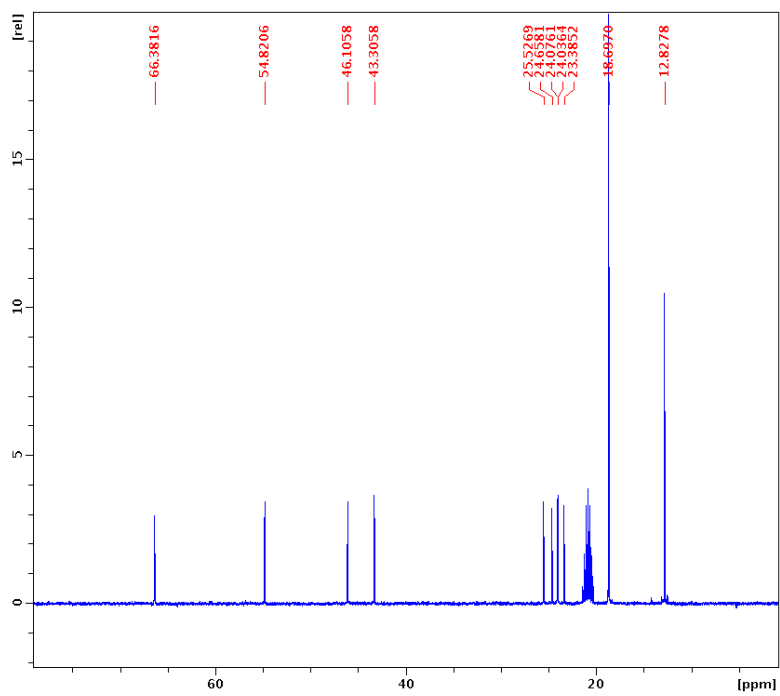


Figure S10.4. ^{13}C NMR of chiral amine **8** in toluene- d_8

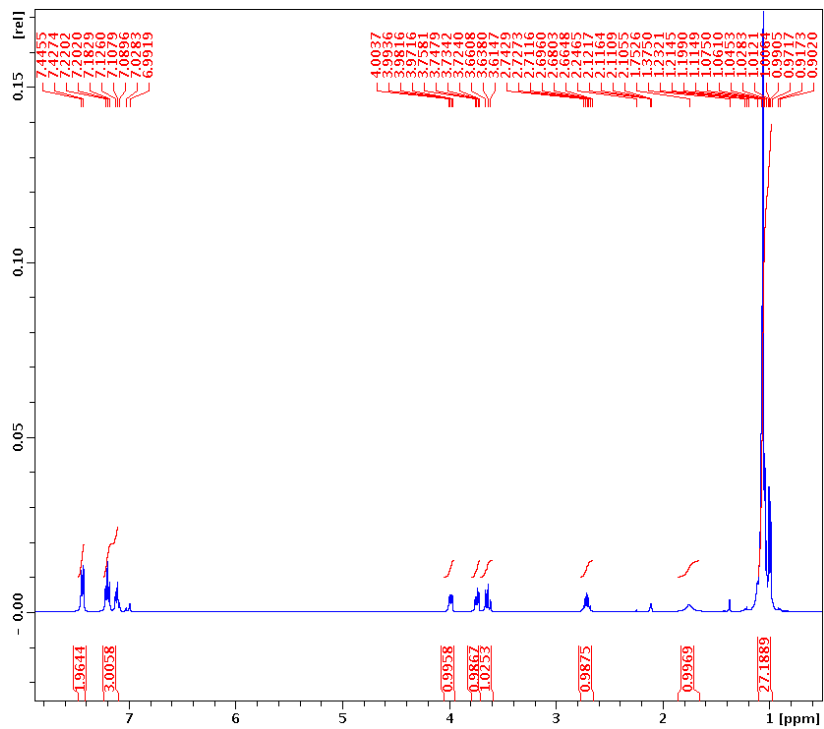


Figure S10.5. ^1H NMR of chiral amine **9** in toluene- d_8

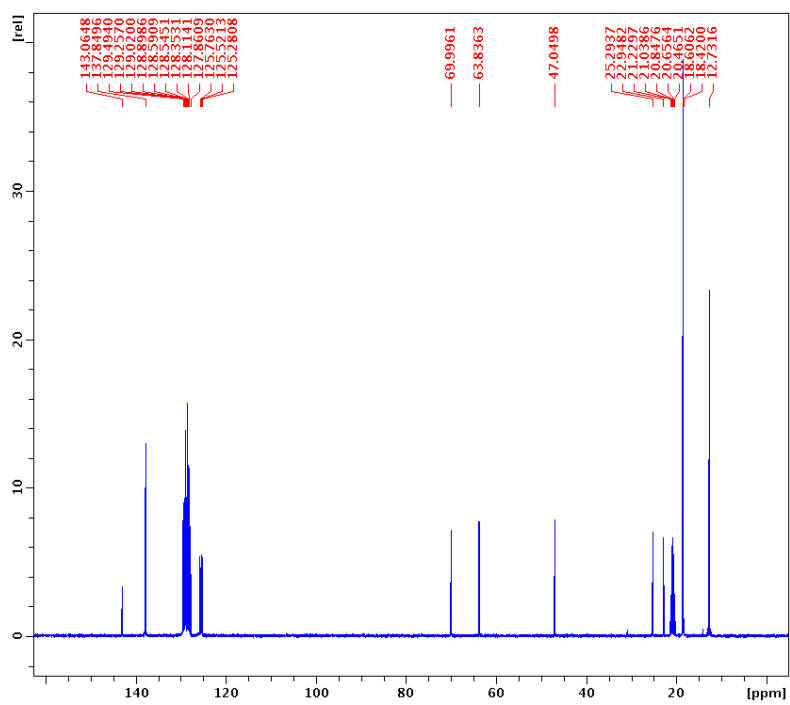


Figure S10.6. ^{13}C NMR of chiral amine **9** in toluene- d_8

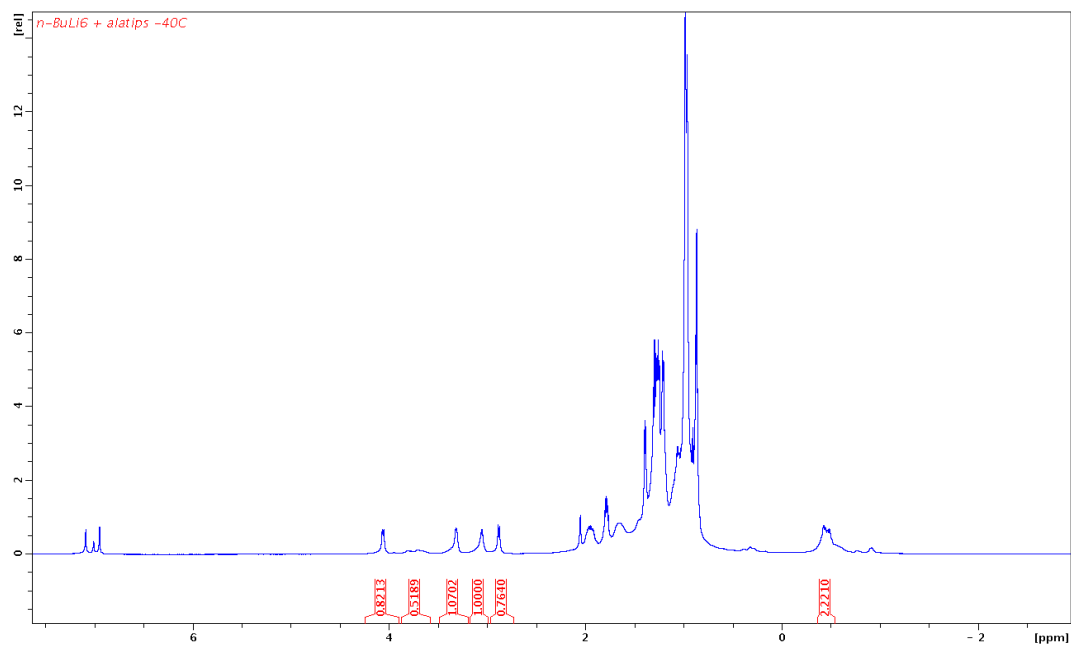


Figure S10.7. ^1H NMR of Mixed Aggregate **10** in toluene- d_8 at $-40\text{ }^\circ\text{C}$

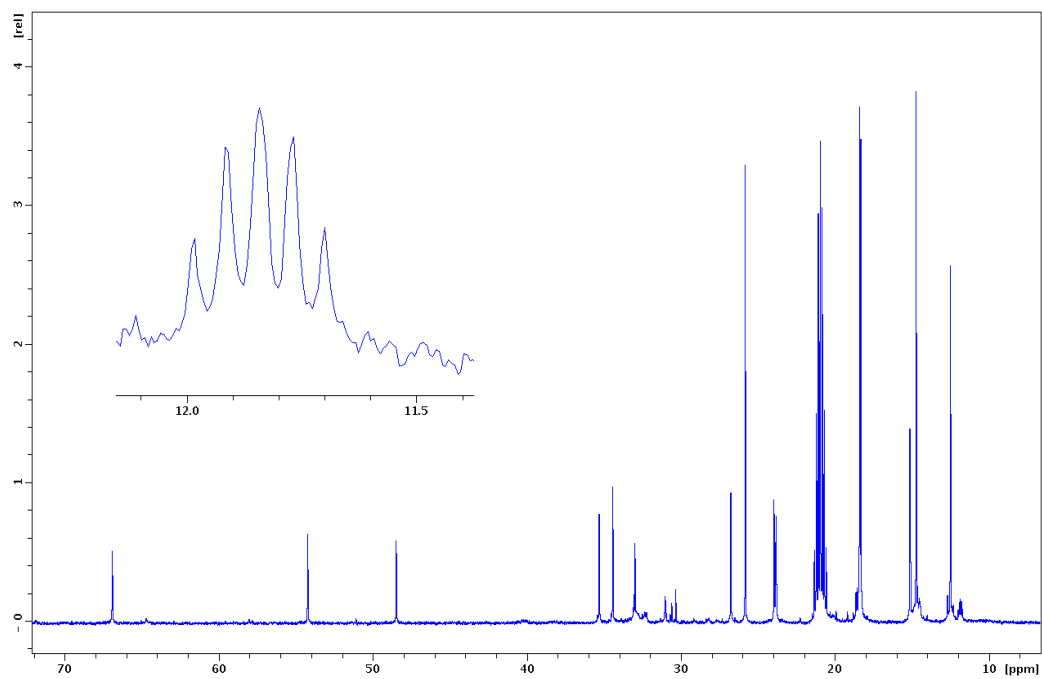


Figure S10.8. ^{13}C NMR of Mixed Aggregate **10** in toluene- d_8 at $-40\text{ }^\circ\text{C}$

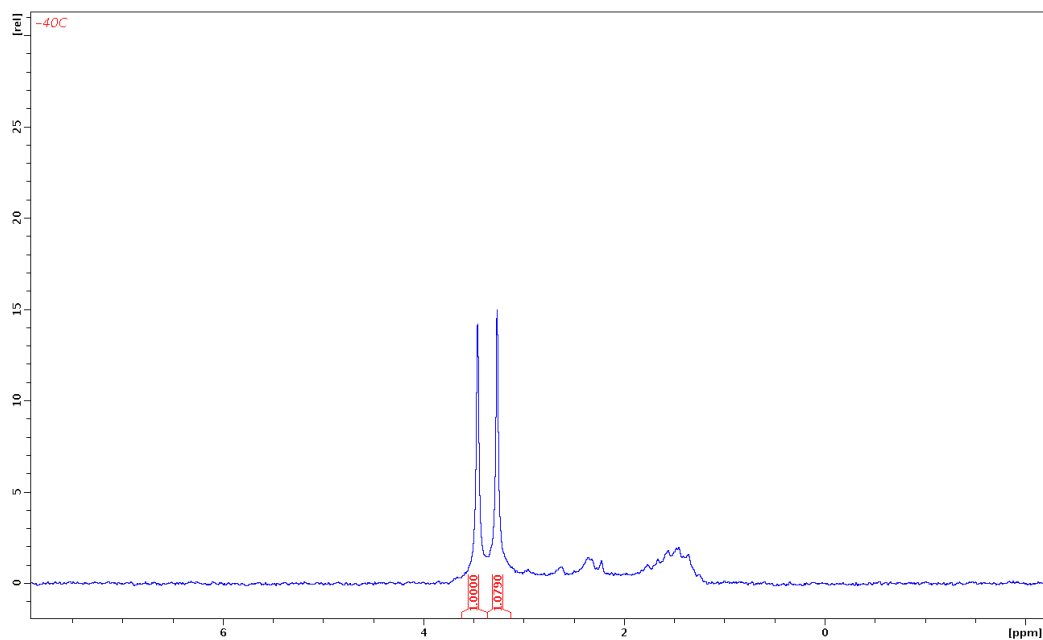


Figure S10.9. ${}^6\text{Li}$ NMR of Mixed Aggregate **10** in toluene- d_8 at $-40\text{ }^\circ\text{C}$

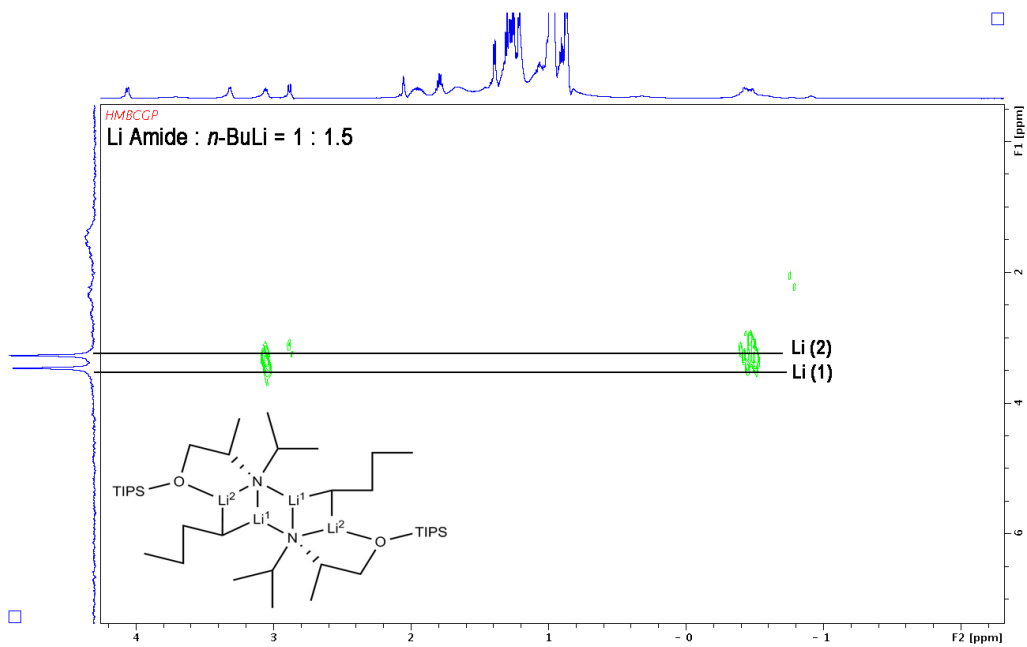


Figure S10.10. ${}^1\text{H}$ - ${}^6\text{Li}$ HMBC of Mixed Aggregate **10** in toluene- d_8 at $-40\text{ }^\circ\text{C}$

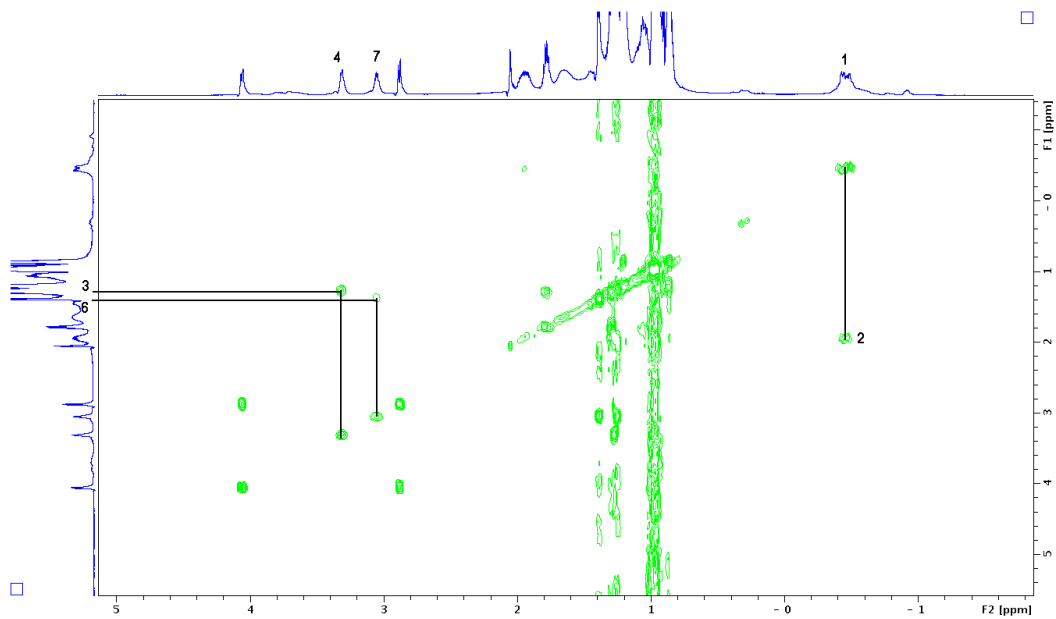


Figure S10.11. ^1H COSY of Mixed Aggregate **10** in toluene- d_8 at $-40\text{ }^\circ\text{C}$

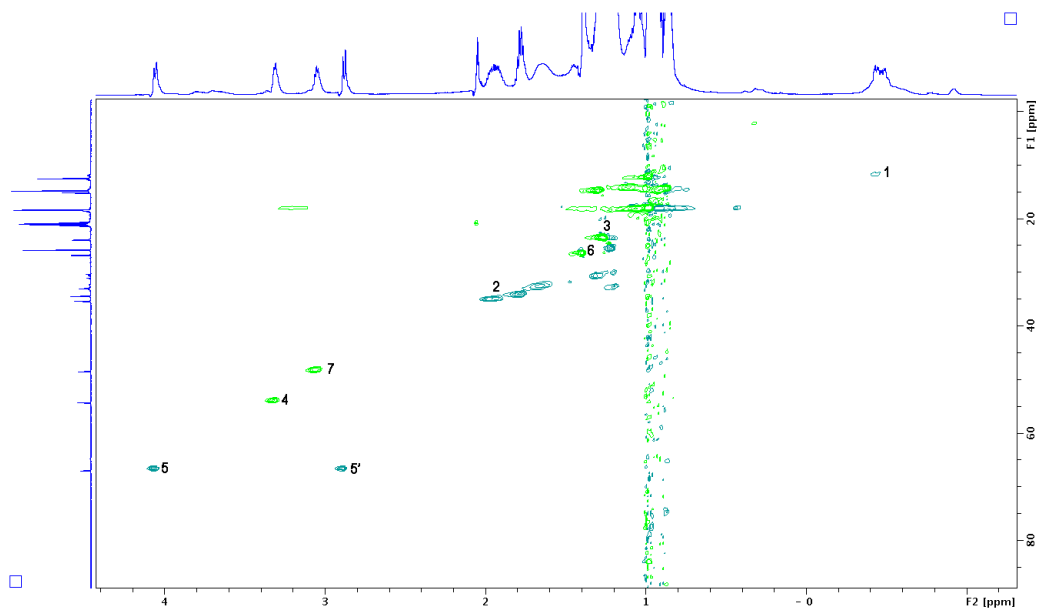


Figure S10.12. ^1H - ^{13}C HSQC of Mixed Aggregate **10** in toluene- d_8 at $-40\text{ }^\circ\text{C}$

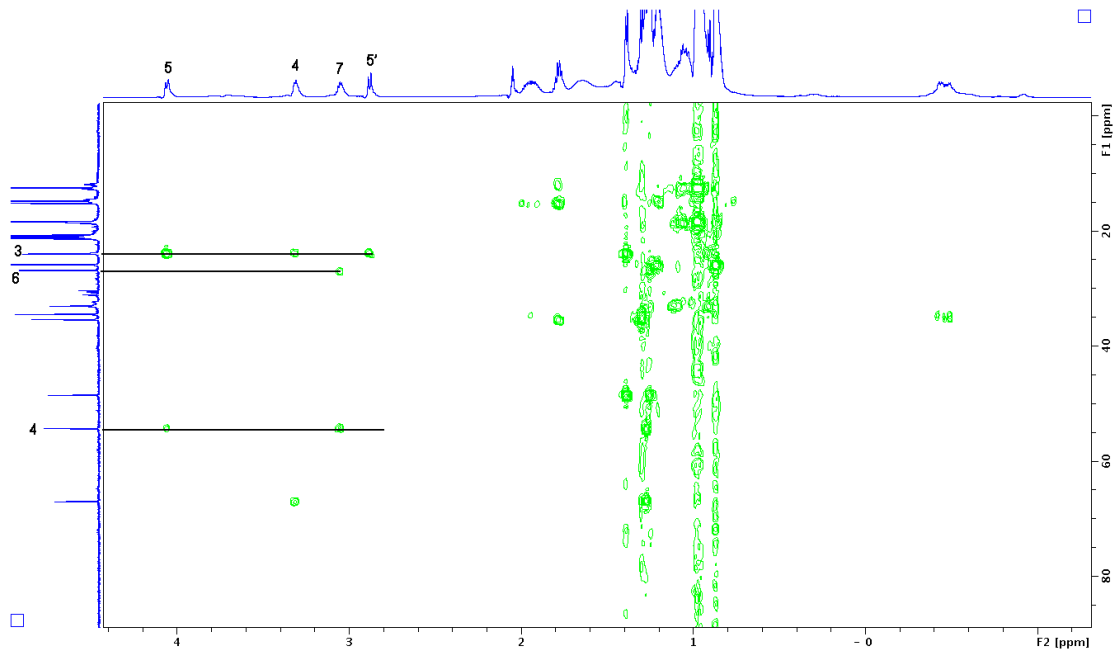


Figure S10.13. ^1H - ^{13}C HMBC of Mixed Aggregate **10** in toluene- d_8 at $-40\text{ }^\circ\text{C}$

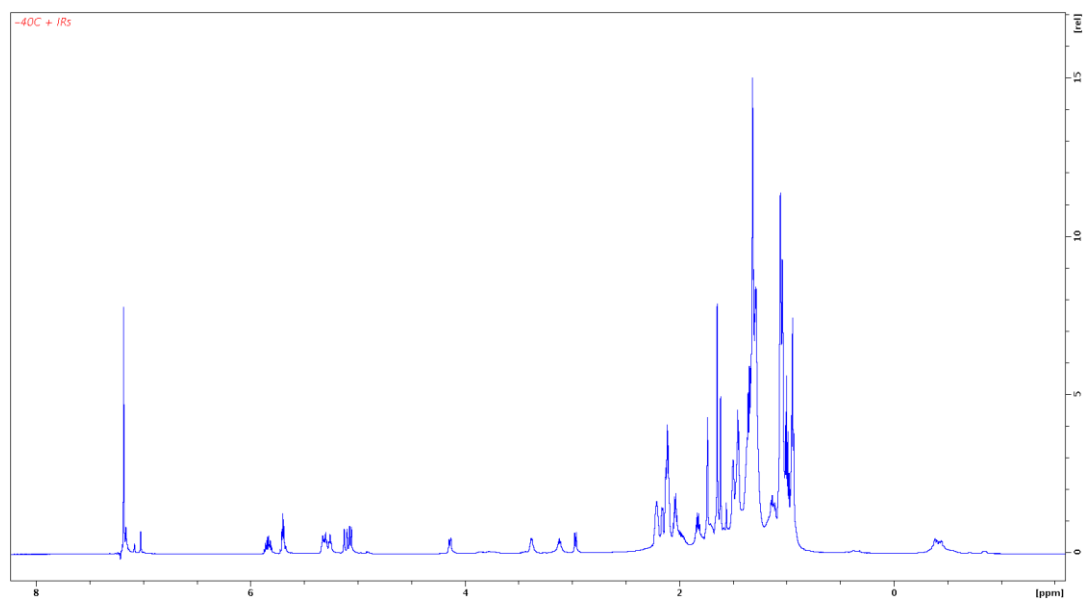
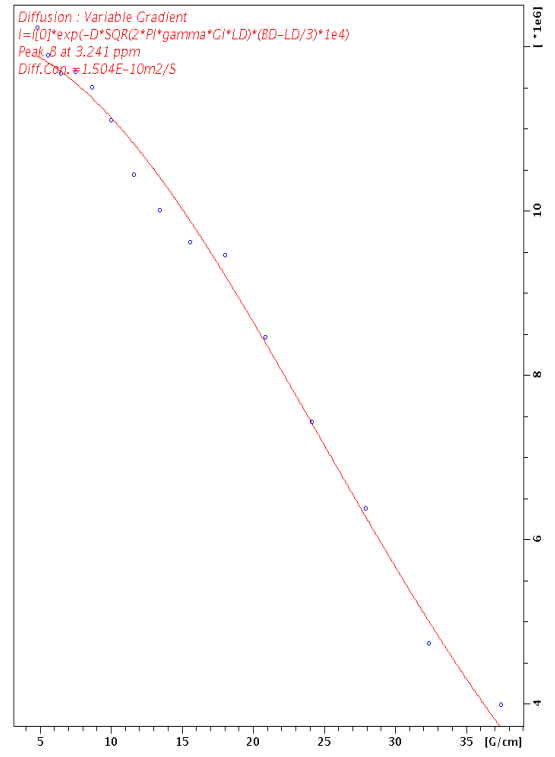
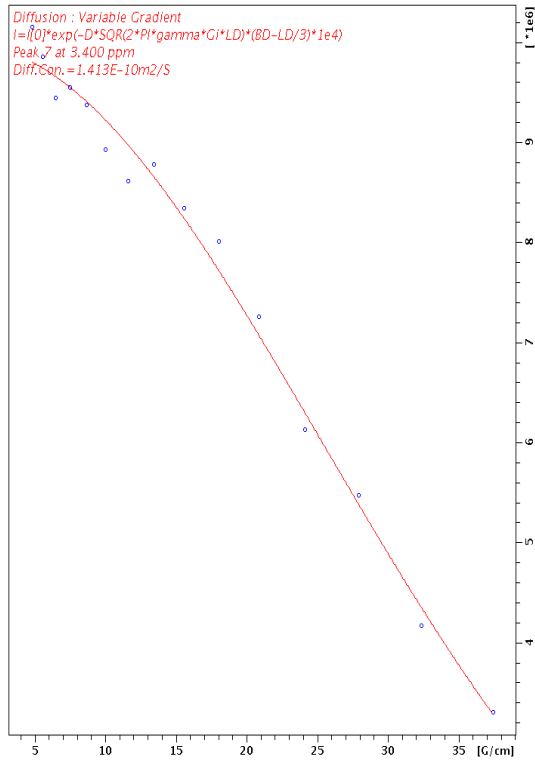
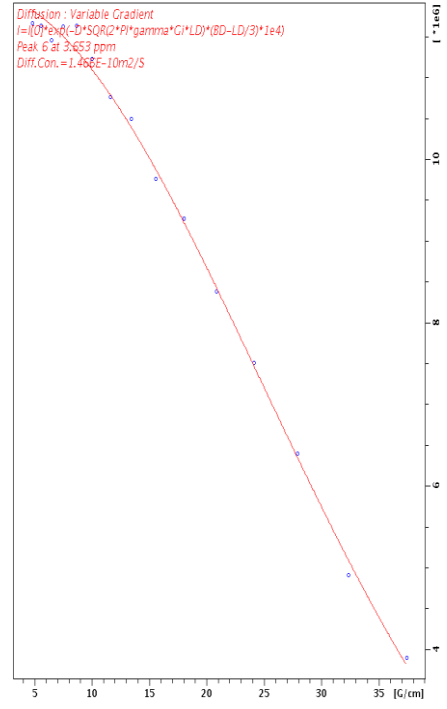
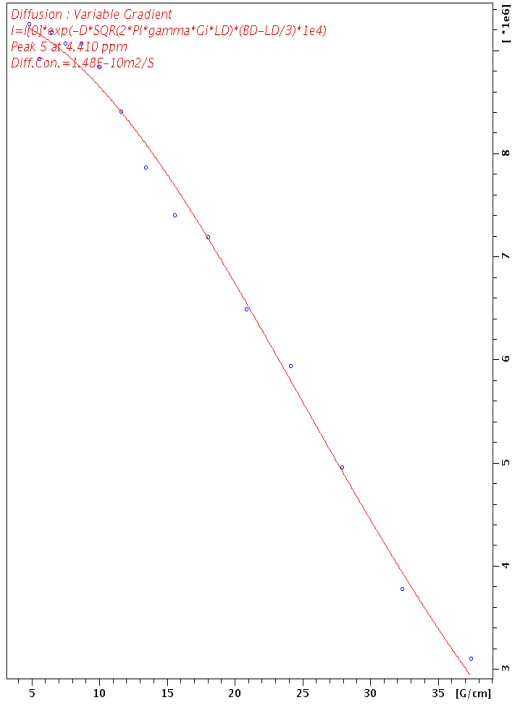


Figure S10.14. ^1H NMR of Mixed Aggregate **10** in toluene- d_8 with Internal References at $-40\text{ }^\circ\text{C}$



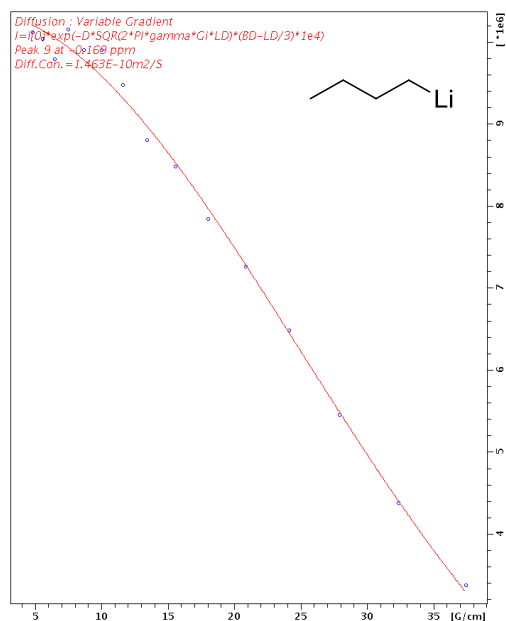


Figure S10.16. ^1H DOSY Decay Curves for Mixed Aggregate **10**

Table S10.1. D-FW Analysis of ^1H DOSY data of Mixed Aggregate **10** toluene- d_8 solution at -40

Compound	FW (g/mol)	$10^{-10}D$ (m^2/s)	log FW	log D	Predicted FW (g/mol)	% error
BEN	78.11	5.960	1.893	-9.225	80.37	-2.9
COE	110.2	4.816	2.042	-9.317	110.8	-0.6
TDE	196.4	3.462	2.293	-9.461	182.3	7.2
SQU	410.7	1.967	2.614	-9.706	427.5	-4.1
10 ^a	683.3 ^b	1.480 ^a	2.835	-9.830	656.5	3.9
10 ^a	683.3 ^b	1.466 ^a	2.835	-9.834	666.0	2.5
10 ^a	683.3 ^b	1.413 ^a	2.835	-9.850	704.0	-3.0
10 ^a	683.3 ^b	1.504 ^a	2.835	-9.823	640.8	6.2
10 ^c	683.3 ^b	1.463 ^c	2.835	-9.835	668.0	2.2
10 ^d	683.3 ^b	1.465 ^d	2.835	-9.834	667.1	2.4

^aThe measured diffusion coefficients are from the resonances of chiral lithium amide. ^b683.3 g mol^{-1} is the formula weight of 2:2 lithiated chiral amine **7**/*n*-BuLi (^6Li labeled) complex **10**. ^cThe measured diffusion coefficient is from the α -methylene protons peak (-0.45 ppm) of *n*-BuLi. ^dThe diffusion coefficient is the average of the above five values.

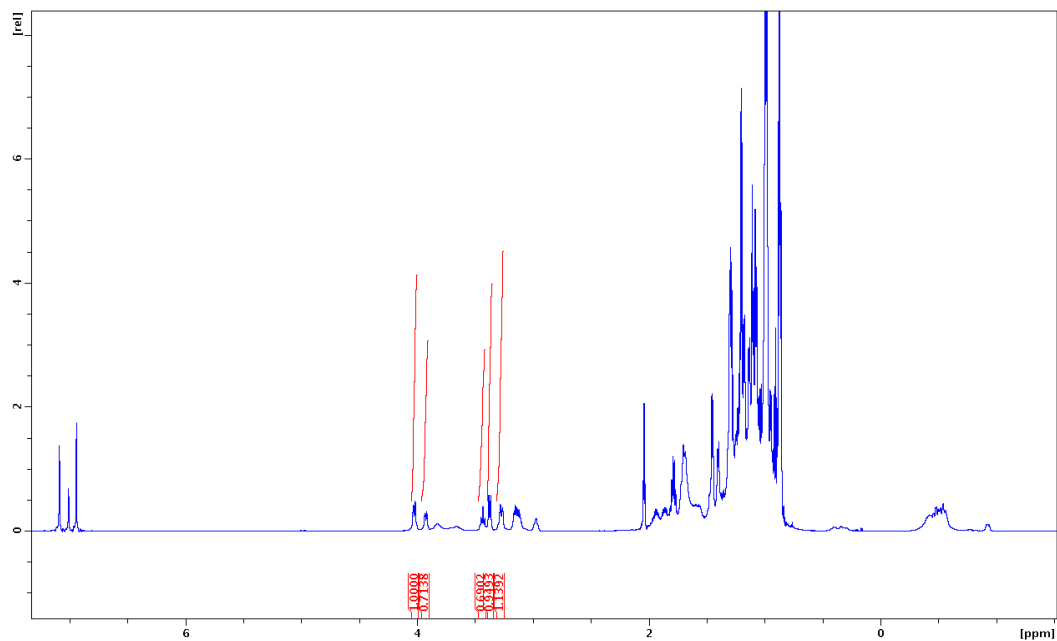


Figure S10.17. ^1H NMR of Mixed Aggregates **11** and **12** in toluene- d_8 at $-40\text{ }^\circ\text{C}$

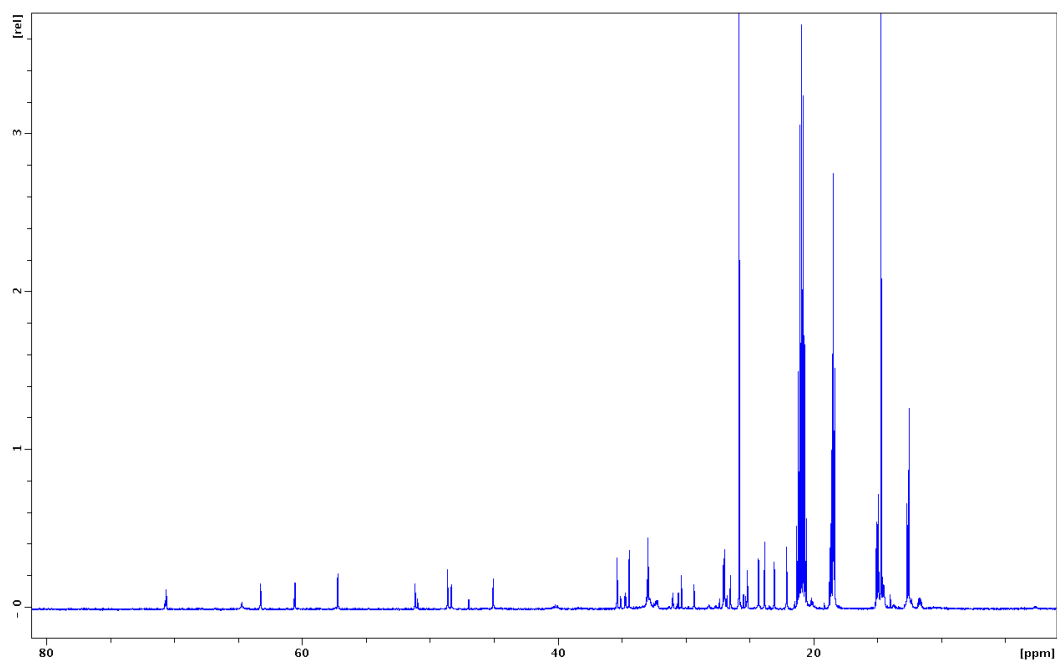


Figure S10.18. ^{13}C NMR of Mixed Aggregates **11** and **12** in toluene- d_8 at $-40\text{ }^\circ\text{C}$

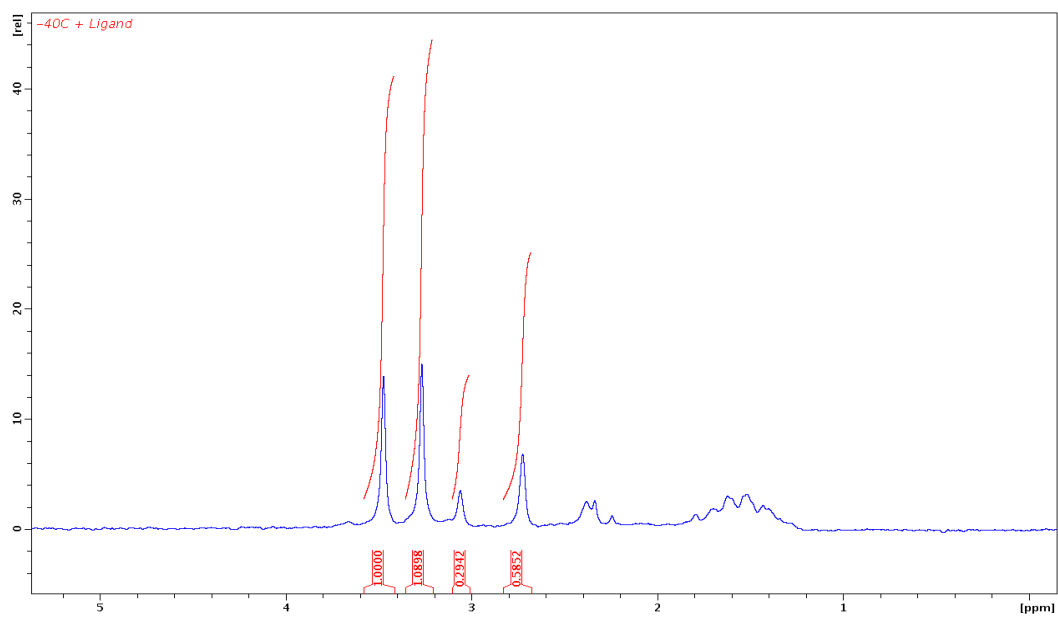


Figure S10.19. ${}^6\text{Li}$ NMR of Mixed Aggregates **11** and **12** in toluene- d_8 at $-40\text{ }^\circ\text{C}$

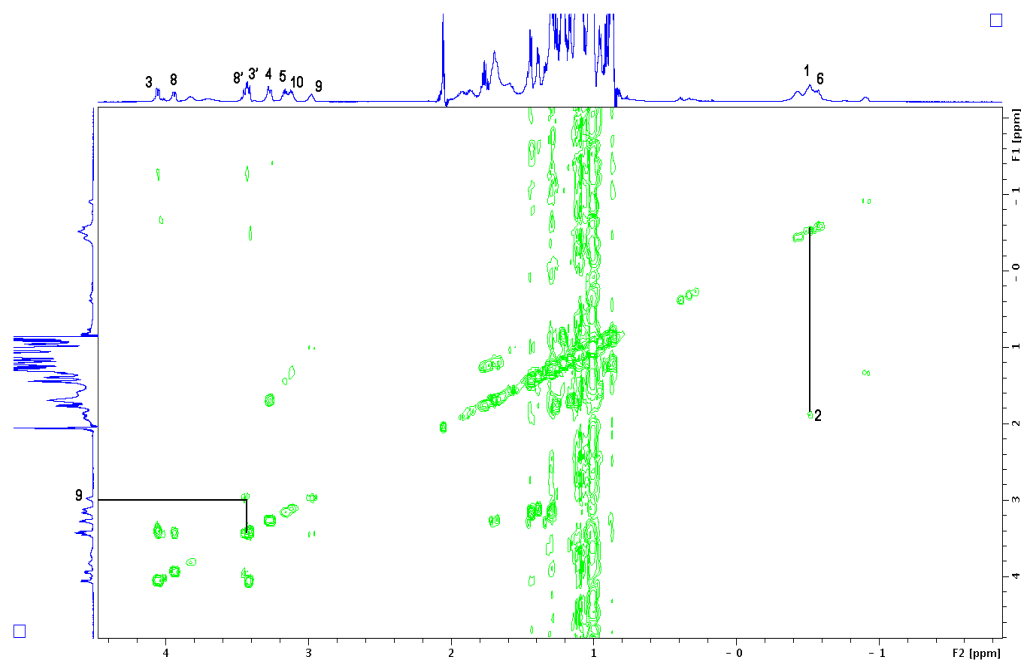


Figure S10.20. ${}^1\text{H}$ COSY of Mixed Aggregates **11** and **12** in toluene- d_8 at $-40\text{ }^\circ\text{C}$

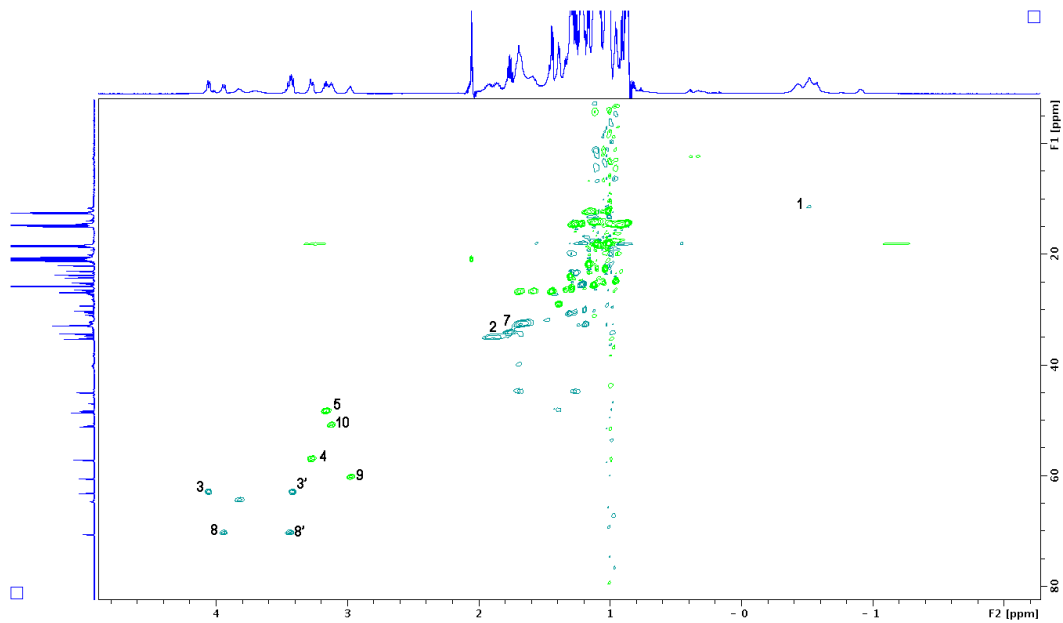


Figure S10.21. ^1H - ^{13}C HSQC of Mixed Aggregates **11** and **12** in toluene- d_8 at $-40\text{ }^\circ\text{C}$

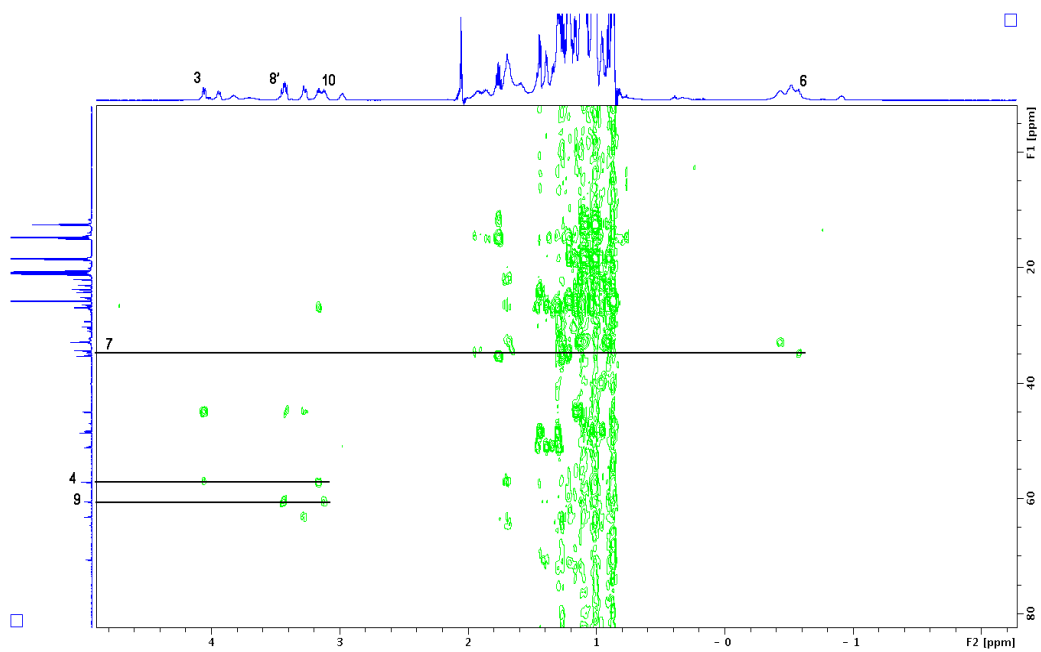


Figure S10.22. ^1H - ^{13}C HMBC of Mixed Aggregates **11** and **12** in toluene- d_8 at $-40\text{ }^\circ\text{C}$

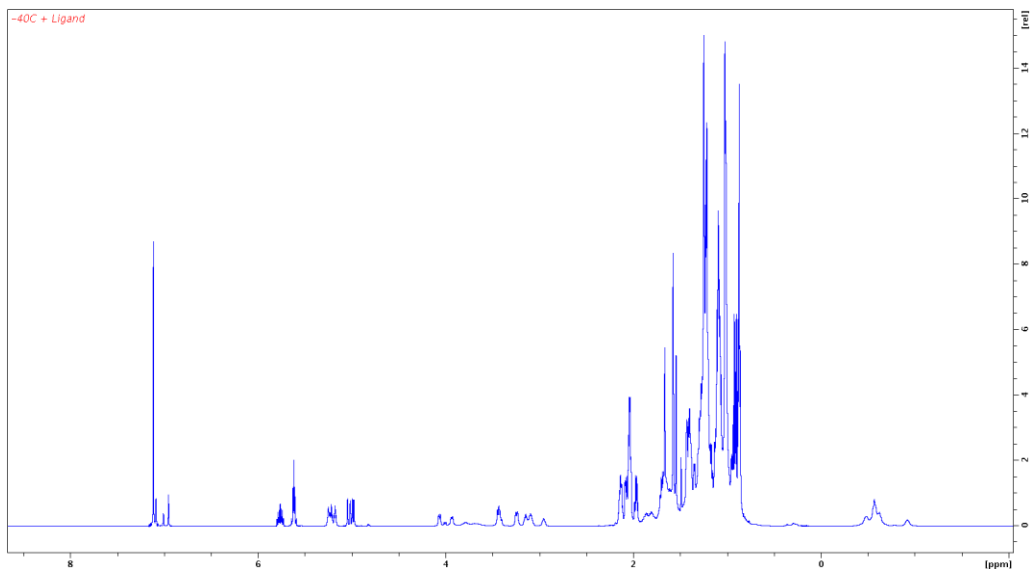
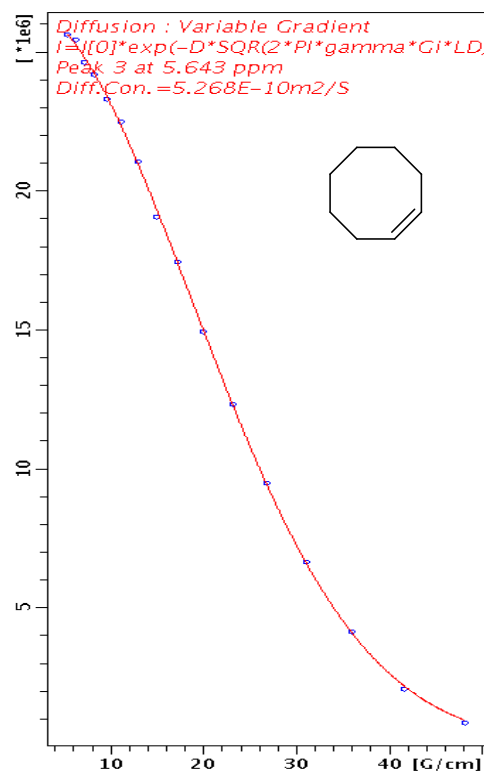
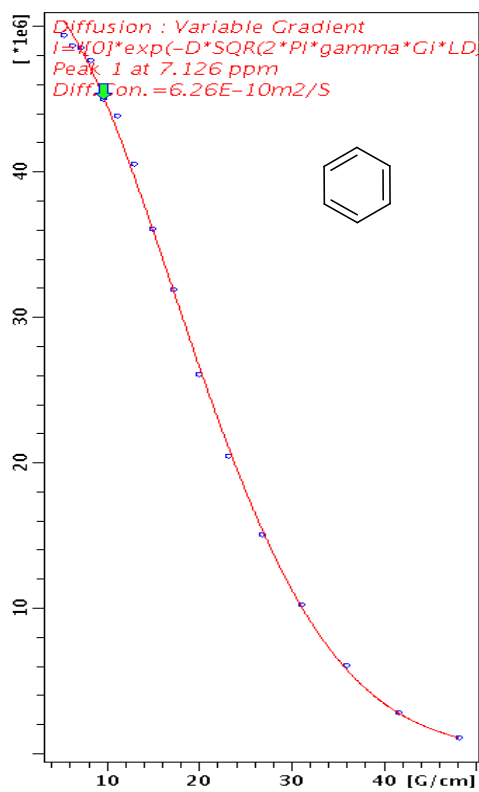


Figure S10.23. ^1H NMR of Mixed Aggregate **11** and **12** in toluene- d_8 with Internal References at -40°C



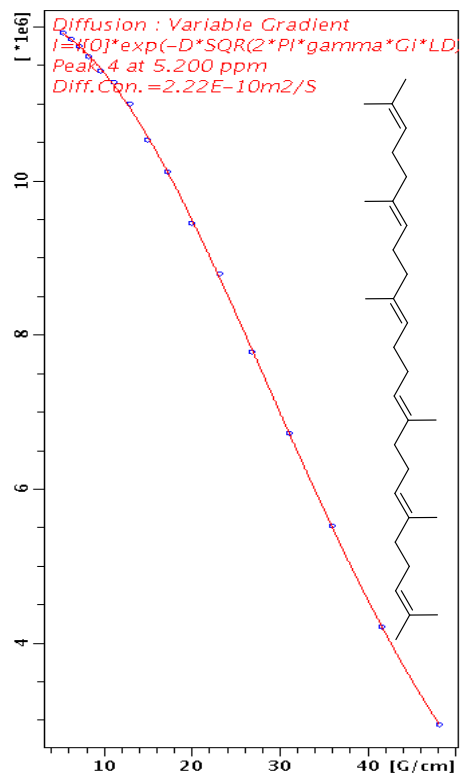
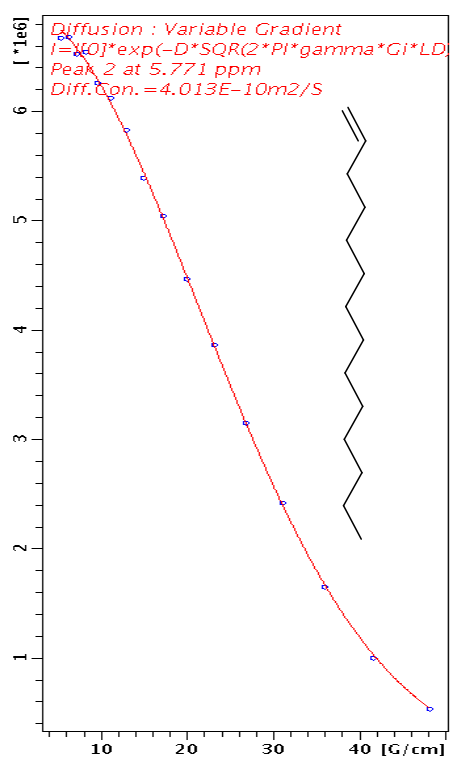


Figure S10.24. ¹H DOSY Decay Curves for Internal References

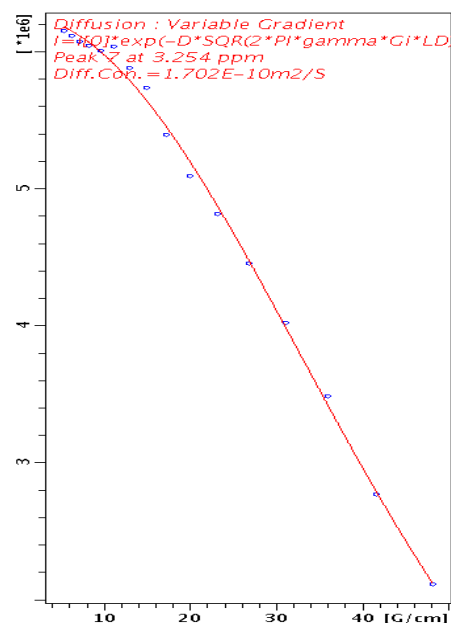
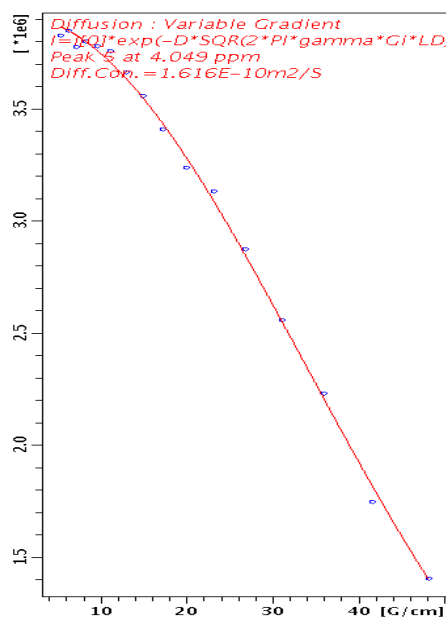


Figure S10.25. ¹H DOSY Decay Curves for Mixed Aggregate 11

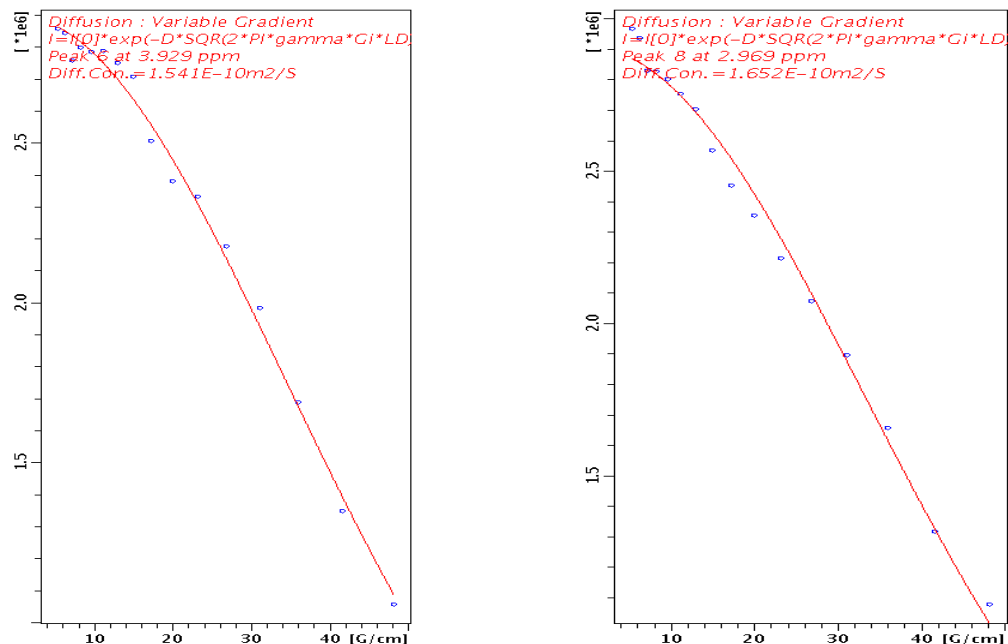


Figure S10.26. ^1H DOSY Decay Curves for Mixed Aggregate **12**

Table S10.2. D-FW Analysis of ^1H DOSY data of Mixed Aggregates **11** and **12** toluene- d_8 solution at -40°C

Compd	FW (g/mol)	10^{-10}D (m^2/s)	log FW	log D	Predicted FW (g/mol)	% error
BEN	78.11	6.260	1.893	-9.203	83.25	-6.6
COE	110.2	5.268	2.042	-9.278	110.0	0.2
TDE	196.4	4.013	2.293	-9.397	170.7	13
SQU	410.7	2.220	2.614	-9.654	444.1	-8.1
11 ^a	767.5 ^b	1.616 ^a	2.885	-9.792	741.7	3.4
11 ^a	767.5 ^b	1.702 ^a	2.885	-9.769	682.1	11
12 ^a	704.4 ^c	1.541 ^a	2.848	-9.812	800.9	-14
12 ^a	704.4 ^c	1.504 ^a	2.848	-9.782	715.8	-1.6
11 ^d	767.5 ^b	1.659 ^d	2.885	-9.780	711.9	7.2
12 ^d	704.4 ^c	1.596 ^d	2.848	-9.797	758.3	-7.7

^aThe measured diffusion coefficients are from the resonances of chiral lithium amide. ^b767.5 gmol^{-1} is the formula weight of 2:2 lithiated chiral amine **8**/ n -BuLi (^6Li labeled) complex **11**. ^c704.4 gmol^{-1} is the formula weight of 2:1 lithiated chiral amine **8**/ n -BuLi (^6Li labeled) complex **12**. ^dThe diffusion coefficient is the average of the above two values.

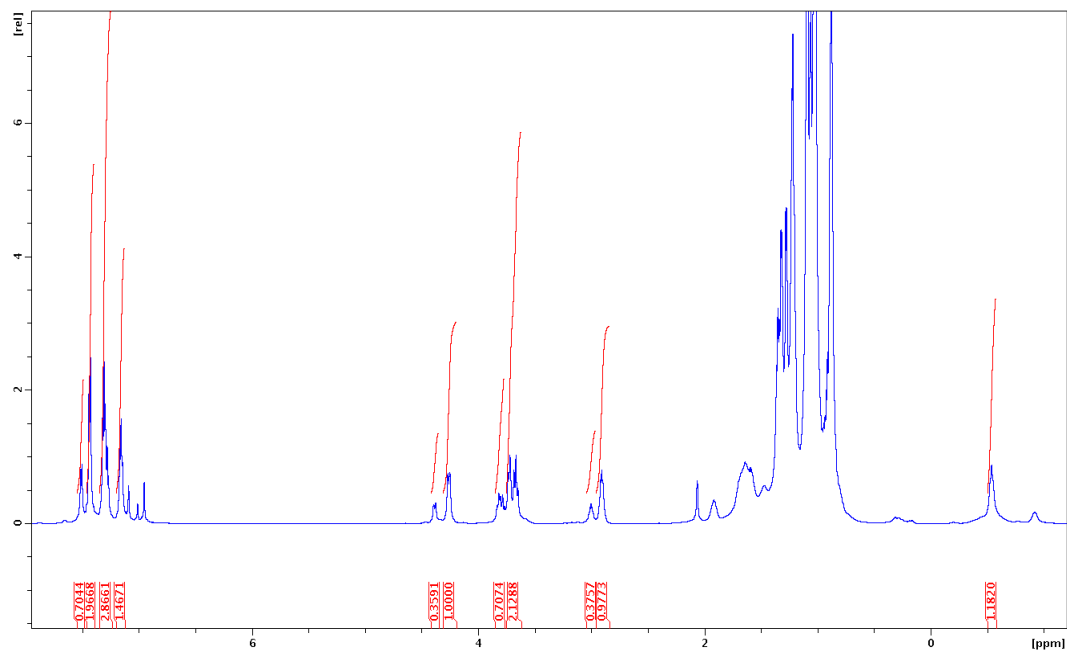


Figure S10.27. ^1H NMR of Complexes **13** and **14** in $\text{toluene-}d_8$ at -40°C

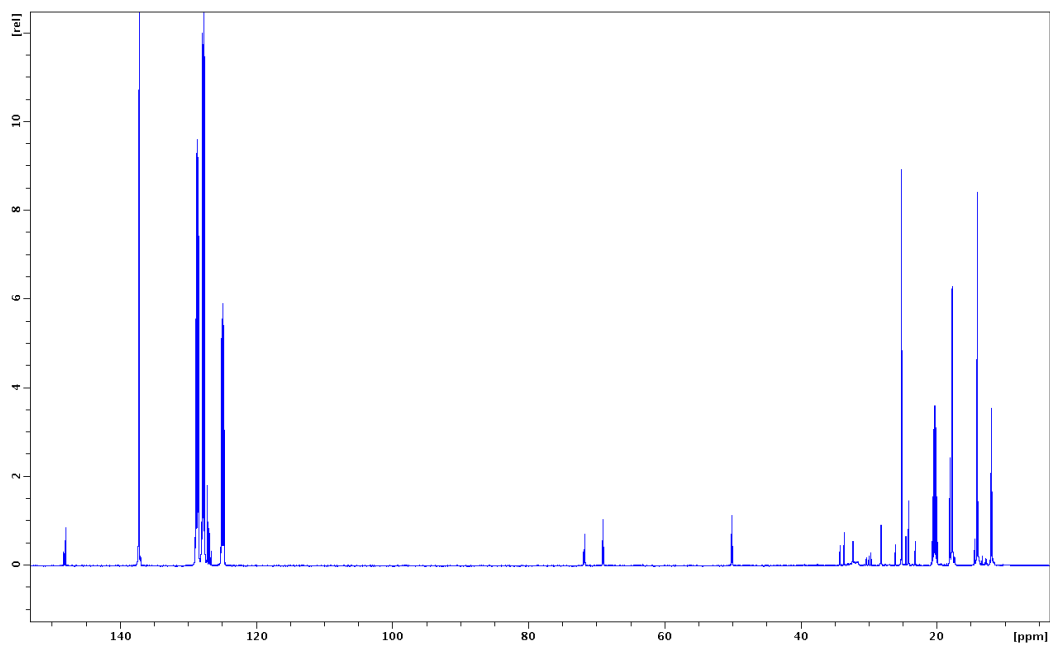


Figure S10.28. ^{13}C NMR of Complexes **13** and **14** in $\text{toluene-}d_8$ at -40°C

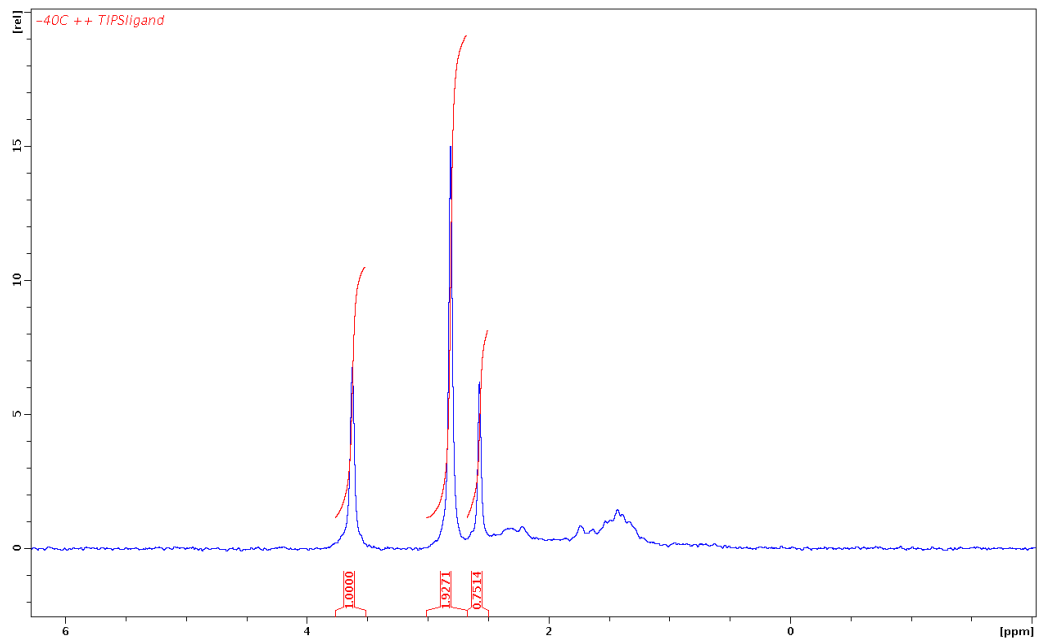


Figure S10.29. ${}^6\text{Li}$ NMR of Complexes **13** and **14** in toluene- d_8 at $-40\text{ }^\circ\text{C}$

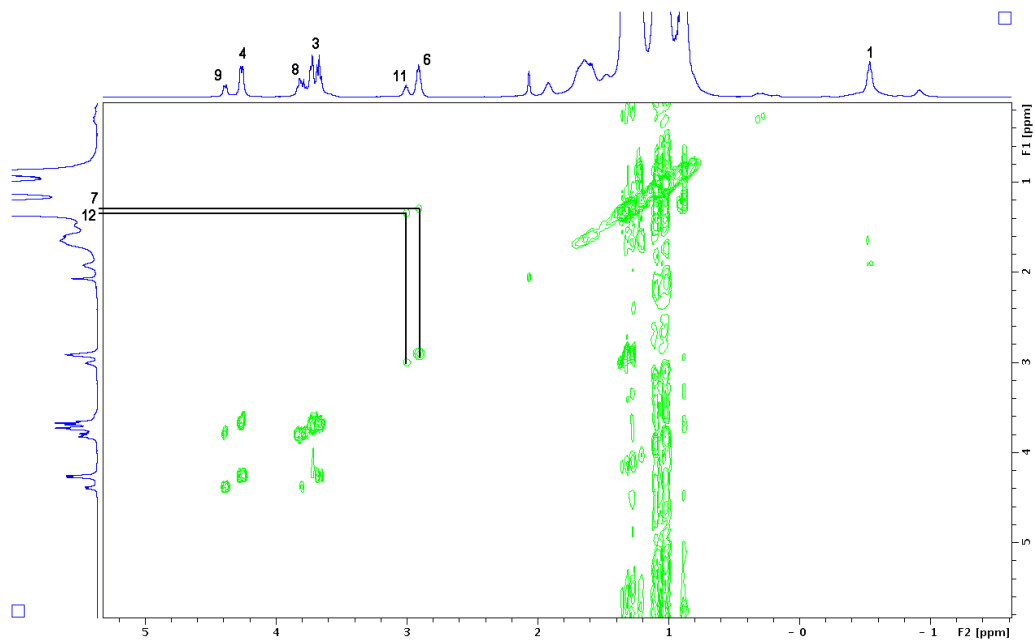


Figure S10.30. ${}^1\text{H}$ COSY of Complexes **13** and **14** in toluene- d_8 at $-40\text{ }^\circ\text{C}$

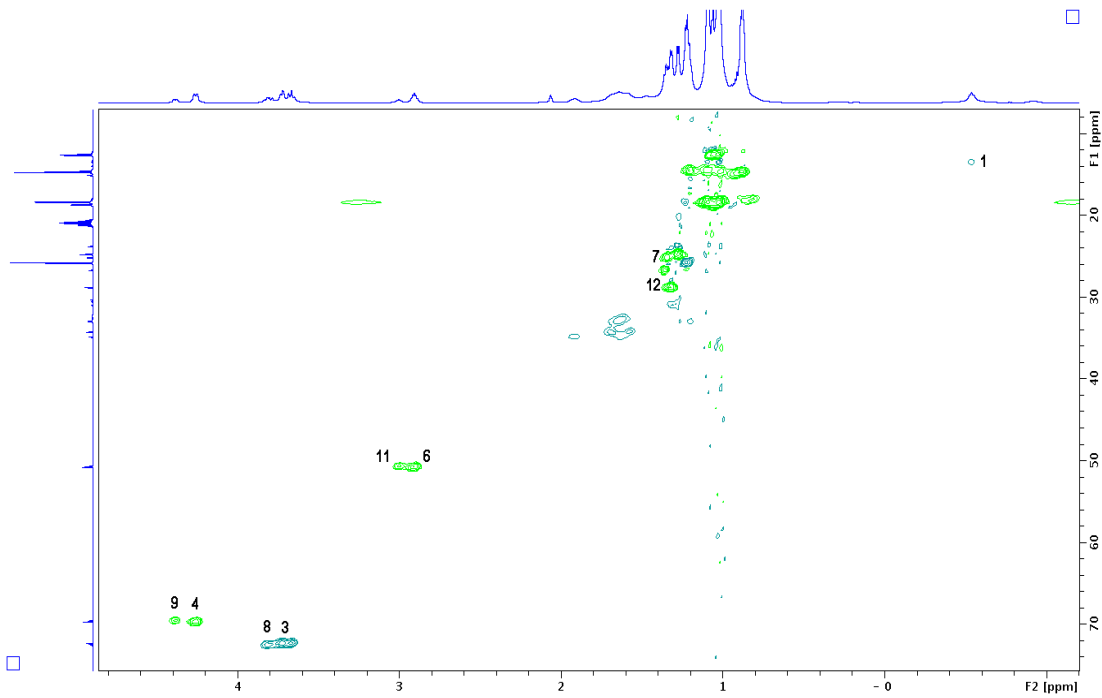


Figure S10.31. ^1H - ^{13}C HSQC of Complexes **13** and **14** in toluene- d_8 at $-40\text{ }^\circ\text{C}$

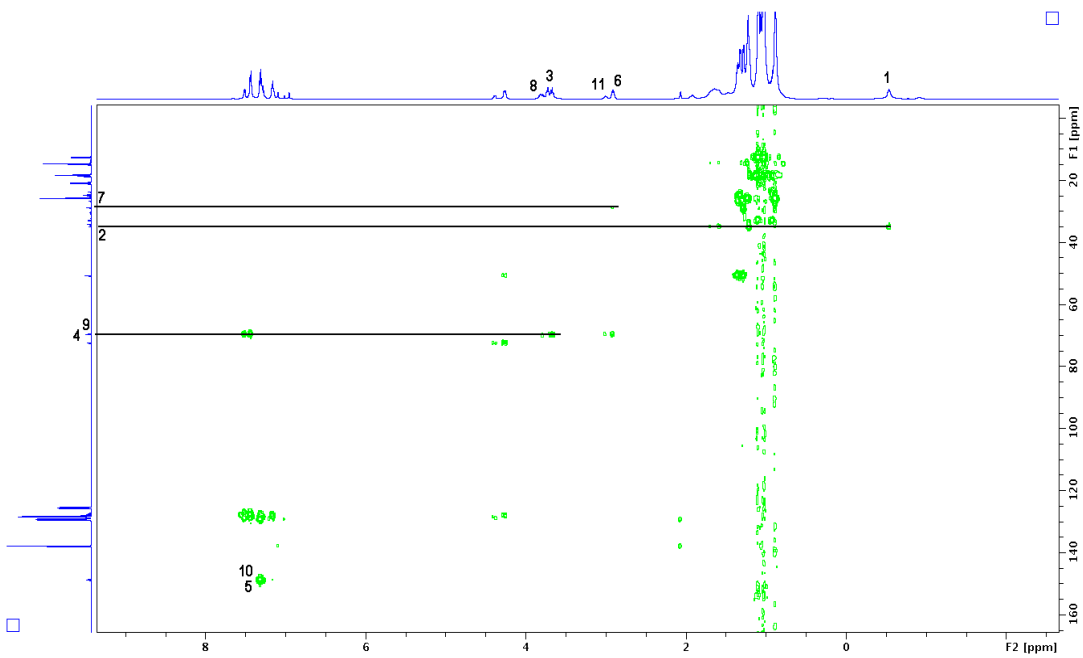


Figure S10.32. ^1H - ^{13}C HMBC of Complexes **13** and **14** in toluene- d_8 at $-40\text{ }^\circ\text{C}$

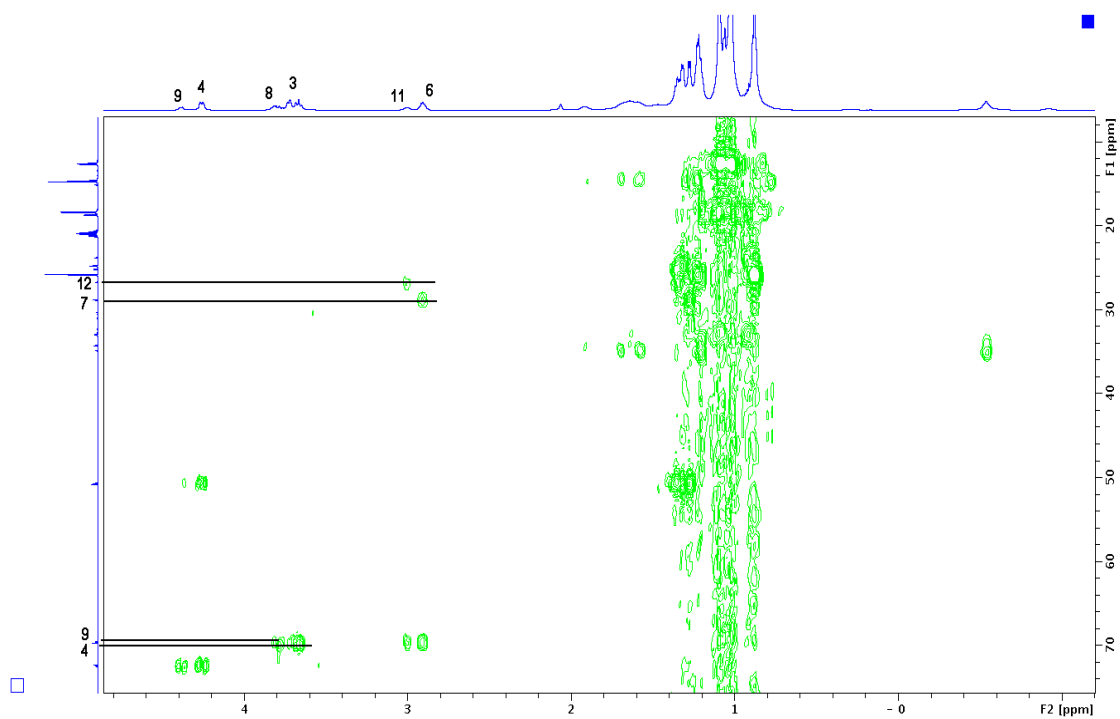


Figure S10.33. ^1H - ^{13}C HMBC of Complexes **13** and **14** in toluene- d_8 at $-40\text{ }^\circ\text{C}$ (Enlarged)

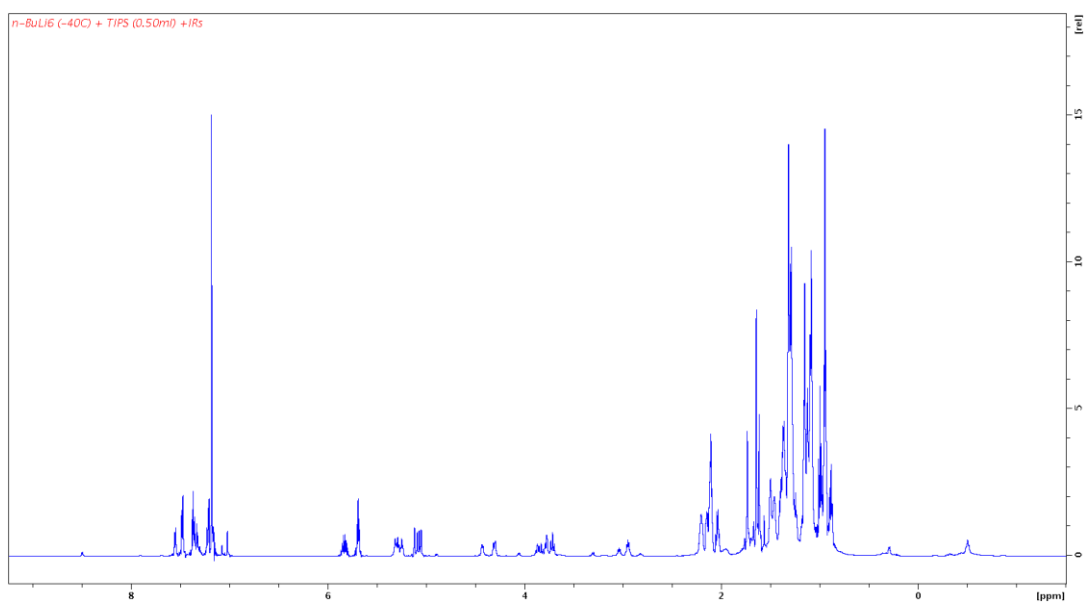


Figure S10.34. ^1H NMR of Complexes **13** and **14** in toluene- d_8 with Internal References at $-40\text{ }^\circ\text{C}$

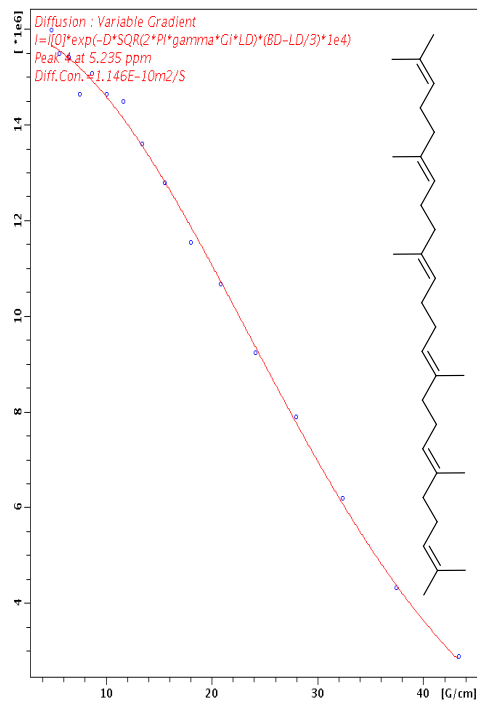
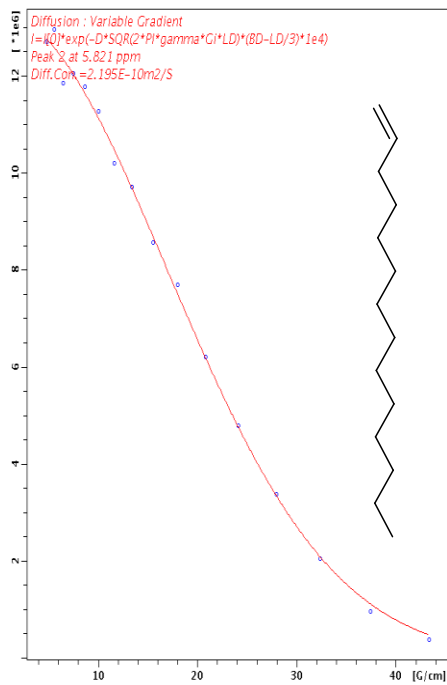
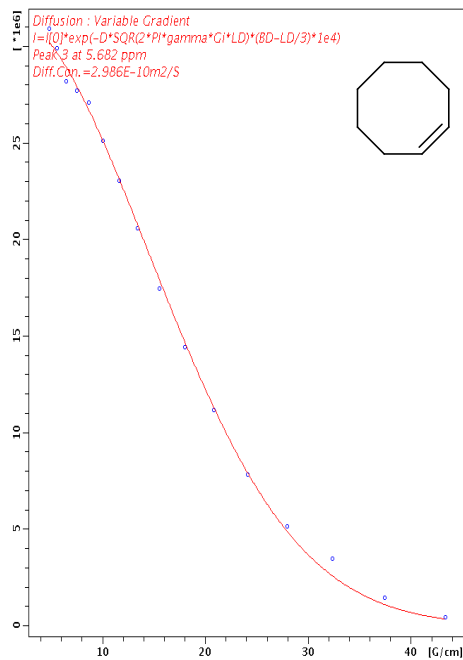
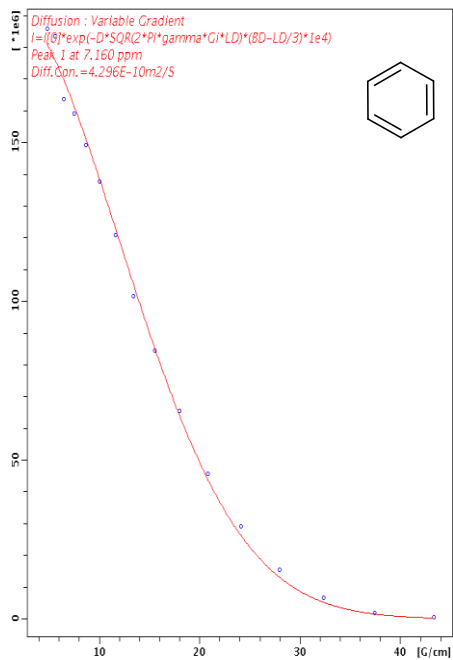


Figure S10.35. ¹H DOSY Decay Curves for Internal References

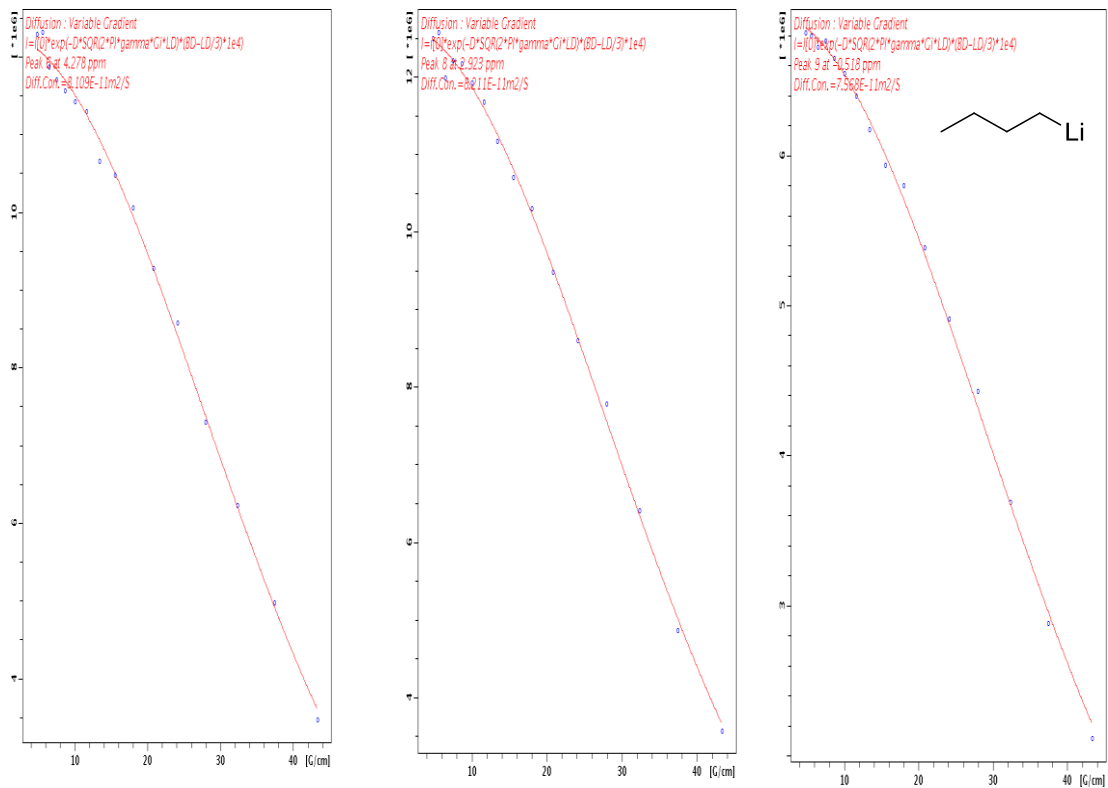


Figure S10.36. ^1H DOSY Decay Curves for Mixed Aggregate **13**

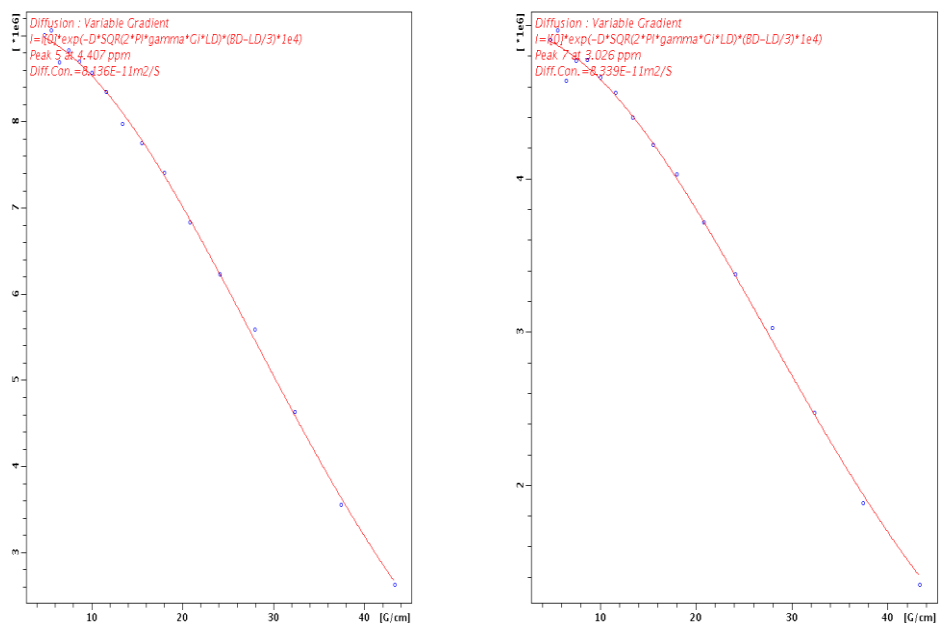


Figure S10.37. ^1H DOSY Decay Curves for Homodimer **14**

Table S10.3. D-FW Analysis of ^1H DOSY data of Complexes **13** and **14** in toluene- d_8 solution at $-40\text{ }^\circ\text{C}$

Compd	FW (g/mol)	10^{-10}D (m^2/s)	log FW	log D	Predicted FW (g/mol)	% error
BEN	78.11	4.296	1.893	-9.367	75.27	3.6
COE	110.2	2.986	2.042	-9.525	121.0	-9.8
TDE	196.4	2.195	2.293	-9.659	180.7	8.0
SQU	410.7	1.146	2.614	-9.941	421.9	-2.7
13 ^a	743.4 ^b	0.811 ^a	2.871	-10.091	662.4	10.9
13 ^a	743.4 ^b	0.821 ^a	2.871	-10.086	651.7	12.3
13 ^c	743.4 ^b	0.757 ^c	2.871	-10.121	724.8	2.5
14	681.2 ^d	0.814	2.833	-10.090	659.5	3.2
14	681.2 ^d	0.834	2.833	-10.079	638.7	6.2
13 ^e	743.4 ^b	0.796 ^e	2.871	-10.099	678.3	8.8
14 ^f	681.2 ^d	0.824 ^f	2.833	-10.084	649.0	4.7

^aThe measured diffusion coefficients are from the resonances of chiral lithium amide. ^b743.4 g mol^{-1} is the formula weight of 2:1 lithiated chiral amine **9**/ n -BuLi (^6Li labeled) complex **13**. ^cThe measured diffusion coefficient is from the α -methylene protons peak (-0.54 ppm) of n -BuLi. ^d681.2 g mol^{-1} is the formula weight of homodimer **14**. ^eThe diffusion coefficient is the average of the above three values. ^fThe diffusion coefficient is the average of the above two values.